SEDIMENT COMPOSITION OF PERIPLATFORM SEDIMENTS AND CALCITURBIDITES AROUND PEDRO BANK, SOUTHWESTERN CARIBBEAN SEA

SEDIMENTZUSAMMENSETZUNG VON PERIPLATFORMSEDIMENTEN UND KALKTURBIDITEN IM BEREICH DER PEDRO BANK, SÜDWESTLICHES KARIBISCHES MEER

Dissertation
zur Erlangung des Doktorgrades
der Mathematisch-Naturwissenschaftlichen Fakultät
der Christian-Albrechts-Universität
zu Kiel, Deutschland

vorgelegt von
Nils Andresen

Kiel 2000

Referent/ in:	**Prof. Dr. W.-Chr. Dullo**
Korreferent/ in:	**Prof. Dr. Chr. Betzler**
Tag der mündlichen Prüfung:	**15. November 2000**
Zum Druck genehmigt: Kiel, den	**15. November 2000**
Der Dekan	**gez. Prof. Dr. Thomas Bauer**

ABSTRACT

Spatial and temporal variations in the carbonate production and sediment export of the Pedro Bank carbonate platform were studied in response to the late Quaternary sea level fluctuations. A set of nine sediment cores were obtained from up- and downcurrent position to Pedro Bank to form a downcurrent offbank transect that covers the proximal toe-of-slope to a distal basinal setting. The sediments studied were deposited between 650 to 2520 meter below recent sea level, and reach back until oxygen isotope stage 9, i.e. until approximately 300-310 ky. The sediments recovered are rather uniform, and consist of foraminifer- and pteropod-bearing aragonite-rich mud- to wackstones. This typical periplatform lithology incorporates calciturbidites, which are of pelagic as well as neritic origin. The pelagic sourced turbidites are generally evident as fine tail-end turbidites, whereas the few neritic calciturbidites are present as coarse pack- to grainstones.

The sediments were analysed on their ability to record the export patterns of neritic sediment from the shallow tops of Pedro Bank. Therefore mineralogical, sedimentological and geochemical analyses were performed. The aragonite and strontium content were found to be good indicators for variations in shallow-water sediment export. The geochemistry data, as well as the grainsize and component distribution patterns, were useful to differentiate between primary sediment input signals and secondary processes such as dissolution and preservation of metastable carbonates at the seafloor.

This study shows that during the last 300 ky (1) sea-level fluctuations, but also the (2) ocean currents, (3) pelagic and neritic sediment production, (4) dissolution of metastable sediment constituents, and (5) input of non-carbonates have had a major control on the sediment dispersal, sediment deposition and composition, especially along the downcurrent margin, where main neritic export occurs. The mineralogical and grain-size composition documents this variability of periplatform sedimentation along the margins off Pedro Bank. In addition, it was found that also the seafloor morphology plays an important role for the spatial and temporal evolution of the periplatform sedimentation in the vicinity of Pedro Bank, which is situated in a tectonically active plate margin setting.

The analyses of a series of periplatform cores taken from the surrounding of Pedro Bank showed that based on mineralogical, grain-size and microfacies studies characteristic depositional environments existed during the last 300 ky, both in space and time. The spatial variability of periplatform sedimentation shown by the mineralogical and grain-size data along a transect off the leeward margin of Pedro Bank exhibits the response of the neritic platform environment to climatic and sea-level changes and its export pattern towards the slopes and into the adjacent basins.

Offbank shedding of neritic sediment components (aragonite and high-Mg calcite) can be observed within a halo of about 20 km at the downcurrent margin, where main export from the platform occurs. During **interglacial highstands in sea level,** the fine sediment fraction (<63 µm) dominates periplatform sediments along the entire leeward transect and no spatial variations could be observed. The sediments are dominated by fine aragonite. Within the subclasses of the coarse fraction (>63 µm) the very fine sand fraction dominates only at proximal sites (<20 km) showing the export potential of the shallow-water realm. More distal sites (>20 km) exhibit a more bimodal distribution pattern in the coarse grain sizes with maximum amounts within the very fine and the medium sand fraction, indication a mixed neritic/pelagic signal. The sediment composition during highstands in sea level revealed that only minor export of coarse neritic grains into the deep surrounding of Pedro Bank takes place. The interglacial periplatform sediments are characterised by a low coarse fraction content and a dominance of coarse planktic grains like planktic foraminifera and pteropods. Microfacies analyses showed that even in proximal depositional settings close to the toe-of-slope, coarse bank-derived grains only occurred at an average of about 4 vol.%. The individual groups of coarse shallow-water grains do not show any clear glacial/interglacial distribution pattern, whereas planktic foraminifera and pteropods, which form major parts of the coarse fraction, show very similar temporal variations with high amounts during glacials and low amounts during interglacial periods.

During **glacial lowstands in sea level** a twofold division is evident in the spatial distribution of the periplatform sediments. A proximal environment (<28 km) with enhanced percentages in coarse fraction content (22-33%) vs. a distal environment (> 28 km) with a strong dominance of the fine fraction (> 90%). The increased coarse fraction content at the proximal sites results from various interacting contemporaneous processes: (1) lower input of fine neritic sediments, (2) increased current winnowing, and (3) redepositional processes at the upper slope during lowered sea-level stands, and the export of this material to “proximal basinal” sites (< 28 km). In the coarse fraction subclasses a similar distribution pattern is found at all sites showing a bimodal distribution. This might show the low neritic influence, and a similar influence of pelagic sedimentation at all sites during glacials. During

glacials, when preservation of metastable carbonate minerals is enhanced at intermediate water depths, aragonite still shows a general decrease with greater offbank distance, whereas HMC shows highest accumulation rates at about 1000-1400 mbsl (= 20-42 km offbank distance), which might result from submarine precipitation of HMC-cements or the erosion and redeposition of these cements from upper slope settings combined with better preservation potential under the influence of intermediate water masses.
The mineralogy, turbidite distribution as well as composition analyses of the periplatform sediments deposited during lowered **interstadial sea-level stand of marine isotope stage 3** might be indicative for enhanced neritic production at the top of Pedro Bank. This productivity might be caused by the inclined bank top morphology with its deepest parts at the northwestern edge.
In upcurrent locations the carbonate mineralogy displays a similar spatial evolution as seen along the downcurrent margin, but with overall reduced amounts. This is due to the lower export potential of the platform regime against the main direction of the Caribbean Current, one important factor for neritic sediment dispersal in the study area. Turbidites and coarse glacial periplatform sediments from upcurrent settings show a slightly higher abundance of typical shallow-water grains, which mirrors the different faunal composition at the top of Pedro Bank with its shallower bank top depths in comparison to the downcurrent margins.
Lagtimes between sea-level and the timing of deposition of sediment export proxies (e.g. $\delta^{18}O$ vs. aragonite) were observed within several sediment cores from the surrounding of Pedro Bank. These lagtimes probably were caused by the inclined bank-top morphology, which results in a different timing of bank-top flooding of Pedro Bank on either the northern or southern margin. This pattern could not be observed in all cores, which might be the result from a variety of other processes such as: (1) early diagenesis, (2) relative position to the bank margin, (3) seafloor morphology and (4) syn- and postdepositional dissolution of metastable carbonates, which might might have affected the metastable sediment constituents to a varying degree.

The study of calciturbidites shows that the highstand "bundling" of calciturbidites is well developed even in the tectonically active setting of the Northern Nicaragua Rise close to the Caribbean plate boundary. The high- to lowstand turbidite frequency for the last 300 ky is the same with 3 times more highstand than lowstand turbidites during the last 3 glacial-interglacial cycles. This consistency might indicate that no major depositional changes occurred within the Pedro Bank carbonate system during this time interval. Turbidite deposition in the vicinity of Pedro Bank is controlled by: (1) late Quaternary sea-level fluctuations, (2) sediment production and overloading of the upper slope, (3) proximity of the core location to the bank margin, (4) local slope morphology and (5) seafloor morphology, which provides a line source for turbidites through gullies and canyons. At the end of these canyon and gully systems the turbidites are deposited in the distal flat-floored basins, which records the history of turbidite shedding at the best.
Fluctuations in sea-level are clearly marked by turbidite deposition during transitional times. This is especially evident during the onset of bank-top flooding, subsequent neritic sediment overproduction, and offbank export, which is usually recorded by the onset of turbidite deposition at various sites along several platform-to-basin transects in down- and upcurrent slope settings.
Only a few calciturbidites within the up- and downcurrent cores, show a distinct amount of bank-derived grains. However, the majority of calciturbidites from the periplatform setting of Pedro Bank show a dominance of a fine aragonitic matrix (ooze) and of coarse pelagic grains, predominantly planktic foraminifera and pteropods. As the neritic grains were not only found at proximal sites, sedimentation of platform-sourced turbidites is probably associated with the local seafloor morphology. Gullies and canyons act as major pathways for these turbidites, which most probably originate from the upper slope to toe-of-slope setting.

The results of the geochemical studies in Pedro Bank periplatform sediments show that the measurement of strontium in periplatform sediments can be used to differentiate between: (1) neritic input (high-Sr-aragonite) and (2) pelagic sources (low-Sr-aragonite) for the aragonite content in the periplatform sediments of Pedro Bank. The shallow, proximal sites clearly mirror the input of neritic-sourced Sr, which is mainly bound in the aragonite of the fine fraction. This becomes evident as both Sr-aragonite varieties display their own temporal trend. At distal sites situated below the depth of beginning dissolution of metastable carbonates at about 1100 mbsl at the NNR, the temporal pattern of low- and high-Sr aragonite become very similar, suggesting that dissolution affected both varieties of Sr-aragonite in the same way.

KURZFASSUNG

Im Rahmen dieser Dissertation wurden die zeitlichen und räumlichen Veränderungen in der Karbonatproduktion, vor allem aber im Sedimentexport der Pedro Bank im Zuge der spatquartären Meeresspiegelschwankungen während der letzten 300.000 Jahre untersucht. Hierfür wurden 9 Sedimentkerne aus stromauf- und abwärts gelegenen Positionen zur Pedro Bank gewonnen, wodurch u.a. ein Tiefenprofil entlang des leewärtigen Hanges und der angrenzenden sedimentären Becken detaillierter untersucht werden konnte, das sich vom Hangfuß bis in die zentrale Achse des Pedro Channels (92 km Entfernung zum Plattformrand) erstreckt. Die untersuchten Sedimente wurden aus Wassertiefen zwischen 650 und 2520 m gewonnen, und reichen stratigraphisch bis in das späte Sauerstoffisotopenstadium 9 zurück. Die untersuchten Sedimente zeigen alle eine sehr ähnliche Lithologie und bestehen überwiegend aus Foraminiferen- und Pteropoden-führenden, aragonitreichen Mud- und Wackestones. Dieser typischen Periplattformsediment-Lithologie sind Kalkturbidite zwischengelagert, die sowohl pelagischer, als auch neritischer Herkunft sind. Die pelagischen Turbidite treten hauptsächlich als feine "Schlammturbidite" auf, während die neritisch geprägten Turbidite durch gröbere Pack- und Grainstones gekennzeichnet sind.
Die Periplattformsedimente wurden daraufhin studiert, inwieweit sie die Exportvorgänge neritischen Sedimentmaterials von der Plattformoberfläche der Pedro Bank aufzeichnen können. Hierfür wurden neben mineralogischen und sedimentologischen, auch geochemische Analysen durchgeführt. Es konnte z.B. nachgewiesen werden, daß Aragonit und Strontium sehr gute Indikatoren für zeitliche Veränderungen im Sedimentexport aus dem Flachwasserbereich darstellen. Desweiteren zeigen die geochemischen, sowie auch die Korngrößen-Analysen und die Ergebnisse der Sedimentzusammensetzung, daß sie brauchbare analytische Hilfsmittel für die Studien in Karbonatsystemen sein können, um z.B. primäre Sedimenteintragssignale von sekundären Prozessen, wie die Lösung oder Erhaltung von metastabilen Karbonaten am Meeresgrund während der letzten 300.000 Jahre zu rekonstruieren.
Die generellen Ergebnisse dieser Studie zeigen deutlich, daß im Untersuchungszeitraum folgende Faktoren die Verteilung und Ablagerung von Sedimenten und vor allem die Sedimentzusammensetzung kontrolliert haben: (1) die Meeresspiegelschwankungen, (2) der Einfluß von Meeresströmungen, (3) die pelagische und neritische Sedimentproduktion, (4) die Lösung und/oder die Erhaltung metastabiler Karbonate, und (5) der Eintrag von nicht-karbonatischem Material.
Diese Veränderungen in der Periplattformsedimentation sind deutlich in der Mineralogie als auch der Zusammensetzung der Korngrößen dokumentiert. Außerdem konnte anhand der vorliegenden Analysen erkannt werden, daß die Meeresbodenmorphologie im Bereich der Plattformhänge und der angrenzenden sedimentären Becken eine weitere wichtige Rolle für die zeitliche und räumliche Entwicklung der Periplattformsedimentation in der Nähe der Pedro Bank spielen. Die Analyse von mehreren Periplattformsedimenten aus der Umgebung der Pedro Bank Karbonatplattform hat gezeigt, daß, basierend auf mineralogischen, Korngrößen-analytischen und Mikrofazies-Studien, charakteristische Ablagerungsräume während der letzten 300.000 Jahre existierten - sowohl im zeitlichen als auch im räumlichen Rahmen. Besonders die räumliche Variabilität in der Periplattformsedimentation, wie sie sich in den den sedimentologischen Analysen entlang eines 92 km langen Tiefenprofiles am leewärtigen Plattformrand zeigen, offenbart die Reaktion des neritischen Ablagerungsraumes zu den Veränderungen im Klima und des Meeresspiegels im Untersuchungszeitraum, und die daraus resultierenden Sediment-Exportmuster auf die angrenzenden Hänge und Becken.

Innerhalb eines Bereiches von 20 km entlang des leewärtigen Plattformrandes kann ein klares Exportmuster von neritischen Sedimentkomponenten (Aragonit und Hoch-Mg-Kalzit [HMC]) beobachtet werden. Während **interglazialer Meeresspiegelhochstände** dominiert dort auch die Feinfraktion (<63 µm) die Periplattformsedimentation, und es konnte auch keine räumliche Variabilität in der Konzentration der Feinfraktion beobachtet werden. Zudem werden die untersuchten Sedimente von metastabilem Aragonit dominiert. Innerhalb der Grobfraktion überwiegen der Feinstsandanteil nur in Ablagerungsräumen von <20 km zum Plattformrand, ein deutlicher Indikator für das Exportvermögen des Flachwassermilieus der Pedro Bank. Der distalere Ablagerungsraum entlang des leewärtigen Plattformrandes (>20 km) zeigt hingegen ein bimodales Korngrößenverteilungsmuster mit höchsten Anteilen in der Feinstsand- und der Mittelsandfraktion. Dieses Muster deutet auf ein gemischt neritisch-pelagisches Sedimentsignal hin. Die Zusammensetzung der Sedimente während Meeresspiegelhochständen offenbarte einen nur sehr geringen Export von grobkörnigerem (>63 µm) neritischen Sedimentmaterial, und eine Dominanz von groben planktischen Sedimentbestandteilen, vor allem von

planktischen Foraminiferen und Pteropoden. Die Mikrofaziesanalyse zeigt auch, daß selbst in proximalen Ablagerungsräumen nahe zum Hangfuß der Plattform grobes, neritisches Sedimentmaterial im Schnitt mit nur 4 Vol.% abgelagert wurde. Die individuellen Flachwasser-Sedimentkomponenten spiegeln ebenfalls kein klares Glazial-Interglazial-Exportmuster wider. Planktische Foraminiferen und Pteropoden hingegen, die den Hauptbestandteil der Grobfraktion stellen, zeigen sehr ähnliche zeitliche Trends mit hohen Anteilen während der Glaziale und niedrigen Gehalten während interglazialer Meeresspiegelhochstände.
Während **glazialer Meeresspiegel-Niedrigstände** hingegen ist eine Zweiteilung im räumlichen Verteilungsmuster der Periplattformsedimente erkennbar. Es kann zwischen einem proximalen (<28 km) Ablagerungsraum mit erhöhten Grobfraktionsanteilen (22-33%) und einem distalen Ablagerungsmilieu (>28 km) unterschieden werden, der durch eine Dominanz der Feinfraktion (>90%) gekennzeichnet ist. Die erhöhten glazialen Grobfraktionsanteile in den proximalen Kernpositionen resultieren aus verschiedenen zeitgleich wechselwirkenden Prozessen: (1) geringer Eintrag von neritischem Sedimentmaterial, (2) erhöhte Strömungssortierung, und (3) Umlagerungsprozesse auf dem oberen Hang während niedriger Meeresspiegelstände und dem Export dieses umgelagerten Sedimentmaterials in den "proximal" gelegenen Ablagerungsraum (<28 km). In den Subfraktionen der Grobfraktion ist entlang des gesamten Tiefentransektes während der Glaziale eine bimodale Verteilung vorhanden. Dies zeigt offensichtlich den geringen neritischen, aber auch den sehr gleichbleibenden pelagischen Eintrag in allen untersuchten Sedimentkernen des Transektes in den Glazialen. Während dieser Zeitabschnitte, wenn metastabile Karbonate unter dem Einfluß intermediärer Wassermassen eine erhöhtes Erhaltungspotential zeigen, nimmt der Gehalt an Aragonit dennoch mit zunehmender Entfernung von der Karbonatbank ab. HMC hingegen zeigt höhere Akkumulationsraten zwischen 1000-1400 m Wassertiefe (= 20-42 km Entfernung zur Pedro Bank), möglicherweise hervorgerufen durch submarin-ausgefällte HMC-Zemente oder die Erosion und Umlagerung dieser Zemente aus dem Bereich des oberen Hanges sowie das bessere Erhaltungspotential in den Glazialen.
Die Mineralogie, die Verteilung und das Auftreten von Turbiditen sowie die Zusammensetzung der Periplattformsedimente während des **Sauerstoffisotopenstadiums 3** deuten außerdem auf eine erhöhte neritische Produktivität auf der Oberfläche der Pedro Bank hin. Diese Produktion von neritischem Sedimentmaterial ist wahrscheinlich aufgrund der geneigten Plattformoberfläche und der daraus resultierenden Tiefenlage mit den tiefsten Teilen der Pedro Bank im Nordwesten der Plattform möglich.

In den stromaufwärts gelegenen Kernpositionen zeigt die Karbonatmineralogie ein ähnliches räumliches Sedimentationsmuster, wie es für für die leewärtige Seite der Pedro Bank beschrieben wurde, jedoch mit deutlich reduzierten prozentualen Anteilen. Dies ist auf das geringe Sedimentexportpotential der Plattform entgegen der vorherrschenden Richtung des Karibikstromes zurückzuführen, der ein Hauptfaktor für die Verteilung von neritischem Sedimentmaterial entlang der Karbonatplattformen des nördlichen Nicaragua Rückens ist. Die Turbidite als auch die gröberen glazialen Periplattformsedimente aus dem stromaufwärts gelegenen Ablagerungsraum zeigen einen leicht höheren Anteil an typischem Flachwassermaterial. Dies spiegelt klar die unterschiedliche Faunenzusammensetzung zwischen der flacheren, windwärtigen und der tieferen, leewärtigen Plattformoberkante wider.
Ein weiteres interessantes Muster, das durch den Vergleich der verschiedenen untersuchten Proxies augenscheinlich wird, ist das Vorhandensein von "Lagtimes" zwischen Meeresspiegel-Proxies (z.B. $\delta^{18}O$) und den Sedimentexport-Proxies (z.B. Aragonit). Solche zeitlichen Differenzen zwischen diesen beiden Proxies konnten in einigen Sedimentkernen aus der Umgebung der Pedro Bank erkannt werden. Diese "Lagtimes" werden wahrscheinlich durch die geneigte Plattformoberfläche mitverursacht. Dies hat zur Folge, daß das initiale Überfluten der Plattformoberfläche im Zuge von Meeresspiegelanstiegen zu unterschiedlichen Zeiten an der nördlichen, tieferen und der südlichen, flacheren Plattformoberkante stattfindet. Dieses Muster wurde jedoch nicht in allen analysierten Sedimentkernen beobachtet, was durch verschiedene Prozesse bewirkt werden kann, wie (1) frühe Sedimentdiagenese, (2) die relative Lage des Ablagerungsraumes zum Plattformrand, (3) die Meeresbodentopographie und (4) syn- und postdepositionale Lösung von metastabilen Karbonaten, die die metastabilen Sedimentanteile in unterschiedlichem Ausmaß in den einzelnen Kernen beeinflußt haben kann.
Eine weitere Studie in dieser Dissertation hat gezeigt, daß die "Hochstands-Bündelung" von Kalkturbiditen auch in einem von aktiver Tektonik geprägtem Ablagerungsmilieu, wie dem des nördlichen Nicaragua Rückens, sehr deutlich ausgeprägt ist. Die Frequenz von Meeresspiegel-Hochstands- zu Tiefstandsturbiditen während der letzten 300.000 Jahre zeigt ein gleichbleibendes Muster mit einem dreifach höheren Anteil an Hochstandsturbiditen während der letzten 3 vollständigen Glazial-Interglazial-Zyklen. Die Einheitlichkeit könnte darauf hindeuten, daß während des untersuchten

Ablagerungszeitraumes keine tiefgreifenden Veränderungen im Ablagerungsmilieu stattgefunden haben. Innerhalb der Untersuchungen konnte festgestellt werden, daß die Ablagerung von Turbiditen in der Umgebung der Pedro Bank von mehreren Faktoren beeinflußt und gesteuert wird: (1) die spätquartären Meeresspiegelschwankungen, (2) die Sedimentproduktion und die Überladung des oberen Hanges, (3) die Nähe der Kernposition zum Rand der Karbonatplattform, (4) die lokale Hangmorphologie und (5) die Meeresbodentopographie, die eine "line source" für Turbidite durch Rinnen und Canyons darstellt. Am Ende dieser Rinnensysteme werden die Turbidite dann in distalen sedimentären Becken mit einer flachen Beckenmorphologie abgelagert, in denen die Ablagerungsgeschichte der Turbiditschüttungen am besten dokumentiert wird.
Schwankungen im Meeresspiegel sind demnach deutlich durch die Ablagerung von Turbiditen in eben diesen Übergangsintervallen des Meeresspiegelganges gekennzeichnet. Dies wird insbesondere während des Überflutungsbeginns der Plattformoberfläche, der darauffolgenden neritischen Sedimentproduktion und dem Export dieses Sedimentmaterials deutlich. Dieses Szenario führt gewöhnlicherweise zum Beginn der Ablagerung von Turbiditen auf den lee- und windwärtigen Hängen und Becken der Pedro Bank entlang der untersuchten Plattform-Becken-Profile.
Die Sedimentzusammensetzung in einigen wenigen Kalkturbiditen zeigt ebenfalls nur einen geringen Anteil von Flachwassermaterial. Generell wird die Mehrheit der untersuchten Kalkturbiditlagen durch das Vorherrschen einer feinen aragonitischen Matrix sowie einem Überwiegen von grobem, pelagischen Sedimentmaterial, vornehmlich planktischer Foraminiferen und Pteropoden, gekennzeichnet. Neritische Sedimentkomponenten werden sowohl im proximalen als auch distalen Ablagerungsraum gefunden. Dies zeigt deutlich, daß die Sedimentation der von der Plattform stammenden Turbidite wahrscheinlich eng mit der lokalen Meeresbodenmorphologie verbunden ist. Die vorher erwähnten Rinnensysteme fungieren daher wahrscheinlich als Hauptlieferwege für die neritischen Turbidite, die hauptsächlich vom oberen Plattformrand oder dem Bereich des Hangfußes stammen.

Die Ergebnisse der geochemischen Analysen an Periplattformsedimenten zeigen, daß der Gehalt an Strontium im Gesamtsediment verwendet werden kann, um zwischen (1) neritischem Sedimenteintrag (High-Sr-Aragonit) und (2) pelagischen Sr-Quellen (Niedrig-Sr-Aragonit) zu unterscheiden. Die flacheren und proximalen Ablagerungsräume spiegeln deutlich den Eintrag von neritischen Sr wider, der hauptsächlich an den Aragonitanteil der Feinfraktion gebunden ist. Dies wird dadurch deutlich, daß die beiden unterschiedlichen Sr-Varietäten einen eigenen zeitlichen Trend in den proximalen Kernen widerspiegeln. In den distalen Ablagerungsräumen, unterhalb der Wassertiefe, in der die Lösung metastabiler Karbonatphasen beginnt (ca. 1100 m am NNR), sind die zeitlichen Muster von Niedrig- und Hoch-Sr-Aragonit sehr ähnlich, was darauf hindeutet, daß Lösungvorgänge beide Sr-Aragonit-Varitetäten gleichmäßig beeinflußt haben.

ACKNOWLEDGEMENTS

The completion of this thesis would not have been possible without the support of numerous persons, whom I want to thank at this place.

First of all I am indebted to Dr. John Reijmer for his perpetual support, supervision, collaboration and scientific input during the entire four years working on this thesis. Without his support many things in this thesis wouldn´t have been possible. I am also very grateful to Professor Wolf-Christian Dullo for giving me the chance to start this thesis at his working group at GEOMAR. Also I want to thank him for supervising this thesis, and for the support during the entire study.

I am very indebted to Prof. Andre Droxler from Rice University, who provided a lot of help and support during this study. He shared his extensive knowledge on the geology, paleoceanography and sedimentology of the Northern Nicaragua Rise carbonate system, made it possible to obtain additional sediment samples from the vicinity of Pedro Bank, which helped to extend the margin-to-basin transect. He also provided the 3.5 kHz seismic lines which were extremely helpful for a major outcome of this study. In addition, I am thankful to him for giving me the chance to visit Rice University during my Ph.D. project, and his hospitality during my stay in Houston.

Prof. Christian Betzler from the University of Frankfurt is thanked for reviewing a previous version of the thesis and for giving valuable suggestions and hints.

Furthermore I want to thank various other scientists for their help and discussions of single results of this thesis, as there are: Gideon Henderson for the U/Th analyses; Ralf Tiedemann and Dirk Reese from the GEOMAR mass spectrometer laboratory for the isotope analyses; the Leibnitz Laboratory for age determinations at the Christian Albrechts University of Kiel for providing the ^{14}C age determinations; Jutta Heinze, who helped with the XRD measurements; Kerstin Wolf who did the XRF-measurements at GEOMAR; Dagmar Rau for preparing the thin-sections; and the laboratory assistants Steffen Zamhöffer, “Alex” Palmeiro-Beck, Johanna Suhonen, Thorsten Bauch and Tina Kuhlmann, who helped with measuring data during the last four years gaining the majority of data presented in this study.

Also I want to thank the members of the “carbonate reef” group at GEOMAR: Jens Zinke, Ingo Gläser, Florian Böhm, Miriam Pfeiffer, Dierk Blomeier and especially Peter Emmermann, who did a comparable study in the Red Sea. I want to thank him for his help onboard the M35/1 cruise to Pedro Bank, his valuable discussions about carbonate sedimentology and microfacies during his time at GEOMAR. In addition, I want to thank the following colleagues at GEOMAR for their fellowship and help, especially Kristina Heilemann, Sven Roth, Arne Sturm, Anja Müller, and Dirk Lukas.

A very special thank goes to my colleague and good friend Rebecca “Bec” Rendle for her support and the fruitful and valuable discussions when comparing the Northern Nicaragua Rise and Great Bahama Bank study areas ... and the four years of daily english “chatting”, which helped much to improve my spoken english.

The shipboard scientific party of the M35/1 cruise to the Northern Nicaragua Rise is thanked for their help with coring and sampling of the Pedro Bank sediment cores onboard R/V Meteor. I also want to thank the master and crew of the R/V Meteor for their technical support. I also would like to thank Dr. Rainer Zahn, chief-scientist during the M35/1 cruise, for his help during the six days at Pedro Bank.

A very special thank goes to Priscilla Huston and Sam Davis, as well as the family Alexandrova in Houston, who offered me to stay at their house during my visit at Rice University. During these eight weeks in Houston we became very good friends and it formed the beginning of a long friendship. From my first day in Houston I was part of the family, and it was not easy to go back to Germany when my visit to Houston ended.
I also want to thank Michelle S. Shearer, a good friend I met during my stay at Rice University. She helped me from the first day I worked at the Geology and Geophysics Department. Thanks for the

great time in Houston! I also want to thank Sookie Kelley and Judy Wagoner from the administration of the Geology and Geophysics Department for their continous help during my stay at Rice.

To GEOMAR and the Geology and Geophysics Department of Rice University, Houston, I am grateful for providing the facilities. Due thanks are also given to the German Science Foundation (DFG), who provided the financial support of this study (DFG Du 129/11).

I would like also to thank my best friend Rolf Muxfeldt for his support, and for being such a great friend all the time. I also would like to thank my very good friends Marlis and Kai Musfeldt for their support and good friendship over all the years. I hope that we will have some more time to spend together now.

To Ms. Hanni Wragge I am indebted for her hospitality and the possibility stay at her house for now more than a year at a special friendship rate. I hope that this friendship grown in the last two years will still last for a long time.

I also want to thank Kathrin for the great time we had since the beginning of this year, and that we will still have a long time to go together.

I want to thank Artur for his financial support, especially during the last phase of this thesis.

Finally, and this is very important to me, I am very grateful to my mother Greta Andresen for all her support during my study and in particular during the entire time of this PhD. Without her hard work over the last 32 years, I wouldn´t be able to be what I am now. “Ja ty kocham”!

CONTENTS

FIGURE LIST

Figures Chapter 7

Figures Chapter 8

Figures Chapter 9

Figures Chapter 10

TABLE LIST

ABBREVIATIONS

MIS	Marine Oxygen Isotope Stage
LSR	Linear Sedimentation Rate
MAR	Mass Accumulation Rate
XRD	X-Ray Diffraction
XRF	X-Ray Fluorescence
mbsl	Meters below sea level
ky	Kilo years (*1.000 years)
Ma	Million years (*1.000000 years)
HMC	High-magnesium calcite
LMC	Low-magnesium calcite
NC	Non-carbonates
AAIW	Antartictic Intermediate Water
NADW	North Atlantic Deep Water
MOW	Mediterranean Outflow Water
SUW	Subtropical Underwater
HST	Highstand Systems Tract
LST	Lowstand Systems Tract
TST	Transgressive Systems Tract
NNR	Northern Nicaragua Rise

TABLE LIST

ABBREVIATIONS

MIS	Marine Oxygen Isotope Stage
LSR	Linear Sedimentation Rate
MAR	Mass Accumulation Rate
XRD	X-Ray Diffraction
XRF	X-Ray Fluorescence
mbsl	Meters below sea level
ky	Kilo years (*1.000 years)
Ma	Million years (*1.000000 years)
HMC	High-magnesium calcite
LMC	Low-magnesium calcite
NC	Non-carbonates
AAIW	Antartictic Intermediate Water
NADW	North Atlantic Deep Water
MOW	Mediterranean Outflow Water
SUW	Subtropical Underwater
HST	Highstand Systems Tract
LST	Lowstand Systems Tract
TST	Transgressive Systems Tract
NNR	Northern Nicaragua Rise

CHAPTER 1

INTRODUCTION

Structure of this thesis
The thesis comprises a sequence of chapters, in which single topics are discussed, and which will later be submitted for publication in scientific journals. Therefore some descriptions of the study area and methods occur repeatedly in different parts of the thesis. The methods are described in chapter 2 in detail, and if necessary additional methodical information is presented in the single subchapters.
Chapter one provides a general introduction to the study area and previous research done along the Northern Nicaragua Rise. Chapter 2 describes the methods used, while in chapter 3 tests on the X-ray diffraction method are shown in more detail. The stratigraphy of all analysed sediment cores is presented in chapter 4. Chapters 5 to 10 deal with the single themes of this study, which include: seafloor topography along platform to basin transects (Ch. 5), accumulation rates (Ch. 6), mineralogy and grain-size studies (Ch. 7), microfacies analysis (Ch. 8), geochemistry studies (Ch. 9), and timing and distribution of calciturbidites (Ch. 10).

1.1. Introduction and main objectives of the study

Shallow-water carbonate platforms, ramps and reefs of the low latitudes are the most important carbonate factories for neritic carbonate production (Schlager & James, 1978). The largest recent shallow-water carbonate production factories that produce large amounts of neritic carbonates to the worlds ocean are the Great Barrier Reef off Australia, the Bahama Bank Platform, the Maldives and Lakkadives and the Trucial coast of the Arabian Sea (e.g. Tucker & Wright, 1990). Beside these hugh carbonate provinces there are several smaller areas that also produce considerable amounts of neritic carbonates, such as several barrier islands and atolls in the Pacific and Indian Ocean, and last but not least the carbonate systems of the Caribbean Sea (Belize Reefs, Saba Bank, Grand Cayman and barrier islands of the Gulf of Mexico). One large carbonate province of the Caribbean Sea is the Northern Nicaragua Rise (NNR) that is thought to have been a large, continuous carbonate system until early Miocene time (Droxler et al., 1998). Today it consists of the carbonate shelfs of Honduras and Nicaragua, the Southern Jamaican Shelf and a series of isolated platforms in between these shelf regions. These isolated carbonate platforms are deeply submerged but highly productive (Triffleman, 1989; Glaser, 1991). Pedro Bank, which is the largest of the NNR´s isolated platforms, and its surrounding basins, forms the focus of this study.

Scientific goals of the Pedro Bank project
The Pedro Bank project was planned as a part of a four week-long scientific cruise onboard *R/V Meteor* carried out in 1996. Using Hydrosweep and Parasound, parts of Pedro Bank and their foreslope morphology as well as the periplatform environment should be mapped. Pedro Bank was choosen because of its inclined bank top morphology. This morphology results in a different flooding history in comparison to those of flat-topped carbonate platforms. In addition, the sediment coverage and the geometry of sediment bodies should be evaluated, especially from the "toe-of-slope" setting. The general aims of the project Pedro Bank, as they were outlined in the primary proposal were:
1. Closing those data gaps of seismic sea- and subbottom morphology in the working area of the Northern Nicaragua Rise that still existed after several american research cruises into the study area, using Hydrosweep, Parasound and SSI Air Guns for 3.5kHz seismics
2. Determine the geometry of the toe-of-slope sedimentary packages, in particular of highstand debris aprons/fans at the toe-of-slope. Also it should be attempted to separate the highstand sediment packages that were shedded during the Holocene and the preceding interglacial (isotope stage 5) by means of high-resolution seismics.
3. To reconstruct the sea level history trough sampling of *in situ* coral skeletons along the upper slope using the submersible JAGO.

4. To establish two offbank sediment core transects along the up- and downcurrent margins of Pedro Bank. In particular the toe-of-slope environment should be sampled extensively for major sedimentary analysis in comparison to studies from similar carbonate environments (Bahamas, Red Sea etc.). Main goal was to determine how the late Quaternary sea level fluctuations were recorded within the carbonate sediments. These new data sets should complement the research done by Glaser & Droxler (1991, 1993) and Triffleman (1992) on the Northern Nicaragua Rise.
5. To estimate the magnitude and rates of sea-level changes using different scientific approaches (foreslope development, sedimentary analysis, dating of *in situ* coral material etc.) and to combine each resulting sea-level curve to a "main sea-level curve" for the study area.
6. To determine slope morphology and slope colonisation, as well as the bathymetric zonation of Pedro Bank.
7. To determine the sedimentary facies of the recent highstand sediments on top of Pedro Bank through sampling of the current shallow-water areas and their living stock in order to obtain an insight into the spectrum of the recent shallow-water environment during an interglacial highstand in sea level.

Aims and objectives of this study

The main objective of the Pedro Bank project was to study the effects of late Quaternary sea-level fluctuations within the context of the evolution of the Pedro Bank carbonate platform. It was attempted to evaluate the sedimentary response of this carbonate system to sea-level fluctuations within the periplatform carbonate sequences. In general the main focus of this thesis was to extend the knowledge of the following topics:
1. Sediment export patterns in downcurrent vs. upcurrent position of the active producing and exporting carbonate platform. To measure temporal and spatial variations in mineralogy, grain size distribution, geochemical composition of the sediments and to give a microfacies overview of the sediments
2. Temporal and spatial distribution patterns of calciturbidites from different settings around Pedro Bank: with an empasis on variations in geochemistry and component composition
3. Variability of the X-ray diffraction measurement method (comparibility of XRD measurements)
Mineralogical, geochemical, microfacies and grain-size analyses were applied on the periplatform sediments recovered to provide information on the export pattern of this deeply submerged and inclined carbonate platform. Furthermore, grain-size and thin-section analyses were used to determine the compositional variability within these periplatform sediments through time (glacials vs. interglacials) and space, e.g. with increasing distance from the active bank margin. These results should be compared to research done on Bahamian periplatform sediments (e.g. Reijmer et al, 1988; Haak & Schlager, 1989; Rendle, 2000) and studies in the Red Sea (Emmermann, 2000). In addition, the point counting carried out on turbidite samples should extend our knowledge on the composition of exported sediment by gravity processes. Finally geochemical analyses were done to obtain information on e.g. the Sr/Ca-ratio of the bulk sediment. This proxy provides another independent indicator for shallow-water input to the periplatform realm as shown by Alexander (1996) for the Great Barrier Reef. In addition, this proxy was used to evaluate the effect of diagenesis on the input signal during sedimentation and burial.
So this part of the Pedro Bank project aimed at understanding how the late Quaternary sea-level fluctuations affected a deeply submerged carbonate platform on the NNR. Previous research mainly focussed on palaeoceanographic questions (e.g Glaser, 1991; Schwartz, 1996; Haddad & Droxler, 1996; Duncan, 1997; Cunningham, 1998), whereas this project was outlined to address the more sedimentological aspects.

Final Dataset

At 25 stations cores were taken, sometimes with minor success, while it showed that the gravity coring device had extreme difficulties to core the sediment found near Pedro Bank because of the existence of very coarse pteropod layers and hardgrounds. During the cruise M35/1 and ultimately during the laboratory analyses it became evident that certain aims of the project could not be reached because of a variety of reasons. In order to use the core set obtained during M35/1 to its full extent, a large variety of sediment cores were opened to specify new aims that could be addressed instead. So, in addition two sediment cores were sampled at Rice University

in Houston (courtesy of Prof. Droxler) to lengthen the downcurrent, leeward transect from 41 km up to an offbank distance of 92 km. Some of the reasons for the impossibility to carry out certain subanalyses and their respective aims are shortly listed below:

1 . As the research group of Dr. Droxler did not received funding and thus did not join the M35/1 cruise, we were not able to gain 3.5kHz sediment seismics, which were significant to obtain high quality coring sites. Also the extensive knowledge of Prof. Droxler on the geology of the Pedro Bank area obviously was not available onboard the R/V Meteor during cruise M35/1.

2 . Only three out of at least five submersible dives could be carried out during the seven day scientific programme due to high waves in the study area. Therefore no bank top samples could be obtained, which were neccessary to determine the sedimentary facies of recent highstand sediments.

3 . The work on the upcurrent, windward sediment transect at the southeastern bank margin of Pedro Bank could not be carried out, as no official authorisation was available to perform scientific work within Jamaican territorial waters. This was due to the sea charts that were used to plan the cruise, which did not indicate the “Pedro Cays” were part of the Jamaican territory. Therefore, the cores retrieved instead from the upcurrent positions do not form an offbank transect as originally planned. The majority of the gravity cores situated more proximal to the upcurrent bank margin did not exceed 350 cm in core length, and thus lacked long-term sedimentary records. This probably was caused by hardgrounds or impenetrable pteropod layers, which were observed quite often in the Caribbean during cruise M35/1. This also resulted in the lack of typical toe-of-slope sediment cores.

4 . Because of the generally more basinal positions of the cores analysed, the facies analysis (point counting) could only be carried out to contentment for one proximal upcurrent coring site (M35034). However, the more basinal position of the other sites is not the only reason for the lack of more coarse neritic sediment material, which is one major outcome of this study.

Although various analyses could not be performed entirely or even failed, the possibility to use previously uninterpreted 3.5kHz data and additional sediment cores from Rice University helped in understanding the sedimentary processes along the slopes and basins of Pedro Bank. Thus it added new insight into the sedimentary response of the Pedro Bank carbonate system with its inclined bank top morphology to the late Quaternary sea-level fluctuations.

1.2 Carbonate platforms and their response to sea level changes - Sediment production and export

During the past 25 years our understanding of sediment production and export from carbonate platforms and their response to sea-level changes has been dramatically improved. During the 1970´s Neumann & Land (1975) stated that continous carbonate production of carbonate systems in the shallow-water realm leads to a permanent sediment export of shallow-water particles into the adjacent basins. The resulting mix of "exported" components with the pelagic rain of planktic foraminifera, pteropods and nannoplankton (mainly coccoliths) was later defined as "periplatform sediments" (Schlager & James, 1978).

The growth or demise of carbonate platforms is highly dependent on their ability to "keep up" with relative sea level changes (Kendall & Schlager, 1981). The maximum productivity and thus maximum benthic carbonate production is almost restricted to the photic zone (Schlager et al., 1994; Bosscher, 1992). As many organisms are phototrophic or live in symbiosis with phototrophic algae, such as scleractinian corals, it is essential for the platforms to keep their bank-tops within the photic zone (Bosscher, 1992; Veron, 1996). As shown by Kendall & Schlager (1981) the study of sediment types, geometry and diagenesis of carbonate shelves and platforms can be the most accurate gauge of changes in sea level.

The Bahamian platform has been the subject of numerous field studies since the early 1960´s (e.g. Purdy, 1963), and since this time, continued research in the Bahamas has made it one of the best studied "modern carbonate system". This has added new basic concepts in to how a carbonate system evolves through time in response to major sea-level fluctuations and palaeoceanographic changes from the Miocene to the Recent (e.g Schlager & Ginsburg, 1981; Eberli & Ginsburg, 1989; Droxler et al., 1990; Wilber et al., 1990; Eberli, 1991; Reijmer et al., 1992; Westphal, 1997; Betzler et al., 1999; Anselmetti et al., 2000; Eberli, 2000; Rendle, 2000).

Several authors have shown that periplatform sediments record the sedimentological response of carbonate systems to sea level fluctuations by using different analytical approaches e.g. carbonate mineralogy and especially the aragonite content (Droxler, 1984; Droxler & Schlager, 1985; Reijmer et al., 1988); compositional changes of periplatform sediments as well as calciturbidites (Haak & Schlager, 1989; Wilber, 1990; Reijmer et al., 1992). Droxler & Schlager (1985) introduced the term of “highstand shedding” of carbonate systems. During times of high sea level, when the tops of shallow-water carbonate systems are flooded, these platforms are able to produce large amounts of sediment (benthic carbonate and inorganically produced carbonate such as whitings) that are exported towards the adjacent slopes and basins. These "highstand" deposits are enriched in the metastable carbonate minerals aragonite and high magnesium calcite (HMC), which are predominantly produced by shallow-water organisms such as corals, red and green algae. This preferential offbank export of carbonate sediments leads to high sedimentation rates close to carbonate platforms in comparison with other open ocean settings. The periplatform sediments deposited during "lowstands" in sea level, when banktops are exposed and the carbonate factory is shut down or minimized to a small fringe at the upper slopes, are characterised by low amounts of aragonite and HMC (Droxler, 1984; Droxler & Schlager, 1985; Reijmer et al., 1988). They are enriched in low magnesium calcite (LMC), the typical carbonate mineral of pelagic nanno- or microfossils (e.g. coccoliths, planktic foraminifera; Milliman, 1974).
In addition to the deposition of these periplatform oozes around the platforms a large number of "calciturbidites" can be found in sediments surrounding the shallow-water carbonate systems (Eberli, 1991). These calciturbidites can be used as an additional proxy to elucidate the sedimentological and environmental changes that took place during major changes in sea level. Haak & Schlager (1989) as well as Reijmer et al. (1992) could show that compositional changes within calciturbidites from the Bahamian Platform reflect major changes of the production factory in response to major Pliocene to Pleistocene sea-level fluctuations.
Several studies on different periplatforms sediments have shown that the aragonite/calcite-ratio can be used as an interglacial/glacial proxy. In most cases the aragonite curve runs more or less parallel to the $\delta^{18}O$-curve (Bahamas: Droxler, 1985; Reijmer et al., 1988; Rendle, 2000); Maldives: Droxler et al., 1990; Great Barrier Reef: Alexander, 1996; and the Caribbean/Pedro Bank: Glaser & Droxler, 1993). Analyses of Alexander (1996) has shown that geochemical proxies (Sr/Ca-ratio) can also be used as a good indicator to differentiate between high- and lowstands in sea level in the proximity of carbonate systems. The origin of the aforementioned aragonite cycles is still strongly debated. Different mechanisms were proposed for the origin of the cycles. Boardman et al. (1986) and others interpreted the aragonite cycles as mainly driven by shallow-water input and thus sediment export. Droxler at al. (1990) and Haddad & Droxler (1996) argue that more globally controlling factors must be taken into account because the saw-tooth pattern of the aragonite curves is very similar worldwide. They assume that the similarity between fluctuations in the $\delta^{18}O$-curve and aragonite content can be explained by submarine dissolution of the metastable carbonates controlled by the existence or non-existence of distinct water masses (AAIW vs. NADW).

1.3 Geology and oceanography of the Caribbean Sea and the study area

1.3.1 General overview on the Caribbean Sea

The present-day Caribbean Sea extends from 9-20° N and 61-87° W, however, the Caribbean plate, which is defined using earthquake epicenters (Molnar and Sykes, 1969), is slightly larger. The plate is bounded, to the north and the south, by strike-slip fault zones such as the Cayman Trench (Fig. 1.1), and to the east and west by subduction zones and their associated volcanic arcs.
The origin of the Caribbean plate is still unknown, but there are several features that distinguish the “Caribbean crust” from normal oceanic crust. Molnar and Sykes (1969) suggested that the Caribbean plate was a rigid lithospheric plate.

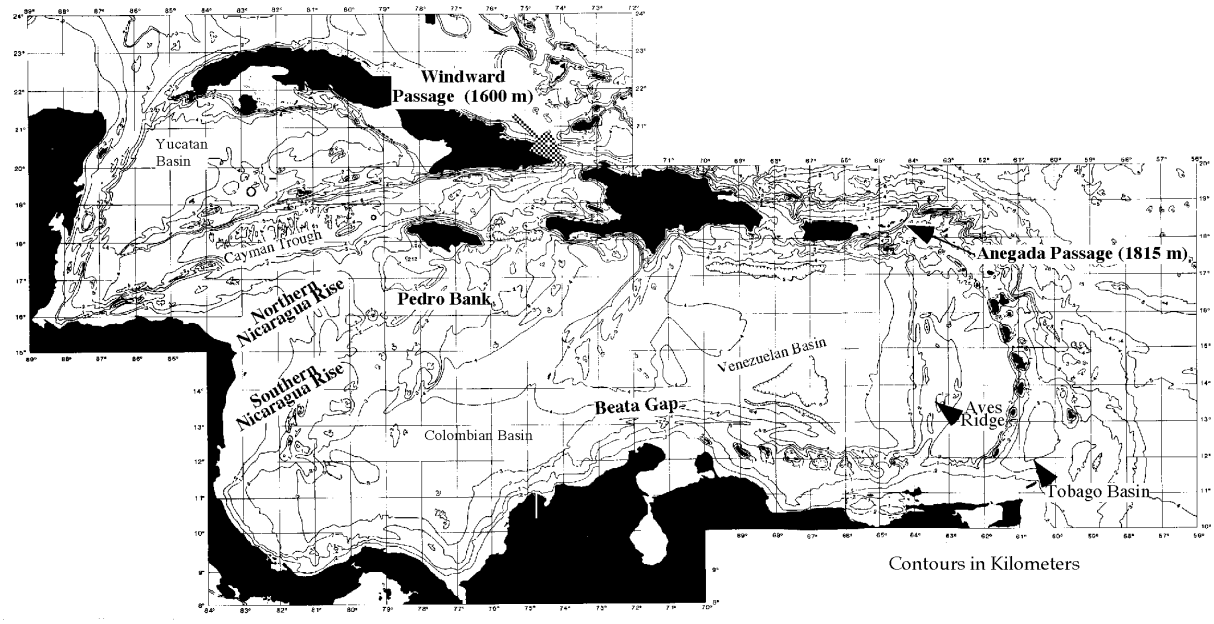

Fig. 1.1: Map of the Caribbean Sea - major basins and major tectonical features. The two major passages for water influx and their respective sill depths are shown.

However, other studies imply that this plate has undergone significant internal deformation, and has not acted as a single plate (Burke et al., 1978, 1984; Burke, 1988). Normal oceans have oceanic crust with a thickness of about 6-7 km and show identifiable magnetic anomaly patterns (Kearey & Vine, 1990). The Caribbean crust, however, does not exhibit these typical features. The thickness of the Caribbean plate varies from 10-15 km (e.g. Houtz & Ludwig, 1977) and lacks clearly identifiable magnetic anomalies (Duncan & Hargraves, 1984). In addition, the Caribbean seafloor lies about 1-2 km shallower than predicted by thermal subsidence studies (Burke et al., 1978). This crustal thickening has been attributed to widespread presence of basaltic sills and flows of late Cretaceous age (e.g. Pindell, 1993). Duncan & Hargraves (1984) as well as other authors suggested that the initially "normal" oceanic crust of the Caribbean moved over the Galapagos hot-spot, where the volcanism led to the crustal thickening ("Pacific hypothesis" [Fig. 1.4a] on the Caribbean plate evolution [e.g. Pindell et al., 1988; Pindell & Barrett, 1990; Stephan et al., 1990; Pindell, 1994; Hoernle et al., 2000]). These sills and flows may also be responsible for obscuring deeper magnetic anomalies throughout much of the Caribbean. Other reseachers, such as Meschede (1998) favor an alternative model (Fig. 1.4b) on the formation of the Caribbean Crust. They see this formation a near-American position between the two Americas (e.g. Sykes et al., 1982; Donelly, 1985; Frisch et al., 1992; Meschede, 1998; Meschede & Frisch, 1998).

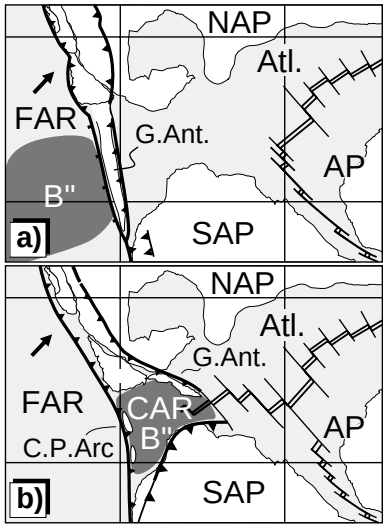

Fig. 1.4: The two hypothesis for the evolution of the Caribbean plate (comparison of palinspastic reconstructions of the Albian at about 100 Ma; Fig. 1a, b in Meschede [1998])
Fig (a) shows the "Pacific hypothesis", modified after Pindell (1994).
Fig (b) shows the alternative hypothesis of the formation of the Caribbean crust in a near-American position.

LEGEND: AP= African Plate; Atl.= Atlantic Ocean; B"= thickened Caribbean oceanic crust; CAR= Caribbean plate; C.P.Arc= Costa Rica-Panama Arc; FAR= Farallon plate; G.Ant.= Greater Antilles; NAP= North American plate; SAP= South American plate.

1.3.2 Regional Geology of the Northern Nicaragua Rise

The present topography of the NNR results from the complex tectonic evolution of the northern Caribbean plate boundary that started during the Jurassic (e.g Burke et al., 1984; Burke, 1988; Pindell & Barrett, 1990; Pindell, 1993).

The Nicaragua Rise (NR) is a topographic high in the western Caribbean Sea. This ENE-WSW orientated feature is about 1350 km long and about 540 km wide. It extends from Honduras and Nicaragua in the west, to Jamaica in the east. This topographical high consists of several shallow-water carbonate banks (Miskito, Bawihka, Diarangen, Rosalind, Serranilla and Pedro Bank) and shelves (central America and southern Jamaica) that are separated by basins and channels (Walton and Serranilla Basin; Diriangen, Rosalind and Pedro Channel). The bank tops occur generally below 30 m of present water depth. Most of these banks show a typical bathymetric feature while their platform top deepen towards the northwest (e.g. Triffleman et al., 1992). Pedro Bank, a submarine horst block (Marshall, 1976), reaches sea level at the small cays in the southeast, and shows maximum water depths of 60-70 m in the northwest.

The Nicaragua Rise is bounded to the north by the actively spreading Cayman Trench (Fig. 1.1) and its associated transfer fault system (Molnar and Sykes, 1969), which began to open about 40 Ma ago (Rosencrantz et al., 1988). The Hess Escarpment marks the southern boundary (Case et al., 1984). The Pedro Bank Fracture Zone (PBFZ) is located south of Pedro Bank. This structural feature separates the Northern Nicaragua Rise (NNR), which is the main working area of this study, from the Southern Nicaragua Rise (Fig. 1.1).

Tectonic and sedimentary evolution of the Nicaragua Rise

The tectonic history of the Nicaragua Rise can be traced back into Jurassic or early Cretaceous time, when the crust of the Nicaragua Rise is suggested to have originated as part of the Greater Antilles volcanic arc (e.g. Arden, 1975; Pindell, 1993). During the Cretaceous the area of the Nicaragua Rise seems to have been a very active feature, which is indicated by volcanics present along the southern margin of Pedro Bank across to Rosalind Bank (Arden, 1969). Pindel & Dewey (1982) suggest northward subduction of Caribbean oceanic crust beneath the Nicaragua Rise in the late Cretaceous. Granodiorites found on Jamaica, the walls of the Cayman Trough and within one of the industrial wells (Pedro Bank-1) are late Cretaceous to Paleocene in age (e.g. Holcombe et al. 1990). They are interpreted to be the result of north-dipping subduction of "normal" Caribbean oceanic crust beneath the Nicaragua Rise.

During the Paleocene and lower Eocene sediment deposition can be traced only in the deeper parts of the intervening seaways between the single carbonate banks (Cunningham, 1998). In the Eocene volcanic activity ceased in Honduras as well as Jamaica (Pindell and Barrett, 1990), which seems to be linked to the possible end of northward-dipping subduction of remnants of the Caribbean crust (Pindell & Barrett, 1990; Pindell, 1993). From the middle Eocene to the middle Miocene the area seems to have gone through a period of tectonic quiescence, thermal subsidence and preferentially carbonate deposition. Until the early Miocene time the Nicaragua Rise was continuously covered by shallow carbonate banks and barrier reefs (or one "megabank" sensu Droxler et al., 1998). From the middle Miocene or even as early as the late Oligocene the whole system of the NNR became instable (Sigurdson et al., 1997). Progressive segmentation and partial drowning due to the break-up of the continous bank from 12-15 Ma (or as early as 15-20 Ma) enabled the initiation of the Caribbean Current (Droxler et al., 1998).

1.3.3 Oceanographic Setting

The study area around Pedro Bank lies within the tropical Caribbean, with normal water salinities of about 36‰ and surface temperatures ranging from 26-29°C (e.g. Triffleman, 1989 for Serranilla Bank located west of Pedro Bank). The dominant surface current within the study area is the Caribbean Current that flows from the southeast (Molinari et al., 1981), and which feds the North Antlantic Gyre´s Western Boundary Current (Gulf Stream). Large parts of the NNR are affected by this current, which is an extension of the Guiana Current that enters the eastern Caribbean through various passages throughout the Lesser Antilles (e.g. Jungfern-Passage, Anageda-Passage & Windward Passage; see Figs. 1.3 and 1.4). Gordon (1986) describes the Caribbean Current as part of the North Atlantic Deep Water (NADW) surface return flow.

Today, Antarctic Intermediate Water (AAIW) is entrained in the upper water layer flow by the fast-moving Caribbean Current as it passes through the Lesser Antilles, linking AAIW to NADW surface return flow (Gordon, 1986; Gordon et al., 1992; Fig. 1.4).

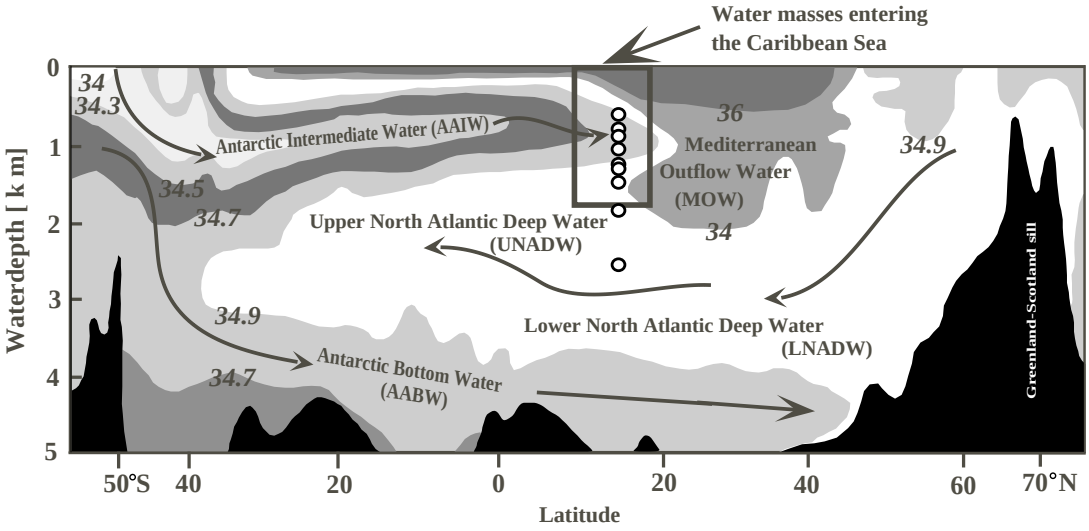

Fig. 1.3: Distribution patterns of Atlantic water masses in respect of their salinity (modified after Haddad & Droxler [1996]). The black box marks the water masses entering the Caribbean today. These water masses are composed of three different Atlantic intermediate water masses: UNADW, MOW and AAIW. In addition, the white circles show the location of the analysed cores with respect to geographical latitude and their depth of deposition.

In the western Caribbean the banks and seaways of the NNR act as gateways for the Caribbean Current to pass through the Yucatan Channel into the Gulf of Mexico and later join with the Gulf Stream (Wüst, 1964; Kinder et al., 1985; Fig. 1.4), a major component of the global thermohaline circulation.

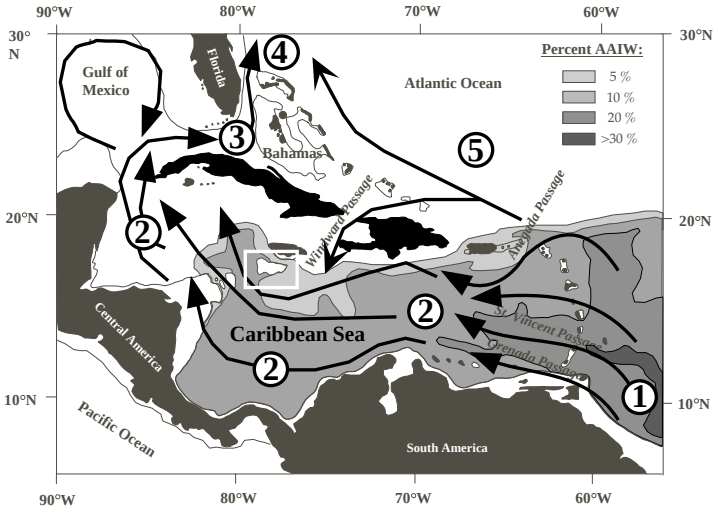

1: Guiana Current + Northern Equat. Current

2: Caribbean Current

3: Florida Current

4: Gulf Stream (Western Boundary Current)

5: Antillean Current

Fig. 1.4: General ocean current system of the Caribbean Sea (indicated by arrows), which is part of the global thermohaline circulation. The study area is indicated by a white rectangle. Encircled numbers display the single current systems of importance for the Caribbean and the global thermohaline circulation.
In addition the percentage of Antarctic Intermediate Water as a share of the Caribbean water mass inventory in a water depth of 800 mbsl is shown (based on T-S-data of Wüst [1964]). This depth represents the nucleus layer of the Caribbean water masses.

The waters that make up the Caribbean Current are highly stratified down to about 1200 mbsl, and this is related to the sill depths that control entry into the Caribbean from the Atlantic (Gordon, 1967). In the northeastern Caribbean the Subtropical Underwater (SUW) exists between 100-300 mbsl with a salinity of 37-37.8‰, but it is absent near Pedro Bank (Schmuker, 2000). Sources ot the SUW are from the Sargasso Sea (Wüst, 1964). In the

southeastern Caribbean Sea the Sub-Antarctic Intermediate Water (SSAIW, 35.2-37‰) occurs below 300 m. The Antarctic Intermediate Water (AAIW, salinity <35‰) occurs between 600-1000 m water depth (Gordon, 1967; Morrison & Nowlin, 1982; Kumar et al., 1991). Below 1800 m, the Caribbean waters are nearly homogenous as the deep Caribbean basins are filled up with North Atlantic Deep Water (NADW), which is nutrient depleted and has a higher salinity than the overlying AAIW (Morrison & Nowlin, 1982).
The estimated volume transport through the Caribbean Current is approximately 30 Sv (1Sv = $10^6 m^2 s^{-1}$). Two-thirds flow through the Lesser Antilles, and one-third enters through the Windward Passage (Kinder et al., 1985). Mean velocity is approx. 50 cm/sec (Gordon, 1967). Based on data of Wüst (1964), a clear westward intensification of the Caribbean Current can be observed across the NNR as well as in Pedro Channel itself. Kinder et al. (1985) describe an increase in surface velocities to the west up to 80 cm/sec. Triffleman et al. (1992) show values of up to 100 cm/sec in Bawhika Channel and over the banks of the NNR.
The deeper stratified layers of Subtropical Underwater (100-200 m depth) and AAIW (600-800 m depth) show average current velocities of 30-40 cm/sec and 15 cm/sec, respectively (Gordon, 1967).

1.3.4 Climate

The Pedro Bank is situated at the western end of the northeast trade wind belt, and therefore easterly winds predominate. During hurricane season (generally between October and December) Pedro Bank may be affected by stormy weather. During the change from “winter” to “summer” in this region severe tropical storms may occur (Sugg, 1966; Jindrich, 1972; Crutcher & Quayle, 1974; Hidore & Oliver, 1991), which might cause the initation of mass gravity movements as well as enhanced export of sediment from the tops of the carbonate platforms along the NNR. The impact of storm activity on the shallow water carbonate systems has been described from various settings such as the the wind- and leeward margins of the Great Bahama Bank (Boss & Neumann, 1993; Bourrouilh-Le Jan, 1998), Virgin Islands (Hubbard et al., 1991), atolls in French-Polynesia (Harmelin-Vivien & Laboute, 1986) and the southeastern Pacific (Bourrouilh-Le Jan, 1998), Jamaican coral reefs (Woodley et al., 1981) and the Grand Cayman Island (Blanchon et al., 1997; Li et al., 1997).

1.4 Previous research along the Northern Nicaragua Rise and Pedro Bank

Research on Pedro Bank started with an ecological description of the reefs by Zans (1958). The reefs on the southern edge of Pedro Bank emerge within a sandy platform realm. The reef crest consists of a *Millepora-Palythoa* association with abundant encrusting coralline algae indicative of high energy conditions. A well-developed *Acropora palmata* zone is found on both sides of the reef crest in fore-reef and back-reef environments. *A. cernivoris*, *Diploria* spp., *Montastraea* spp., *Porites* spp. and *Colpohayllia natans* are abundant on the deeper fore-reef (UNEP/IUCN, 1988). In the early 1970´s the ecological composition and distribution of organisms on top of Pedro Bank was analysed using 155 thin-sectioned banktop grab samples (Dolan, 1972). Cluster analysis of the 13 major components found yielded 4 major facies:

(1) Shallow Reefs dominated by coralline algae and encrusting foraminifera; found on the eastern end of Pedro Bank and coincides with the shallowest parts of Pedro Bank (mean water depth 12 m).
(2) Reefal Areas dominated by corals and *Halimeda*; characterised by sandy bottom with frequent isolated patch reefs which can usually be found on the leeward side of the “Shallow reefs”, and constitute a transitional zone between the latter and the central sand blanket zone (mean water depth 24 m).
(3) Sand Blankets dominated by mollucs, peneroplids and pelletoids; main facies, which covers 2/3 of Pedro Bank from the northeast to the western end. They contain predominantly skeletal carbonate sand detritus (mean water depth 26 m), and
(4) Mud facies dominated by fine sediments; found in peripheral position along Pedro Banks upper slopes (mean water depth 63 m).

In 1987, 1988 and 1992 Rice University, Houston and the University of South Florida in Miami organised a series of oceanographic cruises to the Northern Nicaragua Rise. The objective of these cruises was to improve the knowledge of the carbonate systems along the NNR. Research carried out by Hallock et el. (1988), Triffleman (1989), Triffleman et al. (1991, 1992), Glaser (1991), Glaser & Droxler (1993), Schwartz (1996), Peebles et al. (1997), Duncan (1997) and Cunningham (1998) extended the sedimentological, ecological, biological, palaeontological and primarly the palaeoceanographical knowledge of this carbonate system immensely. These studies focused mainly on Pedro Bank and Serranilla Bank, and the adjacent basins and seaways (Walton Basin, Pedro Channel, Serranilla Basin and Rosalind Channel). A summary of these studies findings is outlined below.

The bank top of Serranilla Bank was the scope of research by Triffleman (1989). Using high-resolution seismic profiles of bank tops, sediment samples, SCUBA-dive observations and dredge hauls it could be shown that this carbonate bank is partially drowned. No reef development could be observed on top of the platform. A sediment cover was nearly non-existent, and if present, it was very thin and consisted of coarse-grained sediments. It has been suggested that this might be the result of a strong surface flow of the Caribbean Current over the top of Serranilla Bank. In addition, a predominance of chloralagal rather then chlorozoan sediments could be observed. The lack of active frame-builders, the presence of abundant bioeroders, the limited development of sediment-producing environments and the high energy environment, may all contribute to the partial drowning of Serranilla Bank. This carbonate system shows all features that it could not keep-up with the Quaternary (perhaps only the Holocene) sea-level rises.

Duncan (1997) researched the geologic and palaeoceanographic evolution of the adjoining Serranilla Basin. The tectonically active Northern Nicaragua Rise and thus also Serranilla Basin represents an important gateway for water masses that are part of the global thermohaline circulation. Besides this Serranilla Basin offers the opportunity to study the palaeoceanographic evolution of the Caribbean Sea during the late Quaternary in a basin bounded by 4 smaller carbonate banks (Serranilla, Rosalind, Diriangen and Bawihka Bank). The geologic evolution was established by using single-channel, high-resolution seismic data. The palaeoceanographic evolution was studied using sediments of box cores and piston cores from the central Serranilla Basin. Duncan (1997) showed that the periplatform sediments indicate a long-term (500 ky to present) increase in currents and a decrease in carbonate dissolution in this part of the Caribbean. These findings support the idea that the basins of the NNR form the link between Southern Ocean circulation and North Atlantic deep water formation. Schwartz (1996) could show the same long-term trends for Pedro Channel (see later).

Turbidites make up a significant portion of the sediments infilling the Serranilla Basin. The Serranilla Basin shows a major difference to other basins along the NNR as well as the Bahama Platform because the turbidites infill the basin against the predominant direction of the Caribbean current. This current system is one of the major controlling factor for offbank transport and deposition along the NNR (Glaser & Droxler, 1991). Duncan (1997) assumed that other factors (e.g. seasonal reversals in surface currents due to storms or tectonic activity) also steered turbidite deposition.

On the base of periplatform ooze analyses from the Walton Basin and Pedro Bank, Glaser & Droxler (1991) showed that these (so called) "partially drowned" carbonate platforms are deeply submerged and highly productive carbonate environments. Glaser & Droxler (1991) showed that sediment accumulation on the Northern Nicaragua Rise is controlled by four main factors: (1) input of carbonate sediments; (2) input of siliciclastic sediments; (3) physical redistribution of sediment by currents and (4) dissolution of carbonate phases. Just like on Serranilla Bank the bank tops of Pedro Bank and the Southern Jamaican Shelf were “submerged” during late Quaternary interglacial sea-level highstands. Pedro Bank exhibits a chlorozoan assemblage of organisms during highstands in sea level, which produces metastable carbonates enriched in aragonite and high-Mg calcite (HMC). Serranilla Bank contrarily is dominated by a chloralgal assemblage (Triffleman, 1989). Surface currents sweeping these deeply submerged platforms and transport large amounts of carbonate to the slopes and adjacent basins (Walton Basin, Pedro Channel). One of the main suppliers of fine-grained aragonite needles is formed by green algae (e.g. *Halimeda*), which dominates the banks of the NNR.

Glaser & Droxler (1991) also showed that metastable bank-derived aragonite and high magnesium calcite that accumulate below 1100 mbsl are partly subjected to dissolution. This dissolution increases with water depth as the water column becomes more and more

undersaturated with respect to these carbonate phases. Haddad & Droxler (1996) compared dissolution patterns of the Bahamian and the Northern Nicaragua Rise periplatform environments and observed different dissolution patterns at intermediate waterdepths. They also showed that in the deeper parts of the intermediate water column on the Northern Nicaragua Rise the dissolution pattern displays a "hybrid" of both, shallow and intermediate dissolution records. The analysis of periplatform sediments also showed that fine grained sediments (>63 µm) are mainly exported during highstands in sea level, whereas coarse neritic sediments are exported or redeposited from upper slope settings preferentially during lowstands in sea level (Glaser & Droxler, 1991). Coarse sediments mainly occur proximal to the platform slopes in waterdepths less than 600 mbsl, which is the result of narrowing of the seaways, increased current flow rates and thus winnowing the finer sediments during glacial periods.
Detailed examinations of high-resolution 3.5kHz profiles showed that the transgressive systems tracts are unresolvable even with this type of seismics due to the rapid flooding of the bank tops. The main difference with the sequence stratigraphic model proposed by Sarg (1988) is therefore that no TST could be found, but only a large HST and a minor LST are evident. The transgressive system tract is only revealed by subtle compositional changes within the sediment column.
Schwartz (1996) analysed sediment cores of intermediate water depths (900-1400 mbsl) from Pedro Channel to quantify differences in depositional patterns between the late-Brunhes (0-185 ky) and the mid-Brunhes epoch (185-525 ky). Based on the effects that global climate shifts had on mass accumulation rates, dissolution records and the abundance of planktic foraminiferal species in the Caribbean, Schwartz (1996) showed that significant differences exist between these two periods. The last 185 ky recorded extreme changes between glacial and interglacial conditions and a consistent behaviour within single isotope stages. The mid-Brunhes mode in contrast to the late Brunhes period represented a time with mild changes between as well as within glacial and interglacial stages. This study also showed that:
- Migration of the North Atlantic Gyre has been more severe in the last 185 ky, bringing more low-nutrient gyre-center waters into the Caribbean during glacials.
- Compressed glacial temperature gradients increase wind stress, creating stronger flow of the Caribbean Current, vigorous mixing and winnowing of finer particles in the upper water layer.
- In the late-Brunhes mode maximum mass accumulation rates concentrate in interglacials, indicating the dominant influence of highstand shedding and nutrient influx, whereas during the mid-Brunhes mode the mass accumulation rates occur around the glacial/interglacial transition. Schwartz (1996) proposed that this might be linked to the flooding of exposed shelves and platform tops during the transgression, which could have released massive amounts of nutrients.
- Dissolution studies (“Composite Dissolution Index”) showed that interglacial dissolution in Pedro Channel is related to the influx of AAIW (Figs. 1.3 and 1.4). The good glacial preservation indicates a lower influx and influence of the Southern Ocean watermasses during the late-Brunhes mode. Dissolution indices from the mid-Brunhes mode point to a poor preservation, which might indicate a more consistent influence of Southern Ocean water masses such as AAIW.
Cunningham (1998) researched the Neogene evolution of the Pedro Channel carbonate system. This work included the renewed aquisition of bathymetric data, which show that the studied area displays a seafloor interrupted by numerous canyons, gullies and portions of drowned carbonate banks. 3.5 kHz echograms indicate that the surrounding banks show two modes of sediment input into the channel: (1) a line source as illustrated by concentric facies belts along the bank margins and (2) a point source as illustrated by local zones with coarse-grained deposits at the base of canyons along the bank margins.
The analysis of seismograms reveals that periplatform sedimentation has dominated within Pedro Channel from the early Miocene to Recent. Analysis of dredge samples support earlier theories by Droxler et al. (1998), who proposed the existence of a neritic carbonate bank that partially drowned in the middle Oligocene and finally in the early Miocene.

CHAPTER 2

STUDY AREA, MATERIALS AND METHODS

2.1 Materials and study area

Nine sediment cores from the northwestern to southeastern periplatform environment around Pedro Bank were studied within this doctoral thesis. In total 718 samples were analysed.

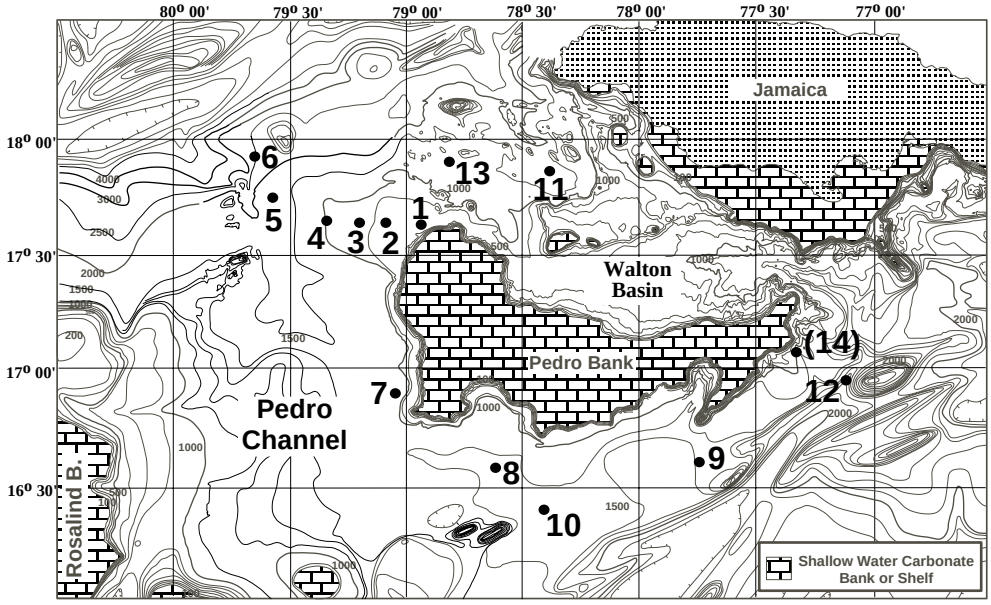

Fig. 2.1: General bathymetry of the periplatform environment of the Southern Jamaican Shelf, Pedro Bank and Rosalind Bank. Cores used within this study are indicated. (Core locations are as follows: 1=M35048**; 2**=M35049**; 3**=M35043**; 4**=M35042**; 5**=PC059**; 6**=PC100**; 7**=M35034**; 8**=M35032**; 9**=M35052**; 10**=PC016**; 11**=PC035**; 12**=PC073**; 13**=**PC108**; (14**=PC076**)).**

The sediments were recovered during the *R/V Meteor* cruise M35/1 in 1996 and two American reseach cruises in 1988 and 1992 onboard *R/V Cape Hatteras* along the Northern Nicaragua Rise. Cores taken during the *Meteor* cruise were recovered by gravity coring, whereas those taken during the *Cape Hatteras* cruise used piston coring. The sediment cores were taken from water depths between 648 mbsl to 2520 mbsl. The offbank distance of the cores range from 5.5 km to about 92 km (see table 2.1 and Fig. 2.1 for exact positions and general locations).
The lithology of the sediments recovered varies. Predominantly mud- to wackestones (Dunham, 1962) were found, which form the typical lithogical composition of periplatform sediments. Fine, neritic material exported from the carbonate platforms and the fine, pelagic rain mainly consist of nannoplankton (coccolithophorids) and only to a minor amount of sand-sized foraminifera (Tucker & Wright, 1990). Intercalated pack- to grainstones are common and usually appear as turbidites. Some of them do not correspond to turbidites, and can be interpreted to be winnowed sediments deposited during times of enhanced bottom water currents (e.g. during glacial times). Turbidites in distal settings, predominantly on the downcurrent slopes, are present as fine endtails of turbidites (mudstones sensu Dunham [1962]). The lithology of each studied core is presented in Appendix 1.

Core (No. in Fig. 2.1)	Relative position (closest distance to active bank margin)	Up-/Down-current position	Latitude (°N)	Longitude (°W)	Water-depth (m)	Topo-graphy
M35032-2 (8)	SW-Edge (25 km)	Upcurrent	16.5925	78.6261	1364	flat floor
M35034-1 (7)	SW-Edge(toe-of-slope / Pedro Channel; 10 km)	Upcurrent	16.9092	79.0694	1211	near toe-of-slope
M35042-2 (4)	NW-Transect (41 km)	Downcurrent	17.6486	79.3094	1023	flat floor
M35043-1 (3)	NW-Transect (28 km)	Downcurrent	17.6441	79.1691	975	local topogr.
M35048-1 (1)	NW-Transect (5.5 km)	Downcurrent	17.6469	78.9144	648	horst struct.
M35049-2 (2)	NW-Transect (19.5 km)	Downcurrent	17.6438	79.0877	893	local topogr.
M35052-2 (9)	SE-Edge (30 km)	Upcurrent	16.5753	77.7028	1445	flat floor
PC 059 (5)	NW-Transect (72 km)	Downcurrent	17.7255	79.6353	1887	canyon slope
PC 100 (6)	NW-Transect (91 km)	Downcurrent	17.9211	79.7166	2520	canyon slope
PC 016 (10)	SW-Edge (35 km)	Upcurrent	16.4097	78.4094	1422	flat floor
PC 035 (11)	Walton Basin (47 km)	Downcurrent	17.8377	78.3939	1642	flat floor
PC 073 (12)	SE-Edge (31 km)	Upcurrent	16.9108	77.145	1894	flat floor
PC 076 (14)	SE.Edge (3.9km)	Upcurrent	17.0585	77.1729	903	upper slope
PC 108 (13)	NW-Edge (30 km)	Downcurrent	17.8619	78.8005	1230	flat floor

Table 2.1: Locations, relative position, number of turbidites and surrounding topography of the sediment cores analysed or mentioned in this study. Cores 10-14 have been analysed in other studies by Glaser (1991) and Schwartz (1996).

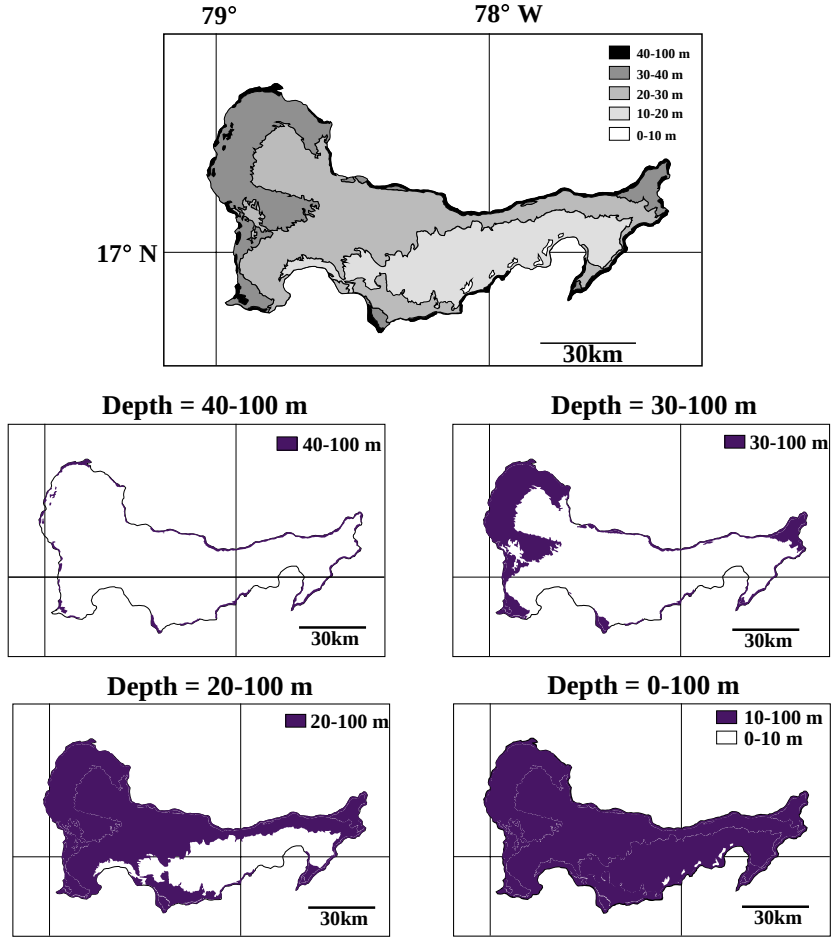

Fig. 2.2: Bathymetry of the platform top of Pedro Bank (redrawn and modified after Dolan, 1972).

Study Area

Pedro Bank represents the largest isolated platform on the Northern Nicaragua Rise. It is located south-east of Jamaica (Fig. 2.1). The platform represents a major submarine horst structure produced by cenozoic tectonism (Arden, 1969). Pedro Bank ranges from 17°39´-16°42´ N and 77°20´-79°4´ W, which results in a total banktop area of about 8000 km^2 for those parts of Pedro Bank, that are less than 50 m deep (Zans, 1958). Pedro Bank is roughly triangular in shape with a maximum of 83 km along it´s east-west axis and 53 km wide at the western end. The main parts of the top of Pedro Bank are situated in waterdepths of 5-40 mbsl and rise from the sea bed at 800 mbsl or more. Bank tops starts at maximum water depths of 60-70 mbsl (Dullo, 1997) and may form smaller "terraces" between 40-70 mbsl (see revised bathymetric map of Pedro Bank after Dolan, 1972; Fig. 2.2). Another typical feature of the carbonate platforms on the NNR is the northward deepening of the platform top (Fig. 2.3). This makes the platforms interesting for comparison with flat-topped platforms as well as carbonate ramp systems.

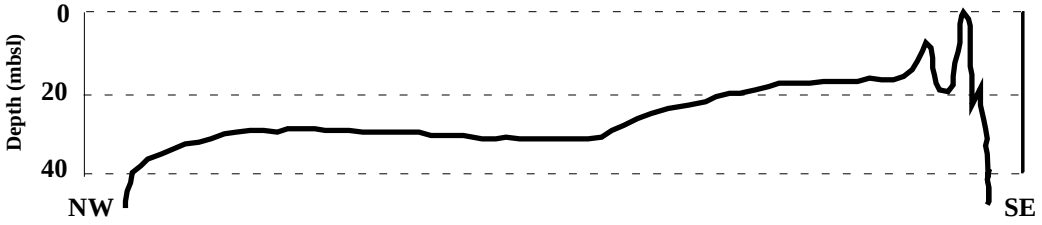

Fig. 2.3: Bank top morphology of Pedro Bank (redrawn from Triffleman, 1992)

The submarine topography of Pedro Bank, however, is fairly flat (Zans, 1958; Dolan, 1972). The bottom is covered with coral rubble, sand and silt with patches of scattered corals and algae increasing to the south-east where reefs and shoals are situated (Zans, 1958; Munro, 1983) forming the Pedro Cays.

2.2 The basic principles and applications of the used methods

All methods are described in detail in this chapter. There will only be a cross-reference to this chapter at the beginning of each consective chapter. Only if additional analyses are shown, which exceed the basic principles explained here, a more detailed view of the method will be given there.

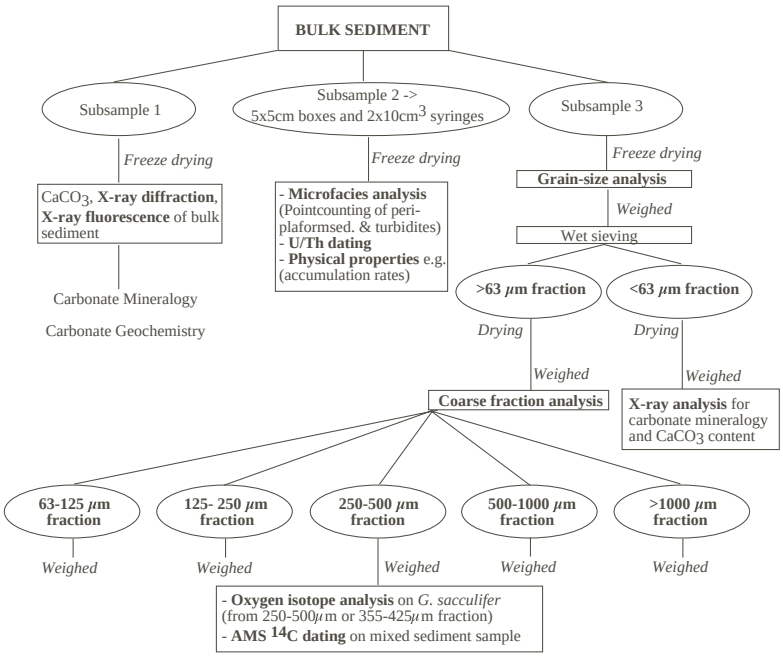

Fig. 2.4: A flow diagram of the different sedimentary analyses carried out on the periplatform sediments.

2.2.1 Sampling strategy and sample preparation

Sampling strategy
Several different analytical techniques were used during this study to reach the envisaged goals. A simplified schematic scheme gives an overview on the general analytical methods used (Fig. 2.4). A first set of sediment cores was already opened onboard the *R/V Meteor* in 1996. Magnetic susceptibility measurements (MST) and colour scanning was applied to all cores opened onboard, to obtain a first estimation on the stratigraphical range.

2.2.2 Stratigraphic analysis

2.2.2.1 Stable oxygen isotope analysis

(I) δ^{18}O and foraminifera
Since the first analysis were done by Emiliani (1954, 1955), stable oxygen isotope measurements are a widely accepted stratigraphic tool to date late Quaternary sediments. The oxygen isotopes of planktic and benthic organisms record the global cycles of oceanic oxygen isotope composition, and thus changes in global climate and sea level (Shackleton and Opdyke, 1973; Imbrie et al., 1984; Ruddiman et al., 1987). Through the SPECMAP-Stack sedimentologists and oceanographers are able to date sediment cores from the seafloor worldwide (e.g. Imbrie et al., 1984). The fractionation process of the different oxygen isotopes shows a specific pattern related to the glacial/interglacial sea level cycle. During glacial stages, water vapour enriched in ^{16}O is evaporated from the ocean´s surface makes it way to the high latitudes where it is precipitated as snow (enriced in ^{16}O) and finally becomes stored as ice in large quantities. Simultaneously the oceans sea level falls and the water becomes enriched in the isotopically "heavier" ^{18}O. During the following deglaciation the ice at the poles melts and sea level rises again. This process releases the ^{16}O stored in the ice back into the sea water, which in turn, leads to a decrease in the oceans ^{18}O. The oceans will become again isotopically "lighter". This glacial/interglacial cycle of sealevel and ice volume is recorded in the carbonate tests of foraminifera and thus reflects the changing isotopic composition of the ocean´s water. This is known as the ice volume effect. A variety of factors influence the isotopic composition of foraminifera. Beside the major ice-volume effect, temperature, evaporation/precipitation, water mass, seasonal depth change as well as vital and size effects of the organisms must be considered, however, the general pattern remains unaffected.
The planktic foraminfera *Globigerinoides sacculifer* was used to obtain the isotopic signature of the surface water in the study area. *G. sacculifer* is known to dwell between 0-5 mbsl and can be found there all year round. This species may possess a distinct final sac-like chamber. This chamber is build up during the end of the life span when the foraminifera starts to sink into deeper water. *G. sacculifer* was selected from the 250-500 µm fraction for cores M35032, -34, -49 and -52, whereas for the remaining 5 sediment cores the size range was restricted to the 355-425 µm fraction to minimize the above mentioned size effect. At least 10 specimens were selected based on the lack of the sac-like final chamber (Duplessy et al., 1981) to exclude that a different isotopic signature from a deeper water mass effects the sea surface signal. Also attention was paid to the preservation condition of the foraminferal test (no mineral coatings or sediment in chambers). In order to remove possible coatings and sediment the forams were crushed carefully and cleaned with Ethanol in an ultrasonic bath.
The oxygen and carbon isotopes were measured using a FINNIGAN mass spectrometer ("Kiel CARBO II device") at GEOMAR. The calcitic tests were dissolved with 100% orthophosphoric acid at 70°C. The released CO_2 was cleaned when passing through various cryo traps and then finally injected directly over a microvolume into the mass spectrometer. The ratio of occurence of stable oxygen and carbon isotopes was then measured relative to a laboratory internal standard gas (HCO_3 from "Burgbrohl"). These measurements were then calibrated to the international isotope standard (PDB-Standard; Craig, 1957) using the NBS 19 carbonate standard of the National Bureau of Standards. The overall reproducibility of measurements (± 1σ) carried out on the GEOMAR´s mass spectrometer averages 0.03‰ for δ^{18}O (and 0.01‰ for δ^{13}C) referred to a laboratory internal standard (Solnhofener Plattenkalk).

(II) Aragonite variations with time as a proxy for $\delta^{18}O$ ("Aragonite stratigraphy")

Input of metastable aragonite into the deep surroundings of modern carbonate platforms is known to be linked to sea-level fluctuations. Extensive export of sediments from the platform into the periplatform environment can be seen during highstands in sea level, when bank tops are flooded, whereas lower aragonite contents, and thus reduced export, are observed during lowstands in sea level, when the platforms are exposed. This pattern has been observed along the Bahama Platform (Droxler et al., 1983; Droxler & Schlager, 1985; Reijmer et al., 1988; Rendle, 2000) as well as many other platforms like the Maldives and the Northern Nicaragua Rise (e.g. Boardman et al., 1986; Droxler et al., 1990; Glaser & Droxler, 1993) and is known as "highstand shedding" (Droxler & Schlager, 1985). Forementioned authors clearly demonstrated the correlation between the amount of fine aragonite in periplatform sediments and the $\delta^{18}O$ record in periplatform sediments. Glaser (1991) showed that this also applies for sediments from Walton Basin north of Pedro Bank. This close correlation justifies the use of aragonite variations with time as a proxy for $\delta^{18}O$ variations, when no oxygen isotope data are available.

Glaser (1991) used this method for cores from intermediate and shallow water depths (<1100 mbsl). Below that depth the aragonite content can also be modified by dissolution of the metastable carbonate phases, as the depth of aragonite undersaturation within Walton Basin (and probably most of the NNR) lies around 1800-2200 mbsl (Droxler et al., 1991). Also it should not be neglected that considerable dissolution of calcium carbonate may occur in the upper 500-1000 m of the ocean, which is well above the chemical lysocline (Milliman et al., 1999). This dissolution can be as much as 60-80% of the original production in the neritic realm.

Research of Emmermann et al. (1999) showed that lagtimes might occur between both proxies (oxygen isotopes and aragonite content), most probably as a result of different platform top morphologies. This might be an additional evidence for a natural lagtime that occurs due to the reorganisation of the bank-top environment after sea level falls and rises (Tipper, 1997).

Despite all these facts this method was applied to cores M35048 (648 mbsl) and PC059 (1887 mbsl) as the aragonite signal displayed useful glacial-interglacial variations.

(III) Age models and correlation of the oxygen isotopes to the SPECMAP-Stack

The final correlation of $\delta^{18}O$-data (or another stratigraphic proxy) and the creation of age-depth models for each core was made by using the specified dates provided by the SPECMAP stack of Imbrie et al. (1984). As regional isotope curves in general display similar trends that might differ from this stacked isotope curve, also data from Glaser & Droxler (1993), Schwartz (1996) and Duncan (1997) from the nearby Walton and Serranilla Basin and Pedro Channel were used to define the specific isotope events. The used dates for the single oxygen isotope events can be seen in Appendix 10.

By pattern matching of the isotope or aragonite signatures of each core against the SPECMAP stacked isotope curve of Imbrie et al. (1984) the sediments were dated relatively to the events of the SPECMAP curve. The actual correlation was made using the computer program "Analyserie" (Paillard, 1996). This program calculates the "SPECMAP-age" by linear interpolation, which results in relative ages for all given depths of the analysed cores. The correlation coefficient between the oxygen isotope curves of cores (or other proxies used) in this study with the SPECMAP curve are good ($r^2 = 0.9$).

2.2.2.2 Biostratigraphy (*Globorotalia menardii* Complex)

The *Globorotalia menardii* complex stratigraphy was determined for all cores by visual inspection of the subfractions 250-500 µm, 500-1000 µm and >1000 µm to prove the presence or absence of the two Globorotaliid species, *G. menardii* and *G. tumida* (Globorotaliid abundance). Using the following categories "no presence, minor presence, common, frequent" the presence/absence of the *Globorotalia menardii* complex could be established, which is in agreement with those of other studies in the Caribbean (e.g. Ericson & Wollin, 1956, 1968; Prell & Hays, 1976; Glaser & Droxler, 1993; Haddad, 1994). As this simple method provided good results, no counting of these species was neccesary, as was also shown by Schwartz (1996) and Duncan (1997). Ericson & Wollin (1956, 1968) observed that Globorotaliid species, which are always present in the late Quaternary in other parts of the worlds ocean, disappeared from the Atlantic Ocean and the Caribbean Sea periodically. The reason for this periodic disappearance is still unknown, but Schwartz (1996) stated that the abundance of

Globorotaliid species in the Caribbean might be related to (1) changes in surface water connections between the Atlantic and Indian Oceans and (2) conditions within the upper water column. Haddad (1994) stated that the abundance of Globorotaliid species may be directly controlled by NADW production. In addition, because NADW production is also linked to the influx of AAIW into the Caribbean, Schwartz (1996) showed that the abundance of Globorotaliid species can be used as a proxy for the influence of AAIW in the Caribbean. It is clear that this biostratigraphic tool seems to be the result of a very complex process, however, the appearance and disappearance of the Globorotaliid species can be used to support isotope stratigraphic interpretations. The zones of presence and absence in the Caribbean were established by Ericson and Wollin (1956). This zonation starts with the letter Z (= Holocene) and then counts back in time (Table 2.2).

***Globorotalia menardii* Complex Biozone**	**Age of boundaries in ky**	**Reference**
Z	0 to 9/12	Ericson & Wollin (1956)
Y	9/12 to 77/84	Ericson & Wollin, (1956); Glaser & Droxler (1993)
X	128	Ericson & Wollin (1956)
W	ca. 160	Glaser & Droxler (1993)
V	ca. 475	Ericson & Wollin (1956)

Table 2.2: The *Globorotalia menardii* complex: Zones, ages and references.

2.2.2.3 Radiocarbon ages (AMS ^{14}C-dating)

To prove the established stratigraphy using oxygen isotopes and the *Globorotalia menardii* complex, radiocarbon dating to samples of the Holocene and the marine isotope stage 3 was applied. For older sediments a new analytical approach using an advanced U/Th-method was used to date marine bulk sediment (see chapter 2.2.2.4). For 9 samples AMS ^{14}C-dating was applied. While the use of this method is limited to the sediments younger than approx. 50.000 years BP, samples were preferentially selected from oxygen isotope stage 3, where the isotope stratigraphy always seems to be precarious because of low sedimentation and accumulation rates. Mixed sediment samples (preferentially planktic foraminifera and pteropods) of the 250-500 µm or the 355-425 µm-fraction were used. These samples were identical to those that were used for oxygen isotope analysis. No monospecies samples were measured.
Radiocarbon analysis were provided by the Leibnitz Laboratory for Age Determinations at the Christian-Albrechts-University in Kiel (Prof. Dr. Grootes). The dates presented are corrected "conventional ages" according to Stuiver & Polach (1977). The global 400-yr reservoir age correction was not applied.
The preparation methods for ^{14}C-measurements are as follows: the samples were cleaned with 30% H_2O_2 in an ultrasonic bath to remove any adhering dust and detrital carbonate as well as a possible organic surface coating. The CO_2 was liberated from the sample with 100% phosphoric acid at 90°C. The CO_2 was reduced with H_2 over about 2 mg of Fe powder as catalyst, and the resulting carbon/iron mixture was pressed into a pellet for the target holder.
The resulting AMS ^{14}C-dates are shown in chapter 4 (Table 4.2), together with the other stratigraphic measurement for each sediment core. The AMS ^{14}C-data were solely used to confirm the ages obtained from the linear interpolation of the oxygen isotope data with the SPECMAP stack, and in general to support the interpretation of stage 3 samples as obtained from the oxygen isotope curve. An exception to the rule is formed by the AMS ^{14}C age that was received for core M35034. This age was used to obtain at least an estimate for stage 3 sedimentation rates.

2.2.2.4 U/Th dating of marine bulk sediment (using TIMS)

Due to the lack of large amounts of shallow water grains (like aragonitic corals) within the periplatform muds off Pedro Bank “normal” TIMS U/Th-dating could not be performed.
In coorperation with Dr. Gideon Henderson (LDEO Palisades, USA / Oxford University, UK) marine bulk sediment from the periplatform setting of Pedro Bank was used for dating. This new method is based on work done by Slowey et al. (1996), who showed that Bahamian periplatform sediments with a high content of aragonite are useful for direct U/Th-dating. From the 14 samples choosen for this technique, five resulted in reliable absolute dates (within an acceptable error range). These samples are from the two most proximal cores at the

northwestern bank margin (M35048, M35049). In all other cores the aragonite content of the sediments was probably high enough, but high clay content and/or high detrital input provided another source for uranium and scavenged thorium from seawater. This resulted in U/Th-ages, that could not be used due to their large age errors.
In addition one sample was taken from a turbidite layer (M35042, 470cm; 1023 mbsl, 41 km offbank distance), to ascertain if contemporaneous or older sediments are deposited along the slopes of Pedro Bank.

Bulk sample dating
Bahamian platform slope sediments can contain up to 90% aragonite (and should have <0.5% detrital material) during highstands in sea level. Slowey et al. (1996) used these type of sediment for U/Th-dating. The bulk sediments were sieved to separate the coarse and fine fraction and thus increase the U-concentration while removing the foraminifera with low U concentrations.
Bulk sediment also needs a correction for U and Th that is incorporated in the detrital material and for Th, scavenged from the seawater. Therefore, aluminium concentrations are measured either by neutron activation prior to dissolution, by directly coupled plasma analysis or by using XRF data obtained on bulk samples. The "quality" of the final ages thus depends on the quality of determinations for detrital material and the value that is used for the correction of scavenged ^{232}Th from seawater. Slowey et al. (1996) used the ^{232}Th/^{230}Th of modern seawater. The used ^{232}Th/^{230}Th value of 10000±4000 is consistent with shallow water measurements close to the Bahamas (Hoff et al., in press) as well as with estimates from young Bahamian sediments (Slowey et al., 1996).
The decay chain of U that is used to date sediment is given by: ^{238}U -> ^{234}U -> ^{230}Th -> ^{226}Ra -> ... -> ^{206}Pb (stable isotope). Ideally, marine carbonates start with a ^{234}U/^{238}U-ratio of 1.148, and this value is decreasing towards 1.000 with time. On the other hand, the carbonates should start with a ^{230}Th/^{234}U-ratio of 0.0, which then increases towards 1.000 with time. This results in two independent chronometers, with advantages and disadvantages. They are given for both chronometers below:

^{234}U/^{238}U-dating
advantages: - Nearly all the U incorporated in the samples to start with is derived from seawater, therefore the ^{234}U/^{238}U-ratio of the samples lies close to 1.148.
disadvantages: - ^{234}U is more mobile than ^{238}U, therefore diagenesis may influence the age.
- the ratio changes only slowly with time so that ages are not very precise, even without diagenesis

^{230}Th/^{234}U dating:
advantages: - Th is immobile in the sediment
- the ratio changes more quickly, therefore the precision is much better
disadvantages: - the most obvious problem with this dating-method is that the ^{230}Th/^{234}U ratio does not start at 0.0. There is initial ^{230}Th in the sediments - some from detrital material, and some scavenged from seawater. Therefore one needs to assess the amount of detrital material and correct for the two sources of ^{230}Th separately. This can be done by measuring the amount of aluminium in the samples.

If the ^{232}Th/^{230}Th-ratio is high, than the corrections for initial ^{230}Th are high as well and the uncertainty on the final age increases drastically. For further details the reader is referred to Slowey et al. (1996), Henderson et al. (1999) and Henderson et al. (2000).

2.2.3 Calcium carbonate and organic carbon content
The measurements of the total carbon content (TC) and total organic carbon content (TOC) was performed on a Carlo Erba CHNO Analyser NA1500 at GEOMAR.
During one automated run of 50 samples four blank containers, seven standard samples (0.1 - 1.0 mg of "acetanilide standard" for samples with high $CaCO_3$ content) and one internal standard with a known percentage of carbon (3.75% TC) were analysed. These blanks and standards were used to produce a calibration curve that finally results in the TC- and TOC-content of the sample. Each sample was measured twice. If both samples differed more than 0.2% for TC or 0.1% for TOC, the sample was remeasured. Assuming that all inorganic carbon

(IC) is bound in calcium carbonate, the weight percentages of calcium carbonate was calculated by using the following formula

$$CaCO_{3(weight\%)} = IC_{(weight\%)} \times 8.3333$$

$$\text{with} \quad IC = TC - TOC$$

The internal standard (Sample SO-109) was measured continously during all analyses performed to obtain a measure of the reproducibility. A standard deviation of 0.11% for 25 standard measurements of this internal standard circumstantiate the availability of the method.

2.2.4 X-ray powder diffraction

X-ray diffraction was used to analyse the carbonate mineralogical composition of bulk sediment as well as the fine fraction. The peak area method (Milliman, 1974), that is the integration of counts under a given peak, provides the best estimate of the content of a known or unknown mineral.

Using a Phillips X-ray machine (PW 1710) at GEOMAR Kiel the relative abundance of the carbonate phases (aragonite, low-magnesium calcite [LMC] and high-magnesium calcite [HMC]), as well as quartz, an indicator for terrigenous input, was measured. The diffractometer at GEOMAR creates X-ray beams using a Co- K_α-Anode with a wave length of 1.7903Å at 40 kV and 35 mA. As the PW1710 is equipped with a multisampler, 35 samples can be measured in one run. Each sample was ovendried at 40°C and ground in a mortar by hand, not longer than 3 minutes to produce sediment with a grain size less than 63 µm. This procedure was used to avoid measurement artefacts that originate from inhomogeneous particle size and transformations of aragonite to LMC due to overgrinding (Milliman, 1974). Each sample was pressed into an aluminium holder and scanned with a speed of 0.01°/s within the range of 25°-40° 2θ. This range covers all main X-ray diffraction peaks of the minerals of interest (Table 2.2).

Mineral	d-value	2θ–angle (Co-Anode)
Aragonite	3.396 Å	30.56°
Low-Mg-Calcite	3.035 Å	34.31°
High-Mg-Calcite	2.996 A	34.77°
Quartz	3.343 Å	31.06°

Table 2.2: d-values and 2θ–angle for main x-ray diffraction peaks of minerals analysed in this study.

Inaccuracies have been observed in the calibrations (used to correct the data) utilised in the X-ray diffraction method. A clear variability between the calibration curves that evolve from the measurement of the same calibration samples on different XRD machines, e.g. GEOMAR, the Universities of Houston (Rice University) and Edinburgh. Thus special emphasis has been put on determining the validity of this analytical method and its associated problems, which will be addressed in detail in chapter 3. However, the general data processing is outlined below.

At the University of Edinburgh a Phillips PW 1011/1050 was used. Measurements on this device were measured with a Cu- K_α-anode at 40 kV and 50 mA. This machine can also run multiple samples. But, the samples have to be prepared as slurry samples on a glass slide.

At Rice University a Phillips-Norelco model 12045 X-Ray diffractometer was used to measure the mineralogical content of the sediment samples. The X-ray source is a Cu-K_α-anode, and samples were run at 35 kV and 20 mA. Samples that were pressed into an aluminium holder, were scanned from 25.5-27.5° and from 28.5-32 2θ at a resolution of 0.01° per step. The measured files are stored on an "old" D´Apple computer automation system. This file format cannot be read directly by the peak evaluation programme MacDiff (Petschick et al., 1996) because of system incompatibilities. Therefore, the output files were converted.

Output files from the XRD-devices at GEOMAR and the Unversity of Edinburgh are provided in the raw data-Format (.rd). These type of files can be read directly by the computer program MacDiff (Petschick et al., 1996), which is able to display and evaluate X-ray diffractograms on Apple Macintosh computers. Fig. 2.5 shows a typical scan of a periplatform sediment from the study area and the peaks of the main carbonate phases.

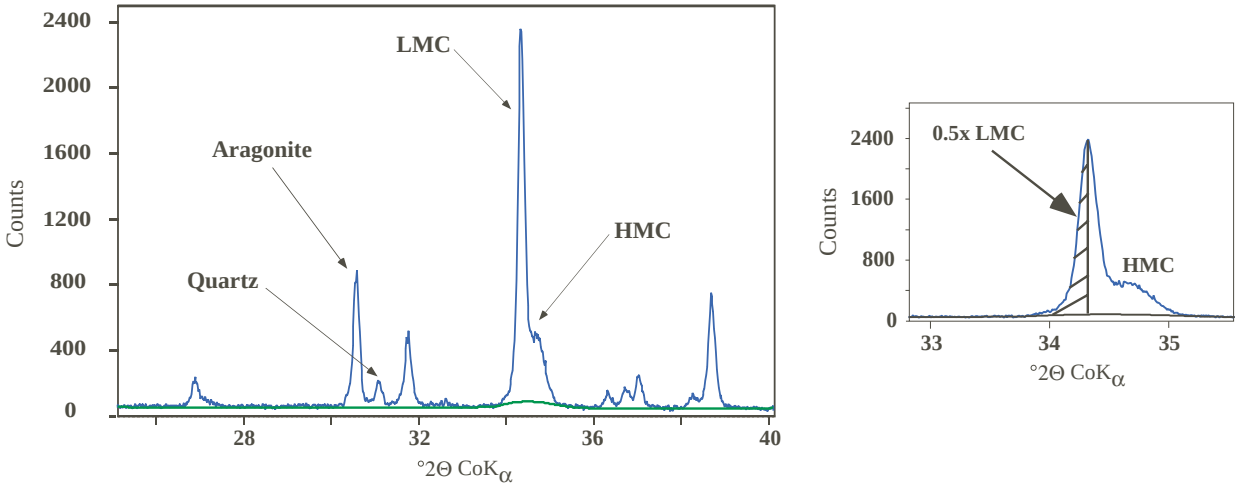

Fig. 2.5: Typical X-ray diffractogram showing the peaks of major carbonate phases and quartz. Small figure shows how half of the LMC peak was defined to calculate HMC-content if HMC is only present as a shoulder on the major LMC peak (method after Droxler, 1984).

Using the computer program MacDiff (Petschick et al., 1996) and the modified peak area method after Droxler (1984) the relative amounts of aragonite, LMC and HMC were calculated as well as the relative intensity of quartz within each sample. The calculation of the peak areas for aragonite, LMC and HMC (see Fig. 2.5) is described below:

(1) Aragonite peak area: direct measurement of peak area (defined by left and right intersection of the peak with the base line)

(2) $\text{LMC peak area} = 2 \times \frac{1}{2} \text{peak area}_{\text{LMC}}$ (= left part of LMC peak)

(3) $\text{HMC peak area} = (\text{total calcite peak area (LMC + HMC)} - (2 \times \frac{1}{2} \text{peak area}_{\text{LMC}}))$

From the integrated peak areas obtained, the aragonite/calcite ratio was determined using the following formula:

$$\text{Aragonite/Calcite} - \text{ratio (\%)} = \frac{\text{peak area}_{\text{aragonite}}}{((\text{peak area}_{\text{aragonite}}) + (\text{peak area}_{\text{calcite}}))} \times 100$$

Finally the relative percentages of the carbonate minerals were calculated using a calibration curve. This calibration curve was established by measuring known weight percentages of mixtures from pure skeletal aragonite and pure synthetic calcite (see Chapter 3). Each sample was measured three times. After each individual measurement of a sample it was rejected, and a new sample was prepared. The resulting standard deviation of these 3 measurements shows a linear increase from 0.08 to 5.16% 2σ with increasing aragonite percentage (Emmermann et al., 1999). The mineralogical data used in this study are based on the Kiel calibration curve and equation (Chapter 3).

2.2.5 Grain size analysis

Grain size is a fundamental attribute of siliciclastic rocks and thus one of the most important descriptive properties of such rocks (Boggs, 1987). In the carbonate environment the application of grain-size analyses is relatively minor. The main reason for this is that carbonate sediments are “born”, not made (James, 1983), and therefore the grain size of carbonates seems to reflect biological processes more than depostional and/or transport processes. This has also been recognised by Tucker & Wright (1993), who stated that “granulometric and morphometric

properties, such as grain size, sorting, roundness and spericity are given less significance in carbonate sedimentology then in the study of siliciclastic deposits". Therefore it is generally accepted that grain types are more useful for environmental interpretations of limestones and carbonate sediments. However, grain size is still important as it forms a primary controlling factor for other derived physical properties such as bulk density, porosity and permeability (Boggs, 1987; Rendle et al., 2000). However, precaution should be taken during interpretation due to the biogenic factors discussed above.
Nonetheless, grain-size distributions in carbonate have been used by various authors to some extent. Purdy (1963) and Mullins et al. (1980) found grain size to be useful obtaining knowledge on the current intensity along the margins of Great Bahama Bank (GBB). However, they also recognised that as the texture of Bahamian sediments is determined not only by the presence of transported material, but also by *in situ* skeletal debris and *in situ* changes in original particle size, the statistical parameters generally used for siliciclastics to describe the environment of deposition are not useful in carbonates.
Although all these provisos exist, recent sedimentary analyses along a platform-to-basin transect on the leeward margin of GBB (Rendle et al., 2000) has shown that the practicability of grain-size distribution analyses within the carbonate environment can be useful, when the interpretation of this data is approachend with care.

Laboratory procedures
(I) Pre-sieving procedures
Fresh or constantly cooled bulk sediment samples were vacuum freeze-dried at about -40°C. These dehydrated samples were weighed to a precision of 0.001 g. Before starting wet sieving, the samples were treated with demineralised water for a few hours to one day to deflocculate the dried sample again and thus ease the wet sieving process.

(II) Wet-sieving
Using the suspended bulk sediment sample wet sieving procedure separates clay and silt sized particles (<63 µm) from the sand sized fraction and coarser particles (>63 µm). This is achieved by washing the suspended sediment through a 63 µm standard sieve with demineralised water. The fine sediment is collected in 1-3 liter bottles in which it settles down within a few days or weeks (depending on the clay and silt-size distribution). After settling the water is removed carefully and the fine fraction is dried at 40°C.

(III) Dry sieving
The dried and weighted coarse fraction samples (>63 µm) were then subsequently splitted into the following five subfraction according to the Wentworth-Udden grain-size scale (Wentworth, 1922) for terrigenous sediments and the weight percentages of each subfraction were determined as part of the entire coarse fraction weight:

very fine sand:	63-125 µm = 1-2 phi;
fine sand:	125-250 µm = 2-3 phi;
medium sand:	250-500 µm = 3-4 phi;
coarse sand:	500-1000 µm = 4-5 phi
very coarse sand to rubble:	>1000 µm = >5 phi.

2.2.6 Physical Properties
Sediment accumulation rates (also called mass accumulation rates [MAR]) for bulk sediment usually are determined through the multiplication of a linear sedimentation rates [LSR] and measured dry bulk density [DBD] (e.g. Backman et al, 1988; see equation 2.1 and 2.2).

Equation 2.1: $$\mathrm{MAR[g/cm\hat{}2/ky]} = \frac{\mathrm{LSR[cm/ky]}}{\mathrm{DBD[g/\,cm\hat{}3]}}$$

where DBD is calculated as follows:

Equation 2.2: $$\mathrm{DBD[g/cm\hat{}3]} = \frac{\text{Weight of dry sediment sample [g]}}{\text{Volume of sample[cm\hat{}3]}}$$

The water content of the samples can be obtained by using equation 2.3:

Equation 2.3: $$\text{Water content [\%]} = \frac{(\text{Weight wet sediment} - \text{Weight dry sediment})\ [\text{g}]}{\text{Weight wet sediment [g]}}$$

2.2.7 X-ray fluorescence: geochemical analysis of bulk sediment

Using a Phillips PW 1480 sequential X-ray spectrometer 27 major and trace elements were analysed from 130 samples within 4 cores. X-ray beams of this device are generated by a rhodium tube. The samples were hand-ground to a size finer than 63 µm, dried overnight at 110°C and then mixed with lithiumtetraborate as catalysator in a ratio of 1:6 (600 mg : 3600 mg) to produce homogenous melting tablets needed for the final analysis.
During the final measurement procedure the melting tablets are exposed to a beam of high energy photons including polychromatic X-rays (more detailed description in Chapter 8).

2.2.8 Microfacies and microscopical analysis of coarse fraction

For microfacies analysis of the bulk sediment, as well as specific turbidite layers, artificial thin sections were prepared. The identification of skeletal and non-skeletal grains was based on Loeblich et al. (1964), Horrowitz & Potter (1971), Dolan (1972), Milliman (1974), Flügel (1983), Dullo (1990), Piller (1994) and Gischler & Lomando (1999).
The components of the coarse fraction were identified using Milliman (1974) and for:
(1) benthic foraminifera: Rose & Lidz (1977), Poag (1981), Murray & Perkins (1991), Triffleman et al. (1991), Hottinger et al. (1993), Bolli et al., (1985), Li & Jones (1997), Li et al. (1997);
(2) planktic foraminifera: Rose & Lidz (1977), Saito et al. (1981), Bolli et al. (1985), Li & Jones (1997), Li et al. (1997);
(3) pteropods: Jung (1973), Be & Gilmer (1977), Herman (1978), Almogi-Labin (1982), Bolli et al. (1985) and
(4) molluscs: Boggild (1930), MacClintock (1967) and Bathurst (1971).

Further information on the classification of the components present in the periplatform sediments of Pedro Bank can be found in chapter 8.

2.2.9 Parasound data and 3.5 kHz seismics

As part of this study several platform-to-basin transects will be presented, obtained with the PARASOUND system onboard *R/V Meteor* (1996) and with 3.5 kHz seismic recorders onboard *R/V Cape Hatteras* (1988) on the Northern Nicaragua Rise.

1. The PARASOUND System operates as a narrow-beam (ca. 4.5°) sub-bottom profiling echosounder that is able to use low frequencies of 2.5-5.5 kHz. The system has a fixed primary frequency of 18 kHz ("Pilot-frequency"), and a selectable set of slightly higher primary frequencies (20.5-23.5 kHz). The "parametric effect", which means the simultaneous transmission of two primary frequencies, generates a narrow pulse of low frequency (difference between both primary frequencies). Electronic compensation for the ships motion as well as for the heave of the ship ensures that the transmitted beam is directed vertically down.

2. The second device that was used for interpretations of the seafloor morphology is a 3.5 kHz seismic recorder, used during the forementioned American research cruises. These data were analog recorded on paper onboard *R/V Cape Hatteras* by the working group of Dr. Droxler from Rice University. The 3.5 kHz echogram data were collected using a hull-mounted array of 9 Raytheon TR-109 kHz transducers and Edo 248E transceivers. For a more detailed technical explanation of this procedure the reader is referred to Cunningham (1998).

CHAPTER 3

ARAGONITE/CALCITE CALIBRATION CURVES

3.1 Introduction

The carbonate mineralogical composition of periplatform sediments can be calculated applying the standard calibration curve (Fig. 3.1) by Milliman (1974) for the aragonite/calcite ratio of the sample. This calibration curve was created using different calibration standards measured on different XRD machines. This might create huge errors, when applying it to samples measured with other X-ray machines. Therefore, before calculating the mineralogical content of a sample, calibration measurements for each specific machine should be made.

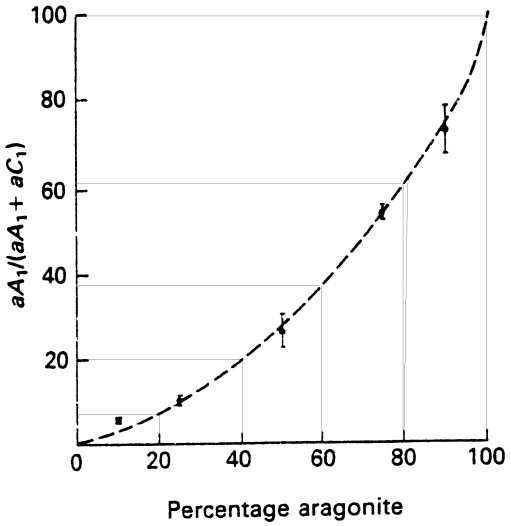

Fig. 3.1: Standard calibration curve for aragonite determination using the peak area method (Milliman, 1974). The known percentage of aragonite is displayed on the x-axis, whereas the aragonite/calcite ratio is displayed on the y-axis. (aA1 = area calculated for the main aragonite peak; aC1 = area calculated for the main calcite peak).
Each data point represents 8-10 analyses of various calcite and aragonite standards. The standard deviation (vertical bars) is considerably less then 5% on an absolute scale (Milliman, 1974).

Starting the analysis of periplatform sediments around Pedro Bank, a major uncertainty was how to compare our own dataset with those of other researchers (e.g. Glaser, 1991; Glaser & Droxler, 1993; Haddad & Droxler, 1996; Schwartz, 1996). To estimate the errors that might arise comparing datasets produced on different machines, a calibration set of 18 samples with known percentages of low-magnesium calcite (synthetic) and aragonite (Red Sea coral) was measured on 3 different XRD-machines: GEOMAR - Kiel, Rice University - Houston and the University of Edinburgh. In addition, sediment samples from three sediment cores from different depositional environments were measured on the X-ray machines at GEOMAR and Rice University to obtain a scale of the absolute error that might arise between measurements on these two machines.

3.2 Material and methods

Mixtures of 18 different weight percentages of pure aragonite and LMC were made to produce the standard calibration set used. A detailed description of the X-ray diffraction method and of the calculation of the aragonite content and the other carbonate phases can be found in chapter 2.

3.3 Results

3.3.1 Calibration curves and equations

The results of measuring identical standard samples at different XRD-machines show clearly that offsets occur. The calibration curves obtained by using a simple exponential curve fit for the calculated aragonite-calcite ratios at Kiel, Edinburgh and Houston are very similar (Fig. 3.2).

The GEOMAR calibration curve produces the highest aragonite values, but those derived from Edinburgh and Houston only show a minor offset from the Kiel curve. All curves result in very similar aragonite amounts for aragonite/calcite ratio percentages from 0-10%, whereas for aragonite-calcite ratio percentages exceeding 10% the curves result in very different aragonite percentages.

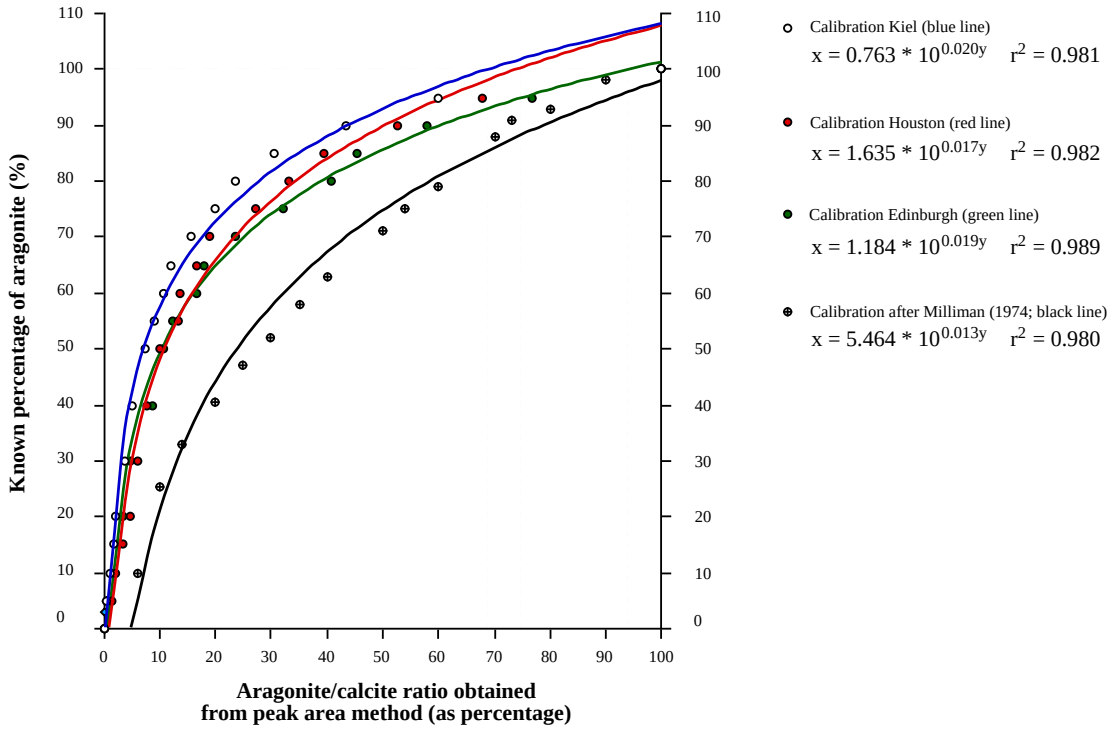

Fig. 3.2: Calibration curves of the calibration measurements at GEOMAR Kiel (blue line), University of Edinburgh (green line) and Rice University (red line).
The calibration curve of Milliman (1974; black line) is also shown. The colored lines show the "best fit" using an exponential equation. All "best fit" curves do not cross the 0/0% and 100/100% data points, which might cause slight errors at the lower and upper measured ranges. The curve with the best fit is that of the XRD-machine of the University of Edinburgh, correlation coefficient r^2=0.989.

Fig. 3.2 shows that the calibration curves do not cross the data points of the endmembers of pure aragonite and pure calcite. This is a mathematical problem caused by the curve fit routine of the CricketGraph computer program that was used to calculate the calibration curves for the individual data points of each apparatus. This discrepancy can be neglected for our datasets as the highest aragonite-calcite ratios that were measured do not exceed 53% (proximal periplatform sediment and turbidites in core M35048). The values lie well below the intersection of the calibration curve with the 100% aragonite content line (dashed line in Fig. 3.2).

All three calibration curves and equations were used to generate an averaged calibration curve, as the same calibration samples were used. This curve and equation might be used to calculate the content of aragonite within carbonate sediments at the three used machines (Fig. 3.3), as it possibly displays a more accurate average of data for this specific calibration data set. For comparison the calibration curve of Milliman (1974) is shown as well. As it is evident from Fig. 3.3 both curves differ significantly from each other. Using the new averaged calibration the calculated aragonite contents are clearly higher than those derived by using the standard calibration dataset of Milliman (1974). Comparison of the new calibration set and Milliman (1974) result in differences in the percentage of aragonite of up to 35% (Fig. 3.3).

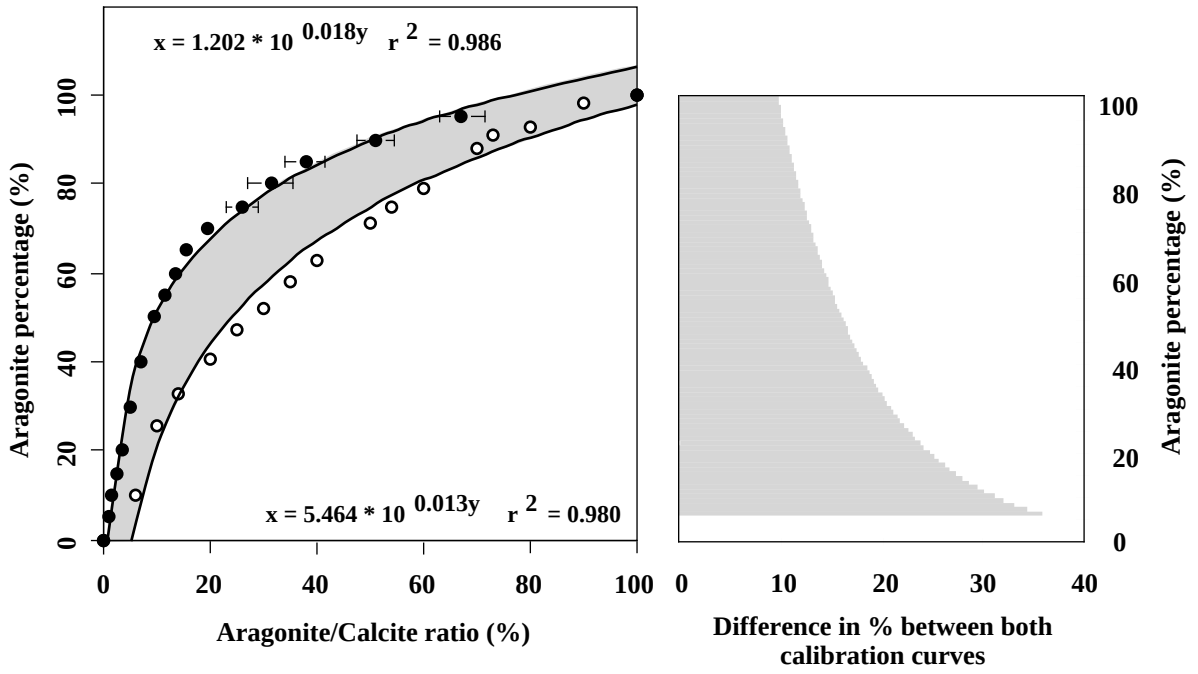

Fig. 3.3: Averaged aragonite/calcite calibration curve derived from the three calibration data sets measured at GEOMAR Kiel, Edinburgh and Houston. The standard deviation of the 3 curves used to calculate this mean curve (see error bars) is neglectable for Ar/Cc-ratios smaller than 20%, but increases with greater aragonite/calcite ratio.
Open circles display the calibration point for the aragonite/calcite calibration of Milliman (1974). The curve fit for these data point were created by the same exponential curve fit routine as done for averaged aragonite/calcite calibration curve shown in this figure. The grey shaded area marks the difference that occurs between both averaged calibration curves. It is obvious that aragonite contents calculated by using the Kiel calibration curve results in higher aragonite percentages. The maximum difference between both curves is found for low aragonite/calcite ratios (see right graph) and adds up to a maximum value of 35%. The smallest difference in the final calculated aragonite content can be seen for higher Ar/Cc-ratios.

3.3.2 Estimation of errors introduced from using different XRD machines

Three sediment cores from the downcurrent basin and slope of Pedro Bank were measured on the Kiel and Houston XRD machines. The content of aragonite, LMC and HMC were calculated independently using the calibration equation obtained for the individual XRD machine (Fig. 3.2). The aragonite, LMC and HMC curves for the proximal core M35048 (with highest aragonite contents) and distal sites PC059 and PC100 (with intermediate and low contents of aragonite) display clear differences and inconsistencies for the Kiel and Houston calibration curves (Fig. 3.4). The most striking differences are found in the high-magnesium calcite contents, preferentially in the deep and distal cores with lowered amounts of aragonite and HMC. The determination of HMC follows the method described in chapter 2. Table 3.1 exhibits the range of differences for aragonite, LMC and HMC contents within the three cores. It is clearly evident from these calculations (Fig. 3.4) that:

1. Sediments with higher amounts of metastables carbonates show minor errors when a comparative analysis is done on different X-ray machines and calculated with machine-specific calibration curves (see M35048). The absolute error for aragonite ranges between 0.16-4.9% (average:1.89%), for LMC between 0.31-6.66% (average: 3.15%) and for HMC between 0-5.68% (average:1.71%).
2. Sediments retrieved from intermediate and deep water depths with clearly lowered amounts of metastable carbonate phases display extremely high differences. The absolute errors for the aragonite content in PC059 and PC100 ranges between 0.16-21.84% (average: 9.6% respectively 9.95%). The error in the content of LMC averages 0.7-32% (average:15.5% respectively 13.5%), whereas the errors for HMC varies between 0-16% (average: 5.9% respectively 4%).

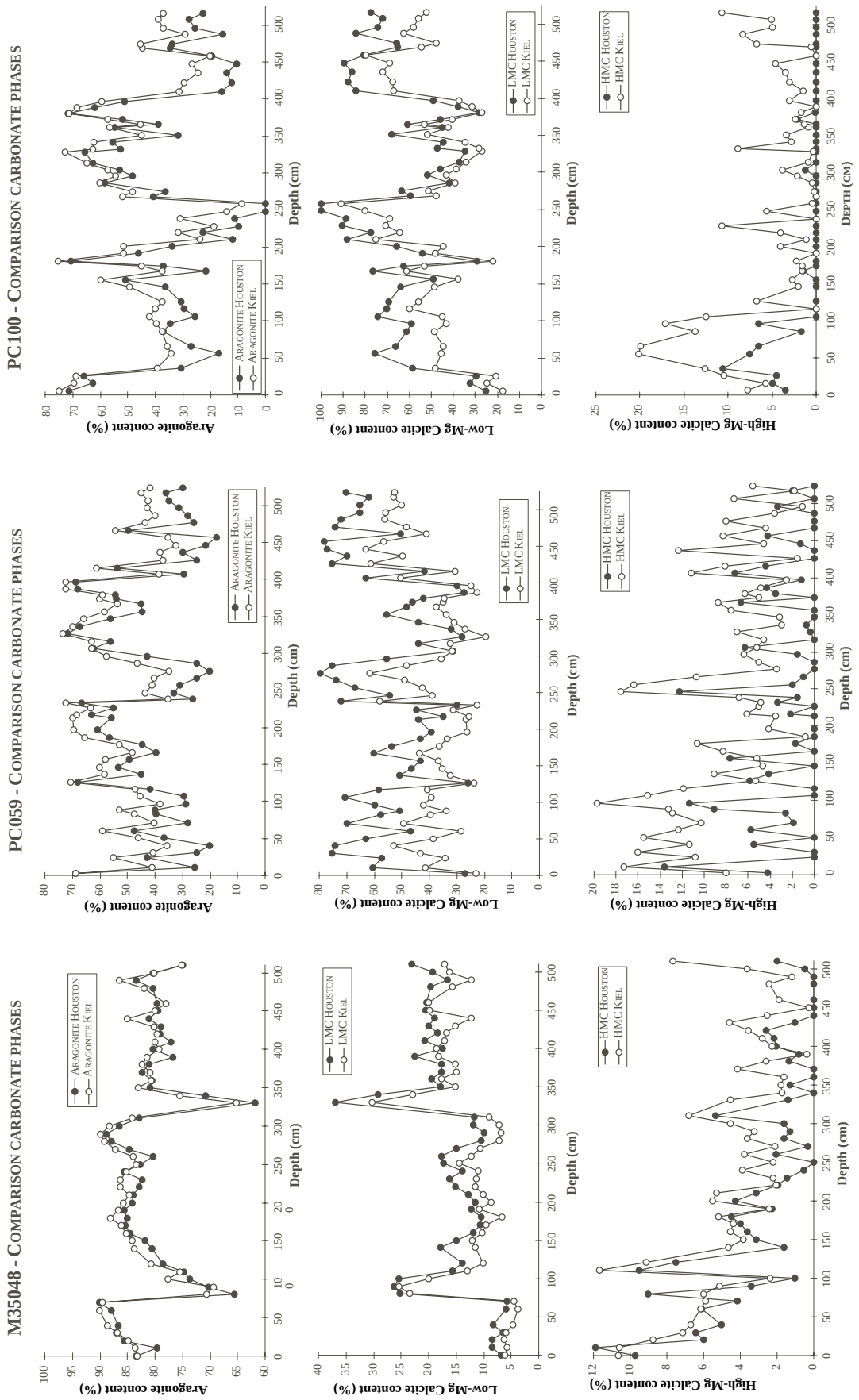

Fig. 3.4: Comparison of carbonate mineral content in one proximal and two deep, distal sediment cores. Values were calculated by using the calibration curves of this study for X-ray machines at Kiel and Houston.

3. Main differences are found in the HMC content of cores PC059 and PC100. In many cases HMC could be detected by the XRD machine in Kiel, whereas no traces of any HMC were found in the identical sample measured in Houston. This seems to be a very delicate problem, as those HMC values are used partly to calculate the "Composite Dissolution Index (CDI)" by Haddad & Droxler (1996) for example. This might result in incorrect interpretations of the calculated indices.

Core	Statistical measure	Differences in aragonite (%) between Kiel and Houston calculations	Differences in LMC (%) between Kiel and Houston calculations	Differences in HMC (%) between Kiel and Houston calculations
M35048	Minimum value	0.16	0.31	0
	Maximum value	4.9	6.66	5.68
	Average	1.89	3.15	1.71
PC059	Minimum value	0.5	0.7	0
	Maximum value	21.84	32.06	16.08
	Average	9.95	15.5	5.9
PC100	Minimum value	0.16	0.7	0
	Maximum value	20	30	13.4
	Average	9.6	13.5	4

Table 3.1: Range of differences in calculations of aragonite, LMC and HMC content of identical samples measured at Kiel and Rice Unversities. Final calculations of the carbonate mineralogical content in similar samples is based on the calibration equations obtained from measurements of similar standard samples on the individual machines (see chapter 3.3.1).

3.4 Discussion

This "methodical" study shows that it is nearly impossible to compare absolute carbonate mineralogical data that were "produced" from different authors, using different X-ray diffraction methods on different machines. The method probably gives a good estimate of the relative changes of the carbonate mineral content, but the absolute amount of the individual carbonate minerals cannot be determined with great accuracy.
The calibration curves obtained through our studies differs significantly from the well-known Milliman (1974) curve. This might result in variations in the the relative percentage of aragonite of up to 35% (Fig. 3.3). Disadvantage of the new averaged calibration curve is the relative large variability for sediments with aragonite percentages exceeding 80%. Other studies by Greinert (1999), however, obtained similar results using other boundary conditions. For his geochemical studies Greinert (1999) produced an independent aragonite-calcite calibration curve (Fig. 3.5) using inorganically grown calcite and aragonite. The Greinert (1999) calibration curve resembles our curve (Fig. 3.3) and thus differs in the same way from the Milliman (1974) curve. Milliman (1974) already showed within his studies on the aragonite-calcite calibration that generally the influence of different types or phases of aragonite, but primarly the source of low-magnesium calcite, results in very different diffraction behaviour, as the different types of calcite unfortunately crystallize differently.
A major problem that occurs when applying the X-ray diffraction method and establishing a calibration curve to calculate the content of certain carbonate minerals, evolves from using different X-ray machines and probably also from using different calculation programmes. During earlier studies the peak intensity was measured by graphical integration of a measured peak. At present, computer programmes such as MacDiff (Petschick et al., 1996) can be used to determine the areas of the individual peaks.
Reijmer (1991) already noted that some differences might evolve measuring the same samples on different machines and using different peak area calculation programmes. The HMC content for example, could differ of up to 10.4% to those percentages calculated by Droxler (1984) using the same samples. Reijmer (1991) attributed these differences in the calculated content of carbonate minerals to differences in peak resolution, e.g. to the analytical setup that was used

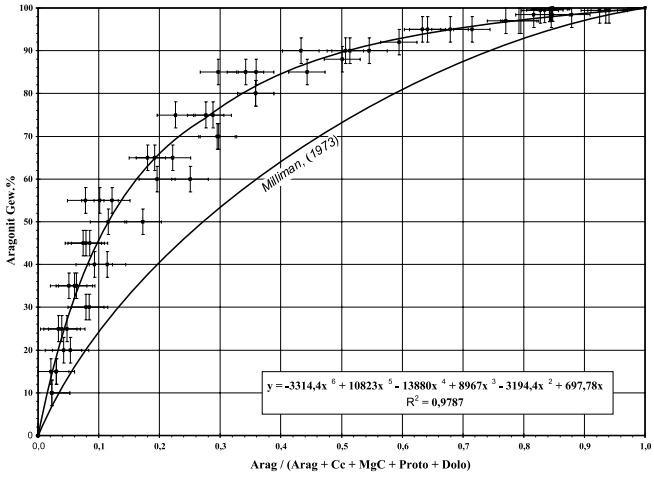

Fig. 3.5: Aragonite calibration curve from Greinert (1999) and Milliman (1974). It is evident that the aragonite/calcite calibration curve of Greinert (1999) resembles the Kiel aragonite/calcite calibration curve (Fig. 3.3). The differences between the Greinert (1999) and Milliman (1974) curve are very similar to those obtained in this study (Fig 3.3).

for XRD analysis. This difference also occured in our study (see chapter 3.3.2; Fig. 3.4 and Table 3.1). Reijmer (1991) concluded that "fortunately these discrepancies do not affect the aragonite curve and its use as a correlation tool". The reason for this is that the calcuation of the aragonite/calcite ratio HMC and LMC are added up to "whole calcite", which indeed do not affect to aragonite/calcite calibration. Studies by Haddad & Droxler (1996) and Schwartz (1996) used the content of HMC as a major factor to calculate the "Composite Dissolution Index" (CDI) of sediments. This index provided information on the absence or presence of corrosive water masses and therefore on times of carbonate preservation and dissolution at intermediate waterdepths. The content of HMC in the cores studied is in general very low. As shown in Table 3.1 the differences in the content of HMC in the distal cores measured on two different machines might be up to 16%. These differences are, therefore probably high enough to affect the original calculation of the CDI by Haddad & Droxler (1996). As a consequence this would lead to changes in the preservation/dissolution cycles as proposed by these authors. To what extent these changes affect the interpretation of Haddad & Droxler (1996) remains to be researched.

3.5 Conclusions

1. For each X-ray diffraction machine a specific calibration curve should be established calculating the carbonate mineral content of sediments and the same analytical setup should be used.

2. Some differences might occur when different types of aragonite and calcite are used to calculate the calibration curve. Therefore, the same calibration samples of aragonite and calcite should be used, although the calibration set should be adapted to the types of sediments. While the sediment composition, including periplatform sediments, differs from location to location no general standard sample for both carbonate mineral phases can be provided.
The Milliman (1974) curve tried to meet these needs, but the calibration curve from this study and the one provided by Greinert (1999) differ significantly from the Milliman standard curve. Both new aragonite/calcite calibration curves, however, agree very well despite the fact that different calcite and aragonite standards were used to calculate these curves. The curves presented here probably forms a significant improvement of the Milliman (1974) curve. It should be used when determining the aragonite and calcite content of periplatform sediment samples, at least for the three XRD machines, where the calibration set was measured. But in general standard samples should be adapted to the sediments or rocks that are in the focus of the own research.

3. Differences between individual machines might occur when analysing the carbonate mineral content, but the overall trends seen in the individual cores remain largely unaffected. Problems might evolve calculating the HMC content in sediments where HMC only occurs in very low percentages in periplatform sediments. HMC then often only shows itself as a tiny shoulder of the major LMC peak. Problems can be avoided when a precise identification of the major carbonate peaks takes place using precise analytical tools like the MacDiff X-ray evaluation programme (Petschick et al., 1996).

CHAPTER 4

STRATIGRAPHY
-
OXYGEN ISOTOPE STRATIGRAPHY, BIOSTRATIGRAPHY AND ABSOLUTE DATING (AMS ^{14}C AND U/TH DATING OF BULK SEDIMENTS)

4.1 Introduction

This chapter presents the stratigraphy and sedimentation rates for all sediment cores analysed. In addition, the problems of establishing the stratigraphies for each core will be dicussed. For six out of nine cores an oxygen isotope stratigraphy could be established. For cores M35032, M35048 and PC059 the content of fine aragonite or the calcium carbonate content of the fine fraction was used to establish a stratigraphy.
The applied methods, such as oxygen isotope stratigraphy, biostratigraphy, AMS ^{14}C-dating and U/Th absolute dating of bulk sediments that were used to establish the stratigraphy for nine late Quaternary sediment cores from the periplatform setting around Pedro Bank are described in detail in chapter 2. Here only the results will be presented and discussed.

4.2 Results

Sediment cores M35048, -49, -43, -42, PC059 and PC100 form an offbank transect along the northwestern margin of Pedro Bank (see Fig. 2.1). The remaining cores M35032, -34 and -52 are located off the southwestern to southern margin of Pedro Bank. As a proposed offbank transect from the southern margin could not be established during Meteor 35/1 cruise, these southern cores were treated independently. All the southern cores are from intermediate water depths ranging from 1211 to 1445 mbsl, with an offbank distance varying from 10 to 30 km.
Within the stratigraphic graphs larger gaps along the displayed proxy may occur. These gaps originate from the presence of numerous turbidite layers within the sediment cores. In this chapter the presence of turbidites is not indicated specifically except for core M35052. For a detailed presentation of the stratigraphic position of single turbidites the reader is referred to chapter 10 and the lithologic columns in Appendix 1. To facilitate the comparison of the single sediment cores, all graphs use the same x-axis (i.e. 1000 cm core depth), as the largest core is 965 cm long (M35052). This might occasionally result in a “stretched view” of the presented proxy. The age-depth plots for all cores are shown in the appendix. The average sedimentation rates are listed separately at the end of the results section in table 4.5.

4.2.1 Results of absolute age determinations (AMS ^{14}C- and U/Th-dating)

For 9 samples AMS ^{14}C-dating was applied, whereas 14 samples were choosen to apply U/Th-dating on marine bulk sediments. While the use of the AMS ^{14}C-method is limited to the sediments younger than approximately 50.000 years, U/Th was used to obtain knowledge on the age of highstands sediments from the last 3 full glacial/interglacial cycles (back to ± 300 ky).

The data shown in tables 4.1 to 4.3 were solely used to confirm the ages obtained from the linear interpolation of the oxygen isotope data (or another δ^{18}O proxy) with the SPECMAP stack, and in general to support the interpretation of stage 3 samples as obtained from the forementioned correlation to the SPECMAP stack. An exception to the rule is formed by the AMS ^{14}C age that was received for core M35034. This age was used to obtain, at least, an estimate for stage 3 sedimentation rates.

Core	Depth (cm)	Interpreted Isotope Event/Stage	Estimated age from correlation to SPECMAP	AMS Age Conventional ^{14}C Age (no res. age correct.)
M35032 (*1)	80	Stage 3	28	28650 ± 250
M35034 (*2)	230	Stage 3	no estimation possible	48350 ± 2890
M35042 (*3)	80	Stage 3	36.3	31390 ± 330
M35043 (*4)	90	Stage 3	40.5	35130 ± 540
M35048 (*5)	50	early Holocene	6	7160 ± 60
M35049 (*6)	110	Stage 3	43	43390 +1540/-1290
M35052 (*7)	100	S tage 3	33.8	29740 ± 310
PC059 (*8)	30	Stage 3	31.68	30580 ± 350
PC100 (*9)	76	Event 3.1	28	27020 ± 220

Table 4.1: Results of AMS ^{14}C age determinations. Indicators (*1 - *9) are the link to the AMS ^{14}C ages shown in Figs. 4.1 - 4.9.

Core	Depth (cm)	^{238}U concentr. (ppm)	^{232}Th concentr. (ppb)	$^{232}Th/^{230}Th$ (atom ratio)	$^{234}U/^{238}U$ age (ky) uncorr. (2σ in brackets)	$^{230}Th/^{238}U$ ages (ky) (2σ in brackets)
M35034-1	230	1.916	2854±87	58653±1527	111(±28)	-
M35042-2	80	0.913	2717±47	50932±723	153(±31)	-
M35042-2	100	1.011	3056±88	57231±2665	174(±28)	-
M35042-2 (TB)	470	5.889	649±9	6480±56	278(±21)	303(±18)
M35043-1	130	1.357	2371±41	58993±2941	68(±21)	-
M35043-1	150	1.579	1476±22	39767±628	83(±13)	-
M35043-1	430	2.268	1638±54	39784±1552	156(±12)	-
M35048-1 (*10)	180	5.313	286±5	4797±66	87(±9)	91(±10)
M35048-1 (*15)	290	8.019	242±7	2360±47	105(±9)	120(±6)
M35048-1 (*16)	500	5.648	382±5	4249±39	225(±18)	225(±12)
M35049-2 (*11)	170	4.771	1303±15	20812±235	15(±7)	83(±34)
M35049-2 (*12)	210	4.115	863±15	16016±395	72(±9)	94(±29)
M35049-2 (*13)	270	4.763	1030±19	16051±406	89(±8)	104(±29)
M35049-2 (*14)	320	4.040	379±4	6151±73	136(±11)	172(±16)

Table 4.2: U and Th isotopic composition and ^{234}U and ^{230}Th ages of 14 periplatform samples off Pedro Bank. Dash indicates that the content of detrital U and/or scavenged Th was too high to obtain a reliable U/Th age. Indicators (*10 - *16) are the link to the AMS ^{14}C ages shown in Figs. 4.1 - 4.9. TB = Turbidite sample.

Core	Depth (cm)	$^{230}Th/^{238}U$ age (ky) uncorr.	Age error (2σ)	Al_2O_3 (%)	Clay fraction	Corrected $^{230}Th/^{238}U$ age (ky)	Age error (2σ)	Corr. initial $\delta^{234}U$	$\delta^{234}U$ error (2σ)
M35048-1	180	91	±10	0.38	0.018	95.1	9.0	165.5	7.5
M35049-2	170	83	±34	1.86	0.090	100.2	48.8	271.8	51.9
M35049-2	210	94	±29	1.31	0.063	113.0	46.4	235.0	43.0
M35049-2	270	104	±29	1.22	0.059	99.6	33.7	205.0	27.5
M35049-2	320	172	±16	0.68	0.033	180.6	14.5	210.4	16.1

Table 4.3: Results for corrected U/Th absolute age determinations of marine bulk sediments age dates. Age improvement was achieved by using the aluminium concentrations of XRF analysis of bulk samples. Clay fraction was calculated assuming clay has 11% Al. The error of the corrected ages increased dramatically (last column). The corrected ages are still the better ones to give an estimate of the sediment age, as they are more accurate, even though they seem to be less precise (pers. comm. G. Henderson).

4.2.2 Stratigraphy of individual cores

(I) Core M35032 (southwestern margin)

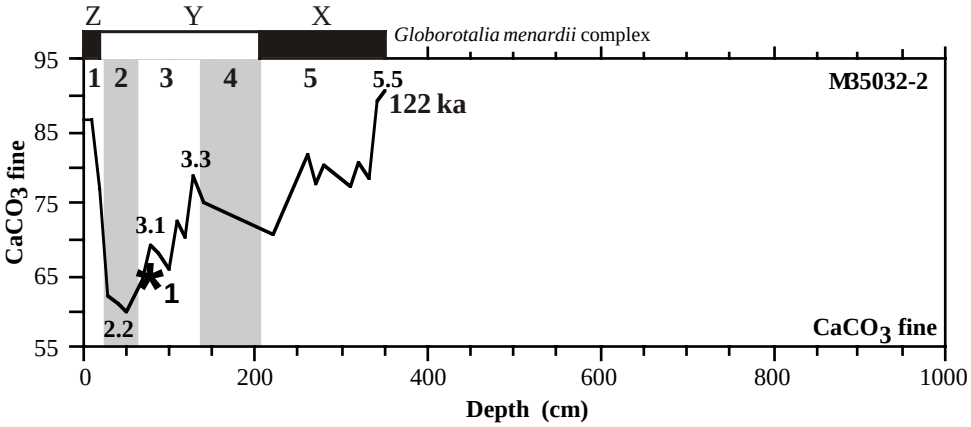

Fig. 4.1: Stratigraphy of core M35032 based on calcium carbonate content in the fine fraction. One AMS ^{14}C age is displayed (*1; see table 4.1), which confirms the interpretation of stage 3. Major oxygen isotope events are indicated. The *Globorotalia menardii*-complex zonation is displayed above. Shaded intervals indicate glacial isotope stages (stage numbers are displayed in the upper part of the shaded section).

Due to the presence of coarse-grained turbidite layers and related diagenetic reactions within the sediments, the oxygen isotope analysis resulted in an useless $\delta^{18}O$ signature (see also core M35048). The calcium carbonate content of the fine fraction was used instead to construct a proper stratigraphy.
Core M35032, which contains 5 turbidite layers (**not** indicated in Fig. 4.1), possibly reaches down to the Eemian (isotope stage 5e = 122 ky). The stratigraphy of this core seems to be heavily disturbed by the erosive action of turbidites. Isotope event 5.1 is not apparent, when determining the onset of the biostratigraphic zone X of the *Globorotalia menardii* complex, which indicates an age of 77-83 ky (Ericson & Wollin, 1956; Glaser & Droxler, 1993). Therefore it might be concluded that lower parts of interglacial stage 5 (and upper parts of stage 4) have been removed by erosion.

(II) Core M35034 (southwestern margin)

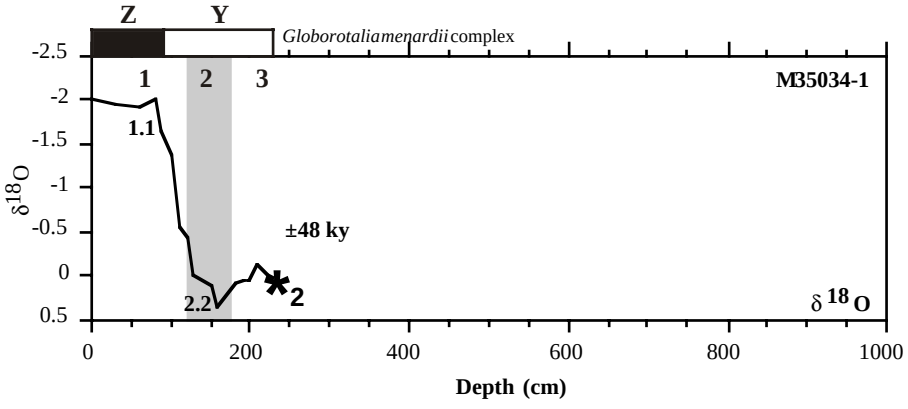

Fig. 4.2: Stratigraphy of core M35034 resulting from oxygen isotope analysis. Based on AMS ^{14}C dating the base of the core is dated at 48 ky. Major oxygen isotope events are indicated. The *Globorotalia menardii* complex zonation is displayed on top. Shaded intervals indicate glacial isotope stages.

Core M35034-1 displays the shortest sedimentary record of the nine analysed cores. The bottom of the core was dated using AMS ^{14}C absolute dating to obtain a maximum age for the sediments deposited. The age of 48.350 ± 2890 yr is placed within the lower detection range of AMS-dating, and therefore has to be interpreted with caution. However, M35034 displays the highest sedimentation rates of about 8 cm/ky during certain time slices during the Holocene and even might reach values of up to 12 cm/ky when not corrected for turbidite input (see Table 4.4 and Appendix 3).
Also in this core, the oxygen isotopes do not show the expected amplitude for the section between isotope events 2.2 and 3.1. However, the AMS ^{14}C obtained for the lower part of the core gives an idea of the stratigraphic range.

(III) Core M35042 (northwestern margin)

Core M35042 probably displays the most complete stratigraphic record of all cores. The oxygen isotope stratigraphy is in excellent correlation with the *Globorotalia menardii* complex biostratigraphy. Even though this core contains 8 turbidite layers (mainly fine tails of turbidites; not displayed in Fig. 4.3), these turbidites did not affected the stratigraphy as it was apparent in other cores of this study.

The fine tail of the turbidite layer within interglacial stage 7 (470 cm) was sampled and dated by TIMS U/Th dating of bulk sediment. The obtained absolute $^{230}Th/^{238}U$- age of 303±18 ky (or 278±21 ky for $^{234}U/^{238}U$-age) implies, that no contemporaneous sediments were redeposited in this turbidite. Obviously older sediments that might have been deposited during the preceding interglacial isotope stage 9 and/or glacial stage 8 were redeposited.

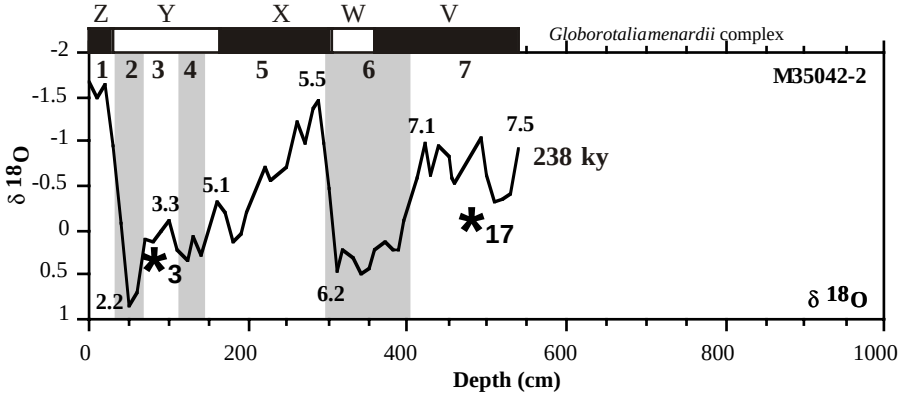

Fig. 4.3: Stratigraphy for core M35042 based on oxygen isotope analysis. Oldest sediments are about 238 ky old (= isotope event 7.5). The AMS ^{14}C age (*3) confirms the interpretation of stage 3 as derived from oxygen isotope stratigraphy. Major oxygen isotope events are indicated. The *Globorotalia menardii* complex zonation is displayed on top. Shaded intervals indicate glacial isotope stages (stage numbers are displayed in the upper part of the shaded area).

(IV) Core M35043 (northwestern margin)

When establishing the stratigraphy for core M35043 using oxygen isotopes a major problem arises for the time slice between isotope event 3.3 and 5.1 (see Fig. 4.5). Within the oxygen isotope curve heavier isotopes, which should be indicative for glacial stage 4 were not found. Only a minor drop towards heavier isotope values was observed. In addition, isotope event 5.1 is indicated not by a clear rise towards lighter isotope values. Instead a twofold peak is evident.

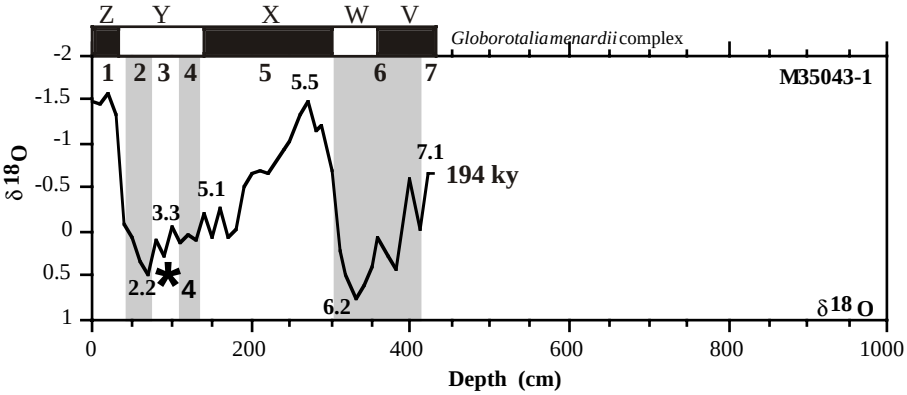

Fig. 4.4: Stratigraphy for core M35043 based on oxygen isotope analysis. Oldest sediment are of isotopic event 7.1 (=194 ky). The AMS ^{14}C age (*4) confirms the interpretation of stage 3 as derived from oxygen isotope stratigraphy. Major oxygen isotope events are indicated. The *Globorotalia menardii* complex zonation is displayed on top of the graph. Shaded intervals indicate glacial isotope stages (stage numbers are displayed in the upper part of the shaded area).

The final decision to classify this twofold peak as isotope event 5.1 is supported by the latest appearance of the Globorotaliid species of zone X at about 150-160 cm core depth. Subsequently the stage boundary between interglacial stage 5 and glacial stage 4 was defined to be roughly at 130-140 cm core depth, even though the isotope values recorded are not of glacial-to-interglacial amplitude.

(V) Core M35048 (northwestern margin)

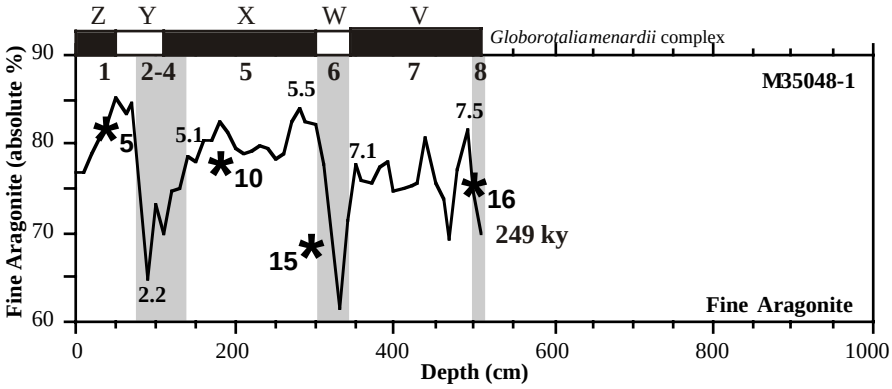

Fig. 4.5: Stratigraphy for core M35048 based on the aragonite content. Oldest sediments are from isotopic event 8.2 (=249 ky). The AMS ^{14}C age (*5) confirms the interpretation of Holocene age as derived from oxygen isotope stratigraphy. Major oxygen isotope events are indicated. The *Globorotalia menardii* complex zonation is displayed on top. Absolute U/Th-ages are displayed (*10, *15, *16) confirming the interpretation using the fine aragonite content in bulk sediment as a δ^{18}O proxy. Shaded intervals indicate glacial isotope stages (stage numbers are displayed in the upper part of the shaded areas).

The oxygen isotopes analyses on *G. sacculifer* failed to establish a proper stratigraphy. Instead the content of fine aragonite in bulk sediment was used. The close proximity of this core to the bank top and it´s shallow water depth assured that the samples choosen for the U/Th dating method had high enough U-concentrations to provide, at least, a very good estimate of the time of deposition or time of sediment production.
The sedimentation rate pattern of core M35048 exhibits an excellent highstand shedding pattern. Core M35048 displays the highest sedimentation rates within interglacial times, and lowest rates during glacials for cores from the downcurrent side of Pedro Bank (e.g. 5.4 cm/ky during the Holocene or up to 8.5 cm/ky if not corrected for turbidites; 0.6 cm/ky during glacial stage 2; see Table 4.4 and Appendix 3). This is probably due to the close proximity of this core to the active platform edge. During highstands in sea level this location received high amounts of metastable carbonates, whereas during glacials most of the sediment is winnnowed due to stronger current activity, which may be enhanced close to the platform edge (Glaser, 1991; Schwartz, 1996; Duncan, 1997).

(VI) Core M35049 (northwestern margin)

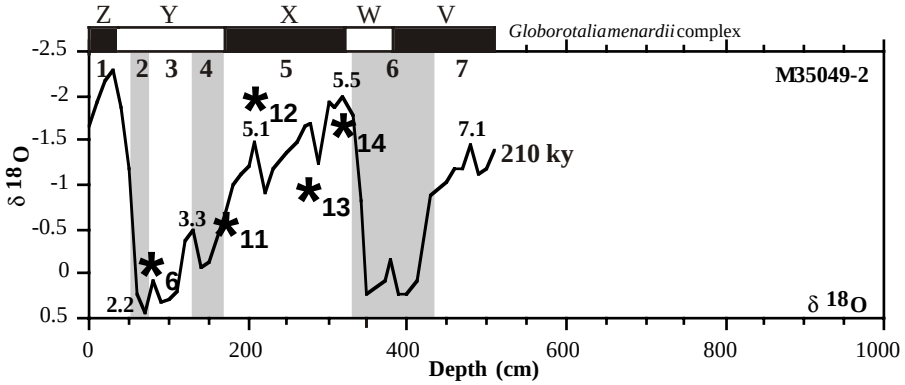

Fig. 4.6: Stratigraphy for core M35049 based on oxygen isotope analysis. Oldest sediments recovered fall within isotope stage 7 (=210 ky). Absolute age determinations are indicated with numbered asteriks (for ages see Tables 4.2 and 4.3). The AMS ^{14}C age (*6) confirms the interpretation of stage 3 as derived from oxygen isotope stratigraphy. Absolute U/Th-ages (*11 - *14; Tables 4.2/4.3) show that already at 893 mbsl U/Th analysis do not provide reliable U/Th-age. The *Globorotalia menardii* complex is displayed above. Shaded intervals indicate glacial isotope stages (stage numbers are displayed in the upper part of the shaded areas).

Core M35049 displays a well-developed oxygen isotope curve, which, together with the biostratigraphy, can be used to construct a reliable stratigraphy. The absolute dates of TIMS

U/Th-dating (see Table 4.2 and 4.3) shows the limited use of sediment cores from intermediate water depths for direct TIMS U/Th-dating. The content of detrital U and Th, as well as scavenged Th at this water depth can not be recalculated to produce reliable absolute U/Th-ages (see discussion).

(VII) Core M35052 (southern margin)

Core M35052 represents the longest sediment core recovered during Leg 35/1 of R/V *Meteor* at Pedro Bank. Large turbidites are present but they do not jumble the stratigraphic record for this core (at least down to the stage 7/8 boundary). The core probably reaches down to isotope event 9.1. This interpretation is based on comparison with isotope values measured by Schwartz (1996) in core PC-52, which showed similar low isotope values and amplitudes within this time slice. On the other hand it seems be a typical feature for low latitude cores, that isotope events 8.5 and 9.1 exhibit almost the same isotopic values. This was also observed by Bassinot et al. (1994), which would strengthen the interpretation given for core M35052.
Another major point that has to be mentioned, is the large extension of marine isotope stage 3 in this core. Sedimentation rates for stage 3 are much higher than for any other interglacials within this core. Although there is a large turbidite present at the beginning of stage 3, this turbidite does not account for the high (turbidite-free) sedimentation rate of 3.5 cm/ky (Table 4.4). At present there is no explanation for this extended stage 3.

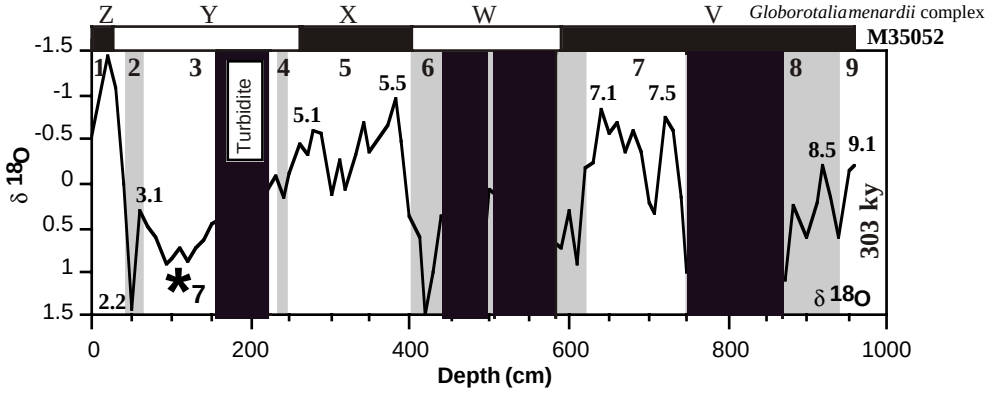

Fig. 4.7: Stratigraphy for core M35052 based on oxygen isotope analysis. Oldest sediments can be attributed to isotopic event 9.1 (=310 ky). The AMS ^{14}C age (*7) confirms the interpretation of stage 3 as derived from oxygen isotope stratigraphy. Major oxygen isotope events are indicated. The *Globorotalia menardii* complex is displayed on top of the graph. Shaded intervals indicate glacial isotope stages (stage numbers are displayed in the upper part of the shaded area).
The core contains four large turbidites (indicated by black bars), which probably makes the interpretation of the lower part of the core somehow uncertain as there are also no biostratigraphic markers that can be used.

(VIII) Core PC059 (northwestern margin, Pedro Channel)

The entire core is about 526 cm long, but only the upper 480 cm were analysed, while the remainder of the core is heavily disturbed. The stratigraphy of core PC059 is based on the content of aragonite in the fine fraction (Fig. 4.8). Oxygen isotope analysis failed on planktic, as well as on benthic foraminifera, probably due to diagenetic overprint of the foraminiferal tests. It seems apparent that the core top is probably lost, or that during the Holocene a major hiatus is present (Holocene sedimentation rate is 0.58 cm/ky; Table 4.4). Glacial stage 2, 4, 6 and 8 show very low sedimentation rates. This might be the result of increased current velocities within Pedro Channel, that may have affected sedimentation at this core location (eastern slope of the central canyon in Pedro Channel).

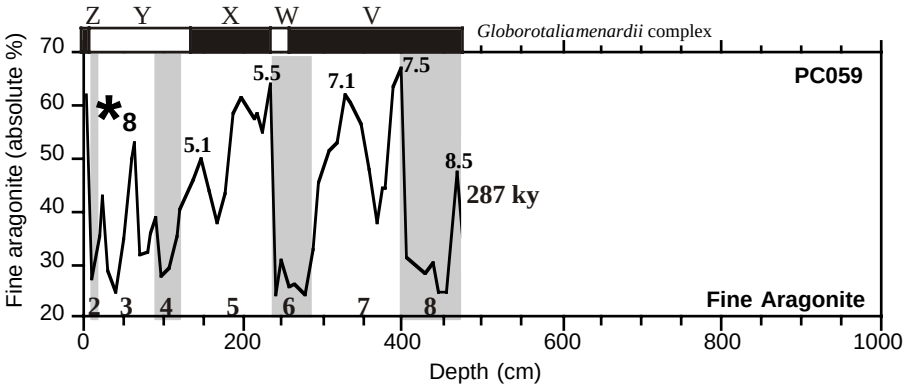

Fig. 4.8: Stratigraphy for core PC059 based on content of fine aragonite. Oldest sediment reach down to isotope event 8.5 (=287 ky). The AMS ^{14}C age (*8) confirms the interpretation of stage 3 as derived from "aragonite stratigraphy". Major oxygen isotope events are indicated. The *Globorotalia menardii* complex zonation is displayed on top. Shaded intervals indicate glacial isotope stages (stage numbers are displayed in the upper part of the shaded area).

(IX) Core PC100 (northwestern margin, Pedro Channel)

This core probably displays the longest statigraphic record within this study, even though core PC100 is disturbed by a hiatus between isotopic event 5.3 to 6.2 (99 to 135 ky). This seems to be confirmed by the small range of biostratigraphic zone X of the *Globorotalia menardii* complex, in comparison to other cores from this sedimentary environment.

The isotope values for interglacial stages 5, 7 and 9 are heavier than expected resulting in a much lower glacial-interglacial oxygen isotope amplitude. The obtained oxygen isotope pattern could be used to construct a reliable age model for PC100 in conjunction with the biostratigraphy.

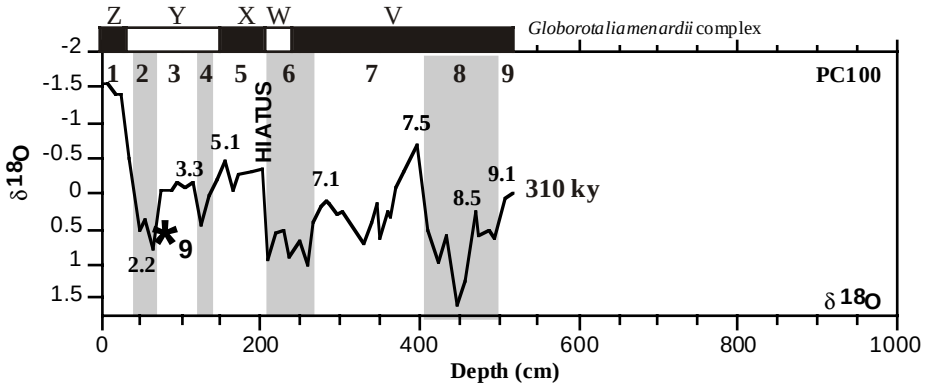

Fig. 4.9: Stratigraphy for core PC100 based on oxygen isotope analysis. Oldest sediments can be attributed to isotope stage 9 (=310 ky). The AMS ^{14}C age (*9) confirms the interpretation of stage 3 as derived from oxygen isotope stratigraphy. Major oxygen isotope events are indicated. The *Globorotalia menardii* complex zonation is displayed on top of the graph. The assumed hiatus from ca. 99-135 ky is also indicated. Shaded intervals indicate glacial isotope stages (stage numbers are displayed in the upper part of the shaded area).

4.2.3 Linear Sedimentation Rates (LSR)

Based on the stratigraphic framework shown in chapter 4.2.2 linear sedimentation for the late Quaternary marine isotope stages of each sediment core were calculated on a turbidite-free basis (Table 4.4). These sedimentation are the basis for the calculation of the mass accumulation rates shown in chapter 6.

The spatial evolution of the sedimentation rates for distinct interglacial and glacials isotope stages within the last approximately ~250 ky (MIS 1-7) along the offbank transect off the northwestern bank margin displays clear trends (Fig. 4.10). It is obvious that interglacial periods show a very similar spatial pattern of decreasing sedimentation rates with greater offbank distance. Highest sedimentation rates within MIS 1, 5 and 7 are found within the proximal sites. In contrast the spatial evolution of LSR during glacial MIS 2, 4, and 6 show

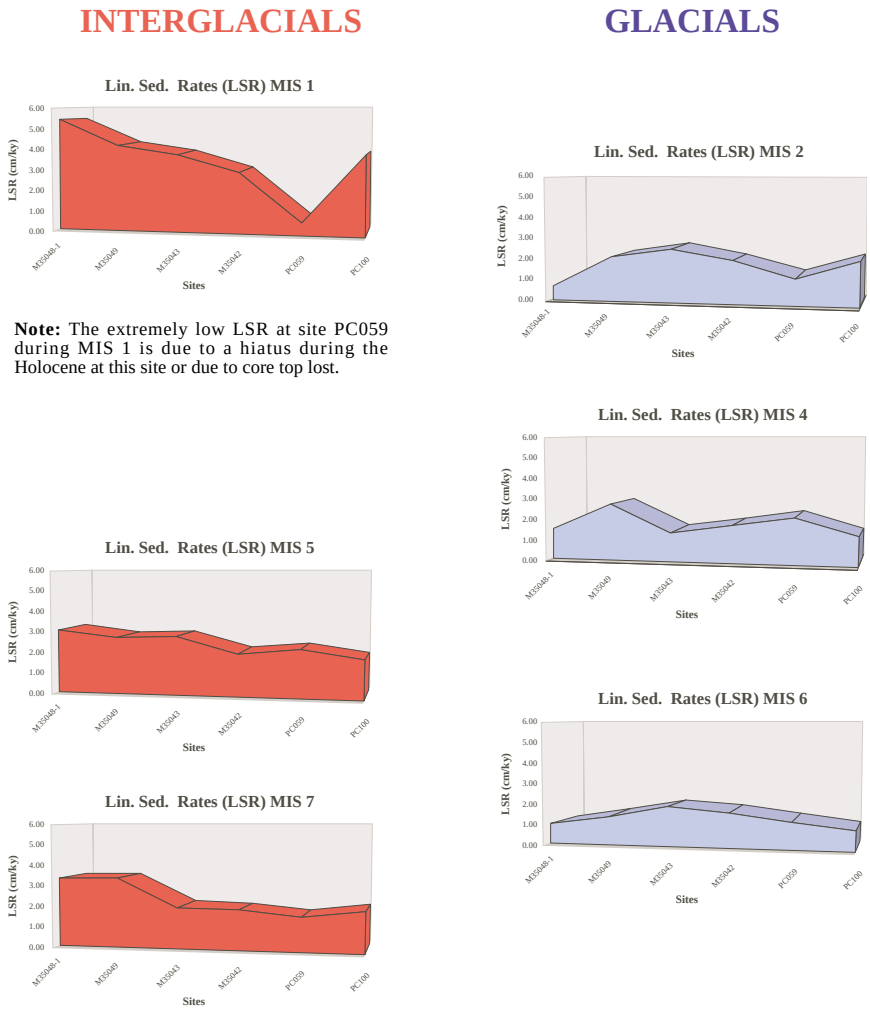

Note: The extremely low LSR at site PC059 during MIS 1 is due to a hiatus during the Holocene at this site or due to core top lost.

Fig. 4.10: Evolution of linear sedimentation rates (LSR) along the northwestern bank margin offbank transect. The spatial evolution of LSR´s for single interglacial and glacial marine isotope stages (MIS) is shown. The LSR´s are corrected for turbiditic input. Note the similarity of decreasing sedimentation rates with increasing offbank distance during interglacials. In contrast, the glacials display a inhomogeneous spatial distribution of the LSR´s. Maximum sedimentation rates occur during glacial MIS 2 and 6 at sites M35043, and during MIS 4 at site M35049.

maximum linear sedimentation rates for depositional sites at greater offbank distance, such as at site M35043 during MIS 1 and 6 and at site M35049 during MIS 4. The implications that can be drawn from this spatial evolution of LSR´s along the downcurrent margin of Pedro Bank will be discussed in chapter 4.3

Sediment Core	MIS 1	MIS 2	MIS 3	MIS 4	MIS 2-4	MIS 5	MIS 6	MIS 7	MIS 8	MIS 9
M35032	-	-	-	-	-	-	-	-	-	-
M35034	3.83	2.17	(1.7)	-	-	-	-	-	-	-
M35042	2.92	2.08	1.71	1.83	1.81	2.05	1.71	2.02	-	-
M35043	3.75	2.58	0.94	1.42	1.37	2.86	1.47	2.86	-	-
M35048	5.42	0.67	0.77	1.5	0.9	3.09	0.97	2.34	1.25	-
M35049	4.17	2.17	1.69	2.75	2.0	2.74	1.4	3.4	-	-
M35052	2.92	1.75	3.5	1.75	2.79	2.42	1.74	2.05	1.64	1.8
PC059	(0.58)	1.29	1.17	2.25	1.42	2.32	1.33	1.66	1.55	-
PC100	3.83	2.17	1.29	1.42	1.49	1.9	1.0	2.0	1.33	2.0

Table 4.4: Average linear sedimentation rates (in cm/ky) for marine isotope stages (MIS) derived from the stratigraphy shown in this chapter.

4.3 Discussion

1. Oxygen isotope analysis

As the locations of sediment cores recovered for this study were also choosen in order to obtain a large number of turbidites the stratigraphic interpretations were sometimes somewhat problematic.

The isotope values obtained from oxygen isotope analysis on *G. sacculifer* in general show expected glacial-interglacial amplitudinal changes. This was also shown for various other periplatform settings along the Nicaragua Rise (Glaser & Droxler, 1993; Schwartz, 1996; Duncan, 1997; Cunningham, 1999). The Holocene-Last Glacial $\delta^{18}O$-amplitude varies between 2 and 2.5‰ for most cores. Cores M35049 and M35052, however, showed amplitudes of 2.8‰ and 3‰ respectively. Within two up- and downcurrent sediment cores, Glaser (1991) found amplitudes from 2.2 to 2.3‰. Schwartz´s (1996) analyses of cores from the Pedro Channel, obtained Holocene-to-glacial amplitudes of 1.7 to 2.1‰. The most western cores analysed on the Nicaragua Rise within the Serranilla Basin showed the lowest amplitudes of 1.6-1.9‰ (Duncan, 1997). As the oxygen isotopes measured on planktic organisms depends on various factors such as temperature and evaporation/precipitation, this westward decrease in the Holocene-to-glacial oxygen isotope amplitude may be related to the influence of the surface water composition on the isotopes (in sense of temperature and/or evaporation/precipitation).

Three other cores, M35049 & M35052 (this study) and PC089 (Glaser & Droxler, 1993) show extraordinarily high oxygen isotope interglacial/glacial amplitudes (2.8-3‰). As these cores are taken from different water depths (500-1500 mbsl) with varying proximity to the platform (8 to 25 km), and different relative position to the platform (up- and downcurrent), there is no uniform explanation for this raised amplitude. It probably resulted from varying local factors such as local upwelling or diagenesis that modified the isotope signature within these three cores. The low amplitudes found in the oxygen isotopes during the transition from MIS 9 to glacial MIS 8 at about 300 ky (cores M35052 and PC100) can be explained by changes in the orbitally controlled variations in insolation that drive the Plio- to Pleistocene glaciations (Imbrie et al., 1984). During marine isotope stages prior to stage 11 (Matuyama chron from 0.735-2.47 Ma) an obliquity-dominated cyclity (41 ky cycles) prevailed on the Northern hemisphere (Ruddiman et al., 1986), which resulted in more severe changes between glacial and interglacial periods. From as early as 0.735 Ma (MIS 19), but more apparently after 0.45 Ma (MIS 11), a more eccentricity-dominated cyclicity (100 ky cycles) is evident (Ruddiman & Raymo, 1988; Kroon et al., 2000). This obliquity rythmicity resulted in lower amplitudes between glacial and interglacial isotope stages and less dramatic changes within these stages (Schwartz, 1996).

2. U/Th isotopic analysis

The TIMS U/Th dating method provided five reliable dates out of 14 analyses. A number of causes can be given for the age deviations found in the 9 samples which provided unreliable absolute ages (pers. comm. G. Henderson):

1. The aragonite content after preparation was too low,
2. The content of detrital material and/or the content of scavenged Th from seawater within the samples was too high. This can be observed in the $^{232}Th/^{230}Th$ (atom ratio) in Tables 4.2/4.3. The high content of detrital U and scavenged Th seems to be the major problem when using TIMS-U/Th-dating on marine bulk sediments. In general the $^{230}Th/^{234}U$-ratio does not start at 0.0. There is an initial ^{230}Th content in the sediments, some from detrital material and some scavenged from seawater. If the measured $^{232}Th/^{230}Th$-ratio is high, then the corrections for initial ^{230}Th are large and the uncertainty on the final calculated age is also large.

The $^{232}Th/^{230}Th$-ratio values should be < 1000 (see Slowey et al., 1996), but values up to 6500, as measured within the five samples that provided good absolute ages, also seem to fall within an acceptable range. The remaining 10 samples show values from approx. 16000 to 59000, which makes a reliable correction for those samples nearly impossible.

Gallup (1997) described the results of “high-precision Uranium-series analysis of fossil corals and Nicaragua Rise sediments”. She dealt with TIMS uranium-series analysis of bulk sediments taken north of Pedro Bank (Walton Basin). In that study two cores were used from 500 and 1000 mbsl (cores PC035 and PC089). The main objective was to date the sediment with TIMS ^{230}Th-methods, or as a second alternative, to use the sediments measured $\delta^{234}U$ value as a chronometer, assuming that the past marine $\delta^{234}U$ values have not varied significantly from the modern value (Gallup, 1997). Unfortunately geochemical inconsistencies between and within

the cores occurred, which made it impossible to determine the absolute chronostratigraphy for these cores (Gallup, 1997). Inconsistencies on those two cores were (Gallup, 1997): (1) ^{232}Th concentrations are a function of either water-column depth or chemistry, (2) excess ^{230}Th in core PC-37 comes from the overlying water column and causes the difference between oxygen-isotope and ^{230}Th ages, and (3) down-core PC-89 sediments have likely gained secondary uranium early in their history.
Gallup (1997) propopsed that absolute ages, calculated using the ^{234}U/^{238}U-dating technique, result in useful dates as the "primary uranium from the last interglacial sediments from the Nicaragua Rise constrain the marine δ^{234}U value to have been within 6‰ of the modern value for most of the last 200 ky, which in turn confirms the conclusions of simple models based on the residence time of uranium in the ocean (Edwards, 1988; Hamelin et al., 1991; Richter & Turekian, 1993)". In contrast to this observation Gallup (1997) also stated that the absolute dating using ^{230}Th/^{234}U-ratios inhibits too many error sources, which does not provide reliable absolute ages.

3. Absolute age of a turbidite layer
One fine tail-end of a turbidite (M35042, 470 cm), consisting of >99% calcium carbonate and >84% aragonite, was dated through TIMS U/Th dating. This sample contained a high ^{238}U concentration of 5.889 ppm and its ^{232}Th/^{230}Th atom ratio of 6480±56 was reasonably low. The resulting ^{230}Th/^{238}U-age of 303±18 ky (^{234}U/^{238}U-age of 278±21 ky) suggests that this turbidite layer contains sediments of late interglacial stage 9 or early stage 8, which were redeposited during isotope stage 7. This might be an indication of the erosive forces of gravity flows, which may disturb the sedimentary record further upslope. This type of event might have caused the hiatus present in PC100. Similar events have also been showed by Emmermann (2000) from the periplatform environment of the Sanganeb Atoll (Sudanese Red Sea).

4. Linear sedimentation rates
The observed pattern of decreasing sedimentation rates with increasing offbank distance during interglacials obviously reflects the decreasing input of neritic (preferentially fine aragonitic) material during highstand in sea level ("highstand shedding"). In contrast the glacials display an inhomogeneous spatial distribution of the sedimentation rates. This pattern might indicate shifting depocenters during glacial periods, as lower or lowest sedimentation rates can be observed at most proximal sites. The low sedimentation rates at proximal sites can be explained by current winnowing of fine sediment at times of enhanced bottom current activity near to the margin of Pedro Bank during lowered glacial sea levels (e.g. Glaser & Droxler, 1993; Schwartz, 1996; chapter 6 and 7). The higher sedimentation rates at the more distal, basinal sites might be the result of redistribution of these current winnowed sediments further upslope. This would result in thicker packages of "drift deposits" in the distal areas during lowstands in sea level, and might also be an explanation for the relatively high amounts of fine aragonite observed during glacial stages in the periplatform sediments (Chapters 6 and 7). A similar process has been proposed recently by Anselmetti et al. (2000) for periplatform sediments along the leeward margins of the GBB, which are shed into the Straits of Florida. In this area drift deposits can be identified in the seismic, whereas in this study the assumption of drift deposits is solely based on the spatial variability of sedimentation rates in a 92 km-long depth transect along the downcurrent margin of Pedro Bank i.e., the area of main neritic offbank export (Glaser & Droxler, 1993; Chapters 6 and 7).

4.4 Conclusions

Due to possible diagenetic overprints, which might be caused by turbidite layers (formation of hard- or firmgrounds within coarser-grained turbidite layers as assumed for core M35048) or other up to now unknown processes, three out of the nine cores analysed could not be dated using the oxygen isotopes of the planktic foraminifera species *Globigerinoides sacculifer*. Instead the content of aragonite in the fine fraction or the content of calcium carbonate in the fine fraction was used to establish a reliable stratigraphy. In addition, the biostratigraphy of the *Globorotalia menardii* complex (sensu Ericson & Wollin, 1956; used by Glaser, 1991; Schwartz, 1996; Duncan, 1997) was found to be a useful tool in defining certain interglacial events or glacial/interglacial boundaries.

AMS ^{14}C-dating confirmed the presence of stage 3 sediments in 8 sediment cores. The obtained ages vary from 27.020 ± 220 yr BP (core PC100) to 48.350 ± 2890 yr BP. (core M35034) and are in good accordance with those dates calculated from the correlation of the stratigraphic proxies ($\delta^{18}O$ and aragonite) to the SPECMAP standard isotope curve. One sample proposed to be of Holocene age (M35048, 50 cm) was dated and gave an age of 7160±60 yr BP.

U/Th age dating only gave a reliable age estimate for 5 out of 14 samples as the detrital content and thus the $^{232}Th/^{230}Th$ were generally too high to produce reliable absolute ages.

The dating of a fine end-tail turbidite deposited during interglacial stage 7 suggests that sediments of interglacial stage 9 or early glacial stage 8 have been redeposited. This might indicate the erosive forces of gravity flows, which may disturb the sedimentary record further upslope and also downslope as shown by the hiatus present in PC100.

From the spatial evolution of linear sedimentation rates along an offbank transect on the downcurrent margin of Pedro Bank, evidences could be found for the possible existence of drift deposits during glacial periods at more basinal sites. These indications imply that huge amounts of fine neritic material might have been redeposited further downslope. This mechanism would also explain the high glacial percentages of fine neritic aragonite within the periplatform sediments.

CHAPTER 5

SEAFLOOR TOPOGRAPHY ALONG PEDRO BANK MARGIN-TO-BASIN TRANSECTS

5.1 Introduction

Parasound data and 3.5 kHz seismic recordings from the northwestern and southwestern periplatform environment of Pedro Bank were used for this study. Both records show a variety of topographic features along the tectonically active northwestern edge of Pedro Bank. The analysis of these features is important to understand the sediment distribution processes at the toe-of-slope to basin transition.
For the Bahamian slopes, Mullins et al. (1979) and Schlager & Chermak (1979) showed that 3.5 kHz echograms can be used to map sediment types and to interpret sedimentary processes. Cunningham (1998) used analogous and digital bathymetric and echosound data to gain information on the Neogene evolution of the Pedro Channel carbonate system. The 3.5 kHz echograms, Multi-channel seismics (MCS) and Hydrosweep data, in combination with data obtained from piston cores, box cores and dredge hauls, provided an excellent insight into the bathymetric distribution in most of Pedro Channel. In addition, he provided a sediment facies distribution map of Pedro Channel based on 3.5 kHz sounding (Fig. 5.3) The bathymetric research done by Cunningham (1998) resulted also in a new bathymetric map. Cunningham (1998) stated that "aside from the regions covered by Hydrosweep (and this area is limited with respect to the size of Pedro Channel with a maximum depth of 1500-2000 mbsl), the final bathymetric map (Fig. 5.1) does a poor job of reflecting the complexity of the seafloor in Pedro Channel, but it provides a good quality generalised bathymetric map".

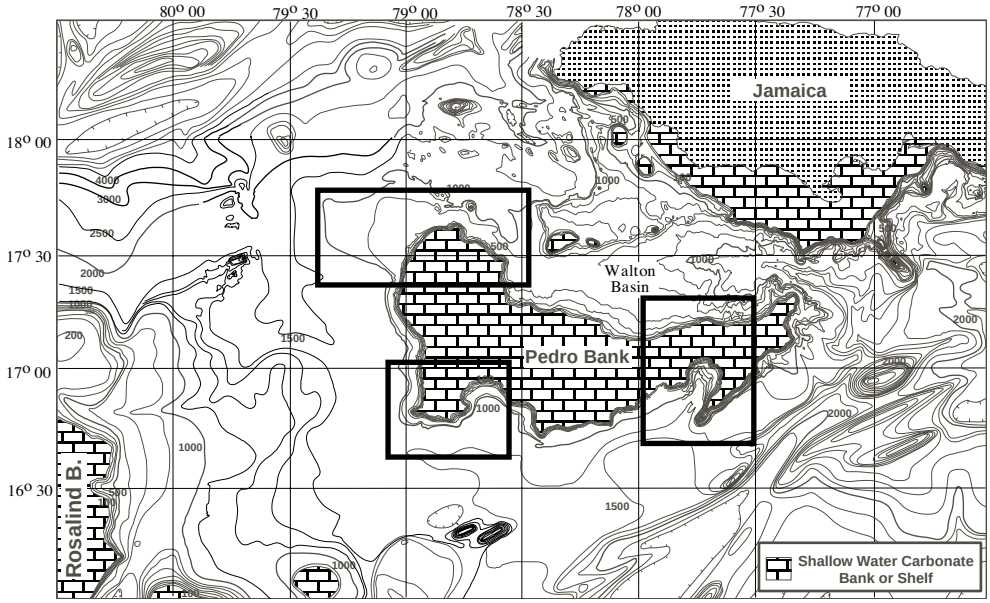

Fig. 5.1: Bathymetric map of the surrounding of Pedro Bank (modified after Cunningham, 1998). Rectangles mark the areas, where 3.5 kHz and Parasound surveys were conducted for this study.

The main area of interest in this study (the northwestern offbank transect) is not covered by the work of Cunningham (1998). Parasound survey and new 3.5 kHz seismics of Rice University (courtesy of A. Droxler) from the northwestern and southeastern periplatform environment, could be used to obtain more information on the complex bathymetric zonation along several slope-to-basin transects along the northeastern part of Pedro Channel. The use of Hydrosweep data was rejected because of shallow-water depths near to the bank margins and the low quality of the recorded data because of too much backscattering.

Both seismic tools might help in understanding depositional processes along the bank margins of Pedro Bank, which are situated in a tectonically active plate boundary setting. Therefore, here the results of various platform-to-basin transects are shown prior to the results of the main mineralogical and grain-size studies, as the seafloor morphology in the vicinity of Pedro Bank seems to be a major controlling factor for offbank transport and thus for deposition of neritic material shed offbank during highstands in sea level.

5.2 Material and Methods

Both applied methods are described in chapter 2.2.9. In addition, profiles of the uppermost bank margin (platform top - steep wall to upper slope) will also be shown. These were recorded during submersible dives with the research submersible JAGO by Prof. Dullo in 1996. Parts of the data have already been published by Dullo (1997). Additional work and interpretation are based on personal communication with Prof. Dullo.
Within the presented study several 3.5 kHz seismic lines taken during the research cruise CH0288, onboard *R/V Cape Hatteras*, will be used to study a couple of bank-to-basin transects with respect to slope and basin morphology (see Fig. 5.2). In total 5 perpendicular and 3 margin parallel transects from northwestern Pedro Bank will be shown. In addition, one 3.5 kHz transect from the southeastern bight near the Pedro Cays (Line PB48) and an ± perpendicular offbank transect from the northern bank margin into Walton Basin (Line PB49) will be presented.
During research cruise 35/1 of *R/V Meteor* Parasound surveys were carried out. The data could be used to display another two perpendicular offbank transects along the northwestern margin of Pedro Bank (PS Line A+B; Fig. 5.2), as well as two ± perpendicular offbank transects from the toe-of-slope to basin within the southwestern bight (PS Line C+D; Fig. 5.2). Start positions, endpoints and directions of the 3.5 kHz seismic lines and Parasound profiles are listed in Appendix 9.

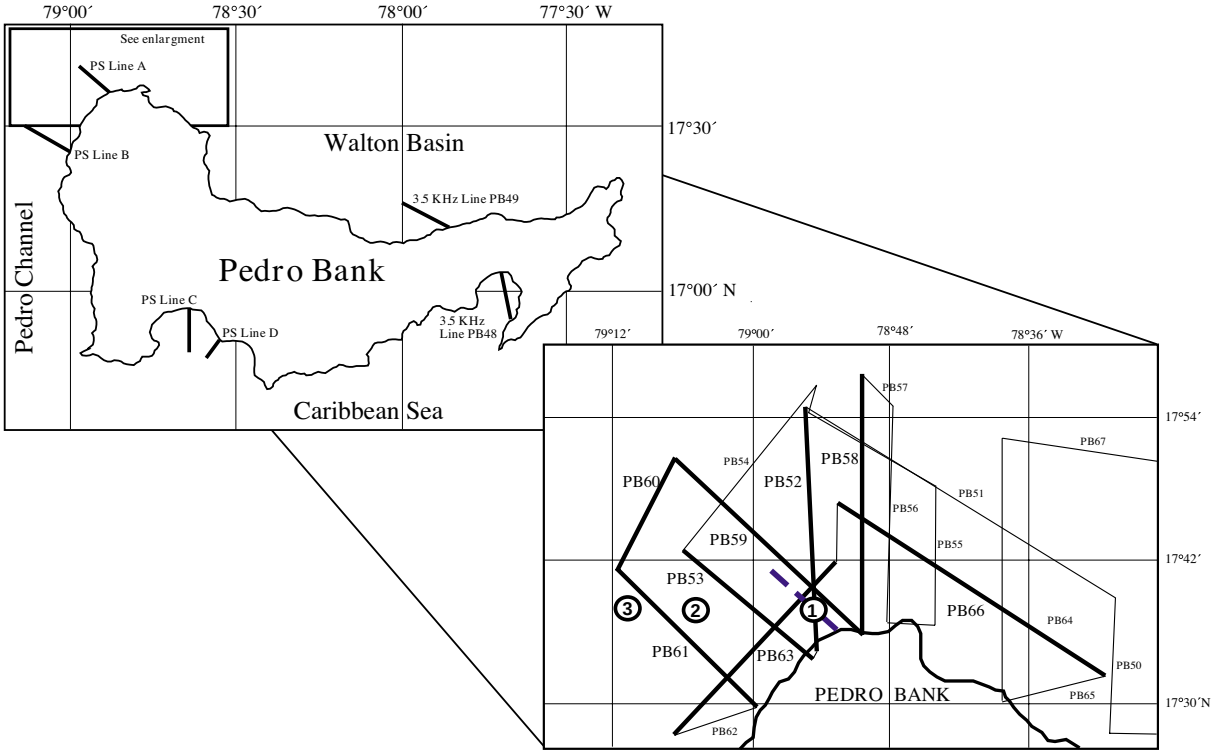

Fig. 5.2: Position of Parasound profiles (=PS Lines) and 3.5 kHz seismic lines of Rice University (see enlarged map of the northwestern bank margin).
Bold Lines and annotations mark seismic lines used within this study. The dashed line within the enlarged map show PS Line A. Encircled numbers mark the position of three sediment cores used within this study (1=M35048; 2=M35049 and 3=M35043).

5.3 Research history

5.3.1 Previous seismic survey on the Northern Nicaragua Rise

The 3.5 kHz seismic facies of the periplatform environment off Pedro and Serranilla Bank was mapped and calibrated with data from piston and box cores as well as dredge hauls (Cunningham, 1998). Based on these 3.5 kHz echograms four different facies types were identified and mapped throughout Pedro Channel and interpretations were made on the sediment types that were associated with each of the observed seismic facies (Fig. 5.3, after Cunningham [1998]). The interpretation and nomenclature of the echograms types recognised in the 3.5 kHz seismics is also based on Mullins et al. (1979) and Schlager & Chermak (1979).

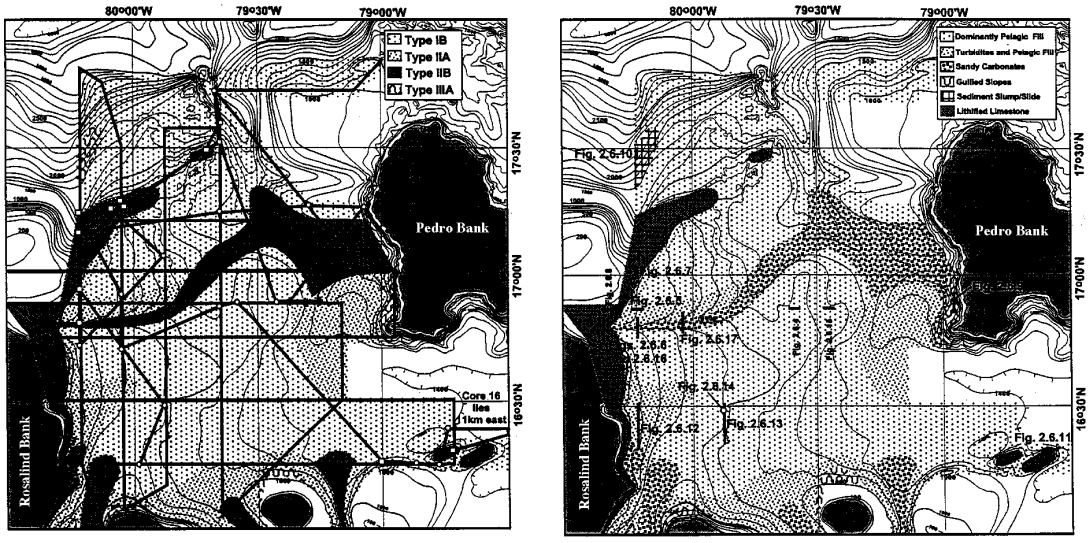

Fig. 5.3: Seismic facies map and lithologic interpretation of 3.5 kHz seismic as done by Cunningham (1998).

The predominant facies within Pedro Channel is periplatform fill (seismic facies IB; Cunningham, 1998), which primarly consists of muddy pelagic sediments, with a non-pelagic component containing rare, fine-grained, thin-bedded turbidites. Facies IIA displays a zone that combines turbidite and periplatform fill, and is located basinwards of the bank, at or near the toe-of-slope (Cunningham, 1998). Facies IIB reflects a "sandy bottom facies". Lithologically this facies consists of coarse-grained lag deposits containing current winnowed sands and 0-10% muddy pelagics (Mullins et al., 1979; Cunningham, 1998). Finally, facies IIIA is typical of sediment slumps and irregular topography such as submarine canyons and/or gullied slopes (Cunningham, 1998).

5.3.2 Foreslope morphology of the upper Pedro Bank margin

The upper slope morphology (i.e. the upper 400 mbsl) cannot be displayed due to the low resolution of Parasound and 3.5 kHz seismic data, when the slope angle becomes too steep. During dives with research submersible JAGO in 1996 along the northwestern margin of Pedro Bank three morphological transects of the foreslope could be obtained (see Fig. 5.4). The upper 360 m of the foreslope could, therefore be subdivided into three different sections:
(1) a deeper sediment slope, followed further upslope by (2) a cemented slope, which then merges into (3) the "steep wall" (Dullo, 1997). At about 60-70 mbsl the platform top starts as the morphology abruptly changes into a "terrace-like plateau". This morphology shows large similarity to other foreslope morphologies recorded throughout the Caribbean and the Atlantic Ocean (James & Ginsburg, 1979; Grammer & Ginsburg, 1992). Slope angles that were measured along these three diving profiles vary as follows:

lower sediment slope: 20-25° (deeper than 320 mbsl)
upper cemented slope: 40-50° (between 180/190 mbsl and 320 mbsl)
cliff or steep wall: 75-90° (between 180/190 mbsl and 60/70 mbsl).

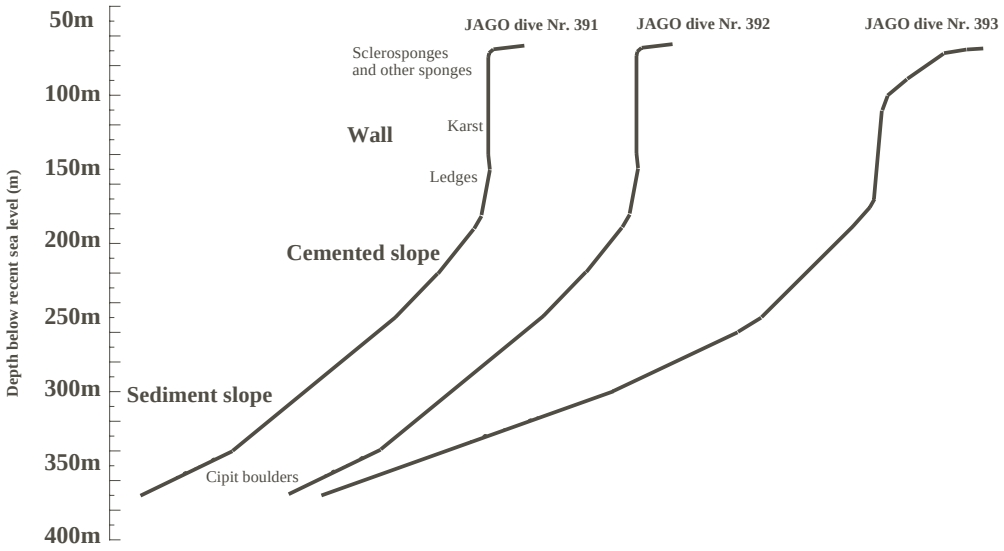

Fig. 5.4: Platform slope morphology of the upper 400 mbsl as derived from submersible dives along the northwestern margin of Pedro Bank (Dullo, 1997).

5.4 Results

5.4.1 3.5 kHz seismic echograms along northwestern margin

(A) Perpendicular transects

Five 3.5 kHz seismic lines from CH0288 were used; Lines PB52, 53, 58, 59 and 61 (see Fig. 5.5, A-E). Line 61 starts in about 600 mbsl at the lower, upper slope. All others start at the platform top in about 50 m water depth. The length of the transects ranges from 25 to 37 km offbank distance and cover a water depth range from 50 mbsl to about 1230 mbsl. Slope angles calculated from the 3.5 kHz echogram might be slightly lower to those calculated from the Parasound data. The latter are more accurate as they were registered digitally every two minutes.

Line PB 61 (Fig.5.5 A)

Along this profile the upper slope starts at a water depth of ~835 mbsl with an average slope angle of 3°. The upper slope shows small gullies that might act as sedimentary traps for coarse material.

The toe-of-slope region, at 1030 mbsl, exhibits a slightly irregular topography, with elevations of up to 50-60 m along a horizontal range of about 2 km. This results in a slope angle of about 2.2°, and could act as a minor barrier for offbank transport of coarse material. This topography is not as irregular as in the other perpendicular profiles of Lines PB 52, 58 or 58, situated further to the north.

Line PB 53 (Fig. 5.5 C)

This offbank profile is one of the best examples to show the topographical complexity and variability of the northwestern bank margin off Pedro Bank. The slope is fairly gentle along a distance of approx. 25 km, which is very different to the other northwestern margin offbank transects. This type of a gentle slope is seen in transects along the southwestern margins (see 5.4.2) and the northern margin (from Pedro Bank into the adjacent Walton Basin: Line PB49).

Line PB 59 (Fig. 5.5 B)

The angle of the upper slope further northeast of Line PB61 increases to 5.6°. This offbank transect shows a rough topography within the first 15 km from the bank margin with several gullies and submarine elevations. Slope angles of these small-scale features vary between 3.9° and 6.6°. The most prominent features in the slope topography are major bank parallel gullies or canyons that could prevent coarse sediment transport further downslope.

Line PB 52 (Fig. 5.5 D)
This 37 km long, N-S profile along the most northern edge of Pedro Bank displays two smaller slopes parallel to the bank margin with an average slope angle of 2.1° and 2.2°, respectively. The more proximal gully probably acts as a barrier for (coarse) neritic sediment transport from the platform top to the basin.

Line PB58 (Fig. 5.5 E)
This N-S profile about 4 km east of Line PB52 shows a similar slope topography and slope angle (2.5°) to that seen in Line PB52. Along the two northernmost transects (Lines PB 52 and 58), sedimentary basins were observed, which are not present in other transects within the same area (Lines PB 59 and 61). This might suggest the variability of the periplatform topography along the northwestern margin of Pedro Bank. The "mini-sedimentary basins", like the basin at about 10-15 km offbank distance (930 mbsl), probably are the best recorders of ancient offbank transport and periplatform deposition history. Sediment core M35049 is located within one of these mini-sedimentary basins and shows one of the best sedimentary records in this study.
All five offbank profiles show that the upper slope angle increases from the SW to the NE. Slope angles that were recorded during this study start with an average upper slope angle of 2.4° to 3° in the more southern profiles and increases to a value of 12.1° along the more northwestern profiles. This observed change might control the way in which sediments can be exported further downslope (see discussion).

(B) Bank-margin parallel transects

Line PB63 (Fig. 5.6 A) and Line PB60 (Fig. 5.6 B)
The bank margin transects along the western side of Pedro Bank´s northwestern edge are formed by the proximal parallel transect PB 63 and distal parallel transect PB 60. Both display a gullied toe-of-slope. These gullies or canyons show typical irregular, overlapping hyperbolical echoes, similar to those described along the southwestern margin of Pedro Bank in the direction of Pedro Channel (Cunningham, 1998). Slope angles of the gullies vary between 3.1° and 4.6°, but within single structures, the slope angle might increase to more than 13° (see line PB60).

Line PB64 (Fig. 5.6 C)
Transect PB 64 along the eastern side of the northwestern edge also displays a gullied slope. However, the gullies are not as prominent as those evident along Lines 60 and 63. The topographic features on the seafloor are more widely spaced, whereas along Lines 60 and 63 the gullies are smaller in extension, resulting in a steeper slope morphology. As a result, slope angles are lower along Line PB64 and vary between 1.6° to 3.1°

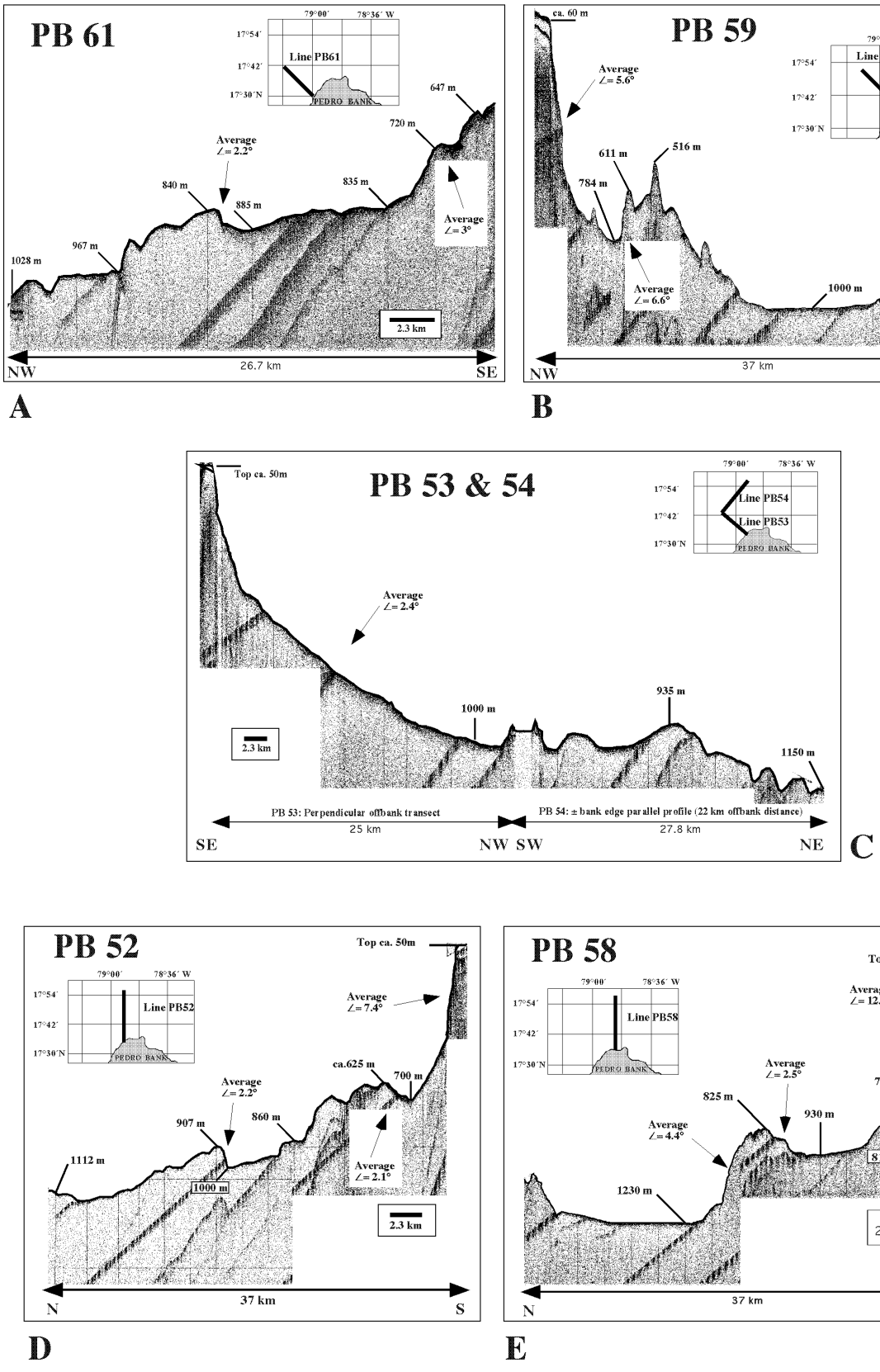

Fig. 5.5 A-E: 3.5 kHz profiles running perpendicular to the northwestern margin of Pedro Bank. Relative position of the individual profiles is indicated in the small map within each figure. Several depths below sea level and average slope angles of prominent features are shown.

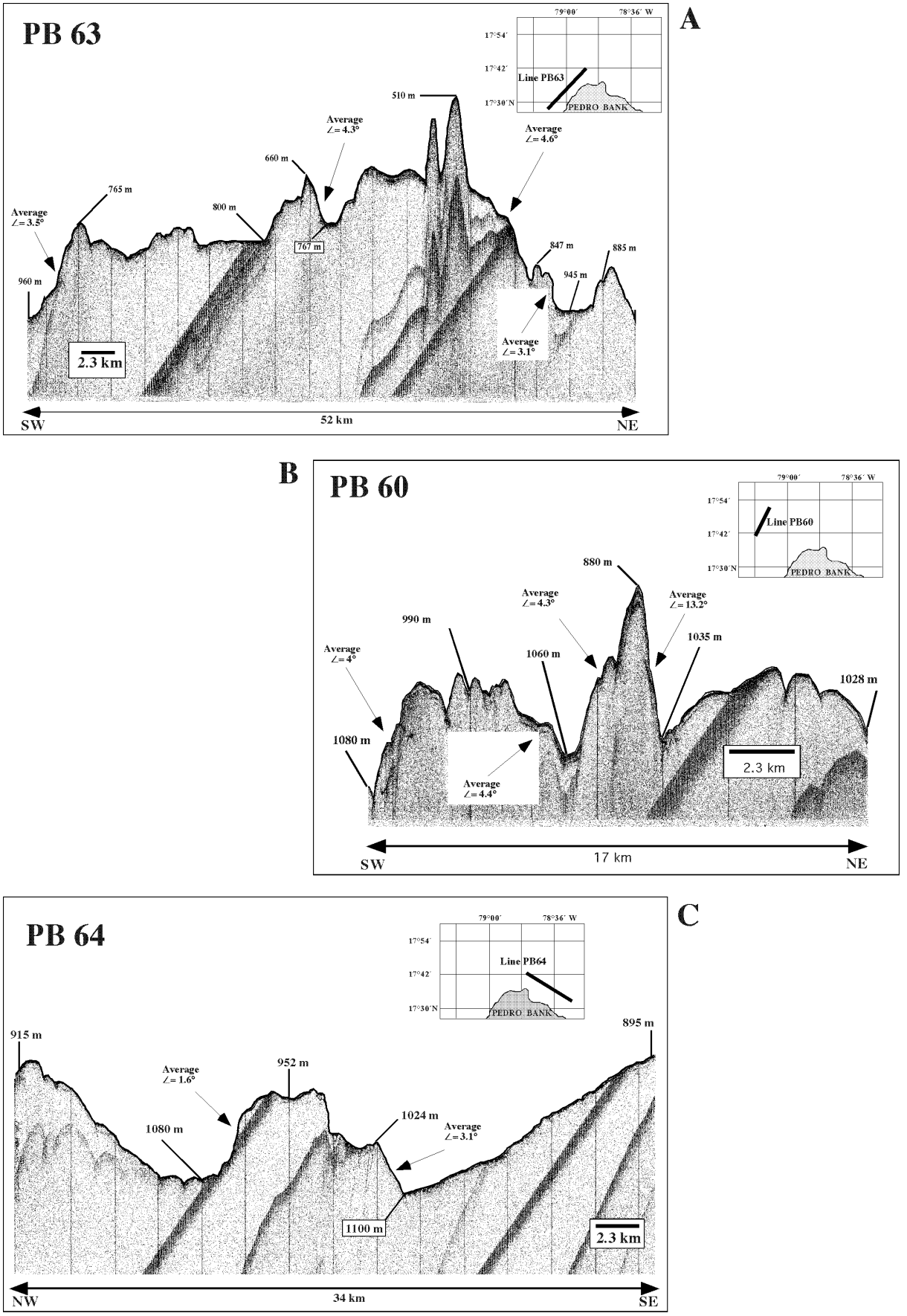

Fig. 5.6 A-C: 3.5 kHz profiles of the seafloor parallel to the northwestern margin of Pedro Bank. Relative position of the individual profiles is indicated in a small map within each figure. Several depths below sea level and average slope angles of prominent features are shown.

5.4.2 Parasound profiles along northwestern margin (PS Lines A & B)

PS Line A
This northernmost Parasound line (Fig. 5.7) is located between Lines PB59 and PB53, and shows similar topographic features to those observed along Line PB59. The vertical differences in seafloor elevation results in slope angles of 5.5° to 5.7°, which are fairly consistent with the 6.6° in slope angle calculated for Line PB59. Further downslope another prominent bank margin parallel gully is present with an average slope angle of 3.9°. The upper slope angle averages 10.7° and lies within the upper range of upper slope angles found along Pedro Bank´s northwestern margin and shows again the variability of the slope-to-basin topography.
The bank parallel profile, the right part of PS Line A (Fig. 5.7), shows the topography of the upper slope in a water depth of 450 to 300 mbsl. This part, which equates with the cemented slope described by Dullo (1997; see Fig. 5.4), is situated at the base of the "steep wall" and marks the actual bank margin. Slope angles for gullies striking perpendicular to the bank margin reach values between 18.5° and 23.5°. These steep walled gullies or canyons might act as transport channels for coarse material, possibly entrained in turbidite currents, which enter the distal basins if these channels continue far downslope.

PS Line B
PS Line B displays the southwesternmost slope-to-basin profile from the northwestern bank margin. In comparison to Line PB61, the closest 3.5 kHz profile, slope angles for the upper slope (7.9°), and for bank parallel gullies (5.7°), show higher values than observed further north (Fig. 5.6A). The prominent "horst structure" probably restricts the transport of neritic sediment further downslope (Fig. 5.6B). The reflectors from the Parasound recording show that at the base of this horst structure towards the bank margin, sediment slumps (discontinuous, hummocky/wavy reflectors) are present. This supports the interpretation for turbiditic downslope transport as well as sediment mass movements along this part of the toe-of-slope.

5.4.3 Profiles along the southwestern, southeastern and northern bank margin

Southwestern slope-to-basin profiles (PS Lines C and D; Fig. 5.7)
In comparison to the slope-to-basin transitions on the northwestern side of Pedro Bank, the two Parasound profiles taken along the southwestern margin show no prominent gullies or canyons, but rather display a very gentle slope. This is probably the reason why they do not have the capability to trap coarse neritic sediment shedded from the platform margins. The lithology and grain size composition of sediment cores taken from this area support this interpretation (e.g. M35032 of this study; PC016 from Glaser, 1993). Upper slope angles vary between 6.1° to 8°, which falls within the range seen along the southern transects of the northwestern bank margin.

Southeastern offbank profile (Line PB48; Fig. 5.8 A)
Seismic line PB 48 shows the slope variability along bank-to-basin transects around Pedro Bank. This cross-section across the southeastern bight near the Pedro Cays show upper slope/toe-of-slope angles between 11.5° to 17.8°, which is fairly high when compared to other bank-to-basin transects presented in this study. Therefore, sediment produced along this part of Pedro Bank might be transported far downslope because the seafloor features seems to extend far downslope (as it can be derived from the bathymetric map of Cunningham, 1998).

Northern slope-to-basin profile (Line PB49; Fig. 5.8 B)
This offbank profile displays a very gentle slope topography. Gullies or canyons running parallel to the bank margin are absent. Offbank sediment transport is probably not blocked along the northern margin of Pedro Bank.

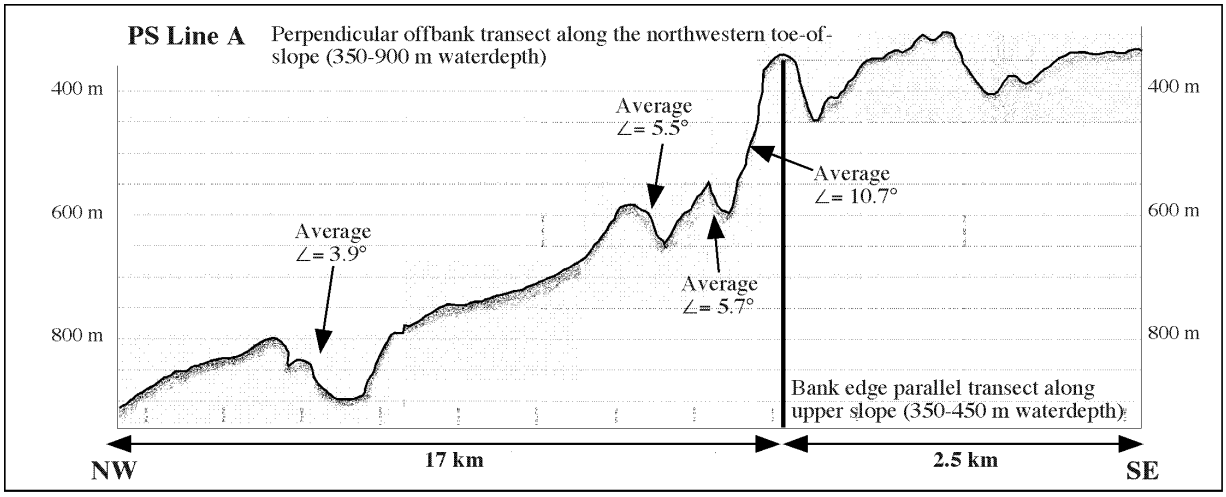

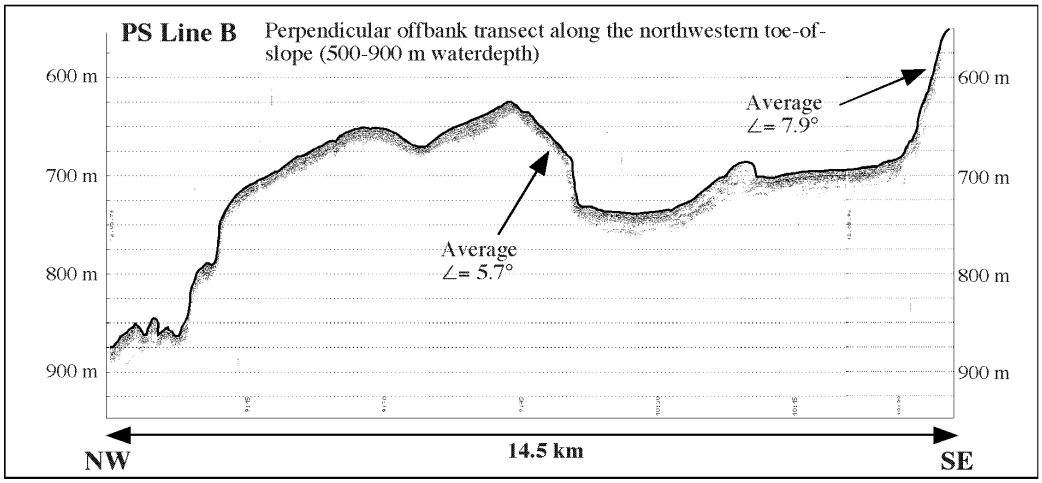

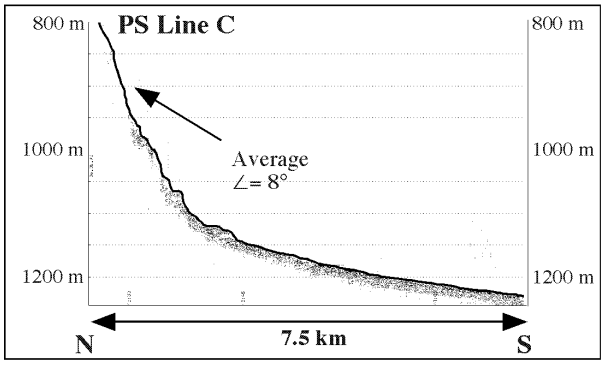

PS Line C

Perpendicular transect along the toe-of-slope in the southwestern bight of Pedro Bank (1250-800 m waterdepth); upper slope morphology could not be recorded with Parasound as slope angle is to steep (bank margin is less than 0.2 km away from the most northern position of this graph in the upper left)

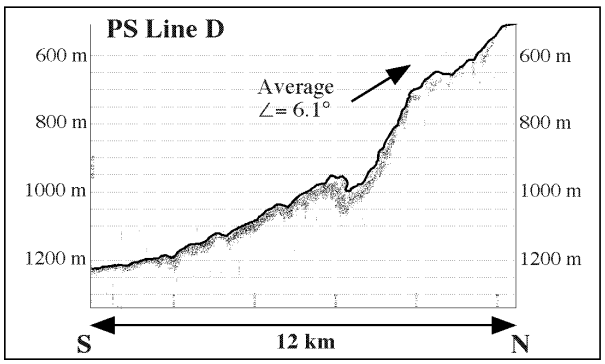

PS Line D

Perpendicular transect along the toe-of-slope in the southwestern bight of Pedro Bank (1250-500 m waterdepth); upper slope morphology could not be recorded with Parasound as slope angle is to steep (bank margin is less than 0.2 km away from the most northern position of this graph in the upper right)

Fig. 5.7 A-D: Parasound profiles from the northwestern (Lines A and B) and southwestern (Lines C and D) margin of Pedro Bank. Average slope angles are indicated.

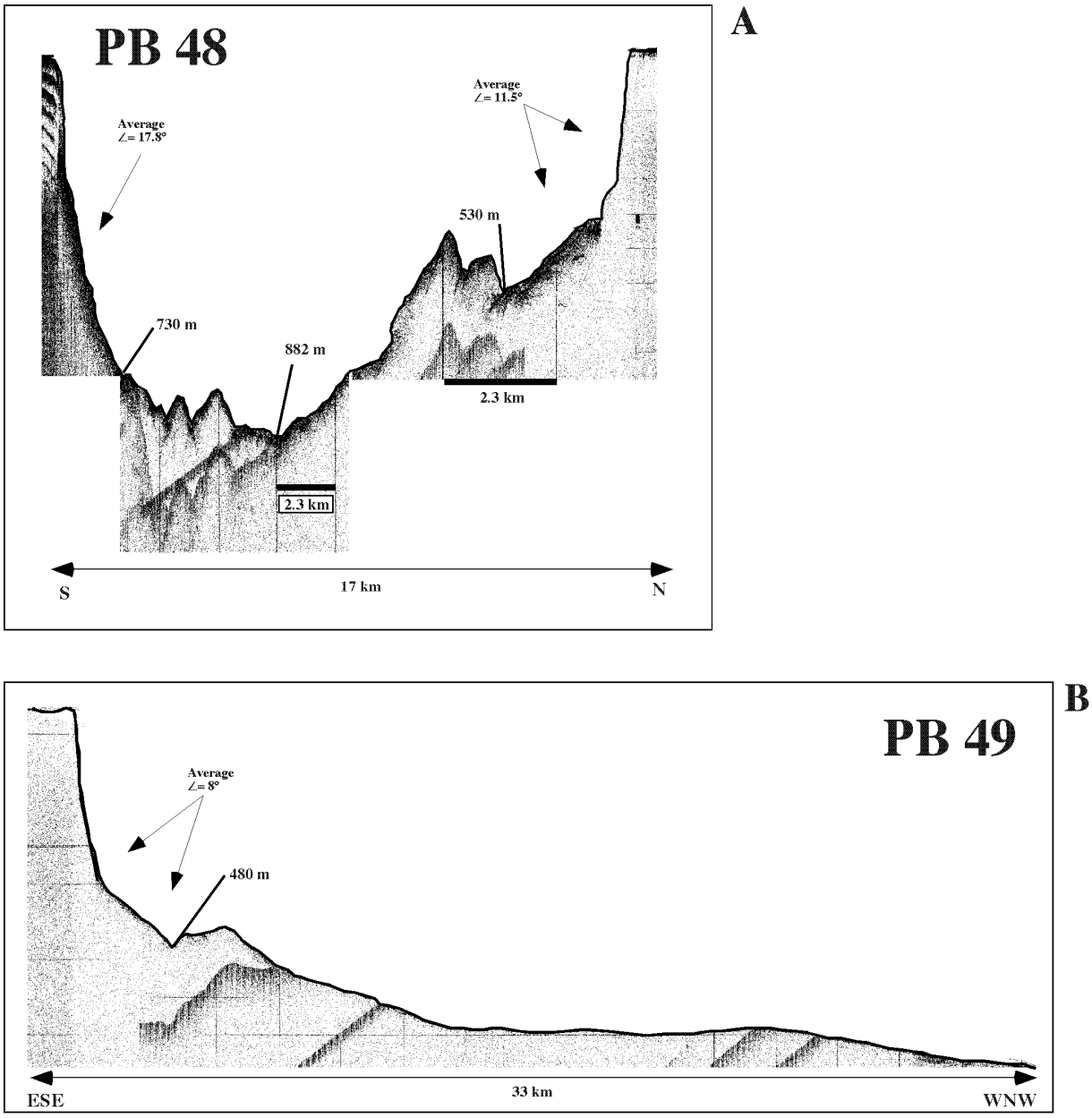

Fig. 5.8: 3.5 kHz echograms from the southeastern bank margin (A) and the northern margin (B) of Pedro Bank. Whereas the southeastern bank margin displays several prominent seafloor features with average slope angles of up to 17.8°, the northern bank-to-basin transect displays a very gentle slope without major gullies or canyons.

5.5 Discussion

Studies of Cunningham (1998) provided, for the first time, a more detailed insight into the complexity of the seafloor topography within the deep periplatform setting of Pedro Channel (the widest seaway of the Northern Nicaragua Rise). His research, which was primarly based on 3.5kHz seismic interpretation, cross-correlated with sediment cores, box cores and dredge hauls, clearly indicated that the banks east and west of Pedro Channel provide both a line and point source for sediment into the adjacent periplatform environment. This line source concept is illustrated by concentric facies belts along the bank margins, which is a typical pattern for most carbonate platforms that produce and shed sediment along much of their margins (e.g. shown for the GBB by Mullins & Neumann (1979), Schlager & Chermak (1979), Boardman & Neumann (1984) and Harwood & Towers (1988)). On the other hand, local zones of coarser-grained deposits at the base of canyons along the bank margins depict the point source concept.

These canyons might receive excess coarse-grained sediments, which then is funneled down through the canyons and eventually expelled as turbidites onto the channel floor (Cunningham, 1998).
The research done in this study, along various parts of the Pedro Bank margin, aimed to understand the complex topography along various margin/slope-to-basin transects and the impact of the seafloor topography on the depositional environment of periplatform sedimentation along the margins. The various offbank transects along the northwestern margin of Pedro Bank showed a "rough" topography with a few bank parallel canyons or gullies that probably act as major or minor barriers for coarse-grained sediment export. This might explain the absence of coarser-grained neritic material even within proximally located sites (see Chapters 6, 7 and 9). Cunningham (1998) stated that the margins of Pedro Bank, Serranilla Bank and Alice Shoal are "likely dissected by numerous gullies that trend perpendicular to the strike of the bank margins". These gullies source sediment from the bank tops and shed it into Pedro Channel. They also might act as pathways for coarse grained material (Cunningham, 1998) to be transported into distally located flat-floored basins. This again might explain the high number of turbidites at the more distal sites PC016, PC035, PC108 (Glaser, 1991) and site M35042 and their sometimes slightly raised content of coarse neritic biota (see also Chapters 8 and 10).
As shown, the slope topography along the southwestern bank margin (Figs. 5.7 and 5.8) is much more gentle and shows no major canyons or gullies. This more gentle topography is probably also responsible for the presence of neritic turbidites at the more distal site PC016 (Glaser, 1991; Cunningham, 1998) located about 30 km from the southern margin (see also Chapter 8).
In comparison to the major areas studied in this project (northwestern and southwestern margin) other profiles from the southeastern and northern margin display a different margin-to-basin transition. Within the southeastern bight (Fig. 5.8A) a rough slope topography could be observed, but as no sediment data from the inner bight are available an interpretation cannot be substantiated, but it shows again the complexity of the slopes around the margin of Pedro Bank. The margin along the northern side of Pedro Bank (towards Walton Basin) shows a very gentle slope morphology without major rises, gullies or canyons. The northern margin reflects the margin of Pedro Bank were main export into the basin occurs and sedimentary highstand wedges have been described (Glaser & Droxler, 1991). This high export of sediment and their deposition on the upper slope (e.g. high proximal sedimentation and thinning of sediment packages away from the bank) might have resulted in obscuring an older bathymetric relief on the upper slope. A similar process has been described for older, hidden subsurface structures in bathymetric lows of Pedro Channel (Cunningham, 1998).
In addition to factors such as (1) the input of pelagic carbonates and bank-derived fine aragonite and magnesium calcite, (2) the input of siliciclastic sediments, (3) the dispersal and removal of sediments by the Caribbean Current and (4) partial seafloor dissolution of metastable carbonates (Glaser & Droxler, 1993), it seems that the seafloor topography adds up as another major controlling factor for the deposition of neritic (and pelagic) sediments. All seafloor features described, such as the presence of gullies and canyons and the basinward thickening of sediment packages (in Pedro Channel) point to a negative sediment budget for the slopes of Pedro Channel (Cunningham, 1998). Schlager & Camber (1986) found that a negative sediment budget indicates an erosional depositional setting in carbonate systems. This means that there is little sediment deposition on the slope, as the sediment bypasses the slope via troughs, gullies and canyons, before being deposited on the basin floor. As it will be shown within chapters 6, 7 and 10 this trend, which was first described by Cunningham (1998), can be supported by a variety of studies within this project. This shows furthermore the importance of the seafloor topography for the composition and the dispersal of periplatform sediments along the margins and within the basins of carbonate platforms, not only along the Northern Nicaragua Rise.

5.6 Conclusions

Various platform-to-basin transects along the northwestern, southwestern, southeastern and northern margin of Pedro Bank revealed a more detailed insight into the complexity of the seafloor morphology along this carbonate platform situated in a tectonically active plate-boundary setting near the Cayman Through. The study shows that the seafloor topography

seems to be another major controlling factor for sediment distribution and composition along the periplatform environments on the Northern Nicaragua Rise.
Small bank parallel gullies and/or canyons are evident along the northwestern bank margin. The average slope angle within smaller-scaled seafloor features in proximity to the upper slope varies between 1.6° to 13°. These features probably act as morphological barriers for further offbank transport of coarser-grained, neritic material, which cannot be transported in suspension far away from their sources e.g. fine aragonite and/or magnesium calcite. This is probably the main reason, why sediments from the northwestern bank margin almost completely lack coarse-grained neritic biota from the top of Pedro Bank (see Chapter 8).

Bank parallel seismic transects along the northwestern edge of Pedro Bank showed that the margin is dissected by gullies that trend perpendicular to the strike of the margin. These gullies provide a point source for coarse grained sediments, which are transported to distal sites, such as the main Pedro Channel or other sedimentary basins. This might explain the presence of coarse-grained, neritic material at a few distal sites (as e.g. PC108 and PC035), although in general the distal sites are characterised by fine-tailend turbidites (see also Chapter 10).

The margin-to-basin transects along the southwestern margin, in contrast to the northwestern margin, show a very gentle slope morphology. Major gullies or canyons are missing. Therefore, coarse material can be transported over long distances to distal sites through turbidites (such as site PC016).

CHAPTER 6

PHYSICAL PROPERTIES AND ACCUMULATION RATES

6.1 Introduction

Linear sedimentation rates derived from the direct calculations of time vs. deposited sediment thickness gives a gross overview on the real amount of sediment that has been deposited during distinct time intervals. In order to gain more information on sedimentation processes, mass accumulation rates were introduced by van Andel et al. (1975) and Ehrmann & Thiede (1985). Mass accumulation rates show depositional changes on the base of a weight unit ($g/cm^2/ky$) and allow the comparison of sediment input of differently compacted sediments.
The calculation of sediment accumulation rates is strongly dependent on the reliability of the stratigraphy. In addition, an exact determination of the physical properties of the sediment is a must to gain useful data for mass accumulation rates of sediments. In this chapter, which presents mass accumulation rates for the periplatform setting around Pedro Bank, care has therefore been taken to address the above mentioned factors. Previous accumulation rate data (Glaser, 1991; Schwartz, 1996) from the Walton Basin and Pedro Channel were determined by using a calculated porosity profile of one sediment core. The depth/time values were then applied to all other cores. Bulk density as well as water content were not available for these analyses. In order to test the calculated proxy porosity and the derived mass accumulation rates for various sediment components, the water content, wet and dry bulk densities for nine sediment cores, from the up- and downcurrent periplatform environment, were determined. This chapter describes the temporal and spatial variability in mass accumulation rates of pelagic, neritic and non-carbonate sediment components, as well as changes in the fine (<63 µm) and coarse (>63 µm) sediment fraction.

6.2 Methods

The methods used to determine the data shown in this chapter are described in subchapter 2.3.6. The relative position of the sediment cores to Pedro Bank are shown in Fig. 2.1. Wet and dry bulk density (DBD and WBD) and the water content of the samples were calculated and multiplied with the grain size and mineralogy data. All data were plotted with respect to water depth as well as distance from the active bank margin in order to evaluate the factors that might influence the sedimentation of single sediment components in periplatform sediments around carbonate platforms on the Northern Nicaragua Rise.

6.3 Results

Average water content ranges between 28-37%, whereas average DBD vary between 1.05 - 1.3 g/cm^3. The overall range of DBD in all samples analysed range from 0.75 g/cm^3 (M35032) to 1.46 g/cm^3 (M35048). For detailed physical property data see Appendix 6.

6.3.1 Mass accumulation rates of bulk sediment (Fig. 6.2; 6.8A)

The mass accumulation rates (MAR) of the bulk sediment represent the general sedimentation trends around the up- and downcurrent margins of Pedro Bank. The general trend seen in the bulk accumulation rates is similar to the accumulation rate (AR) patterns of the fine fraction and the fine aragonite, which form the main constituents of the bulk sediment.
Interglacial bulk AR show an overall decreasing trend with increasing offbank distance and water depth. They vary from 2.5 $g/cm^2/ky$ to 7$g/cm^2/ky$ during marine oxygen isotope stages (MIS) 1, 5, 7 and 9. Core M35034 shows the highest interglacial bulk AR, 6.9 $g/cm^2/ky$ for MIS 1, even though this core location at the southwestern margin of Pedro Bank, should only be influenced to a minor extent by sediments shedded from the shallow bank top. This value agrees with accumulation rates observed in the most proximal core at the downcurrent margin

(M35048). The bulk AR of the two other upcurrent cores (M35032 and M35052) fit into the overall trend of AR found in downcurrent cores. Along the downcurrent offbank profile a higher interglacial stage-to-stage variability of bulk AR (3.5-7 g/cm^2/ky) can be seen within the first 20 km from the bank margin (=650-900 mbsl). With increasing offbank distance the AR of interglacial stages becomes more similar to each other, i.e. the stage-to-stage variability of AR´s decreases. Core M35042 (42km, 1023 mbsl) for example shows interglacial AR that only vary between 2.49-3.11 g/cm^2/ky (Δ=0.62 g/cm^2/ky). This is five times lower than those found in proximal core M35048 with 3.53-6.58 g/cm^2/ky (Δ=3.05 g/cm^2/ky).
Glacial bulk AR show no clear trends. The AR vary between 0.5-3g/cm^2/ky. Only stage 4 in M35049 (3.65g/cm^2/ky) and stage 2 in M35034 (4.62g/cm^2/ky) show high glacial bulk AR. When comparing glacial with interglacial bulk AR, the downcurrent cores M35048 and M35049 display the largest interglacial-glacial variability (Fig. 6.1), with 52% to 56% less accumulation during glacials (Fig. 6.8A). The more distal cores located further downslope show a more or less similar decrease with 12-24% less bulk accumulation during glacial periods (Fig. 6.8A).

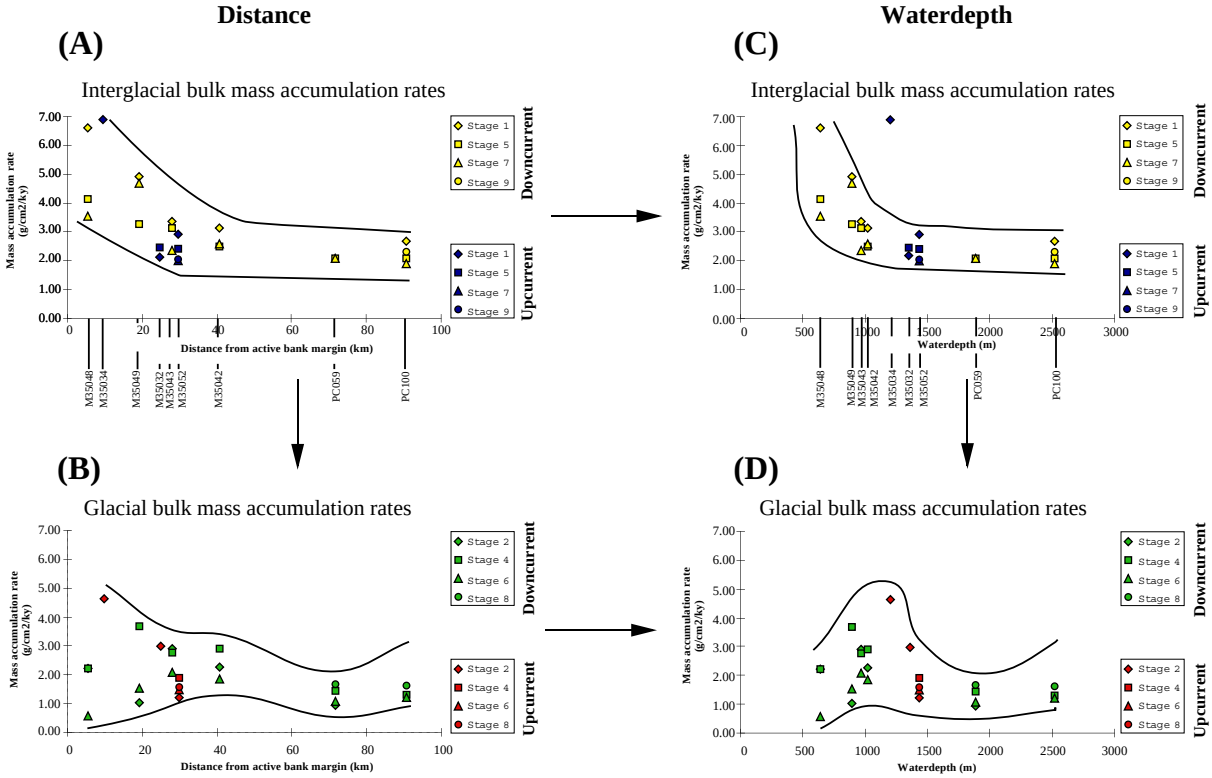

Fig. 6.1: Interglacial/glacial variability of bulk accumulation rates with increasing distance (A,B) and water depth (C, D). All graphs show the same y-axis. AR for various interglacial and glacial isotope stages are shown. Upcurrent cores are shown in red (interglacial) or blue (glacial), whereas downcurrent cores are highlighted in yellow (interglacial) or green (glacial) colour. Lines are self-defined to display the general evolution of AR with increasing offbank distance and waterdepth. The core locations are indicated in Fig. A for offbank distance and in Fig. C for waterdepth (not shown within the following figures 6.2 to 6.7). The lines show the general trends seen in all analysed cores.

The accumulation trends of single interglacial substages (stages 1, 5 and 7) show that all three interglacials contain differerent spatial accumulation patterns along the northwestern offbank transect. Stage 1 shows a continuously decreasing trend in bulk AR with increasing offbank distance to about 25 km (< 975 mbsl). Then, the AR values level off at ~3 g/cm^2/ky. Interglacial stage 5 shows not only an overall lower accumulation than during stage 1, but also a smaller variability with increasing offbank distance (2-4 g/cm^2/ky). In contrast to stage 1 and 5, interglacial MIS 7 displays no significant trend in the AR. A lower limit of about 2 g/cm^2/ky is reached far downslope at site PC059 (72 km offbank distance).

6.3.2 Mass accumulation rates of coarse and fine fraction

Fine Fraction (Fig. 6.2 and Fig. 6.8B)

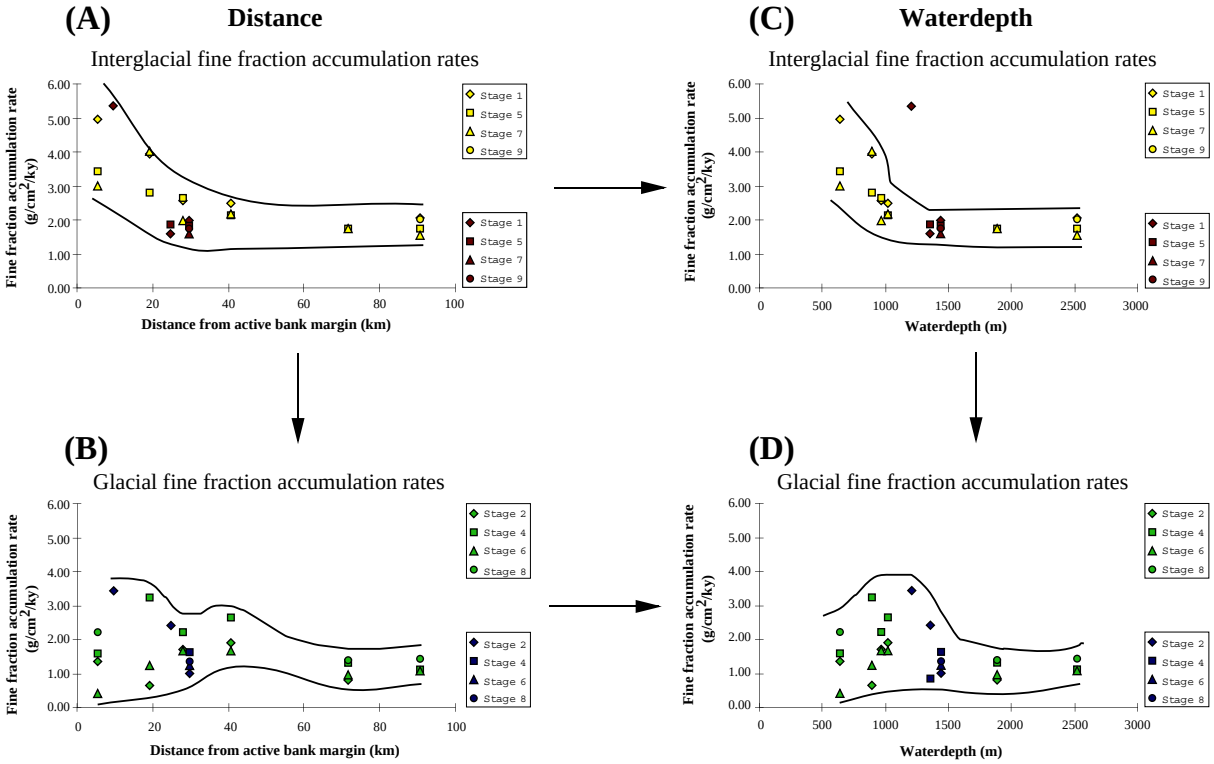

Fig. 6.2: Interglacial/glacial variability of the fine fraction AR with increasing distance (A,B) and water depth (C, D). All graphs show the same y-axis. AR for various interglacial and glacial isotope stages are shown. Upcurrent cores are shown in red (interglacial) or blue (glacial), whereas downcurrent cores are highlighted in yellow (interglacial) or green (glacial) colour. Lines are self-defined to display the general evolution of AR with increasing offbank distance and water depth.

The fine fraction generally displays the same trends described for the bulk sediment. This is due to a dominance by the fine fraction (76-86%) within the periplatform sediments.
The interglacial fine fraction AR decrease from 3.8 to 1.4 g/cm^2/ky with increasing offbank distance (Fig. 6.2). The Holocene (MIS 1) AR of proximal upcurrent core M35034 equals the AR observed in the most proximal downcurrent core M35048. Core M35032 and M35052 show slightly lower AR in comparison to similar downcurrent cores. This pattern of lowered AR along the upcurrent margin shows the main sediment export direction from Pedro Bank.
Glacial AR of the fine fraction show the same irregular pattern as observed for bulk AR. The largest variability in glacial-to-interglacial AR (Fig 6.8B) along the northwestern offbank transect can be seen within “proximal” cores M35048 and M35049. Both show a lowered AR by 64-52% during glacial periods. Within the remaining four cores M35043, M35042, PC059 and PC100 the AR are lowered by 9-22%.

Coarse Fraction (Fig. 6.3 and Fig. 6.8C)

During interglacial periods a strong relationship between AR and offbank distance can be seen, independent of up- or downcurrent position. Highest interglacial AR are evident during the Holocene, and a continuously decreasing trend with increasing offbank distance (1.7 - 0.7 g/cm^2/ky) is evident. During MIS 1 coarse fraction AR of the proximal upcurrent core M35034 is in excellent agreement with the values for proximal downcurrent core M35048.

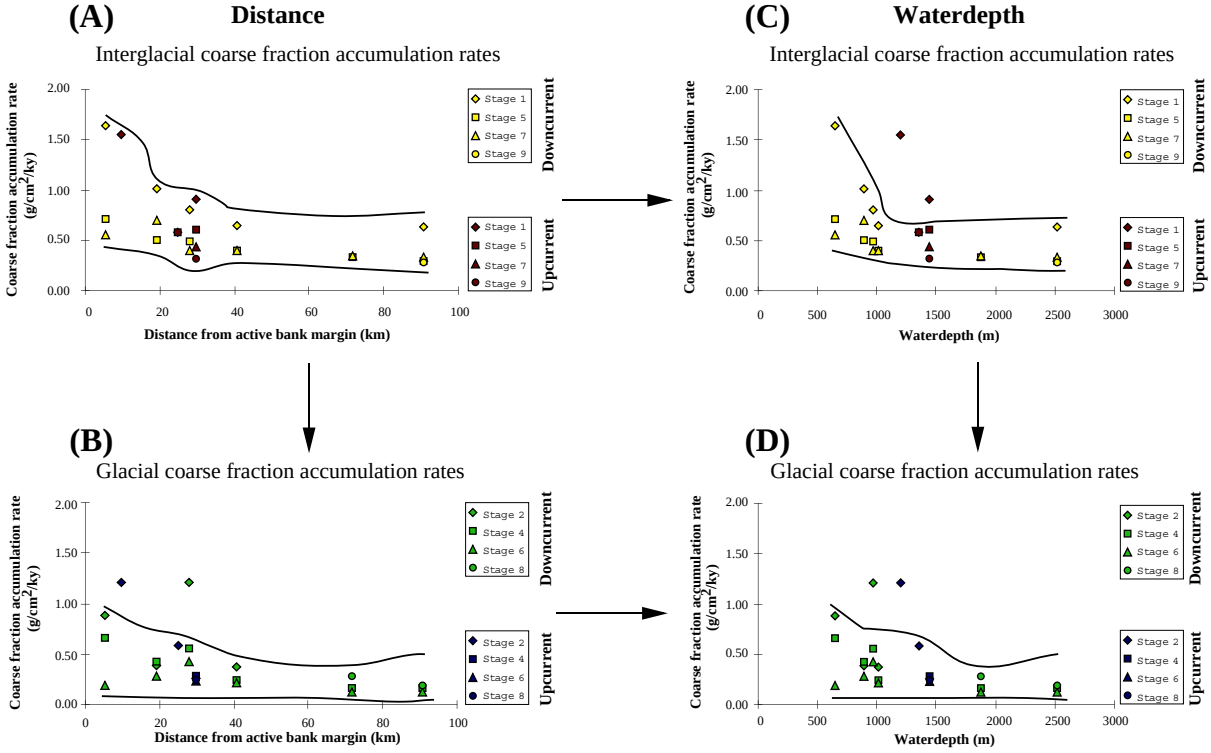

Fig. 6.3: Interglacial/glacial variability of coarse fraction AR with increasing distance (A,B) and water depth (C, D). All graphs show the same y-axis. AR for various interglacial and glacial isotope stages are shown. Upcurrent cores are shown in red (interglacial) or blue (glacial), whereas downcurrent cores are highlighted in yellow (interglacial) or green (glacial) colour. Lines are self-defined to display the general evolution of AR with increasing offbank distance and water depth.

Distal upcurrent cores M35032 and M35052 show similar values for equally distant cores from the downcurrent side. At about 40 km from the platform edge an interglacial lower limit value of approx. 0.6-0.7 g/cm^2/ky is reached, which probably shows the pelagic background accumulation of coarse sediment. The proximal core M35048 shows the highest interglacial-to-interglacial variability in the Holocene ranging from ~0.5 g/cm^2/ky to about 1.7 g/cm^2/ky. Cores located further away than ~20 km from the active margin show a clearly reduced variability of only 0.3-0.4 g/cm^2/ky between interglacial stages 1, 5, 7 and 9.
During glacial periods a similar trend of uniform AR can be observed from a distance of >40 km (deeper than 1500 mbsl). Glacial AR at an offbank distance <40 km and/or <1500 mbsl do not show a clear pattern. Downcurrent cores are characterised by varying accumulation rates within single interglacial stages. Upcurrent cores show, at least for the glacial stage 2, a decreasing trend. The observed decrease in the AR of the coarse fraction during interglacials with increased offbank distance can be also seen during glacials.
The by 27-50% lower AR during glacials (in comparison to the interglacial stages; Fig. 6.8) indicates that more coarse fraction (in total mass per time unit) was deposited during interglacials. However, based on their percentual proportions more coarse fraction is found in proximal and/or shallow sediment cores during glacials (see Chapter 7; Glaser, 1991). Therefore the spatial trends in the content of the coarse is more sensible for interpretations using the absolute percentages (Chapter 7).

6.3.3 Mass accumulation rates of neritic carbonates (Aragonite and HMC)

Fine Aragonite (Fig. 6.4 and Fig 6.8D)

The fine aragonite MAR mirror the export of neritic components from the top of shallow water carbonate systems. Fig. 6.4 shows that no clear correlation exists between up- and downcurrent interglacial AR of fine aragonite. An exception is formed by the Holocene AR at proximal

upcurrent site M35034, which perfectly fits into the offbank accumulation pattern of downcurrent sites.

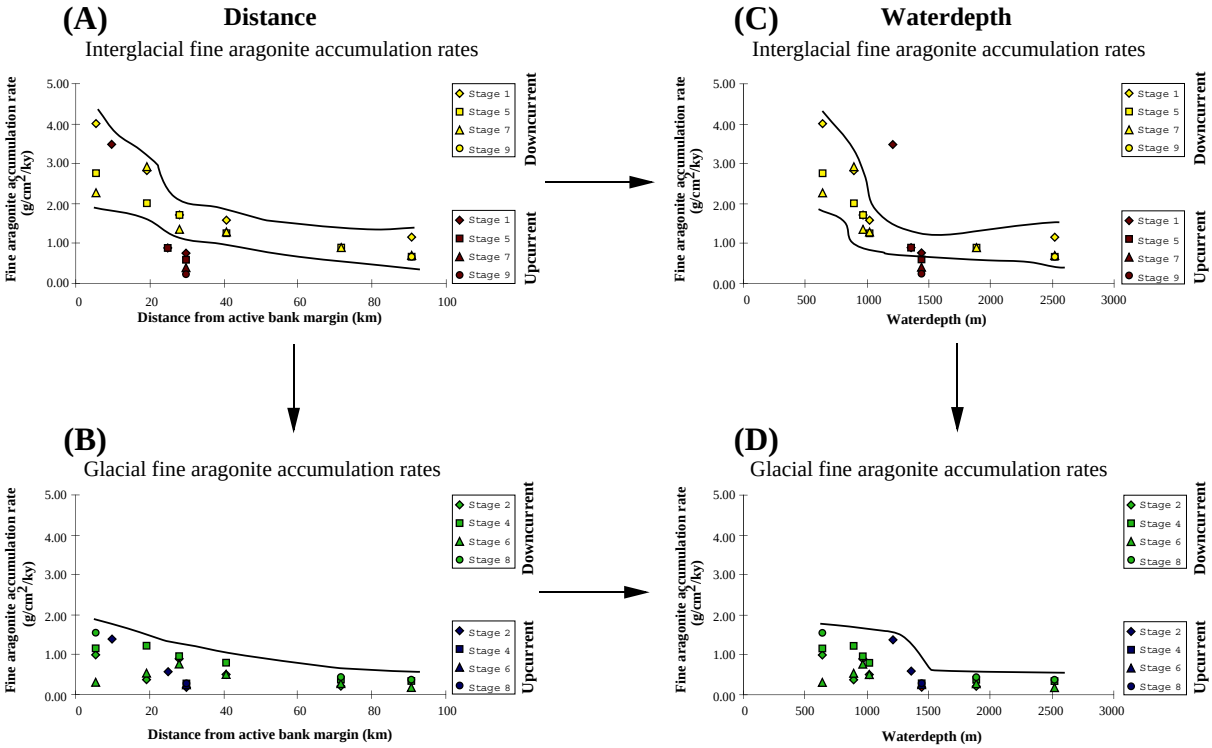

Fig. 6.4: Interglacial/glacial variability of fine aragonite AR with increasing distance (A,B) and water depth (C, D). All graphs show the same y-axis. AR for various interglacial and glacial isotope stages are shown. Upcurrent cores are shown in red (interglacial) or blue (glacial), whereas downcurrent cores are highlighted in yellow (interglacial) or green (glacial) colour. Lines are self-defined to display the general evolution of AR with increasing offbank distance and water depth.

Interglacials

On the downcurrent side the fine aragonite AR show a clear decrease with greater offbank distance for the different interglacial marine isotope stages. During stage 1 the largest AR variability can be observed (proximal: 4 g/cm^2/ky vs. distal: 1.1 g/cm^2/ky). Stage 5 already shows a much smaller accumulation rate variability along the offbank transect. Values for aragonite accumulation rates range from 2.75 - 0.67 g/cm^2/ky. Stage 7 exhibits accumulation rates between 0.7-2.25 g/cm^2/ky. All these interglacial stages show a generally decreasing trend with greater offbank distance. Upcurrent cores M35032 and M35052 show AR between 0.2-0.8 g/cm^2/ky, which are the lowest calculated mass accumulation rates.

Glacials

Highest accumulation rates of ~1.38-1.54 g/cm^2/ky are found in the most proximal cores M35048 and M35034. The overall pattern shows that the AR decrease with increasing distance from the platform margin. For water depths exceeding approx. 1000 mbsl, the AR for fine aragonite drop significantly. Most of the isotope stages show irregular variations along the offbank transect. This might indicate that local factors play a role in generating the observed signal of glacial aragonite accumulation rates. The AR along the northwestern offbank transect (Fig. 6.8) indicate the relative variability of interglacial-to-glacial changes in the direction of the main export from Pedro Bank. Only the most proximal core M35048 shows a decrease in accumulation of up to 67% during glacials. The remaining five cores, which cover an offbank transect of more than 70 km and an increase in water depths from 900 - 2500 mbsl, show a decrease in glacial fine aragonite accumulation rates of 46-58% in comparison to their respective interglacial accumulation rates (Fig. 6.8D).

Fine HMC (Fig. 6.5 and Fig. 6.8E)

This neritic sediment component plays a very important role in the periplatform sediments around carbonate platforms, while HMC is mainly affected by dissolution at intermediate water depths (Glaser, 1991; Glaser & Droxler, 1993; Haddad & Droxler, 1996; Schwartz, 1996). Therefore, HMC accumulation rates should show these dissolution effects at least when looking at the HMC distribution with respect to water depths.

Interglacials

During the Holocene downcurrent cores show a decreasing trend in AR with increasing offbank distance, with 0.35-0.15 g/cm^2/ky. The water depth distribution pattern clearly shows a decrease down to a waterdepth of ~1000 mbsl, where the AR reaches a lower limit value of approx. 0.15 g/cm^2/ky. This depth dependency seems to be supported by AR for upcurrent cores M35032 and M35052 from intermediate waterdepths (1350-1450 mbsl). HMC AR for these cores are the same (0.15 g/cm^2/ky) during the Holocene. One exception is formed by the high Holocene AR in core M35034, which also lead to a high HMC AR of approx. 0.5 g/cm^2/ky.

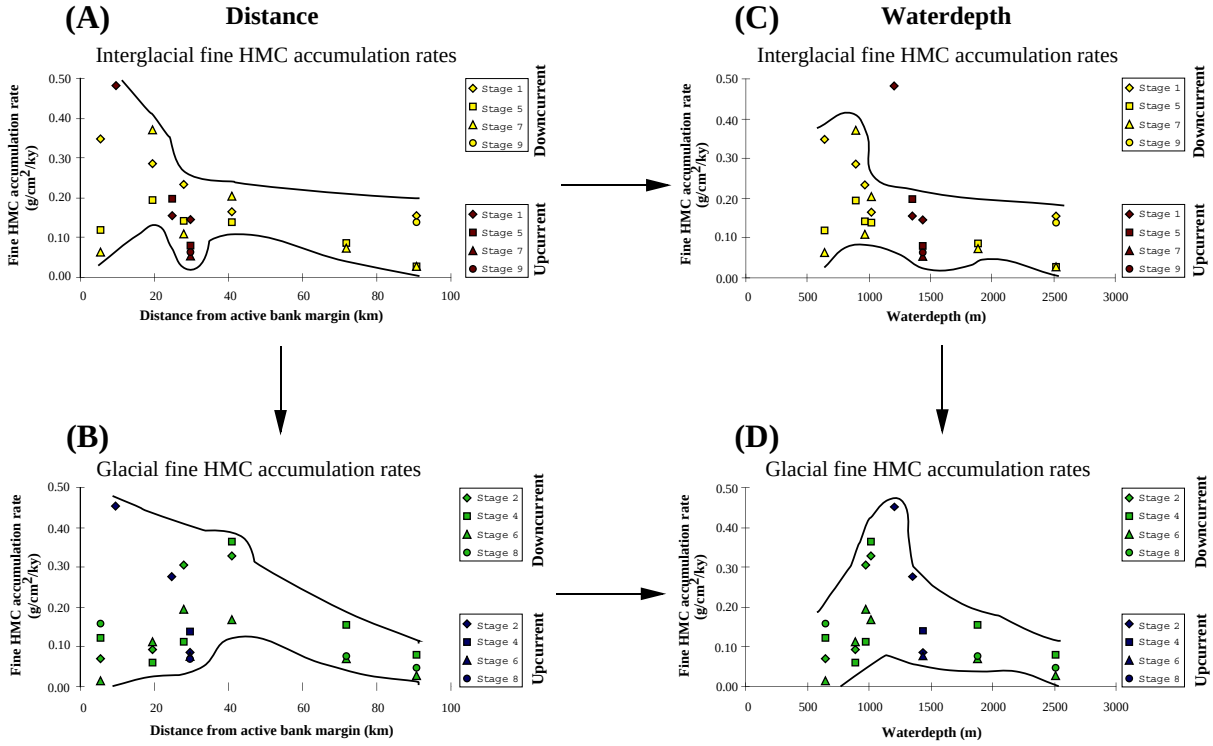

Fig. 6.5: Interglacial/glacial variability of fine HMC AR with increasing distance (A,B) and water depth (C, D). All graphs show the same y-axis. AR for various interglacial and glacial isotope stages are shown. Upcurrent cores are shown in red (interglacial) or blue (glacial) colours, downcurrent cores in yellow (interglacial) or green (glacial). Lines are self-defined to display the general evolution of AR with increasing offbank distance and water depth.

Interglacial stages 5 and 7, however, show a very different distributional pattern. During these interglacial stages proximal cores show low AR, whereas maximal AR are found at an offbank distance of ~20 km (or 900-1000 mbsl). At distances larger than 20-25 km (or >1000 mbsl) accumulation rates show a constant decrease.

Glacials

Minimum AR during single isotope stages can be found between 600-900 mbsl (0-0.18 g/cm^2/ky). From 900-1350 mbsl accumulation rates increase to values between 0.1-0.45 g/cm^2/ky. Below 1350 mbsl fine HMC accumulation rates decrease to minimum values between 0.03-0.16 g/cm^2/ky (Fig. 6.5). The glacial-to-interglacial differences (Fig. 6.8E, lower graph)

in the AR of fine HMC indicate a spatial separation between cores deposited in 500-900 mbsl and those in waterdepths exceeding 900 mbsl. Cores M35048 and M35049 display reduced glacial AR of 48-69% in comparison to the interglacial average, whereas cores exceeding 900 mbsl show raised AR of 24-69% during glacial periods.

6.3.4 Mass accumulation rates of fine pelagic carbonates (Fig. 6.6)

The accumulation rates of fine low-Mg calcite (LMC) in periplatform sediments should be controlled by the productivity of pelagic biota (preferentially coccoliths), as they form the major fine LMC component within the cored sediment types.

Interglacials

Cores deposited in upcurrent position show a slight increase in AR of LMC with increasing water depth. The AR show a very homogeneous distribution between 0.2-0.6 g/cm^2/ky. Only stage 9 AR in core M35052 (upcurrent) and PC100 (downcurrent), show high AR of 0.9 g/cm^2/ky. Single interglacial stages show no clear trends with greater offbank distance.

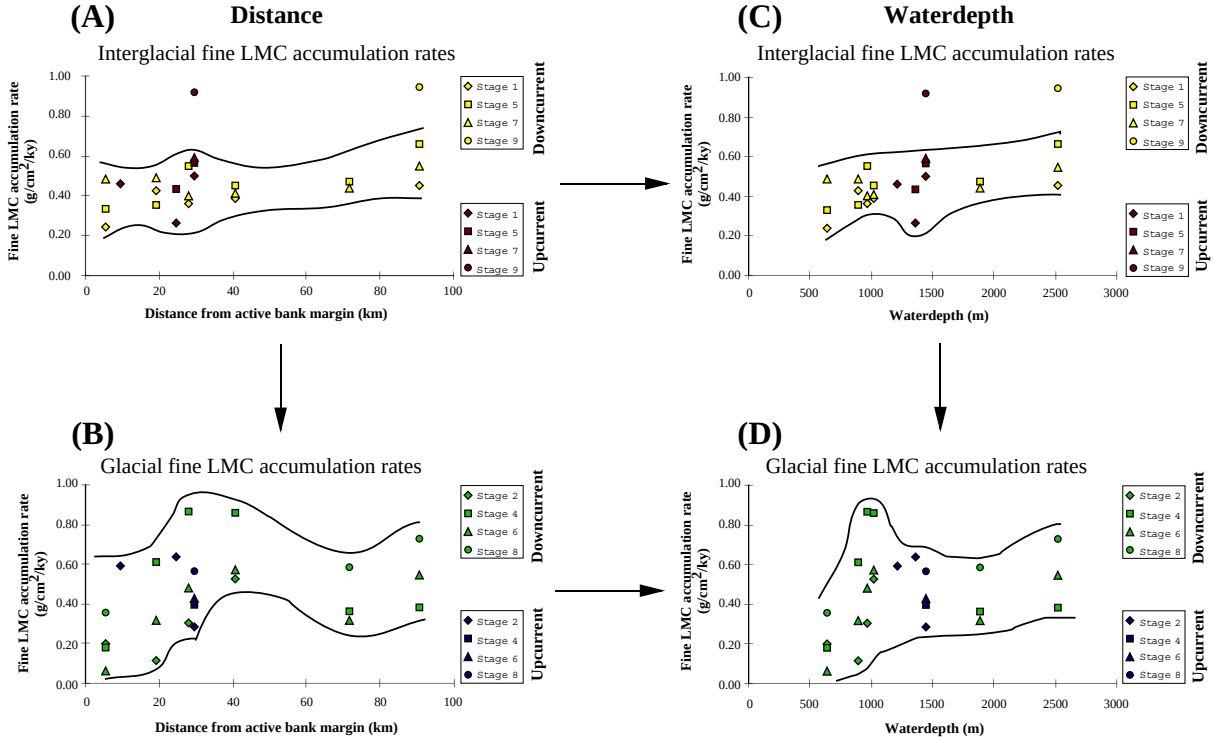

Fig. 6.6: Interglacial/glacial variability of fine LMC AR with increasing distance (A,B) and water depth (C, D). All graphs show the same y-axis. AR for various interglacial and glacial isotope stages are shown. Upcurrent cores are shown in red (interglacial) or blue (glacial), whereas downcurrent cores are highlighted in yellow (interglacial) or green (glacial) colour. Lines are self-defined to display the general evolution of AR with increasing offbank distance and water depth.

Glacials

During glacial periods AR of fine LMC show a much higher variability with values ranging from almost 0 to more than 0.8 g/ cm^2/ky. The proximal core M35048 shows lowest values between 0.06-0.35 g/cm^3/ky. AR generally increases slightly with increasing water depth. Up- and downcurrent values show the same distribution pattern with variable LMC AR from 0.3-0.65 g/cm^2/ky except for the increased AR observed during stage 4 in core M35043 and M35042 (>0.8 g/cm^2/ky).

6.3.5 Mass accumulation rates of fine non-carbonates (Fig. 6.7 and Fig 6.8F)

Interglacials

The downcurrent cores display a very uniform distribution of AR varying between 0.15-0.4 g/cm^2/ky. Upcurrent cores M35052 and M35034 show higher rates for non-carbonates, 0.5-0.95 g/cm^2/ky, whereas M35032, from the southwestern margin, shows similar values to those observed in the downcurrent cores. The general pattern that emerges, is that higher amounts of non-carbonates can be found in upcurrent locations.

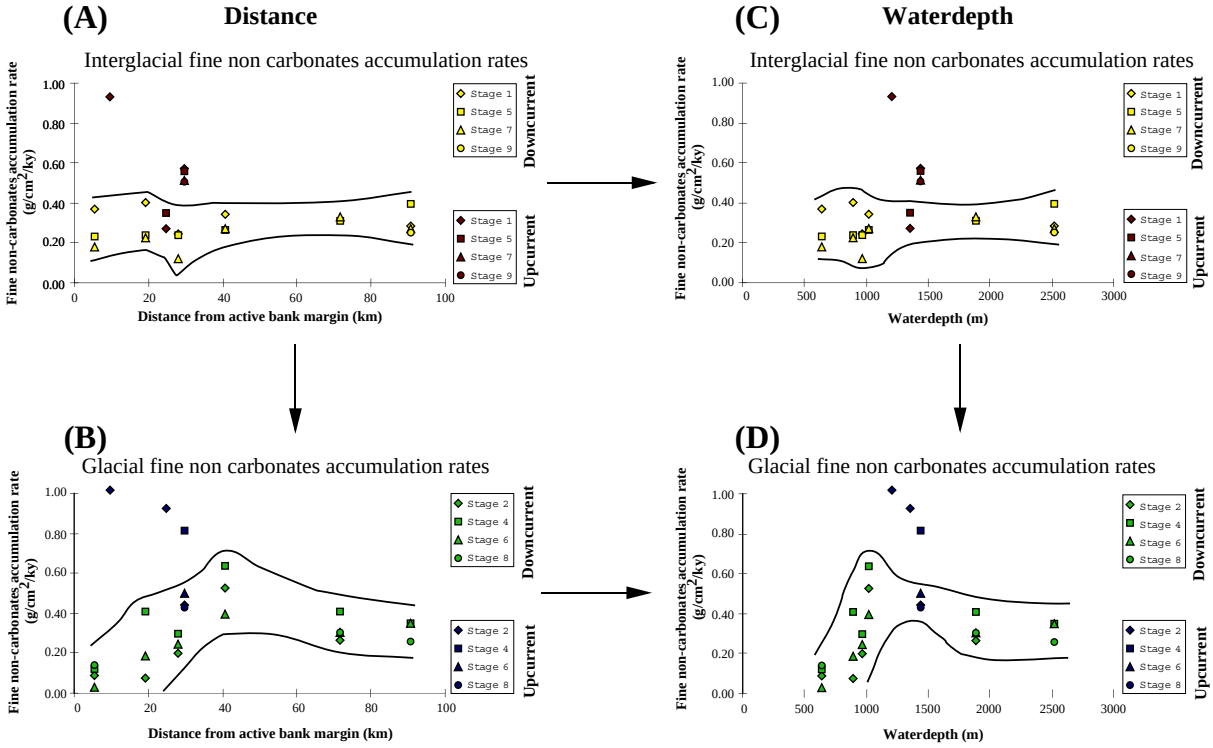

Fig. 6.7: Interglacial/glacial variability of fine non-carbonate AR with increasing distance (A,B) and water depth (C, D). All graphs show the same y-axis. AR for various interglacial and glacial isotope stages are shown. Upcurrent cores are shown in red (interglacial) or blue (glacial), whereas downcurrent cores are highlighted in yellow (interglacial) or green (glacial) colour. Lines are self-defined to display the general evolution of AR with increasing offbank distance and water depth.

Glacials

Lowest AR can be found in the most proximal core M35048 (0-0.15 g/cm^2/ky) within the downcurrent cores. Further downslope, up to a distance of ~40 km (= 900-1100 mbsl), glacial accumulation rates increase to 0.65 g/cm^2/ky. At distal sites PC059 and PC100 they decrease again to reach a near constant value of 0.3-0.4 g/cm^2/ky (cores PC059 and PC100). Upcurrent cores show glacial AR that are 2 to 5 times higher than rates found in equivalent downcurrent cores. Highest rates are found during the last glacial in cores M35034 and M35032 with rates up to 1 g/cm^2/ky. Accumulation rates for glacial stages 2, 6 and 8 in M35052 show nearly identical values, ranging from 0.43-0.49 g/cm^2/ky. The overall AR pattern along the downcurrent offbank transect (Fig. 6.8F, upper graph) shows that during interglacials all cores are supplied with about the same amount of fine non-carbonates (0.2-0.3 g/cm^2/ky), while during glacial times a clear increase is found with increasing offbank distance (0.09-0.52 g/cm^2/ky). The maximum value of 0.52 g/cm^2/ky within core M35042 is probably a result of its special location at the outer end of the very large submarine plateau off the northwestern bank margin. This change to higher AR at more distal sites can also be observed when comparing the glacial-to-interglacial differences (Fig. 6.8F, lower graph). Whereas the “proximal” cores M35048 and M35049 show a lowered glacial accumulation of non-carbonates by 65-22%, the remaining downslope cores show enhanced accumulation of 23-79% during glacial periods.

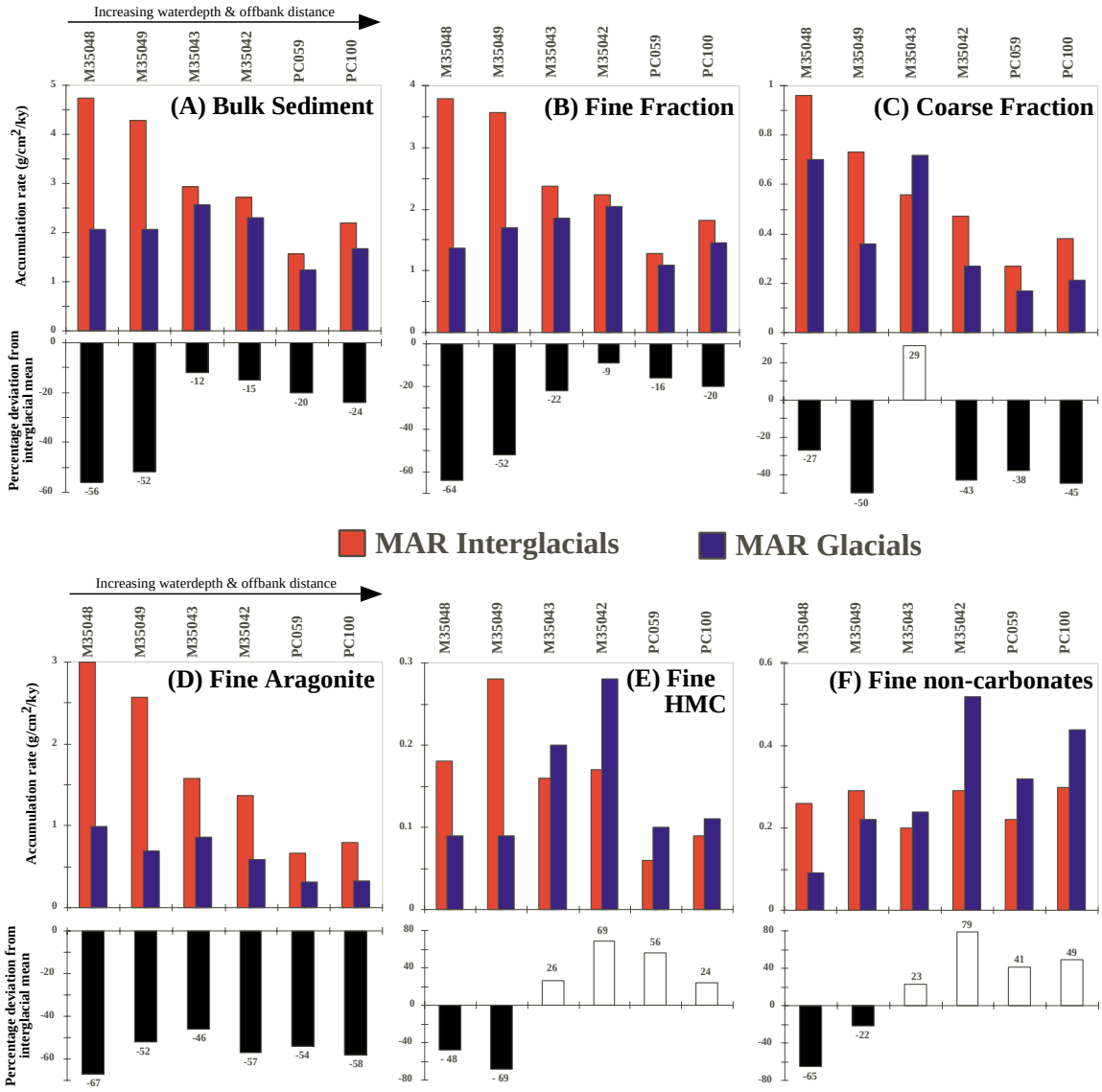

Fig. 6.8: Differences of averaged interglacial-to-glacial AR for the sediment cores along the northwestern transect. The upper graph shows the absolute AR during interglacials (red bar) and glacials (blue bar). The lower part of each graph shows if a negative (=less accumulation during glacials; black bar) or a positive deviation (=more accumulation during glacials; white bar) of the single sediment components is evident in comparison to the interglacial mean. (A= bulk sediment; B= fine fraction; C=coarse fraction; D=fine aragonite; E=fine HMC; F= fine non-carbonates). For discussion see chapter 6.4.

6.4 Discussion

In contrast to studies by Schwartz (1996) and Duncan (1997) the accumulation rates within this study were not calculated on a depth-to-depth basis. The latter method might show more single accumulation events, but is also highly dependent on the quality of the age model of each core and the quality of the choosen isotopic events. The accumulation rate data shown here were calculated analogous to Glaser (1991) for each single marine isotope stage, which can be determined more precisely.

6.4.1 Mass accumulation rates of sediment components

One major difference to studies on periplatform sediments on the Northern Nicaragua Rise by Glaser & Droxler (1993), Schwartz (1996) and Duncan (1997) became clear by means of the

accurate determination of dry bulk densities. Forementioned studies used mass accumulation rates that were determined using a dry bulk density model based on calculated average densities from other sediment cores from the deep surroundings of Pedro Bank. Schwartz (1996) described dry bulk densities of 0.9-1.1g/cm^3. This study shows that the range for dry bulk density varies between 0.76-1.46 g/cm^3 in sediment cores that cover a wide depositional range. Therefore, the mass accumulation rates used within the forementioned studies might differ from those presented in this study. Although differences exist in the physical properties the calculated accumulation rates of the bulk sediment and single sediment components of this study and previous studies from Pedro Channel, Walton Basin and Serranilla Basin, still agree fairly well (Glaser & Droxler, 1993; Schwartz, 1996; Duncan, 1997; see table 6.1). One major difference found is that sediment cores studied by Schwartz (1996) show a higher content of fine LMC- and fine non-carbonates. This might indicate the reduced influence of the input from the carbonate platforms at these core locations within Pedro Channel.

Sediment components	Range of accum. rates after Schwartz (1996) or Glaser & Droxler (1993)	Range of accum. rates within this study
Bulk sediment	0.2 - 6.7 g/cm^2/ky (Pedro Channel) 0.7 - 6.0 g/cm^2/ky (Walton Basin)	0.5 - 7 g/cm^2/ky
Coarse Fraction	0.01 - 1.8 g/cm^2/ky	0-1.7 g/cm^2/ky
Fine Fraction	0.2 - 6.6 g/cm^2/ky	0.2 - 5.5 g/cm^2/ky
Fine Aragonite	0.05 - 2.75 g/cm^2/ky	0.16 - 4 g/cm^2/ky
Fine High-Mg Calcite	0 - 0.35 (0.85) g/cm^2/ky	0 - 0.5 g/cm^2/ky
Fine Low-Mg Calcite	0.05 - 2.85 g/cm^2/ky	0-1 g/cm^2/ky
Fine Non-carbonates	0.05 - 0.45 g/cm^2/ky	0 - 0.6 g/cm^2/ky

Table 6.1: Range in accumulation rates of bulk sediments and single sediment components of this study and other studies near Pedro Bank (Glaser & Droxler, 1993; Schwartz, 1996).

Core M35034, situated on the southwestern margin of Pedro Bank, however, shows a somewhat dualistic behaviour. It should show only minor influence from the actively producing carbonate platform, and thus should be classified as a typical upcurrent core. The calculation of sedimentation- and accumulation rates, however, classify this core as one with a downcurrent depositional pattern. Transport from the platform along its southwestern margin is probably controlled by the topography of the margin and the slope (with channels that funnel neritic sediments to proximal located depositional sites; see chapter 5). This might explain why the sedimentation rates in this core agree well with those for the proximal downcurrent core M35048, and thus fit in the "periplatform sediment halo" model of Glaser & Droxler (1993).

Bulk sediment

The accumulation rates of bulk sediment clearly show their dependence on distance from the platform. During interglacials preferential offbank transport occur in the direction of the surface flow of the Caribbean Currrent (Glaser & Droxler, 1993), which can be seen in the accumulation rates for single interglacial isotope stages. The larger variability seen in a halo of ~20km in downcurrent direction probably shows different export pattern during various interglacial stages within the last 300 ky. This might also indicate the control of seafloor topography on the distribution of sediments around Pedro Bank (see also discussion Chapter 5). Further downslope the interglacial accumulation rates tend to be very similar, suggesting that the depositional history in these cores (at an offbank distance > 20 km) is probably very similar. At these positions sedimentation patterns are dominated by open-ocean pelagic sedimentation processes, but to a minor extent still receive fine neritic sediments.

During glacials no clear trend in bulk accumulation rates could be observed. Single glacial accumulation rates might be very high, such as for MIS 4 at site M35049 and MIS 2 at site M35034. This trend was also observed proximal to Diarangen and Bawhika Bank (Duncan, 1997). Redeposition of winnowed sediment from proximal sites during lowered sea level at more distal sites where drift deposits occur (Chapter 4), might explain this pattern.

Fine Fraction

Distance seems to play a major role in the distribution of fine, neritic components along the Pedro Bank carbonate platform. Large amounts of platform-derived sediments occur at a distance of up to 10 km in upcurrent and < 20 km in downcurrent position. Maximum changes in accumulation rates occur at water depths shallower than 900-1000 mbsl, whereas deeper than 1000 mbsl, accumulation rates tend to normalise around a lower limit of about 1.5-2 g/ cm^2/ky for the fine fraction. This value remains constant to locations at 92 km downslope (or 2500 mbsl). This lower limit value probably represent the overall open ocean accumulation rate of fine sediment around Pedro Bank. During glacials the accumulation rates are mainly controlled by the influence of enhanced bottom water current activity (Glaser & Droxler, 1993; Schwartz, 1996), which results from the restriction of the seaways during lowered glacial sea levels. More proximal and thus shallower sites (<500/600 mbsl) will be strongly affected by these current effects, but the accumulation rates found do not show lowered accumulation rates, probably because they originate from positions that were not close enough to the platform margin to show sediment removal due to current winnowing.

Coarse Fraction

The accumulation pattern of the 9 new Pedro Bank sediment cores clearly show that the Holocene deposition and accumulation of coarse (> 63µm) sediments greatly depends on the actual distance to the active bank margin. They are fairly independent of the up- or downcurrent position of the depositional site (see Fig. 6.5 (A) and (C)). Besides this pattern, other interglacial stages (MIS 5, 7 and 9) show a relatively constant accumulation pattern. A similar trend was observed by Glaser (1991) for the accumulation trends of coarse pelagic calcite in sediments from downcurrent Walton Basin and in single upcurrent cores from the southeastern margin of Pedro Bank. The conformity of coarse fraction accumulation rates from different basin and slope settings around the entire Pedro Bank carbonate platform shows the consistency of this input signal.

Glacial accumulation rates of the coarse fraction show a decreasing trend with greater offbank distance. Higher accumulation rates were observed for MIS 2 at sites M35034 and M35043. The latter might be caused by local factors such as, seafloor morphology and/or changing current activity.

Fine aragonite

Fine aragonite is the main component in periplatform sediments, registering changes in neritic production on top of the shallow carbonate platforms (e.g. Pilkey & Rucker, 1966; Milliman, 1974; Droxler, 1984), which is generally steered by major eustatic sea-level changes (e.g. Boardman & Neumann, 1984; Droxler & Schlager, 1985; Droxler et al., 1988a, 1988b; Reijmer et al, 1988; Glaser & Droxler, 1993). The amount of metastable carbonates in periplatform sediments might be modified by dissolution at intermediate water depths after deposition. This was shown for sediments in basins surrounding Pedro Bank by Haddad & Droxler (1993) and Schwartz (1996). In addition, biologically mediated dissolution of calcium carbonate in the upper 500-1000 m of the ocean, well above the chemical lysocline, as proposed by Milliman et al. (1999), might also have changed the signal. To what extend the aforementioned processes modified the input pattern found remains unclear because no data is available on the production on top of Pedro Bank, thus hampering precise budget calculations.

Large amounts of metastable carbonates are exported from the deeply submerged platforms on the Northern Nicaragua Rise into the surrounding basins (Glaser & Droxler, 1993; Schwartz, 1996; Duncan, 1997). This study supports those findings, but in addition, two further patterns become evident (see Fig. 6.6 A and C):

(1) Up to a distance of about 20 km the accumulation of fine bank-derived aragonite during interglacials is controlled by the export potential of the shallow carbonate platform. This holds for the downcurrent, leeward sites, but also includes accumulation within “upcurrent” site M35034 from the southwestern margin. As mentioned before, site M35034 somehow holds a special depositional location, as the depositional processes around the southwestern part of Pedro Bank seems to be more influenced by the local topography (see Chapter 5) resulting in the much higher accumulation rates observed at this site.

(2) In downslope positions, at water depths exceeding about 1000 mbsl, the changing influence of corrosive intermediate water masses (Haddad & Droxler, 1996; Schwartz, 1996) and local topography (Cunningham, 1997), in conjunction with changing current regimes, may steer for

the sudden interglacial decrease in aragonite accumulation rates. The high glacial accumulation rates of fine aragonite in proximal cores indicate that relatively large amounts of metastable carbonate were produced and deposited on the the platform margin during lowered glacial sea levels of 120-150 mbsl (Chappell & Shackleton, 1986; Dullo et al., 1996).
The present day topography of Pedro Bank shows a steep upper cemented slope from 320 mbsl to 180 mbsl (Dullo, 1997; see Fig. 5.4). At present, living populations of green algae e.g. *Halimeda* are found in water depths between 50 mbsl and 110 mbsl (Great Bahama Bank: Grammer et al., 1993; Freile et al., 1995; Jamaica: Liddell et al., 1988; Miskito Channel, Nicaragua Rise: Hine et al., 1988). During a maximum sea level lowstand at 120-150 mbsl the upper slope around Pedro Bank could still have been a productive area. *Halimeda* colonies were even observed on the steep rocky escarpment (>45°) of Great Bahama Bank (Grammer et al., 1993). So, even the steep cemented slope of Pedro Bank (40-50°; Dullo, 1997) could have functioned as a productive area for fine aragonite during sea-level lowstands. An intensification of the Caribbean Current during glacial times caused the winnowing of fine-grained sediments at water depths < 600 mbsl (Glaser, 1991). The shallowest core studied was taken from 648 mbsl and shows only limited winnowing of fine aragonite.

Fine High-Mg calcite
The accumulation of HMC within periplatform sediments deposited under the influence of changing surface-, intermediate- and deep-water masses is controlled by at least 3 factors:
(1) The production fluctuations in shallow- and deep-water biota, whose tests consists of high-Mg calcite (e.g. red calcareous algae, certain shallow water benthic foraminifera such as in miliolids and peneroplids, that dominate in Caribbean lagoonal deposits (Wantland, 1975), sponges, echinoderms and octocorallia). High input may be expected during highstands in sea level, when the bank tops are flooded enabling the production and export of these type of biota to the surround deep-water environment.
(2) Dissolution (or preservation) of HMC at intermediate water depths (>1100 mbsl; shown for Northern Nicaragua Rise sediments by Haddad & Droxler, 1996). The higher susceptibility to dissolution of HMC with more than 13 Mol% $MgCO_3$ in comparison to metastable aragonite is well known (Chave et al, 1962; Walter & Morse, 1984). Studies in the Caribbean by Haddad & Droxler (1996) could tie the composite dissolution indices (CDI) in the Walton Basin with the formation of NADW meaning that higher dissolution due to more corrosive [CO_3^{2-}]-poor Antarctic Intermediate Water (AAIW) entrainment preferentially took place during interglacial times with strong North Atlantic Deep Water (NADW) formation (Raymo et al., 1990; Hodell, 1993). So these watermass fluctuations probably steer the dissolution of metastable carbonates within the eastern Caribbean and the Bahamas (Droxler et al., 1991; Haddad & Droxler, 1996).
(3) The formation of submarine magnesium-calcite cements. The formation of these HMC-cements was described by Grammer et al. (1993) from steep marginal slopes of the GBB and by Ginsburg & James (1976) for the Belize Barrier Reef. Another source for HMC might be the formation of HMC cements in periplatform sediments during early diagenesis as shown for late Quaternary to late Miocene sediments from the GBB (Schlager & James, 1978; Westphal, 1997; de Mol et al., 1998).
Higher HMC-input rates during interglacials at the proximal sites (< 20 km) suggest that the distance from the active bank margin might play a role in the input pattern observed. This pattern clearly evolves in sediments of M35034, which show the highest Holocene accumulation rates. These high rates coincide with the high rates observed in other proximal downcurrent cores, eventhough sediments at site M35034 were deposited under the influence of intermediate water masses (1211 mbsl), which, if corrosive water masses were present, should result in lower accumulation rates due to dissolution of metastable carbonates. The high sedimentation rates during the Holocene are therefore probably a result of oversupply of metastable high-Mg calcite, so that dissolution did not affected HMC to a greater extent. In contrast to this special pattern, accumulation rates in water depths exceeding ~1000-1100 mbsl are very uniform, which points to a similar impact of dissolution on sediments deposited at more distal and deeper sites.
During glacial periods water depth, and thus the influence of intermediate water masses, seems to have had a major influence on the distributional pattern of fine HMC accumulation rates (Fig. 6.7). Glacial times with generally higher percentages in HMC content (Chapter 7) represent times of enhanced preservation of metastable carbonates in Caribbean intermediate water masses (Haddad & Droxler, 1996; Schwartz, 1996). The highest glacial HMC accumulation rates

observed in sediments deposited in water depths between 1000-1400 mbsl suggest this higher preservation potential. If these high amounts of HMC result from erosion and redeposition of upper slope deposits (biota as well as submarine cements) or in-situ cementation at intermediate waterdepth cannot be resolved. Rendle (2000) suggested that the first process caused the higher HMC-content at shallow sites (< 650 mbsl) along the leeward margin of GBB during glacial periods.

Fine Low-Mg calcite

Interglacial accumulation rates of LMC show very consistent values of 0.2-0.6 g/cm^2/ky for all cores, which suggests that open ocean productivity was very similar throughout the entire study area - independent of the water depth or distance from the active platform margin. An exception to this rule is formed by the high accumulation rates of ~1 g/cm^2/ky during isotope stage 9 in distal upcurrent core M35052 and distal downcurrent core PC100. In both cores only the interval from isotopic events 9.0 to 9.1 (299-310ky) is present. Isotope stage 9 lies within the mid-Brunhes climatic interval of Jansen et al. (1986) and the mid-Brunhes epoch (> 185 ky) of Schwartz (1996), a period of long-term climatic changes, characterised by less dramatic changes between interglacial and glacial stages, compared to the late-Brunhes epoch (< 185 ky) with severe glacial/interglacial changes. Accumulation rates in Pedro Channel during the mid-Brunhes epoch often centered near the glacial/interglacial transition (Schwartz, 1996). This might explain these extraordinary high accumulation rates observed during the end of isotope stage 9.

During glacials a general trend towards higher LMC accumulation rates with increasing offbank distance and water depth is evident. In addition, higher glacial accumulation rates were found during mid-Brunhes isotope stage 8 in comparison to late-Brunhes glacial stages 6, 4, and during the LGM. This also supports the findings of Schwartz (1996), who stated that during the mid-Brunhes mode a reversion from high accumulation rates in interglacials to high accumulation rates during glacials could be observed in comparison to the late-Brunhes period. The higher glacial accumulation of LMC with increasing offbank distance may result from low-productivity "Sargasso Sea" conditions during glacials (Prell & Hays, 1976) with low nutrients, to which most coccolithophores species are adapted (MacIntyre et al., 1976). The surface water masses close to the platform margins might be affected e.g. by local topographic upwelling processes (Schwartz, 1996) that could create higher nutrient levels, which would favour the existence of aragonite producing *Halimeda* meadows near to the plaform margins during the glacials. So, the spatial differences observed with increasing offbank distance, might point to variations in the surface water masses in the vicinity of the platform margins that could also have caused increased glacial aragonite accumulation rates as found at the proximal sites analysed in this study.

Fine Non-carbonates

The accumulation rate of fine non-carbonates reflects either (1) riverine input of clays from South American rivers (Bowles & Fleischer, 1985; Reid et al., 1996; Schwartz, 1996; Flood & Piper, 1997; Franz, 1999), or (2) originates from the Lesser Antilles as volcanogenic sediments (Sigurdsson et al., 1980; Reid et al., 1996) or (3) reflects eolian input from the Sahara (Reid et al., 1996). The non-carbonates can be transported over long distances through surface currents or within the nepheloid layer (Schwartz, 1996), a water layer in the deep ocean basins that contains significant amounts of suspended sediments and can reach 200 to 1000 m in thickness (Bates & Jackson, 1997).

Analysis of glacial and interglacial stage accumulation rates revealed the following pattern:

(1) In up- and downcurrent cores interglacial non-carbonate accumulation rates are more or less uniformly low. Once again MIS 2 at site M35034 forms an exception to this rule reflecting its high sedimentation rates caused by regional morphology and topography.

(2) During glacial stages 2, 4, 6 and 8 two patterns can be observed in the accumulation rates of non-carbonates: (A) Upcurrent sites display highest accumulation rates, which can be explained by their proximity to the source area of the South American rivers. In addition, dilution by other sediment components, like neritic sediments, is minimized because of their upcurrent location. (B) Highest accumulation rates are observed at site M35042. The distal position within central Pedro Channel and the relatively shallow depositional depth (1023 mbsl) might be responsible for overall highest accumulation rates of non-carbonates at this site. This once again shows the importance of local topography as a major controlling factor on the deposition of periplatform

sediments near Pedro Bank. In general, the trends seen in the accumulation of non-carbonates can be related to (1) current strength and winnowing (Schwartz, 1996), (2) the westward intensification of the Caribbean Current (Hallock et al., 1988) and (3) topographic upwelling (Schwartz, 1996; Cunningham, 1998), which have the potential to alter the strength of flow.

6.4.2 Spatial variability in glacial-to-interglacial accumulation rates along a leeward offbank transect

Fig. 6.8 shows the temporal and spatial changes of the single components of periplatform sediments at the leeward, downcurrent margin of Pedro Bank, the main depositional center near Pedro Bank (Glaser & Droxler, 1993). In the following chapter the changes in periplatform sediment accumulation along the platform-to-basin transect (Fig. 6.8) will be discussed and compared with the literature data of Glaser (1991), Glaser & Droxler (1993), Schwartz (1996) and Duncan (1997).

The **fine fraction**, which forms the main proportion of the **bulk sediment** is the main contributor to the periplatform sediments (e.g. Boardman et al., 1986; Glaser & Droxler, 1993; Milliman et al., 1993; Robbins et al., 1997) and shows a distinct spatial difference along the slope-to-basin transect. The most obvious glacial-interglacial changes along the transect occur at "proximal" sites M35048 and M35049, where glacial accumulation of the fine fraction is lowered by 52-64%. The glacial accumulation rates within the remaining downslope sites M35043-42-PC059-PC100 display lowered rates between 9-22% for fine fraction. In contrast, average overall interglacial accumulation rates show a clearly decreasing trend with increasing offbank distance. All these trends indicate the strong influence of neritic export from the bank top of Pedro Bank, as was also shown by Glaser & Droxler (1993) for the northern Walton Basin. Our study demonstrates that the halo of neritic sediment export can extend to an offbank distance of up to 20 km at the northwestern margin.

The observed decrease in the accumulation of the **coarse fraction** during interglacials with greater offbank distance can be also seen during glacials. This decrease of 27-50% comparing glacial-to-interglacial accumulation rates indicates that more coarse fraction (in total mass per time unit) was deposited during interglacials. It does not agree with the findings of Glaser (1991), and those in chapter 7 that during glacials a higher coarse fraction percentage can be found in proximal and/or shallow sediment cores. This might be the result of comparing accumulation rate data and data based on the relative percentage of a sediment proxy. Therefore, the spatial variability of the coarse fraction and grain size data is discussed in detail in chapter 7.5.3.

Aragonite accumulation rates show a decrease during interglacials and glacials with greater offbank distance and waterdepth. These observations confirm the findings of others for various regions (Pedro Bank: Droxer et al., 1991; Glaser & Droxler, 1993; Bahamas (windward): Droxler et al., 1988; Reijmer et al., 1988; Haddad & Droxler, 1996; Bahamas (leeward): Rendle (2000); Bermuda: Berner & Berner, 1976). Low concentrations in aragonite accumulation were observed during glacials, when production on the top of carbonate platforms is shut down or reduced to a small fringe along the upper slope (Kendall & Schlager, 1981; Handford & Loucks, 1993; Schlager et al., 1994). Along the slope-to-basin transect it can be observed that at each site the accumulation of aragonite is about 2-3 times lower during glacials, regardless of the relative position to the active bank (Fig. 6.8). This becomes also evident through the very similar patterns a reduced glacial accumulation of 46-67% in comparison to the average interglacial accumulation of neritic aragonite. The slightly higher average glacial AR at proximal sites M35048-49-43 might point to minor production of neritic carbonates during lowered glacial sea levels (see Chapter 7)

Along the slope-to-basin transect the high- and lowstand accumulation rates of fine **high-Mg calcite** as well as fine non-carbonates present a very similar pattern. A proximal depositional environment (sites M35048 and M35049) and an intermediate to distal depositional environment (M35043, M35042, PC059 and PC100) can be distinguished. The source area of these two sediment components, neritic vs. terrigenous, however, differs significantly. During interglacials high average accumulation rates for high-Mg calcite are found at sites M35048, M35049, M35043 and M35042, with the latter two located on the wide and flat plateau along the northwestern margin of Pedro Bank. This type of HMC-deposition agrees with the literature, whereby preferential input occurs during interglacials (e.g. Boardman et al., 1986; Glaser & Droxler, 1993; Haddad & Droxler, 1996). This links the HMC deposition at all 4

sites, at shallow to intermediate water depths (offbank distance <42 km), to the production of HMC-biota on top of Pedro Bank. The deep sites PC059 and PC100 only receive minor amounts of HMC during interglacials. This might be due to their location near or within intermediate water masses that might have undergone intensive dissolution of metastables carbonates during interglacials (Haddad & Droxler, 1996; Schwartz, 1996). At sites M35043 and -42 deposited in 975-1023 mbsl interglacial dissolution under the influence of "shallow intermediate" water masses (Haddad & Droxler, 1996) might explain the slightly lowered HMC accumulation during highstands in sea level. The HMC accumulation during glacials shows a reversed pattern, with lowest accumulation rates at the most proximal sites. Cores deposited around 1000 mbsl display highest glacial HMC accumulation, and sites from the deep Pedro Channel on average display a somewhat higher accumulation rate than proximal sites. This results in a zonation of (1) a proximal environment, with a lower average glacial HMC accumulation (-48 to -69%), and (2) a zone exceeding 975 mbsl (intermediate to deep intermediate watermasses), which indicate higher glacial accumulation of HMC by 24-69%. This pattern results from enhanced preservation of metastable carbonate phases during glacial periods in the eastern Caribbean (Haddad & Droxler, 1996). As mentioned earlier in this section, magnesium calcite cements can be formed during glacial periods on steep marginal slopes (Grammer et al., 1993; Dullo et al., 1996, 1998), at shallow slope sites (Westphal, 1997; deMol et al., 1998) and at the deep seafloor (Schlager & James, 1978). To what extent these cements affect the accumulation rates, both in absolute amounts and in a spatial context, remains unclear. The formation of cements on the upper slopes during lowstands in sea level and their subsequent erosion, however, might have resulted in a higher preservation potential at intermediate water depths. This might hold for the increased glacial accumulation of HMC at deep sites PC059 and PC100 from the central Pedro Channel. The low HMC accumulation rates within both proximal and shallow sites (648-893 mbsl) during glacials may result from the very low glacial sedimentation rates. In addition, enhanced current winnowing due to strenghtening of the Caribbean Current during glacials (Glaser & Droxler, 1993) might have modified the signal in the most proximal and shallow site M35048 by removing fine sediment.

The interglacial-to-glacial and spatial variability of **fine non-carbonates (NC)** along the northwestern slope of Pedro Bank shows a distinct difference between high- and lowstand accumulation. During interglacials the accumulation of NC is fairly consistent along the entire transect (0.2-0.3 g/cm^2/ky). The spatial variations define three depositional environments:

(1) Very proximal sites (M35048) receive only minor amounts of NC during glacials (67% lower than during interglacials). This might result from the increase in current activity close to the bank, resulting in winnowing of fine sediment particles (Glaser & Droxler, 1993).

(2) Sites at proximal to intermediate offbank distance (10-30 km; M35049 and M35043). They show a transitional environment for the deposition of NC along the downcurrent offbank transect. Glacial accumulation of fine non-carbonates increases slightly, indicated by the change from a slightly negative glacial-to-interglacial accumulation budget at site M35049 to a slightly positive budget at site M35043 (Fig. 6.8F). This pattern might be the result of redeposition of fine NC in greater offbank distance, where the influence of current winnowing might decrease. Also local topography might play an important role for the deposition of NC at both sites.

(3) Distal sites (>30-40 km offbank distance). Glacial mass AR show a clearly enhanced accumulation of NC (41-49%). This pattern might be explained by the lowered current strengths distally to the margins of Pedro Bank. These locations might promote the deposition of non-carbonates that most probably originate from South American rivers (e.g. Reid et al., 1996; Schwartz, 1996; Flood & Piper, 1997; Franz, 1999). The data obtained from these studies confirm the simple sequence-stratigraphic principles, which proposed a higher siliciclastic input into the oceans during lowered, glacial sea levels (e.g. Vail et al., 1991 cum lit.).

6.5 Conclusions

In general a strong influence of offbank shedding of neritic sediment components (aragonite and high-Mg calcite) can be observed within a halo of about 20 km at the downcurrent margin of main neritic export.

The most obvious changes on a glacial-to-interglacial comparison along the leeward offbank transect for all sediment components, neritic and pelagic ones, occur at the shallow sites, which

are located within the above mentioned sediment halo. It is obvious that these shallower sites are less affected by dissolution processes, which might modify the original input signal.
HMC, as the less stable carbonate phase, clearly shows the increasing influence of more corrosive water masses during interglacial periods along the offbank transect. Aragonite shows these dissolution effects only to a minor extent, probably resulting from oversupply into the periplatform realm during interglacial highstands in sea level. During glacials, when preservation of metastable carbonate minerals is enhanced at intermediate water depths, aragonite still shows a general decrease with greater offbank distance. During glacial periods HMC shows highest accumulation rates at about 1000-1400 mbsl, which might be originating from submarine precipitated HMC-cements. The erosion of these type of cements within upper slope settings and their redeposition at basinal sites might form another input source for this metastable carbonate.

Single sediment component accumulation rates within the periplatform oozes off Pedro Bank show distinct spatial differences along a downcurrent offbank transect. The sites can be separated into a proximal, from offbank shedding influenced depositional realm, and a distal, more pelagic influenced depositional realm. However, the single sediment components might show slight differences in this separation of proximal vs. distal environments, which is due to variations in:
1. the current strengths,
2. the input of pelagic and non-carbonate sediments causing dilution of the neritic sediment components,
3. the preservation and dissolution of metastable carbonates, beginning at about 1000-1100 mbsl in the vicinity of the Pedro Bank carbonate platform, and
4. the seafloor morphology as shown in chapter 5. This feature plays an important role in the distribution of sediments, especially for the downcurrent margin of PB.

CHAPTER 7

MINERALOGY AND GRAIN-SIZE ANALYSES
ALONG A BANK-TO-BASIN TRANSECT IN DOWNCURRENT POSITION
TO PEDRO BANK (NORTHERN NICARAGUA RISE)

7.1 Introduction

Carbonate sediments represented one of the major sediment types in earth history. Shallow-water environments were widespread during certain periods of the Phanerozoic. Large amounts of carbonates accumulated along large carbonate platforms in extensive low-latitude shallow seas (Tucker & Wright, 1990). At present about 90% of the calcium carbonate production originates from calcitic plankton (coccolithophorids and foraminifera) [Tucker & Wright, 1990]. On the "deep" seafloor (100-4500 mbsl) this pelagic ooze accounts for 80% of the global deposition of marine $CaCO_3$ (Tucker & Wright, 1990). During highstands in sea level pelagic and neritic environments sequester approximately same amounts of carbonates, whereas during lowstands in sea level the decreased neritic zone produces and accumulates approximately an order of magnitude less carbonate (Milliman & Droxler, 1996). Overall the shallow-water enviroment, reefs and carbonate platforms accounts for about 6% of the global carbonate production (Tucker & Wright, 1993).
Carbonate slopes are characterised by various depositional processes and receive sediments from the platform and/or the pelagic realm. Four processes are interacting in this depositional environment: deposition, erosion, cementation and dissolution. The stability of sediment packages deposited on the slopes depends on sediment type, grain size and slope angle (Kenter, 1990). Modern carbonate platforms mainly export fine sediments (<63µm) to the slopes and basins as shown for the Bahama Platform (Boardman & Neumann, 1984, 1986; Boardman et al., 1986; Droxler & Schlager, 1985; and others), the Northern Nicaragua Rise (e.g. Triffleman et al., 1992; Glaser, 1991; Glaser & Droxler, 1993), and the Maldives (Droxler et al., 1990). Kenter (1990) showed that muddy carbonates are not able to maintain slope angles that exceed 5°. Coarse grained deposits, however, are able to build slopes of up to 32°. Redepositional processes along modern carbonate platforms might be a major factor controlling sedimentation and composition of periplatform sediments. The study of the spatial and temporal variability of the grain size frequency distribution along platform-to-basin transects might give an insight into the depositional processes along modern carbonate slopes.
The mineralogical composition of periplatform sediments have been studied in numerous modern carbonate environments such as the Bahamian Platform, isolated carbonate platforms of the Northern Nicaragua Rise or the carbonate platforms of the Maldives (Boardman & Neumann, 1984, 1986; Boardman et al., 1986; Droxler & Schlager, 1985; Triffleman et al., 1992; Glaser, 1991; Glaser & Droxler, 1993; Droxler et al., 1990). A dominance of low-magnesium calcite (LMC) and quartz was be observed in glacial times, but also high amounts of high-magnesium calcite (HMC) could be found in glacials. Latter might originate of submarine HMC cements and/or redeposition of upper slope shallow-water debris from the preceeding interglacial (Rendle, 2000). Interglacial periods with highstands in sea level are characterised by sediments enriched with the metastable carbonates aragonite and HMC. They are produced by shallow water organisms and then exported to the adjacent slopes and basins after degradation into finer particles, known as the "highstand shedding" of carbonate systems sensu Schlager et al. (1994). The mineralogy of metastable carbonates in the deep surroundings of carbonate systems were also used to detect carbonate dissolution or preservation of sediments deposited within intermediate water masses. Droxler et al. (1990), Droxler & Haddad (1996) and Schwartz (1996) showed that metastable carbonates (such as HMC) along with frequency distributions of pteropods and their preservation stage might be a tool to differentiate times of carbonate preservation or dissolution. Glaser (1991) stated that sediments deposited deeper than 1100 mbsl in the surroundings of Pedro Bank might be subjected to dissolution of metastable carbonates. The sediment cores analysed in this study cover a wide depositional range in offbank distance and waterdepth. Therefore they contain a varying input from the platform by metastable carbonates such as aragonite or HMC.

In contrast to the well studied mineralogical composition of carbonate platform and periplatform sediments, little is known about the grain size distribution along platform margins, although grain size analysis is a common tool in the analysis of siliciclastic sedimentary rocks. Siliciclastic sediments are generally described using grain size, shape and/or fabric (e.g. Boggs, 1987). So far, only limited documentation has been made of these parameters for carbonate sediments. Therefore the major part of this chapter aims to describe grain-size varations through space and time along the slopes of an isolated carbonate platform.

Objectives

This chapter covers the sedimentary analysis of periplatform sediments around Pedro Bank. A series of cores along two offbank transects were retrieved during the Meteor 35 research cruise in 1996 - one in a downcurrent (northwestern) position to the bank edge and a second one along the southwestern (upcurrent) side of Pedro Bank.
Main objective of this study was to gain insight into the export pattern of this inclined carbonate platform by using a microfacies approach (see Chapter 8). Glaser (1991) established the use of sedimentological and mineralogical parameters to obtain a carbonate stratigraphy for periplatform sediments off Pedro Bank and their ability to record fluctuations in dissolution of metastable carbonate phases. Schwartz (1996) extended the analysis to sediment cores from Pedro Channel. Glaser & Droxler (1993) demonstrated that Pedro Bank is far away from being a partially drowned carbonate platform and unequivocally showed that this carbonate platform is deeply submerged, but highly productive. Glaser (1991) ascertained that in addition to distance from the closest bank or shelf margin and the up- versus downcurrent position, waterdepth also influences the distribution of carbonate accumulation rates along the deep surroundings of Pedro Bank.
In this study the main focus lies on the description of changes in mineralogy and grain size along a roughly 100 km long offbank transect along the northwestern margin of Pedro Bank.

7.2 Dataset and Methods

Dataset

Nine sediment cores from the periplatform environment around Pedro Bank were analysed. These cores were taken from waterdepths ranging from 648 to 2520 mbsl and offbank distances ranging from 5.5 to 92 km (see Table 7.1 and Fig. 7.1).

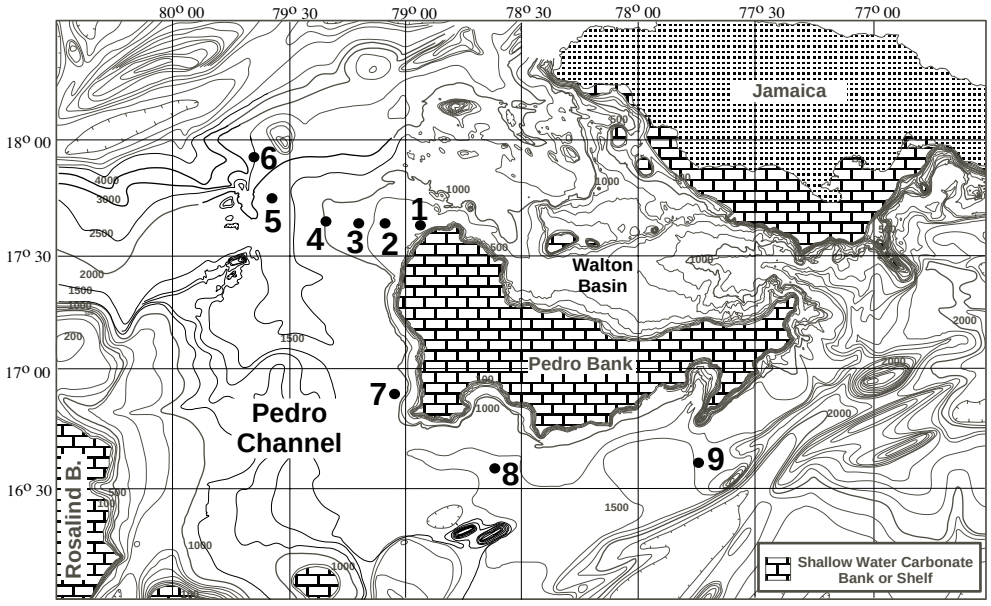

Fig. 7.1: Bathymetric map for the Pedro Bank area with core locations. Bathymetry is based on revised data collected during several American research cruises to the Northern Nicaragua Rise and modified after Cunningham (1998). Core abbreviations are as follows: 1=M35048; 2=M35049; 3=M35043; 4=M35042; 5=PC059; 6=PC100; 7=M35034; 8=M35032; 9=M35052)

Six cores (1-6) are located along the northwestern margin of Pedro Bank forming a platform-to-basin transect on the downcurrent side of Pedro Bank. Cores M35034 (7), M35032 (8) and M35052 (9) were recovered from the southwestern to southeastern margin and will be used independently to show sedimentational processes along the upcurrent margin. These sites cover an offbank distance from 10 to 30 km and a depth range from 1211 to 1442 mbsl. Sediments from a more proximal upcurrent position to Pedro Bank were not retrieved as coring activities failed. This was possibly due to the existence of hard layers along the upper slope/toe-of-slope preventing seismic penetration. The recovered upcurrent sediments were therefore solely deposited under the changing influence of different intermediate water masses such as NADW and AAIW and possibly contained similar dissolution patterns of metastable carbonates as shown by Glaser & Droxler (1993) and Haddad & Droxler (1996).

For the mineralogical and sedimentological analysis of the nine cores (see Table 7.1 for general data on cores), 602 sediment samples were taken. Within each core they were taken equidistantly spaced at 10 cm.

Core (No. in Fig. 7.1)	Relative position (closest distance to active bank margin)	Up-/Down-current position	Position Latitude (°N)	Position Longitude (°W)	Water depth (m)	Length of core (cm)
M35032-2 (8)	SW-Edge (25 km)	Upcurrent	16.5925	78.6261	1364	354
M35034-1 (7)	SW-Edge (10 km)	Upcurrent	16.9092	79.0694	1211	231
M35042-2 (4)	NW-Transect (41 km)	Downcurrent	17.6486	79.3094	1023	556
M35043-1 (3)	NW-Transect (28 km)	Downcurrent	17.6441	79.1691	975	431
M35048-1 (1)	NW-Transect (5.5 km)	Downcurrent	17.6469	78.9144	648	517
M35049-2 (2)	NW-Transect (19.5 km)	Downcurrent	17.6438	79.0877	893	513
M35052-2 (9)	SE-Edge (30 km)	Upcurrent	16.5753	77.7028	1445	965
PC 059 (5)	NW-Transect (72 km)	Downcurrent	17.7255	79.6353	1887	571
PC 100 (6)	NW-Transect (91 km)	Downcurrent	17.9211	79.7166	2520	519

Table 7.1: Core locations, relative position, waterdepths and core length of the nine analysed sediment from the periplatform environment around Pedro Bank

Methods

The following methods were used in this study: (1) stratigraphical analysis: oxygen isotope analysis of *G. sacculifer*, U/Th-dating of marine bulk sediment, AMS ^{14}C-dating of mixed Holocene and stage 3 coarse-fraction samples, (2) determination of calcium carbonate content of the fine fraction and bulk sediment, (3) X-ray powder diffraction of the fine fraction to determine the carbonate mineralogical composition of sediments, and (4) grain-size analysis by (a) wet sieving, separating the coarse and fine fine fraction and (b) dry sieving of the coarse fraction. All analytical procedures and error estimates are described in greater detail in chapter 2. Data of Glaser (1991) that were used for comparison purposes might cause problems due to using (1) different coring devices (piston vs. gravity coring), (2) different X-ray machines and (3) calibration standards that were needed to calculate the mineralogical composition and content of carbonate phases in periplatform oozes (see Chapter 4). The data sets from Glaser (1991) thus were not recalculated, as this could not to be done without introducing additional errors (see Chapter 4).

7.3. Results

7.3.1 Presentation of Data

This chapter covers a wide range of data, mineralogical as well as sedimentological, of nine sediment cores. They will be described for one platform-to-basin transect (downcurrent) and 3 single upcurrent located sediment cores. The presented values were calculated using the stratigraphic interpretations shown in chapter 4. Interglacial and glacial values are averaged for each core for mineralogy, content of coarse vs. fine fraction and grain size subfractions along the northwestern transect and single sediment cores from the southern periplatform environment. Oxygen isotope stages 2, 3 and 4 have been, where possible, seperated in the stratigraphy. Interstadial stage 3 is thought to have had sea level stands of up to 40 m below

present day sea level (e.g. Chappell et al., 1996), which would result in the flooding of small areas at the inclined top of Pedro Bank. When using, as generally done, the timespan of isotope stages 2-4, this would result in a mixed "glacial/interglacial" mineralogical and grain size signal. The interglacial, glacial and interstadial means are shown with increasing offbank distance, which also accounts for increasing waterdepths.
The carbonate mineralogical data are calculated percentages of the fine carbonate component within the bulk sediment (which therefore do not add up to 100%). They were determined using the following equation:

$$\text{Carbonate component}_{\text{(in bulk sediment)}} =$$

$$\text{Carbonate component}_{\text{(raw data in percent)}} \times \text{Carbonate content ratio}_{\text{(fine fraction)}} \times \text{fine fraction ratio}$$

with

$$\text{Carbonate content ratio}_{\text{(fine fraction)}} = CaCO_3 \,/\, 100$$

$$\text{fine fraction ratio} = \text{Fine fraction percentage} / 100$$

In addition characteristic data for each core will be shown based on specific parameters (e.g. fine aragonite content or the weight percentage of the 125-250µm) versus time or depth (Figs. 7.8 to 7.16). The ultimate aim is to describe the temporal changes of single sediment proxies defining characteristical depositional environments

7.3.2 Spatial mineralogical variability along platform-to-basin transects

(A) Downcurrent Transect (Fig. 7.2)

Interglacials
Aragonite content decreases continuously (64-36%) with increasing distance and waterdepth along this transect. LMC shows an increase from on average 8.5% in proximal cores to 30% for distal site PC100. Mid-distanced cores M35043 and -42 show similar amounts of LMC (±15%). HMC varies between 3.3% in the most proximal core to slightly raised values of 5.5-6.5% for cores located between 20-42 km offbank distance or 893-1023 mbsl. Further downslope (1887-2520 mbsl) the average HMC content decreases again to values of approx. 3.5%. The content of fine non-carbonates displays a constant increase with increasing waterdepth and offbank distance (6.5-16.5%).

Glacials
During glacials the distribution of aragonite within the bulk sediments shows a slightly different pattern than during interglacials. The most proximal core contains high amounts of aragonite (49%). M35049 and -43 (20-28 km offbank distance) show nearly identical aragonite amounts of 34%, as well as the next two cores along the downslope transect (M35042 and PC059) with 25% aragonite. The minimum amount along the transect is found at the most distal site PC100 with 20% aragonite on average during glacials. The content of LMC in glacial periods is generally higher than during interglacial periods. The amount of LMC increases downslope (10-38%), with M35042 and PC059 showing more or less identical amounts (28%) although they differ by 40 km distance or 800 m waterdepth. The HMC content is in general higher during glacial periods, although the difference between interglacials and glacials at certain sites is neglectable (e.g. M35048 and -49). It seems that also waterdepth plays an role in the spatial distribution pattern of HMC. The most obvious increase in the glacial HMC content is evident at site M35042 (1023 mbsl), where the average amount of HMC raises from 6.2% to 12%. The most distal and deepest sites PC059 and PC100 display again lowered amounts of HMC (see Fig. 7.2). The observed increase in HMC during glacials between 900-1100 mbsl can also be seen in the HMC accumulation rates (see Chapter 6). The amount of fine non-carbonates increases along the entire transect, except for proximal core M35048, which shows a nearly identical amount of terrigenous input. The amounts of non-carbonates at proximal sites M35048 and -49 are almost identical with about 13%, M35042 contains on average 25% non-carbonates, and distal sites PC059 and PC100 show maximum glacial amounts of about 30% on average.

Stage 3
The spatial distribution of stage 3 samples (Fig. 7.2) will not be described in detail. However, the stage 3 samples at proximal site M35048 is worth to mention, as this sample probably was deposited during isotope event 3.3, an interstadial highstand in sea level. The main point of interest therefore is given by the relatively high amount of aragonite (61%) for this distinct sample, which might be important for the flooding history of Pedro Bank during marine isotope stage 3.

(B) Upcurrent sites (Fig. 7.3)
The cores from the upcurrent margin of Pedro Bank are located at 10, 25 and 30 km offbank distance, but were deposited in a very small depth range between 1211 and 1445 mbsl. This waterdepths covers a depth range, which was not recovered along the northwestern transect. The sediments recovered were deposited under the influence of intermediate water masses. This water layer is probably characterised by variable influence of NADW and AAIW during certain periods of the late Quaternary, which resulted in preservation and dissolution cycles recorded in the the content of metastables carbonates, as shown by Haddad & Droxler (1996) and Schwartz (1996). Even though an offbank transect for the southern edge of Pedro Bank could not be established, the sediments recovered might at least show changes in intermediate water masses during the late Quaternary.

Interglacials
The average content of fine aragonite in bulk sediment shows a constant decrease with increasing offbank distance/waterdepth (51-21%). Highest amounts were found in the most proximal core (M35034, 10 km offbank distance) and correlate with the amounts in core M35042 (offbank distance 42 km). This might indicate the sediment export potential along the downcurrent margins of Pedro Bank. At the most distal site M35052 21% fine aragonite is found on average during interglacials. This is nearly 75% less than at the most distal core PC100 on the downcurrent side. LMC also displays a continuous increase with increasing offbank distance. The amounts vary during interglacial between 7-30%. The content of HMC during glacials averages about 7% within the southwestern, proximal located cores M35032 and -34, whereas distal core M35052 only shows an average interglacial content of 3.5%. The content of fine non-carbonates varies between 17% for southwestern cores M35032 and -34, and shows a maximum interglacial average content of nearly 30% at site M35052. These values are higher than maximal values along the downcurrent transect in interglacials.

Glacials
During glacial periods the mineralogy of periplatform sediments along the upcurrent margin of Pedro Bank shows the following characteristics: average amounts of fine aragonite decrease (29-15%) with increasing offbank distance/waterdepth (Fig. 7.3A). This equals an interglacial-to-glacial reduction in the aragonite contents of one-third to a half (Fig. 7.3B). The content of fine LMC shows lowest amounts in proximity of the platform (13% in M35034), whereas M35032 and -52 show very similar values of about 25-27%. The content of LMC in glacials is clearly higher than in interglacial periods in cores M35034 and -32, whereas most distal core M35052 shows very similar amounts of LMC during glacials and interglacials. The average content of HMC shows a continuous decrease with increasing waterdepth (9% to 6%; Fig. 7.3A) at upcurrent sites. The amount of fine non-carbonates in the southern cores raises from about 30% in M35034 to a maximum of 42% during glacials at site M35052 (Fig. 7.3A). The input of non-carbonates is therefore about twice as high as during interglacial times (44-81%; Fig. 7.3B).

Stage 3
The averaged amounts of carbonate minerals show a close relationship to glacial averages calculated within the same cores. This also applies to proximal core M35034.

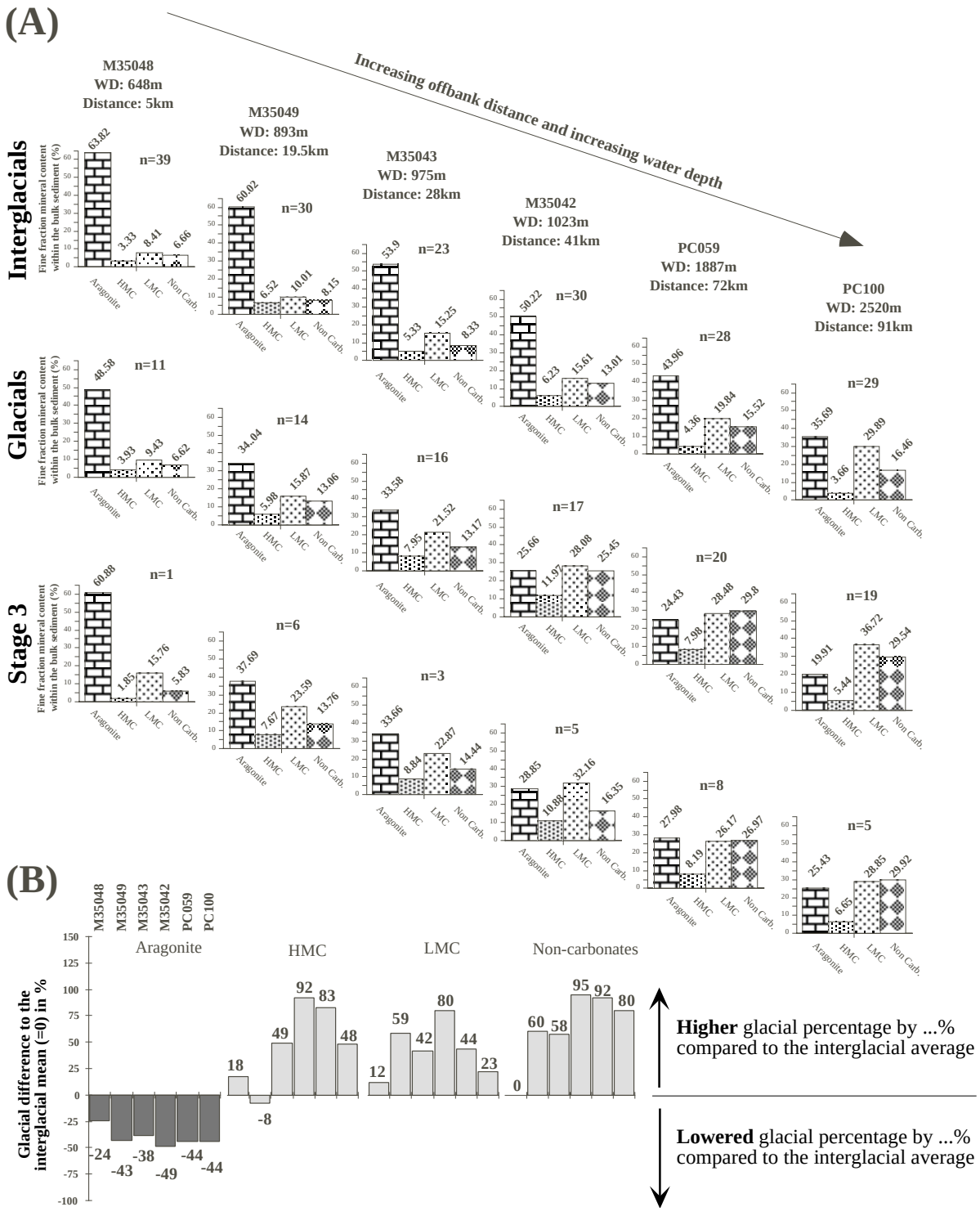

Fig. 7.2: Spatial mineralogy distribution along the northwestern offbank transect (A) and percentual glacial-to-interglacial comparison (B).
From the lower figure the spatial trends of carbonate phases and non-carbonates are clearly visible. Aragonite as an indicator for neritic export to the basins show reduced glacial input along the entire transect. HMC shows a bimodal distribution with little change at proximal sites and largest glacial-to-interglacial differences at mid-distanced site M35042. LMC and non-carbonates show clearly enhanced percentages during glacials along the entire transect, but lowest differences for most proximal site M35048, which is probably influenced by current winnowing, whereas the other sites probably receive major amounts of this winnowed sediment material.

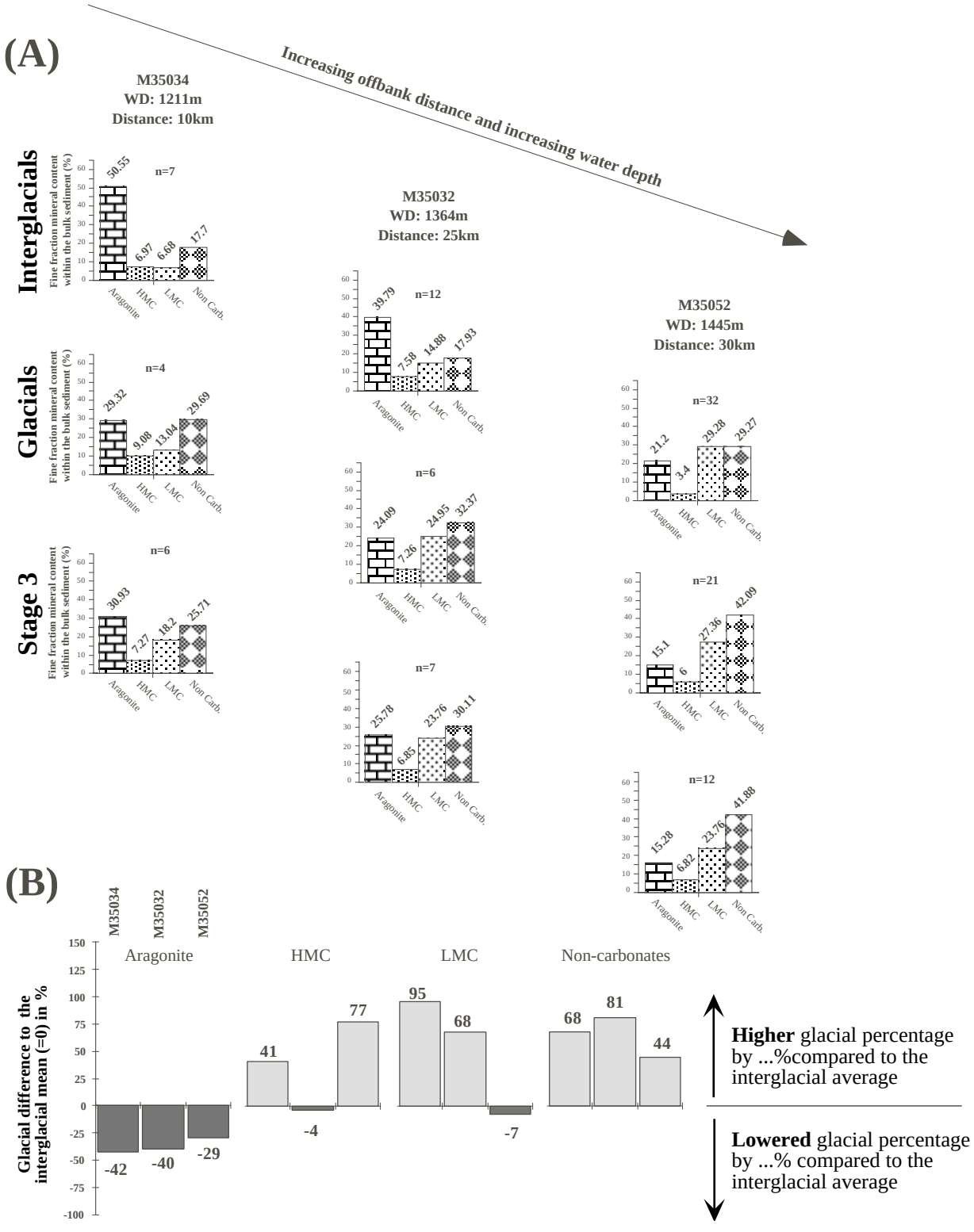

Fig. 7.3: Spatial mineralogy distribution of upcurrent periplatform sites (A) and percentual glacial-to-interglacial comparison (B).
Although the cores do not display a real offbank transect, they still show the decreasing influence of neritic export and increasing influence of pelagic and terrigenous sediment components with greater offbank distance. Data for site M30532 must be treated with care, as this core is disturbed intensively due to the erosive forces of turbidites.

7.3.3 Spatial grain size variability along platform-to-basin transects

(A) Downcurrent Transect

(A.1) Coarse vs. Fine Fraction (Fig. 7.4)

In the cores studied, the amount of fine fraction varies between 76% and 85%. Independent from up- or downcurrent location the lowest fine fraction contents are found at proximal sites (M35034 and M35048). Along the downcurrent side the fine fraction content is almost the same (79-85%) as in the upcurrent cores (76-79.5%).

Interglacials

The proportion of the coarse and fine fraction during interglacials along the northwestern transect shows only minor variations. The coarse fraction varies between 16.7% and 19.3%. Highest values are found in cores M35048, M35043 and PC059 with about 19%. These slighlty raised values for the latter three cores may depend on local factors, as the three cores represent different depositional environments.

Glacials and Stage 3

During glacial times the cores along the transect can be subdived into three different groups. At most proximal site M35048 14% more coarse fraction was deposited during glacials, whereas sites -49 and -43 show a minor increase of only 5.5% and 8% respectively (Fig. 7.4A). At downslope sites 42, 59 and 100 in contrast about 5-6% less coarse fraction was deposited. This trend is also visible when looking at the glacial-to-interglacial percentual difference of the coarse fraction content (Fig. 7.4B). At site 48 about 77% more coarse fraction is recorded during glacials in comparison to the interglacial mean. Sites 49 and 43 show "only" 34-45% more coarse fraction, whereas sites 42, 59 and 100 show very similar reduction of about 29-33% less coarse fraction in glacial periods (Fig. 7.4B). The same spatial pattern, i.e. a threefold divison of the sites, can be seen during marine isotope stage 3.

(A.2) Subfractions of the coarse fraction (Fig. 7.6)

Interglacials

The most proximal core M35048 shows a strong dominance of fine sands (more than 75%), and a gradual decline to coarser subfractions, and thus displays a negative skewness within the coarse subfractions. With increasing offbank distance the distributional pattern within interglacials becomes more bimodal, as subfractions such as the very fine and medium sands occur more frequently. The fine sand fraction shows a continuous decrease (50-29%) along cores situated on the relatively flat plateau on the northwestern margin (M35048 to -42), whereas PC059 and PC100, situated on the flanks of Pedro Channel, show similar amounts within the 63-125µm fraction (± 32%). The fine sand fraction shows relatively constant amounts between 24-28% along the whole transect. The medium sand content is lowest in proximal core M35048 (17%), increasing towards M35043 (30%) and varies in other cores situated further downslope around 30-32%. A similar spatial distribution pattern can be seen in the coarse sand fraction. The very coarse sand fraction shows no distinct changes along the entire offbank transect (0.89-1.89%).

Glacials

The glacial sediments on average show a very similar distributional pattern for the subfractions along the entire offbank transect. All grain-size distribution curves from the most proximal core M35048 downslope to PC059 (1887 mbsl, 72 km offbank distance) show a dominance of the very fine to fine sand fractions and decreasing values with increasing grain size classes.
Along the transect the single grain-size classes show the following variations: the 63-125µm fraction show only minor variations with 35-39.5%. The fine sand content (125-250µm) is stable with 27-31% for cores situated on the flat plateau, whereas the values for cores located further downslope on the flanks of Pedro Channel decrease to 24.5%. The medium sand content varies from 23.5 to 25% within most cores. Both, the coarse and very coarse fraction show a minor increase with increasing offbank distance, respectively from 6.5-10% and 0.96-1.91%.

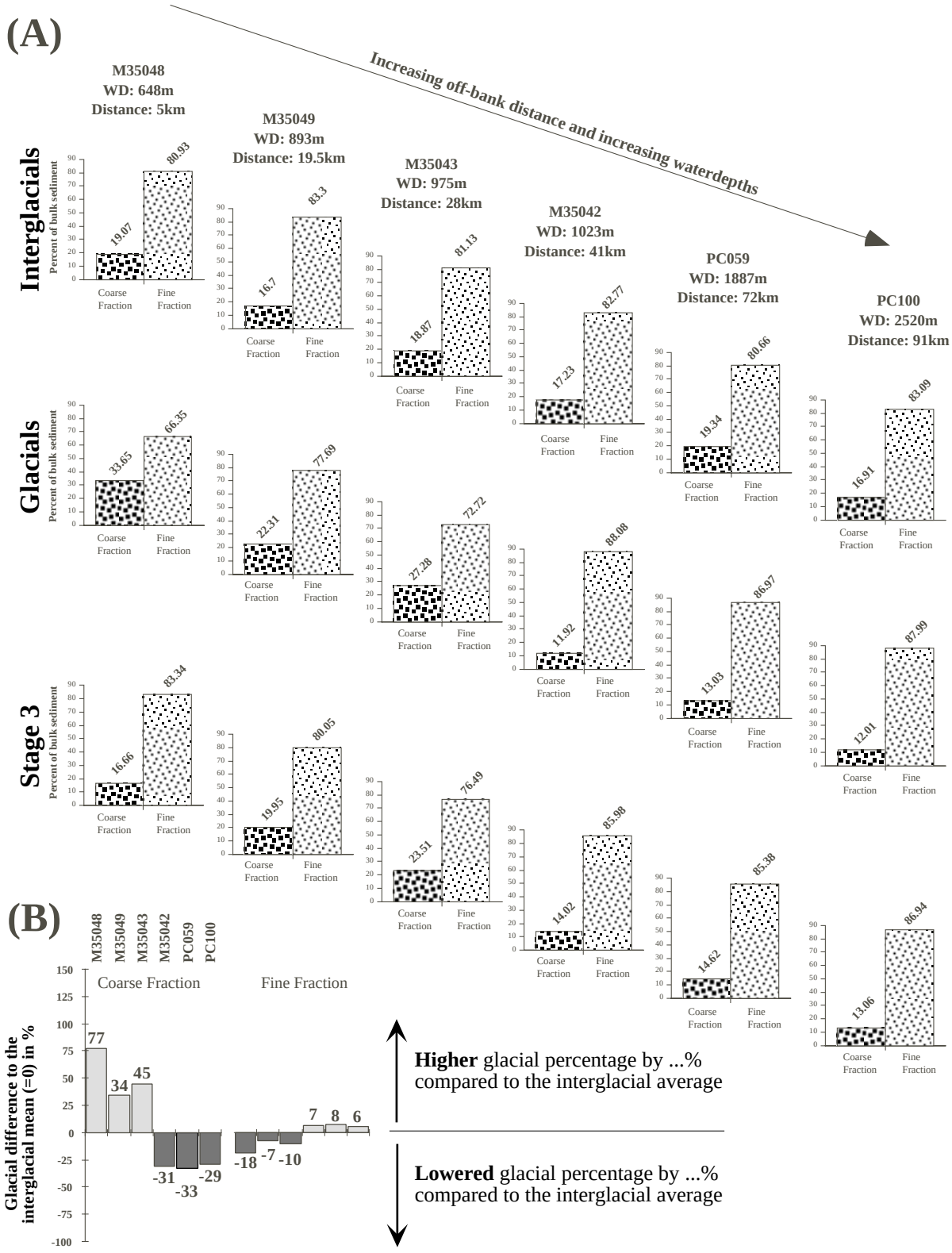

Fig. 7.4: Spatial coarse vs. fine fraction distribution along the northwestern offbank transect (A) and percentual glacial-to-interglacial comparison (B).
During interglacials no major changes in the content of coarse and fine fraction occurs along the entire offbank transect. Glacial periods, however, show two distinct environments. Cores within M35048, -49 and -43 (<28 km offbank distance) display raised glacial coarse fraction contents, which might be the result of lower input of fine neritic components, current winnowing or redepositional processes. The other more distal sites also show a very similar coarse vs. fine fraction pattern, which might reflect a similar influence of open ocean sedimentation at these sites.

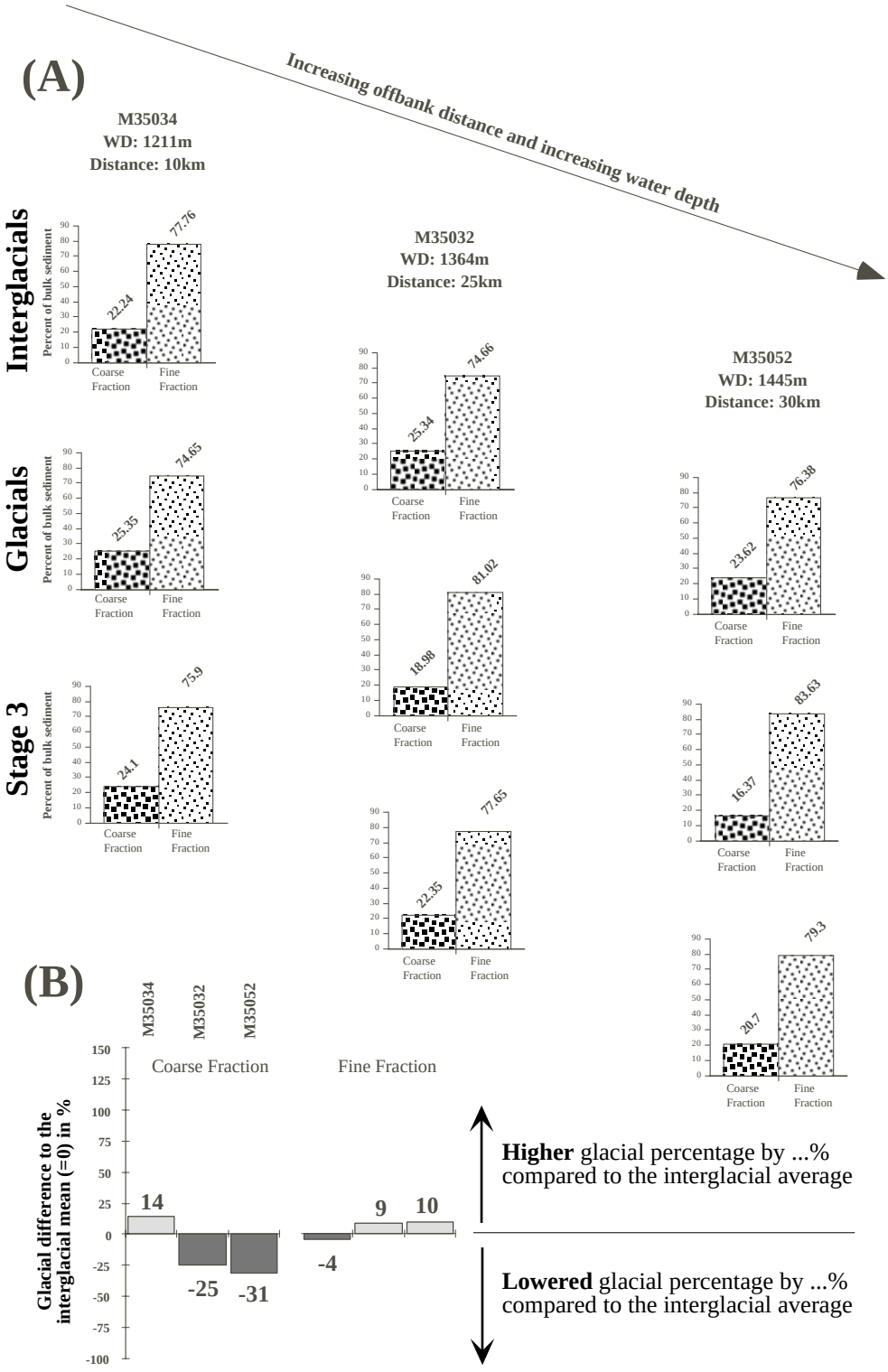

Fig. 7.5: Spatial coarse vs. fine fraction distribution of upcurrent periplatform sites (A) and percentual glacial-to-interglacial comparison (B).
The interglacial content of coarse and fine fraction is very similar in all analysed upcurrent sediment cores, showing no real trend. During glacials an obvious decrease in the coarse fraction content can be observed. The higher percentage at most proximal site might be indicative for a stronger influence of redeposited material closer to the slopes of Pedro Bank, which might be subjected to redeposition of coarser grained material. Also this higher coarse fraction content at the proximal site M35034 can be the result of enhanced current activity, resulting in winnowing of fine sediments. Probably both factors will induce the observed pattern.

A comparison of the interglacial and glacial averages (Fig. 7.6B) shows that the most obvious changes occur in the proximal cores M35048 and -49 in the 63-125µm and 250-500µm fraction. Within the fine sand fraction the glacial-to-interglacial difference is only minor (2-15%) The absolute percentages for the >1000µm fraction remain very low (0-2%) and very coarse sand fraction only varies on a subordinate scale, therefore the high percentual changes probable are an artefact.

Stage 3
The proximal cores M35048 and -49 show similar coarse subfractions distribution patterns with a clear dominance of the 63-125µm fraction (45-48%). This might suggest the export of fine metastable carbonates during interstadial stage 3 (see discussion).

(B) Upcurrent Sites

(B.1) Coarse vs. Fine Fraction (Fig. 7.5)

Interglacials
Similar to the downcurrent transect, the interglacial coarse and fine fraction content within the upcurrent cores shows minor changes that are independent from their relative location to the platform edge (22.2-25.3% respectively 77.8-74.7%). The absolute coarse fraction contents however, are higher by about 6% in comparison to the downcurrent margin.

Glacials
Along the upcurrent side the tendency of highest coarse fraction contents in proximal cores and a decreasing trend with increasing offbank distance also can be observed. The proximal core M35034 shows a coarse fraction content of about 25%, which is lower than the 33% found in the most proximal core M35048 on the downcurrent margin. M35032 and -52 show coarse fraction contents between 16-19% (Fig. 7.5), which is lower than those amounts observed in cores at similar distance from the downcurrent margin (Fig. 7.4). Fig. 7.5B shows that only proximal core M35034 exhibits a minor increase by 14% compared to averaged interglacial contents, whereas M35032 and -52 show a similar decrease of 25-31% in the amount of coarse fraction. Cores M35032 and -52 probably contain a more pelagic signal, while at proximal site M35034 probably redepositional processes might be recorded.

Stage 3
During marine isotope stage 3 the average coarse fraction amount displays a small decrease with increasing offbank distance (24-21%).

(B.2) Subfractions of the coarse fraction (Fig. 7.7)

Interglacials
The distribution pattern of the coarse subfraction within core M35034 shows a dominance of fine sands. With increasing distance the amount of the 63-125µm and 125-250µm fraction decreases steadily. The very coarse sand fraction (>1000µm) displays only minor spatial changes.

Glacials
The averaged glacial distribution patterns shows a more bimodal distribution pattern (in M35032, M35052) indicated by maximal amounts in the medium sand size subclass. The very coarse sand fraction (>1000µm) shows slightly increased values (1.6-2.6%), which might suggest reworking.
Fig. 7.7B shows that the very fine and fine sand fraction have slightly increased percentages during glacial periods (by 8-20% in comparison to the interglacial mean), whereas medium and coarse sand contents decrease by 9-27%. The most distinct changes are evident in the very coarse sand fraction (increase by 65-141%), but these high percentages probably are the result of slight changes on a subordinate scale.

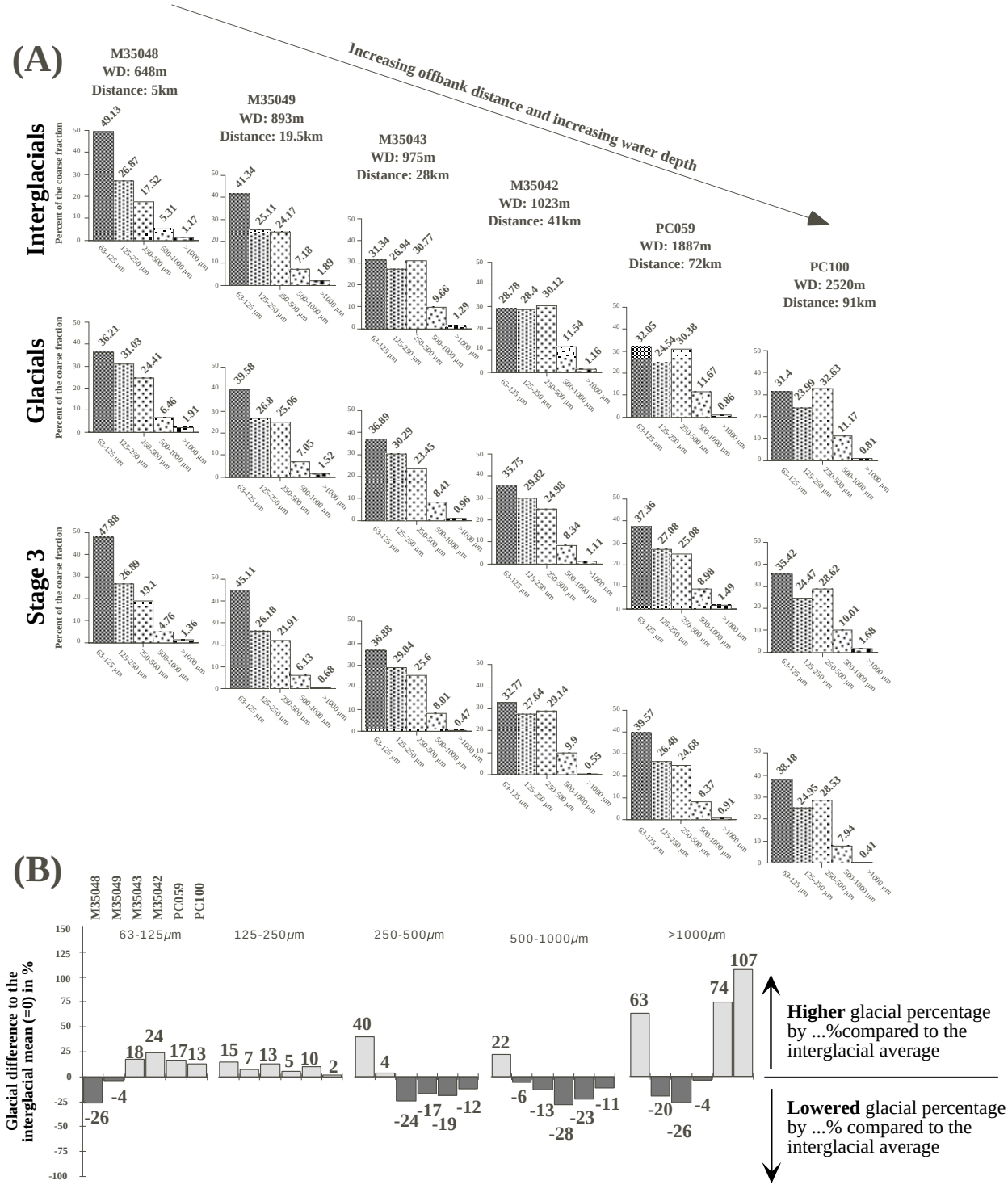

Fig. 7.6: Spatial subfraction distribution pattern along the northwestern offbank transect (A) and percentual glacial-to-interglacial comparison (B).
During interglacials it is evident that proximal sites are mainly composed of fine sediment material from the bank top, displayed through their highest percentages in the very fine to fine sand fraction ("normal" sorting pattern). The more distally sites are located, the greater the pelagic influence becomes evident through a more bimodal distribution with maximum amounts in the very fine sands (neritic) and the medium sand fraction (pelagic signal). During glacials generally a normal sorting with a decrease of each consecutive coarse grain size class is evident. This shows that all sites are probably influenced by the same depositional processes. The high content in the very fine sand fraction might occur from the input of fine LMC in form of nannoplankton such as coccolithophorids).

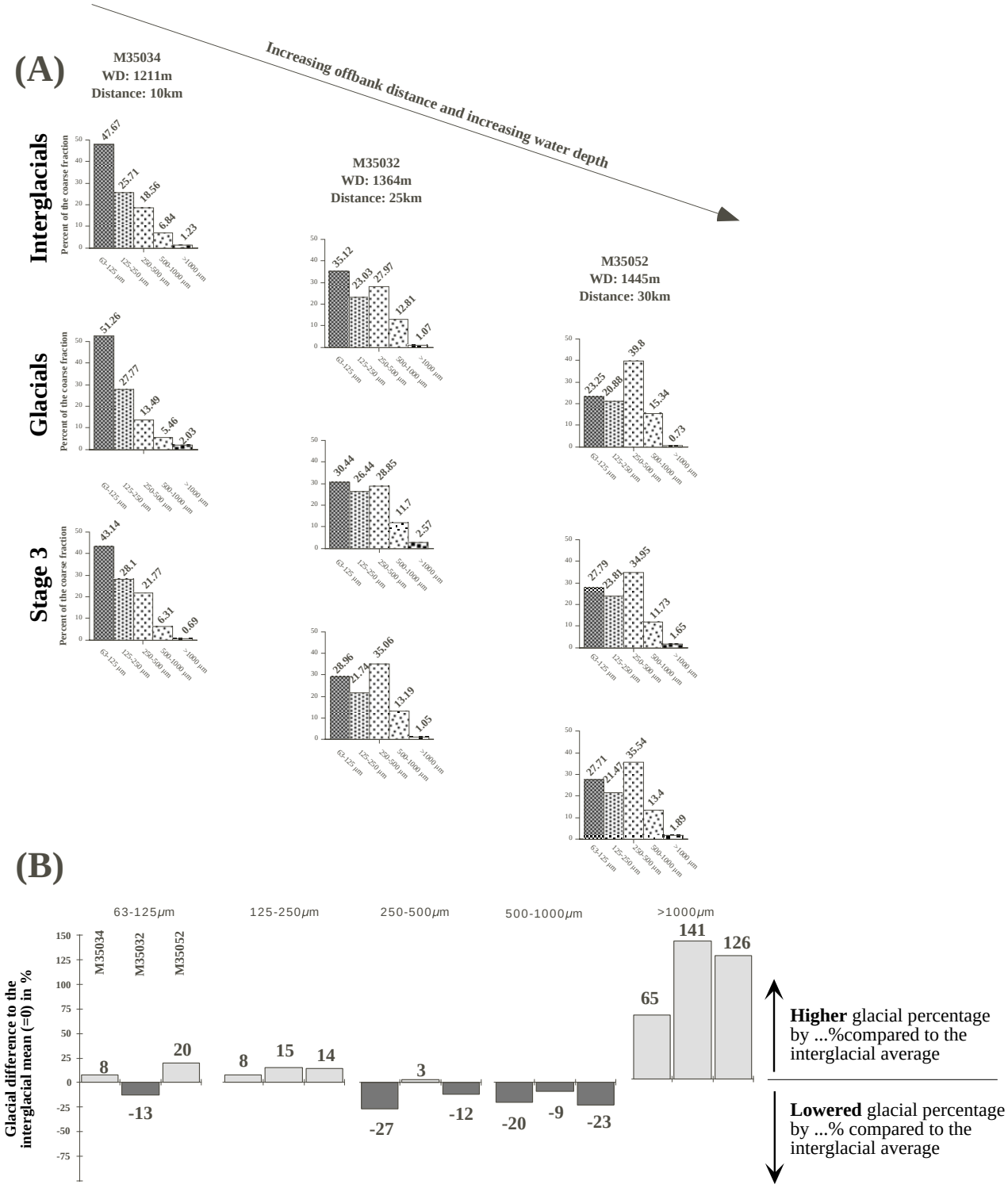

Fig. 7.7: Spatial subfraction distribution pattern of upcurrent periplatform sites (A) and percentual glacial-to-interglacial comparison (B).
In upcurrent cores interglacial and glacial coarse fraction distribution pattern are quite similar. During both periods sediments at proximal site M35034 show a normal sorting pattern with decreasing percentages with each consecutive coarser grain size class. At more distal sites M35032 and M35052 a bimodal distribution pattern is evident indicating a more pelagic influenced deposition at both sites.

Stage 3
During marine isotope stage 3 the most proximal core M35034 shows highest amounts in the very fine sand fraction and constantly decreasing amounts with increasing grain size classes. The grainsize distribution patterns for the more distal cores M35032 and -32 are remarkably similar despite their varying position to Pedro Bank.

7.3.4 Temporal variability of mineralogical proxies

(A) Downcurrent Transect

(A.1) Shallow (<700 m) and proximal (<6 km) cores - M35048 (Fig. 7.8)
The most shallow and proximal core shows a clear input signal with high amounts of fine aragonite in the bulk sediment (60-80%) during interglacials (sea level highstands) and lowered values (30-40%) during glacial periods. HMC exhibits low amounts (0-8%) in this proximal position. Highest amounts can be found in sediments younger than 6 ky and at the stage 3/4 and 7/8 boundaries. The overall pattern shows that HMC increased towards the core top. The LMC content decreases from stage 8 to the present (maximum value about 25% during early stage 7). During the Holocene LMC values fall below 10%. Quartz intensities in the fine fraction varies only minor during glacial and interglacial intervals.

(A.2) Cores from intermediate waterdepth (893-1023 mbsl) and intermediate offbank distance (19-42 km) - M35049 (Fig. 7.9), -43 (Fig. 7.10) and -42 (Fig. 7.11)
These cores show similar amounts of aragonite, with higher aragonite contents in interglacials (50-70%), whereas glacial periods display lower values between 20-30%. The content of HMC steadily increases further downslope. At site M35042 the overall highest amounts in HMC are observed. In general the amount of HMC is lower during interglacial and higher during glacial periods, with maximum values during late stage 6. The content of LMC generally peaks during glacial times, and shows low amounts during interglacial periods. This pattern was observed in all cores along the submarine plateau off the northwestern margin of Pedro Bank. The quartz intensity shows higher intensities during glacial stage 2-4, 6 and 8. Interglacial quartz intensities are characterised by small amplitudes. The intensity of quartz in general mirrors the content of fine non-carbonates.

(A.3) Deep (1887-2520 m) and distal (72-92 km) cores - PC059 (Fig. 7.12) and PC100 (Fig. 7.13).
Although the sediments at sites PC059 and PC100 were deposited in depths exceeding 1800 mbsl the fine aragonite content still shows a well developed highstand shedding pattern. Interglacials are characterised by higher amounts of aragonite (30-55%), whereas glacials show lowest values between 5-25%. The aragonite signal shows a typical saw tooth pattern as known from the isotope curve. The HMC content in PC059 shows an increasing trend from the beginning of interglacials towards the end or the maximum of the next glacial. This results in higher HMC content during glacial periods, whereas interglacials show lower values. Both deep cores show a generally decreasing trend in the amount of LMC from the end of stage 8 towards the recent. Higher amounts of LMC (30-50%) are present in glacial periods (stage 6 and 8), whereas interglacial LMC contents vary between 10-30%, with lowest values during the Holocene. The content of fine non-carbonates and the quartz both show the same trends with highest amounts in glacials and interglacial substage 7.4.

(B) Upcurrent Sites

M35034 (Fig. 7.14), M35032 (Fig. 7.15) and M35052 (Fig. 7.16) from intermediate waterdepths (1214 - 1445 mbsl)
The temporal changes within upcurrent sediment cores from intermediate waterdepths will only be described in detail for M35052. Core M35034 recorded only limited time slice from the early stage 3 to the Holocene, whereas the stratigraphy for core M35032 is interrupted by numerous turbidite layers hampering a proper interpretation.
The content of fine aragonite in the bulk sediment of core M35052 displays a relative clear “highstand shedding pattern” from the Holocene to glacial isotope stage 6 with 25-30% for

Figure 7.8

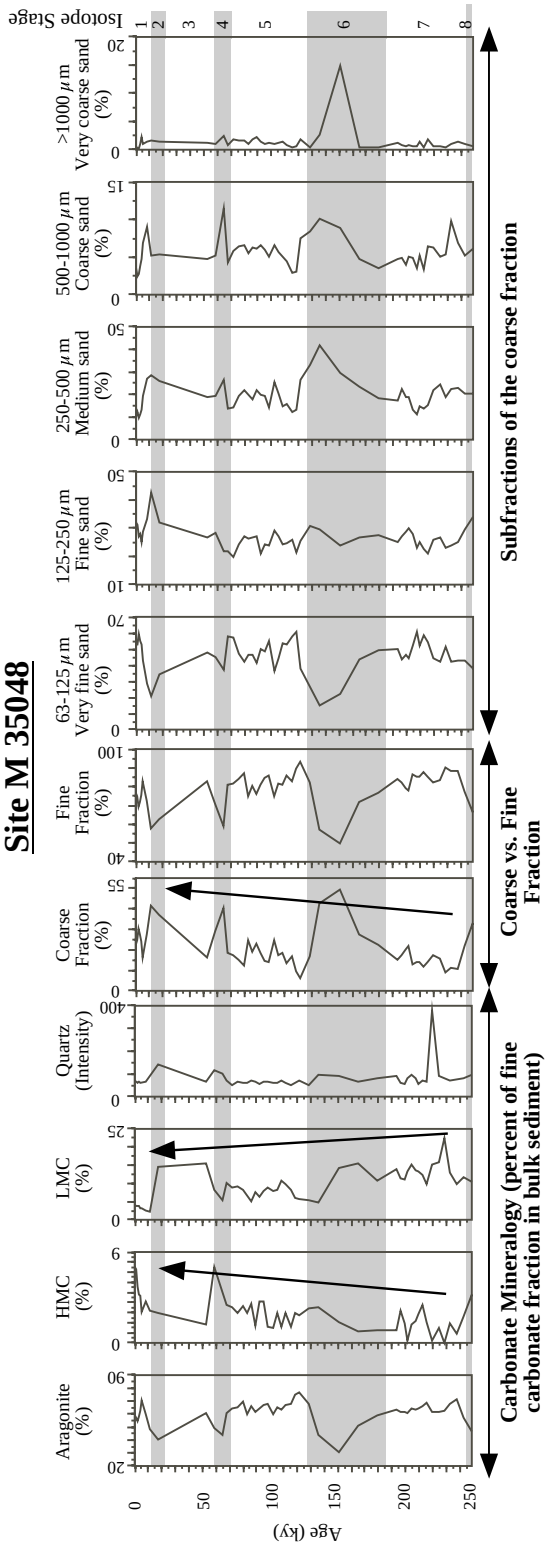

Figure 7.9

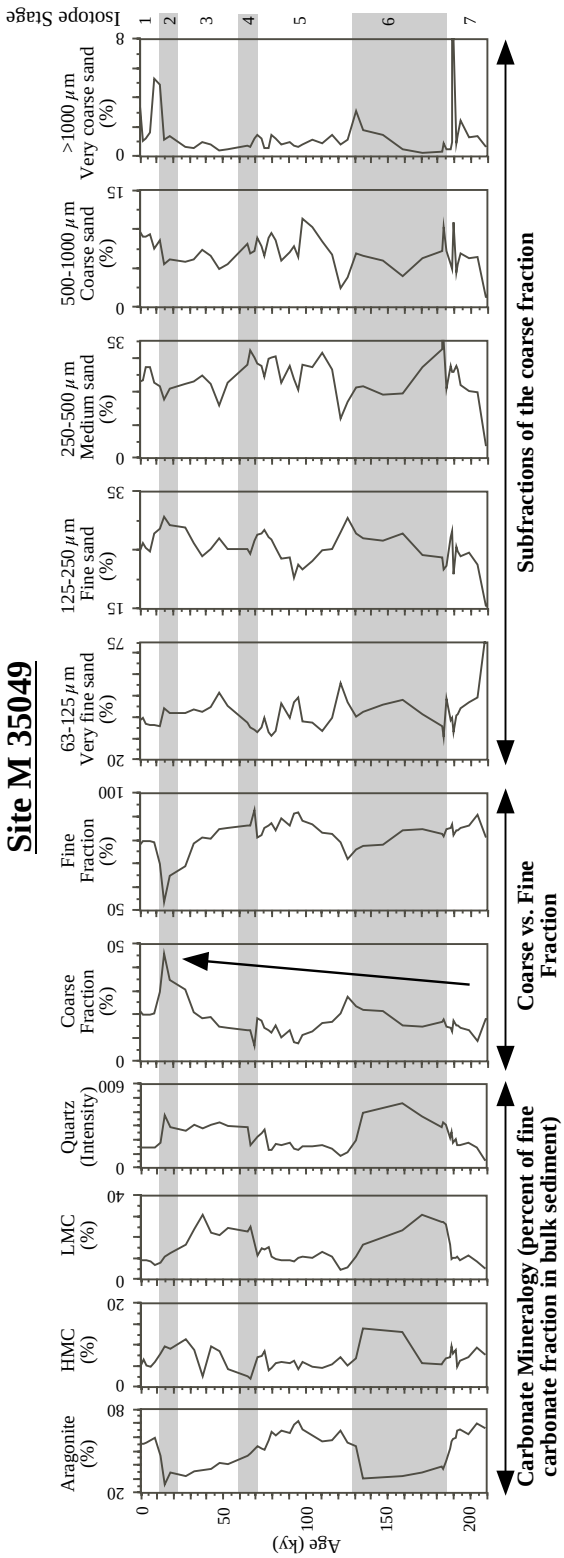

Fig. 7.8 and 7.9: Temporal variations of mineralogical and grain size proxies at proximal downcurrent sites M35048 (Fig. 7.8) and M35049 (Fig. 7.9). Long-term trends of single sediment proxies are indicated by arrows.

Figure 7.10

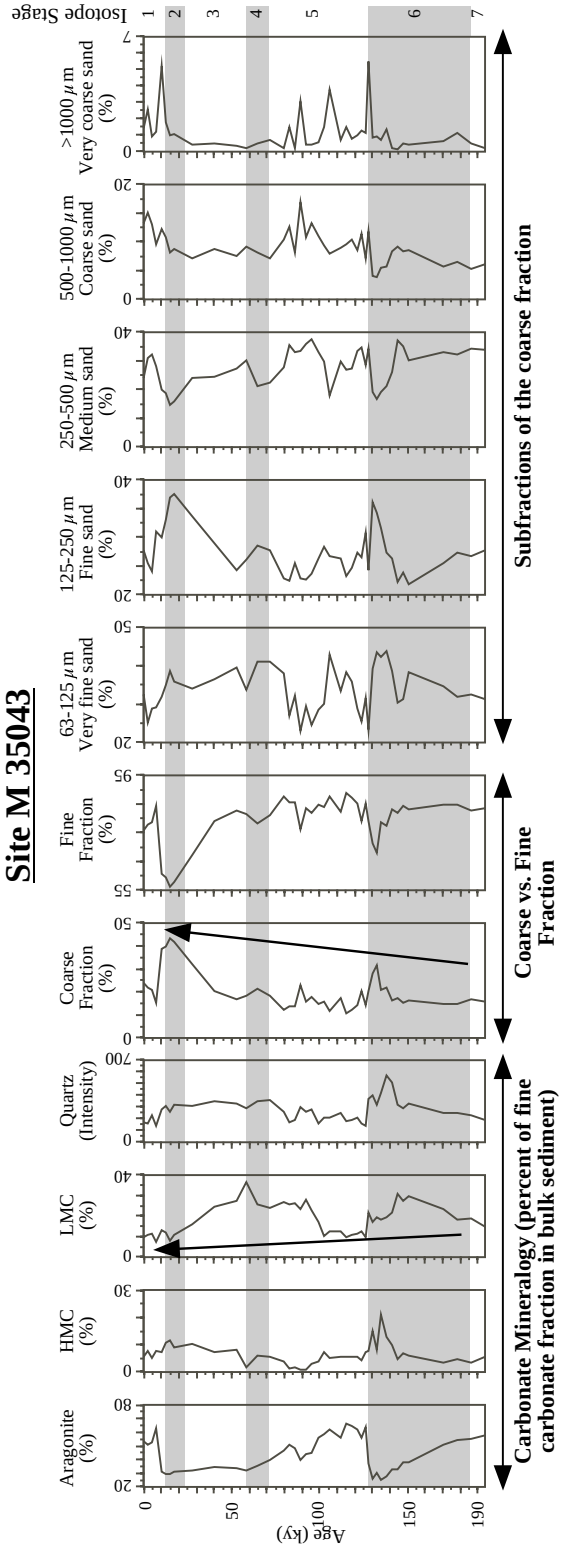

Figure 7.11

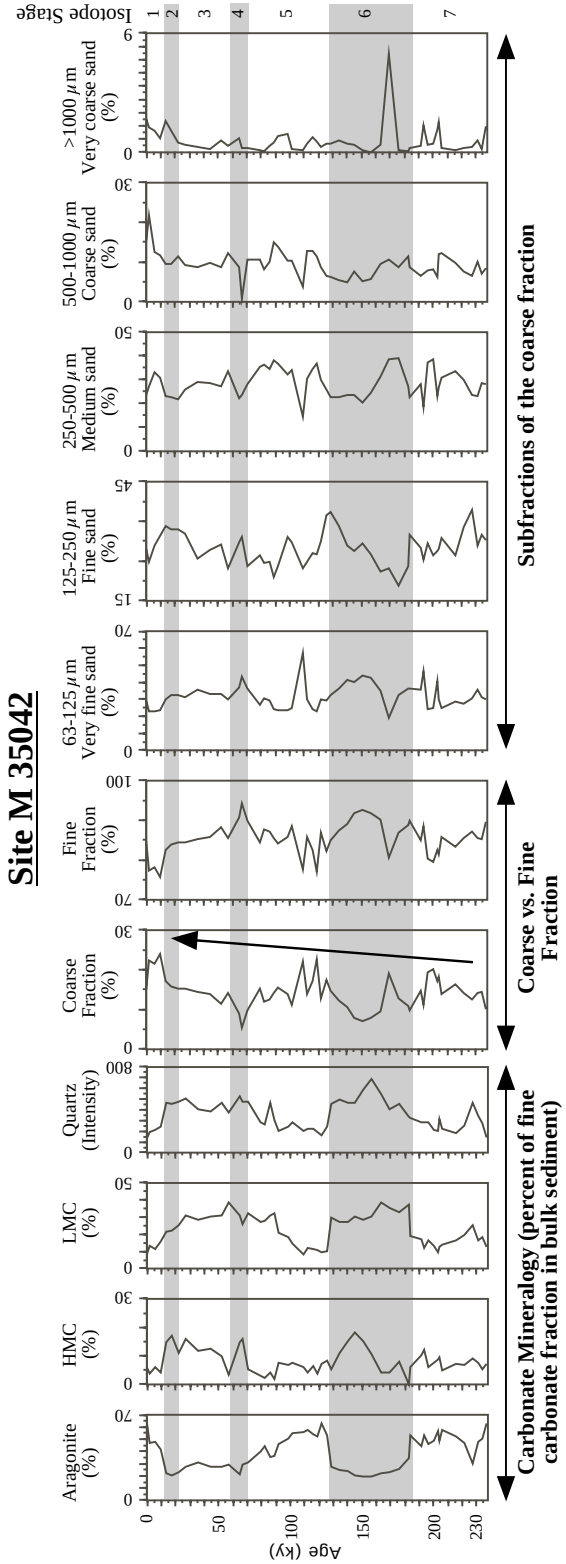

Fig. 7.10 and 7.11: Temporal variations of mineralogical and grain size proxies at intermediate-distanced, downcurrent sites M35043 (Fig. 7.10) and M35042 (Fig. 7.11). Long-term trends of single sediment proxies are indicated by arrows.

Figure 7.12

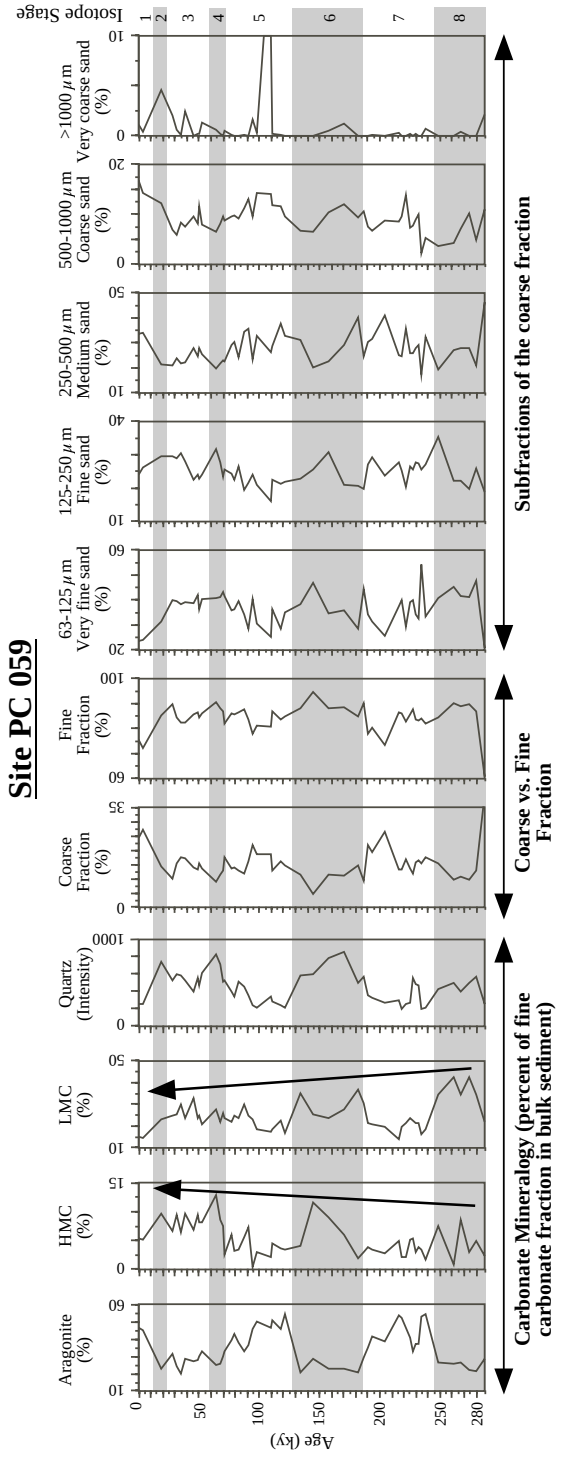

Figure 7.13

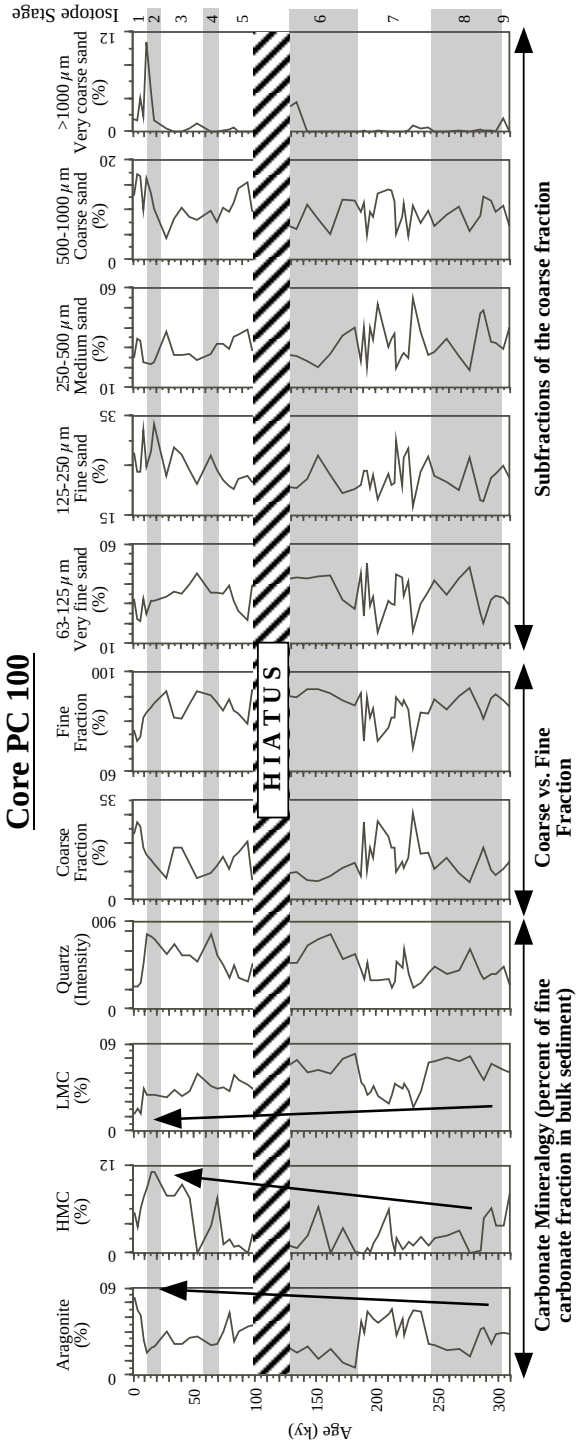

Fig. 7.12 and 7.13: Temporal variations of mineralogical and grain size proxies at distal downcurrent sites PC059 (7.12) and PC100 (7.13). Long-term trends of single sediment proxies are indicated by arrows.

interglacials and 10-15% for glacials, which are clearly lower than those observed on the downcurrent side of Pedro Bank. Sediments older than isotope stage 6 do not show a clear highstand/lowstand pattern, as the interglacial-glacial amplitudes are reduced to 10%. The content of fine aragonite during interglacials shows a decreasing trend from stage 1 to 9. HMC contents within core M35052 vary with higher amounts during glacials and at certain times during isotope stage 3. The LMC content within M35052 shows an overall decreasing trend from stage 9 to stage 1. The input variations of LMC do not show any clear link with glacial/interglacial periods. The intensity of fine quartz and of fine non-carbonates show low

intensities at the beginning of interglacials with an increasing trend towards the next glacial, and a generally decreasing trend from middle of stage 3 towards the recent. During the Last Glacial Maximum no strong peaks could be observed.

7.3.5 Temporal variability of single grain size proxys

During the analysis it became evident that, in contrast to the trends seen in the mineralogy, the trends and evolution of the observed grain size proxies are mainly controlled by offbank distance as well as local topography. Therefore the grouping of cores varies from that choosen for the mineralogical proxy data.

(A) Downcurrent Transect

(A.1) Proximal (<6 km) sediment cores - M35048 (Fig. 7.8)

In this proximal core high amounts of coarse fraction are observed during glacial periods (peaks of 40-50% coarse fraction content). Another general trend is a slight coarsening upward sequence within each interglacial. The fine fraction shows highest amounts during interglacials and almost mirrors the single events of the isotope stratigraphy. The analysis of the coarse fraction subclasses shows that the very fine sand fraction dominates during interglacial times with maximal amounts of 60%, whereas during glacial stages 2 and 6 lowest percentages (15-20%) are observed. The fine sand fraction shows major peaks in conjunction with stage boundaries, preferentially during transgressive phases in sea level. The very coarse sand fraction shows similar amounts of about 2.5% during interglacials and glacials. Only at 151 ky (isotope event 6.4) a sudden peak of 15% is apparent.

(A.2) Cores from intermediate offbank distance between 19-28 km - M35049 (Fig. 7.9) and M35043 (Fig. 7.10)

Both cores show a very similar temporal trend in the coarse fraction distribution. From the oldest sediments deposited in these cores towards the Last Glacial Maximum a long-term increase of the coarse fraction content is evident. A general glacial/interglacial cyclicity could not be observed, but major changes (of about 15-20%) occur near stage boundaries. The 63-125µm fraction in M35049 shows no clear glacial-interglacial cyclicity, but high abundances during interglacial isotope events such as 3.3, 5.1, 5.3, 5.5, 7.1 and 7.3 were observed. This trend is not visible in M35043, which shows maxima in the very fine sand fraction during glacial stages 2, 4 and late stage 6. Temporal changes of the fine sand fraction (125-250µm) in M35043 mirrors those seen for the very fine sand fraction. This is not evident in M35049, in which the 125-250µm fraction shows a different temporal pattern. A clear glacial-interglacial cyclicity is not visible. Both cores were probably deposited in more or less the same depositional environment, but already the two finest grain size subclasses show a very different temporal evolution. This shows the high variability of grain size proxies within periplatform sediments. The medium and coarse sand fraction shows the same trends in M35049. Contents are higher in interglacials and lower in glacials as well as during stage 3. The interval around the stage boundaries are those which display distinct changes (see stage 7/6 or 6/5 boundary). The subfraction changes in core M35043 differ significantly from those in M35049 with
(1) increased amounts at the very beginning of stage 5 (probably within the transgression) and (2) a high medium sand content during early stage 6, whereas the 500-1000µm fraction shows overall minimum values. While this fraction mainly contains planktic components, this variability probably results from changes in open ocean productivity of foraminifera and pteropods. The content of the very coarse sand fraction shows distinct peaks in both cores along the stage 2/1 and 6/5 transgression and several maxima (3-4%) within stage 5 of core M35043. One major peak occurs at the end of stage 7 (± event 7.1) in more proximal core M35049, but in general the very coarse sand fraction doesn´t show any glacial-interglacial variability.

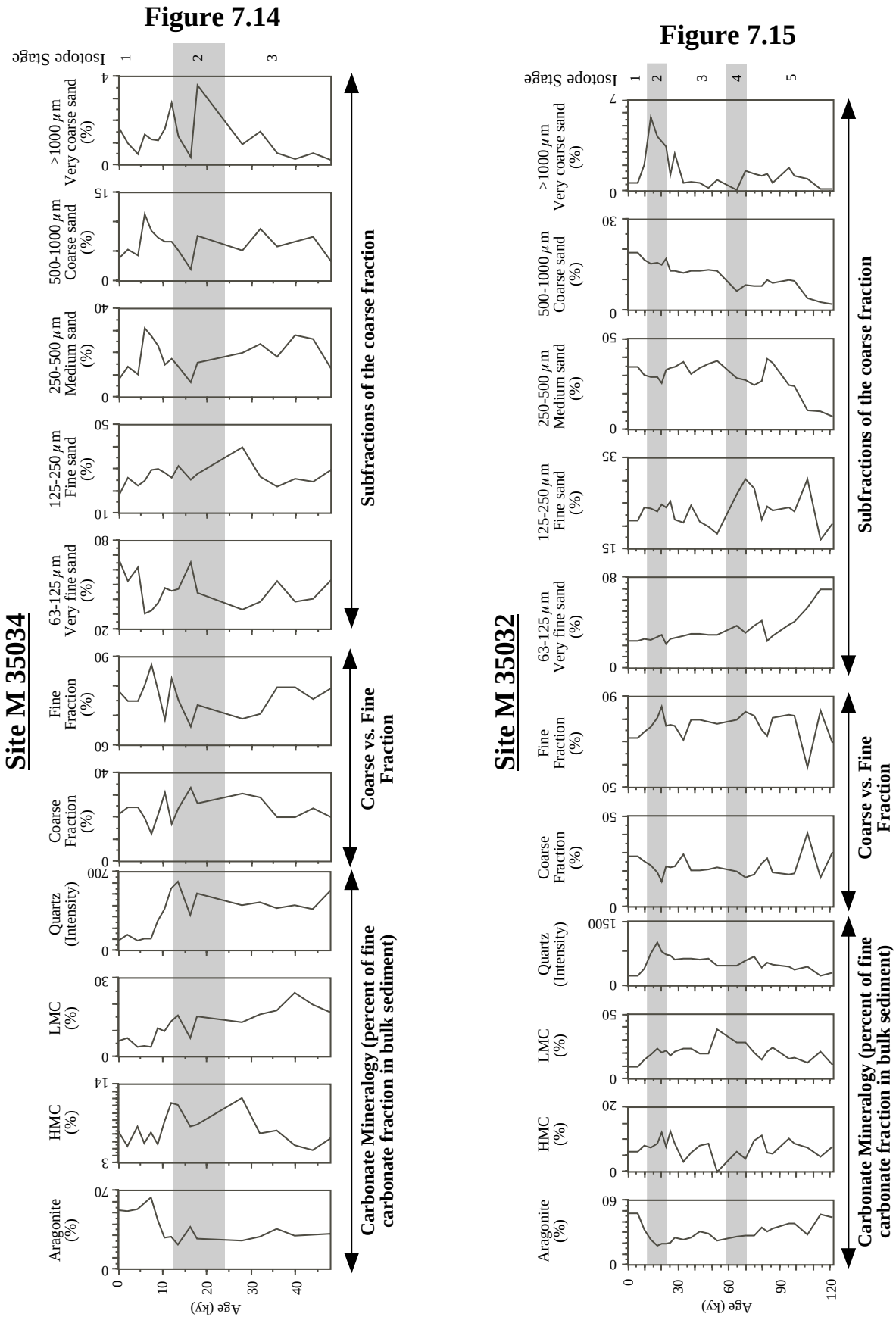

Fig. 7.14 and 7.15: Temporal variations of mineralogical and grain size proxies at upcurrent sites M35034 (Fig. 7.14) and M35032 (Fig. 7.15). Long-term trends of single sediment proxies are not evident due to the short stratigrahic range of these sediment cores.

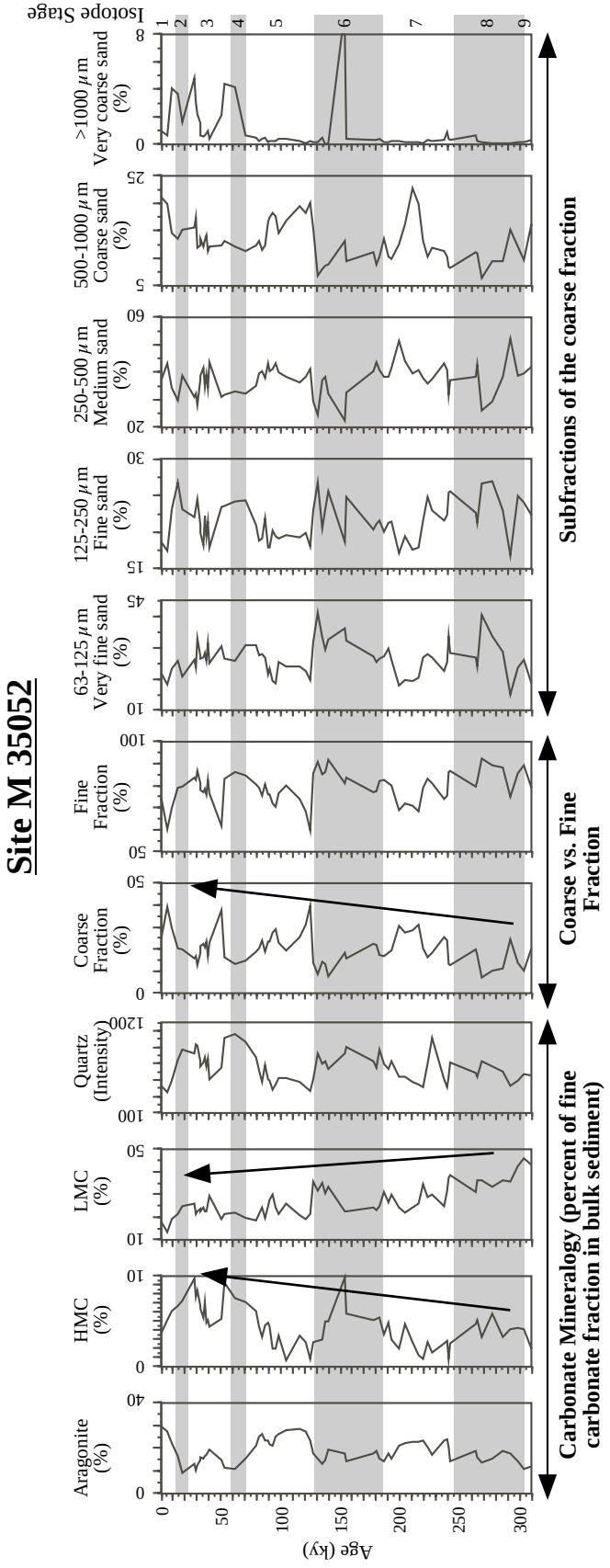

Fig. 7.16: Temporal variations of mineralogical and grain size proxies at upcurrent site M35052.
Long-term trends of single sediment proxies are indicated by arrows.

(A.3) Distal (42-92 km) sediment cores - M35042 (Fig. 7.11), PC059 (Fig. 7.12) and PC100 (Fig. 7.13)

The temporal variability of the coarse fraction is more or less similar within these three distal cores. Lower values can be found during glacial periods, whereas higher amounts and also a higher variability is evident during interglacial times. Interglacial amounts vary between 15-30%, glacials between 5-15%. Highest amount of ±30-35% are found within the most distal core PC100 during interglacial stage 7. The fine fraction content shows highest amounts during glacial stages 4, 6 and 8 and around isotope event 3.1 in PC059 and PC100.

At these 3 sites the very fine sand fraction displays slightly raised amounts during glacials. Each core shows its own temporal variability, which probably might be controlled by locally changing subbottom morphology of the Pedro Channel area (Cunningham, 1997). The same holds for the coarser subfractions. Each sediment core shows its own specific trend along single subfractions. An exception to this rule is given by the 250-500µm fraction with its lower amounts during glacial times and raised contents during interglacials. Distinct peaks can be observed in all cores (around 100 ky, 120 ky, early stage 6 (170-180 ky), 200-210 ky and 280-290 ky) indicating that sedimentation of this subfraction might be linked to open ocean productivity changes as the medium sand size fraction is mainly composed of planktic foraminifera and pteropod fragments.

(B) Upcurrent Sites

M35034 (Fig. 7.14), M35032 (Fig. 7.15) and M35052 (Fig. 7.16) from intermediate waterdepths (1214 - 1445 mbsl)
The temporal changes are only described in more detail for M35052, while M35034 (too short stratigraphic range) and M35032 (disturbed stratigraphy) do not provide detailed information with enough temporal resolution. The temporal variations in the coarse fraction of M35052 mirrors the isotope curve. The single subfractions, the 63-125µm and 125-250µm fraction, show very similar trends to those described for the fine fraction, whereas the 250-500µm and 500-1000µm fraction mirrors the trend displayed by the coarse fraction content. The very coarse sand fraction content is generally lower than 2% besides 4 major maxima of 4-10% occuring during glacial stages 2, stage 4 and at isotope event 6.4 (151 ky).

7.5 Discussion

Periplatform sediments off the northwestern and southern slopes and basins around Pedro Bank record the Quaternary cycles in their sedimentological and geochemical character. This was shown for the Walton Basin (Glaser & Droxler, 1993), Pedro Channel (Schwartz, 1996), as well as Serranilla Basin (Duncan, 1997). Schwartz (1996) and Duncan (1997) determined the controls on Quaternary cycles based on a variety of different sediment components. Schwartz (1996) showed that each sediment component can be used as a proxy for one or more oceanographic factors. As it can be deduced from this study the main controlling factors for sediment composition in the basins of the Northern Nicaragua Rise (NNR) are:
(1) pelagic and neritic production,
(2) dissolution of metastables constituents,
(3) the input of non-carbonates and
(4) the influence and the effects of oceanic currents.
Long term sedimentation trends of periplatform sediments in response to late Quaternary sea-level fluctuations and climatic changes have been extensively described for different basins of the NNR (Glaser & Droxler, 1993; Schwartz, 1996; Duncan, 1997). The interpretation of single sediment proxies under sedimentological and paleoceanographical aspects showed that slight differences can be observed when comparing different basins located on the eastern and western extensions of the NNR. The sediment cores analysed in this study confirm this picture both, in the northwestern transect as well as for upcurrent site M35052.
The main difference to previous studies on the NNR is the detailed investigation of a platform margin-to-basin transect on the leeward (downcurrent) margin. It provides a more detailed insight into the depositional processes and the spatial differences of periplatform sedimentation along the active margins of the Pedro Bank carbonate platform. The interpretation of such platform-to-basin transects are an essential requirement for the study of the response of sedimentary systems to sea-level changes (Eberli et al., 1997).

7.5.1 Long-term trends of mineralogical and grain-size proxies

(I) Neritic production
Neritic production is manifested in the sediment composition by the abundance of metastables carbonates like aragonite and HMC. Both can be used as proxies for sea level and sediment export, dissolution, and nutrients within the water column (Schwartz, 1996). Unfortunately the input of these components, such as aragonite, are controlled by more than one of the above mentioned factors, which makes the interpretation of these sedimentational and paleoceanographical proxies sometimes somehow speculative.
The content of fine (bank-derived) aragonite peaks at the beginning of interglacials (Figs.7.8 - 7.16). Thus, aragonite content mainly seems to be controlled by the flooding of the production sites, a pattern also found in sediment cores from Serranilla Basin (Duncan, 1997). Within cores from Pedro Channel an increase in aragonite contents was observed at the end of interglacials prior to stage 5 (Schwartz, 1996). One possible explanation for this pattern might be that sediment cores from the northwestern margin of Pedro Bank are all located within the main sediment export direction from the shallow bank top (Glaser, 1991), whereas the cores studied by Schwartz (1996) are not situated within such a basinal position. In addition,

corrosive intermediate water masses (NADW vs. AAIW) might have modified the input signal due to enhanced dissolution during interglacials (e.g. Haddad & Droxler, 1996; Schwartz, 1996). Possibly an oversaturation of aragonite is existent along the northwestern margin, which prevents or diminishes the dissolution effects of surface sediments. The content of fine HMC is an indicator for sea level fluctuations and/or preservation or dissolution of HMC (Haddad & Droxler, 1996; Schwartz, 1996). HMC originates from production on the bank top or from fine HMC cements formed at the seafloor (e.g. Schlager & James, 1978; Glaser & Droxler, 1993), and is more susceptible to dissolution at intermediate water depth than aragonite (Schlager & James, 1978; Walter & Morse, 1984). The long term trends in the content of HMC show distinct differences for the analysed cores:
(1) Shallow site M35048 (648 mbsl) shows a long-term increase in HMC from IS 8 to 1.
(2) Intermediate cores (893-1023 mbsl) display no general long-term change, but a more or less clear interglacial/glacial cyclicity, whereas
(3) sites from a depth exceeding 1445 mbsl (M35052, PC059 and PC100) display a long-term increase in the HMC-content since interglacial MIS 9 to the recent.
The trend observed in the proximal core M35048 might indicate a change within the production of HMC-organisms on top of Pedro Bank, i.e. a compositional change of biota. In what way biologically mediated dissolution of calcium carbonates above the chemical lysocline (Milliman et al., 1999) modified this long-term trend, remains unclear. However, the steady increase in the HMC contents points to an enhanced preservation of metastable HMC since isotope stage 8 in shallow sediments of M35048. The sediments deposited in water depth between 893-1023 mbsl, do not show any major variational trends in the input of metastable carbonates. The depositional depth of these cores is near to 1100 mbsl, a depth assigned by Glaser & Droxler (1993), Schwartz (1996) and Haddad & Droxler (1996) as the upper level from where partial dissolution of metastable carbonates starts in the basins on the NNR. Thus it is unclear why the fine aragonite and fine HMC content do not show any distinct long-term trends as observed in a variety of other sediment cores from intermediate waterdepths on the NNR (Glaser & Droxler, 1993; Schwartz, 1996). However, within the three cores M35049, -43, and -42 a similar cyclicity of the HMC signal could be observed, which seems to correlate with the preservation/dissolution cycles described by Haddad & Droxler (1996) for intermediate waterdepths in the Caribbean. In general these observed preservation/dissolution intervals were in good correlation to the results of Haddad & Droxler (1996) during the Holocene and glacial stages 2, 4 and 6 in all three cores. However, the preservation cycles proposed by Haddad & Droxler (1996) within interglacial stage 5 could not be identified in the HMC content of the new studied cores. Probably other factors that were used to calculate the "composite dissolution index" (such as pteropod abundance), were more influencing during stage 5. Therefore the HMC content alone might not be able to display these climatic induced changes of different intermediate water masses that seems to be mainly responsible for the preservation of dissolution of carbonates (changing entrainment of corrosive AAIW into the Caribbean and production changes of NADW; Raymo et al., 1990; Schwartz, 1996). Finally sediment cores deposited under the influence of intermediate and deep water masses (>1445 mbsl) exhibit a long-term increase in the content of HMC, which clearly show an increase in the preservation potential from stage 9 to the recent interglacial, a trend already observed by Schwartz (1996).

(II) Planktonic production - Nutrients and current winnowing
While fine calcite monitors the rain of coccoliths from the overlying photic zone the content of fine LMC can be used as a proxy for changes in surface water productivity (= nutrients) and the evolution of current strength (= winnowing) (Schwartz, 1996). Glaser & Droxler (1993) stated that during the last 200 ky current velocities in Nicaraguan Rise channels were increased due to the restriction of the seaways during lowered glacial sea level. Assuming a constant coccolith production (McIntyre, 1976; Glaser & Droxler, 1993), lower glacial than interglacial percentages and accumulation rates in fine LMC could be explained by sediment winnowing. In nearly all cores, except for M35049 and -42, in which no clear trend is visible, a long-term decrease exists in fine LMC input. This trend was also observed within shallow and deep cores from the Walton Basin (Glaser & Droxler, 1993), Pedro Channel (Schwartz, 1996) and Serranilla Basin (Duncan, 1997). This trend suggests increased current activity during the Late Brunhes Epoch (0-185 ky; Schwartz, 1996).
The coarse fraction content shows the following long-term trends: within cores from shallow and intermediate waterdepths (648-1445 mbsl; M35048-49-43-42 and M35052) an overall

long-term increase during the last 300 ky can be observed. The same trend was observed by Schwartz (1996) for cores from Pedro Channel and interpreted as a long-term increase in the availability of nutrients. This is based on the assumption that most of the coarse fraction of Pedro Channel sediments consist of planktonic foraminifera, and to a minor extent of pteropods. Thus, the accumulation and/or the percentage of the coarse fraction can be considered as a qualitative proxy for surface water nutrient flux (Schwartz, 1996), as calcitic planktonic foraminifera are not subjected to dissolution or winnowing because of their size. Dilution by fine bank-derived or siliciclastic input, as well as by the removal of fines due to current winnowing (Glaser & Droxler, 1993), might also play a role in modifying the relative percentages of the coarse fraction. Local upwelling along the bank margins or flooding of the shallow bank tops and thus increased productivity are minor causes for the aforementioned nutrient increase (Duncan, 1997). Major causes for these long-term trends are the changes in intermediate water masses and circulation pattern changes within the Caribbean, which ultimately reflect global changes in NADW production, AAIW entrainment into the Caribbean, and increased trade wind intensity along with glacial/interglacial climatic changes (Glaser & Droxler, 1993; Schwartz, 1996; Duncan, 1997).

(III) Non-carbonate input - current transport

The abundance of non-carbonates show a clear glacial-interglacial cyclicity with higher amounts during the glacial stages 2, 4, 6 and 8. One major exception to this rule is isotope event 7.4, an extreme sea-level lowstand within interglacial stage 7, with a sea level stand of about -80 mbsl (e.g. Haddad, 1994). In all cores a long-term increase in the content of fine non-carbonates could be observed. This increase during the last 200 ky may be related to the general decrease in fine LMC, which has been interpreted as a long-term current strengthening (Schwartz, 1996). Most of the non-carbonates orginate from the large South American rivers Orinoco, Magdalena and Amazon. These rivers preferentially shed large amounts of sediment into the Atlantic Ocean and the Caribbean Sea during glacial periods (Reid at al., 1996; Schwartz, 1996; Flood & Piper, 1997; Franz, 1999). So, the increased current transport might have been the main control shaping the input patterns of non-carbonates (Duncan, 1997). This is also supported by the fact that higher amounts of non-carbonates are found in the upcurrent cores, which are located closer to the sources of non-carbonates. This pattern is also evident in Serranilla Basin (Duncan, 1997).

7.5.2 Spatial variations in downcurrent core transect

The mineralogical and grain size parameters have been discussed in detail in chapter 6 on the base of averaged interglacial and glacial accumulation rates of single sediment parameters. The glacial-to-interglacial variability of those parameters shown in this chapter are based on the percentages and differ markedly in the spatial context (Figs. 7.2 to 7.7), particularly with regard to the observed variability in the proximal cores. The mineralogical data are shortly discussed, as the controls that steer the sediment mineralogical composition has been already discussed in detail in chapter 6 and preceeding chapter 7.5.1. More emphasis is taken for the discussion of grain size data, as this part of this study reveals new insight into the depositional controls of periplatform sedimentation. However, both, the spatial difference in accumulation rates (Chapter 6) as well as in the percentage of sediment proxies (this chapter), are described and discussed, as they might help in understanding the carbonate sedimentary environment.

(I) Mineralogy

The content of aragonite displays, as expected, highest percentages in proximal sites and lowest amounts at distal sites, and therefore shows the decreasing influence of the export of fine-grained neritic sediments with increasing distance from the carbonate bank. Similar patterns have been described for the Bahamian carbonate slopes (Rendle, 2000) as well as for basins surrounding Pedro Bank (Glaser & Droxler, 1993; Schwartz, 1996). This typical pattern is further shaped by the dissolution of metastable carbonates, which starts at depths exceeding 1100 mbsl during interglacials (Glaser & Droxler, 1993; Chapter 6; see Fig. 6.6c). In general the spatial distribution pattern of aragonite along the northwestern transect shows that the input of bank-derived aragonite overrules the dissolution effects during interglacials in the main direction of sediment export from shallow Pedro Bank. The controls on the dissolution of metastable carbonates have already been described in chapter 6.4 (influence of varying intermediate water masses). HMC is an indicator for offbank transport in proximal cores and at

the same time is an indicator for dissolution of metastable carbonates in sediments deposited at intermediate waterdepths during interglacials (see Chapter 6.4). The exceptionally low average percentage during interglacials at site M35034 might indicate (1) the low export potential of HMC biota, (2) the dilution of HMC by the high amounts of aragonite or (3) the existence of dissolution of calcium carbonate in the upper 500-1000m of the ocean (Milliman et al., 1999).
Both, interglacial and glacial percentages show a spatial increase with greater offbank distance along the transect, which culminates in about 1000 mbsl (site M35042). This pattern is more pronounced during glacials (Fig. 7.17), apparently due to better preservation of HMC at intermediate waterdepths during these periods (Haddad & Droxler, 1996; Schwartz, 1996). The apparent drop in HMC content at distal sites, where sediments were deposited in waterdepths exceeding 1880 mbsl, can be attributed to an increase in dissolution of metastable carbonates below 1800-2000 mbsl (Chen, 1968; Droxler et al., 1988b). Fine LMC mirrors the content of calcitic nannoplankton in the study area (Schwartz, 1996). The general increase of LMC during interglacials and glacials with greater offbank distance reflects the increasing pelagic, and decreasing neritic influence in the mineralogical sediment composition. The percentage of fine non-carbonates shows a similar pattern to LMC with a general percentage increase with greater offbank distance. During glacials this trend is more pronounced due to the preferential input of non-carbonates during these periods (Bowles & Fleischer, 1995; Glaser & Droxler, 1993; Schwartz, 1996).

(II) Grain sizes

In previous studies grain-size variations were primarly described from the siliciclastic environment and used to understand depositional processes and environments (Boggs, 1987 cum lit.). In the carbonate environment, preferentially in ancient carbonate rocks, grainsize is described very broadly using the classification of Dunham (1962), which combines the grain type and the texture, but gives no exact measurement of the grain size. In recent times studies on the evolution of carbonate platforms used the grain-composition, but not grain-size, as an important source of information (e.g. Haak & Schlager, 1989; Reijmer et al., 1992).
Within the carbonate depositional realm the content of the coarse fraction was mainly used in pelagic sediments to obtain knowledge on paleoceanographic changes in the ocean, such as changes in planktonic surface productivity (e.g. Lynts et al., 1973; Prell, 1978; Glaser & Droxler, 1993) or as an indicator for dissolution (Bassinot et al., 1994). Only in recent times more information became available, at least on the content of coarse fraction, for modern periplatform sediments from the Northern Nicaragua Rise periplatform environments (Triffleman et al., 1992; Glaser & Droxler, 1993; Schwartz, 1996; Duncan, 1997) and the Bahama Bank (Westphal, 1997; Rendle et al., 2000).
These studies showed that during highstands in sea level (interglacials) most of the sediment export, preferentially of fine-grained sediments, takes place from the shallow-water carbonate banks (Droxler & Schlager, 1985; Reijmer et al., 1988; Glaser & Droxler, 1993; Schwartz, 1996; Duncan, 1997), while lower accumulation is evident during glacials in the periplatform environment (Droxler & Schlager, 1985; Reijmer et al., 1988; Glaser & Droxler, 1993; Schwartz, 1996; Duncan, 1997; Kendall & Schlager, 1981). The glacial/interglacial spatial evolution of the coarse fraction and coarse subfraction contents shows the large influence of offbank transport on the periplatform sedimentation during interglacials and the impact of gravity-controlled sedimentation (and other paleoceanographical parameters) on the slopes of Pedro Bank during glacial times. This results in the forementioned dominance of the fine fraction during interglacials, whereas during glacial sea level lowstands there is a tendency to coarser sediments, at least at proximal sites.

Interglacials

The study of the coarse fraction content along the northwestern offbank transect reveals no major changes during highstands in sea level (Figs. 7.4 and 7.17). This low spatial variation probably indicates the high export potential of fine-grained sediments from the downcurrent (leeward) margins of Pedro Bank described by Glaser & Droxler (1993) and the consistent (high) surface water production of coarse pelagic components (Prell, 1978; Glaser & Droxler, 1993). These findings agree with those by Hine et al. (1981a, 1981b) and Rendle et al. (2000) describing the leeward bank margin of GBB, although the dominant factor for the dispersal of shallow-water sediments at the GBB is the main wind direction (Wilber et al., 1990), whereas within the study area the Caribbean Current steers the sediment dispersal on the slopes and

within the basins (Glaser & Droxler, 1993; Schwartz, 1996). The small differences that are evident in the coarse to fine fraction percentages along the transect (Figs. 7.6 and 7.17) might be modified by local factors such as the position of the sites relative to platform, local topography, or surface and bottom currents (e.g. Mullins et al., 1980). Other factors that might lead to a similar dominance of the fine fraction along the entire downcurrent transect are, (1) resedimentation of fine fraction sediments from the upper slope or result (2) from offbank transport by possible "density cascading" as known from the GBB (Wilson & Roberts, 1992, 1995).
Within the coarse fraction itself a distinct change in the coarse fraction subdivisions occurs in a spatial context during the interglacials. Whereas in both proximal sites M35048 and -49 normal sorting is evident (decrease in percentages of each coarser grain-sized subdivision; Fig. 7.6), this pattern changes at sites further downslope to a more bimodal distribution with maximum percentages in the very fine sand and medium sand fraction (Fig. 7.6). This change might show the change from a generally bank-input controlled sedimentation at the proximal sites to a mixed neritic/pelagic sedimentation at distal basinal sites.

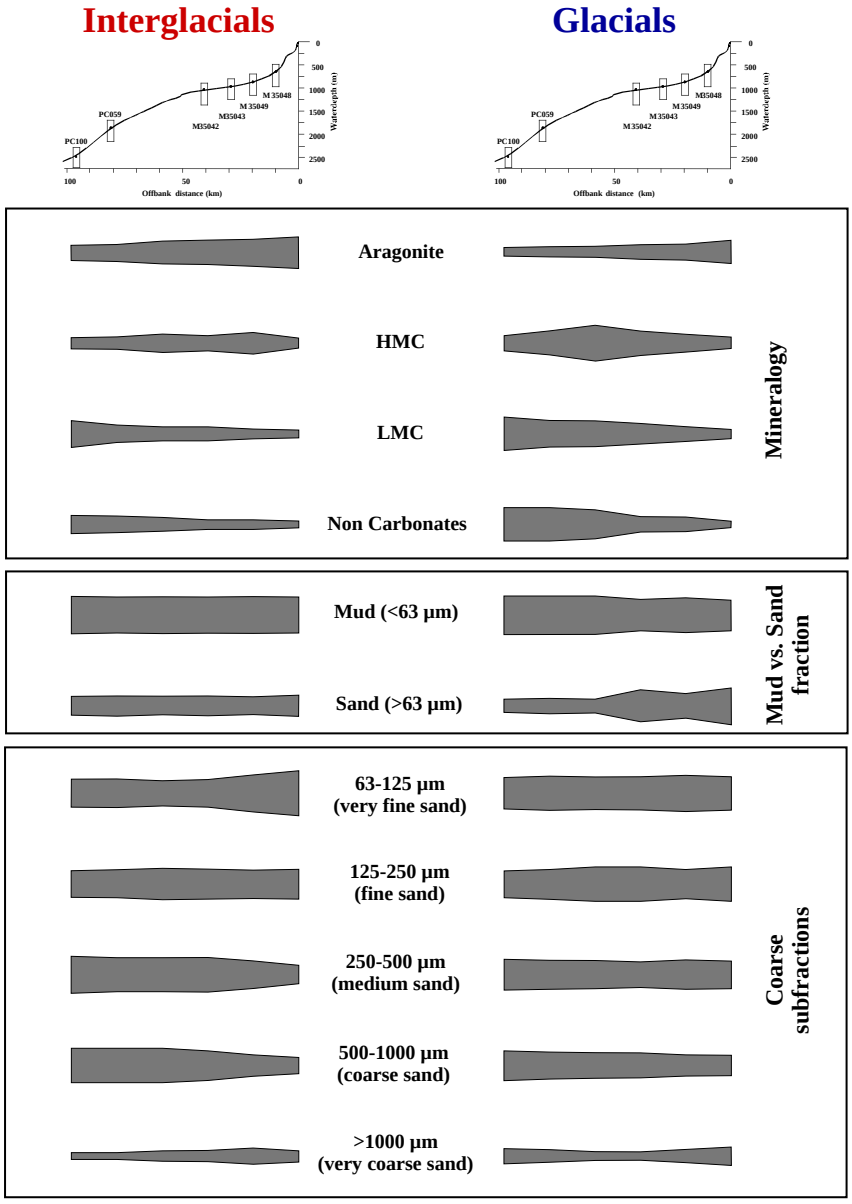

Fig. 7.17: General overview on the spatial variations of mineralogical and grain-size proxies along the downcurrent offbank transect. The scale of the bars shown are displayed using the same relative scale for interglacials and glacials for each component. The variations are based on the data displayed within Figs. 7.2 - 7.7.

Glacials

During sea level lowstands the proximal sites (<30 km; M35048/-49/-43) from 648-975 mbsl exhibit highest coarse fraction contents of up to 34% (M35048), while the distal sites (>40 km; M35042/PC059/PC100) show lowest glacial coarse fraction percentages (Figs. 7.4 and 7.17). The concentration of coarse sediment is therefore more significant during glacials. The high

percentage in the proximal site M35048 can be mainly attributed to current winnowing and related removal of fine sediment constituents at shallow sites due to enhanced flow of the Carribean Current (Glaser & Droxler, 1993). Glaser (1991) estimated that about 75% of the fines deposited during glacials above 600 mbsl have been removed by bottom currents, which explain the observed overall highest coarse fraction content at site M35048 from 648 mbsl. Compressed worldwide climatic belts and increased wind regimes, which intensified ocean circulation (Mullins et al., 1980) lead to an increase in bottom currents during glacials in the Straits of Florida, which caused a similar increase in the coarse fraction content at leeward sites of the GBB during glacials (Rendle et al., 2000). Higher glacial coarse fraction contents in more proximal sites have been also confirmed by Westphal (1997) for Pliocene slope deposits at the GBB. Also the spatial distribution at the leeward margin shows a similar decrease in the coarse fraction with greater offbank distance (Rendle et al., 2000).
Another major sedimentary process that could have caused the higher coarse fraction contents within shallow and particularly proximal sites near Pedro Bank is the erosion and reworking of upper slope deposits along with major trans- or regressions as well as during extended sea level lowstands (e.g. Shanmugan & Moiola, 1982, 1984). Although this pattern is mainly observed in siliciclastic environments (Emery, 1996), it should not be neglected along carbonate slopes (see Chapter 8; indications of reworked clasts in M35034 turbidites). During times of lowered sea level, upper slope deposits were eroded by a variety of processes, e.g. wave action, subaerial erosion or karst phenomens (Cook & Mullins, 1983; Sarg, 1988; Cook & Taylor, 1991). Bypassing of the upper slope (Ginsburg et al., 1991) may also be responsible for the overall higher glacial coarse fraction content up to a distance of 30 km. The irregular, tectonically-derived seabottom morphology along the northwestern slope-to-basin transition at Pedro Bank (see Chapter 5) might enhance bypassing of coarser glacial deposits downslope as far as site M35043. These bypass-slopes have been recognised along the GBB (Schlager & Ginsburg, 1981; Ginsburg et al., 1991). Due to steepening of the slope angle depositional slopes change gradually into bypass-slopes, and finally become erosional slopes (see classical Fig. 10 in Schlager & Ginsburg, 1981). Foreslopes research (Dullo, 1997; Chapter 5) shows that the morphology of the northwestern Pedro Bank slope probably displays a bypass slope.
These reworking processes appears preferentially along with gravity-induced transport mechanisms. However, turbidites leave their coarser load further upslope, whereas in more distal parts of the basin, preferentially the fine endtails of turbidites are deposited (Eberli, 1991). The lithology and the composition of calciturbidites in periplatform sediment cores off Pedro Bank confirms this picture showing that in distal cores M35042, PC059 (and PC100) fine-tail turbidites prevail, whereas in cores further upslope the grain composition shows a tendency to coarser grain sizes (see Chapter 10).
The subdivisions of the coarse fraction in glacials along the downcurrent transect displays a normal sorting pattern in almost all cores, i.e. a decreasing content of each consecutive subfraction with increasing grain size. This indicates that similar depositional processes act at all sites, except for the most distal site PC100 in central Pedro Channel, which shows a bimodal distribution with grain size maxima in the very fine sand and the medium sand fraction, probably showing a different depositional environment with different sediment sources within central Pedro Channel. The peak of very fine sand probably reflects the input of fine neritic material and/or fine pelagic rain, whereas the peak in the medium sand fraction can be attributed to the high input planktic foraminifera and pteropods, which are most common within the 250-500 µm fraction.

7.5.3 Sedimentological response of Pedro Bank flooding during interglacial highstands in sea level - in particular during isotope stage 3

The research on the sea level history during the late Quaternary has come up with various new estimates on the sea level during the last interglacial maximum (isotope event 5.5 = 122 ky) and marine isotope stages 9 and 11. Only minor research has been done on estimating sea level stands during interstadial isotope stage 3. So far, various estimates on stage 3 sea level have been published, which are based on coral datings, tectonically stable or tectonically uplifted coral terraces, on reconstructions of sea levels using combined planktic and benthic $\delta^{18}O$ values, as well as on geochemical analysis such as amino acid racemization (Table 7.3). The interstadial sea level data were yielded from various parts of the world, including Bermuda, Bahamas, Barbados, the Indopacific and Australia and range between -20 mbsl and -80 mbsl during the entire stage 3 (Table 7.3).

The modern physiography of the Pedro Bank platform exhibits a deepening from the southern to northern margins (Dolan, 1972). The author mentioned various areas around the entire Pedro Bank that were as deep as 40-100 m below present sea level (Fig. 2.2). Submersible dives of Dullo (1997) observed the flat bank top of Pedro Bank to start at about 60-70 mbsl at the northwestern margin, confirming these earlier findings (see Fig. 5.4). These parts of Pedro Bank could have flooded during this interstadial stage sea level stands, bringing these parts of the platform into the zone of maximum or at least enhanced carbonate production (Bosscher, 1992). The overall high aragonite content of 61% in the bulk sediment at most proximal downcurrent site M35048 during event isotope event 3.3 (probably the highest sea level stand during stage 3), and the sudden and massive drop in the aragonite content at site M35049 might also be an indicator for a limited production on top of Pedro Bank during the early part of stage 3 (Fig. 7.2).

Locality/Source	Sea level and timing	Reference
Huon Peninsula, New Guinea	-45 to -55 mbsl during 51-36 ky	Chappell (1983)
Bermuda	below -20 mbsl during 34-43 ky	Harmon et al. (1983)
Huon Peninsula compared to equatorial Pacific core V19-30	-44±2 mbsl at 28 ky -41±4 mbsl at 40 ky	Chappell & Shackleton (1986)
Recalculation of isotope values	-40 to -50 mbsl during early stage 3	Labeyrie et al. (1986)
Benthic & planktic $\delta^{18}O$	-50 to -70 mbsl during entire stage 3	Shackleton (1987)
Bass Basin, S. Australia	above -66 mbsl at 30 ky	Blom (1988)
Gulf of Carpenteria	between -40 to -55 mbsl at 54-36 ky	Jones & Torgersen (1988)
Gulf St.Vincent, S. Australia	-22 to -30 mbsl during 45-30 ky	Murray-Wallace et al. (1993)
Benthic & planktic $\delta^{18}O$	approx. 65-70 mbsl at 53 ky	Haddad (1994)
Red Sea	above -65 mbsl in <64 ky	Gvirtzman (1994)
Huon Peninsula	-40 to -60 mbsl at 53 ky -60 to -80 mbsl during <53 ky	Chappell et al. (1996)

Table 7.3: List of published interstadial sea levels during oxygen isotope stage 3 in chronological order (updated list from Murray-Wallace et al., 1993).

Also upcurrent core M35052 is characterised by an extremely raised sedimentation rate during isotope stage 3 (see chapter 4). At the southeastern part of Pedro Bank a remarkable part of the Pedro Bank top is situated in 40-100 mbsl (Dolan, 1972). During stage 3 sea level stand estimates range from -40 to -50 mbsl on average (Table 7.3). These "deeper" parts of Pedro Bank obviously produced remarkable amounts of neritic sediments that can be observed in M35052 (Fig. 7.16). In addition a turbidite layer can be observed shortly after this first interstadial "highstand" in sea level at 53 ky (see Fig. 4.8 and Chapter 10). This turbidite might indicate a first increase in production and export from the bank top, which initiated this gravity-induced transport of sediment further downslope due to overloading of the upper slope and subsequent slope failure. Turbidites are also present during the same part of early stage 3 in PC073 from the southeastern margin of Pedro Bank, further northeast of M35052 (Glaser, 1991), where this deeper terrace is also evident. Both early stage 3 turbidites contain well preserved bank derived biota (Glaser, 1991; Chapter 8), confirming flooding of certain areas of Pedro Bank during stage 3. Core PC016, located in a similar relative position off the southwestern margin of Pedro Bank, where margins of PB lack deeper terraces, do not show any evidence for early stage 3 turbidites or enhanced sedimentation.
A stage 3 flooding of Pedro Bank thus can be substantiated by the existence of further early stage 3 turbidites and by mineralogical evidence from downcurrent periplatform sediment cores as earlier suggested by Glaser (1991). The existence of deeper terraces found in water depths of 60 to 90 mbsl is also known from the Red Sea (Brachert & Dullo, 1990; Gvirtzman, 1994; Dullo & Montaggioni, 1998) and the foreslopes of the island of Mayotte (Dullo et al., 1998). There reef growth also subsequent carbonate production has been assumed during interstadial MIS 3 by Emmermann (2000) based on microfacies and turbidite analyses.

Lagtimes between sea-level and sediment export proxies

During platform flooding a lagtime occurs between highstands in sea level and high production and export of neritic sediment. Emmermann et al. (1999), comparing Red Sea and Pedro Bank periplatform cores, observed small lagtimes at flat-topped platforms, such as Sanganeb Atoll,

and larger lagtimes at Pedro Bank with its inclined bank top. Observations from St. Croix (Adey, 1987), Florida (Shinn, 1980; Shinn et al., 1989) and the Great Barrier Reef (Davies & Montaggioni, 1985) show the existence of a lag time between flooding of old substratum and reef initiation of up to 2500 years. In addition to this reef initiation lagtime further time lags will occur through delayed sediment production on top of a platform and the time that is needed to fill up available accomodation space, before sediment export starts (Emmermann et al., 1999). If other processes influence the differences seen between the oxygen isotope signal and the aragonite content, such as dissolution of metastable carbonate phases above the lysocline (Milliman et al., 1999) or at intermediate waterdepths (Droxler et al., 1988a, 1988b; Droxler et al., 1990; Haddad & Droxler, 1996; Schwarz, 1996), cannot be resolved within this study and needs further detailed studies.
A closer look at cores PC108 and PC035 in downcurrent position to Pedro Bank (Glaser, 1991), validate the interpretation given by Emmermann et al. (1999). Highest amounts in neritic aragonite content show, at least during stage 3, a lagtime in cores PC108 and PC035. Lightest isotope values indicate a highstand in sea level, which is then followed, with a distinct offset in core depth, by maximum input of metastable neritic carbonates. This sequence of processes probably reflects the time needed by the shallow water environment to start production and the adjustment of the biota to the new conditions on top of the carbonate platform (Tipper, 1997). A similar pattern could be described for core M35049 (Emmerman et al., 1999) for interstadial highstand at about 51 ky (isotope event 3.3). In addition, lagtimes existed, in which the aragonite signal preceeds the highstand in sea level as indicated by the oxygen isotope values. This might be attributed to the inclined platform morphology of Pedro Bank (Emmermann et al., 1999). The deep northwestern bank margin (up to 60 mbsl) was probably flooded several thousand years earlier during the major transitions in sea level from full glacial to full interglacial conditions. Correlating sea level curves from Jamaica (Digerfeldt & Hendry, 1987) and Barbados (Fairbanks, 1989), Glaser (1991) could show that already at 10 ky parts of Pedro Bank were flooded by an average of 5 m to 10 m of water, and thus could probably produce recogniseable amounts of neritic carbonates.

7.6. Conclusions

The analyses carried out on several periplatform cores in the surrounding of Pedro Bank showed that characteristic depositional environments during the last 300 ky could be determined based on mineralogical and grain-size studies, both through time and space. The analyses showed in which way the export of neritic sediments developed and interacted with the pelagic and siliciclastic input as a result of late Quaternary climate variations and sea-level fluctuations. One major outcome of this study is the temporal and spatial evolution of mineralogical and grain-size proxies along a 92 km long transect at the northwestern edge of Pedro Bank, the side of main sediment export from the platform top.

Previous research of Glaser & Droxler (1993) and Schwartz (1996) in the vicinity of Pedro Bank could be substantiated. The sediment deposition and composition therefore is strongly controlled by four main factors, which have been already outlined by the forementioned authors: (1) pelagic and neritic sediment production, (2) dissolution of metastable sediment constituents, (3) the input of non-carbonates and (4) the influence and effects of ocean currents. In addition, this study clearly shows that seafloor morphology (Chapter 5) might also play an important role for the distribution of the sediments.

The spatial variability of periplatform sedimentation as seen through the combination of mineralogical and grain-size data along the leeward margin of Pedro Bank is a valuable approach to determine the response of the neritic platform environment to climate and thus sea-level changes and their export pattern to the slopes and basins. The spatial distribution along the leeward, downcurrent margin shows a distinct pattern:

1. During **interglacial highstands in sea level** the fine sediment fraction (<63 µm) dominates periplatform sediments along the entire leeward transect and no spatial variations in the concentration could be observed. The sediments are mainly of neritic origin, preferentially fine aragonite needles, therefore aragonite dominates the mineralogy of the sediments within a

distance of 40 km from the margin. Further downslope aragonite is still the most abundant mineral, but the percentage decreases obviously, while the pelagic carbonate mineral content increase. Within the subordinate coarse fraction classes (>63 µm) the very fine sand fraction dominates only at proximal sites (<20 km), due to the influence of fine neritic sediments shed offbank. More distal sites (>20 km) show a more bimodal distribution pattern in the coarse grain sizes with maximum amounts within the very fine sand and the medium sand fraction. This indicates a mixed neritic/pelagic signal. Due to the dominance of fine-grained sediments at all sites along the transect the interglacial sediments have a low diagenetic potential as a result of low permeability, which has been observed for similar periplatform sediments along the leeward margin of the Bahama Bank (Westphal, 1997; Rendle, 2000).

2. During **glacial lowstands in sea level** a twofold division in the spatial distribution of the periplatform sediments is evident. A proximal environment (<28 km) with enhanced coarse fraction percentages vs. a distal environment (> 28 km) showing a strong dominance of the fine fraction (> 90%). The raised coarse fraction content at proximal sites is the result of various interacting processes: (1) lower input of fine neritic sediments, (2) increased current winnowing, and (3) redepositional processes at the upper slope during lowered sea-level stands, and the export of this material to "proximal basinal" sites (< 28 km). These glacial sediments, therefore, also have a higher diagenetic potential. In the subordinate coarse fraction classes a similar distribution pattern is found at all sites. This might show the low neritic influence, and a similar influence of pelagic sedimentation at all sites during glacials. One exception in this spatial distribution has been observed in the mineralogy of sediments at most proximal site M35048. There a very high content in aragonite during lowered interstadial sea level stands of MIS 3 might be indicative for enhanced neritic production at the top of Pedro Bank. This production might be possible due to the inclined bank top morphology with it´s deepest parts at the northwestern edge. In general the mineralogy of glacial periplatform oozes is dominated by LMC and non-carbonates, especially at more distal depositional sites. Also HMC shows clearly raised percentages, which might be the results of enhanced preservation or the formation and redeposition of HMC-rich submarine cements.

At upcurrent sites a clear spatial distribution pattern cannot be seen, but in general the mineralogy displays a similar spatial evolution as seen along the downcurrent margin, but with overall reduced amounts. This is due to the lower export potential of the platform regime against the main direction of the Caribbean Current, one important factor for neritic sediment dispersal in the study area. The coarse fraction content is slightly higher during interglacials compared to the downcurrent margin, showing the different sediment composition between the up- and downcurrent margin (Chapter 8). During glacials a similar percentual reduction is evident in a spatial context, but in general the percentage is lower than at proximal, downcurrent sites. This also substantiates the lower export and redeposition potential of the upcurrent margin.

As grain size and mineralogy data of the sediments describe the nature of the periplatform sediments only to a certain extent, it is also important to obtain knowledge on the composition of the coarse grain fraction. This is much more important in the carbonate environment, where grain-sizes are also influenced by a "biological growth factor". To understand both data sets in the context of climate and sea-level fluctuations it is necessary to know the origin of these grains (skeletal vs. non-skeletal, neritic vs. pelagic). These analyses are shown in chapter 8, but in general it can be stated that the coarse sediments are dominated by planktic foraminifera and pteropods, and only to a minor extent by bank-derived grains.

Finally, lagtimes between sea-level and sediment export proxies (e.g. $\delta^{18}O$ vs. aragonite) were observed within several sediment cores from the surrounding of Pedro Bank (this study and Glaser, 1991). These lagtimes might be due to the inclined bank top morphology, which results in a different timing of bank-top flooding of Pedro Bank. This pattern could not be observed in all cores, which might be the result of a variety of other postdepositional processes affecting the sediments to a varying degree such as (1) early diagenesis, (2) relative position to the bank margin, (3) seafloor morphology and (4) syn- and postdepositional dissolution of metastable carbonates.

CHAPTER 8

SEDIMENT COMPOSITION OF PERIPLATFORM SEDIMENT AND CALCITURBIDITES OFF PEDRO BANK

8.1 Introduction

The identification of skeletal and non-skeletal sediment constituents in periplatform sediments and calciturbidites is known as a useful tool to record environmental and ecological changes on the top of carbonate platforms (Haak & Schlager, 1989; Reijmer et al., 1992) and other shallow water carbonate systems, e.g. the Bay of Safaga, northern Red Sea (Piller & Mansour, 1990). The visual inspection of certain subclasses of the coarse fraction forms another useful tool to determine sediment composition and their spatial and temporal variability (Sarnthein, 1971; Piller & Mansour, 1990). Both techniques were applied to sediments retrieved from the deep basins surrounding the Pedro Bank carbonate platform. This platform is situated on the Northern Nicaragua Rise, a huge carbonate province extending from the Nicaraguan and Hondurian shelves in the west, to the mixed siliciclastic/carbonate shelf of Jamaica in the east.
The work of Dolan (1972) dealt with the genesis and distribution of recent sediments found on top of the Pedro Bank carbonate platform. This work forms the basic knowledge on the composition of the sediments on top of Pedro Bank.
Using a descriptive sedimentological and palaeoecological approach in periplatform sediments, which already was sucessfully applied by Haak & Schlager (1989) and Reijmer et al. (1992) along the slopes and basins of Tongue of the Ocean and Exuma Sound (Bahama Platform), the concept of highstand shedding (Droxler & Schlager, 1985) of carbonate platforms should be validated. The aspired paleoecological research within this project focusses on two major objectives. The major goal within this thesis was to evaluate and describe the neritic input from the shallow tops to the platform margin along the up- and downcurrent margins of Pedro Bank. A point-count analyses of thin-sections and coarse fraction analyses were applied to quantify the platform input. The second objective was to determine the distribution of coarse neritic material along the individual platform-to-basin transects.

8.2 Methods

8.2.1 Dataset

Thin sections of several turbidite layers as well as periplatform sediment were prepared for nine sediment cores around Pedro Bank (for location of cores see Fig. 2.1) for point-count analysis and microfacies description. Due to the dominance of pelagic input in nearly all sediment cores recovered, detailed point-count analysis was only provided for core M35034 from the southwestern toe-of-slope.
The unconsolidated Late Quaternary periplatform sediments were sampled with 10 cm^3 plastic syringes or large (5x5 cm) boxes. After freeze drying, the samples were impregnated with resin before the final preparation of artificial thin sections. Point count analysis and photographic documentation was obtained using a ZEISS Universal polarisation microscope (Axioplan Pol). For each sample more than 300 grains were counted. For further comparison of the microfacies analysis with mineralogical proxies three facies-indicative groups were assigned: (1) Shallow-water biota, (2) Planktonic (open ocean) biota and (3) the matrix content. The results are shown in chapter 8.3.1. Coarse fraction samples were identified and photographed under a simple binocular microscope. Microfacies and coarse fraction photographs of typical and atypical skeletal and non-skeletal grains are shown on various plates in Appendix 2.

8.2.2 Components

Identification of the components is mainly based on biological and ecological research on the shallow bank-top sediments of Pedro Bank by Dolan (1972). Additionally microfacies research e.g. by Milliman (1974), Piller (1991, 1994), Emmermann (2000) and Gischler & Lomando (1999) were used to identify the shallow-water carbonate and deep-water biota. The identification of components within the coarse fraction further relies on studies by Bathurst

(1971), Sarnthein (1972), Jung (1973), Milliman (1974), Be & Gilmer (1977), Herman (1978), Poag (1981), Saito et al. (1981), Almogi-Labin (1982), Bolli & Saunders (1985), Murray & Perkins (1991), and Triffleman (1991).
Corals and calcareous algae are important biogenic constituents in reefs and shallow water carbonate platforms (Tucker & Wright, 1993). Green algae, such as *Halimeda*, supply huge amounts of fine aragonite needles to the periplatform sediments. The existence of *Halimeda* and *Halimeda* bioherms on top of Pedro Bank is known from Dolan (1972) and also for banks west of Pedro Bank by Hallock et al. (1988) and Hine et al. (1998). Submersible dives by Dullo (1997; personal communcation and video material) around Pedro Bank also showed the presence of *Halimeda* along those parts of the northwestern margin of Pedro Bank in 40-60 mbsl. This fine bank-derived material probably makes up the sedimentary matrix of the sediments within the proximal sediment cores. REM studies of periplatform bulk sediment supports the occurrence of fine aragonite needles in the matrix of these sediments.

Thin section analysis of Pedro Bank periplatform sediments revealed the presence two major component groups within the turbidite layers:

(A) Neritic derived components like fragments of scleractinian corals, bryozoa, coralline red algae, green algae (*Halimeda*), various shallow-water benthic foraminifera (e.g. Miliolids, Peneroplids and Textulariids), echinoderms and encrusting organisms (e.g. *Homotrema rubrum* and *Planorbulina sp.*), as well as non-skeletal components e.g. multilayered ooids and peloids.

(B) The remaining components are of **pelagic origin**, and provide more than 95% of the coarse fraction. This includes planktic foraminifera of the genera *Globigerinoides*, *Globigerina* and *Rotaliida*, but mostly pteropods and pteropod fragments of various genera (*Creseis*, *Limacina*, *Helix*).

The following skeletal and non-skeletal components (except the pelagic ones) were found:

1. Corals

Coral fragments, mainly from scleractinian genera, which are present on top Pedro Bank (Dolan, 1972), are very rare in periplatform sediments and turbidites. They are characterised by their fairly clear, but often anastomising fractures under plane polarised light. Dolan (1972) stated that their general appearance under crossed nicols is of “interlocking tufts” of crystals having high birefringence colours with wavy extinction. These coral fragments are difficult to recognise, and may be mixed up with mollusc debris, when the prismatic structure of molluscs in not evident. Within the coarse fraction spiculae of octocorals (“alcyonarian spiculae”) were rarely found, although these soft corals are described to be common on the top of Pedro Bank (Dolan, 1972). They are identified in thin section and in the coarse fraction by their wide range of colours (translucent through white, yellow, red and purple) and their typical form, which was described by Hoskin (1963) as “ ... like warty sweet gherkin pickles”.

2. Calcarous algae

2.1 Coralline red algae

Red algae are typified by the layers of brownish, sub-cubical cells. On top of Pedro Bank both encrusting and branching genera, such as *Goniolithon* sp. and *Lithothamnion* sp. are present (Dolan, 1972). The encrusting forms usually show contorted cell layers, whereas the branching types contain external layers of cubical cells, which encircle internal curving layers of rectangular cells. As these characteristics can only be seen in well preserved material found near to their living habitat, it was not attempted to differentiate these genera within the thin sections.

2.2 Green algae (*Halimeda*)

Halimeda forms the main contributor of fine aragonite to periplatform environments around tropical and subtropical shallow-water carbonate systems. Hallock et al. (1988) and Hine et al. (1988) described extensive *Halimeda* meadows from the carbonate banks west of Pedro Bank.
The following features characterise this ubiquitous found calcified green algae: circular pores which ramify the segments, thin platy form and brown colour in transmittend light. Another identification is the fine cellular pattern of the outer surface. Altered *Halimeda* fragments are difficult to identify, when their internal pores and tubes become infilled by the aragonitic sediments.

3. Molluscs
Dolan (1972) stated that pelecypods and gastropods are quite common over the entire bank top. Since most grains on top of Pedro Bank were broken to such an extent that the diagnostic morphology of both subgroups were lost, only the general group of molluscs could be distinguished and counted.

4. Foraminifera (benthic)
Dolan (1972) established the distributional patterns of benthic shallow water foraminifera for his ecological research and divided them into six subgroups. Each was of specific enviromental significance: (1) peneroplids, (2) agglutinating miliolids, (3) *Amphistegina* sp., (4) *Homotrema* sp., (5) other encrusting foraminifera and finally (6) "all other foraminifera". Due to the minor presence of the certain subgroups shallow-water benthic foraminifera were counted as one major skeletal group. Some species are presented in Plates 2 and 3.

5. Echinoderms
Echinoderm fragments are easily to distinguish under crossed nicols as they usually exhibit uniform extinction. Echinoderm plates, the most commonly found fragments, have a fine sieve-like texture, whereas spines can be easily identified, especially in cross section where the symmetry is petalloid.

6. Bryozoa
Bryozoan fragments are difficult to identify. In thin sections the most striking feature is a mass of sub-parallel, *en echolon* tubes, usually of a dull brownish colour.

7. Pelletoids
According to Dolan (1972), three types of pelletoids have been recognised on top of Pedro Bank: (1) large fecal pellets containing an obvious melange of intestinal debris; (2) ellipsoids of amorphous micritic material (about 90% of all pelletoids on top of Pedro Bank); and (3) also grains of skeletal material, which have been coated and rounded by micritic material (baroque pellets sensu Hoskin, 1963).

8. Ooids
Multilayered ooids (as described in Piller, 1994) could be identified within a few thin sections. They sometimes occur in grapestones. Any type of grain was counted as an ooid, which was spherical to ellipsoidal in shape, and showed concentric banding (see Plates 2-4).

9. Unidentified "skeletal" grains
This category includes all skeletal grains that could not be identified under the microscope. Transport processes and subsequent abrasion of the outer surface of these grains diminished any surface structures that could have been used to identify these components in the coarse fraction analysis. But also recrystallization and micritization of skeletal grain diminishes the structures that are needed to identify the grains properly in thin sections. It is likely that most of these grains originate from the platform top and are of biogenic origin. Loreau (1982) stated that many of these "unknown grains" may well represent broken or dissaggregated algal material. This was also observed from Alexander (1996) for periplatform sediment off the Great Barrier Reef. In certain turbidite layers, as well as in the point-counted core M35034 this group can be the most distinct group within the sediments, showing the fast alteration of biogenic fragments, which are mostly of aragonitic or high magnesium calcitic origin. In addition, cryptocrystalline grains were also included into this group.

8.3. Results

8.3.1 Point count analysis of "proximal" core M35034
Temporal variations of bank derived components, planktonic components and the matrix content is shown in Fig. 8.2 and 8.3. The point counting results of single components is shown in Appendix 11. The difference between turbidite layers and normal glacial and interglacial background sedimentation displays itself as an increase in the amount of coarse shallow-water material in the turbidites. Analysis of a relatively proximal sediment core (10 km offbank

distance) indicates that the main export of coarser grained bank derived material to the slope and basin environment occurs through turbidites. The amount of shallow-water material in these turbidite layers varies between 20-35%. A large quantity of unidentifiable micritised biogenic components were present, probably of neritic origin. The total amount of bank derived material may add up to a maximum of 60% of the components counted (see chapter 8.3.2). Other cores, however, do not show such high values for offbank transported, coarser-grained material.

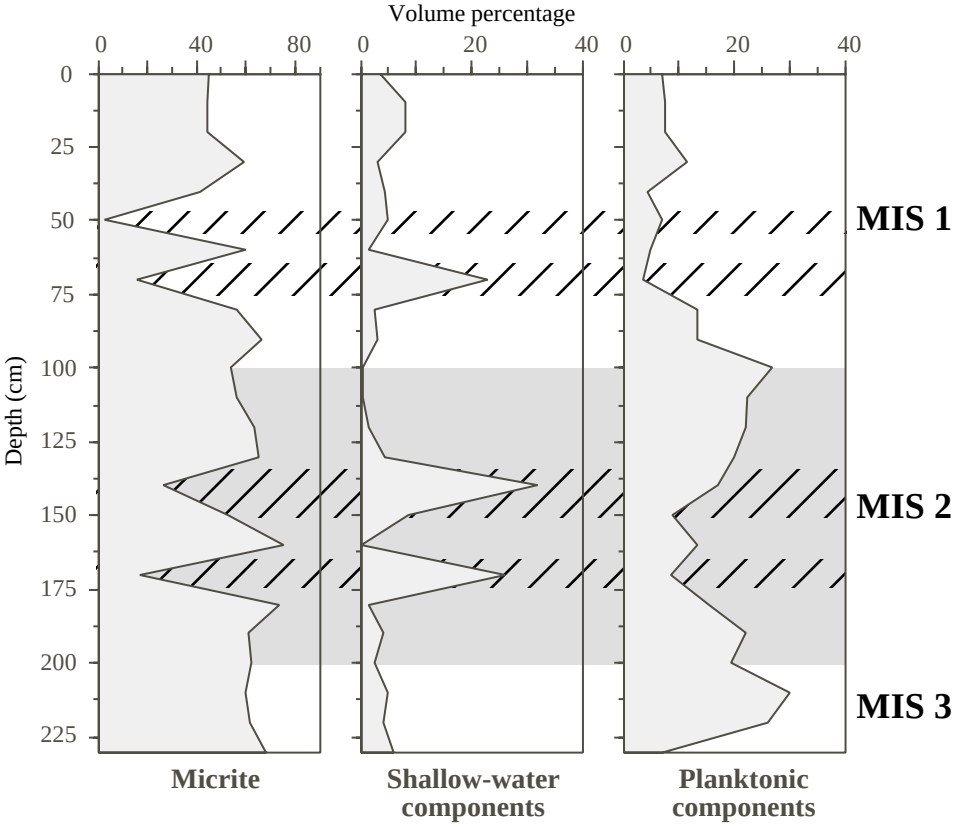

Fig. 8.1: Micrite, shallow-water and planktonic components within sediment core M35034 (turbidite samples included; hatched signature). Turbidites can be clearly distinguished by their raised content in shallow-water material. Marine oxygen isotope stages are shown on the right.

The point-count data of the three facies-indicative groups were compared to sediment mineralogical data measured on bulk sediment samples (Fig. 8.3). The matrix content and the content of planktic components are compared to the content of low magnesium calcite, the variability of bank-derived components to the content of fine aragonite. Main parts of the matrix contains fine silty biodetritus, which was counted as matrix.
During the observed time span (early stage 3 to recent) the micrite content (matrix) varies between 40-70 Vol.%. Higher amounts occur during glacial times. Comparing the content of micrite in thin sections along with the LMC and aragonite signal, it is apparent that the micrite content correlates well with aragonite during interglacial highstands in sea level, whereas a good correlation can be observed with low-magnesium calcite during lowstands in sea level. This shows that the highstand shedding concept (Schlager et al., 1994) also diplays itself in the microfacies distribution of components within proximal cores along the margins of Pedro Bank.
The amount of planktonic components in the bulk sediment increases, similar to the matrix content, during the last glacial (Figs. 8.2 and 8.3). The interglacial values of planktonic components varies between 5-10 Vol.%, whereas the glacial content ranges between 10-20 Vol.%. Highest amounts can be found during the early Holocene and at the end of stage 3 (±24-30 ky).

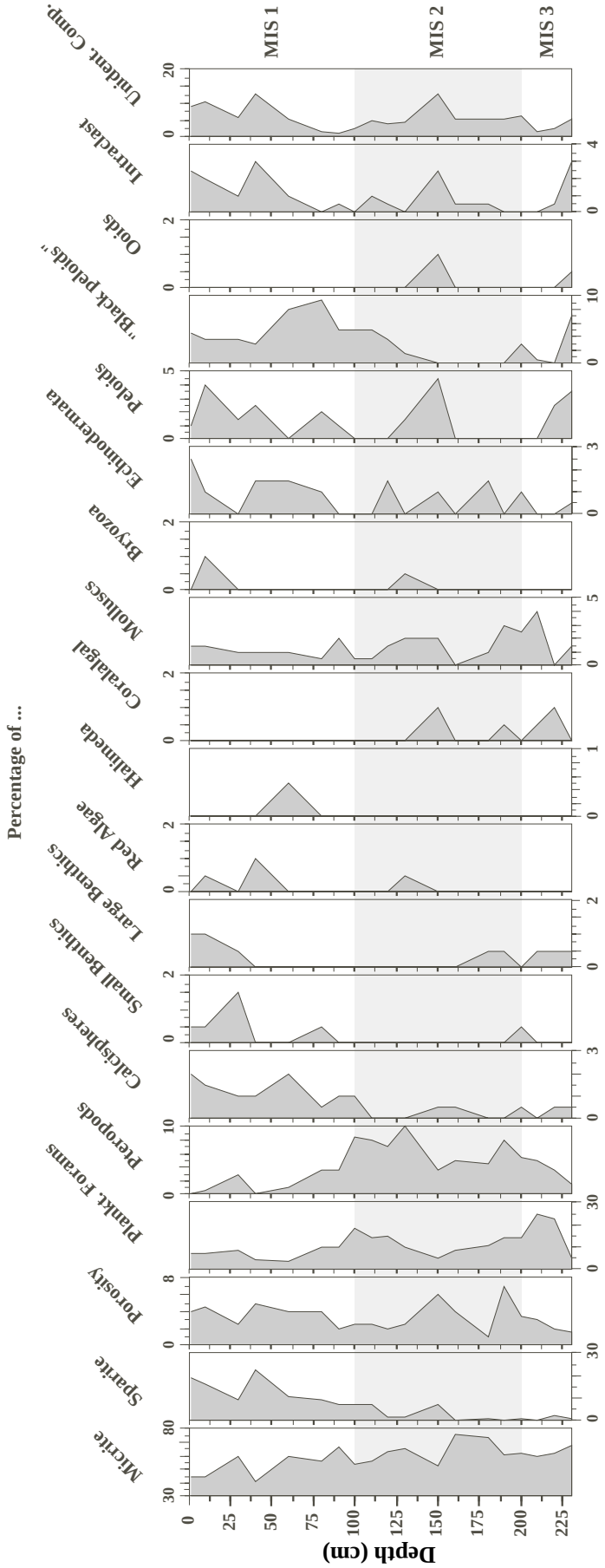

Fig. 8.2: Point count results for single sediment components within proximal, upcurrent core M35034. Plankonic foraminifera and pteropods show a clear interglacial-glacial cyclity with higher amounts during glacial periods, and lowered percentages during interglacial times.

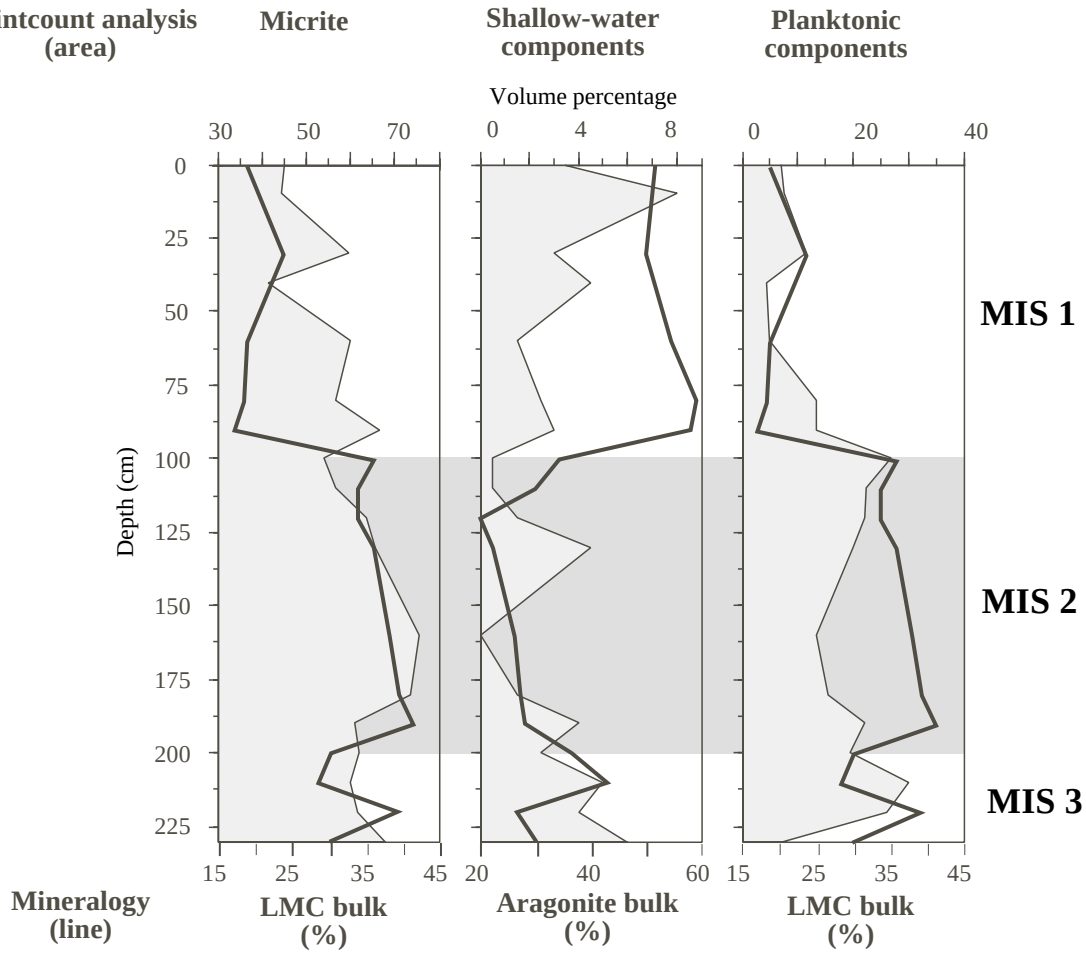

Fig. 8.3: Comparison of mineralogical (line) and point count (area) data. Stratigraphy is shown on the right. Micrite and planktonic components show similar trends seen in the LMC content. Aragonite, as indicator of fine neritic input from the platform, agrees in general with the input of coarse neritic components. It must be noted that the absolute amount of platform-derived components do not exceed 8 vol.% of the sediment content. The difference between the aragonite content of the sediment and the content of coarse platform-derived components probably show the low export potential of coarse material into the periplatform realm, whereas the high aragonite content displays the dominant export of fine aragonite needles, mainly due to the desintegration of the ubiquitous green algae *Halimeda*. In addition, the gentle increase shallow-water components during the Holocene sea-level rise might indicate the adaption of the shallow-water realm during and after the reflooding of Pedro Bank and the time of reorganisation and re-adaption to the new enviromental conditions promoting shallow-water production and export.

The trends seen in the volumetric content of shallow-water biota during the Holocene and the last glacial support the hypothesis of "highstand shedding" of carbonate platforms along the eastern edge of the Northern Nicaragua Rise. The absolute amounts of shallow-water material within sediments along the southwestern margin of Pedro Bank are low. They average about 4 vol.% (maximum of 8 vol.%) during interglacials, and less than 1 vol.% (maximum 5 vol.%) during the last glacial. Similar changes in the input of shallow-water biota in periplatform sediments and the amount of aragonite show that a coupling between the export of fine neritic components and coarse neritic grains is evident, but that these two sediment-export proxies might tell a different story. Both proxies show the same tendencies, but individual peaks cannot be linked with each other.

8.3.2 Point count analysis of turbidites in proximal core M35034

In core M35034, taken close to the toe-of-slope, the composition of glacial and interglacial calciturbidites differs significantly (see Fig. 8.4). This core is the only one from the southern

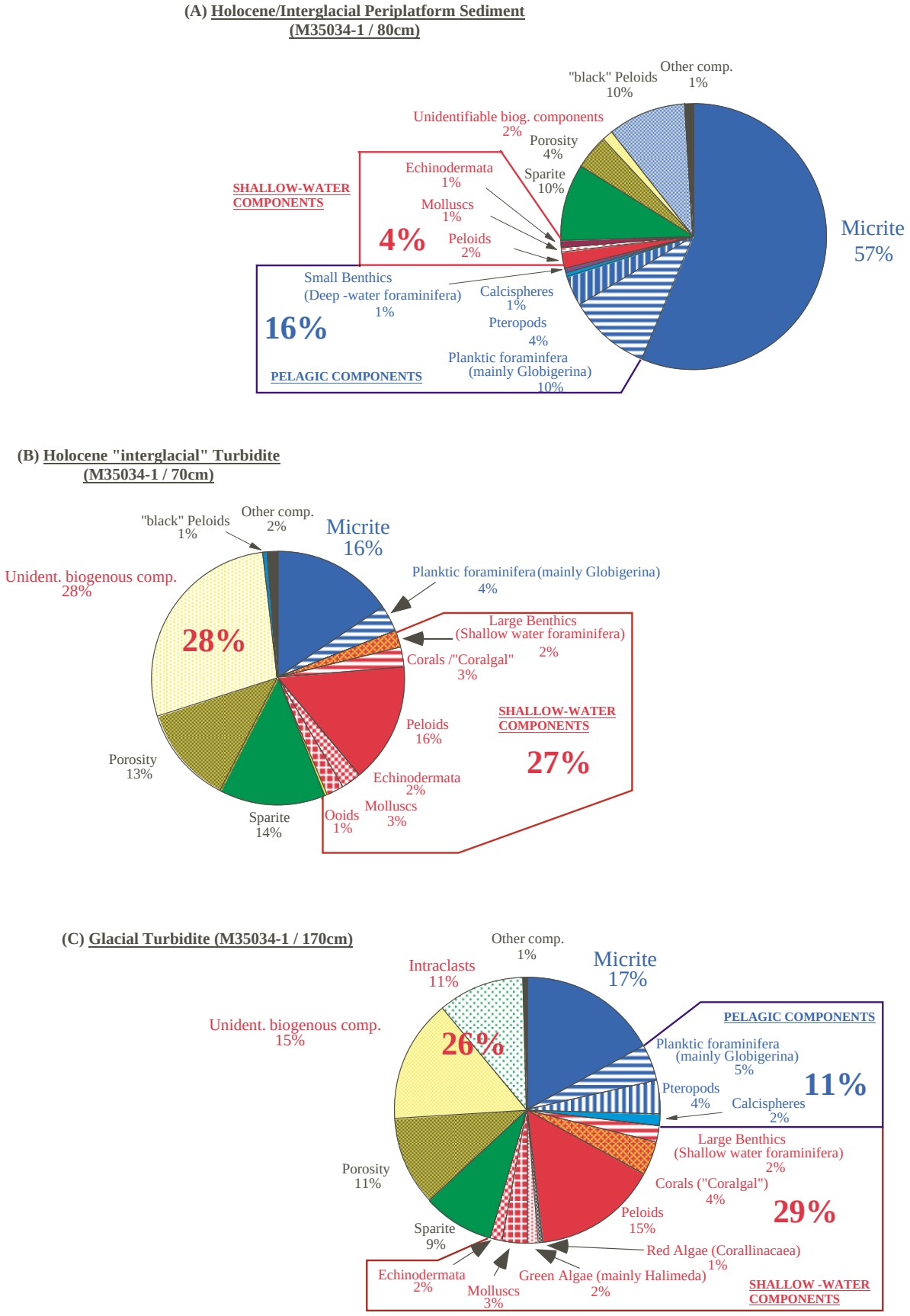

Fig. 8.4: Point count results of an interglacial (B) and a glacial turbidite (C) as well as of a typical interglacial periplatform sediment sample (A) in core M35034.

bank margin of Pedro Bank that contains significant amounts of bank-derived biota. Five turbidites were deposited within the last ~48 ky. Figure 8.4 shows the point-count analysis of a Holocene (interglacial) turbidite (M35034, 70 cm) and a glacial turbidite, which was probably deposited during the transition from isotope events 2.2 to 1.1 (M35034, 170 cm).
The interglacial turbidite contains 27% shallow-water biota (e.g. shallow-water foraminifera, coralagal fragments, peloids, molluscs, echinoderms and ooids). In total 28% of unidentifiable components (most probably micritised algal fragments, which also originate from the bank top) were present. So, the overall content of bank-derived biota in this interglacial turbidite accounts for approximately 55 vol.%.
The glacial turbidite (170 cm) also shows a high amount of bank-derived biota (29%), nearly the same amount as seen in the interglacial turbidite. A major difference in the composition of this glacial turbidite lies in the presence of "intraclasts (see discussion). Both groups add up to about 44% of "bank-derived" material, which is only slightly lower than during interglacials.
In addition to the turbidites the contents of a typical interglacial periplatform sediment was analysed. It shows only minor input of coarse offbank-transported shallow-water material (about 4%). In turbidite layers of other upcurrent cores shallow-water biota were found only sporadically: one layer within M35032 and -52, one in PC016 and 3 layers of platform origin in PC073 (turbidite analysis of PC016 and PC073 from Glaser, 1991).

8.3.3 General periplatform sediment composition within the 500-1000 µm and >1000 µm fraction

The composition of periplatform sediments retrieved from the slopes and deep basins off Pedro Bank show a dominance by planktic foraminifera (of the families Orbulina, Globigerina, Rotaliida and Globigerinida) and pteropods. Typical interglacial and glacial coarse fraction samples from all analysed cores show a high abundance of these planktic organisms within the coarse fraction. Photo tables in Appendix 2 show typical compositions of periplatform sediments and calciturbidites from the slopes and basins off Pedro Bank. In certain coarse fraction samples of the "proximal" downcurrent cores M35048 and -49 an enrichment of peloids could be observed, which could be attributed to highstands in sea level, when the platform top was flooded.

8.3.4 Composition of calciturbidites

8.3.4.1 Downcurrent slopes and basins (M35042,43,48,49, PC059 and PC100)

The periplatform sediments deposited on the downcurrent side of Pedro Bank are dominated by fine constituents of bank-derived material (mainly fine aragonite needles) and coarse pelagic components such as planktic foraminifers and pteropods. This is also mirrored in the composition of turbidites from the northwestern offbank environment. Due to dominance by fine aragonitic muds and coarse pelagic components no quantification of the periplatform sediment and calciturbidite composition was provided. Instead a detailed description of the basic component content within the turbidite layers is provided.
The depositional setting of the six downcurrent cores differs significantly. M35042 is the only core within this depth transect situated in a flat-floored basin. The other cores were recovered from (1) the top of a horst structure (M35048), (2) close to a rough seabottom morphology (M35049 and M35043), or (3) from the flanks of the Pedro Channel canyon (PC059 and PC100).

(A) "Proximal" downcurrent cores (M35048, -49 and -43)

(A.1) M35048 (5.5 km)

Turbidites in core M35048 contain minor bank-derived grains, despite its close proximity to the toe-of-slope. The depositional setting of this core on the flank of a steep horst structure (Fig. 5.7) might restrain the deposition of coarse material at this location.
The turbidite layer in the transition from oxygen isotope stage 2 to 1 (55-73 cm) contains large planktic components at the base, fining upwards to a muddy top. Between 55-70 cm large molluscan fragments as well as planktic foraminifers and pteropods can be found. The top of this turbidite layer shows echinoderm fragments, some larger fragments of algae and

Amphistegina sp. Dark lithoclasts (reworked material?) are also present within the upper 5 cm of the turbidite.
The turbidite layer at 312-321 cm was deposited during the interglacial-glacial transition from stage 6 to 5. This layer contains coarse planktic foraminifera and pteropods. In addition, large mudclasts and resedimented planktic foraminifera (chambers filled with sediment) can be observed. Bank-derived components are sparse, e.g. algal fragments, miliolid and agglutinating foraminifera. The turbidite between 511-517 cm was deposited during the transition from stage 8 to 7. Compared to the two other turbidites, this layer is slightly more dominated by matrix input, but the coarse fraction still consists of planktic foraminifers and pteropods. At 513-514 cm some molluscan fragments and agglutinating foraminifera could be observed. The turbidites between 55-73 cm and from 511-517 cm are also characterised by cemented clasts within the turbiditic layer itself. Within these cemented layers that mainly consists of pteropods, a single coral fragment was found. It could not determined if it was of deep- or shallow-water origin.

(A.2) M35049 (19.5 km)
The fining-upward turbidite layer at 47-69 cm shows a gradual change from wacke/packstone to mudstone. This layer was deposited during the major transgression from stage 2 to 1. The base is dominated by coarse components, respectively planktic forams and pteropods. The turbidite layer at 231-241 cm (within stage 5, probably event 5.3) displays an alteration of small micritised bioclast fragments and coarse layers with pteropods and planktic forams at the top. The coarse components at the base might be of shallow-water origin, but this is not clearly evident as most of the fragments are strongly micritised. The only clear indication for shallow-water input is the presence of a single *Halimeda* fragment. The turbidite at 412-421 cm (transition from 7.1 to 6.6) is characterised by large micritised biodetrital fragments and bryozoan fragments.

(A.3) M35043 (28 km)
The turbidite layer at 226-237 cm (stage 5, probably event 5.3) displays a typical fining-upward turbidite sequence from coarse to fine sand. The fine endtail of the turbidite seems to be missing. Main constituents at the base are large planktic foraminifera and pteropods. These are intercalated with fine biodetritus of non-identifiable components. A typical feature of this turbidite is the alternation of very closely packed layers of fine micritised biogenic components and less densely packed layers with large foraminifera and pteropods.
A horizon with bioclasts between 304-308 cm (transition from 6.2 to 5.5) shows a mixture of large planktic components (forams and pteropods) and large echinoderm fragments. This layer might represent the base of a turbidite. About 90% of the coarse fragments at the base of this layer are planktic foraminifera, whereas the top is dominated by pteropods. The matrix makes up to 30-40%. At a depth of 390-393 cm (transition from 7.1 to 6.6) a turbidite layer is present, which is dominated by coarse components. Planktic foraminifera, as well as some benthic (shallow-water?) and agglutinating foraminifera are present. A few matrix-clasts at the base of this layer may indicate reworking. The top of the turbidite is dominated by fine micritised bioclasts of unknown origin.
The three cores described (A.1 to A.3) are located at a distance of up to 28 km from the platform edge. The turbidite layers roughly contain 50% coarse and 50% fine fraction. This coarse/fine-ratio within the turbidites differs significantly from those further downslope.

(B) "Distal" downcurrent cores (M35042, PC 059 and 100)
M35042 is situated within a flat-floored basin at about the same off-bank distance (41 km) as cores PC035 and PC108. The latter two were first described by Glaser (1991) and will be used for comparison later in this chapter. Cores PC059 and PC100 are situated on the eastern flank of the main axis of Pedro Channel, and thus represent a different depositional setting. The composition of turbidites in these three cores thus varies significantly.

(B.1) M35042 (41 km)
Coarse components found in turbidites of core M35042 contain predominantly coarse planktic components (planktic forams and pteropods). The presence of unidentifiable micritised skeletal fragments indicates shallow-water input, but this could not be verified in the thin sections. Turbidite layers in 119-126 cm, 152-158 cm, 204-207 cm, 287-294 cm and the section between 466-482 cm (with two turbidite layers in between) form the fine tail-ends of turbidites (on

average 9% coarse fraction content). Thin-section analysis show that these layers consists of more than 90-95% of very fine (aragonitic?) mud with sporadic planktic foraminifera and pteropods. One exception to this rule is formed by the turbidite layer at 229-250 cm. The coarse fraction samples (>500 µm) show clear evidence for bank-derived input (see plates in Appendix 2), probably alterered or repeatedly redeposited neritic skeletal fragments. The thin sections of this turbidite show a larger amount of micritised biogenic components.

(B.2) PC059 (72 km)
Turbidites in PC059 are represented as fine tail-end turbidites as seen further upslope in core M35042, but also as coarse turbidite layers, which are dominated by planktic foraminifera and pteropods. These are also more frequently found in downcurrent turbidites (e.g. PC100). The visual examination of the coarse subfractions 500-1000 µm and >1000 µm showed the dominance of coarse planktic biota within turbidites of PC059.

(B.3) PC100 (91 km)
Turbidites in PC100 are coarser than their upslope counterparts. The coarse fraction content varies between 15 to 91% (average: 61%). Pack- to grainstones are the common turbidite lithology. Three fine tail-end turbidites or small muddy "stringers" are also evident. Only one of these fine tail-end turbidites was sampled and shows a coarse fraction content of 15%. The components within the turbidites exclusively consist of planktic foraminifera and pteropod fragments. No micritised components or shallow-water biota were observed.

Summary Downcurrent cores
- Although the downcurrent margin of Pedro Bank is the side of main sediment deposition, the coarse grain fraction of the cores is dominated by planktic components like foraminifera and pteropods. Shallow-water components can only be found to a minor extent in one turbidite layer of core M35042. Some alterated *Halimeda* fragments and agglutinating benthic foraminifera occured within proximal core M35048.
- Cores located within flat-floored basins contain higher amounts of fine-grained material. They probably form the endtails of turbidites (muddy turbidites); coarser base load turbidites are rare.
- Only distal site PC100, located on the steep eastern flank of the Pedro Channel axis, is dominated by coarse turbidite layers, which consists mainly of planktic components. This compositional signal might indicate a different source area of those turbidites and/or different sorting processes at the axis slope of Pedro Channel.

8.3.4.2 Upcurrent slopes and basins (Cores M35034, -32, -52)
Pedro Bank exhibits a specific platform morphology, with an inclined banktop, which deepens towards the north. The shallowest parts of the platform are therefore found at the southwestern to southeastern (upcurrent) part of Pedro Bank. Hence we should be able to trace typical shallow-water components, such as corals, green algae (*Halimeda*), red algae and other bank-derived components at least in turbidite layers within proximal cores from the upcurrent margin of Pedro Bank.

(A) M35034 (10 km)
In core M35034, taken near to the toe-of-slope, the composition of glacial and interglacial calciturbidites differ significantly (see Fig. 8.4). This core is the only one from the southern edge that exhibits noticeable amounts of bank-derived biota. Five turbidites were deposited within the last ~48 ky (see also chapter 8.3.2). The interglacial turbidite contains about 27% of shallow-water biota. If the 30% unidentifiable components (preferentially micritised algal fragments) are of platform origin the percentage mounts to 60% bank-derived material. The glacial turbidite shows 29% shallow-water components, which equals roughly the interglacial percentage. In addition, the glacial turbidite shows a distinct type of components - namely "intraclasts". They may be evidence for upslope sediment reworking.
In addition the typical shallow-water benthic foraminifera *Archais angulatus* and *Amphistegina lessonii* could be observed. The tests of *Archais angulatus*; which are made of HMC, show evidence for major dissolution.

(B) M35032 (25 km)
A good example for offbank transported or redeposited bank-derived material forms the turbidite layer at 192-209 cm. This turbidite layer was probably deposited during the early transgression from isotope event 4.2 to 3.3. The turbidite base contains a variety of shallow-water components, mainly *Halimeda* fragments, but also red algae, coral, echinoderm and molluscan fragments, encrusting foraminifera (*Homotrema* sp.), agglutinating foraminifera and other benthic foraminifera (such as *Amphistegina lessonii*, *Archais angulatus* and *Amphisorus cf. hemprichii*), ooids and grapestones (see plates in appendix). All tests of *Amphistegina* sp. show minor evidence for dissolution. In addition, this layer also contains reworked material in the form of large clasts of micritic periplatform sediment. The other turbidites are characterised by the input of planktic components (foraminifera and pteropods), and to a minor extent of micritic clasts.

(C) M35052 (30 km)
In M35052 turbidites of up to 1.1m in thickness were deposited, a thickness not found in any other analysed core from the deep surroundings of Pedro Bank. The turbidite sequences, which are mainly deposited during glacial stages 6 and 8, contain a large variety of classical turbidite features (fine tail, lamination, base load sensu Bouma, 1962). Typical bank-derived components occur sporadically between 199-216 cm and 852-869 cm. The base of a large stage 6 turbidite (562-584 cm) contains shallow-water material like *Halimeda*, coral, echinoderm and molluscan fragments, red algae, benthic foraminifera such as *Amphistegina gibbosa*, *Amphistegina lessoni* and other shallow-water benthic foraminifera. The laminated sequences in all turbidites are characterised by small planktic foraminifera such as *Orbulina* sp. *and Globigerina* sp., pteropod fragments and small micritised fragments of unknown origin.

Upcurrent cores summary
Turbidite layers in sediment cores retrieved from upcurrent positions off Pedro Bank show the same dominance of pelagic as seen in downcurrent cores. Sporadically very small layers with slightly increased amounts of neritic components (*Halimeda*, corals, geniculate red algae, shallow water benthic foraminifera) occur in the upcurrent sediment cores.

8.4 Discussion

Sediment composition of periplatform sediments and calciturbidites
The microfacies analysis of periplatform sediments from the basins encircling Pedro Bank showed that no high export of coarse-grained, neritic material takes places. This observation is in sharp contrast to studies made in sediments of several Bahamian basins (Haak & Schlager, 1989; Reijmer, 1991) showing abundant coarse-grained, neritic material in the sediments and the calciturbidites. Nonetheless, other studies proved that the theory of highstand shedding of carbonate platforms applies to the periplatform surrounding of Pedro Bank (Glaser & Droxler, 1996; Schwartz, 1996). The export mainly takes place through the high content of bank-derived fine aragonite within the periplatform sediments (Glaser & Droxler, 1993; Chapter 6 and 7) that evolves from the desintegration of *Halimeda* in fine (< 4 µm) aragonite needles. The high abundance of *Halimeda* on top of Pedro Bank was shown by Dolan (1972).
The results of this study displays a dominance of planktic components within the coarse fraction of periplatform sediments. Mainly planktonic foraminfera as well as pteropods were evident. The following planktonic foraminifera were found: *Globigerinoides ruber*, *Globigerinoides sacculifer*, *Orbulina universa*, *Globorotalia menardii*, *Neogloboquadrina dutertrei*, *Globigerinita glutinata*, and others such as *Globigerinella siphonifera*. Schmuker (2000) observed a similar faunal composition in the upper 100 m of the water column at site M35043 along the northwestern margin of Pedro Bank. This association of planktic foraminifera changed through time, for instance the Globorotaloid species that form the *Globorotalia menardii* complex show a periodical occurrence and absence in Caribbean surface waters (chapter 2.2.2.2 “Biostratigraphy”). Pteropods (Gastropoda suborder *Eutheocosomata*), the other main planktic constituent, show a variety of species from different families. They were not specified in detail, but certain genera that are very abundant need to be mentioned:
- spirally coiled forms of the genus Limacina: *L. inflata*, *L. trochiformis* and *L. bulimoides*.

- uncoiled forms from the family Cavoliniidae: *Creseis acicula, Creseis clava and Creseis virgula sp.*.

Studies of Jung (1973) display a similar faunal composition of pteropods with a high abundance of *Limacina inflata, Creseis virgula* and *Creseis acicula*. Along this main pteropod species *Clio pyramidata, Styliola subula, L. bulimoides, L. trochiformis* and *Peraclis reticulata* occur within the Holocene sediments of the Cariaco Basin (southeastern Caribbean Sea). Both planktic species, although they form a major part of the coarse fraction, are not within the scope of this study. The main focus of this study was to reveal changes in the export of neritic skeletal and non-skeletal grains from the top of shallow Pedro Bank.

The main result of this study is that periplatform sediments as well as calciturbidites from the surrounding of Pedro Bank reveal no major input of coarse neritic grains into the periplatform environment. If coarse neritic material was found, as shown for distal sites PC108 and PC016 (Glaser, 1991) or at upcurrent site M35034, this occurrence is linked to bypass processes by turbidites through gullies or canyons connecting the bank margin with these depositional sites. A major role for the distribution of coarse neritic material thus is given by the seabottom morphology around Pedro Bank (Chapter 5). The results of the microfacies analysis of late Quaternary periplatform sediments and calciturbidites will be discussed in association with paleoecological research done on top of the shallow banks of the Northern Nicaragua Rise and the recent barrier reefs off Belize (Gischler & Hudson, 1998; Gischler & Lomando, 1999).

The studies of Dolan (1972) reaveled the presence of a variety of skeletal and non-skeletal grains on top of Pedro Bank including (in order of abundance): *Halimeda*, molluscs, corals, coralline algae, pelletoids, bryozoa, various benthic shallow-water foraminifera (abundant *Peneroplis* sp.), serpulids, sediment aggregates and echinoderms. Each of these components showed a distinct distribution pattern (Dolan, 1972):

(1) Shallow Reefs are dominated by coralline algae and encrusting foraminifera; found on the eastern end of Pedro Bank and coincides with the shallowest parts of Pedro Bank,

(2) Reefal Areas are dominated by corals and *Halimeda*; characterised by sandy bottom with frequent isolated patch reefs which can be found on the leeward side of the shallow reefs, and constitute a transitional zone between the latter and the central sand blanket zone,

(3) Sand Blankets are dominated by mollucs, peneroplids and pelletoids; main facies, which covers two-third of Pedro Bank from the northeast to the western end. They contain predominantly skeletal carbonate sand detritus.

(4) The mud facies is dominated by fine sediments; found in peripheral position along Pedro Banks upper slopes.

The bank top distribution patterns described by Dolan (1972) are to a certain degree mirrored in the abundance of skeletal and non-skeletal components found within the turbidites around Pedro Bank. Only a few coral fragments were found in the cores situated on the southern upcurrent bank margin. These findings partly mirror the distribution pattern described by Dolan (1972). He showed that corals on top of Pedro Bank are most common in peripheral areas of the bank, and have highest abundances along the southwestern to southeastern upcurrent bank margin. A similar explanation should also hold for the occurrence of coralline algae, which are most common along the southern and eastern margins, where shallow living reefs could be observed. Green algae, predominantly the ubiquitous *Halimeda*, were also found in higher abundances within turbidite layers off the upcurrent margin. At the southwestern to southeastern margin, the most shallow part of the Pedro Bank platform top, Dolan (1972) reported meadows with exceptionally high contents of *Halimeda*. This may explain the higher occurrence of *Halimeda* grains within the coarse remains of the sediments in upcurrent position to the bank margin. Nonetheless, *Halimeda* is present all over the bank, which is verified by the occurence of *Halimeda* plates within turbidite layers from the downcurrent margin, such as in cores PC108 and PC035 (Glaser, 1991). The low numbers of *Halimeda* found, even in the proximal cores M35048 and M35049, probably finds its origin in the fast desintegration of the *Halimeda* plates itself.

Benthic foraminifera are typical constituents of shallow-water carbonate sediments (Maxwell, 1968). They are sensitive to environmental conditions, which makes them particularly useful as environmental indicators. Previous studies along the Nicaraguan Rise carbonate platforms have shown that foraminifera compose approximately 6% of banktop and margin sediments (Peebles, 1993). They also display distinct differences in the habitat and the environmental conditions on the different carbonate platforms of the Nicaragua Rise (Dolan, 1972; Marshall, 1976;

Triffleman et al., 1991; Peebles et al., 1997) and Belize Barrier Reefs (Gischler & Lomando, 1999), which is linked to their depth distribution pattern on the bank top. In general the foraminiferal assemblage displays a typical Caribbean assemblage characterised by abundant soritids and miliolids. Peebles et al. (1997) showed that miliolid species show higher abundances on the eastern Nicaragua Rise platforms compared to Pedro Bank on the western side. On top of Pedro Bank, Dolan (1972) observed highest abundances of *Peneroplis* sp., a miliolid species of the family Soritidae. In total 51 species of shallow-water benthic foraminifera were found of the suborders *Textulariina, Miliolina* and *Rotaliina* on Pedro Bank. Nine species account for 91% of the total assemblage, 6 of them showed a depth dependency:

(1) *Rotorbinella rossa, Valvulineria candeiana, Triloculina rotunda* and *Asterigerina carinata* are common in waters less than 12 m deep,

(2) *Ampistegina gibbosa* and *Cibicides pseudoungerianus* mostly occur in waterdepths between 12-20m, and

(3) *Neoconorbina terquemi, Rosalina floridana* and *Archais angulatus* show no depth dependency.

In the thin-sections and the coarse fraction samples of periplatform sediments, as well as calciturbidites, only the miliolid species *Archais angulatus* and *Amphistegina gibbosa* were found. *Amphistegina lessonii*, present in cores from the southwestern periplatform environment (pers. comm. B. Schmuker), has not been observed in the bank top samples by Dolan (1972). The aforementioned shallow-water species were predominantly found in cores from upcurrent locations, whereas downcurrent cores only showed very minor quantities, even in the calciturbidite layers.

A good indicator for the source area of bank-derived components and for the preferential offbank transport direction are the textulariid foraminifera species present in thin sections. They were found predominantly in cores from the downcurrent slopes and basins. Although a more detailed taxonomic determination was not possible, the observed agglutinating miliolids have great similarity to those described by Dolan (1972), being *Textularia agglutinans* and *Bigenerina irregularis*. Both species occur on the eastern Nicaragua Rise carbonate platforms in minor quantities (Triffleman et al., 1991; Peebles et al., 1997). The common abundance of textulariid benthic foraminifera in periplatform sediments and calciturbidites in downcurrent cores is in good agreement with the studies of Dolan (1972). He stated that these benthic foraminfera are most common in the sand blanket facies, which is the main sedimentary facies at the northwestern part of Pedro Bank. In this environment the textulariid benthic foraminifera have a ready supply of test building material (Dolan, 1972).

Another indicator for offbank transport are pelletoids formed in the sand blankets of the northern and northwestern part of Pedro Bank. In specific samples of the proximal downcurrent cores M35048 and 49 an enrichment of pelletoids could be observed during interglacial highstands in sea level, when the bank top was flooded. Dolan (1972) showed that pelletoids can make up to 10% of the sediments in the sand blanket facies.

Haak & Schlager (1989) and Reijmer et al. (1992) showed for sediments from Tongue of the Ocean and Exuma Sound (Great Bahama Bank) that compositional variations in calciturbidites record facies transitions on the top of the platform through time, and that these compositional changes can be linked to Tertiary and Quaternary sea-level fluctuations. Based on the compositional variations it was even possible to distinguish between high- and lowstand turbidites (Haak & Schlager, 1989). In addition the compositional signal of the turbidite layers paralleled the highstand bundling pattern of Droxler & Schlager (1985). Also the turbidite composition correlates well with the aragonite variations in the periplatform oozes (Droxler et al., 1983; Boardman & Neumann, 1984), showing that the bundling pattern is controlled by sea level fluctuations.

In this study no differentiation between high- and lowstand turbidites could be made based on their composition due to the low amount of coarse-grained turbidite layers combined with the low amount of bank-derived shallow-water grains. 101 turbidite layers were present within 13 periplatform sediment cores (Chapter 10), but the majority of the coarse grains were of planktic origin, or they were present as fine-grained turbidites, which makes the identification of exported neritic material extremely difficult. Even in a proximal core (M35034), located in about 10 km proximity to the southwestern bank margin, no clear differentiation could be made between turbidites deposited during high- and lowstands (Fig. 8.3). Both, high- and lowstand turbidites contain low amounts of bank-derived grains, and a large quantity of unidentifiable micritised grains, which are probably of neritic origin. Although the composition is quite

similar, the mechanisms that are responsible for the initiation of calciturbidites might be different. Highstand turbidites are generally triggered due to overloading and oversteepening of the upper slope deposits (Grammer et al., 1993), whereas glacial turbidites might be initiated due to reworking processes during major trans- or regression phases in sea level and subsequent reworking of upper slope deposits (Shanmugan & Moiola, 1984; see also chapter 10). The occurrence of ”intraclasts” within glacial turbidite layers at proximal site M35034 might be an indicator for the aforementioned reworking processes. The pattern found at site M35034 might be typical for a glacial turbidite in the carbonate system, but it is an exception for turbidites found near the slopes and in the basins surrounding Pedro Bank.
The composition of the periplatform ooze at site M35034 and the mineralogical signal within this core show a clear relationship. The amount of bank-derived grains and the amount of fine aragonite (Fig. 8.3) are in good accordance, whereas the input of planktonic components agrees well with the LMC content. Micrite, which probably displays a mixed neritic (fine aragonite) and pelagic signal (”pelagic rain” of coccoliths), shows a good correlation to the amount of fine aragonite during the Holocene. During glacial MIS 2 and interstadial MIS 3, when neritic input into the periplatform environment was low, a good correlation exists between micrite and the amount of fine LMC. A similar pattern could be observed for the late Quaternary Great Bahama Bank (Haak & Schlager, 1989) and the Pliocene/Pleistocene platform transition of the GBB (Reijmer et al., 1992). The observed low percentage of shallow-water derived grains at site M35034 suggests that offbank transport of coarse grained material to the slopes and the basins is mainly provided by sporadic events such as turbidites.

8.5 Conclusions

Microfacies and coarse fraction analyses of periplatform oozes revealed that only minor export of coarse neritic grains into the deep surrounding of Pedro Bank takes place. This is in sharp contrast to studies from other shallow-water carbonate platforms, such as the Great Bahama Bank or the Red Sea. Due to this low amount of neritic offbank transported material only minor microfacies analyses could be carried out. These analyses showed that even in proximal depositional settings close to the toe-of-slope coarse bank-derived grains could be found on average only at about 4 vol.% within the periplatform background sediments. Single groups of coarse shallow-water grains do not show any clear glacial/interglacial distribution pattern. Planktic foraminifera and pteropds, which form major parts of the coarse fraction, show similar temporal variations with high amounts during glacials and low amounts during interglacial periods.

Calciturbidites, found within a few up- and downcurrent sites, show a distinct amount of bank-derived grains. However, the majority of calciturbidites from the periplatform setting off Pedro Bank show a dominance of fine aragonitic matrix (ooze) and of coarse pelagic grains, predominantly planktic foraminifera and pteropods. As the neritic grains were not only found at proximal sites, sedimentation of platformal-sourced turbidites is probably associated with the local seafloor morphology (see Chapter 5). Gullies and canyons act as major pathways for these turbidites, which most probably originate from the upper slope to toe-of-slope settings.
For proximal site M35034, the only site where point-count analyses could be made, no clear differentiation between high- and lowstand turbidites could be observed. Both contain similar amounts of bank-derived grains, however, the mechanisms responsible for the initiation of these layers are quite different. Highstand turbidites are most probably triggered due to overloading of upper slope deposits, whereas glacial turbidites might be initiated due to reworking processes during excursions in sea level along with major trans- or regressions on the slopes of Pedro Bank.

Although no detailed data about the recent highstand sediment composition on top of Pedro Bank could be obtained, the abundance of specific skeletal and non-skeletal neritic grains mirror the bank-top distribution pattern of certain biota on top of Pedro Bank as observed by Dolan (1972). The distribution of green algae, textulariid foraminifera and pelletoids within distinct up- and downcurrent sediment cores show a close relationship to their preferential production area on the platform.

CHAPTER 9

GEOCHEMISTRY OF PERIPLATFORM SEDIMENTS - STRONTIUM CONTENT AS GEOCHEMICAL INDICATOR FOR SHALLOW-WATER INPUT?

9.1 Introduction

The temporal and spatial variations in metastable carbonates (such as aragonite and HMC) of periplatform carbonates are primarly controlled by shallow-water sediment export (Boardman & Neumann, 1984; Boardman et al., 1986), but also can be modified by postdepositional processes like dissolution or precipitation of metastable carbonates at the seafloor (Schlager & James, 1978; Droxler, 1985; Droxler et al., 1991; Sabine & MacKenzie, 1995; Haddad & Droxler, 1996), in the water column (Sabine & MacKenzie, 1995; Milliman et al., 1999), or in marine pore fluids (Walter & Burton, 1990).
This study on the Caribbean carbonate system of Pedro Bank adds further data to the geochemical studies of periplatform carbonates of the Great Barrier Reef (Alexander, 1996) and the Red Sea (Emmermann, 2000). In periplatform sediments aragonite might source (1) from the neritic realm through the desintegration of e.g. corals and calcareous green algae (high-Sr-aragonite), or (2) the pelagic realm (pteropods and pelecypod shells; low-Sr-aragonite). Therefore the discrimination between pelagic low-Sr-aragonite vs. neritic high-Sr-aragonite facilitate the evaluation of the rates of neritic and pelagic aragonite sources in periplatform sediments in more detail (Boardman et al. (1986) on the Bahamas; Alexander (1996), Queensland margin (Great Barrier Reef); Emmermann (2000), Red Sea).
A major goal of these studies was the determination of the content of bank-derived strontium (Sr) within the periplatform sediments as a proxy for shallow-water input. Strontium occurs in marine sediments in carbonate, phosphate and barite (Church, 1970) and alumosilicates (Goldberg & Arrhenius, 1958), but the main part is contributed by carbonates. In carbonates (e.g. aragonite) strontium can substitute Ca to a minor amount in the mineral lattice as the ion radius as well as the ionic charge is quite similar (Ahrens, 1952). The use of Sr as an indicator for shallow-water input is possible while pelagic components (coccoliths, planktic foraminifera and pteropods) generally show low strontium contents of 1500-1800 ppm (Turekian, 1964; Milliman, 1974), whereas other biota like molluscs, corals and calcareous algae and non-skeletal grains (inorganically precipitated ooids and shallow-water marine cements) show higher strontium contents of up to 10000 ppm (Milliman, 1974). Boardman et al. (1986) proposed that glacial-interglacial variations of high-Sr aragonite within Bahamian periplatform sediments would display changes in the export from the shallow-water environment to the deep basins and slopes. As both curves of high- and low-Sr aragonite displayed different patterns, Boardman et al. (1986) concluded that both signals must be primary signals unaffected by aragonite dissolution (Droxler et al., 1986), which should have affected both signals in the same way.
Within this study four cores, three on the downcurrent side and one on upcurrent position near Pedro Bank were analysed for their Sr-content and major and other minor elements. Using these geochemical proxies a further insight can be given into the bulk composition of carbonates and terrigenous components and their temporal variations of Northern Nicaragua Rise periplatform sediments.

9.2 Materials and methods

9.2.1 Materials

Within the downcurrent proximal cores M35048, M35049 and distal core PC100, 97 samples were taken for XRF analysis on bulk sediment samples. In M35049 the analysis was made along the entire core (48 samples), while in M35048 (25 samples) and PC100 (24 samples) every second sample was measured. In upcurrent core M35052 all samples down to isotope event 6.2 (33 samples) were analysed. These cores were choosen to cover a wide range of

depositional environments like up- vs. downcurrent position for input of terrigenous components, and proximal vs. distal positions for neritic offbank transport. All samples used are periplatform sediments, i.e. no turbidite samples were included.

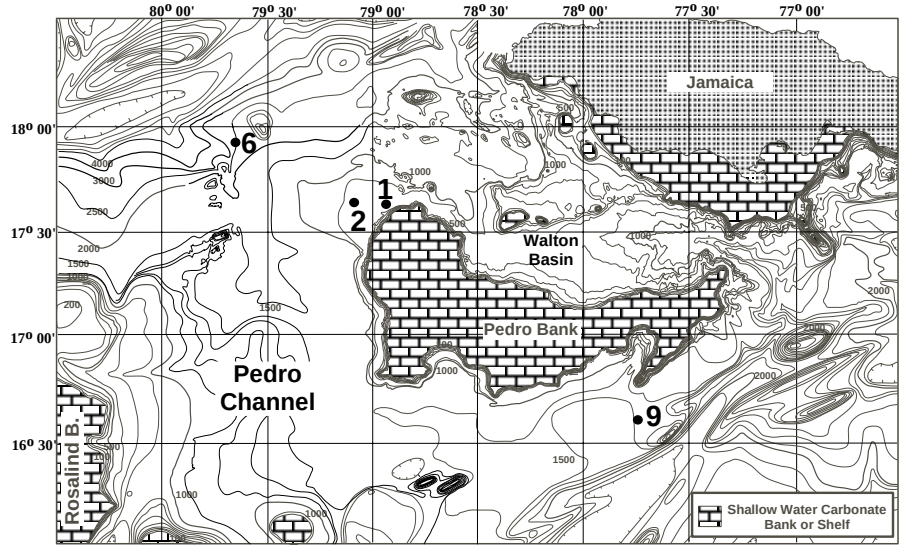

Fig. 9.1: General bathymetry along the periplatform environment of the South Jamaican Shelf, Pedro Bank and Serranilla bank. Cores used within this study are indicated: 1=M35048; 2=M35049; 6=PC100; 9=M35052.

9.2.2 Methods

The analytical principle behind XRF analysis is the bombardement of a sample with a beam of high energy photons (including polychromatic X-rays). The sample subsequently emits secondary radiation with wavelenghts and intensities dependent on the elements present. Measuring the intensities of the characteristic radiation for a distinct element results in a value that reflects its concentration in the sample using Braggs equation. The obtained chemical data from XRF spectrometry do not claim to produce direct evidence of the identities, natures or properties of the minerals (Alexander, 1996), but the obtained overall element information of the samples can be used to calculate estimates of the mineral proportions in an unknown sample (Jones, 1987). Analysis were performed using a Phillips PW 1480 sequential X-ray spectrometer. A simple overview on the sample preparation is given in chapter 2.2.7.
During the XRF analysis two internationally approved standard samples were measured repeatedly (Standard AN and KH; Govindaraju, 1994). Those standards were choosen as they were the only ones with increased amounts of strontium, the element of main interest in this study. Standard AN is a gypsum and the KH-standard is a limestone from the quarry Hoppenstedt near Magdeburg (Germany).

Element	Nominal percentage in standard AN	Nominal percentage in standard KH	Average of repeated measurements	Standard deviation within repeated analysis. In brackets abs.error in %.	Error in comparison to the nominal percentage
Sr	1400ppm	-	1378 ppm	72 ppm (5%)	1%
SiO_2	-	8.6%	8.92%	0.04% (>1%)	3.7%
Al_2O_3	-	2.39%	2.32%	0.01% (>1%)	3 %
Fe_2O_3	-	0.55%	0.8%	0.01% (1%)	45%
MnO	-	0.08%	0.11%	0%	25%
MgO	-	0.74%	0.86%	0.01% (1%)	16%
CaO	40.7%	-	36.67%	2.77% (8%)	9.9%
	-	47.8%	52.88%	0.01% (>1%)	19.6%
K_20	-	0.41%	0.42%	0.01% (2%)	2%
TiO_2	-	0.13%	0.12%	0% (0%)	7%
Ba	-	50 ppm	44 ppm	15 ppm (35%)	12%

Table 9.1: Nominal percentages of distinct oxides and minor elements within XRF standards AN and KH (after Govindaraju, 1994)

Absolute percentages for the analysed major and minor elements are shown in Table 9.1 together with the calculated standard deviations and errors. It has to be mentioned that there is no standard available for very high strontium contents, which are generally found in periplatform sediments. The inhouse, machine-dependent calibration curve for Sr is calibrated for values up to 4000 ppm. For values exceeding this upper range linear extrapolation was used to calculate the final content of the elements (personal communication D. Rau, GEOMAR).
Standard deviations within the repeated measurements of the standards are below 2% for SiO_2, Al_2O_3, Fe_2O_3, MnO, MgO, K_2O and TiO_2 (Table 9.1). The deviation of strontium averages 5% for standard AN, but the absolute error for AN in comparison to the nominal content of AN averages only 1%. The largest deviation shows the measurement of CaO. This probably can be attributed to the very high calcium carbonate content of the periplatform samples and the CaO content of the standards used. The internal calibration program of the XRF-machine applies a linear interpolation, which then subsequently results in relative large measurement errors for CaO (personal communication D. Rau).

Calculation of High- and Low-Sr aragonite
The amounts of high- and low-Sr aragonite in the periplatform sediments were calculated using the approach of Kenter (1995) and Boardman et al. (1986). The high-Sr aragonite should record the interglacial-glacial variations of neritic components, whereas the content of low-Sr aragonite should display variations in the input of pelagic aragonite sources (such as pteropods and other planktic components). In order to calculate the "theoretical" strontium content of a sediment in which all aragonite is high-Sr-aragonite, it is necessary to know the Sr values found within the study area, as biogenic sources and thus the Sr values may vary. The following Sr values for the end members within the mixing triangle **High-Sr-aragonite - Low-Sr-aragonite - Low-Sr-calcite** were used (Fig. 9.2):

1. As *Halimeda* is thought to be the main contributor of neritic aragonite to the periplatform sediments along the Northern Nicaragua Rise (Dolan, 1972; Hine et al., 1988; Liddell et al., 1988; Triffleman, 1989, and Dullo, 1997), the maximum value of 9700 ppm (Milliman, 1974; green algae 7700-9700 ppm) for **high-Sr-aragonite** was choosen. This value agrees with values given by Boardman et al. (1986) for Bahamian periplatform oozes that also are dominated by green algae.
2. Pteropod and distinct bivalve shells are the main contributors to the end member of **low-Sr-aragonite**. The minimum value of 1500 ppm for pteropods was taken following Milliman (1974).
3. As coccoliths and planktic foraminifera are the main contributors to **Low-Sr-calcite** a mean value of 1700 ppm (Turekian, 1964; Milliman, 1974) was choosen for low-Sr-calcite.

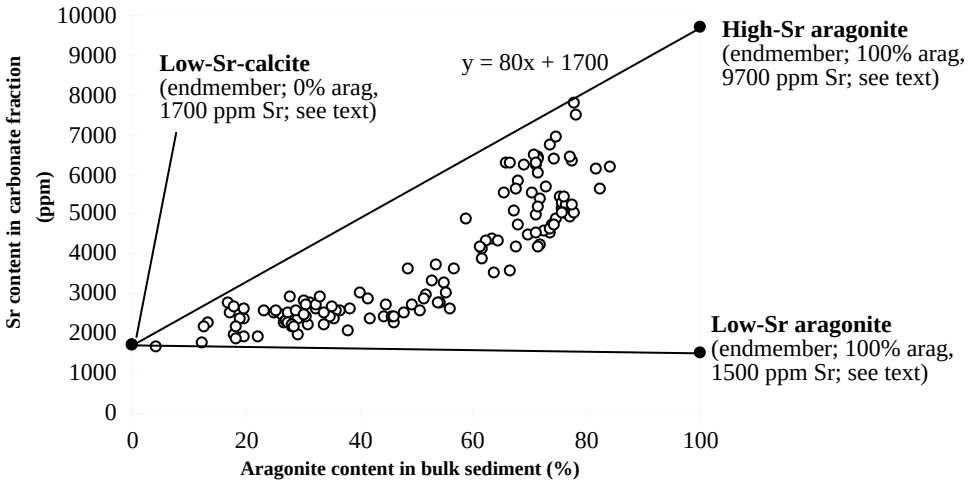

Fig. 9.2: Mixing lines between High-Sr-aragonite (upper) and Low-Sr-aragonite and Sr/Ar-values for Northern Nicaragua Rise sediment samples. The endmembers of the mixing lines were obtained using Sr and aragonite contents of typical major sediment contributors from the platform and pelagic setting along the Northern Nicaragua Rise. The equation y= 80x+1700 is used to calculate the theoretical strontium content (see text).

To calculate the high-Sr- and low-Sr-aragonite percentages from the measured bulk Sr-content the following equations were used (modified after Kenter, 1985 and Boardman et al., 1986 in Emmermann, 2000), which are adapted for the periplatform sediment composition of the Northern Nicaragua Rise:

Equation 9.1: Calculation of the theoretical strontium content in the sample (Sr_{max}):
Sr_{max} = 80x aragonite bulk content + 1700 (see Fig. 9.2)

Equation 9.2: Calculation of high-Sr-arag. percentage of the sample using the analysed Sr content (Sr_{bulk}):
High-Sr-aragonite (%) = (Sr_{bulk} / Sr_{max}) x aragonite bulk content

Equation 9.3 Calculation of the low-Sr-aragonite content:
Low-Sr-aragonite (%) = aragonite bulk content - High-Sr-aragonite

A correlation matrix was calculated for mineralogical data and geochemical proxies using the statistics program "STATVIEW". Single coefficients (r-value) will be presented in the results section (Figs. 9.9 to 9.12), the entire correlation matrices can be found in Appendix 7. The 95% significance levels for the correlation matrices vary between r>0.285 and r>0.404 for all cores. The 99% significance level varies between between r>0.365 and r>0.505. Only correlation coefficients with r>0.6 were considered in this study to be significant.

9.3. Results

9.3.1 Sr-contents in periplatform sediments

The strontium contents in the samples were corrected for their absolute occurrence within the carbonate fraction. This was done while it is assumued that nearly all of the strontium measured in the bulk sediment samples, originates from platform top biota, such as the green algae *Halimeda* (Dolan, 1972; Hine et al., 1988). In general this holds true for cores situated in the main direction of sediment export, whereas sediments in upcurrent position might contain a mixed signal from neritic aragonite, pelagic calcite and some Sr from terrigenous input from the rivers Amazon, Orinoco and Magdalena, which was transported through the Caribbean Sea along by the Caribbean Current (Bowles & Fleischer, 1985; Schwartz, 1996; Flood & Piper, 1997; Franz, 1999).

9.3.1.1 General trend in strontium contents

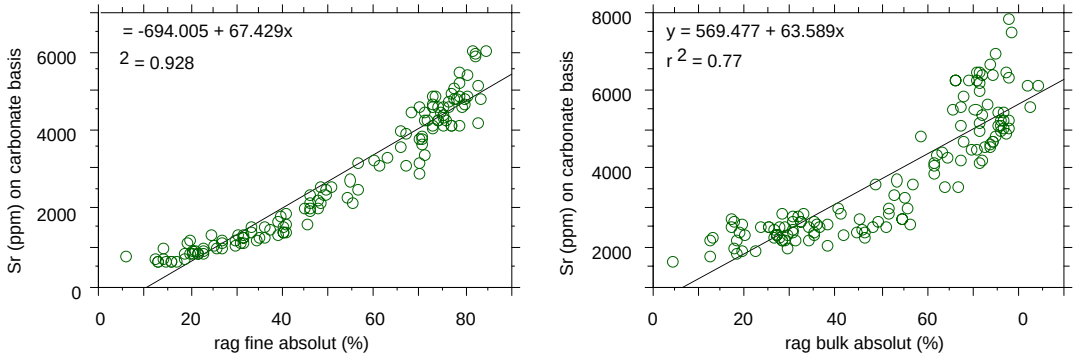

Fig. 9.3: Regression plots for corrected Sr contents (in the carbonate fraction) vs. bulk and fine aragonite content in the periplatform sediments from the slopes and basins near Pedro Bank.

The amount of Sr in bulk periplatform sediments from the deep basins around Pedro Bank varies between 1084 and 6767 ppm for uncorrected bulk sediment samples and between 1668-7793 ppm for Sr-contents based on the carbonate fraction. The regression analysis of the aragonite content (mineralogical proxy) vs. Sr content in the carbonate fraction (geochemical proxy) shows a strong positive correlation between the Sr-content and fine aragonite (r^2=0.93) and with aragonite in bulk sediment (r^2=0.77; Fig. 8.3). This good correlation suggest that most of the strontium is derived from biogenic carbonate sources (e.g. the degradation of *Halimeda* plates into fine (>4µm) aragonite needles). This trend varies among the cores (see Chapter 9.3.1.2).

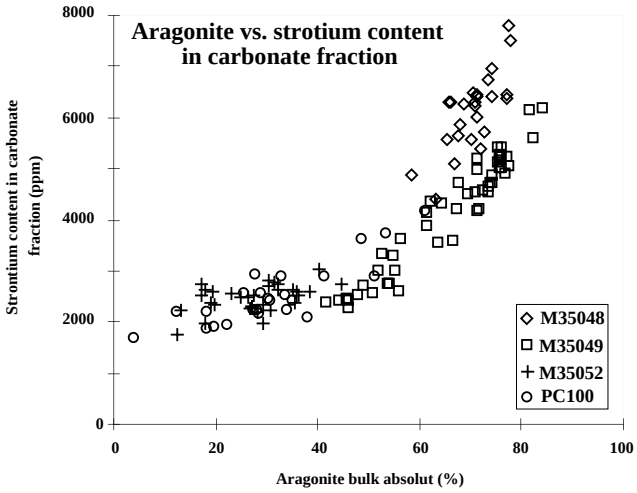

Fig. 9.4: Aragonite vs. strontium contents in the 4 periplatform sediment cores off Pedro Bank. Open symbols show downcurrent cores, crosses upcurrent core M35052.

Proximal downcurrent cores M35048 and -49 show a mean for Sr in the carbonate fraction of 6107 ppm, respectively 4139 ppm. Distal downcurrent core PC100 (92 km offbank distance) shows a mean for Sr values based on the carbonate fraction of only 2527 ppm, which could point to a general origin of these Sr from pelagic biogenic components. The glacial-to-interglacial amplitudes vary from about 3400-3900 ppm in proximal cores to about 2500 ppm in distal downcurrent cores, and display, as expected, minimal amplitudes in upcurrent core M35052 of about 1250 ppm (Table 9.2).
Fig. 9.4 shows the distribution of Sr content vs. bulk aragonite content of four cores. A general decrease in Sr contents with increasing distance from the platform can be observed with lowest values of about 1700 ppm in core PC100.

Sediment Core	Mean for Strontium	Minimum Sr content	Maximum Sr content	Interglacial-glacial difference
M35048	6107 ppm	4386 ppm	7793 ppm	3407 ppm
M35049	4139 ppm	2279 ppm	6162 ppm	3883 ppm
PC100	2526 ppm	1668 ppm	4172 ppm	2504 ppm
M35052	2463 ppm	1764 ppm	3016 ppm	1252 ppm

Table 9.2: Descriptive statistics for strontium content in the carbonate fraction of periplatform bulk sediments off Pedro Bank.

9.3.2 Aragonite vs. strontium contents within single cores

The Sr contents in periplatform sediments show values of 4500-7800 ppm Sr during interglacials in proximal downcurrent cores, 2000-4000 ppm in distal downcurrent cores and 2000-3000 ppm Sr in the upcurrent core (Figures 9.5 to 9.8). Amounts of 2000-3500 ppm Sr are typical for glacial periods except for proximal core M35048, which shows glacial values of 4000-5000 ppm Sr. The Sr variations agree well with the aragonite curves obtained from XRD analysis. The correlation between aragonite and Sr content within the bulk sediment for each core is shown in the following paragraphs.

(A) Proximal downcurrent core M35048 (5.5 km)

The lowest correlation factor between shallow-water input proxies (r^2=0.68 for uncorrected Sr values, r^2=0.58 for Sr in carbonate fraction) was observed in this core, although it shows a strong neritic input. The Sr and aragonite contents are the highest within the analysed cores and the terrigenous influx at this core location is minimal. Comparing the variations of Sr and aragonite with core depth it becomes clear that certain peaks in the aragonite curve occur with slight offsets within the Sr curve. This might indicate that diagnetic processes have affected the sediments after deposition. During interglacial periods the Sr content in the carbonate fraction varies between 5500 and 7800 ppm, during glacials from 4500-5000 ppm Sr. The highest Sr

values are found during isotope event 5.5 (7800 ppm), the lowest during the preceding sea level lowstand of isotope event 6.2 (4400 ppm).

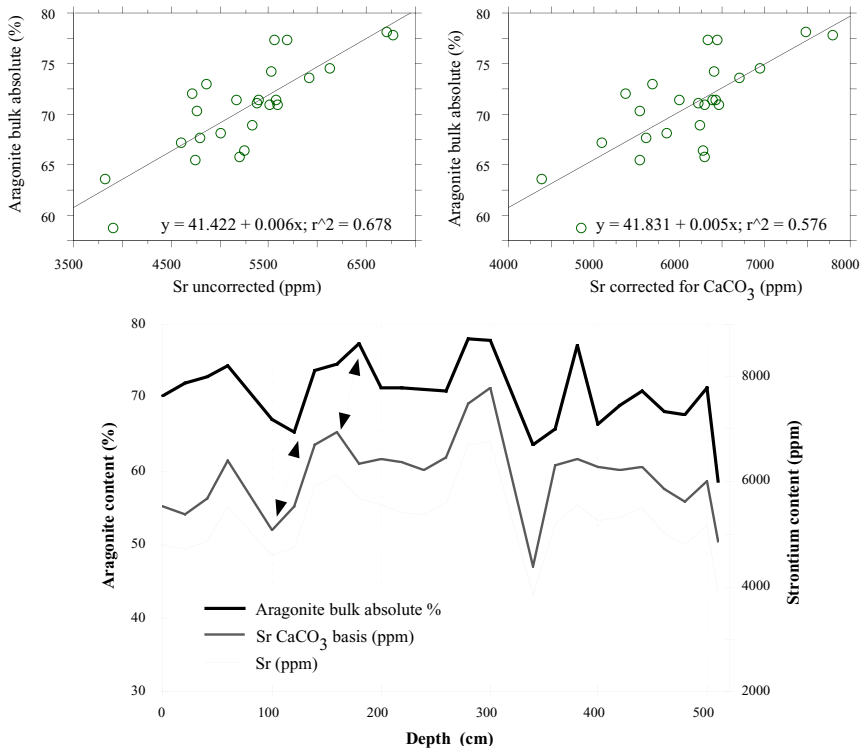

Fig. 9.5: Upper graphs show regression analysis for aragonite vs. Sr content in M35048. Left graph displays uncorrected Sr contents, right graph Sr contents corrected for calcium carbonate fraction. Lower graph shows the distribution of aragonite (thick line) and strontium contents within proximal core M35048. down to isotope event 8.2 (249 ky). Note the small offsets between both proxies e.g. at 100-120 cm, 180-200 cm (arrows).

(B) "Proximal" downcurrent core M35049 (19.5 km)

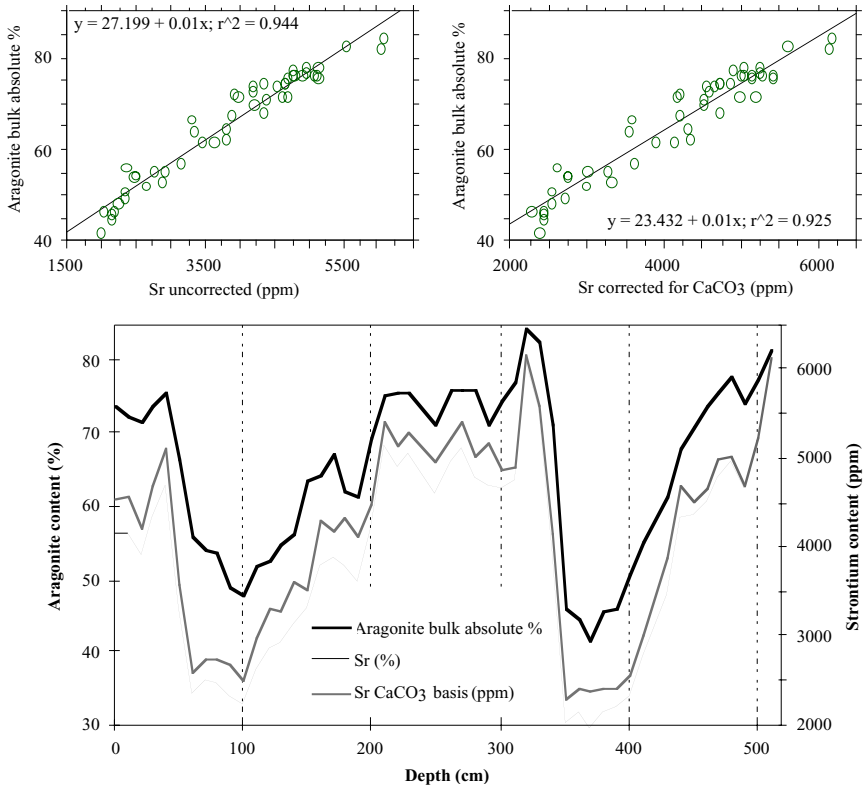

Fig. 9.6: Upper graphs show regression analysis for aragonite vs. Sr content in M35049. Left graph displays uncorrected Sr contents, right graph Sr contents corrected for calcium carbonate fraction. Lower graph displays the variations of aragonite (thick line) and strontium contents within proximal sediment core M35049 down to isotope event 7.3 (210 ky). Note the excellent fit of the mineralogical and geochemical proxies.

XRF analysis was made along the entire core as it display a very good stratigraphy. As shown in Fig. 9.6, the correlation of both, uncorrected and corrected Sr values with the aragonite content is good (r^2=0.944, r^2=0.925 respectively). The strontium values sometimes even show

a better resolution for certain isotopic subevents than the fine or bulk aragonite content. See for example the MIS 2 interval between 50-100 cm.
The interglacial Sr values for M35049 vary between 4300-6300 ppm. Glacial periods are characterised by Sr values ranging from 2500-3000 ppm. Stage 3 shows Sr amounts of 3500-4500 ppm.

(C) Distal downcurrent core PC100 (92 km)

The influence of bank-derived aragonite still can be seen at an offbank distance of 92 km downcurrent to Pedro Bank. During interglacial stage 1 and 5 relatively high Sr values of 3500-4200 ppm are evident, which can be attributed to neritic input.
Lowered amounts of Sr are observed (maximum of ±2800 ppm Sr) with increasing age (i.e. interglacial stages 7 and 9). This might be indicative for a different or lowered export of neritic material during interglacials in sediments older than isotope stage 6. Glacial Sr values range from 1500-2500 ppm and also show a decreasing trend with increasing age.
Although core PC100 is located relatively far away from the margins of Pedro Bank, the correlation between aragonite and Sr is still considerably high (r^2=0.86 for raw uncorrected Sr, r^2=0.73 for corrected Sr). This probably supports the assumption that Sr is mainly bound to the carbonate fraction, and that the influence of terrigenous input to the Sr signal is negligible. A different pattern can be seen in the core from the upcurrent location (core M35052).

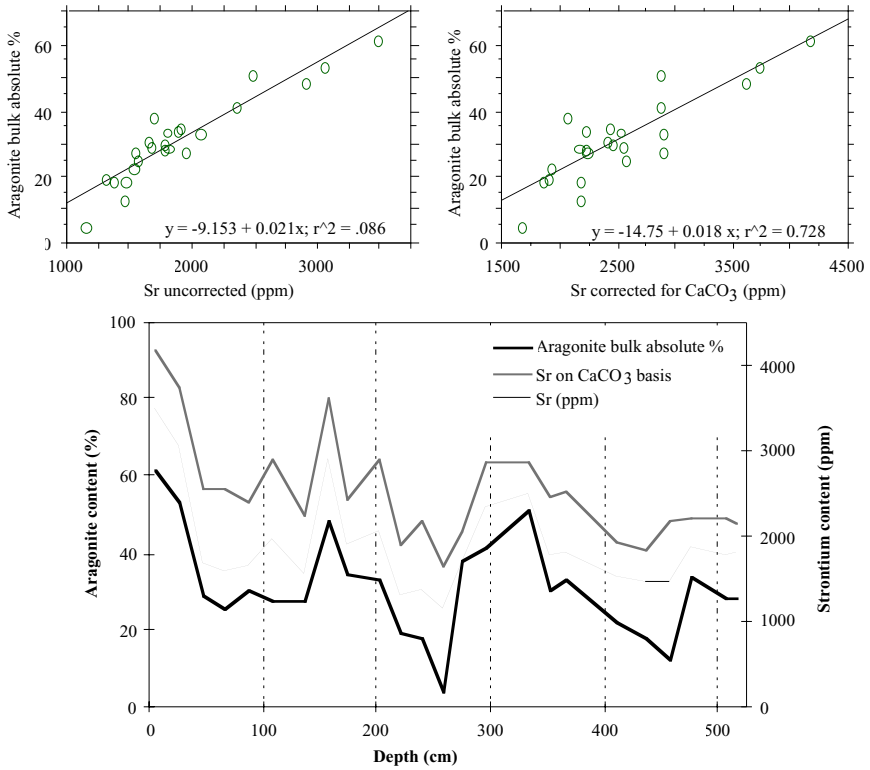

Fig. 9.7: Upper graphs show regression analysis for aragonite vs. Sr content in PC100. Left graph displays analysis for uncorrected Sr contents, right graph Sr contents corrected for calcium carbonate fraction. Lower graph displays the variations of aragonite (thick line) and strontium contents within distal downcurrent sediment core PC100 down to isotope event 9.1 (310 ky).

(D) Upcurrent core M35052 (30 km)

For this upcurrent sediment core it becomes clear that the assumption that most of the Sr is bound within the carbonate fraction, does not apply for every core location (Fig. 9.8). The correlation factor for aragonite vs. corrected Sr contents drops down to r^2=0.22, whereas there is an excellent correlation of r^2=0.88 for uncorrected raw Sr values. Sr in the upcurrent sediments therefore also seems to be influenced by Sr that is bound to terrigenous input.
The maximal interglacial-glacial Sr amplitude of only 1200 ppm, interglacial Sr values of 2200-3000 ppm and Sr values of 1800-2200 ppm during glacial periods, clearly point to another source for Sr within this core than a neritic one. Pteropods and other pelagic biota as well as terrigenous input probably contribute more Sr to the sediments in this upcurrent location to Pedro Bank than for the more proximal sites. This is partly supported by the fact that the coarse fraction, which probably accounts for most of the coarse pelagic input, shows a good correlation with the content of low-Sr-aragonite of r=0.88 (see chapter 9.3.3).

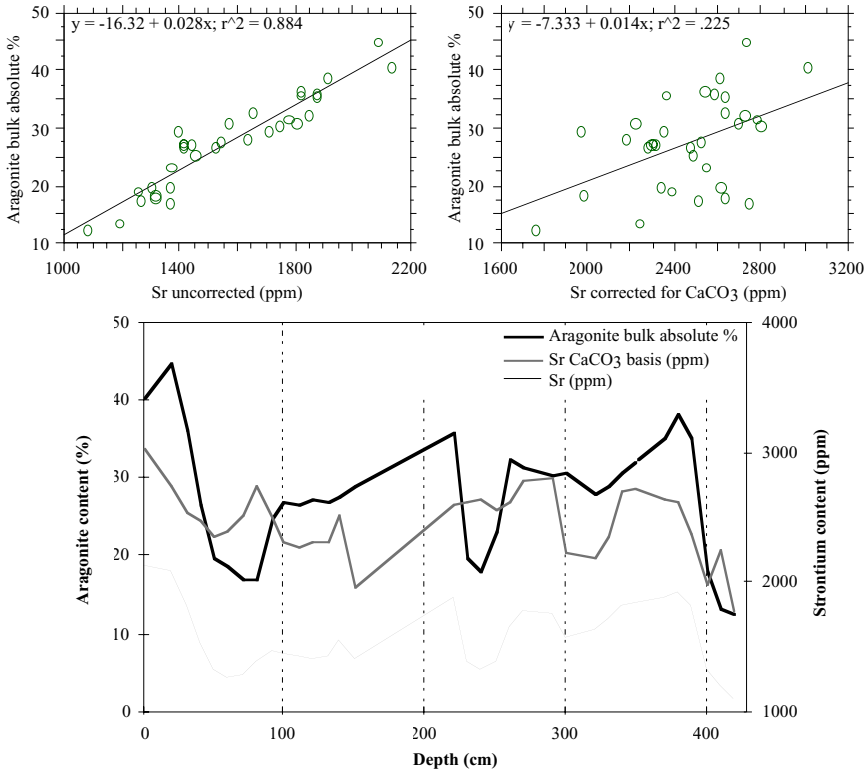

Fig. 9.8: Upper graphs show regression analysis for aragonite vs. Sr content in M35052. Left graph displays analysis for uncorrected Sr contents, right graph Sr contents corrected for calcium carbonate fraction. Lower graph displays the variations of aragonite (thick line) and strontium contents within upcurrent sediment core M35052 down to isotope event 6.2 (135 ky).

9.3.3 High- vs. low-Sr aragonite

In this paragraph the primary data will be presented (Figs. 9.9 to 9.12) that were used for the calculation of high- and low Sr-aragonite calculated with formulas given in paragraph 9.2. These are: (1) bulk aragonite content and Sr content within the carbonate fraction, (2) high- and low-strontium aragonite itself and furthermore, (3) the content of the coarse fraction as one main signal that probably contains large amounts of biota, which might be responsible for the low-Sr-aragonite signal. In addition, the correlation between the individual proxies will be shown. As the variations in the distribution of high- and low-strontium aragonite do not show similar trends throughout all analysed sediment cores, each core is described separately.

(A) Proximal downcurrent cores M35048 and M35049

Variations in the distribution of high- and low-strontium aragonite in core M35048 are shown in Fig. 9.9. From the 60-80% aragonite in bulk sediment, 40-75% originates from high-Sr-aragonite sources within the neritic environment on top of Pedro Bank. The excellent correlation between bulk aragonite, Sr in the carbonate fraction and the high-Sr-aragonite content verifies this statement (correlation factors r= 0.76, r=0.8 respectively).

The almost perfect correlation between Sr in the carbonate fraction and high-Sr-aragonite (r=0.99; Fig. 9.10) shows that the Sr in the carbonate fraction mainly stems from the export of fine neritic aragonite. Only 2-21% of the Sr in the bulk aragonite is of low-Sr-aragonite sources, which show a contenting correlation with the coarse fraction content of r=0.54. This might indicate that pteropods, which are bounded within the coarse fraction, are a major contributor of low-Sr-aragonite. High- and low-Sr-aragonite show a negative correlation coefficient of r=-0.8, which suggests that both proxies display a primary signal.

The other proximal downcurrent core M35049, offbank distance 19.5 km, shows an excellent correlation between bulk aragonite content and high-Sr-aragonite of r=0.97. This suggests a major dependence of the bulk aragonite signal on the input of neritic aragonite. The negative correlation between high- and low-Sr-aragonite is still evident, but not as clear as in core M35048 (r=-0.25). The correlation factor between low-Sr-aragonite and the coarse fraction content remains constant at r=0.55.

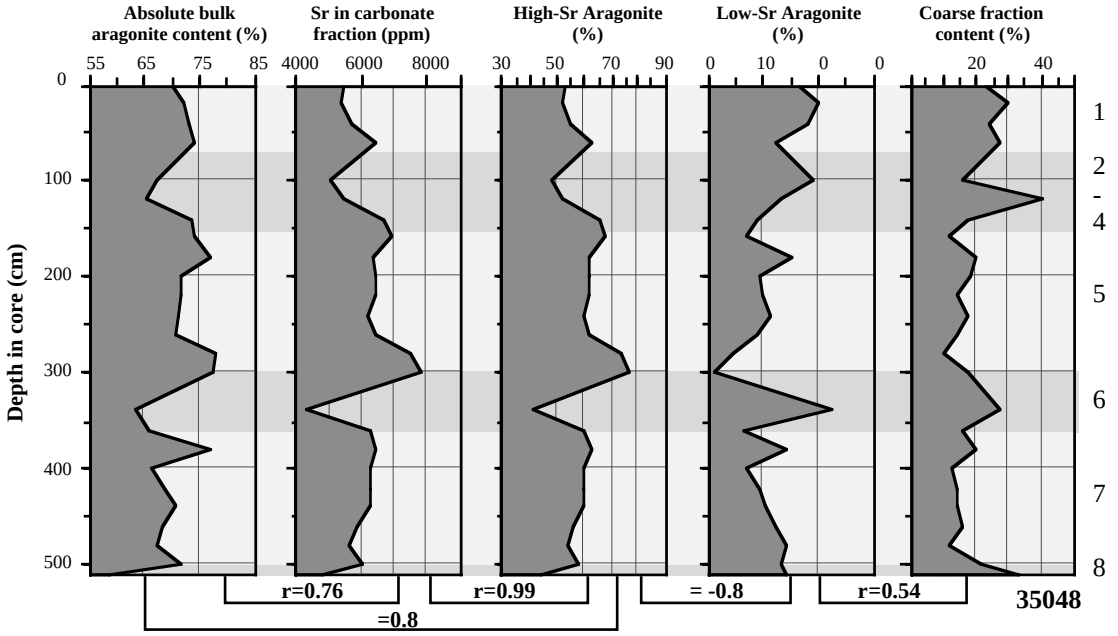

Fig. 9.9: Distribution of mineralogical (aragonite bulk content), geochemical (Sr in carbonate fraction, High- and low-Sr-aragonite) and sedimentological (coarse fraction content) proxies vs. depth within proximal downcurrent core M35048. Correlation coefficients (r) are shown at the base, isotope stages (I.S.) on the right.

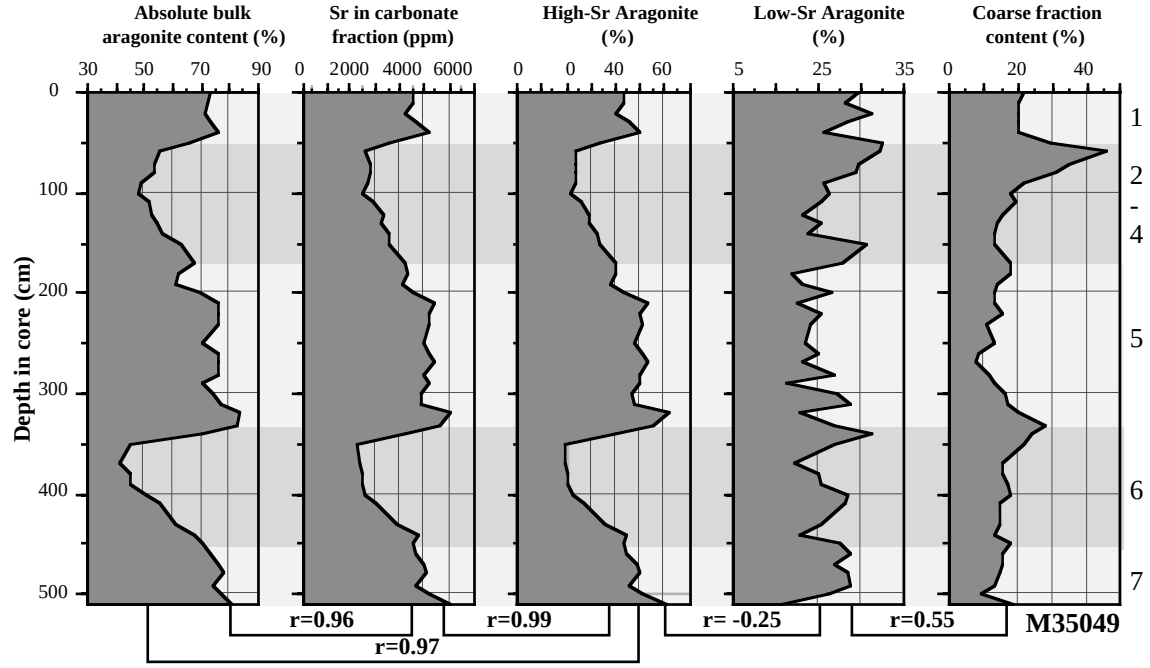

Fig. 9.10: Distribution of mineralogical (aragonite bulk content), geochemical (Sr in carbonate fraction, High- and low-Sr-aragonite) and sedimentological (coarse fraction content) proxies vs. depth within proximal downcurrent core M35049. Correlation coefficients (r) are shown at the base, isotope stages (I.S.) on the right.

(B) Distal downcurrent core PC100

The signal of high- and low-Sr-aragonite within this distal and deep downcurrent site displays a different story in the evolution of the Sr-signals. The correlation between the bulk aragonite content and the Sr in the carbonate fraction or the high-Sr-aragonite remains good (r=0.85, r=0.95 respectively). Most of the aragonite probably is of neritic sources (r=0.97 for Sr in carbonate fraction vs. high-Sr-aragonite). However, it is evident that the content of low-Sr-aragonite also shows an excellent correlation of r=0.92 (Fig. 8.11) with the aragonite bulk signal. In addition, the high- and low-Sr-aragonite display a good correlation of r=0.76. The increased correlation between low-Sr-aragonite and the coarse fraction content (r=0.72) suggests that at this distal site the influence of pelagic Sr-sources is enhanced.

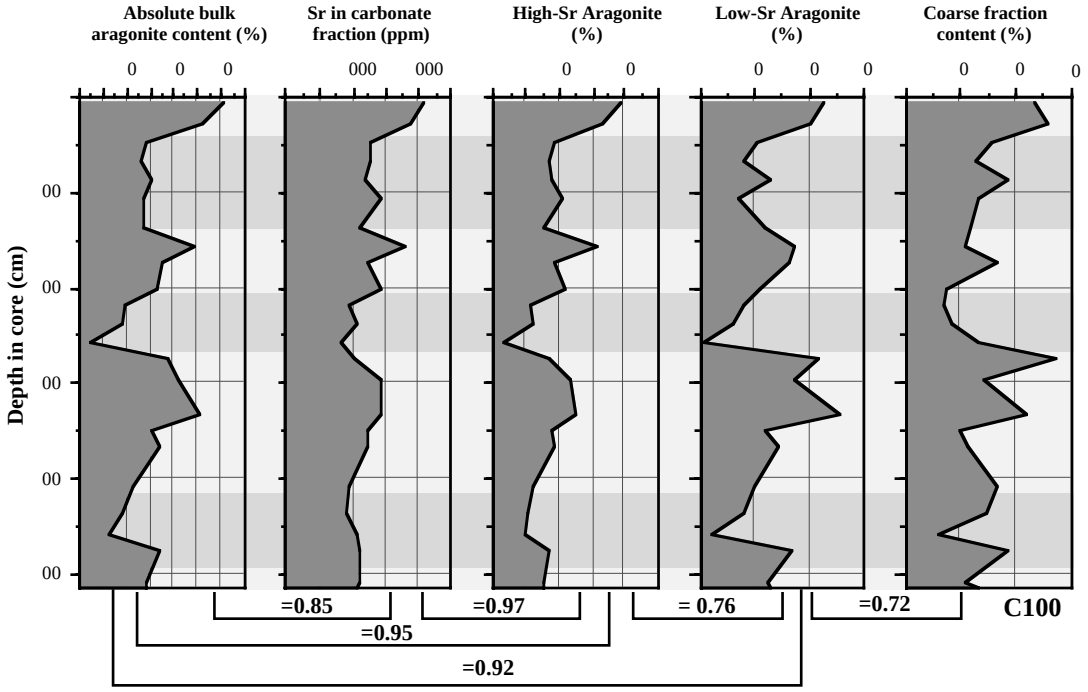

Fig. 9.11: Distribution of mineralogical (aragonite bulk content), geochemical (Sr in carbonate fraction, High- and low-Sr-aragonite) and sedimentological (coarse fraction content) proxies vs. depth within distal downcurrent core PC100. Correlation coefficients (r) are shown at the base, isotope stages (I.S.) on the right.

(C) Upcurrent core M35052

The upcurrent margins and basins receive lower amounts of neritic sediments. This can be seen in the lowered content of aragonite and Sr within the periplatform sediments. This core was retrieved from an intermediate waterdepth of 1445 mbsl, and therefore, metastable carbonates could have been affected by dissolution.

A low correlation can be observed between the bulk aragonite signal and the Sr content in the carbonate fraction (r=0.48, r^2=0.22). It seems that the source of Sr is not only of neritic origin. This observation might be correct for most of the sediment deposited in the upcurrent basins of Pedro Bank. The core also shows similar trends for high- and low-Sr-aragonite input (r=0.72), which probably can be attributed to a similar process such as dissolution affecting both signals. The good correlation between the coarse fraction content and the percentage of low-Sr-aragonite (r=0.88) indicates that most of the low-Sr-aragonite measured in the bulk sediments is of pelagic origin. Pteropods, which form a major component within sediments retrieved from the Northern Nicaragua Rise (see Chapter 8; Glaser, 1991; Schwartz, 1996), probably are the main source for low-Sr-aragonite.

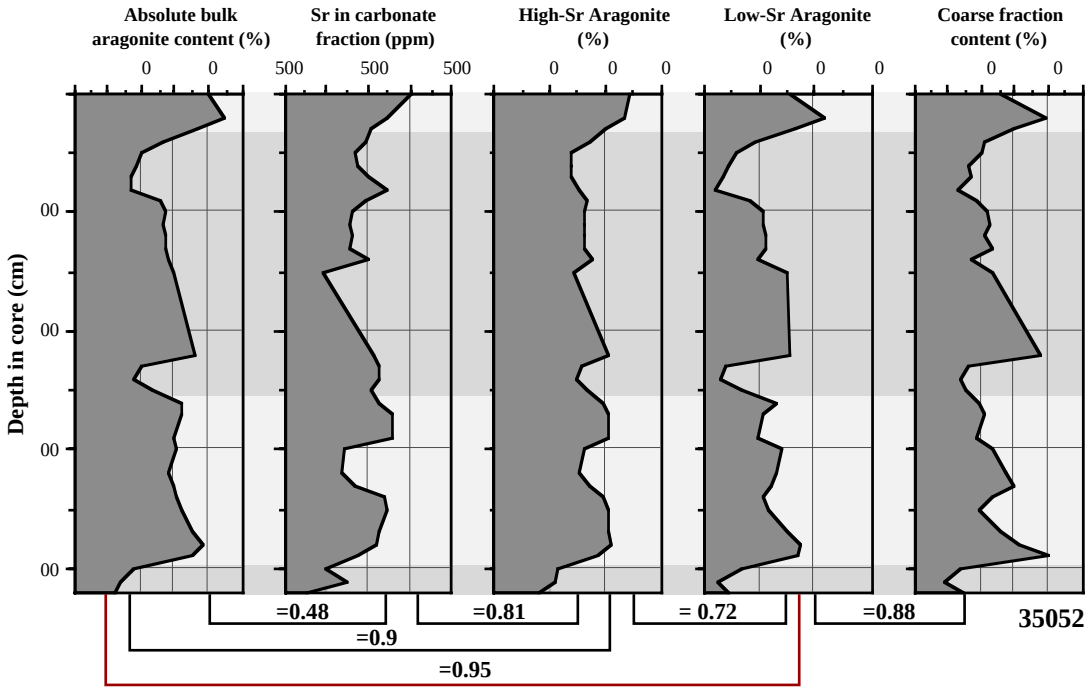

Fig. 9.12: Distribution of mineralogical (aragonite bulk content), geochemical (Sr in carbonate fraction, High- and low-Sr-aragonite) and sedimentological (coarse fraction content) proxies vs. depth within proximal downcurrent core M35052. Simple correlation coefficients (r) are shown at the base, isotope stages (I.S.) on the right.

9.3.4 Terrigenous input (Fig. 9.13)

The main siliciclastic components within the bulk periplatform sediments are SiO_2 and Al_2O_3. Within the three downcurrent cores a clear increase of major and minor elements with increasing offbank distance is evident. These elements show a high positive correlation (r>0.8) with the non-carbonates of these cores (see correlation matrix for geochemistry and mineralogy proxies in Appendix 7). These oxides and elements are SiO_2, Al_2O_3, TiO_2, K_2O, Fe_2O_3, and Zn. The only core that shows a slightly lower correlation of distinct major elements to the content of non-carbonates (r=0.6-0.7) is the most proximal core M35048. Within this core Al_2O_3, K_2O and Fe_2O_3 are positively correlated with the content of non-carbonates. Furthermore there is a good correlation (r=0.6-0.83) between the content of SiO_2 and MgO, Na_2O and K_2O. The average amounts of SiO_2 (1.4%) and Al_2O_3 (0.5%), the main indicators for terrigenous input (Ward et al., 1995), are low but increase rapidly with increasing distance along the downcurrent cores M35049 and PC100 (e.g. SiO_2: 5.2 - 12.1%; Al_2O_3: 1.9 - 4.5%). They show highest contents within the bulk periplatform sediments in upcurrent position (SiO_2: 16.2%; Al_2O_3: 5.6%). M35052, the only core from an upcurrent position displays the maximum content for all these oxides. This might indicate significant terrigenous input to the periplatform sediments. The mean values in SiO_2 (16.8%), Al_2O_3 (5.6), Na_2O (1.8), Fe_2O_3 (2.6) and K_2O are the highest averages seen in all analysed cores, pointing to a different composition of the sediments in up- and downcurrent position. TiO_2 shows an excellent correlation with Al_2O_3 of r=0.99 within distal downcurrent core PC100 and upcurrent core M35052, which probably receive more terrigenous material than neritic influenced core sites, and thus dilution from neritic sources is lowered. The excellent correlation indicates that both elements might have the same primary source.

The content of MgO varies between 0.9 to 2.5% within all cores. Within distal up- and downcurrent sites the MgO content displays similar trends as those seen for terrigenous components (Fig. 9.13). In downcurrent proximal sediment cores (M35048 and -49) the MgO content is not in phase with geochemical terrigenous proxies such as Al_2O_3. In downcurrent proximal cores the correlation of HMC and MgO is good (M35048: r=0.91; M35049: r=0.7), whereas in the distal core PC100 the correlation is very weak with r=0.28 (Fig. 9.14). This probably indicates that the MgO signal in proximal cores is influenced by other sources than in distal up- and downcurrent cores (see discussion). M35052, in his upcurrent location to Pedro

Bank, shows a weak correlation coefficient of r=0.6 for MgO and HMC (not shown in figures), which probably indicates a mixed input signal of different sources (see discussion).

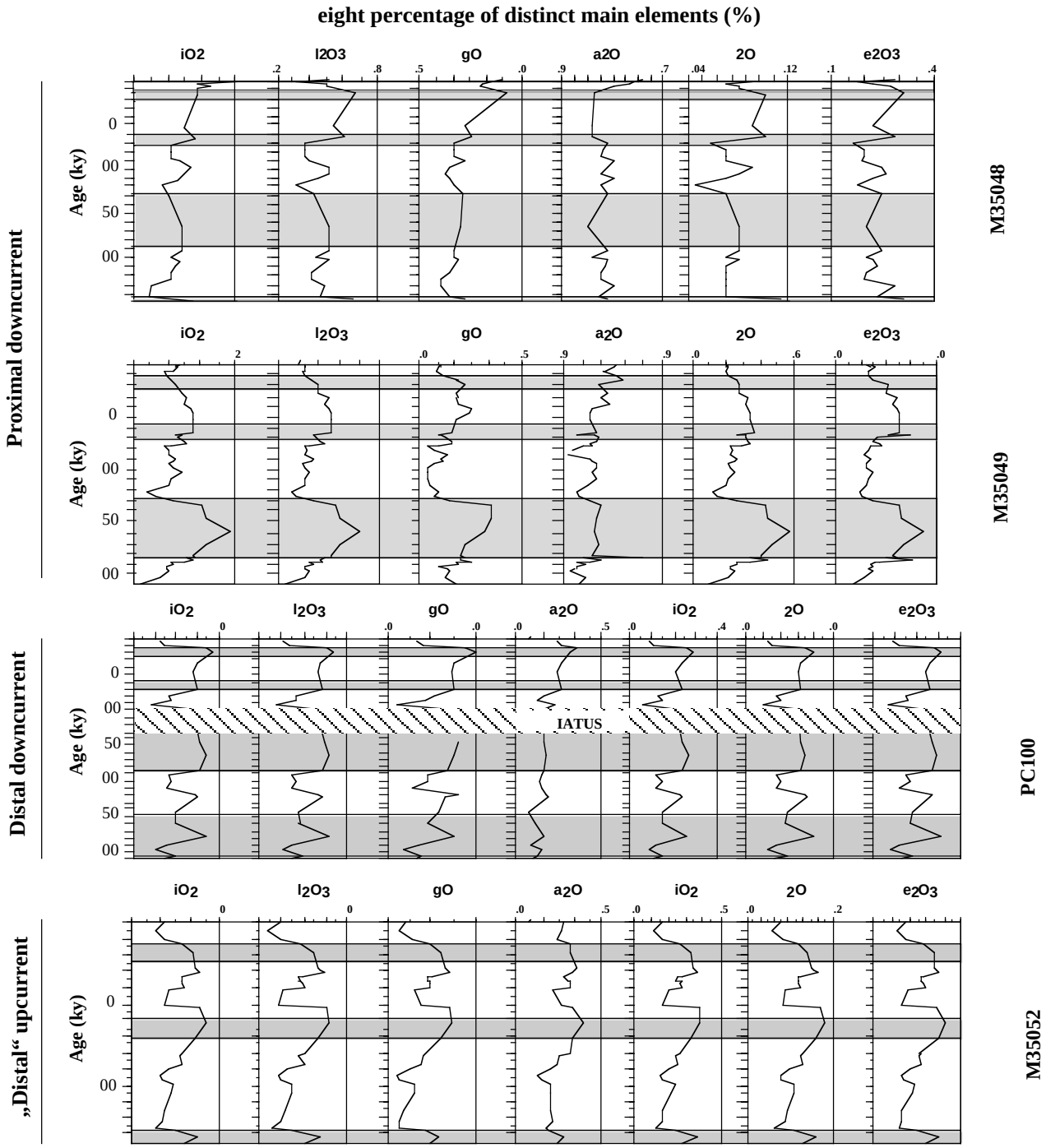

Fig. 9.13: Distribution of main oxides (mainly of terrigenous sources) within the analysed sediment cores. Note the similarity in the abundance of the different proxies within each core. The content of MgO probably displays a mixed signal of neritic and terrigenous origin (see chapter 9.3.5).

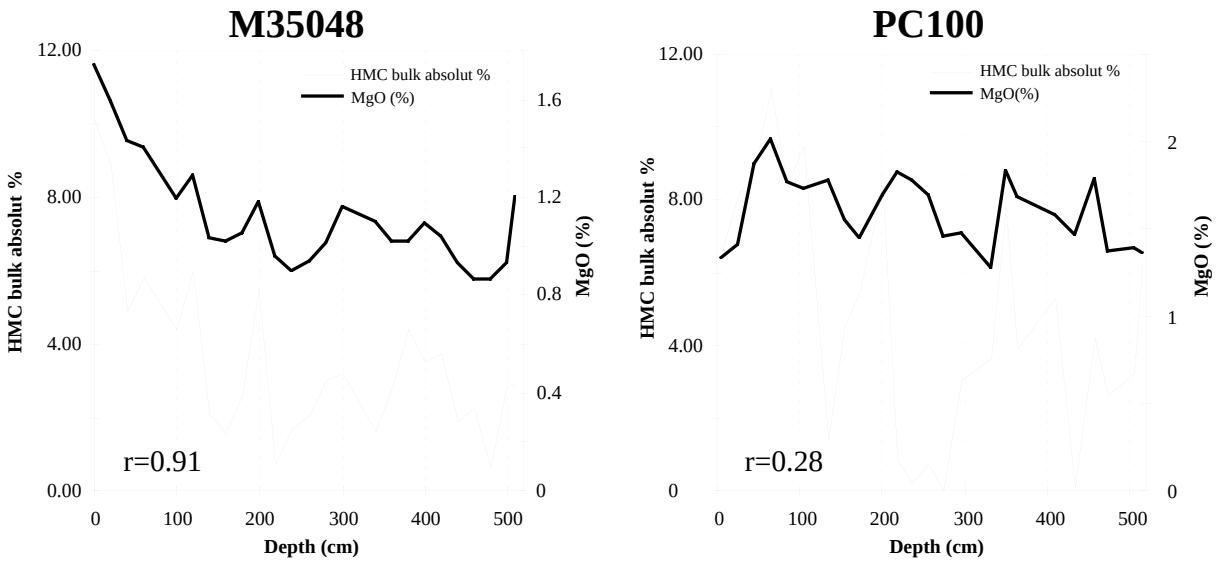

Fig. 9.14: Contents of MgO and HMC within a proximal (M35048) and a distal (PC100) sediment core. Note the excellent correlation for the proximal core (r=0.91), whereas the fit of both proxies in distal core PC100 is relatively low (r=0.28).

9.4 Discussion

9.4.1 Strontium as an indicator for shallow-water input

The results of the geochemical analysis revealed distinct differences in the content of bank-derived strontium. The average strontium concentration in the carbonate fraction in most proximal cores range from 4140 to 6100 ppm, with maximum amounts of about 7800 ppm. They fall in the same range as those observed in Bahamian periplatform sediments by Boardman et al. (1986), but are significantly lower than those observed by Alexander (1996) at the GBR and Emmermann (2000) in the Red Sea. This might be caused by the dominance of shallow-water, reef-derived skeletal grains in these environments (Piller & Mansour, 1990; Piller, 1994; Brachert, 1999), which generally have lower Sr-concentrations. Both areas also display a mixed carbonate-siliciclastic environment. The Bahamian and the Northern Nicaragua Rise shallow-water environments in contrast are dominated by green algae, such as *Halimeda* or *Penicillus*, ooids or inorganically precipitated aragonite (whitings), resulting in the overall higher amounts of aragonite with high strontium values in the periplatform oozes.

1. Correlation between Sr- and aragonite content

Strontium in periplatform oozes might originate from two sources: the neritic input of high-Sr-aragonite and the pelagic input of low-Sr-aragonite. The aragonite contents were correlated with the raw uncorrected Sr content and the Sr content in the carbonate fraction (chapter 9.3.2), as it was assumed that most of the Sr is bound in the carbonates within the carbonate system of Pedro Bank. The highest correlation coefficients between aragonite and Sr were found in downcurrent core M35049 (r^2=0.944), although it is not the most proximal site. This high correlation supports the rationale that high Sr concentrations indicate enhanced neritic carbonate content and thus shallow-water input from an active producing carbonate system (Alexander, 1996). The clear interglacial-glacial variations recorded in the Sr contents with high amounts during interglacial and low contents of Sr during glacial periods shows the influence of late Quaternary sea level changes on the shallow carbonate production and their export (Glaser & Droxler, 1991; Alexander, 1996; Emmermann, 2000). This indicates that highstand shedding (Droxler & Schlager, 1985; Schlager et al., 1994) dominated the aragonite and strontium input patterns observed in the carbonates of the proximal periplatform cores.

The lower correlation between Sr concentrations and the aragonite content at the most proximal site M35048 suggests that the sediments might have undergone early diagenetic processes (chapter 4). The sediment deposited at this shallow and most proximal downcurrent sites should show a good correlation between the two “neritic input” proxies of aragonite and Sr. Although

there is a good fit of both proxies (Fig. 9.5), the low correlation coefficient of "only" r^2=0.678 (compared to the other cores of this study) points to a possible "diagenetic overprint" of the sediments. This might explain why isotope analysis on planktic foraminifera failed for this core. Sediments found at site M35048 are relatively coarse in comparison to the other downcurrent sites studied in this thesis (see Chapter 7). This might indicate a higher diagenetic potential of the sediments (Westphal, 1997; Rendle, 2000). Westphal (1997) showed that coarse glacial periplatform deposits along the margins of Great Bahama Bank, with their higher permeabilities, can be subjected to intense diagenetic alteration. These glacial deposits contained a high percentage of HMC-cements, indicative for diagenetic alteration of the sediments. The observed first cementation of coarse turbidite layers at site M35048 (see Chapter 8) thus also might be an indicator for the finding that diagenetic processes have affected M35048 sediments to a certain degree.

2. High- and low-Sr-aragonite and their correlation to sediment components

The shallow cores M35048 and M35049 show different patterns between the high- and low-Sr-aragonite with no or negative correlation (r=-0.8 to r=-0.25; Figs. 9.9 and 9.10). These results show that both proxies are not controlled by the same process such as selective dissolution, which would result in a more synchronous pattern (Boardman et al., 1986). Thus, each of the single Sr-aragonite proxies displays its own "input history", with high-Sr-aragonite showing the input from the neritic realm, and low-Sr-aragonite the pelagic sources such as pteropods and pelycopod shells. The nearly identical correlation coefficient between the low-Sr-aragonite and the coarse fraction content in both cores (r=0.55; Figs. 9.9/9.10) might point to a similar relationship between low-Sr and coarse fraction content at both sites. The reason for the lower correlation in comparison to the deep distal cores PC100 and M35052 (r=0.72 to r=0.88; Figs. 9.11/9.12) might be caused by the relative high amount of neritic input at proximal sites diluting the pelagic signal (see Chapters 6 and 7). In contrast the deep and distal sites (PC100, M35052) show a very similar correlation between the content of high-and low-Sr-aragonite (r=0.72 to r=0.76). This indicates that similar controlling factors might have influenced both proxies at the deep sites. It seems likely that selective dissolution of the different aragonite varieties caused the observed correlation pattern. The results thus agree with studies by Glaser & Droxler (1991), Haddad & Droxler (1996) and Schwartz (1996), who showed that dissolution of metastable carbonates occurs on the Northern Nicaragua Rise in depths exceeding 1100 mbsl. Boardman & Neumann (1986) and Droxler (1986) argued whether bank top shedding or dissolution of metastable carbonates shaped the observed aragonite pattern in an relatively shallow site from Northwest Providence Channel (CH-8201-07; 675 mbsl). Boardman et al. (1986) favoured the "input model" and stated that the observed aragonite pattern is a primary depositional signal and not the result of dissolution cycles of metastable carbonates. Droxler et al. (1986) instead favoured a strong influence of dissolution to be responsible for the fluctuations in metastable aragonite. The high- and low-Sr-aragonite input pattern found in shallow, proximal cores from the Pedro Bank periplatform environment show that the aragonite signal is mainly controlled by the input of neritic carbonates thus supporting the interpretation of Boardman et al. (1986). In contrast, the high- and low-Sr-aragonite pattern observed at the deep and distal sites (below 1100 mbsl) supports the findings of Droxler et al. (1986) and others (Haddad & Droxler, 1996; Schwartz, 1996) of a strong impact of dissolution shaping the observed pattern of metastable aragonite.

Thus this study shows that various factors must be considered when interpreting the found pattern of metastable carbonates at each depositional sites. The main factors are the relative position to the active bank margin, the depth of deposition and, obviously resulting from both forementioned factors, the influence of paleoceanographical and environmental factors, such as water masses, depth of lysocline for metastable carbonates or early diagenesis.

9.4.2 Terrigenous components

The geochemical signature of the cores shows the increasing influence of terrigenous components with greater offbank distance. In addition, upcurrent cores show highest amounts in terrigenous components. This is due to their position closer to the main source of terrigenous input into the Caribbean Sea from the South American rivers (Bowles & Fleischer, 1985; Schwartz, 1996; Flood & Piper, 1997; Franz, 1999). The non-carbonate fraction within the periplaform sediment is displayed in the content of SiO_2, Al_2O_3, TiO_2, K_2O, Fe_2O_3, Zn and, depending on the core location, also by MgO. These elements are predominantly terrestrially

derived. Al_2O_3, Fe_2O_3 and TiO_2 originate from aluminosilicates and oxyhydroxides, whereas Na_2O and K_2O are mainly present in feldspar (albite and orthoclase), smectice and halite (Calvert & Pedersen, 1993; Ward et al., 1995). The high correlation coefficients of the aforementioned elements to the non-carbonate fraction (see Appendix 7) thus shows their close relationship to the terrigenous sediment fraction. In proximal cores, however, the correlation is relatively weak, due to the strong influence of neritic sedimentation resulting in dilution of the terrigenous sediment fraction. In proximal positions current winnowing might restrain fine terrigenous components to be deposited during times of lowered sea levels (see chapters 6 and 7). Distal downcurrent or upcurrent depositional sites are situated closer to the source areas, which becomes evident in their higher correlation coefficients between typical siliciclastic proxies like silicium, aluminium and other elements (see Fig. 9.13 and correlation matrices in the Appendix 7). The glacial-interglacial cyclicity of terrigenous sediment components with higher contents during sea level lowstands support the sequence stratigraphic models of Vail et al. (1991) predicting higher input of siliciclastics into the worlds ocean during glacial times.
The magnesium content was determined through mineralogical (XRD) and geochemical (XRF) analyses. HMC can be of skeletal origin (e.g. Milliman, 1974), and thus is an indicator for neritic input (Ward et al., 1995). The authors showed that MgO is associated with the carbonate fraction in an inner-shelf embayment of the Great Barrier Reef (GBR). HMC can also precipitate inorganically as cement on the seafloor (e.g. Gevirtz & Friedmann, 1966; Milliman et al., 1969; Schlager & James, 1978; Ellis & Milliman, 1985; Wilber & Neumann, 1993), preferentially during glacial periods. A third source for Mg might be the terrigenous fraction while it also occurs with oxyhydroxides and aluminosilicates (Ward et al., 1995). The high correlation (r=0.91) between the content of MgO and HMC in the bulk sediment at proximal site M35048 shows that both proxies are influenced to a major extent by the input of skeletal high magnesium calcite or the precipitation of Mg-rich cements (see Fig. 9.14 and Appendix 7). In the deep and distal cores (such as PC100; Fig. 9.14), the correlation between HMC and MgO is only very weak with r=0.28. The MgO content at these distal sites is probably driven by other Mg sources, most likely the terrigenous input by the Caribbean Current sites (Bowles & Fleischer, 1985; Schwartz, 1996; Flood & Piper, 1997; Franz, 1999), which is substantiated by the high correlation factors (r>0.947) between MgO and the non-carbonates at both distal sites. Therefore the results of the geochemical and mineralogical study of periplatform sediments along platform-to-basin transect can be used easily for the characterisation and identification of sediment sources.

9.5 Conclusions

The results of this study show that the measurement of strontium in periplatform sediments can be used to differentiate between (1) the influence of neritic input (high-Sr-aragonite) and (2) of pelagic sources (low-Sr-aragonite) in the periplatform sediments of Pedro Bank. However, a strong necessity exists that the calibration for the high- and low-Sr-aragonite calculation is adapted to the type of sediments found in the study area (see Boardman et al., 1986; Droxler et al., 1986).

The shallow, proximal sites clearly show the input of neritic-sourced Sr, which is mainly bound in the fine exported aragonite. This becomes evident as both, high- and low Sr-aragonite display there own temporal trend. In addition, the geochemical analyses might indicate first diagenetic alterations within coarser-grained proximal sediment cores.
At distal sites, which are situated below the depths of beginning dissolution of metastable carbonates (about 1100 mbsl at the NNR), the distribution pattern of low- and high-Sr aragonite become very similar, suggesting that dissolution affected both varieties of Sr in the same way.

In addition, the results of this geochemical study show that the terrigenous sediments fraction in periplatform sediments of the Pedro Bank carbonate system increases with greater offbank distance. Highest concentrations can be found in upcurrent locations to Pedro Bank, due to their closer proximity to the main source areas of terrigenous input into the Caribbean Sea, the South American rivers. This high amount of non-carbonates might also play an important role for the dilution of bank-derived sediments shedded offbank along the upcurrent margins, resulting in the overall lower percentages of neritic sediment material at these locations (Chapter 6 and 7).

CHAPTER 10

TIMING AND DISTRIBUTION OF CALCITURBIDITES AROUND A DEEPLY SUBMERGED CARBONATE PLATFORM (PEDRO BANK, NORTHERN NICARAGUA RISE, CARIBBEAN SEA)

10.1 Introduction

10.1.1 Turbidites and sea level

Sediment gravity flows such as turbidites are a common sedimentological feature on the slopes and within basins of siliciclastic and carbonate systems. In the siliciclastic system these gravity flows preferentially occur during sea level lowstands, when large quantities of shelf sediments are deposited on the slopes and redeposited into the basins (e.g. Vail et al., 1977; Vail, 1987; Mitchum, 1977; Schlager, 1993) due to the exposure of the shelf and the subsequent erosion. Carbonate systems show usually a reversed pattern, because sediments are exported to the slope and basins during highstands in sea level, when the bank tops are flooded and highly productive (e.g. Droxler, 1984; Droxler & Schlager 1985; Reijmer et al., 1988).
Previous studies on the Bahama platform, a tectonically quiescent passive margin area, have shown that late Quaternary calciturbidites occur with a much higher frequency during interglacials ("highstand bundling" sensu Droxler & Schlager, 1985). The compositional changes within turbidite layers also show the link between their increased content of bank-derived biota and highstands in sea level (e.g. Haak & Schlager, 1989; Reijmer et al. 1992).

10.1.2 Modern physiography of Pedro Bank

The bank top morphology of Pedro Bank exhibits an inclined platform (Zans, 1958; Triffleman et al., 1992) in which main parts of the bank lie within waterdepths of 20-40 mbsl. This means that main parts lie below the zone of "maximum productivity", the upper 10 m of the water column, sensu Bosscher (1992). Submersible dives along the steep forereef/platform slope at the northwestern part of Pedro Bank showed that the deepest part of the banktop lies in about 60-65 mbsl (Dullo, 1997), which is about 20-25 m deeper than indicated by previous studies (e.g. Triffleman et al., 1992). The extension of this "terrace" is not known, but it can be assumed that smaller areas around the northern to northwestern edge of Pedro Bank can form minor flat areas that may have been flooded during sea level stands of - 40 to -60 meters below present sea level (e.g. during MIS 3; Pinter & Gardner, 1989; Bard et al., 1990; Chapter 7). Similar areas are also shown on the bathymetric map of Pedro Bank by Dolan (1972). This map displays several small fringes on the northwestern, northern, southeastern and southwestern margin of Pedro Bank along where the bank top is situated between 40-100 mbsl (Dolan, 1972).

10.1.3 Objectives of this study

This study present new data on the distribution pattern of sediment gravity flows ("turbidites") and on the depositional timing of those turbidite layers in respect to their relative position, their offbank distance to the Pedro Bank carbonate system, and in addition, the local topography of the sedimentary basins they were retrieved from. It will be shown that seafloor morphology (flat floored basins vs. regional tectonically derived morphology) and relative changes in sea level play a major role in the distribution pattern of turbidites in the periplatform setting off Pedro Bank. The inclined bank top morphology of Pedro Bank might lead to different triggering times of turbidites on the deeper northern and shallower southern bank margin of this carbonate platform.

10.2 Methods

10.2.1 Sampling procedure

For this study thirteen sediment cores taken from the periplatform setting around Pedro Bank (Northern Nicaragua Rise, eastern Caribbean Sea) were used. They contain 2 to 17 turbidite layers. The cores were taken in 1988, 1992 and 1996 during two American (R/V *Cape Hatteras*

cruises CH0288 and CH9204) and one German (R/V *Meteor* cruise M35/1) research cruise (Fig. 10.1, Table 10.1).

Core (No. in Fig. 10.1)	Relative position (closest distance to active bank margin)	Up-/Down-current position	Latitude (°N)	Longitude (°W)	No. of Turbi-dites	Topo-graphy
M35032-2 (8)	SW-Edge (25 km)	Upcurrent	16.5925	78.6261	6	flat floor
M35034-1 (7)	SW-Edge(toe-of-slope / Pedro Channel; 10 km)	Upcurrent	16.9092	79.0694	5	near toe-of-slope
M35042-2 (4)	NW-Transect (41 km)	Downcurrent	17.6486	79.3094	8	flat floor
M35043-1 (3)	NW-Transect (28 km)	Downcurrent	17.6441	79.1691	2	local topogr.
M35048-1 (1)	NW-Transect (5.5 km)	Downcurrent	17.6469	78.9144	3	horst struct.
M35049-2 (2)	NW-Transect (19.5 km)	Downcurrent	17.6438	79.0877	2	local topogr.
M35052-2 (9)	SE-Edge (30 km)	Upcurrent	16.5753	77.7028	7	flat floor
PC 059 (5)	NW-Transect (72 km)	Downcurrent	17.7255	79.6353	8	canyon slope
PC 100 (6)	NW-Transect (91 km)	Downcurrent	17.9211	79.7166	16	canyon slope
PC 016 (10)	SW-Edge (35 km)	Upcurrent	16.4097	78.4094	10	flat floor
PC 035 (11)	Walton Basin (15 km)	Downcurrent	17.8377	78.3939	17	flat floor
PC 073 (12)	SE-Edge (31 km)	Upcurrent	16.9108	77.145	7	flat floor
[PC 076 (14)]	[SE-Edge (3.9 km)]	[Upcurrent]	[17.0585]	[77.1729]	[5]	[upper slope]
PC 108 (13)	NW-Edge (30 km)	Downcurrent	17.8619	78.8005	10	flat floor

Table 10.1: Core locations, relative position, number of turbidites and surrounding topography of the thirteen analysed sediment cores. Site PC076 is also shown. For this core no stratigraphy could be established, therefore the timing of turbidites could not be determined. However, the grain-size data of the turbidites were included for the those of a proximal depositional setting.

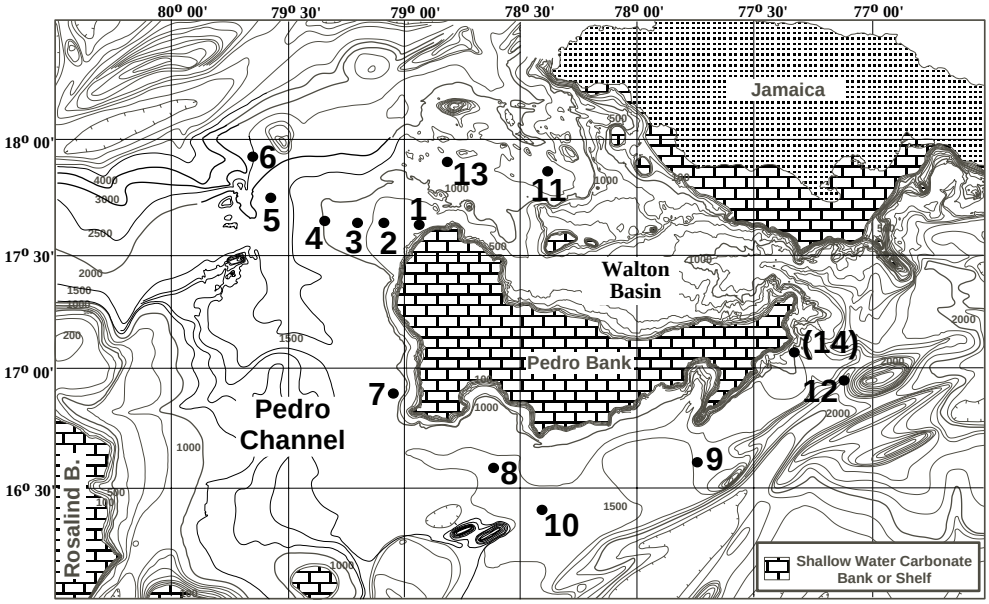

Fig. 10.1: Bathymetric map for the Pedro Bank area with core locations used within this study. Bathymetry after Cunningham (1998). Core abbreviations are as follows: 1=M35048; **2**=M35049; **3**=M35043; **4**=M35042; **5**=PC059; **6**=PC100; **7**=M35034; **8**=M35032; **9**=M35052; **10**=PC016; **11**=PC035; **12**=PC073; **13**=PC108; (**14**=PC076).

All sediment cores were described visually using the Dunham classification (Dunham, 1963). Normal background sediment samples were taken at equal distance of 10 cm. Turbidite layers were sampled additionally, trying to cover the entire sedimentological range within each turbidite layer.

10.2.2 Analytical Methods

The following methods were used to analyse the sediments, which are all described in further detail within chapter 2:
- detailed core descriptions (Appendix 1)
- wet sieving to distinguish the absolute contents of the fine (<63µm) and coarse (> 63µm) fraction.
- dry sieving of the coarse fraction into 5 subclasses using the standard sieves for 63µm, 125µm, 250µm, 500µm and 1000µm
- $\delta^{18}O$-measurements on the planktic foraminifer *Globigerinoides sacculifer* to construct age models for each core
- X-ray diffraction analysis of the fine fraction to determine the mineralogical composition of the sediments (mainly carbonate mineralogy)
- description and photographic documentation of artificial thin sections of the soft sediments to show microfacial changes within the turbidites
- bathymetric (Parasound system) and seismic data (3.5Khz seismics of Rice University) to determine the seabottom morphology around Pedro Bank.

10.2.3 Timing of turbidite shedding

Within the scope of this study it was necessary to define the timing of highstands and lowstands in sea level, in order to determine the time of deposition of the turbidites. In sequence stratigraphy different seismic features (e.g. onlap, offlap, incisions) are used to define high- and lowstands in sea level (Vail et al., 1977; Sarg, 1988). Using the oxygen isotope stratigraphy we are able to define very precisely different positions in sea level. Therefore, a turbidite was classified as a "highstand turbidite" when a layer was deposited during an interglacial marine isotope stage. The stage boundaries were used given by the SPECMAP-Stack of Imbrie et al. (1984). Lowstand turbidites were classified using the glacial isotope stages and their assigned stage boundary ages (Fig. 10.2). In addition a second subdivision was made with respect to major transgressive and regressive phases along the stage boundaries. The major transgressions were defined between the lowest glacial sea level and the highest sea level at the beginning of the following interglacial (e.g.from lowstands 2.2 to highstand 1.1 or from isotope event 6.2 to event 5.5). The reverse scenario defined the regressive phases. Turbidites deposited during these phases maybe counted repeatedly - firstly for the deposition within a major transgressive or regressive phase, and secondly regarding to their relative age as a high- or lowstand turbidite. To determine whether a turbidite was deposited within a regressive or transgressive phase of sea level, the interpolated ages for those depths in which turbidites were deposited (and of the non-turbidite samples above and below those layers) were compared to the SPECMAP curve ages. The main glacial-interglacial and interglacial-glacial transitions could then easily be determined, and the specific turbidites could be classified as of transgressive or regressive origin.
Pedro Bank does not represent a flat-topped platform that is flooded along the entire margin at the same time. This might result in a different stratigraphic distribution of turbidites along the up- and downcurrrent margins. However, this special morphology offers the opportunity to determine the effect of rising or falling sea level on the timing of turbidites on the up- and downcurrent margins of the platform.

10.2.4 Identification of turbidites

Layers were classified as turbidites using the following criteria. These criteria follow the definitions outlined by Crevello & Schlager (1980) and Droxler & Schlager (1985):
(1) sharp basal contacts,
(2) generally coarse-sized grains at the base fining upwards into periplatform muds; packstone or grainstone texture,
(3) very bright colors,
(4) Very bright colors and only very fine silty and clayey material ("muddy turbidites" or endtails of large turbidites, which left their coarse load nearer to their source area),
(5) graded bedding in layers of rubble, sand and silt,
(6) parallel lamination or ripple cross-lamination in sand.

10.3 Results

10.3.1 Overall turbidite distribution

The overall glacial/interglacial distribution of turbidite layers surrounding Pedro Bank only partly show the highstand bundling pattern as described by Droxler & Schlager (1985) for the

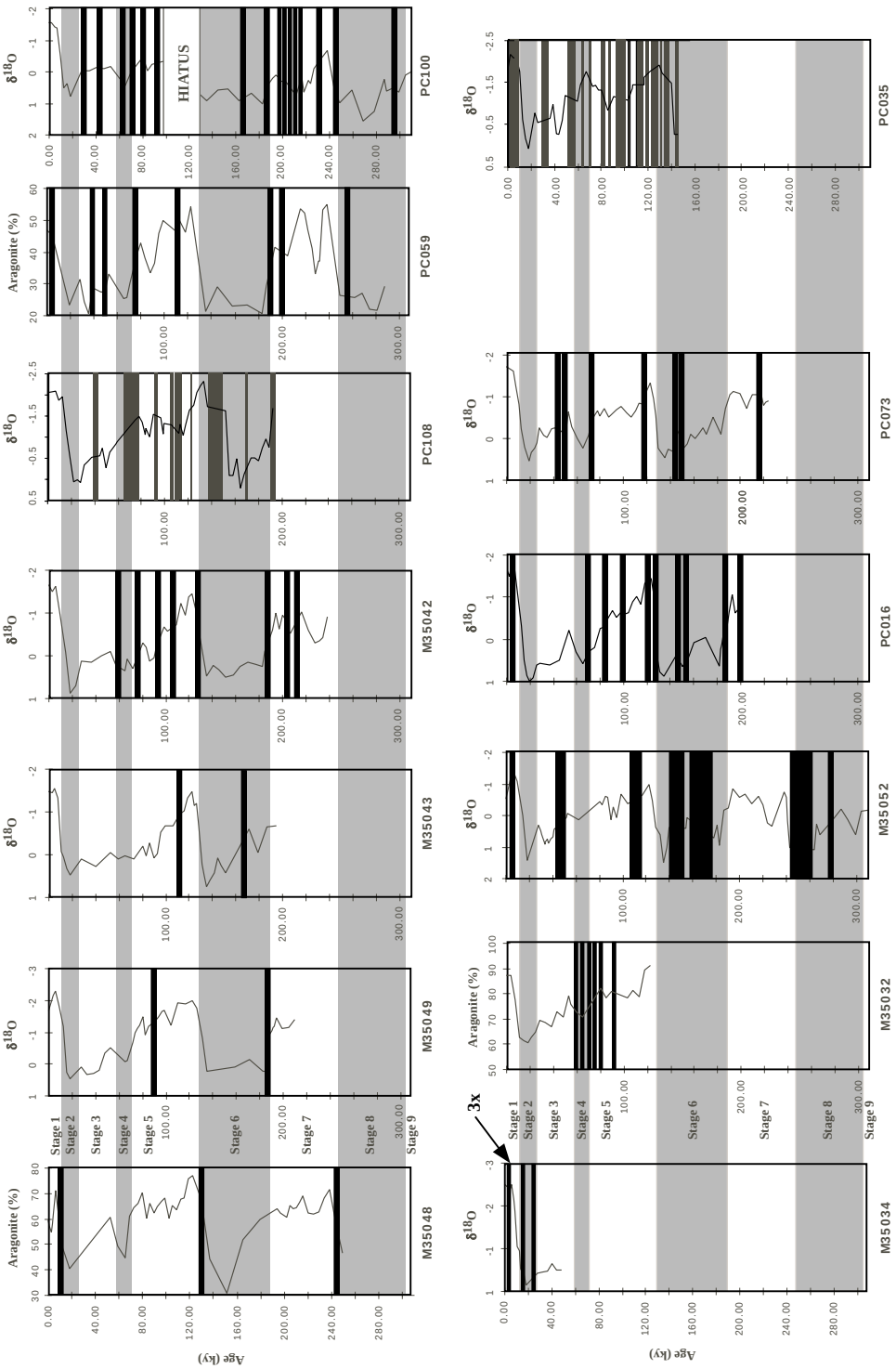

Fig. 10.2: Overview on the turbidite distribution in 13 periplatform cores around Pedro Bank. In total 101 turbidite layers were observed. Turbidites are displayed within the stratigraphic column of each sediment core ($\delta^{18}O$ or aragonite content.). The upper column and the most right core in the lower column represent downcurrent sediment cores, the lower column shows the upcurrent cores. Core locations are shown in Fig. 10.1. The data for cores PC035, PC073 and PC108 are taken from Glaser (1991), the data for core PC016 are unpublished data from Droxler (Rice University).

Tongue of the Ocean, Bahama Platform (TOTO). This is based on the fact that the studied area lacks the number of turbidites in the sedimentary record as present within periplatform sediments from the TOTO, while the periplatform environment of Pedro Bank is not fully surrounded by active producing carbonate banks as it is in the TOTO. Despite the lack of massive turbidite deposition and the fact that Pedro Bank is located within a tectonically active margin area, the turbidite distribution pattern of this deeply submerged carbonate bank still exhibits a clear highstand bundling pattern.

Out of 101 turbidites layers within 13 periplatform sediment cores around Pedro Bank 61% are deposited during interglacial "highstands" in sea level, and 26% during glacial lowstands (Fig. 10.3). About 13% of all turbidites were deposited during MIS 3. During this interstadial sea level estimates range between -50 to -90 m below the Holocene sea level ($\delta^{18}O$ data, Haddad, 1994) and/or between -30 to -65 m below recent sea level (coral reef terraces, Shackleton, 1987; Pinter & Gardner, 1989; Bard et al., 1990). Assuming that at least parts of Pedro Bank with its banks tops in -40 to -60 mbsl were flooded during this interstadial "highstand", about 75% of all turbidites were deposited during highstands in sea level.

About 61% out of 44 turbidite layers have been triggered during "regressive" phases in sea level (Fig. 10.3), therefore during the transition phases from full interglacial to glacial conditions. Similar observations were made by Crevello & Schlager (1989) for Exuma Sound (Bahamas). The remaining 39% percent of turbidite layers are deposited during the major transgressive phases in sea level, during the transition from full glacial to interglacial conditions. A similar pattern was observed by Droxler & Schlager (1985) in the TOTO.

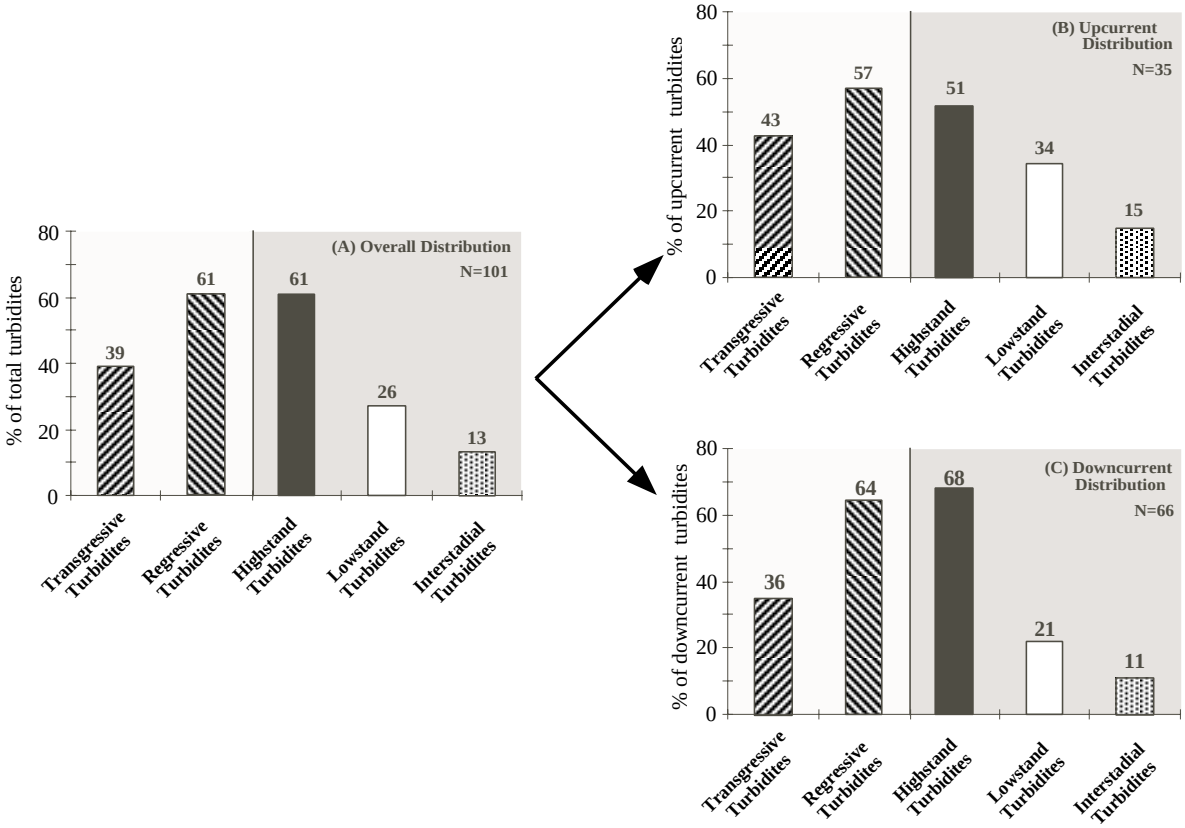

Fig. 10.3: Overall (A), up (B)- and downcurrent (C) turbidite distribution. The preferential turbidite deposition during interglacial periods with highstands in sea level is clearly visible. Note the similarity in the high- vs. lowstand turbidite distribution, as well as in the transgressive vs. regressive depositional trends in up- and downcurrent cores. In the main direction of sediment export on the downcurrent side, nearly 80% of all turbidites were deposited during interglacial and interstadial highstands in sea level.

10.3.2 Up- vs. downcurrent turbidite distribution

Comparing up- and downcurrent distribution patterns it becomes clear that more or less the same turbidite distribution pattern occurs on both sides of the platform (Fig. 10.3). Most of the turbidites are deposited during highstands in sea level, 51% (upcurrent) vs. 68% (downcurrent)

respectively (Figs. 10.4, 10.5 and 10.6), and mainly during regressive interglacial-glacial transitions in sea level (57% and 64%, respectively). Although about 15% more turbidites were deposited on the upcurrent side (34%) during glacial lowstands than on the downcurrent side (21%), it seems that the relative position to Pedro Bank does not play a major role in the timing and subsequent deposition of the individual turbidites. It is evident that the "highstand bundling" pattern sensu Droxler & Schlager (1985) can be seen more accurately on the leeward, downcurrent side of Pedro Bank being the side of main sediment export. In addition, the basin and slope morphology may play a major role in the distribution of turbidite layers (Chapter 5).

10.3.3 Turbidite distribution patterns and basin morphology

Three groups of sediment cores exist, each with their own specific turbidite distribution pattern.

(A) Sediment cores M35042, PC108, PC016 and PC035

These four cores show a more or less identical turbidite distribution pattern (Fig. 10.4). Three out of 4 cores are located around the northwestern edge of Pedro Bank.

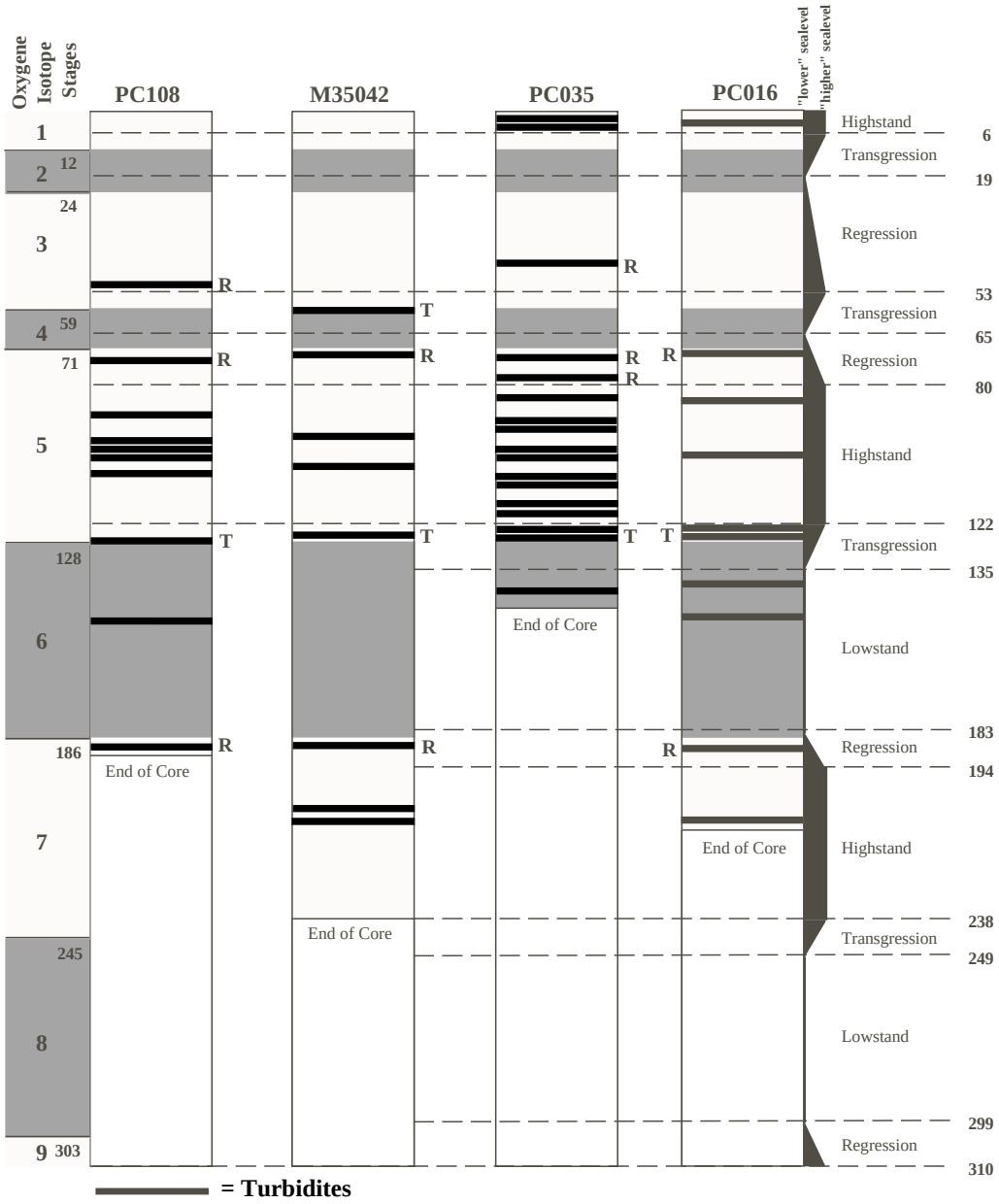

Fig. 10.4: Distribution and timing of turbidites in sediment cores retrieved from flat floored basins. Glacials are marked by a dark gray pattern. Isotope stages are shown on the left. Bold numbers indicate SPECMAP ages in ky after Imbrie et al. (1984). Sea-level phases are shown on the right (R= Turbidite deposited during regressive sea level phase, T= Turbidite deposited during transgressive sea level phase).

Core M35042 is linked to depositional processes of Pedro Bank and partly from Pedro Channel, whereas PC108 is mainly influenced by input from Pedro Bank itself. PC035 possibly is additionally influenced by Walton Bank and the southern Jamaican Shelf, as well as Pedro Bank. This might explain the high number of turbidites present in this core during stage 5. PC016 is situated about 35 kilometers off the southern edge of Pedro Bank and therefore reflects a distinctly different depositional and sedimentological environment. Although the cores are situated at different relative positions with respect to Pedro Bank, the seismics show that all of these cores have been recovered from “flat floored basins”.
The following patterns seem to be similar for these cores:

- 1) the first turbidite layer in the each highstand bundle occurred during the “initial last third” (Andresen et al., 1999) of sea level transgressions, corresponding to the initial bank top flooding of Pedro Bank at each glacial to interglacial stage boundary.
- 2) the last turbidite layers in each highstand bundle occur within the regressional phase from the last interglacial highstand to the glacial lowstand. This can be seen very well for interglacial-to-glacial transitions from stage 7 to 6 and 5 to 4.

3) Furthermore, these cores exhibit much more turbidites within interglacials then observed in all other cores.

(B) Other cores around Pedro Bank

The remaining cores show a very irregular calciturbidite distribution pattern (M35032, M35034, M35043, M35049, M35052, PC059, PC100, PC073; Figs. 10.5 and 10.6). The turbidite layers occur more random during sea level high- and lowstands as well as regressions and transgressions. The possible reasons for these irregular patterns will be given in the discussion, but is yet not fully understood.

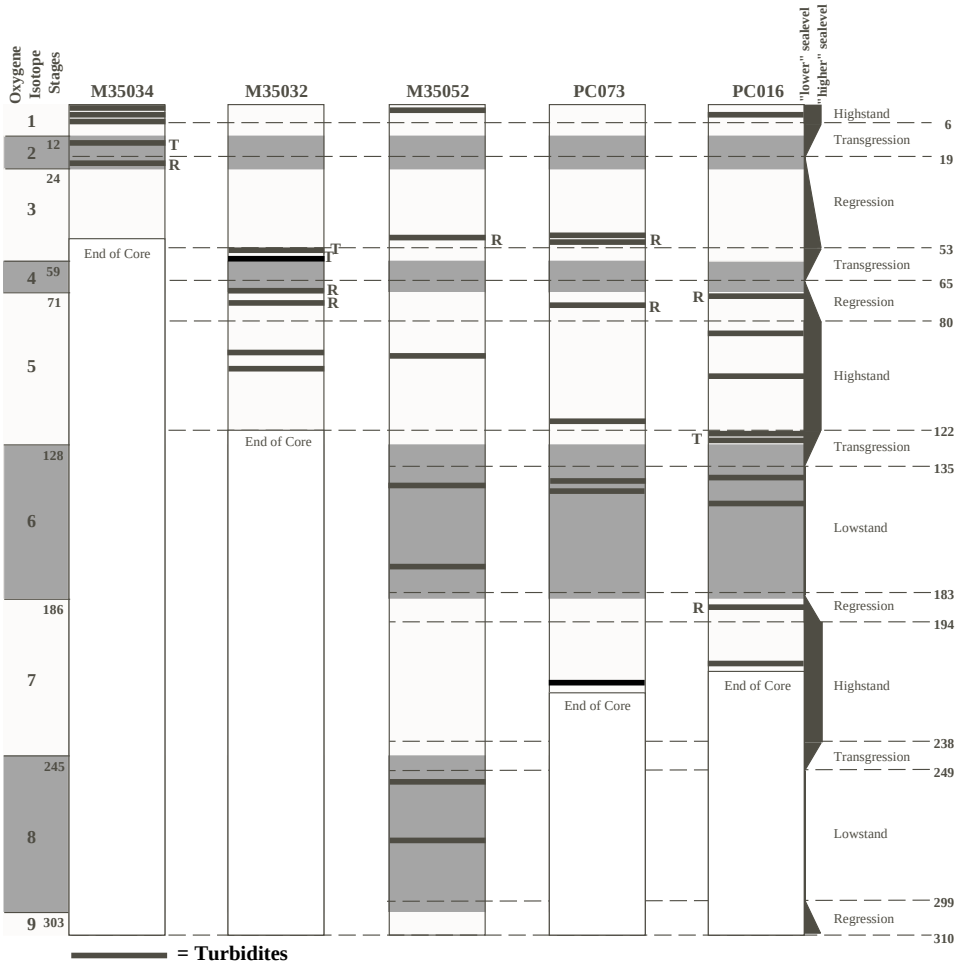

Fig. 10.5: Distribution and timing of turbidites in upcurrent sediment cores of Pedro Bank. Glacials are marked by a dark gray pattern. Isotope stages are shown on the left. Bold numbers on both sides indicate SPECMAP ages in ky after Imbrie et al. (1984). Sea-level phases are shown on the right (R= Turbidite deposited during regressive sea level phase, T= Turbidite deposited during transgressive sea level phase).

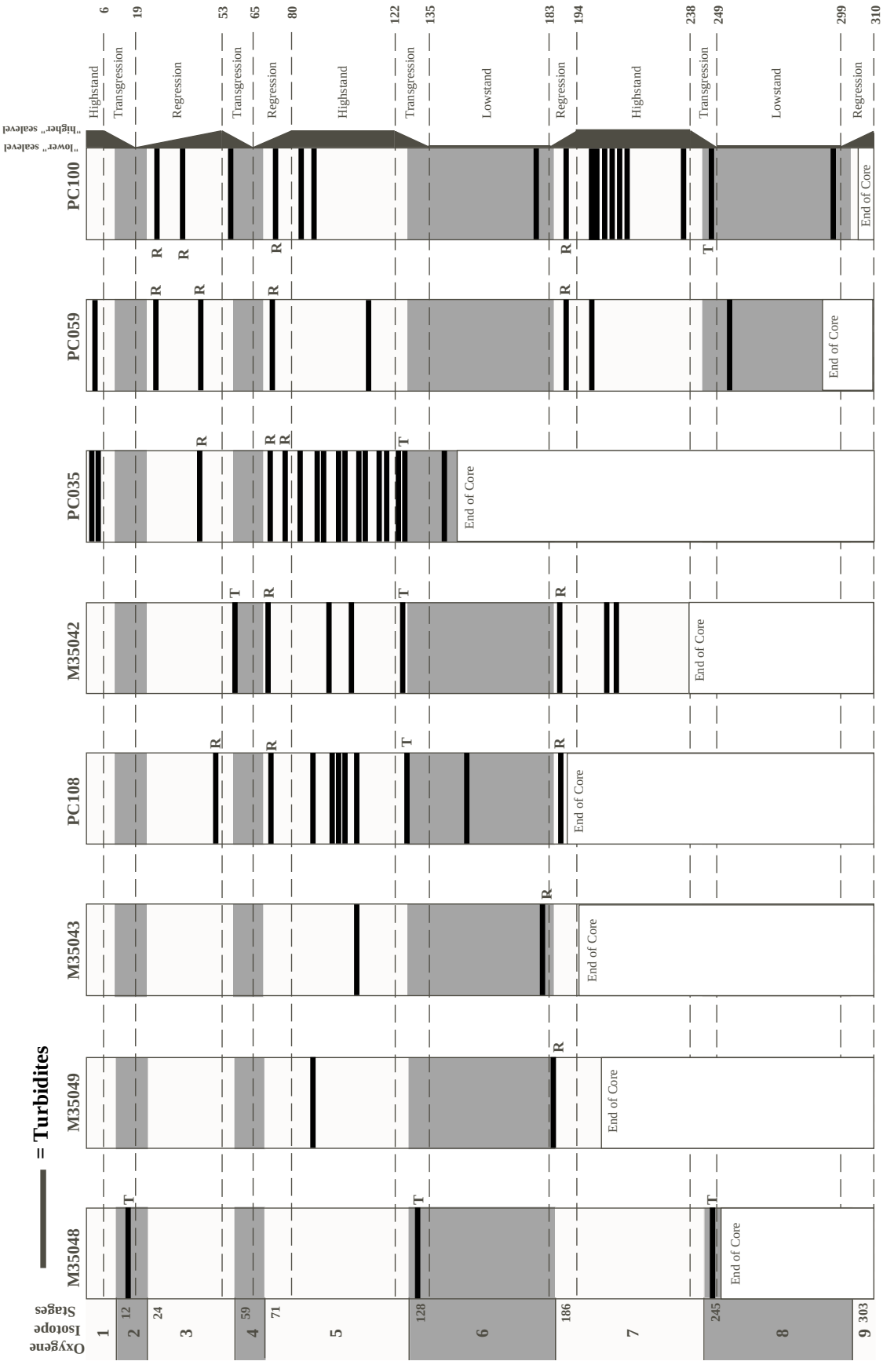

Fig. 10.5: Distribution and timing of turbidites in downcurrent sediment cores. Glacials are marked by a dark gray pattern. Isotope stages are shown on the left. Bold numbers indicate SPECMAP ages in ky after Imbrie et al. (1984). Sea-level phases are shown on the right (R= Turbidite deposited during regressive sea level phase, T= Turbidite deposited during transgressive sea level phase).

(C) Core M35048

In core M35048, the most proximal core within the northwestern off-bank transect, turbidites were deposited exclusively at the very beginning of major glacial-interglacial transitions (Fig. 10.6). These turbidite layers mainly contain pteropods and planktic foraminifera, and to a very minor amount shallow-water components.

10.3.4 Turbidite frequency

In order to compare the turbidite frequency between interglacial and glacial marine isotope stages the number of turbidites per isotope stage were counted in the sediment cores. The frequency of the turbidite layers was calculated by dividing the amount of turbidite layers by the time of each specific isotope stage (Fig. 10.7). Eighty-one out of the 101 turbidite layers were deposited during the last 186ky, i.e. during oxygen isotope stages 1-6. The turbidite frequency within the last two full glacial-to-interglacial transitions shows that the interglacial to glacial turbidite ratio is about 3:1 (Table 10.2). Only 20 turbidites were deposited during marine isotope stages 7 and 8. Despite this low number of turbidites deposited during these marine isotope stages, which probably results in the 3 times lower interglacial to glacial frequency of turbidites, the same trend in the interglacial/glacial ratio (2.7:1) can be observed as for interglacial and glacial isotope stages 1-6.

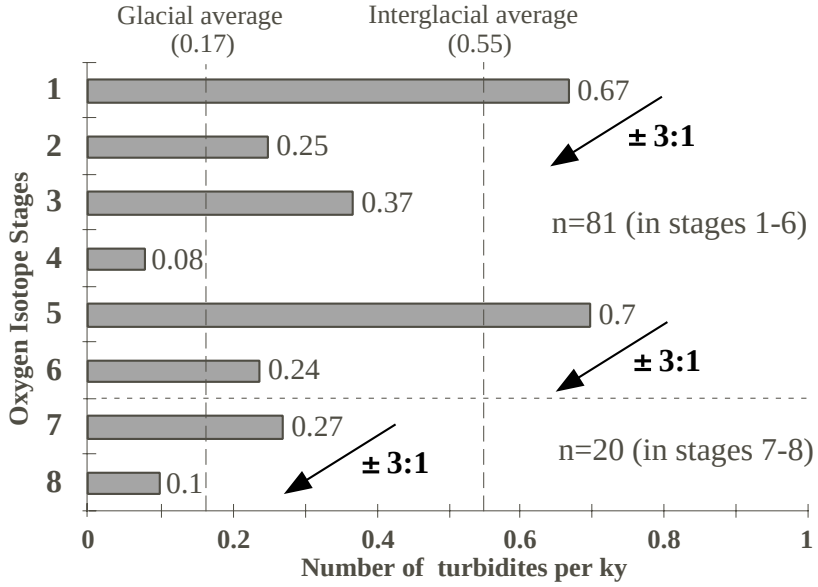

Fig. 10.7: Frequency of turbidites deposited during oxygen isotope stages 1-8 (approx. 300 ky to recent). The turbidite ratio during the last 3 interglacial-glacial cycles is very similar with about 3:1, which shows the validity of the highstand shedding concept.

Interglacial vs. Glacial	Ratio of interglacial. vs. glacial turbidites	Average turbidites per 1000 yr
Stage 1 vs. Stage 2	2.7 : 1	
Stage 1 vs. Stage 2-4	2.9 : 1	
Stage 5 vs. Stage 6	2.9 : 1	
Stage 7 vs. Stage 8	2.7 : 1	
Interglacials		0.55
Glacials		0.17

Table 10.2: Averaged ratio of interglacial vs. glacial turbidites off Pedro Bank.

10.3.5 Turbidite composition

The composition of the individual turbidites was achieved by visual inspection and description of artificial thin sections of the turbidites (Chapter 8). The samples contained only minor amounts of bank-derived shallow water components. The sediments are matrix dominated, mainly micrite, with minor planktonic foraminifera and pteropod input. The composition of the

individual turbidite layers in up- and downcurrent position of Pedro Bank show the following characteristics:

(I) Downcurrent side (M35042, -43, -48, -49, PC059 & PC100; PC035 & PC108)
The periplatform sediments and turbidites deposited on the downcurrent side of Pedro Bank are dominated by fine constituents of bank-derived material, mainly fine aragonite. Although the downcurrent margin of Pedro Bank is the side for main sediment export, the coarse grain fraction of these cores is dominated by planktic foraminifera and pteropods, as well as most of the turbidite layers. Shallow-water components can be found in minor quantities in one turbidite layer of core M35042. Other shallow-water components can be found to a minor extent in turbidites of core PC108 (Glaser, 1991), situated within a flat-floored basin in a distance of about 30 km. Some alterated *Halimeda* fragments and agglutinating benthic forams occured within proximal core M35048.
Sediment cores located within flat floored basins usually contain higher amounts of fine-grained material. They probably form the endtails of turbidites (muddy turbidites). Coarser base load turbidites are rare. Depending on the bottom topography (canyons or gullies; point sources for bank material), shallow-water grains can be found in flat-floored basins even at large distances to the active bank margin (e.g. PC108). At site PC100, located on the steep eastern flank of the Pedro Channel axis, turbidite layers are dominated by coarse material consisting exclusively of planktic components. This compositional signal might indicate a different source area of those turbidites and/or different sorting processes at the axis slope of Pedro Channel.

(II) Upcurrent side (Cores M35034, -32, -52, PC016 and PC073)
The shallowest parts of the platform are found at the southwestern to southeastern upcurrent margin of Pedro Bank. Therefore, we should be able to trace typical shallow water biota, such as corals, green algae (*Halimeda*), red algae and other bank-derived grains at least within proximal upcurrent turbidite layers. However, the turbidite layers retrieved from upcurrent positions off Pedro Bank also show a dominance of planktic foraminifera and pteropod shell fragments as observed in the downcurrent cores. Probably due to the depth distribution of the bank top of Pedro Bank (extensive areas in 0-20 mbsl along the upcurrent margin), sporadically very small layers with slightly increased amounts of neritic components (Halimeda, corals, geniculate red algae, shallow-water benthic foraminifera) occur in the upcurrent sediment cores.
More distal sediment cores described by Glaser (1991) exhibit at least within a few turbidites typical bank-derived components, although these cores were deposited in large distance to the bank margin. Probably the seabottom topography plays an important role in the turbidite distribution.

10.3.2.5 Grain-size variations within turbidites

In order to classify turbidite layers found on their grain-size variations, the fine vs. medium vs. coarse sand content was used to determine possible changes with respect to relative offbank distance and/or a different depositional environment (Fig. 10.8).
Using the coarse fraction grainsize data the turbidites retrieved can be subdivided into three depositional environments: (1) proximal, (2) distal to the active platform and (3) a very deep and distal environment on the main axis flank of central Pedro Channel (core PC100).

(1) The proximal environment is formed by cores located in about 5.5 km (M35048) and 3.7 km (PC076) offbank distance. The coarse load of these turbidite layers is dominated by medium to coarse sand sediments. The coarse fraction content of core PC076 ranges from 25-53% (average: 36%) and for core M35048 form 49-57% (average: 52%).

(2) A second cluster is formed by cores deposited at an offbank distance of about 10 km (M35034) to 72 km (PC059), outside of the proximal “coarse sediment halo”. The coarse grain sizes within these turbidites are dominated by the fine sand fraction. The turbidites with the coarsest grains show up to 40% medium and less than 20% coarse sand.

(3) In core PC100 the turbidites show a different grain size composition. The coarse grain size distribution shows a tendency to more medium sand sized dominated turbidites, which

apparently is connected to the distal position to the carbonate platform and the influence of open ocean sedimentation.

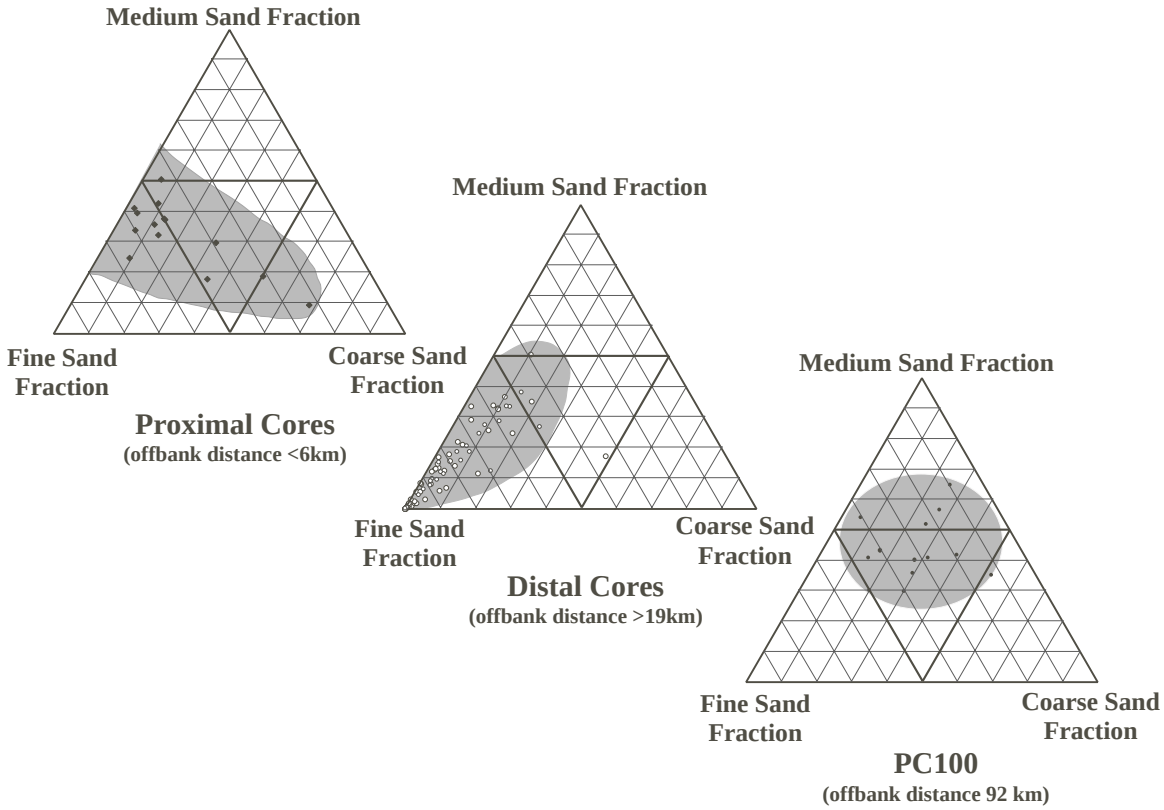

Fig. 10.8: Coarse grain size composition of turbidite layers in dependency on offbank distance from the active bank margin of Pedro Bank.

10.4 Discussion

1. Highstand Bundling and frequency of turbidites

The results of this study support earlier findings of Glaser (1991) from the Walton Basin, which showed a clear coherence of turbidite deposition near carbonate platforms with sea level fluctuations, a hypothesis first described by Droxler & Schlager (1985) from the Tongue of Ocean, Bahamas. A major difference between the Bahamas and Pedro Bank is the setting of Pedro Bank in a tectonically active area. On average 3 times more (75%) turbidites were deposited during interglacial MIS 1, 5 and 7 than during glacial MIS 2, 6 and 8 (see Fig. 10.7). Although this the oberserved turbidite frequency is much lower than the one observed by Droxler & Schlager (1985) in periplatform sediments of the Bahama Bank carbonate platform, this percentage supports the "highstand bundling" theory of Droxler & Schlager (1985). Turbidite bundling, however, is rather an exception to the rule around Pedro Bank (see cores PC108, PC035, M35042). The depositional site probably plays an important role in the turbidite occurence, as more turbidites were found in cores situated in flat-floored sedimentary basins, which are probably fed through submarine canyons or gullies. These morphological features obviously canalize the turbidites into the basins, a mechanism already proposed by Cunningham (1998) on the base of extensive seafloor studies in Pedro Channel (see also Chapter 5).

The turbidite deposition pattern during the last 200 ky also support the hypothesis that "sea-level fluctuations have a stronger influence on the initiation of gravity flows and override the effects of tectonic activity" along the northeastern Nicaragua Rise (Glaser, 1991) near the active margin of the Caribbean plate (Arden, 1976; Burke et al., 1980; Sykes et al., 1982; Mann et al., 1985; Meschede, 1999). Here, at the northwestern bank margin recent earthquakes epicenter could be localized (Wadge & Wooden, 1982). Nonetheless, turbidite initiation seems to be predominantly driven by the production on the bank top as suggested by Glaser (1991), and not result from variation in tectonic activity in the source area (Klein, 1985). Research on turbidite emplacement in the Horseshoe abyssal plain (Iberian margin) also showed the low impact of

tectonic activity on turbidite initiation (Lebreiro et al., 1997). The authors showed that one of the largest earthquakes recorded in human history (Lisbon in 1755) only resulted a thin turbidite layer. In addition, the low amount of eroded lithoclasts in the turbidites around Pedro Bank also suggests another triggering mechanism for gravity flows than tectonic activity, as a higher amounts of lithoclasts are indicative for tectonically induced calcareous turbidites (Eberli, 1991).

2. Distribution and timing of turbidites

A clear trend that can be observed is that more turbidites are deposited during major regressive phases in sea level (61%; Fig. 10.3). This turbidite distribution pattern was also noted by Shanmugan & Moiola (1984) for turbidite layers throughout the Phanerozoic in the Pacific Ocean. Major turbidity currents should occur during the initial stage of sea-level lowering, when carbonate sediments still were unaffected by meteoric cementation. The lowered wave base resulted in slope instabilities, slumps, debris flows and turbidity currents. The large amounts of neritic sediments, which are probably stored on the slopes after a long highstand in sea level were very sensitive to these changing physical conditions resulting in redeposition of the sediments. This type of process was observed by Crevello & Schlager (1980) for Exuma Sound (Bahamas) at the end of interglacial MIS 5. Cook & Taylor (1991) also linked carbonate slope failure to sea level lowering.

Turbidites triggered during major transgressive phases in sea level probably also might result from enhanced production on top of the platform, followed by deposition of these carbonates on the slopes and followed by overloading of the slopes leading to turbidite initiation. This mechanisms seems explain various turbidite events present in the cores PC035, PC108, M35042, PC073 and M35052 shortly after bank tops were flooded during MIS 5 and interstadial MIS 3 (see also Chapter 7). Combining the turbidite data of this study, data of Glaser (1991) and unpublished data of Droxler (Rice University), a striking pattern evolves for the distribution and timing of turbidites from up- and downcurrent positions of Pedro Bank. Four sediment cores (M35042, PC016, PC035 and PC108; see Fig. 10.6) are located at about 30-45 km offbank distance in different flat-floored sedimentary basins, and each of this depositional sites is probably influenced by different sedimentary processes. Despite these different position to Pedro Bank the four cores show a very similar distribution and timing of turbidite layers during the last 200 ky. The first turbidite layer during each highstand occurrs during the “initial last third” of sea level transgression, corresponding to the initial bank top flooding of Pedro Bank at each glacial-interglacial transition, e.g. at about 10 ky during the last glacial/interglacial transition (Glaser, 1991). A similar process and timing of slope failure (at about 7-6 ky, when banks top were flooded) has been described by Grammer et al. (1993) for the Bahamas. Turbidites at the beginning of interglacials were also observed in late Quaternary periplatform sucessions in Tongue of the Ocean (Droxler & Schlager, 1985) and from the leeward margin of Bahama Bank (Eberli et al., 1997). Droxler & Schlager (1985) showed that the abundance of turbidites increased close to the glacial-interglacial boundaries (MIS 2 to 1 and 6 to 5) during the initial bank top flooding. Turbidite initiation seems therefore be closely tied to bank top production, offbank transport and slope failure due to overloading. This pattern is enhanced by the dominance of fine-grained neritic sediment export at the Bahama Bank and Pedro Bank platform. These fine sediments are not able to build up slopes exceeding 5° (Kenter, 1990).

The last turbidite layers in each highstand occur within the major regression from the last interglacial highstand to the glacial lowstand. The triggering process for those turbidites is probably the same process of turbidite initiation by slope failure.

Another pattern that is worth mentioning is the timing of turbidites at the most proximal downcurrent site M35048. At this position turbidites are solely recorded during the early transgression of the last 3 major glacial-interglacial transitions (Fig. 10.5). Although these turbidites contain preferentially planktic components, bank-derived biota and lithoclasts are also evident in minor amounts (see Chapter 7). The timing of turbidites and to some degree the composition of the turbidite layers point to another depositional process causing these turbidites namely the reworking of upper slope deposits during the initial phase of the transgression. This pattern was only found at a proximal downcurrent site close to the bank margin. The mixture of glacial and interglacial sediment deposited during lowstands in sea level probably become instable during the initial phase of sea level rise.

An additional interesting feature is the presence of turbidites during the beginning of interstadial MIS 3 in various up- (PC073, M35052) and downcurrent cores (PC108, PC035). These turbidites likely indicate enhanced production along smaller parts of Pedro Bank situated in depths of at least -40 to -50 mbsl and subsequent turbidite initiation (see also Chapter 7.5.3).

3. Up vs. downcurrent pattern

As the majority of sediment cores in this study originates from an downcurrent setting, it is hard to discuss, if preferentially more turbidites occur along the downcurrent margins. However, Duncan (1997; pers. comm. with Schwartz) stated that turbidite frequency is essentially the same on the upcurrent and downcurrent side of Pedro Bank, although enhanced production on the downcurrent margin should result in a higher turbidite deposition along this margin. On the other hand, Duncan (1997) showed that turbiditic infill of Serranilla Basin occurs in upcurrent direction. He concluded that other factors than the preferential sediment dispersal and export in downcurrent direction, which is mainly controlled by the surface flow of the Caribbean Current, might also control turbidite initiation. Duncan (1997) stated as possible reasons for this upcurrent turbidite infill: (1) seasonal reversals in the surface currents caused by storms, (2) mobilization of neritic sediments from drowned (<400 mbsl) carbonate banks that might have been productive during glacials and (3) canyon systems in the surrounding of Serranilla Bank. Our study shows a minor difference in turbidite deposition between up- and downcurrent position to Pedro Bank. Along the upcurrent margin slightly less turbidites are initiated during highstands and slightly more during lowstands in sea level (Fig. 10.3). If this is caused by steeper slopes on the upcurrent bank margin or the higher wave energy at this site of the platform or one of the other factors suggested by Duncan (1997) cannot be resolved.

4. Composition of turbidites

The composition of turbidites was used to define their time of deposition and their provenance (Haak & Schlager, 1988; Reijmer et al., 1992) along the margins of the flat-topped Great Bahama Bank carbonate platform. The different bank-top morphology of Pedro Bank (deepening to the north: Dolan, 1972; Triffleman et al., 1992) and the abundance of green-algae on the top of Pedro Bank (Hallock et al., 1988; Hine et al., 1998; Dullo, 1997) instead of a coralgal community observed on the Bahamas is a direct result of the “submerged” morphology of Pedro Bank. This causes that typical shallow water components were observed only to a minor extent in Pedro Bank turbidites (see Chapter 8). The desintegration products of abundant green algae (such as *Halimeda*) provide the main amount of neritic carbonates that is exported to the slopes. This is also mirrored in the high abundance of fine-grained turbidites in the basins with high amounts of metastable carbonates (Glaser, 1991; Chapter 8). These fine-grained turbidites are found in more distal settings, whereas coarser grain sized turbidite layers were found further upslope (Fig. 10.8). The coarse grains of the turbidites is dominated by pelagic components such as planktic forams and only to a minor amount by coarse bank-derived grains (see Chapter 8). This differentiation in the deposition of coarse base load turbidites on the upper slope or in a proximal setting and of fine-grained turbidites in more distal parts of the basin, is a normal pattern that evolves from the mechanisms of turbidity current transport (Bouma, 1962; Einsele, 1991 cum lit.). Coarse base loads of turbidites fall out of the suspension in a more proximal position while fine tailends of turbidites proceed to more distal settings. This pattern has also been observed in slope-to-basin sucessions along the leeward margin of Great Bahama Bank (Rendle, personal communication, 2000). Only most distal site PC100, located in central Pedro Channel, exhibits a reverse to this general pattern with a coarser turbidite composition. This material was most likely orginally deposited further upslope at the outer end of the northwestern plateau at about 1100-1200 mbsl, and then redeposited as a mixture of coarse pelagic components with fine-grained hemipelagic sediment (Fig. 10.8).

10.5 Conclusions

Turbidite deposition in the vicinity of Pedro Bank is controlled by various factors:
(1) Late Quaternary sea level fluctuations, (2) production & overloading of upper slope, (3) the proximity of the core location to the bank margin and last but not least (4) different local slope morphologies and seafloor morphology acting as a line source pathway through gullies and canyons for turbidites deposited in the distal flat-floored basins. This supports earlier findings

from other parts of the Pedro Bank margin (Glaser, 1991) and Pedro Channel from Cunningham (1998).

The seafloor morphology might prevent transport of coarse bank-derived sediment far away from the platform margins (Chapter 5). This process might be responsible for the observed dominance of pelagic sediment grains in turbidite layers at most of the distal up- and downcurrrent sites.

Highstand "bundling" of calciturbidites is well-developed even in the tectonically active setting of the Northern Nicaragua Rise close to the Caribbean plate boundary. This is also supported by findings of Lebreiro et al. (1997) from the Iberian continental margin, who showed that even large-scale earthquakes result in no or only very small and thin turbidite layers.
Throughout the last three glacial-interglacial cycles (roughly 300 ky) the turbidite input frequency during interglacials is three times higher than during glacials. This consistent pattern might indicate that no major depositional changes occurred for the Pedro Bank carbonate system during this time interval.

Changes in sea-level are clearly marked by turbidite deposition. This is especially evident during transgressive phases in sea level and renewed bank-top flooding, subsequent neritic sediment overproduction, and offbank export. This transition is usually recorded by the onset of turbidite deposition at various sites along several platform-to-basin transects in down- and upcurrent slope settings. However, slightly more turbidites are deposited during regressive phases in sea-level, probably as a result of sediment reorganisation on the the slope resulting in slope failure.

CHAPTER 11

SUMMARY OF CONCLUSIONS

Sediment Export I (Mineralogy, Grain Size and Microfacies)

The analysis of several periplatform cores taken from the surrounding of Pedro Bank showed that based on mineralogical, grain-size and microfacies studies characteristic depositional environments existed during the last 300 ky, both in space and time. The spatial variability of periplatform sedimentation shown by the mineralogical and grain-size data along a transect off the leeward margin of Pedro Bank exhibits the response of the neritic platform environment to climatic and sea-level changes and its export pattern towards the slopes and into the adjacent basins. As outlined by Glaser & Droxler (1993) and Schwartz (1996) sediment deposition and composition is controlled by four main factors: (1) pelagic and neritic sediment production, (2) dissolution of metastable sediment constituents, (3) the input of non-carbonates and (4) ocean currents. In addition, the results of this thesis clearly show that seafloor morphology also plays an important role in the distribution of periplatform sediments as well as turbidites.

Offbank shedding of neritic sediment components (aragonite and high-Mg calcite) can be observed within a halo of about 20 km at the downcurrent margin, where main export from the platform occurs. During **interglacial highstands in sea level,** the fine sediment fraction (<63 µm) dominates periplatform sediments along the entire leeward transect and no spatial variations in the concentration could be observed. The sediments are dominated by fine aragonite. Within the subclasses of the coarse fraction (>63 µm) the very fine sand fraction dominates only at proximal sites (<20 km) showing the export potential of this shallow-water realm. More distal sites (>20 km) show a more bimodal distribution pattern in the coarse grain sizes with maximum amounts within the very fine sand and the medium sand fraction. This indicates a mixed neritic/pelagic signal. The sediment composition during highstands in sea level revealed that only minor export of coarse neritic grains into the deep surrounding of Pedro Bank takes place. The interglacial periplatform sediments are characterised by a low coarse fraction content and a dominance of coarse planktic grains like planktic foraminifera and pteropods. Microfacies analyses also showed that even in proximal depositional settings close to the toe-of-slope coarse bank-derived grains only occured at an average of about 4 vol.%. The individual groups of coarse shallow-water grains do not show any clear glacial/interglacial distribution pattern, whereas planktic foraminifera and pteropds, which form major parts of the coarse fraction, show very similar temporal variations with high amounts during glacials and low amounts during interglacial periods.

During **glacial lowstands in sea level** a twofold division is evident in the spatial distribution of the periplatform sediments. A proximal environment (<28 km) with enhanced percentages in coarse fraction content vs. a distal environment (> 28 km) with a strong dominance of the fine fraction (> 90%). The raised coarse fraction content at the proximal sites results from various interacting contemporaneous processes: (1) lower input of fine neritic sediments, (2) increased current winnowing, and (3) redepositional processes at the upper slope during lowered sea level stands, and the export of this material to “proximal basinal” sites (< 28 km). In the coarse fraction subclasses a similar distribution pattern is found at all sites showing a bimodal distribution. This might show the low neritic influence, and a similar influence of pelagic sedimentation at all sites during glacials. During glacials, when preservation of metastable carbonate minerals is enhanced at intermediate water depths, aragonite still shows a general decrease with greater offbank distance, whereas HMC shows highest accumulation rates at about 1000-1400 mbsl (= 20-42 km), which might be the result of submarine precipitated HMC-cements or the erosion and redeposition of these cements from upper slope settings and their better preservation potential under the influence of intermediate water masses.

The mineralogy, the turbidite distribution as well as composition analyses of the periplatform sediments deposited during lowered **interstadial sea level stands of MIS 3** might be indicative for enhanced neritic productivity at the top of Pedro Bank. This production might be possible due to the inclined bank top morphology with its deepest parts at the northwestern edge.

In upcurrent locations the carbonate mineralogy displays a similar spatial evolution as seen along the downcurrent margin, but with overall reduced amounts. This is due to the lower export potential of the platform regime against the main direction of the Caribbean Current, one important factor for neritic sediment dispersal in the study area. Turbidites and coarse glacial periplatform sediments from upcurrent settings show a slightly higher abundance of typical shallow-water grains, which mirrors the different faunal composition at the top of Pedro Bank with its shallower bank top depths in comparison to the downcurrent margins.

Lagtimes between sea-level and the timing of deposition of sediment export proxies (e.g. $\delta^{18}O$ vs. aragonite) were observed within several sediment cores from the surrounding of Pedro Bank. These lagtimes probably were caused by the inclined bank top morphology, which results in a different timing of bank-top flooding of Pedro Bank on either the northern or southern margin. This pattern could not be observed in all cores, which might be the result of a variety of other processes such as (1) early diagenesis, (2) relative position to the bank margin, (3) seafloor morphology and (4) syn- and postdepositional dissolution of metastable carbonates, which might might have affected the metastable sediment constituents to a varying degree.

Sediment export II (Turbidites)

Highstand "bundling" of calciturbidites is well-developed even in the tectonically active setting of the Northern Nicaragua Rise close to the Caribbean plate boundary. The high- to lowstand turbidite frequency for the last 300 ky is the same with 3 times more highstand than lowstand turbidites during the last 3 glacial-interglacial cycles. This consistency might indicate that no major depositional changes occurred within the Pedro Bank carbonate system during this time interval. Turbidite deposition in the vicinity of Pedro Bank is controlled by various factors: (1) late Quaternary sea-level fluctuations, (2) sediment production and overloading of the upper slope, (3) the proximity of the core location to the bank margin, (4) local slope morphology and (5) seafloor morphology, which provides a line source for turbidites through gullies and canyons. At the end of these canyon and gully systems the turbidites are deposited in the distal flat-floored basins, which records the history of turbidite shedding at best. In contrast this rough seafloor morphology might also prevent transport of coarse bank-derived sediment far away from the platform margins.

Fluctuations in sea-level are clearly marked by turbidite deposition during transitional intervals. This is especially evident during the onset of bank-top flooding, subsequent neritic sediment overproduction, and offbank export, which is usually recorded by the onset of turbidite deposition at various sites along several platform-to-basin transects in down- and upcurrent slope settings.

Only a few calciturbidites within the up- and downcurrent cores, show a distinct amount of bank-derived grains. However, the majority of calciturbidites from the periplatform setting of Pedro Bank show a dominance of a fine aragonitic matrix (ooze) and of coarse pelagic grains, predominantly planktic foraminifera and pteropods. As the neritic grains were not only found at proximal sites, sedimentation of platform-sourced turbidites is probably associated with the local seafloor morphology. Gullies and canyons act as major pathways for these turbidites, which most probably originate from the upper slope to toe-of-slope setting.

Geochemistry

The results of this study show that the measurement of strontium in periplatform sediments can be used to differentiate between (1) neritic input (high-Sr-aragonite) and (2) pelagic sources (low-Sr-aragonite) for the aragonite content in the periplatform sediments of Pedro Bank.

The shallow, proximal sites clearly mirror the input of neritic-sourced Sr, which is mainly bound in the aragonite of the fine fraction. This becomes evident as both Sr-aragonite varieties displays their own temporal trend. At distal sites situated below the depth of beginning dissolution of metastable carbonates at about 1100 mbsl at the NNR, the temporal pattern of low- and high-Sr aragonite become very similar, suggesting that dissolution affected both varieties of Sr-aragonite in the same way.

CHAPTER 12

REFERENCES

Adey, W. H. (1987) Coral reef morphogenesis: a multidimensional model. *Science*, **202**, 831-837.

Ahrens, L. H. (1952) The use of ionization potentials. Part1: Ionic Radii of the elements. *Geochimica Cosmochimica Acta*, **2**, 155-169.

Alexander, I. T. (1996) Late Quarternary sedimentation off the Queensland continental margin (northeast Australia) in response to sea-level fluctuations. [unpublished Ph.D. Thesis], University of Edinburgh, Edinburgh, Scotland, 492 pp.

Almogi-Labin, A. (1982) Stratigraphic and paleoceanographic significance of late Quarternary pteropods from deep-sea cores in the Gulf of Aqaba (Elat) and northernmost Red Sea. *Marine Micropaleontology*, **7**, 53-72.

Andresen, N., Reijmer, J. J. G. and Droxler, A. W. (1999) Timing, distribution, and composition of calciturbidites in the deep surrounding of Pedro Bank, Northern Nicaragua Rise, Caribbean Sea. In: *Paleoceanology of reefs and carbonate platforms: Miocene to Modern, Vol. 32* (Ed. by Camoin, C. F. and Dullo, W.-C.), pp. 11-13. Publication ASF, Paris, Aix-en-Provence.

Anselmetti, F. S., Eberli, G. P. and Ding, Z.-D. (2000) From the Great Bahama Bank into the Straits of Florida: A margin architecture controlled by sea-level fluctuations and ocean currents. *Geological Society of America Bulletin*, **112**(6), 829-844.

Arden, D. D. (1969) Geologic history of the Nicaraguan Rise. *Transactions - Gulf Coast Association of Geological Societies*, **19**, 295-309.

Arden, D. D. (1975) Geology of Jamaica and the Nicaragua Rise. In: *The Ocean Basins and Margins* (Ed. by Nairn, A. E. M. and Stehli, F. G.), Plenum Press (New York), *Vol. 3*, pp. 617-661.

Backman, J., Duncan, R. A., Peterson , L. C. et al. (1988) Introduction. In: *Proceedings of the Ocean Drilling Program, Part A: Initial reports* (Ed. by Backman, J., Duncan, R. A., Peterson, L. C., *et al.*), Ocean Drilling Program (College Station, TX), *Vol. 115*, pp. 5-15.

Bard, E., Hamelin, B. and Fairbanks, R. G. (1990) U-Th ages obtained by mass spectrometry in corals from Barbados: Sea level during the past 130,.000 years. *Nature*, **346**, 456-458.

Bassinot, F. C., Labeyrie, L. D., Vincent, E., Quidelleur, X., Shackleton, N. J. and Lancelot, Y. (1994) The astronomical theory of climate and the age of the Brunhes-Matuyama magnetic reversal. *Earth and Planetary Science Letters*, **126**, 91-108.

Bates, R. L. and Jackson, J. A. (1997) *Glossary of geology*. American Geological Institute, 788 pp.

Bathurst, R. G. C. (1971) *Carbonate sediments and their diagenesis*. Elsevier (Amsterdam, Netherlands), 620 pp.

Bé, A. W. H. and Gilmer, R. W. (1977) A zoogeographic and taxonomic review of euthecosomotous Pteropoda. In: *Oceanic Micropaleontology* (Ed. by Ramsay, A. T. S.), Academic Press (New York), *Vol. 1 & 2*, pp. 733-808.

Berner, R. A. and Berner, E. K. (1976) Aragonite dissolution on the Bermuda pedestal: its depth and geochemical significance. *Earth and Planetary Science Letters*, **30**, 169-178.

Betzler, C., Reijmer, J. J. G., Bernet, K., Eberli, G. P. and Anselmetti, F. S. (1999) Sedimentary patterns and geometries of the Bahamian outer carbonate ramp (Miocene-Lower Pliocene, Great Bahama Bank). *Sedimentology*, **46**, 1127-1143.

Blanchon, P., Jones, B. and Kalbfleisch, W. (1997) Anatomy of a fringing reef around Grand Cayman: Storm rubble, not coral framework. *Journal of Sedimentary Research*, **67**(1), 1-16.

Blom, W. M. (1988) Late Quaternary sediments and sea levels in Bass Basin, southeastern Australia - A preliminary report. *Search*, **19**, 94-96.

Boardman, M. R. and Neumann, A. C. (1984) Sources of periplatform carbonates: Northwest Providence Channel, Bahamas. *Journal of Sedimentary Petrology*, **54**(4), 1110-1123.

Boardman, M. R., Neumann, A. C., Baker, P. A., Dunlin, L. A., Kenter, R. J., Hunter, G. E. and Kiefer, K. B. (1986) Banktop responses to Quaternary fluctuations in sea level recorded in periplatform sediments. *Geology*, **14**, 28-31.

Boggild, O. G. (1930) The shell structure of the molluscs. *Kgl. Danske Vitenskab. Selskab. Mat. Fys. Medd.*, **9**, 231-325.

Boggs, S. J. (1987) Chapter 5: Sedimentary textures. In: *Principles of Sedimentology and Stratigraphy*. pp. 105-122.

Bolli, H. M., Saunders, J. B. and Perch-Nielsen, K. (1985) *Plankton stratigraphy*. Cambridge University Press (Cambridge, UK), 1032 pp.

Boss, S. K. and Neumann, A. C. (1993) Impact of hurricane Andrew on carbonate platform environments, northern Great Bahama Bank. *Geology*, **21**, 897-900.

Bosscher, H. (1992) Growth potential of coral reefs and carbonate platforms. [Ph.D. Thesis], Vrije Universiteit, Amsterdam, 160 pp.

Bouma, A. H. (1962) *Sedimentology of some Flysch deposits*. Elsevier (Amsterdam), 168 pp.

Bourrouilh-Le Jan, F. G. (1998) The role of high-energy events (hurricanes and/or tsunamis) in the sedimentation, diagenesis and karst initiation of tropical shallow water carbonate platforms and atolls. *Sedimentary Geology*, **118**, 3-36.

Bowles, F. A. and Fleischer, P. (1985) Orinoco and Amazon river sediment input to the eastern Caribbean basin. *Marine Geology*, **68**, 53-72.

Brachert, T. C. (1990) Non-skeletal carbonate production within a deep ocean basin: The "hard layer" of the glacial Red Sea. *Facies*, **40**, 211-228.

Burke, K. (1988) Tectonic evolution of the Caribbean. *Annual Review of Earth and Planetary Science*, **16**, 201-230.

Burke, K., Cooper, C., Dewey, J. F., Mann, P. and Pindell, J. L. (1984) Caribbean tectonics and relative plate motions. In: *The Caribbean-South American plate boundary and regional tectonics* (Ed. by Bonini, W. E., Hargraves, R. B. and Shagam, R.), Geological Society of America Memoir , *Vol. 162*, pp. 31-63.

Burke, K., Fox, P. J. and Celal Singör, A. M. C. (1978) Buoyant ocean floor and the evolution of the Caribbean. *Journal of Geophysical Research*, **83**, 3949-3954.

Burke, K., Gruppi, J. and Celal Singör, A. M. C. (1980) Neogene structures in Jamaica and the tectonic style of the northern Caribbean plate boundary zone. *Journal of Geology*, **88**, 375-386.

Calvert, S. E. and Pedersen, T. F. (1993) Geochemistry of Recent oxic and anoxic marine sediments: implications for the geological record. *Marine Geology*, **113**(67-88).

Case, J. E., Holcombe, T. L. and Martin, R. G. (1984) Map of geologic provinces in the Caribbean region. In: *The Caribbean-South American plate boundary and regional tectonics* (Ed. by Bonini, W. E., Hargraves, R. B. and Shagam, R.), Geological Society of America Memoir , *Vol. 162*, pp. 1-30.

Chappell, J. (1983) A revised sea-level record for the last 300.000 years from Papua New Guinea. *Search*, **14**, 99-101.

Chappell, J., Omura, A., Ezat, T., McCulloch, M., Pandolfi, J., Ota, Y. and Pillans, B. (1996) Reconciliation of late Quaternary sea levels derived from coral terraces at Huon Peninsula with deep-sea oxygen isotope records. *Earth and Planetary Science Letters*, **141**, 227-236.

Chappell, J. and Shackleton, N. J. (1986) Oxygen isotopes and sea level. *Nature*, **324**, 137-140.

Chave, K. E., Deffeyes, K. S., Weyl, P. K., Garrels, R. M. and Thompson, M. E. (1962) Observations on the solubility of skeletal carbonates in aqueous solutions. *Science*, **137**(3523), 33-34.

Chen, C. (1968) Pleistocene pteropods in pelagic sediments. *Nature*, **219**, 1145-1149.

Church, T. M. (1970) Marine Barite. [unpublished Ph.D. thesis], University fo California, 325 pp.

Cook, H. E. and Mullins, H. T. (1983) Basin Margin. In: *Carbonate Depositional Environments* (Ed. by Scholle, P. A., Bebout, D. G. and Moore, C. H.), American Association of Petroleum Geologists, *Vol. 11*, pp. 539-619.

Cook, H. E. and Taylor, M. E. (1991) Carbonate slope failures as indicators of sea level lowerings. *American Association of Petroleum Geologists Bulletin*, **75**(3), 556.

Craig, H. (1957) Isotopic standards for carbon and oxygen correction factors for mass spectrometric analysis of CO_2. *Geochimica Cosmochimica Acta*, **12**, 133-149.

Crevello, P. D. and Schlager, W. (1980) Carbonate debris sheets and turbidites, Exuma Sound, Bahamas. *Journal of Sedimentary Petrology*, **50**(4), 1121-1148.

Crutcher, H. L. and Quayle, R. G. (1974) Mariners world-wide climatic guide to tropical storms at sea. Direction of Commander, Naval Weather Service Command, Navair 50-1C-61, Washington DC, U.S.A. (US Government Printing Office).

Cunningham, A. D. (1998) Neogene evolution of the Pedro Channel carbonate system, Northern Nicaragua Rise. [unpublished Ph.D. thesis], Rice University, Houston, 354 pp.

Davies, P. J. and Montaggioni, L. (1985) Reef growth and sea-level change: The environmental signature. In: *5th international coral reef symposium*, *Vol. 3*, pp. 477-515.

deMol, B. S. G., Westphal, H. and Reijmer, J. J. G. (1998) Correlation between geophysical and sedimentological properties in ODP Leg 166 Site 1005A. In: *15th International Sedimentological Congress*, pp. 290-291, Alicante, Spain.

Digerfeldt, G. and Hendry, M. D. (1987) An 8.000 year Holocene sea-level record from Jamaica: implications for interpretation of Caribbean reef and coastal history. *Coral Reefs*, **5**(165-169).

Dolan, P. (1972) Genesis and distribution of recent sediments on the Pedro Bank, south of Jamaica. [unpublished Ph.D. thesis], University College, London.

Droxler, A. W. (1984) Late Quaternary glacial cycles in the Bahamian deep basins and in the adjacent Atlantic Ocean. [unpublished Ph.D. thesis], University of Miami, Coral Gables, 119 pp.

Droxler, A. W. (1985) Last Deglaciation in the Bahamas: A dissolution record from variations of aragonite content. In: *The carbon cycle and atmospheric CO_2 natural variations Archean to present* (Ed. by Sundquist, E. T. and Broecker, W. S.), Geophysical Monograph , *Vol. 32*, pp. 195-207.

Droxler, A. W., Bruce, C. H., Sager, W. W. and Watkins, D. H. (1988a) Pliocene-Pleistocene variations in aragonite content and planktonic oxygen-isotope record in Bahamian periplatform ooze, Hole 633A. In:

Proceedings of the Ocean Drilling Program, Scientific Results (Ed. by Austin, J. A. and Schlager, W.), Ocean Drilling Program (College Station, TX), *Vol. 101*, pp. 221-236.

Droxler, A. W., Burke, K., Cunningham, A. D., Hine, A. C., Rosencrantz, E., Duncan, D. S., Hallock, P. and Robinson, E. (1998) Caribbean constraints on circulation between Atlantic and Pacific Oceans over the past 40 Million years. In: *Tectonic boundary conditions for climate reconstructions* (Ed. by Crowley, T. and Burke, K.), Oxford Monographs on Geology and Geophysics (Oxford), *Vol. 39*, pp. 160-191.

Droxler, A. W., Haddad, G. A., Mucciarone, D. A. and Cullen, J. L. (1990) Pliocene-Pleistocene aragonite cyclic variations in holes 714A and 716B (The Maldives) compared with hole 633A (The Bahamas): Records of climate-induced $CaCO_3$ preservation at intermediate water depths. In: *Proceedings of the Ocean Drilling Program, Scientific Results* (Ed. by Duncan, R. A., Backman, J., Peterson, L. C., *et al.*), Ocean Drilling Program (College Station, TX), *Vol. 115*, pp. 539-577.

Droxler, A. W., Morse, J. W., Glaser, K. S., Haddad, G. A. and Baker, P. A. (1991) Surface sediment carbonate mineralogy and water column chemistry: Nicaragua Rise vs. Bahamas. *Marine Geology*, **100**, 277-289.

Droxler, A. W., Morse, J. W. and Kornicker, W. A. (1988b) Controls on carbonate mineral accumulation in Bahamian basins and adjacent Atlantic ocean sediments. *Journal of Sedimentary Petrology*, **58**(1), 120-130.

Droxler, A. W. and Schlager, W. (1985) Glacial versus interglacial sedimentation rates and turbidite frequency in the Bahamas. *Geology*, **13**, 799-802.

Droxler, A. W., Schlager, W. and Whallon, C. C. (1983) Quaternary aragonite cycles and oxygen isotope record in Bahamian carbonate ooze. *Geology*, **11**, 235-239.

Dullo, W.-C. (1990) Facies, fossil record, and age of Pleistocene reefs from the Red Sea (Saudi Arabia). *Facies*, **22**, 1-46.

Dullo, W.-C. (1997) Die Plattformhangmorphologie der Pedro Bank in der Karibik. *Geol. Bl. NO-Bayern*, **47**(1-4), 303-320.

Dullo, W.-C., Camoin, G. F., Blomeier, D., Colonna, M., Eisenhauer, A., Faure, G., Casanova, J. and Thomassin, B. A. (1998) Morphology and sediments of the foreslopes of Mayotte, Comoro Islands: direct observations from a submersible. *Special Publications of the International Association of Sedimentologists*, **25**, 219-236.

Dullo, W.-C., Camoin, G. F., Blomeier, D., Eisenhauer, A. and Thomassin, B. A. (1996) Sea-level changes and evolution of the foreslopes of the Comoro Islands: direct observations from submersible. In: *Global and regional controls on biogenic sedimentation. I. Reef evolution. Research Reports* (Ed. by Reitner, J., Neuweiler, F. and Gunkel, F.), Göttinger Arbeiten zur Geologie und Paläontologie (Göttingen), *Vol. SB2*, pp. 19-22.

Duncan, D. S. (1997) The geologic and paleoceanographic evolution of the Serranilla Basin: Northern Nicaragua Rise, Caribbean Sea. [unpublished Ph.D. thesis], University of South Florida, Coral Gables, FL, 195 pp.

Duncan, R. A. and Hargraves, R. B. (1984) Plate tectonic evolution of the Caribbean region in the mantle reference frame. In: *The Caribbean-South American plate boundary and regional tectonics* (Ed. by Bonini, W. E., Hargraves, R. B. and Shagam, R.), Geological Society of America Memoir (Boulder, CO), *Vol. 162*, pp. 81-93.

Dunham, R. (1962) The classification of carbonate rocks according to depositional texture. In: *Classification of Carbonate Rocks - A symposium* (Ed. by Ham, W. E.), American Association of Petroleum Geologists Memoir (Tulsa, OK), , pp. 108-121.

Duplessy, J. C., Be, A. W. H. and Blanc, P. L. (1981) Oxygen and carbon isotopic composition and biogeographic distribution of planktonic foraminifera in the Indian Ocean. *Palaeogeography, Palaeoclimatology, Palaeoecology*, **33**(1-3), 9-46.

Eberli, G. P. (1991) Calcareous turbidites and relationship to sea-level fluctuations and tectonism. In: *Cycles and Events in Stratigraphy* (Ed. by Einsele, G., Ricken, W. and Seilacher, A.), Springer Verlag (Berlin), pp. 340-359.

Eberli, G. P. (2000) The record of Neogene sea-level changes in the prograding carbonates along the Bahamas transect - Leg 166 synthesis. In: *Proceedings of the Ocean Drilling Program, Scientific Results* (Ed. by Swart, P. K., Eberli, G. P., Malone, M. J., *et al.*), Ocean Drilling Program (College Station, TX), *Vol. 166*, pp. 167-177.

Eberli, G. P. and Ginsburg, R. N. (1989) Cenozoic progradation of northwestern Great Bahama Bank, a record of lateral platform growth and sea-level fluctuations. In: *Controls on carbonate platform and basin development* (Ed. by Crevello, P. D., Wilson, J. L., Sarg, J. F., *et al.*), Society of Economic Paleontologists and Mineralogists Special Publication (Tulsa, OK), *Vol. 44*, pp. 339-351.

Eberli, G. P., Swart, P. K. and Malone, M. J. et al. (1997) *Proceedings of the Ocean Drilling Program, Initial Reports*. Ocean Drilling Program (College Station, TX).

Edwards, R. L. (1988) High-precision Th-230 ages of corals and the timing sea-level fluctuations in the late Quaternary. [unpublished Ph.D. thesis].

Ehrmann, W. and Thiede, J. (1985) History of Mesozoic and Cenozoic sediment fluxes to the North Atlantic Ocean. *Contributions to Sedimentology*, **15**, 1-109.

Emery, D. (1996) Carbonate systems. In: *Sequence Stratigraphy* (Ed. by Emery, D. and Myers, K. J.), Cambridge University Press (Cambridge, England), pp. 211-237.

Emiliani, C. (1954) Depth habitats of some species of pelagic foraminifera as indicated by oxygen isotope ratios. *American Journal of Science*, **252**, 149-158.

Emiliani, C. (1955) Pleistocene temperatures. *Journal of Geology*, **63**, 538-578.

Emmermann, P. (2000) Mineralogy, geochemistry and microfacies of Late Quaternary periplatform sediments: Carbonate export cycles and secondary processes - Sanganeb Atoll and Abington Reef, Sudan, Central Red Sea. [unpublished Ph.D. thesis], Christian-Albrechts-Universität, Kiel, Germany, 169 pp.

Emmermann, P., Reijmer, J. J. G. and Andresen, N. (1999) Sedimentation rates of Quarternary periplatform sediments based on aragonite/calcite ratios: Sudanese Red Sea vs. Pedro Bank, Caribbean. In: *On the determination of sediment accumulation rates* (Ed. by Bruns, P. and Haas, C.), Trans Tech Publications (Zürich, Switzerland), *Vol. 5*, pp. 67-86.

Ericson, D. B. and Wollin, G. (1956) Micropaleontological and isotopic determinations of Pleistocene climates. *Micropaleontology*, **2**, 257-270.

Ericson, D. B. and Wollin, G. (1968) Pleistocene climates and chronology in deep-sea sediments. *Science*, **162**, 1227-1234.

Fairbanks, R. G. (1989) A 17.000-year glacio-eustatic sea level record: influence of glacial melting rates on the Younger Dryas event and deep ocean circulation. *Nature*, **342**, 637-642.

Flood, R. D. and Piper, D. J. W. (1997) Amazon fan sedimentation: the relationship to equatorial climate change, continental denudation, and sea-level fluctuations. In: *Proceedings of the Ocean Drilling Program, Scientific Results* (Ed. by Flood, R. D., Piper, D. J. W., Klaus, A., *et al.*), Ocean Drilling Program (College Station, TX), *Vol. 155*, pp. 653-675.

Flügel, E. (1982) *Microfacies analysis of limestones*. Springer Verlag (Berlin), 375 pp.

Franz, S. O. (1999) Pliozäne Zeitreihen zur Rekonstruktion der Tiefenwasserzirkulation und der siliziklastischen Amazonasfracht im Äquatorialen Westatlantik (Ceara Schwelle, ODP Leg 154). [unpublished Ph.D. thesis], Christian-Albrechts Universität, Kiel, 118 pp.

Freile, D., Milliman, J. D. and Hillis, L. (1995) Leeward bank margin Halimeda meadows and draperies and sedimentary importance on the western Great Bahama Bank slope. *Coral Reefs*, **14**, 27-33.

Frisch, W., Meschede, M. and Sick, M. (1992) Origin of the Central American ophiolites: evidence from paleomagnetic results. *Geological Society of America Bulletin*, **104**(10), 1301-1314.

Gallup, C. D. (1997) High-precision Uranium-series analyses of fossil corals and Nicaragua Rise sediments: The timing of high sea levels and the marine δU-234 value during the past 200.000 years. [unpublished Ph.D. thesis], University of Minnesota, , 205 pp.

Gevirtz, J. L. and Friedmann, G. M. (1966) Deep-sea carbonate sediments of the Red Sea and their implications on marine lithification. *Journal of Sedimentary Petrology*, **36**(1), 143-151.

Ginsburg, R. N., Harris, P. M., Eberli, G. P. and Swart, P. K. (1991) The growth potential of a bypass margin, Great Bahama Bank. *Journal of Sedimentary Petrology*, **61**(6), 976-987.

Ginsburg, R. N. and James, N. P. (1976) Submarine botryoidal aragonite in Holocene reef limestones, Belize. *Geology*, **4**, 431-436.

Gischler, E. and Hudson, J. H. (1998) Holocene development of three isolated carbonate platforms, Belize, Central America. *Marine Geology*, **144**, 333-347.

Gischler, E. and Lomando, A. J. (1999) Recent sedimentary facies of isolated carbonate platforms, Belize-Yucatan system, Central America. *Journal of Sedimentary Research*, **69**(3), 747-763.

Glaser, K. S. (1991) Late Quaternary periplatform sediments and environments on the Northeastern Nicaragua Rise, Caribbean Sea. [unpublished Ph.D. thesis], Rice University, Houston, 244 pp.

Glaser, K. S. and Droxler, A. W. (1991) High production and highstand sheeding from deeply submerged carbonate banks, Northern Nicaragua Rise. *Journal of Sedimentary Petrology*, **61**(1), 128-142.

Glaser, K. S. and Droxler, A. W. (1993) Controls and development of Late Quaternary periplatform carbonate stratigraphy in Walton Basin (Northeastern Nicaragua Rise, Caribbean Sea). *Paleoceanography*, **8**(2), 243-274.

Goldberg, E. D. and Arrhenius, G. O. S. (1958) Chemistry of Pacific pelagic sediments. *Geochimica Cosmochimica Acta*, **13**, 153-212.

Gordon, A. L. (1967) Circulation of the Caribbean Sea. *Journal of Geophysical Research*, **72**, 6207-6223.

Gordon, A. L. (1986) Interocean exchange of thermocline water. *Journal of Geophysical Research*, **91**, 5037-5046.

Gordon, A. L., Weiss, R. F., Smethie, W. M., Jr. and Warner, M. J. (1992) Thermocline and intermediate water communication between the South Atlantic and Indian Oceans. *Journal of Geophysical Research*, **97**, 7223-7240.

Govindaraju, K. (1994) 1994 compilation of working values and sample description for 383 geostandards. Geostandards Newsletter, **18**, 1-158.

Grammer, G. M. and Ginsburg, R. N. (1992) Highstand versus lowstand deposition on carbonate platform margins: Insight from Quaternary foreslopes in the Bahamas. *Marine Geology*, **103**, 125-136.

Grammer, G. M., Ginsburg, R. N. and Harris, P. M. (1993) Timing of depostition, diagenesis, and failure of steep carbonate slopes in response to a high-amplitude/ high-resolution fluctuation in sea level, Tongue of the Ocean, Bahamas. In: *Carbonate sequence stratigraphy: recent developments and applications* (Ed. by Loucks, R. G. and Sarg, J. F.), American Association of Petroleum Geologists Memoir (Tulsa, OK), *Vol. 57*, pp. 107-131.

Greinert, J. (1999) Rezente submarine Mineralbildungen - Abbild geochemischer Prozesse an aktiven Fluidaustrittsstellen im Aleuten- und Cascadia-Akkretionskomplex. [unpublished Ph.D. thesis], Christian-Albrechts Universität, Kiel, 196 pp.

Gvirtzman, G. (1994) Fluctuations of sea level during the past 400.000 years: the record of Sinai, Egypt (northern Red Sea). *Coral Reefs*, **13**, 203-214.

Haak, A. B. and Schlager, W. (1989) Compositional variations in calciturbidites due to sea-level fluctuations, late Quaternary, Bahamas. *Geologische Rundschau*, **78**(2), 477-486.

Haddad, G. A. (1994) Calcium carbonate dissolution patterns at intermediate water depths of the tropical oceans during the past Quaternary. [unpublished Ph.D. thesis], Rice University, Houston, TX.

Haddad, G. A. and Droxler, A. W. (1996) Metastable $CaCO_3$ dissolution at intermediate water depths of the Caribbean and western North Atlantic: Implications for intermediate water circulation during the past 200.000 years. *Paleoceanography*, **11**(6), 701-716.

Hallock, P., Hine, A. C., Vargo, G. A., Elrod, J. A. and W.C., J. (1988) Platforms of the Nicaraguan Rise: Examples of the sensitivity of carbonate sedimentation to excess trophic sources. *Geology*, **16**, 1104-1107.

Hamelin, B., Bard, E., Zindler, A. and Fairbanks, R. G. (1991) 234U/238U mass spectrometry of corals: How accurate is the U-Th age of the last interglacial period. *Earth and Planetary Science Letters*, **106**, 169-180.

Handford, C. R. and Loucks, R. G. (1993) Carbonate depositional sequences and systems tracts - Responses of carbonate platforms to relative sea-level changes. In: *Recent Advances and Applications of Carbonate Sequence Stratigraphy* (Ed. by Loucks, R. G. and Sarg, R.), American Association of Petroleum Geologists Memoir (Tulsa, OK), *Vol. 57*, pp. 3-41.

Harmelin-Vivien, M. L. and Laboute, P. (1986) Catastrophic impact of hurricanes on atoll outer reef slopes in the Tuamotu (French Polynesia). *Coral and Reefs*, **5**, 55-62.

Harmon, R. S., Mitterer, R. M., Kriausakul, N., Land, L. S., Schwarcz, H. P., Garrett, P., Larson, G. J., Vacher, H. L. and Rowe, M. (1983) U-series and amino acid racemization geochronology of Bermuda: Implications for eustatic sea-level fluctuations over the past 250.000 years. *Palaeogeography, Palaeoclimatology, Palaeoecology*, **44**(1-2), 41-70.

Harwood, G. H. and Towers, P. A. (1988) Seismic sedimentologic interpretation of a carbonate slope, northern margin of the Little Bahama Bank. In: *Proceedings of the Ocean Drilling Program, Scientific Results* (Ed. by Austin, J. A., Schlager, W. and Comet, P. A.), Ocean Drilling Program (College Station, TX), *Vol. 101*, pp. 263-277.

Henderson, G. M., Lindsay, F. and Slowey, N. C. (1999) Variation of bioturbational mixing depth with water depth on marine slopes: A study on the slopes of the Little Bahama Bank. *Marine Geology*, **160**(1-2), 105-118.

Henderson, G. M., Rendle, R. H., Slowey, N. C. and Reijmer, J. J. G. (2000) U-Th dating and diagenesis of Pleistocene highstand sediments from the Bahama slope. In: *Proceedings of the Ocean Drilling Program, Scientific Results* (Ed. by Swart, P. K., Eberli, G. P., Malone, M. J., *et al.*), Ocean Drilling Program (College Station, TX), *Vol. 166*, pp. 23-31.

Herman, Y. (1978) Calcareous microfossils; pteropods. In: *Introduction to Marine Micropaleontology* (Ed. by Haq, B. and Boersma, A.), Elsevier (New York), , pp. 151-159.

Hidore, J. J. and Oliver, J. E. (1993) *Climatology - An atmospheric science*. MacMillan Publishing Company (New York, U.S.A.).

Hine, A. C., Hallock, P., Harris, M. W., Mullins, H. T., Belknap, D. F. and Jaap, W. C. (1988) Halimeda bioherms along an open seaway: Miskito Channel, Nicaraguan Rise, SW Caribbean Sea. *Coral Reefs*, **6**(3-4), 173-178.

Hine, A. C., Wilber, R. J., Bane, J. M., Neumann, A. C. and Lorenson, K. R. (1981a) Offbank transport of carbonate sands along open, leeward bank margins: northern Bahamas. *Marine Geology*, **42**, 327-348.

Hine, A. C., Wilber, R. J. and Neumann, A. c. (1981b) Carbonate sand bodies along contrasting shallow bank margins facing open seaways in northern Bahamas. *American Association of Petroleum Geologists Bulletin*, **65**(2), 261-290.

Hodell, D. A. (1993) Late Pleistocene paleoceanography of the South Atlantic sector of the Southern Ocean: Ocean Drilling Program hole 704A. *Paleoceanography*, **7**, 79-118.

Hoernle, K., Werner, R., Morgan, J. P., Garbe-Schönberg, D., Bryce, J. and Mrazek, J. (2000) Existence of complex spatial zonation in the Galápagos plume for at least 14 m.y. *Geology*, **28**(5), 435-438.

Hoff, J. A., Edwards, R. L., Buesseler, K. O. and Belastock, R. A. (in press) TIMS measurements of 230Th and 232Th in liter-sized samples of seawater from the Northwest Atlantic Ocean. *Geochimica Cosmochimica Acta*.

Holcombe, T. L., Ladd, J. W., Westbrook, G., Edgar, N. T. and Bowland, C. L. (1990) Caribbean marine geology: Ridges and basins of the plate interior. In: *The Caribbean Region* (Ed. by Dengo, G. and Case, J. E.), Geological Society of America (Boulder, CO), *Vol. H*, pp. 231-260.

Horrowitz, A. S. and Potter, P. E. (1971) *Introductory petrography of fossils*. Springer Verlag (New York), 302 pp.

Hoskin, C. M. (1963) Recent carbonate sedimentation on Alacran Reef, Yucatan, Mexico. Office of Naval Research, Washington, D.C., Foreign Field Research Program, 19.

Hottinger, L., Halicz, E. and Reiss, Z. (1993) *Recent foraminiferida from the Gulf of Aqaba, Red Sea*. Slovenska Akademija Znanosti in Umetnosti (Ljubljana, Yugoslavia), 179 pp.

Houtz, R. and Ludwig, W. J. (1977) Structure of the Colombia Basin, Caribbean Sea, from profiler-sonobuoy measurements. *Journal of Geophysical Research*, **82**, 4861-4867.

Hubbard, D. K., Parsons, K. M., Bythell, J. C. and Walker, N. D. (1991) The effects of hurricane Hugo on the reefs and associated environments of St. Croix, U.S. Virgin Islands - a preliminary assessment. *Journal of Coastal Research*, **8**, 33-48.

Imbrie, J., Hays, J. D., Martinson, D. G., McIntyre, A., Mix, A. C., Morley, J. J., Pisias, N. G., Prell, W. L. and Shackleton, N. J. (1984) The orbital theory of Pleistocene climate: Support from a revised chronology of the marine $\delta^{18}O$ record. In: *Milankovitch and Climate, Part I* (Ed. by Berger, A. L. et al.), D. Reidel Publishing Company, pp. 269-305.

James, N. P. (1983) Reef environment. In: *Carbonate depositional environments* (Ed. by Scholle, P. A., Bebout, D. G. and Moore, C. H.), American Association of Petroleum Geologists Memoir (Tulsa, OK), *Vol. 33*, pp. 345-440.

James, N. P. and Ginsburg, R. N. (1979) *The seaward margin of Belize barrier and atoll reefs*. International Association of Sedimentologists Special Publication (Blackwell Scientific Publications), *Vol. 3*, 191 pp.

Jansen, J. H. F., Kuijpers, A. and Toelstra, S. R. (1986) A Mid-Brunhes climatic event: Long-term changes in global atmospheric and ocean circulation. *Science*, **232**, 619-622.

Jindrich, V. (1972) Biogenic buildings and carbonate sedimentation, Dry Tortugas reef complex, Florida. [unpublished Ph.D. thesis], State University of N.Y., Binghamton, 96 pp.

Jones, M. P. (1987) *Applied mineralogy: A quantitative approach*. Graham and Trotman (Oxford), 259 pp.

Jones, M. R. and Torgersen, T. (1988) Late Quaternary evolution of Lake Carpentaria on the Australia-New Guinea continental shelf. *Australian Journal of Earth Science*, **35**(3), 313-324.

Jung, P. (1973) Pleistocene pteropods, Site 147, Leg 15, Deep Sea Drilling Project. In: *Initial reports of the Deep Sea Drilling Project* (Ed. by Terence, E. N., Saunders, J. B., Bolli, H. M., *et al.*), Deep Sea Drilling Project (College Station, TX), *Vol. 15*, pp. 753-767.

Kearey, P. and Vine, F. J. (1990) *Global Tectonics*. Blackwell Scientific Publications (Oxford, UK), 302 pp.

Kendall, C. G. S. C. and Schlager, W. (1981) Carbonates and relative changes in sea level. *Marine Geology*, **44**, 181-212.

Kenter, J. A. M. (1990) Carbonate platform flanks: Slope angle and sediment fabric. *Sedimentology*, **37**(5).

Kenter, R. J. (1985) Sea-level fluctuations recorded as rythmic deposition in the Northwest Providence Channel, Bahamas. [unpublished M.Sc. thesis], Miami University, Oxford, Ohio, 106 pp.

Kinder, T. H., Heburn, G. W. and Green, A. W. (1985) Some aspects of the Caribbean circulation. *Marine Geology*, **68**, 25-52.

Klein, G. d. V. (1985) The frequency and periodicity of preserved turbidites in submarine fans as a quantitative record of tectonic uplift in collision zones. *Tectonophysics*, **119**(1-4), 181-193.

Kroon, D., Reijmer, J. J. G. and Rendle, R. H. (2000) Mid-late Quaternary variations in the oxygen isotope signature of *Globigerinoides ruber* in the subtropical Atlantic on the leeward side of Great Bahama Bank. In: *Proceedings of the Ocean Drilling Program, Scientific Results* (Ed. by Eberli, G. F., Swart, P. K., Malone, M. J., *et al.*), Ocean Drilling Program (College Station, TX), *Vol. 166*, pp. 13-22.

Kumar, S. P. et al. (1991) Hydrographic characteristics and circulation in the Caribbean Sea during April and May 1990. *Caribbean Marine Studies*, **2**, 69-80.

Labeyrie, L. D., Pichon, J. J., Labracherie, M., Ippolito, P., Duprat, J. and Duplessy, J. C. (1986) Melting history of Antarctica during the past 60.000 years. *Nature*, **322**, 701-706.

Lebreiro, S. M., McCave, I. N. and Weaver, P. P. E. (1997) Late Quaternary turbidite emplacement on the Horseshoe abyssal plain (Iberian margin). *Journal of Sedimentary Research*, **67**(5), 856-870.

Li, C. and Jones, B. (1997) Comparison of foraminiferal assemblages in sediments on the windward and leeward shelves of Grand Cayman, British West Indies. *Palaios*, **12**, 12-26.

Li, C., Jones, B. and Blanchon, P. (1997) Lagoon-shelf sediment exchange by storms - Evidence from foraminiferal assemblages, east coast of Grand Cayman, British West Indies. *Journal of Sedimentary Research*, **67**(1), 17-25.

Liddell, W. D., Ohlhorst, S. L. and Boss, S. K. (1988) The significance of Halimeda as a space-occupier and sediment-producer, 1-750 m, North Jamaica. In: *Coral Reef Symposium, Vol. 3*, pp. 127-132.

Loeblich, A. R. J., Tappan, H., Barker, R. W., Cole, W. S., Douglas, R. C., Reichel, M. and Thompson, M. L. (1964) Treatise on invertebrate paleontology; Part C, Protista 2 Sarcodina, chiefly 'Thecamoebians' and Foraminiferida, V. 1-2, Geological Society of America (New York), *Vol. 1a*, pp. C1-C510.

Loreau, J. P. (1982) Sédiments aragonitiques et leru genèse. *Mémoires du Muséum National d´Histoire Naturelle*, Tome XLVII.

Lynts, G. M., Judd, J. B. and Stehmann, C. F. (1973) Late Pleistocene history of Tongue of the Ocean, Bahamas. *Geological Society of America Bulletin*, **84**, 2665-2684.

MacClintock, C. (1967) *Shell structure of patelloid and bellerophontoid gastropods (Mollusca)*. Peabody Museum of Natural History, Yale University (New Haven, CT, United States), 140 pp.

MacIntyre, A., Kipp, N. G., Be, A. W. H., Crowley, T., Kellog, T., Gardner, J. V., Prell, W. and Ruddiman, W. F. (1976) Glacial North Atlantic 18.000 years ago: A CLIMAP reconstruction. In: *Investigation of*

late Quaternary paleoceanography and paleoclimatology (Ed. by Cline, R. M. and Hays, J. D.), Geological Society of America Memoir , *Vol. 145*, pp. 43-76.

Mann, P., Draper, G. and Burke, K. (1985) Neotectonics of a strike-slip restraining bend system, Jamaica. *Society of Economic Paleontologists and Mineralogists Special Publications*, **37**, 211-226.

Marshall, P. R. (1976) Some relationships between living and total foraminiferal faunas on Pedro Bank, Jamaica. In: *First International Symposium on benthonic foraminifera of continental margins: Part A. Ecology and Biology* (Ed. by Schafer, C. T. and Pelletier, B. R.), Maritime Sediments Special Publication , *Vol. 1*, pp. 61-70.

Meschede, M. (1998) The impossible Galapagos connection: geometric constraints for a near-American origin of the Caribbean plate. *Geologische Rundschau*, **87**, 200-205.

Meschede, M. and Frisch, W. (1998) A plate-tectonic model for the Mesozoic and early Cenozoic history of the Caribbean plate. *Tectonophysics*, **296**(3-4), 269-291.

Milliman, J. D. (1974) *Marine carbonates*. Springer Verlag (Berlin-Heidelberg-New York), 375 pp.

Milliman, J. D. and Droxler, A. W. (1996) Neritic and pelagic carbonate sedimentation in the marine environment: ignorance is not bliss. *Geologische Rundschau*, **85**, 496-504.

Milliman, J. D., Freile, D., Steinen, R. P. and Wilber, R. J. (1993) Great Bahama Bank aragonitic muds: mostly inorganically precipitated, mostly exported. *Journal of Sedimentary Geology*, **63**(4), 589-595.

Milliman, J. D., Ross, D. A. and Ku, T.-L. (1969) Precipitation and lithification of deep-sea carbonates in the Red Sea. *Journal of Sedimentary Petrology*, **39**(2), 724-736.

Milliman, J. D., Troy, P. J., Balch, W. M., Adams, A. K., Li, Y.-H. and Mackenzie, F. T. (1999) Biologically mediated dissolution of calcium carbonate above the chemical lysocline? *Deep-Sea Research*, **I**(46), 1653-1669.

Mitchum, R. M. (1977) Seismic stratigraphy and global changes of sea level; Part 11, Glossary of terms used in seismic stratigraphy. In: *Seismic stratigraphy - applications to hydrocarbon exploration* (Ed. by Payton, C. E.), American Association of Petroleum Geologists Memoir, *Vol. 26*, pp. 205-212.

Molinari, R., Spillane, M., Brooks, I., Atwood, D. and Duckett, C. (1981) Surface currents in the Caribbean Sea as deduced from Lagrangian observations. *Journal of Geophysical Research*, **86**, 6537-6542.

Molnar, P. and Sykes, L. R. (1969) Tectonics of the Caribbean and Middle America regions from focal mechanisms and seismicity. *Geological Society of America Bulletin*, **80**, 1639-1684.

Morrison, J. M. and Nowlin, W. D. (1982) General distribution of water masses within the eastern Caribbean Sea during the winter of 1972 and fall of 1973. *Journal of Geophysical Research*, **87**(C6), 4207-4229.

Mullins, H. T., Boardman, M. R. and Neumann, A. C. (1979) Echo character of off-platform carbonates. *Marine Geology*, **32**, 251-268.

Mullins, H. T., Neumann, A., C., Wilber, R. J., Hine, A. C. and Chinburg, S. J. (1980) Carbonate sediment drifs in northern straits of Florida. *American Association of Petroleum Geologists Bulletin*, **64**, 1701-1717.

Mullins, H. T. and Neumann, A. C. (1979) Deep carbonate bank margin structure and sedimentation in the northern Bahamas. In: *Geology of continental slopes* (Ed. by Doyle, L. J. and Pilkey, O. H.), Society of Economic Paleontologists and Mineralogists Special Publication, *Vol. 27*, pp. 165-192.

Munro, J. L. (1983) *Caribbean coral reef fishery resources*. ICLARM Studies and Reviews, *Vol. 7*, .

Murray, J. W. and Perkins, C. R. (1991) *Ecology and paleoecology of benthic foraminifera*. Longman Scientific & Technical (Harlow, Essex), 397 pp.

Murray-Wallace, C. V., Belperio, A. P., Gostin, V. A. and Cann, J. H. (1993) Amino acid racemization and radiocarbon dating of interstadial marine strata (oxygen isotope stage 3), Gulf St. Vincent, South Australia. *Marine Geology*, **110**, 83-92.

Neumann, A. C. and Land, L. S. (1975) Lime and deposition and calcareous algae in the Bight of Abaco, Bahamas: A budget. *Journal of Sedimentary Geology*, **45**, 763-768.

Paillard, D., Labeyrie, L. and Yiou, P. (1996) AnalySeries 1.0 a7 PPC, Macintosh program performs time-series analysis. *EOS Transactions*, **77**, 379.

Peebles, M. W., Hallock, P. and Hine, A. C. (1997) Benthic foraminiferal assemblages from current-swept carbonate platforms of the Northern Nicaragua Rise, Caribbean Sea. *Journal of Foraminiferal Research*, **27**(1), 42-50.

Petschick, R., Kuhn, G. and Gingele, F. (1996) Clay mineral distribution in surface sediments of the South Atlantic: sources, transport, and relation to oceanography. *Marine Geology*, **130**, 203-229.

Pilckey, O. H. and Rucker, J. (1966) Mineralogy of Tongue of the Ocean sediments. *Journal of Marine Research*, **24**, 276-285.

Piller, W. E. (1994) The Northern Bay of Safaga (Red Sea, Egypt): An actuopalaeontological approach. IV. Thin section analysis. *Beiträge zur Paläontologie von Österreich*, **18**, 1-73.

Piller, W. E. and Mansour, A. M. (1990) The northern Bay of Safaga (Red Sea, Egypt): An actuopalaeontological approach. II. Sediment analysis and sedimentary facies. *Beiträge zur Paläontologie von Österreich*, **16**, 1-102.

Pindell, J. and Dewey, J. F. (1982) Permo-Triassic reconstruction of western Pangea and the evolution of the Gulf of Mexico/Caribbean region. *Tectonics*, **1**, 179-211.

Pindell, J. L. (1993) Regional synopsis of Gulf of Mexico and Caribbean evolution. In: *GCS/SEPM 13th Annual Regional Conference Proceedings*, pp. 251-274.

Pindell, J. L. and Barrett, S. F. (1990) Geological evolution of the Caribbean region; A plate tectonic perspective. In: *The Caribbean Region* (Ed. by Dengo, G. and Case, J. E.), The Geological Society of America (Boulder, CO), *Vol. H*, pp. 405-432.

Pindell, J. L., Cande, S. C., Pitman III, W. C., Browley, D. B., Dewey, J. F., Labreque, J. and Haxby, W. (1988) A plate-kinematic framework for models of Caribbean evolution. *Tectonophysics*, **155**, 121-138.

Pinter, N. and Gardner, T. W. (1989) Construction of polynomial model of glacio-eustatic fluctuation; estimating paleo-sea levels continously through time. *Geology*, **17**(4), 295-298.

Poaq, W. C. (1981) *Ecologic Atlas of Benthic Foraminifera of the Gulf of Mexico*. Academic Press, 174 pp.

Prell, W. L. (1978) Upper Quaternary sediments of the Colombia Basin; spatial and stratigraphic variation. *Geological Society of America Bulletin*, **89**(8), 1241-1255.

Prell, W. L. and Hays, J. D. (1976) Late Pleistocene faunal and temperature patterns of the Colombia Basin, Caribbean Sea. In: *Investigation of late Quaternary paleoceanography and paleoclimatology* (Ed. by Cline, R. M. and Hays, J. D.), Geological Society of America Memoir, *Vol. 145*, pp. 201-220.

Purdy, E. G. (1963) Recent calcium carbonate facies of the Great Bahama Bank. 2. Sedimentary facies. *Journal of Geology*, **71**(4), 472-497.

Raymo, M. E., Ruddiman, W. F., Shackleton, N. J. and Oppo, D. W. (1990) Evolution of global ice volume and Atlantic-Pacific $\delta^{13}C$ gradients over the last 2.5 m.y. *Earth and Planetary Science Letters*, **97**, 353-368.

Reid, R. P., Carey, S. N. and Ross, D. R. (1996) Late quaternary sedimentation in the Lesser Antilles island arc. *Geological Society of America Bulletin*, **108**(1), 78-100.

Reijmer, J. J. G. (1991) Sea level and sedimentation on the flanks of carbonate platforms. [unpublished Ph.D. thesis], Vrije Universiteit, Amsterdam, 162 pp.

Reijmer, J. J. G., Schlager, W., Bosscher, H., Beets, C. J. and McNeill, D. F. (1992) Pliocene/Pleistocene platform facies transition recorded in calciturbidites (Exuma Sound, Bahamas). *Sedimentary Geology*, **78**, 171-179.

Reijmer, J. J. G., Schlager, W. and Droxler, A. W. (1988) Site 632: Pliocene-Pleistocene sedimentation cycles in a Bahamian basin. In: *Proceedings of the Ocean Drilling Program, Scientific Results* (Ed. by Austin, J. A. J. and Schlager, W.), Ocean Drilling Program (College Station, TX), *Vol. 101*, pp. 213-220.

Rendle, R. H. (2000) Quaternary slope development and sedimentology of the western, leeward margin of Great Bahama Bank (ODP Leg 166). [unpublished Ph.D. thesis], Christian-Albrechts-Universität, Kiel, 182 pp.

Rendle, R. H., Reijmer, J. J. G., Kroon, D. and Henderson, G. M. (2000) Mineralogy and sedimentology of the Pleistocene to Holocene on the leeward margin of Great Bahama Bank. In: *Proceedings of the Ocean Drilling Program, Scientific Results* (Ed. by Swart, P. K., Eberli, G. P., Malone, M. J., *et al.*), Ocean Drilling Program (College Station, TX), *Vol. 166*, pp. 61-76.

Richter, F. M. and Turekian, K. K. (1993) Simple models for the geochemical response of the ocean to climatic and tectonic forcing. *Earth and Planetary Science Letters*, **119**, 121-131.

Robbins, L. L., Tao, Y. and Evans, C. A. (1997) Temporal and spatial distribution of whitings on Great Bahama Bank and new lime mud budget. *Geology*, **25**(10), 947-950.

Rose, P. R. and Lidz, B. (1977) *Diagnostic foraminiferal assemblages of shallow-water modern environments, South Florida and the Bahamas*. Comparative Sedimentology Laboratory, Division of Marine Geology and Geophysics, Rosentiel School of Marine and Atmospheric Science, University of Miami (Miami, Fl, United States), 55 pp.

Rosencrantz, E., Ross, M. I. and Sclater, J. G. (1988) Age and spreading history of the Cayman Trough as determined from depth, heat flow and magnetic anomalies. *Journal of Geophysical Research*, **93**(B3), 2141-2157.

Ruddiman, W. F., Cameron, D. and Clement, B. M. (1987) Sediment disturbance and correlation of offset holes drilled with the hydraulic piston corer: Leg 94. In: *Initial Reports of the Deep Sea Drilling Program* (Ed. by Ruddiman, W. F., Kidd, R. B., Thomas, E., *et al.*), U.S. Govt. Printing Office (Washington), *Vol. 94*.

Ruddiman, W. F., Raymo, M. and McIntyre, A. (1986) Matuyama 41.000-year cycles: North Atlantic Ocean and northern hemisphere ice sheets. *Earth and Planetary Science Letters*, **80**, 117-129.

Ruddiman, W. F. and Raymo, M. E. (1988) Northern hemisphere climate regimes during the past 3 Ma: possible tectonic connections. *Philosophical Transactions of the Royal Society of London, Series B: Biological Sciences*, **B318**(1191), 411-430.

Sabine, C. L. and MacKenzie, F. T. (1995) Bank-derived carbonate sediment transport and dissolution in the Hawaiian Archipelago. *Aquatic Geochemistry*, **1**, 189-230.

Saito, T., Thompson, P. R. and Breger, D. (1981) *Systematic index of Recent and Pleistocene planktonic foraminifera*. University of Tokyo (Tokyo, Japan), 189 pp.

Sarg, J. F. (1988) Carbonate Sequence Stratigraphy. In: *Sea Level Changes - An Integrated Approach* (Ed. by Wilgus, C. K., Hastings, B. S., Kendall, C. G. S. C., *et al.*), Society of Economic Paleontologists and Mineralogists Special Publication, *Vol. 42*, pp. 155-181.

Sarnthein, M. (1971) Oberflächensedimente im Persischen Golf und Golf von Oman. II. Quantitative Komponentenanalyse der Grobfraktion. *Meteor Forschungs-Ergebnisse*, **C5**, 1-113.

Schlager, W. (1993) Accomodation and supply; a dual control on stratigraphic sequences. *Sedimentary Geology*, **86**(1-2), 111-136.

Schlager, W. and Camber, O. (1986) Submarine slope angles, drowning unconformities and self-erosion of limestone escarpments. *Geology*, **14**, 762-765.

Schlager, W. and Chermak, A. (1979) Sediment facies of platform basin transition, Tongue of the Ocean, Bahamas. In: *Geology of continental slopes* (Ed. by Doyle, L. J. and Pilkey, O. H.), Society of Economic Paleontologists and Mineralogists Special Publication , *Vol. 27*, pp. 193-208.

Schlager, W. and Ginsburg, R. N. (1981) Bahama carbonate platforms - the deep and the past. *Marine Geology*, **44**, 1-24.

Schlager, W. and James, N. P. (1978) Low-magnesian calcite limestones forming at the deep-sea floor, Tongue of the Ocean, Bahamas. *Sedimentology*, **25**, 675-702.

Schlager, W., Reijmer, J. J. G. and Droxler, A. W. (1994) Highstand shedding of carbonate platforms. *Journal of Sedimentary Research*, **B64**(3), 270-281.

Schmucker, B. (2000) Recent planktic foraminifera in the Caribbean Sea: Distribution, ecology and taphonomy. [unpublished Ph.D. thesis], ETH, Zürich, 179 pp.

Schwartz, J. P. (1996) Late Quaternary periplatform sediments and paleoenvironmental analysis of Pedro Channel, Northeastern Nicaragua Rise, Caribbean Sea. [unpublished M.A. thesis], Rice University, Houston, 206 pp.

Shackleton, N. J. (1987) Oxygen isotopes, ice volume and sea level. *Quaternary Science Reviews*, **6**, 183-190.

Shackleton, N. J. and Opdyke, N. D. (1973) Oxygen isotope and palaeomagnetic stratigraphy of equatorial Pacific core V28-238: oxygen isotope temperatures and ice volumes on a 10^5 year and 10^6 year scale. *Quaternary Research*, **3**, 39-55.

Shanmugan, G. and Moiola, R. J. (1982) Eustatic control of turbidites and winnowed turbidites. *Geology*, **10**, 231-235.

Shanmugan, G. and Moiola, R. J. (1984) Eustatic control of calciclastic turbidites. *Marine Geology*, **56**, 273-278.

Shinn, E. (1980) Geologic history of Grecian Rocks, Key Largo Coral Reef Marine Sanctuary. *Bulletin of Marine Science*, **30**, 646-656.

Shinn, E. A., Steinen, R. P., Lidz, B. H. and Swart, P. W. (1989) Whitings, a sedimentologic dilemma. *Journal of Sedimentary Petrology*, **59**(1), 147-161.

Sigurdsson, H., Leckie, R. M. and Acton, G. D. (1997) Site 1000. In: *Proceedings of the Ocean Drilling Programm, Initial Reports* (Ed. by Sigurdsson, H., Leckie, R. M. and Acton, G. D.), Ocean Drilling Program (College Station, TX), *Vol. 165*, pp. 231-234.

Sigurdsson, H., Sparks, R. S. J., Carey, S. N. and Huang, T. C. (1980) Volcanogenic sedimentation in the Lesser Antilles arc. *Journal of Geology*, **88**, 523-540.

Slowey, N. C., Henderson, G. M. and Curry, W. B. (1996) Direct U-Th dating of marine sediments from the two most recent interglacial periods. *Nature*, **383**, 242-244.

Stephan, J. F., Mercier de Lepinay, B., Calais, E., *et al.* (1990) Paleogeodynamic maps of the Caribbean: 14 steps from the Lias to Present. *Bulletin de la Societe Geologique de France, Huitieme Serie*, **6**(6), 915-919.

Stuiver, M. and Polach, H. (1977) Discussion: Reporting of ^{14}C data. *Radiocarbon*, **19**(3), 355-363.

Sugg, A. L. (1966) The hurricane season of 1965. *Monthly Weather Report*, **94**, 183-191.

Sykes, L. R., McCann, W. R. and Kafka, A. L. (1982) Motion of the Caribbean plate during the last 7 million years and implications for earlier Cenozoic movements. *Journal of Geophysical Research*, **87**, 10656-10676.

Tipper, J. C. (1997) Modelling carbonate platform sedimentation - Lag come naturally. *Geology*, **25**(6), 495-498.

Triffleman, N. J. (1989) Morphology, sediments and depositional environments of a partially drowned carbonate platform Seranilla Bank - Southwest Caribbean Sea. [unpublished M.Sc. thesis], University of South Florida, Coral Gables, 115 pp.

Triffleman, N. J., Hallock, P. and Hine, A. C. (1992) Morphology, sediments, and depositional environments of a small carbonate platform: Serranilla Bank, Nicaraguan Rise, Southwest Caribbean Sea. *Journal of Sedimentary Research*, **62**(4), 591-606.

Triffleman, N. J., Hallock, P., Hine, A. C. and Peebles, M. W. (1991) Distribution of foraminiferal tests in sediments of Serranilla Bank, Nicaraguan Rise, Southwestern Caribbean. *Journal of Foraminiferal Research*, **21**(1), 39-47.

Tucker, M. E. and Wright, P. V. (1990) *Carbonate Sedimentology*. Blackwell Scientific Publications (London), 481 pp.

Turekian, K. K. (1964) The marine geochemistry of strontium. *Geochimica Cosmochimica Acta*, **28**, 1479-1496.

UNEP/IUCN (1988) *Coral Reefs of the World - Volume 1: Atlantic and Eastern Pacific - Bahamas.* IUCN, *Vol. 1*.

Vail, P. R. (1987) Seismic stratigraphy interpretation procedure. In: *Atlas of Seismic Stratigraphy* (Ed. by Bally, A. W.), American Association of Petroleum Studies in Geology, *Vol. 27-1*, pp. 1-10.

Vail, P. R., Audemard, F., Bowman, S. A., Eisner, P. N. and Perez-Cruz, C. (1991) The stratigraphic signatures of tectonics, eustasy and sedimentology - an overview. In: *Cycles and events in Stratigraphy* (Ed. by Einsele), Springer Verlag (Berlin-Heidelberg-New York), pp. 617-658.

Vail, P. R., Mitchum, R. M. and Thompson, S. (1977) Global cycles of relative changes of sea-level. In: *Seismic stratigraphy - applications to hydrocarbon exploration* (Ed. by Payton, C. E.), American Association of Petroleum Geologists Memoir, *Vol. 26*, pp. 83-97.

Van Andel, T. H., Heath, G. R. and Moore, T. C. (1975) Cenozoic history and paleoceanography of the central equatorial Pacific. *Geological Society of America Memoirs*, **143**, 1-134.

Veron, J. E. N. (1996) Evolution in corals. In: *Paleobiology and biology of corals* (Ed. by Staney, G. D. J.), The Paleontological Society , pp. 7-37.

Wadge, G. and Wooden, J. L. (1982) Late Cenozoic alkaline volcanism in the northwestern Caribbean; tectonic setting and Sr isotopic characteristics. *Earth and Planetary Science Letters*, **57**(1), 35-46.

Walter, L. M. and Burton, E. A. (1990) Dissolution of Recent platform carbonate sediment in marine pore fluids. *American Journal of Science*, **220**, 601-643.

Walter, L. M. and Morse, J. W. (1984) Reactive surface area of skeletal carbonates during dissolution; effect of grain size. *Journal of Sedimentary Petrology*, **54**(4), 1081-1090.

Wantland, K. F. (1975) Distribution of Holocence benthic foraminifera on the Belize Shelf. In: *Belize Shelf - Carbonate Sediments, and Ecology* (Ed. by Wantland, K. F. and Pusey, W.), American Association of Petroleum Geologists (Tulsa, OK), pp. 332-399.

Ward, I. A. K., Larcombe, P. and Cuff, C. (1995) Stratigraphic control of the geochemistry of Holocene inner-shelf facies, Great Barrier Reef. *Marine Geology*, **129**, 47-62.

Wentworth, C. K. (1922) A scale of grade and class terms for clastic sediments. *Journal of Geology*, **30**, 377-392.

Westphal, H. (1997) Sediment input and diagenesis of periplatform carbonates on a leeward slope of Great Bahama Bank. [unpublished Ph.D. thesis], Christian-Albrechts Universität, Kiel, 163 pp.

Wilber, R. J., Milliman, J. D. and Halley, R. B. (1990) Accumulation of bank-top sediment on the western slope of Great Bahama Bank: Rapid progradation of a carbonate megabank. *Geology*, **18**, 970-974.

Wilber, R. J. and Neumann, A. C. (1993) Effects of submarine cementation on microfabrics and physical properties of carbonate slope deposites, Northern Bahamas. In: *Carbonate Microfabrics* (Ed. by Rezak, R. and Lavoie, D. L.), Springer (New York), pp. 79-94.

Wilson, P. A. and Roberts, H. H. (1992) Carbonate-periplatform sedimentation by density flows: A mechanism for rapid off-bank and vertical transport of shallow-water fines. *Geology*, **20**, 713-716.

Wilson, P. A. and Roberts, H. H. (1995) Density cascading: off-shelf sediment transport, evidence and implications, Bahama Bank. *Journal of Sedimentary Research*, **A 65**(1), 45-56.

Woodley, J. D., Chornesky, E. A., Clifford, P. A., *et al.* (1981) Hurricane Allens impact on Jamaican coral reefs. *Science*, **214**, 749-755.

Wüst, G. (1964) *Stratification and Circulation of the Antillean-Caribbean Basins. Part 1: Spreading and Mixing of the Water Types with an Oceanographic Atlas*. Columbia University Press (New York, U.S.A.), 202 pp.

Zans, V. A. (1958) The Pedro Cays and Pedro Bank: Report of survey of the Cay (1955-1957). Geological Survey of Jamaica, pp. 57.

Appendices

Appendix 1 **Core lithology**
Appendix 2 **Thin-section and coarse fraction plates**

Data Appendices

Appendix 3 **Stratigraphy, $\delta^{13}C$ and TOC content**
Appendix 4 **Mineralogy**
Appendix 5 **Grain size analyses**
Appendix 6 **Physical properties & Mass accumulation rates**
Appendix 7 **Geochemistry analyses**
Appendix 8 **Turbidite analyses**
Appendix 9 **Seismic analyses**
Appendix 10 **Age correlation data (Specmap- and Bassinot-stack)**
Appendix 11 **Pointcount data**

Appendix 1 - Core lithology

Core M35032-2

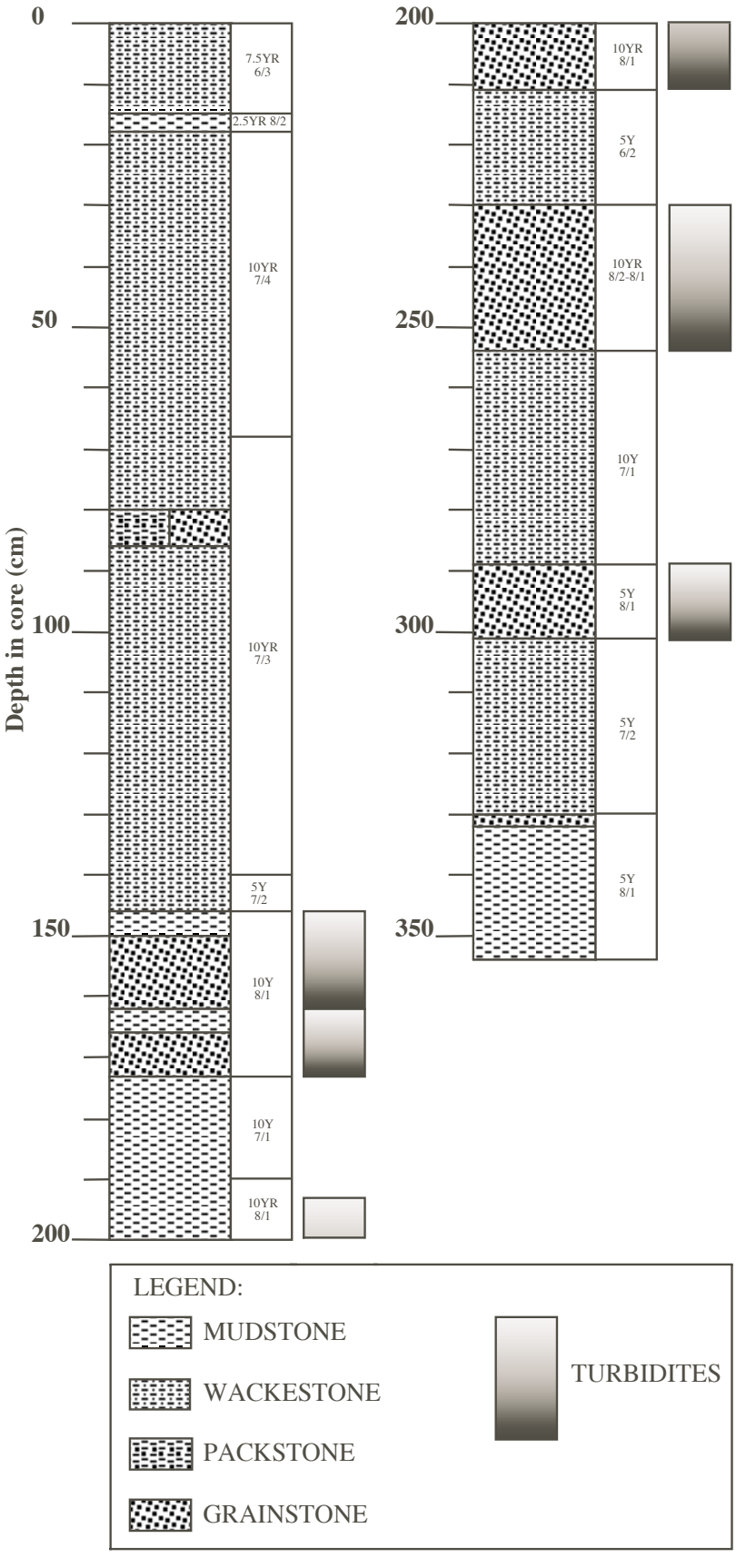

Annotation: Several lithologies within one depth slice indicate a gradational lithological change

Core M35034-1

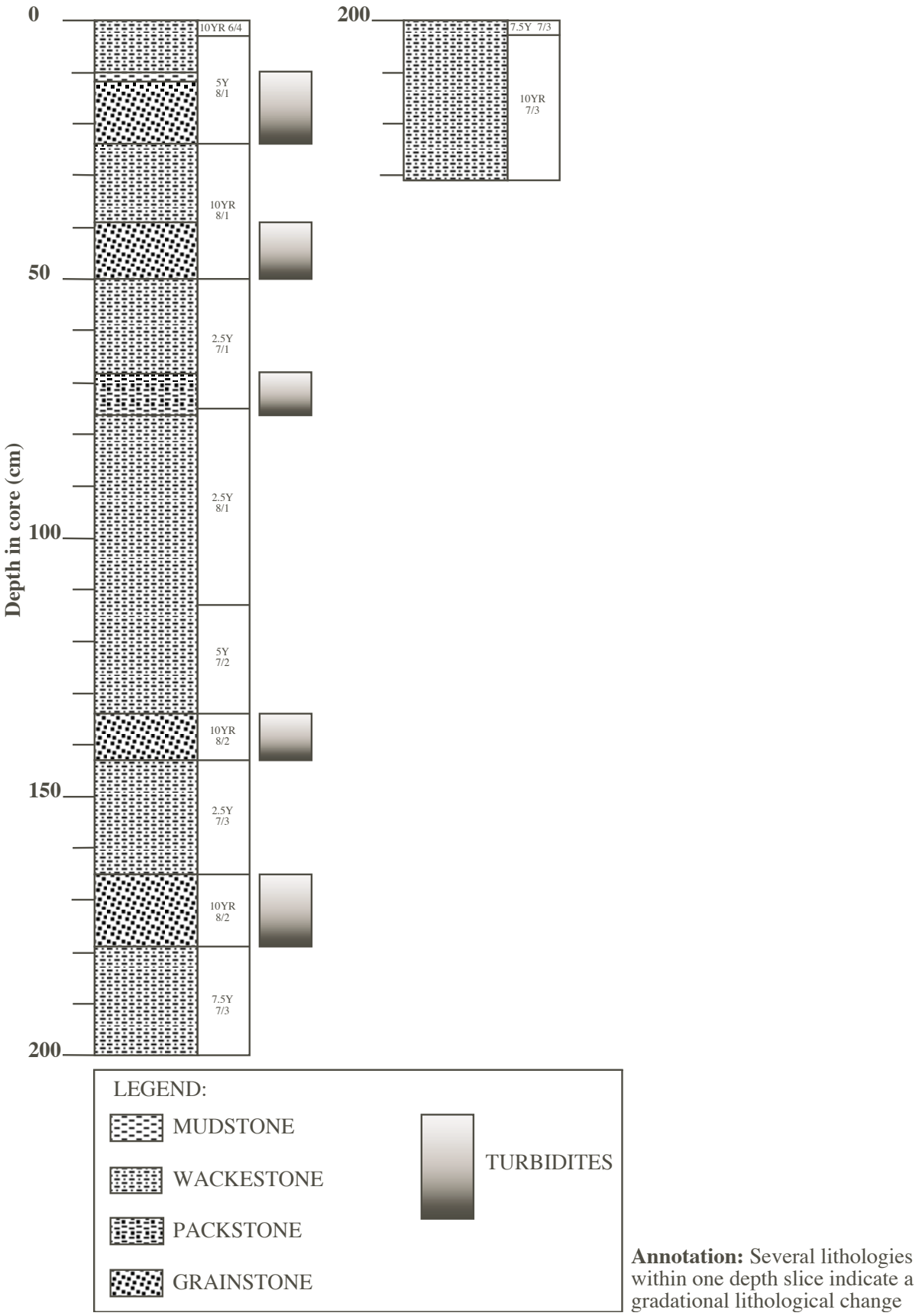

Annotation: Several lithologies within one depth slice indicate a gradational lithological change

Core M35042-2

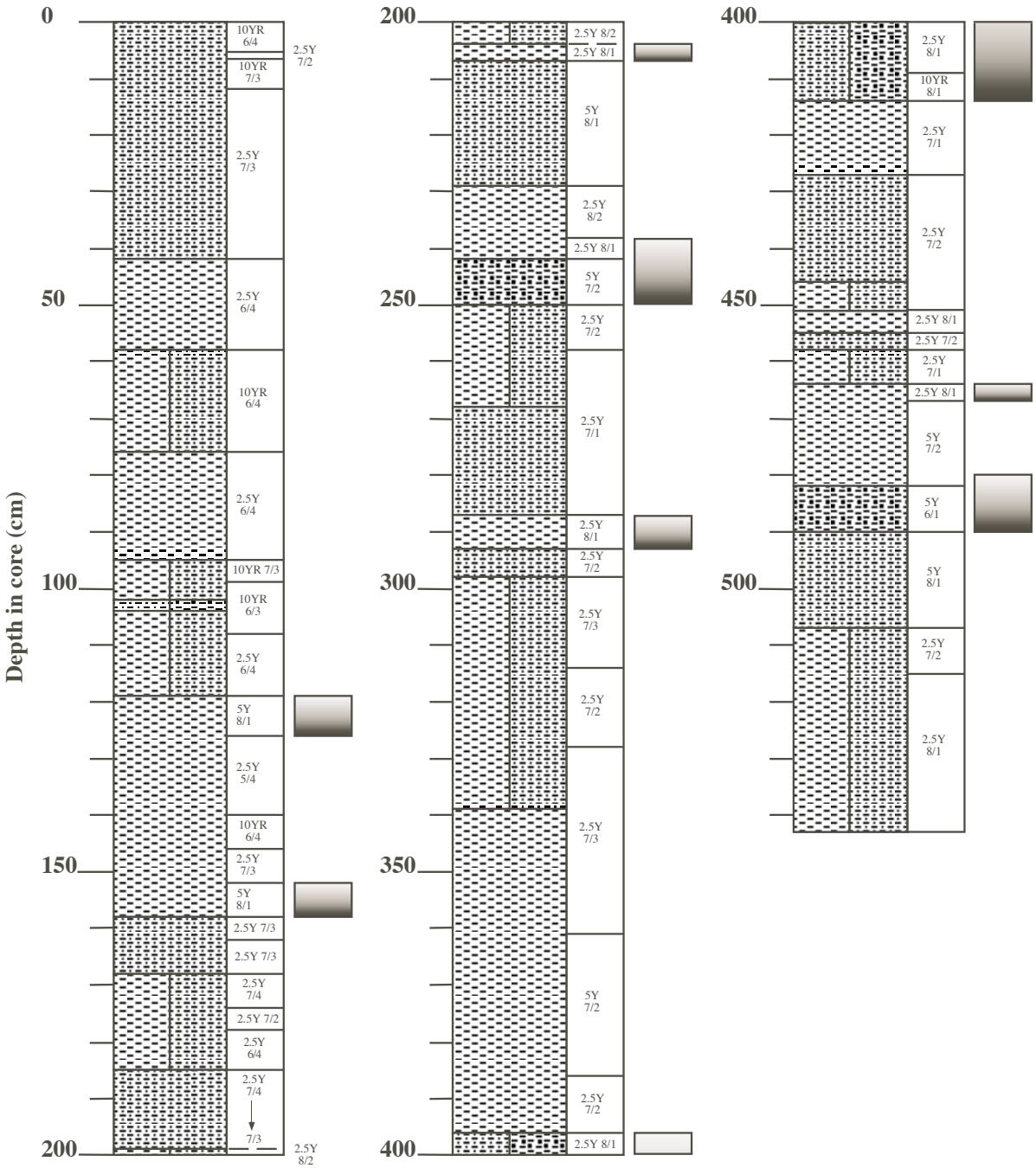

LEGEND:

- MUDSTONE
- WACKESTONE
- PACKSTONE
- GRAINSTONE
- TURBIDITES

Annotation: Several lithologies within one depth slice indicate a gradational lithological change

Core M35043-1

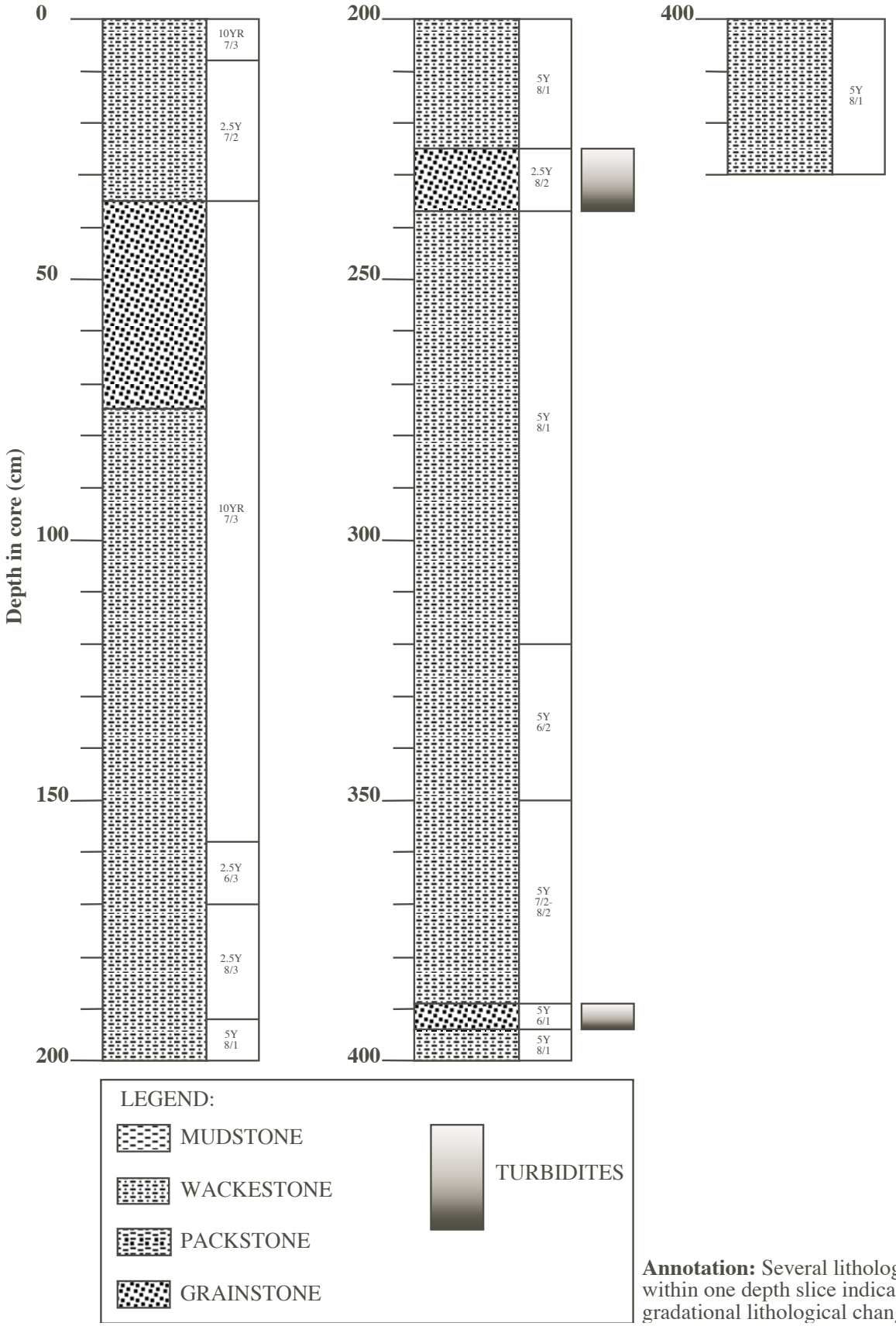

Annotation: Several lithologies within one depth slice indicate a gradational lithological change

Core M35048-1

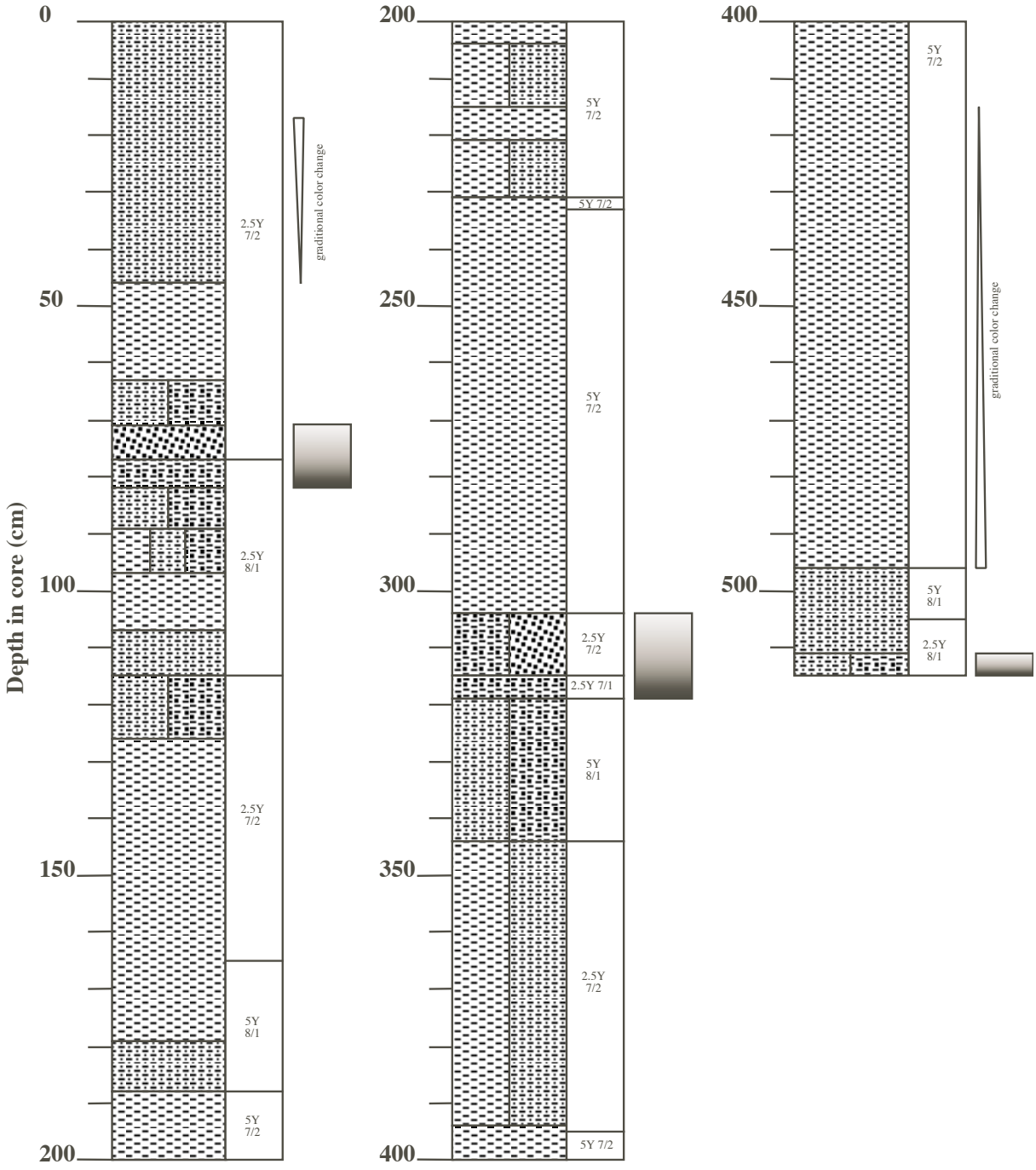

LEGEND:

- MUDSTONE
- WACKESTONE
- PACKSTONE
- GRAINSTONE
- TURBIDITES

Annotation: Several lithologies within one depth slice indicate a gradational lithological change

Core M35049-2

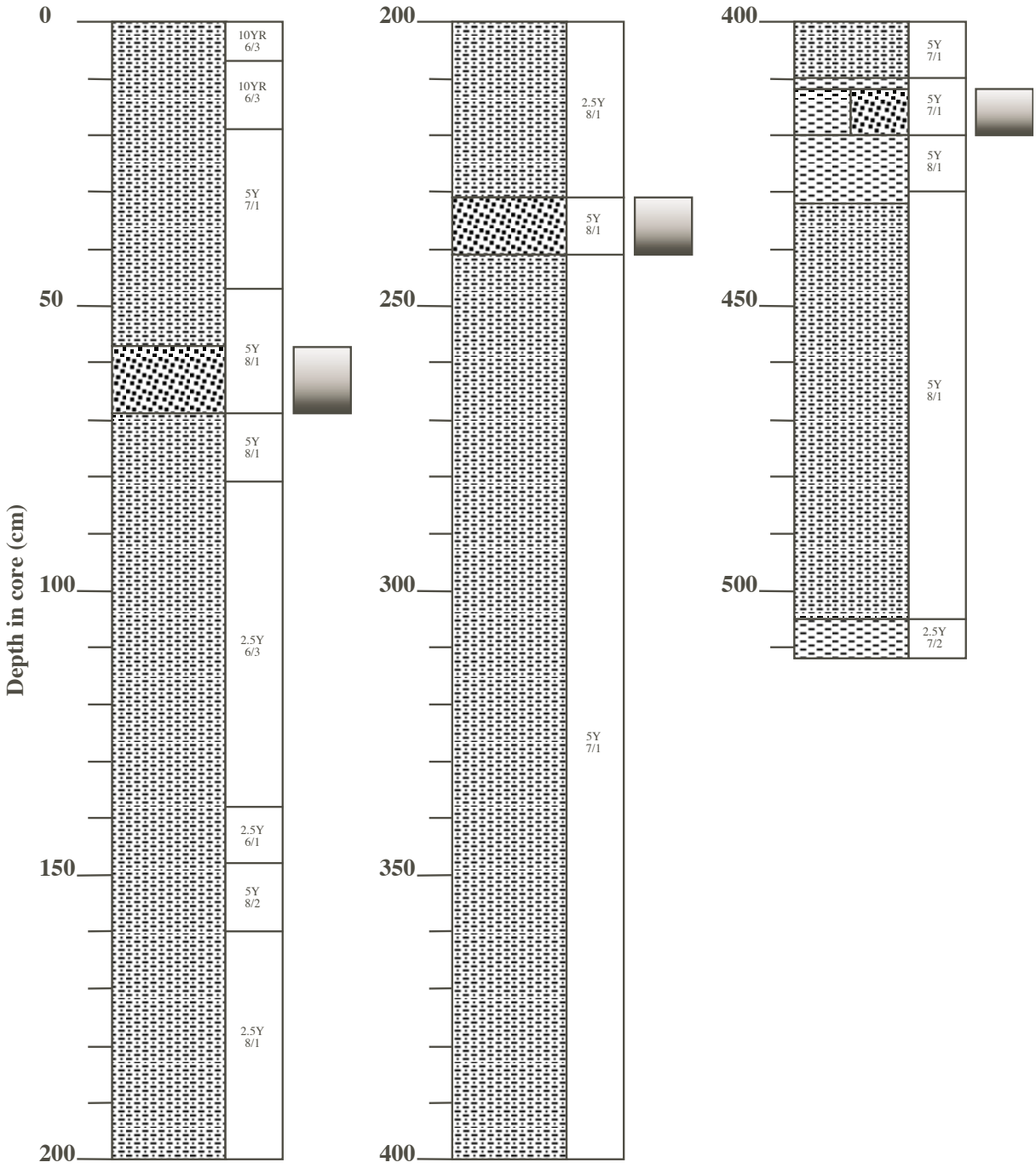

Annotation: Several lithologies within one depth slice indicate a gradational lithological change

Core M35052-2 (Part 1)

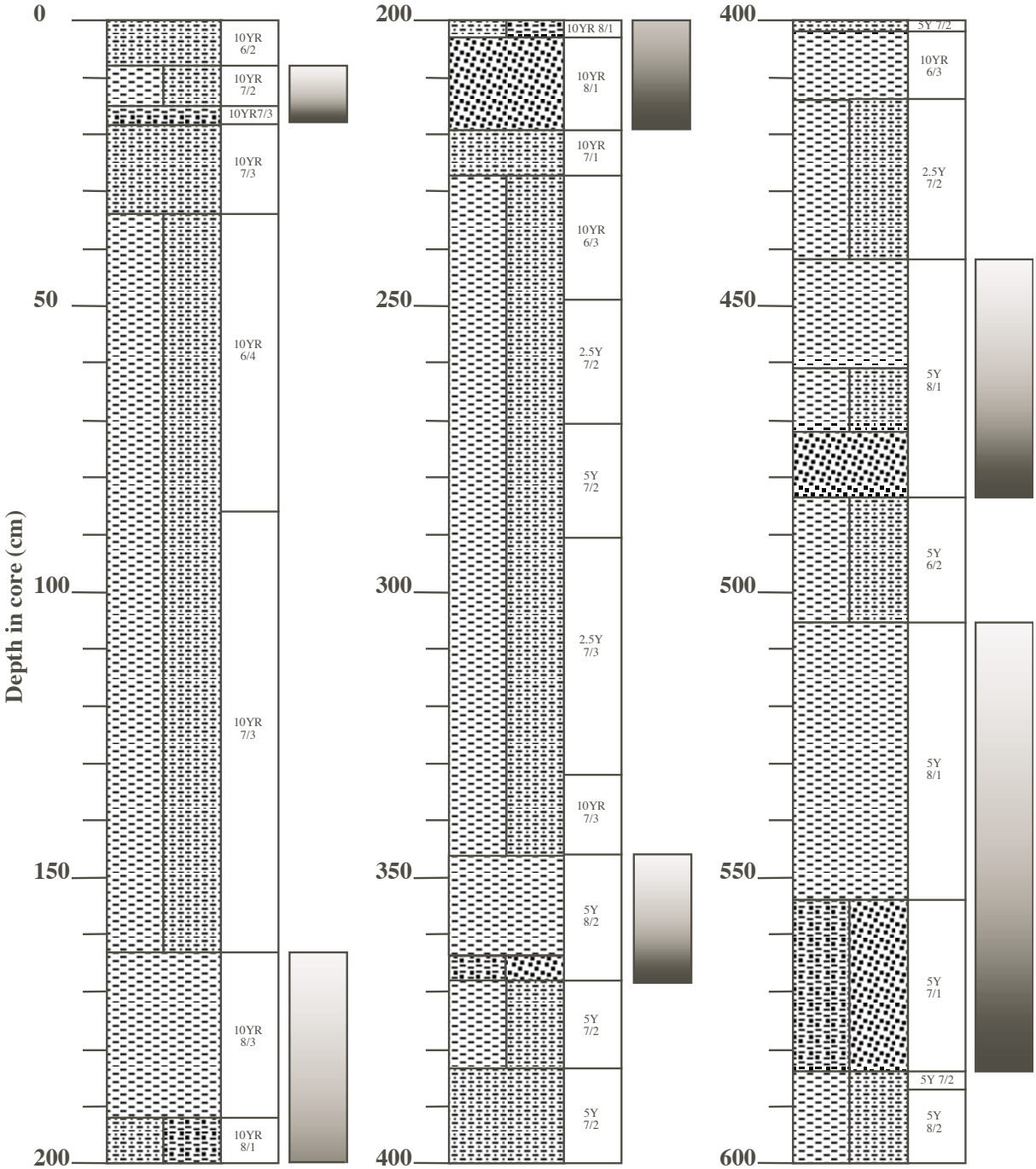

Core M35052-2 (Part 2)

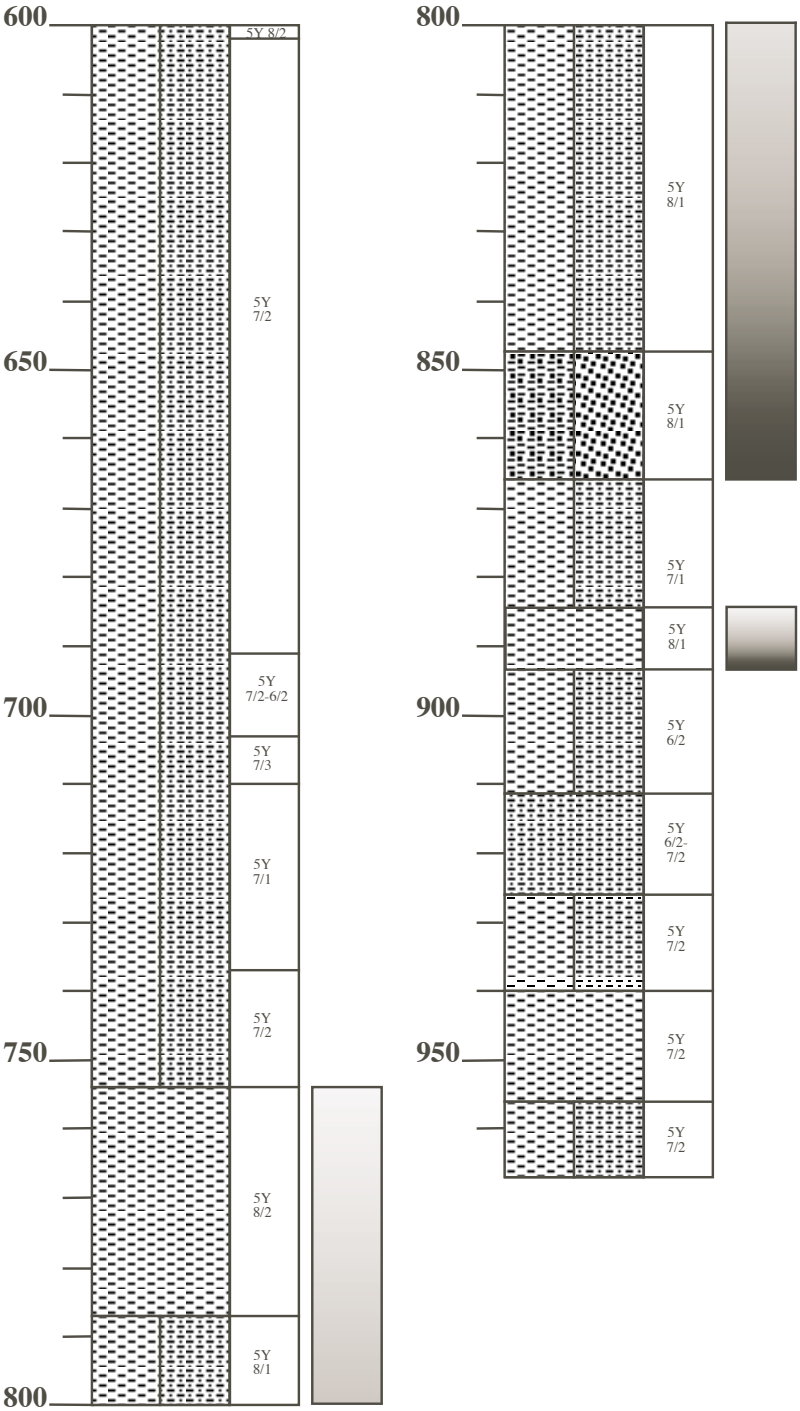

LEGEND:

- MUDSTONE
- WACKESTONE
- PACKSTONE
- GRAINSTONE
- TURBIDITES

Annotation: Several lithologies within one depth slice indicate a gradational lithological change

Core PC 059

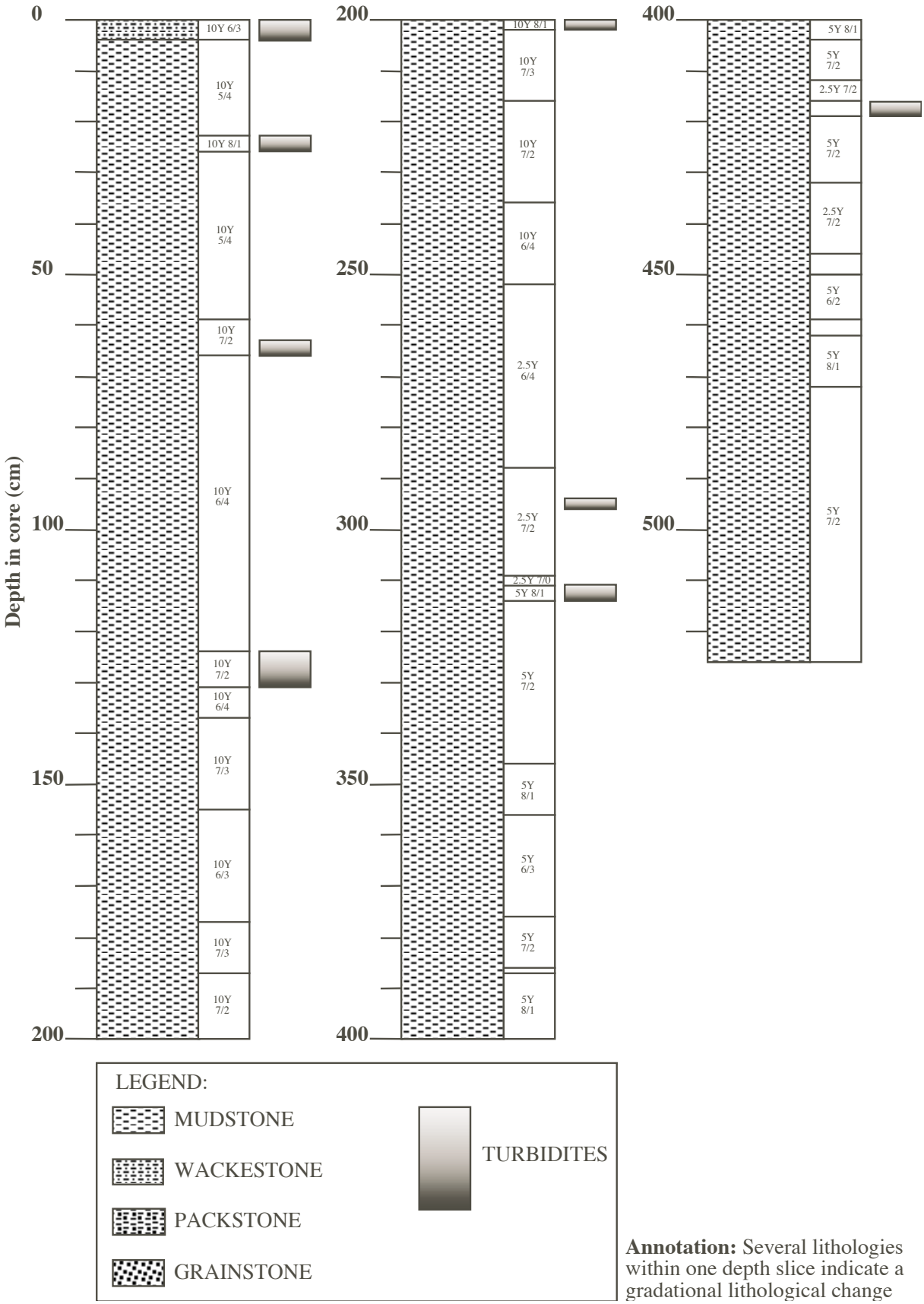

Annotation: Several lithologies within one depth slice indicate a gradational lithological change

Core PC 100

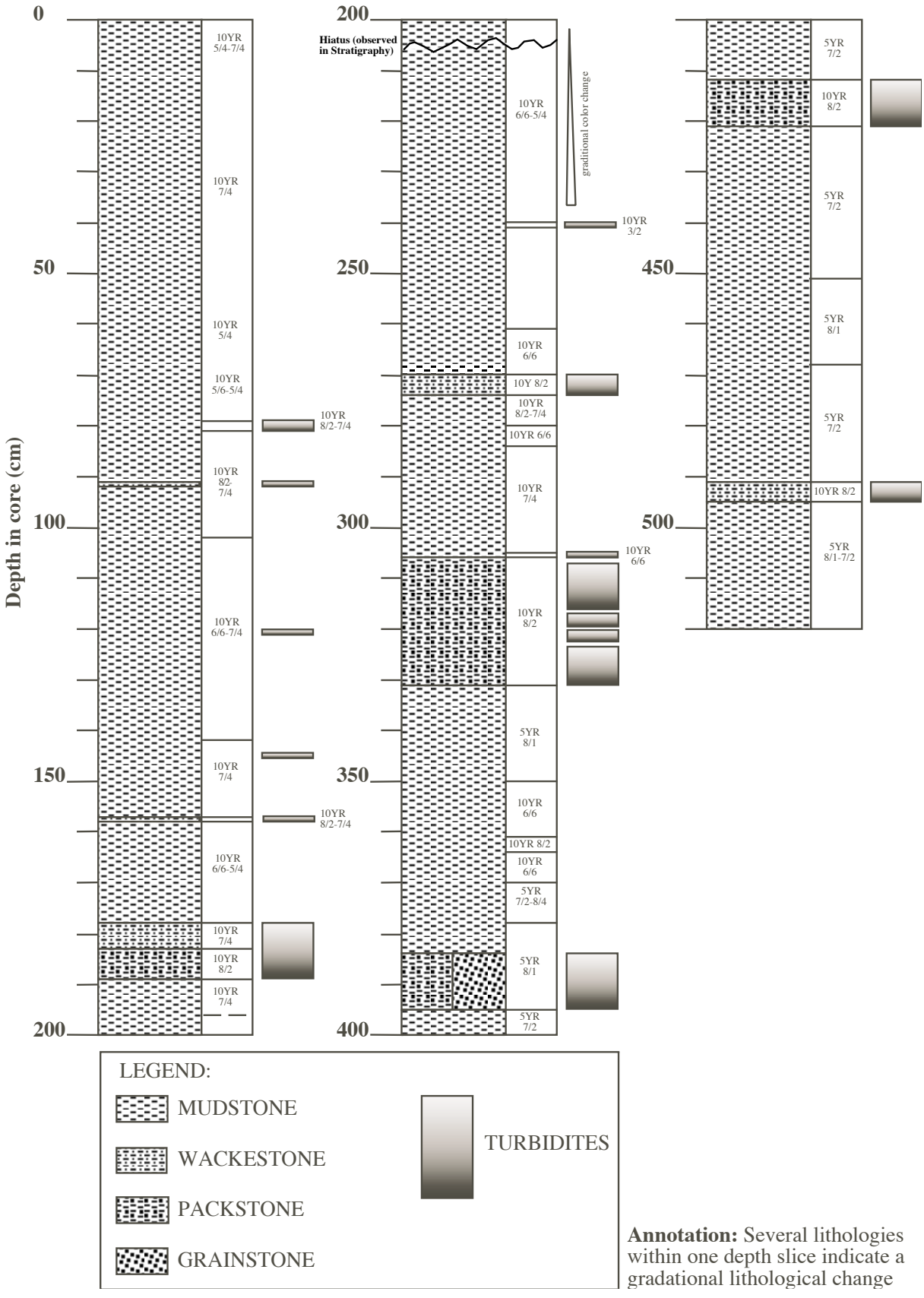

Annotation: Several lithologies within one depth slice indicate a gradational lithological change

Appendix 2 - Plates

Plate 1
Thin-sections of periplatform sediment and turbidite - Overview

Fig. 1.1: **M35032, 1 cm, 53x magnification**
Typical fine-silty mudstone with large pteropods (A) and planktic foraminifera (B). Holocene periplatfrom sediment.

Fig. 1.2: **M35034, 10 cm, 53x magnification**
Wackestone composed of fine-silty biodetritus and large planktic foraminifera (Genus *Globigerinoides* (A))

Fig. 1.3: **M35032, 250 cm, 53x magnification**
Base of turbidite. Packstone, composed predominantly of planktic foraminifera and large pteropods (A).

Fig. 1.4: **M35034, 74 cm, 105x magnification**
Turbidite-periplatform sediment (A) transition. The lithology changes abrupt from a turbiditic grainstone to a mudstone. The periplatform sediment shows a fine-silty matrix. At the base of the turbidite layer shell fragments (B) and multilayered ooids can be found.

Fig. 1.5: **M35034, 50 cm, 53x magnification**
Typical view of a peloidal, biodetrital turbiditic packstone. Most of the grains are probably of skeletal origin, but the grains are already strongly micritisised, bluring their typical identification features.

Fig. 1.6: **M35042, 415 cm, 210x magnification**
For explanation see Fig. 1.6

Fig. 1.7: **M35034, 52 cm, 53x magnification**
For explanation see Fig. 1.6

Fig. 1.8: **M35049, 240 cm, 105x magnification**
Sand-sized skeletal grainstone near the base of a turbidite layer. The majority of grains is of pelagic origin (pteropods and planktic foraminifera), but also typical shallow-water biota are evident (*Halimeda* fragment at upper picture margin).

Plate 1

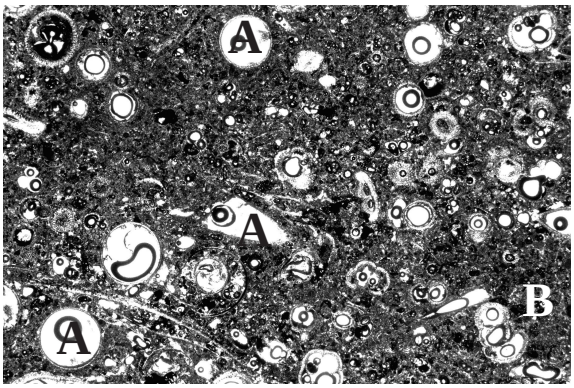

1.1

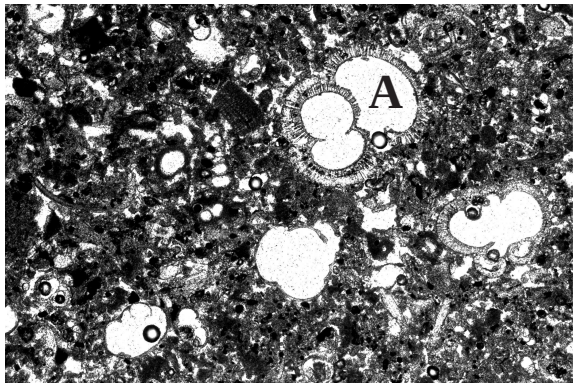

1.2

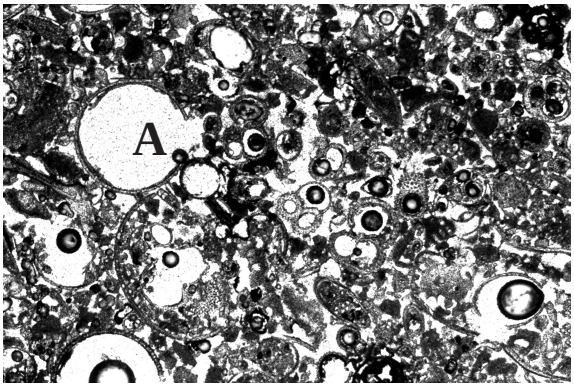

1.3

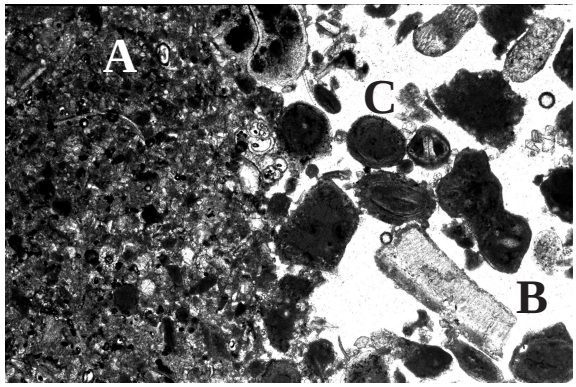

1.4

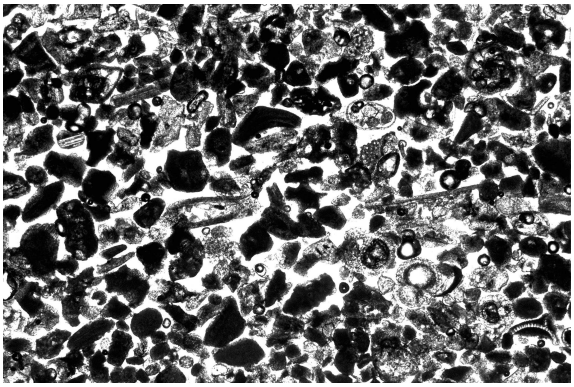

1.5

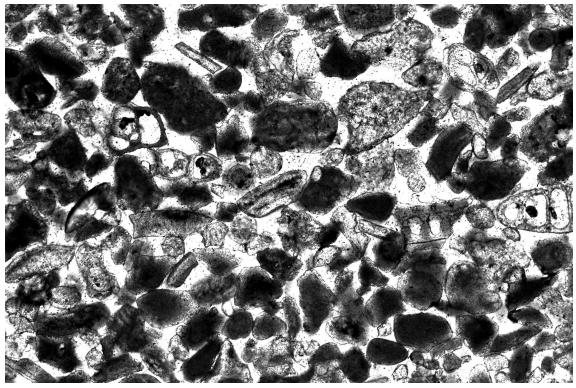

1.6

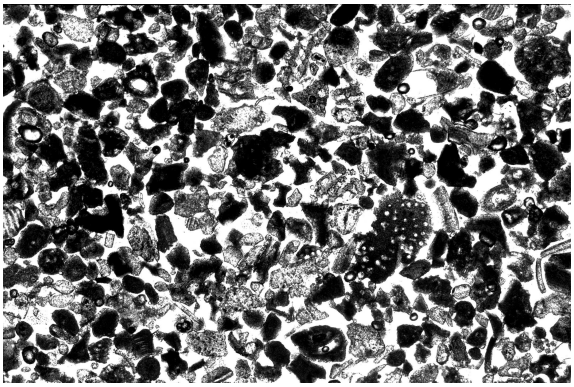

1.7

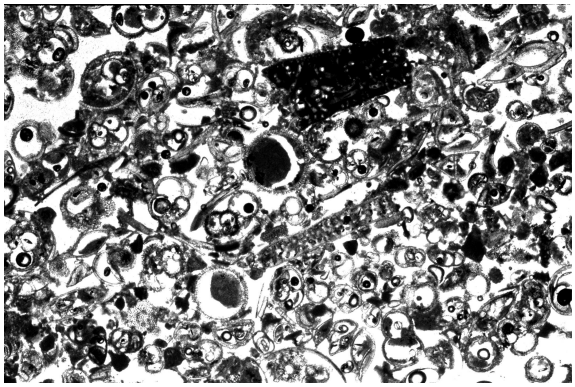

1.8

Plate 2
Shallow-water grains I

Fig. 2.1: **M35034, 75.5 cm, 210x magnification**
Calciturbidite layer (grainstone), with different mulitlayered ooids (A).

Fig. 2.2: **M35034, 44 cm, 105x magnification**
Calciturbidite layer; peloidal pack- to grainstone with a large miliolid foraminifera (*Pyrgo*). The test is well preserved and is characterised by a dark color in thin-sections, which is typical for miliolid foraminifera.

Fig. 2.3: **M35052, 866 cm, 210x magnification**
Base of a pelagic dominated turbidite; transverse equatorial section through a sessile foraminfera of the genus *Planorbulinella* sp./ *Planorbulina* sp.

Fig. 2.4: **M35034, 48 cm, 210x magnification**
Holocene calciturbidite layer; packstone; in the center of the picture a vertical section through a sessile foraminifera (cf. *Planorbulinella* sp.) can be seen.

Fig. 2.5: **M35038, 175-181 cm, 210x magnification**
Base of a shallow water grain enriched turbidite layer. The core is not incorporated in this study. A geniculate red algae (A) is affixed to a shell fragment (B). The other grains present are of pelagic origin.

Fig. 2.6: **M35032, 196.5 cm, 105x magnification**
Top of a calciturbidite layer. Bryozoan fragment (A) and other micritised grains (Rotaliid species, Globigerinid species). Notify the cracks within the sediment, which might act as pathway for fluid flow through the coarse calciturbidite layers.

Fig. 2.7: **M35038, 175-181 cm, 105x magnification**
Longitudinal section through an echinoderm spine (A).Also a benthic foraminifera (cf. *Amphistegina gibbosa*. (B)) is shown. The typical massive test with small chambers is indicative for shallow-water origin.

Fig. 2.8: **M35032, 193 cm, 210x magnification**
Tangentiall section through neritic benthic foraminifera within fine silty biodetrital matrix. This foramifera is most likely of soritid origin, but the genus could not be determined more exact.

Plate 2

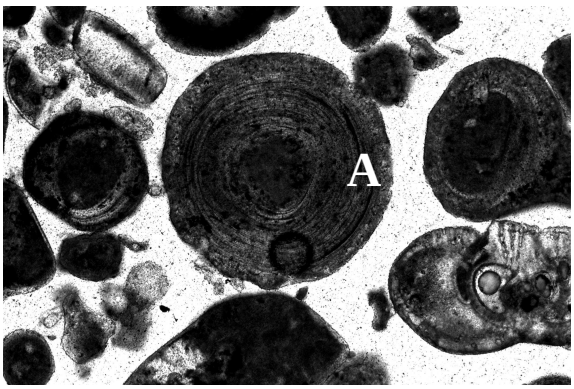

2.1

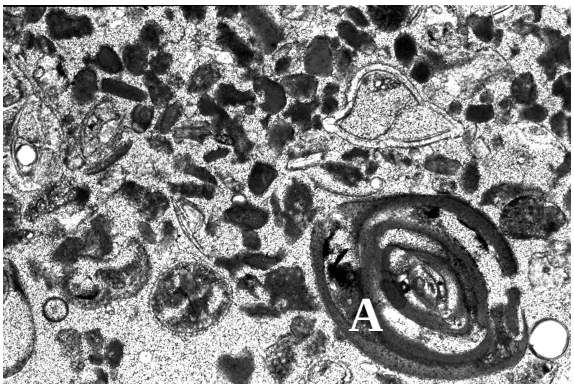

2.2

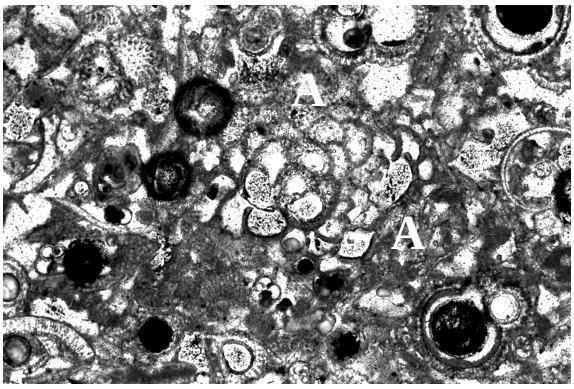

2.3

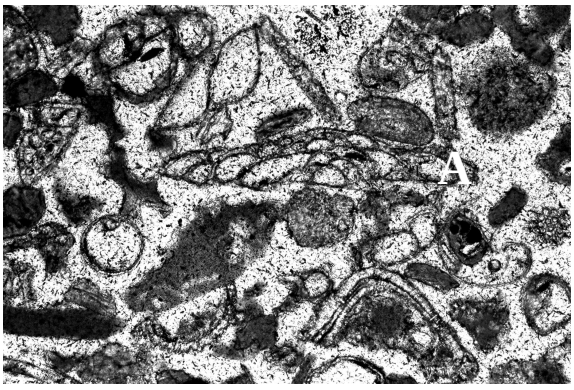

2.4

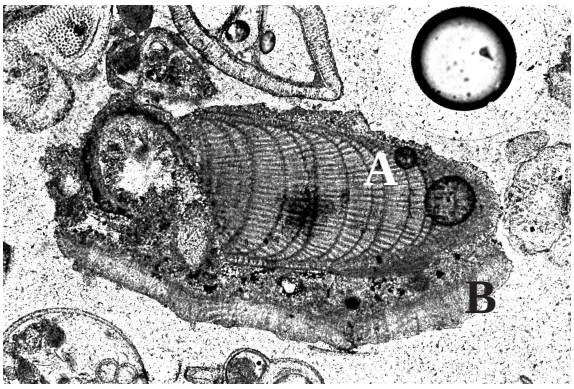

2.5

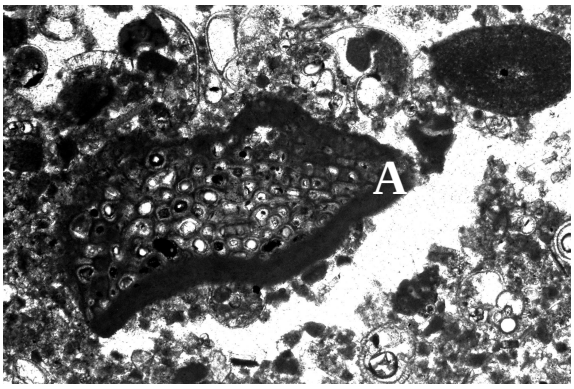

2.6

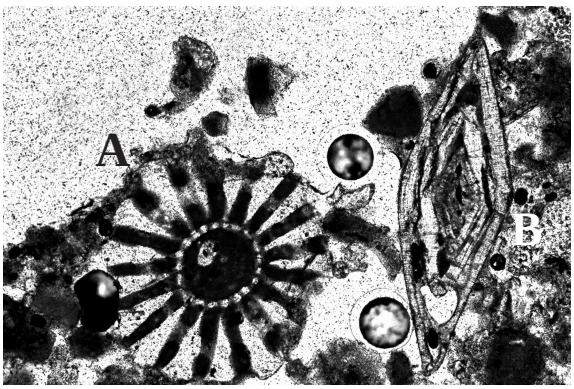

2.7

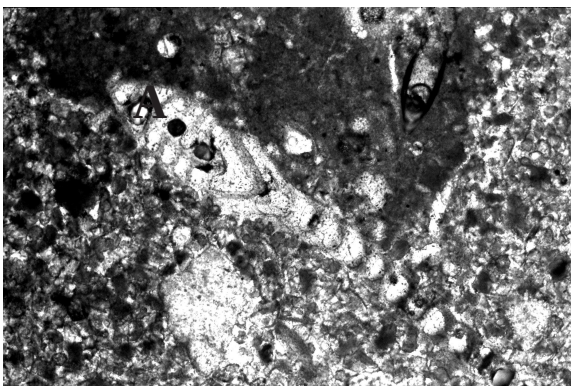

2.8

Plate 3
Shallow-water grains II

Fig. 3.1: **M35032, 195 cm, 105x magnification**
Thin-section photograph of a peloidal calciturbidite layer with two large *Halimeda* fragments (A).

Fig. 3.2: **M35032, 201.5 cm, 105x magnification**
Base of turbidite layer from the upcurrent margin. Fine biodetrital matrix with large skeletal, neritic fragments: (A) coralline algae, (B) coral fragment.

Fig. 3.3: **M35034, 70 cm, 53x magnification**
Coarse-grained calciturbidite packstone. Among various pelagic components, such as pteropods and planktic foraminifera, various neritic components are evident: tangential section through cf. *Sorites* sp. (A); (B) molluscan shell fragment, and peloids (C).

Fig. 3.4: **M35034, 74 cm, 210x magnification**
Typical neritic fragments at the base of a calciturbiditewith (A) Green algae, cf. *Lithophyllum* sp., (B) Grapestone, composed of multilayered ooids, (C) fragment of a scleractinian coral. In addition, a variety of partly or strong micritised components (D), such as shell fragements, planktic foraminifera or micritised algal fragments is evident.

Fig. 3.5: **M35052, 582 cm, 210x magnification**
Calciturbidite grainstone from the southern upcurrent margin. This layer consists predominantly of planktic foraminifera, but also typical shallow-water skeletal grains, such as benthic foraminifera of the genus *Nodosaria* sp. are present.

Fig. 3.6: **M35032, 196.5, 53x magnification**
Fine top of a calciturbidite. The turbidite consists of a fine biodetrital matrix, where single grains cannot be identified due to strong micritisation. Within this fine matrix a large neritic textulariid foraminifera, cf. *Textularia agglutinans* was found.

Fig. 3.7: **M35032, 193 cm, 210x magnification**
Top-tailend of a calciturbidite. The matrix is of fine silty biodetritus. Within this matrix a molluscan shell fragment (A) is evident, with an encrusting sessile foraminfera (B) attached to it.

Fig. 3.8: **M35048, 18 cm, 210x magnification**
Peloids (A) with a typical micritic rim (B) within a fine biodetrital matrix of a Holocene periplatform mud.

Plate 3

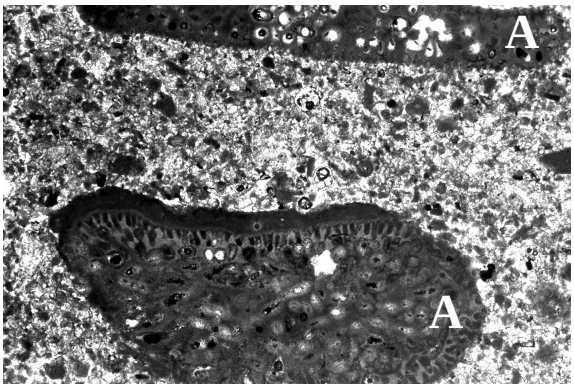

3.1

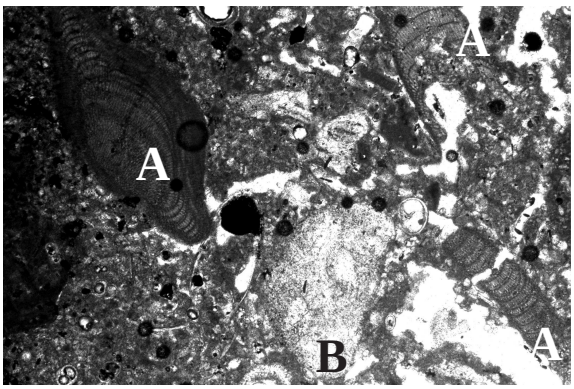

3.2

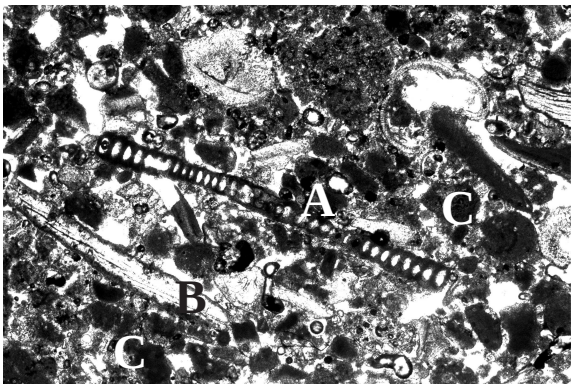

3.3

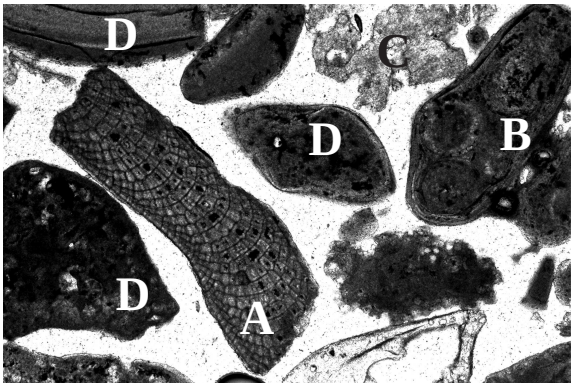

3.4

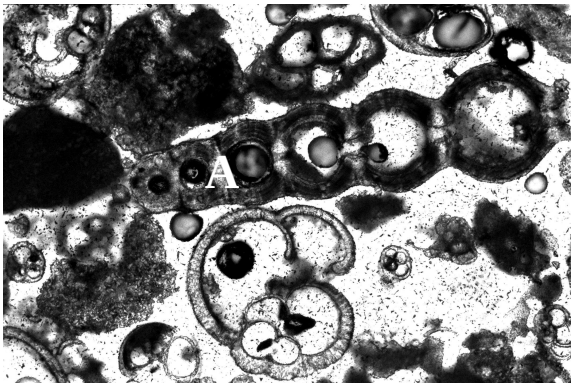

3.5

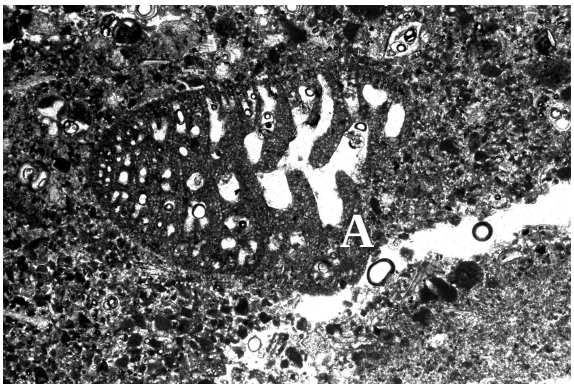

3.6

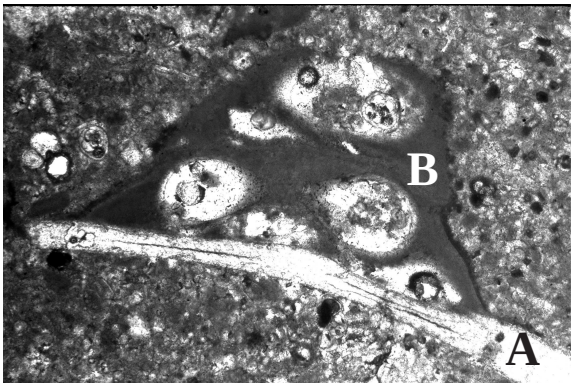

3.7

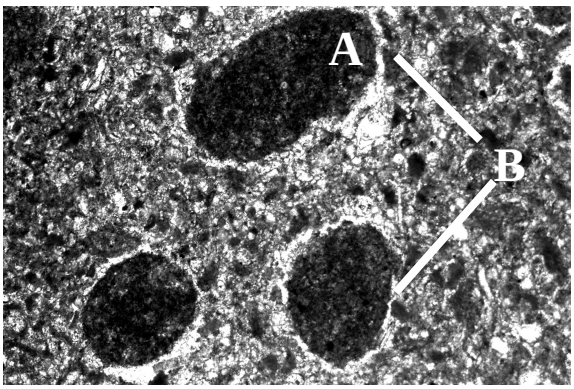

3.8

Plate 4
Shallow-water grains III

Fig. 4.1: M35048, 4 cm, 210x magnification
Holocene periplatform wackestone. The matrix consists primarly fine biodetrital skeletal grains, such as planktic foraminifera, shell fragments anda fine aragonitic (?) matrix. In addition, large round to ellipsoidal peloids (A) can be found.

Fig. 4.2: M35038, 175-181 cm, 105x magnification
This sediment core was not included into the general data set of this thesis, but it exhibited one very typical neritic calciturbidite layer. Within this coarse grainstone turbidite layer typical planktic foraminifera such as *G. ruber*, *G. sacculifer* or rotaliid foraminifera are evident, but also typical shallow-water grains can be found, such as green algae (A), cf. *Lithophyllum* sp., a transerve section through an echinoid spine (B), or an equatorial section of *Operculina* sp., a typical shallow-water benthic foraminifera.

Fig. 4.3: M35038, 175-181 cm, 105x magnification
Same turbidite layer as shown in Fig. 4.2 with other typical shallow-water grains: (A) cf. *Gypsina* sp. and a subaxial section through an *Amphistegina* sp (B).

Fig. 4.4: M35034, 70 cm, 105x magnification
Typical shallow-water grains within a calciturbidite layer along the southwestern toe-of-slope setting: (A) Echinoderm fragment, (B) bryozoan fragment and (C) grapestone composed of two mulitlamellar ooids.

Fig. 4.5: M35034, 74 cm, 105x magnification
Base of a calciturbidite layer. Beside a fine silty biodetrital matrix and some planktic components, also a transverse section through an annelid worm tube (B) and a transverse section of a typical benthic foraminfera, cf. *Archais angulatus* is evident.

Fig. 4.6: M35034, 75 cm, 105x magnification
Base of turbiditic grainstone. This layer consists primarly of micritised mulitlamellar ooids (A).

Plate 4

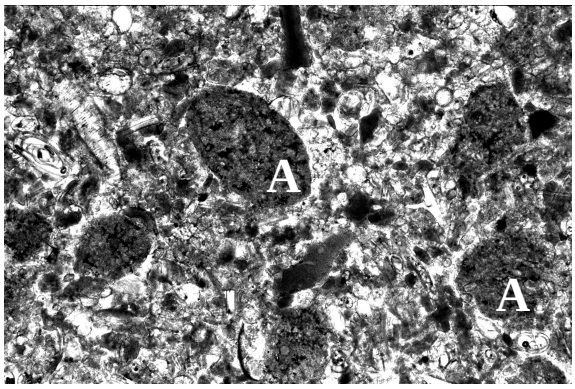

4.1

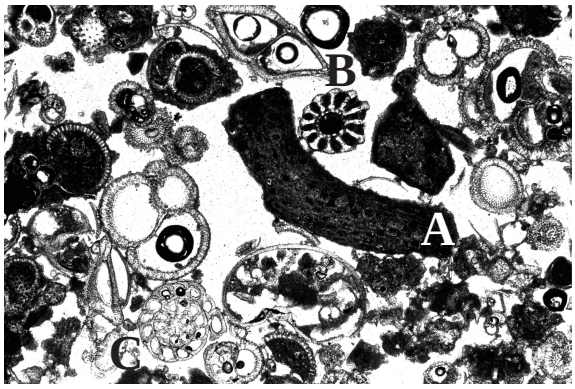

4.2

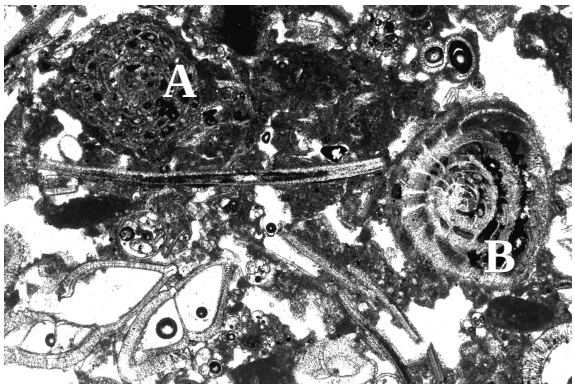

4.3

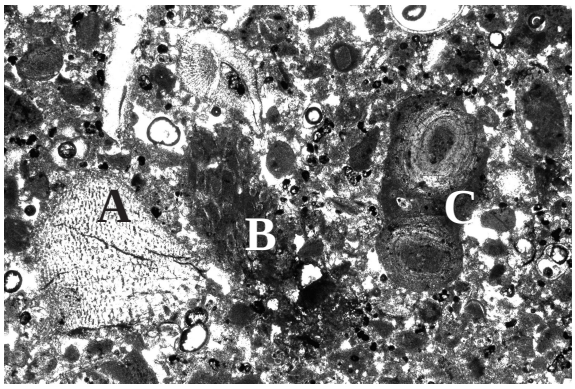

4.4

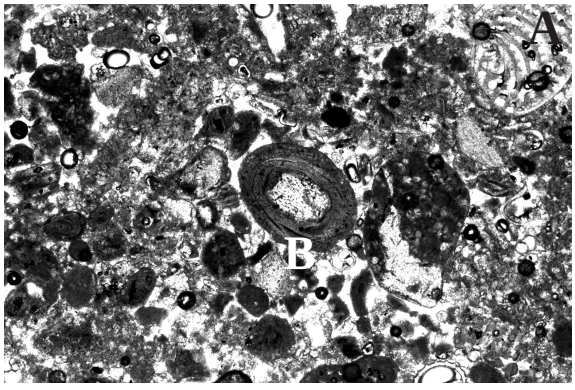

4.5

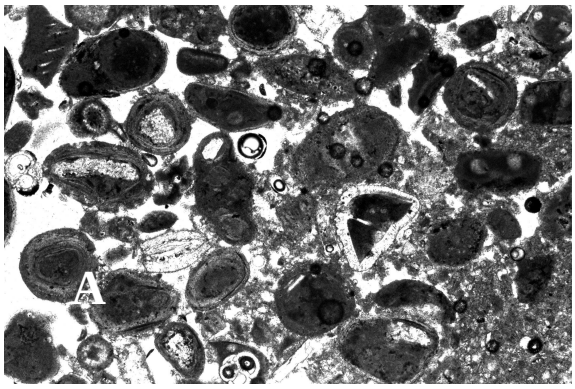

4.6

Plate 5
Interglacial coarse fraction samples

These plates show the interglacial composition of the coarse fraction. The dominant components within the periplatform sediments are planktic foraminifera (A) (genera *Globigerinoides*, *Globigerina* and *Globorotalia*) and pteropods (B). In addition, minor amounts of miliolid foraminifera (C), *Nodosaria* sp. (D), or echinoderm spines (E) can be found. In proximal periplatform sediments (e.g. M35048) an enrichment in peloids (F) was evident.

Fig. 5.1: M35032, 330 cm, 250-500μm, 84x magnification

Fig. 5.2: M35034, 90 cm, 250-500μm, 84x magnification

Fig. 5.3: M35042, 10 cm, 355-425μm, 84x magnification

Fig. 5.4: M35048, 190 cm, 355-425μm, 84x magnification

Fig. 5.5: M35048, 230 cm, 355-425μm, 84x magnification

Fig. 5.6: M35048, 390 cm, 355-425 μm, 84x magnification

Plate 5

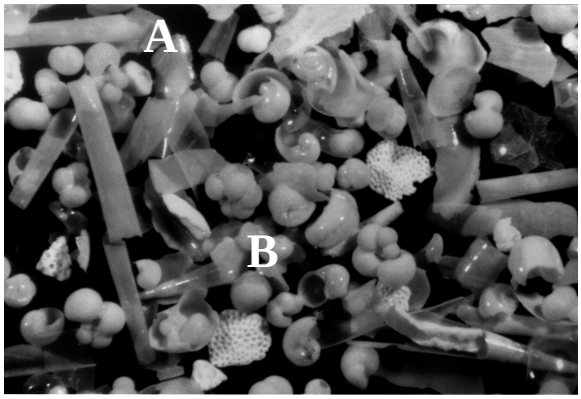

5.1

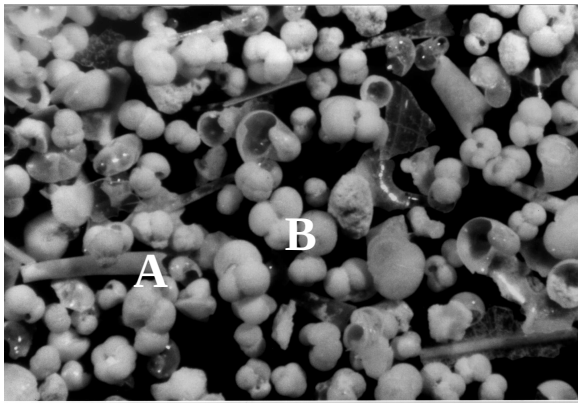

5.2

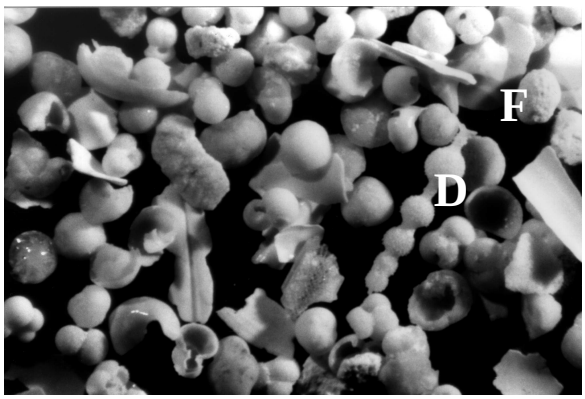

5.3

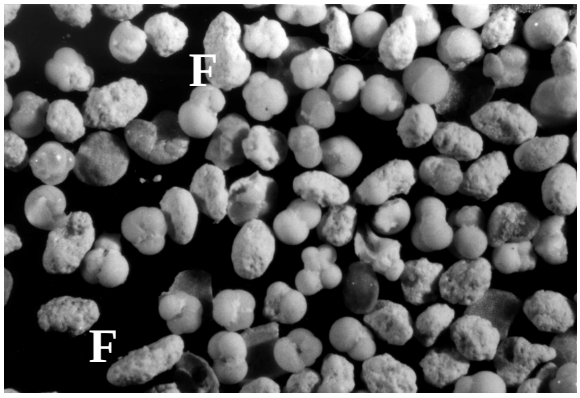

5.4

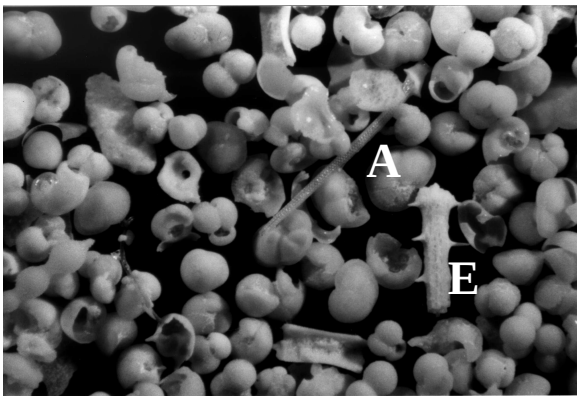

5.5

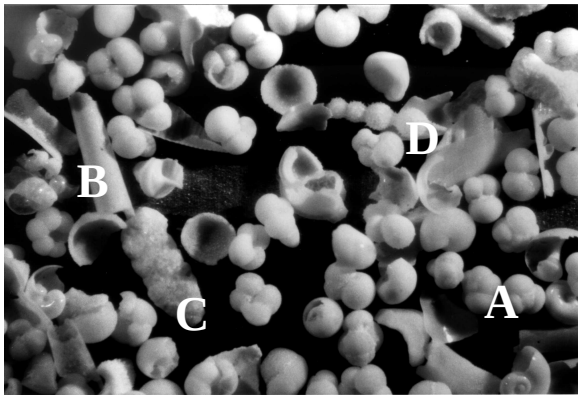

5.6

Plate 6
Glacial coarse fraction samples

These plates show the glacial composition of the coarse fraction. The composition of these samples is rather uniform, with planktic foraminifera and pteropods being the most abundant skeletal grains. In very minor amounts unidentifiable microcrystalline grains and (probably) deep-water benthic foraminifera are evident.

Fig. 6.1: M35032, 180 cm, 250-500μm, 84x magnification

Fig. 6.2: M35034, 130 cm, 250-500μm, 84x magnification

Fig. 6.3: M35042, 125 cm, 355-425μm, 84x magnification

Fig. 6.4: M35048, 120 cm, 355-425μm, 84x magnification

Fig. 6.5: M35048, 330 cm, 355-425μm, 84x magnification

Fig. 6.6: M35048, 510 cm, 355-425μm, 84x magnification

Plate 6

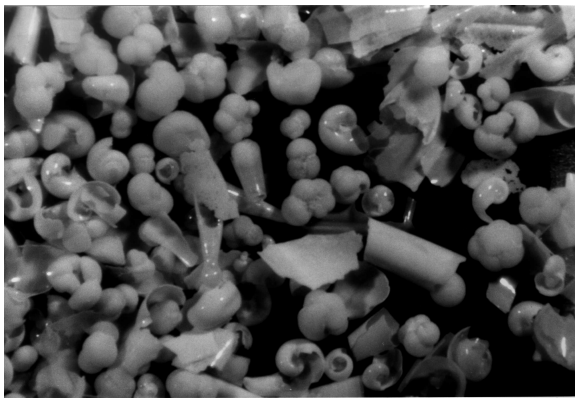

6.1

6.2

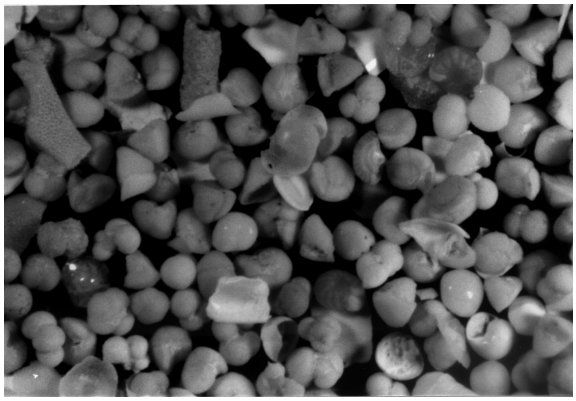

6.3

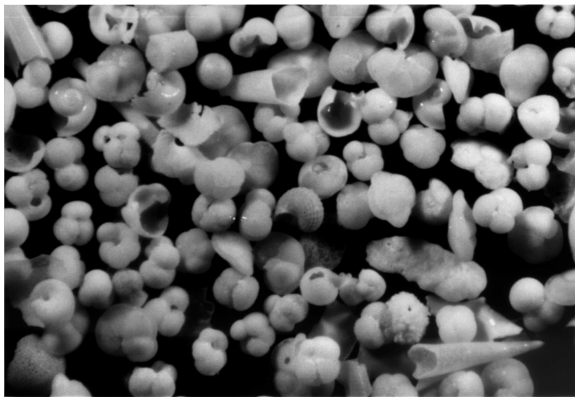

6.4

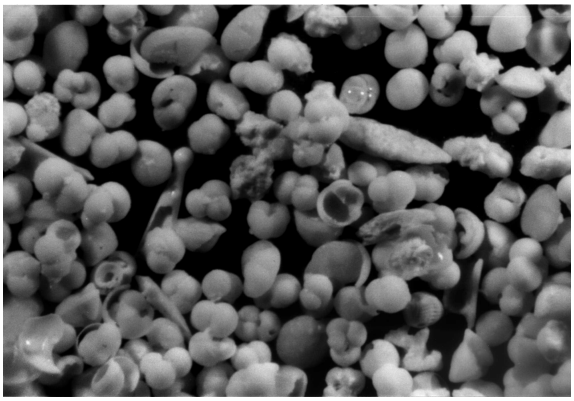

6.5

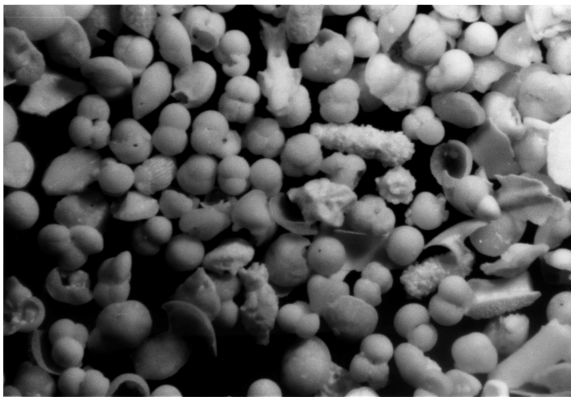

6.6

Plate 7
Turbidite coarse fraction samples I

Typical coarse fraction samples of the >500 μm fraction of calciturbidite layers. Only a few turbidites showed typical neritic components within the coarser fractions of the calciturbidite. Typical grains that are evident are:
(A) sponge fragments, (B) echinoderm spines and plates, (C) coral fragments, (D) pelecypod shells, (E) gastropod shells, (F) microcrystalline grains and (G) other benthic foraminifera.

Fig. 7.1: M35032, 205 cm, 500-1000μm, 53x magnification

Fig. 7.2: M35032, 205 cm, >1000μm, 34x magnification

Fig. 7.3: M35032, 205 cm, 500-1000μm, 53x magnification

Fig. 7.4: M35032, 205 cm, >1000μm, 34x magnification

Fig. 7.5: M35032, 205 cm, 500-1000μm, 53x magnification

Fig. 7.6: M35034, 70 cm, 500-1000μm, 53x magnification

Fig. 7.7: M35048, 516 cm, 500-1000μm, 34x magnification

Fig. 7.8: M35048, 516 cm, 500-1000μm, 53x magnification

Plate 7

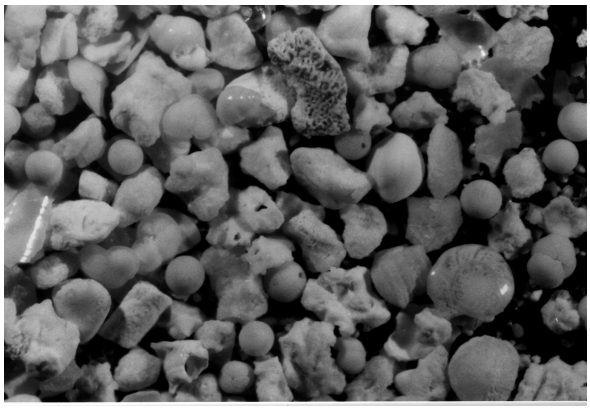

7.1

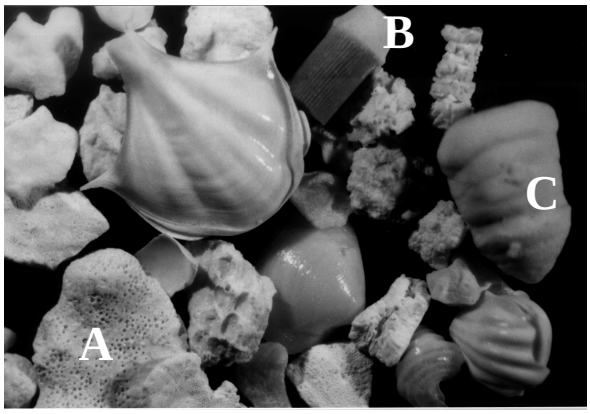

7.2

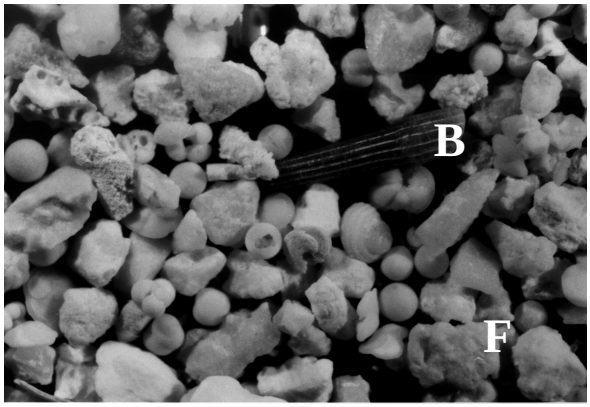

7.3

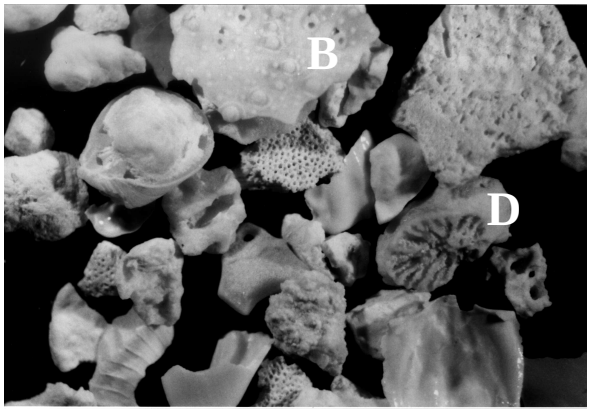

7.4

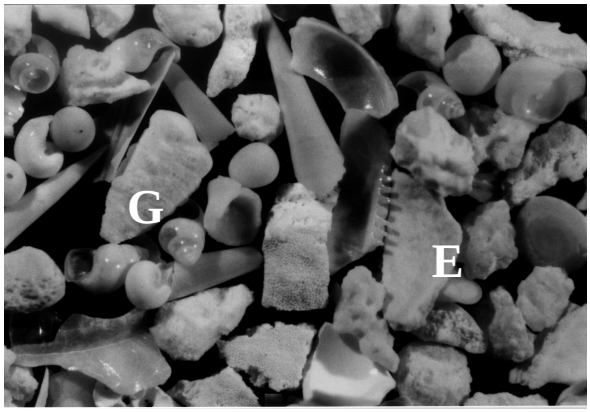

7.5

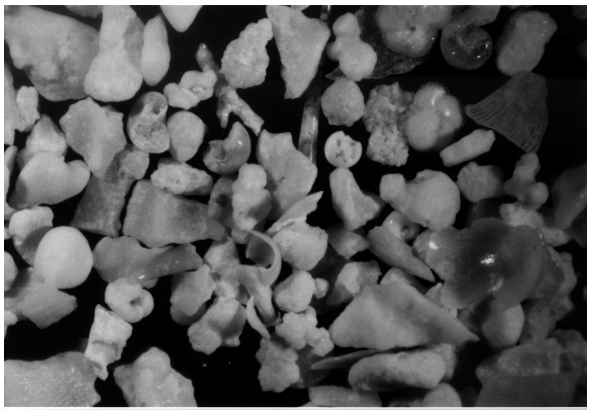

7.6

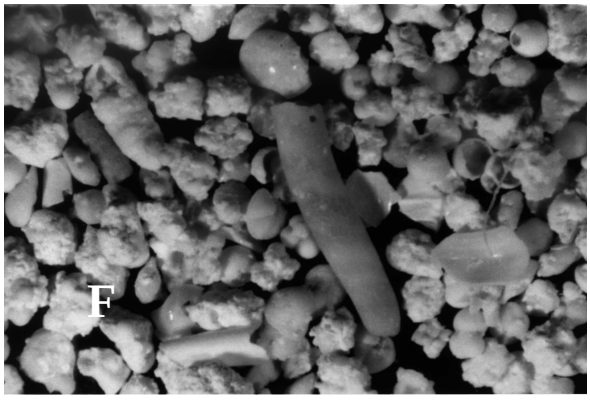

7.7

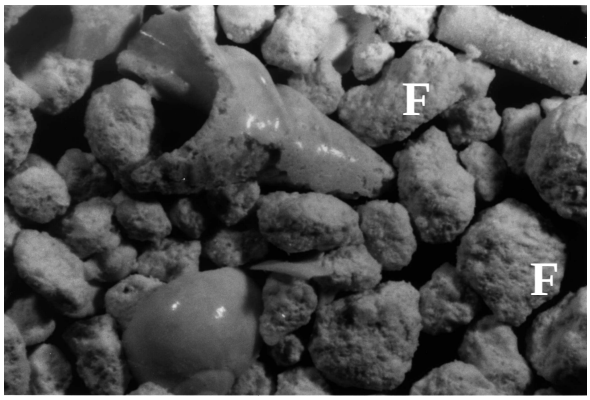

7.8

Plate 8
Turbidite coarse fraction samples II

Typical coarse fraction samples of the >500 μm fraction of calciturbidite layers. Only a few turbidites showed typical neritic components within the coarser fractions of the calciturbidite layers. Other typical grains that are evident are: (A) microcrystalline grains and (B) compacted worm tubes (Fig. 8.1 to 8.3).
Generally the coarse grains of the turbidite layers found within the analysed periplatform oozes of Pedro Bank are dominated by planktic foraminifera and pteropods. Fig. 8.4 to 8.7 show this typical composition.

Fig. 8.1: M35042, 236 cm, 500-1000μm, 53x magnification

Fig. 8.2: M35042, 236 cm, >1000μm, 53x magnification

Fig. 8.3: M35042, 480 cm, 500-1000μm, 53x magnification

Fig. 8.4: M35043, 230 cm, 500-1000μm, 53x magnification

Fig. 8.5: PC100, 386 cm, 500-1000μm, 84x magnification

Fig. 8.6: PC100, 414 cm, 500-1000μm, 53x magnification

Fig. 8.7: M35052, 210 cm, 500-1000μm, 53x magnification

Plate 8

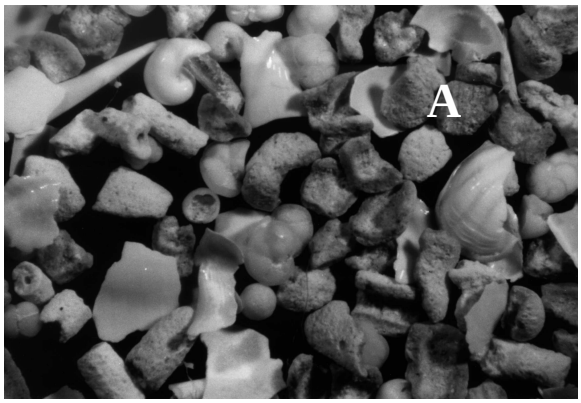

8.1

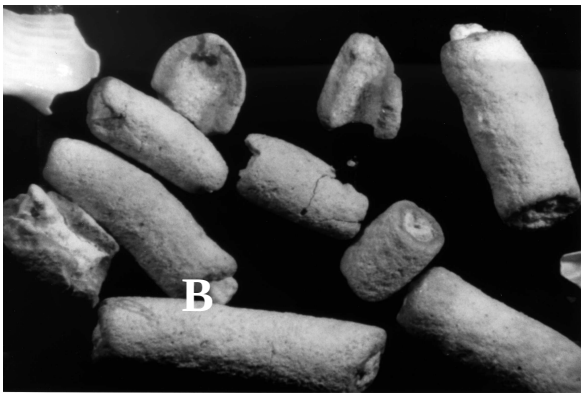

8.2

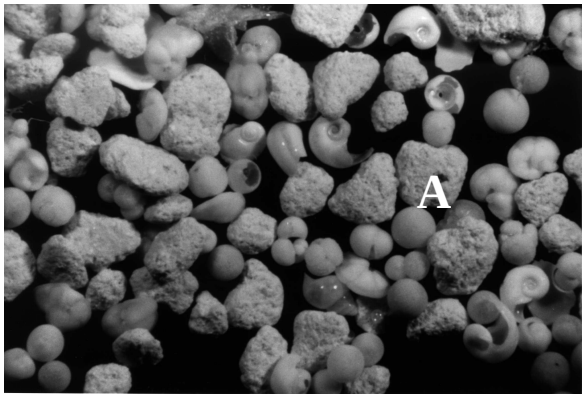

8.3

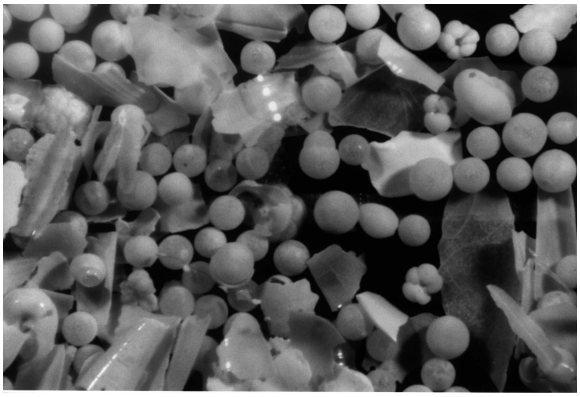

8.4

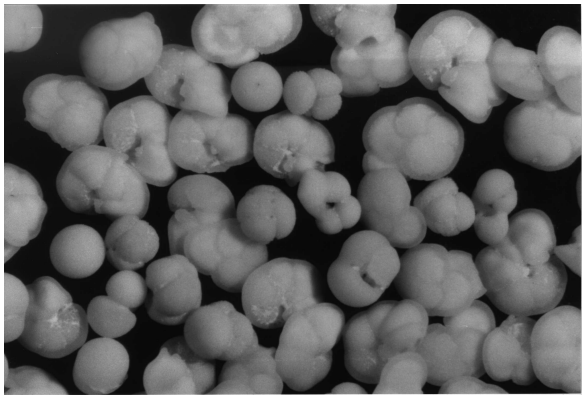

8.5

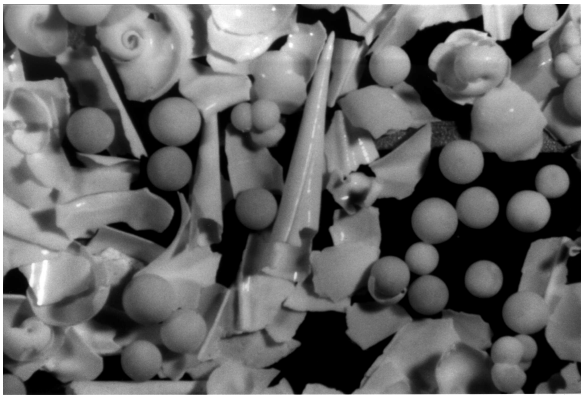

8.6

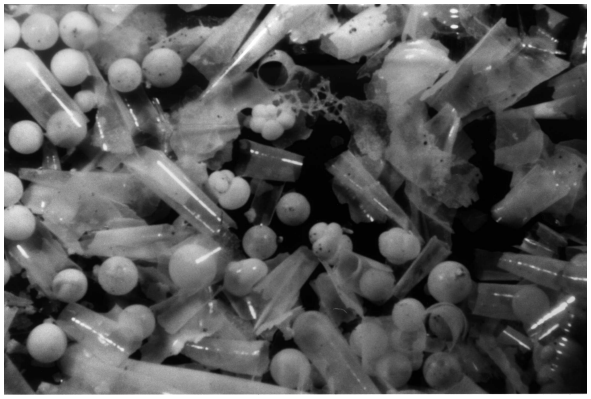

8.7

Data appendices

Appendix 3 - Stratigraphy, $\delta^{13}C$ and TOC content

Depth (cm) and Marine Isotope Stage (MIS)	$\delta^{18}O$ (*G. sacculifer*)	$\delta^{13}C$ (*G. sacculifer*)	Age (ky) Isotopes	Sedim. Rate (cm/ky)	*Globorotalia menardii* complex Zone
M35032-2					
MIS 1					
0	-1.86	1.74	0.00	2.67	Z
10	-1.86	1.74	6.00	2.67	Z
20	-0.57	1.87	10.00	2.67	Y
MIS 2					
30	-0.68	1.87	14.00	3.58	Y
40	0.66	2.08	18.00	3.58	Y
50	0.65	2.28	20.50	3.58	Y
60	0.56	2.15	23.00	3.58	Y
MIS 3					
70	0.56	2.29	25.50	1.69	Y
80	0.19	2.14	28.00	1.69	Y
90	0.48	2	33.00	1.69	Y
100	0.58	2.23	38.00	1.69	Y
110	0.61	2.1	43.00	1.69	Y
120	0.39	2.04	48.00	1.69	Y
130	0.23	2.13	53.00	1.69	Y
MIS 4					
140	0.29	2.09	65.00	1.04	Y
180	-0.24	1.61	70.00	1.04	Y
MIS 5					
220	-0.14	1.74	75.00	2.27	X
260	-0.51	1.61	80.00	2.27	X
270	-0.12	1.82	83.17	2.27	X
280	-0.07	1.55	86.33	2.27	X
310	-0.17	1.92	95.83	2.27	X
320	-0.39	1.75	99.00	2.27	X
330	-0.02	1.81	106.67	2.27	X
340	-0.1	1.62	114.33	2.27	X
350	-0.46	1.62	122.00	2.27	X
M35034					
MIS 1					
0	-2.01	1.96	0	6.46	Z
30	-1.95	2.05	2.25	6.46	Z
60	-1.91	2.15	4.5	6.46	Z
80	-2.01	1.86	6	6.46	Z
90	-1.64	1.99	7.5	6.46	Z
100	-1.37	1.8	9	6.46	Y
110	-0.56	1.86	10.5	6.46	Y
MIS 2					
120	-0.44	1.91	12	4.2	Y
130	-0.03	2.11	13.5	4.2	Y
150	0.1	2.2	16.5	4.2	Y
160	0.35	2.34	18	4.2	Y
MIS 3					
180	0.08	2.12	28	2.2	Y
190	0.06	2.25	32	2.2	Y
200	0.03	2.17	36	2.2	Y

Depth (cm) and Marine Isotope Stage (MIS)	$\delta^{18}O$ (*G. sacculifer*)	$\delta^{13}C$ (*G. sacculifer*)	Age (ky) Isotopes	Sedim. Rate (cm/ky)	*Globorotalia menardii* complex Zone
210	-0.14	1.99	40	2.2	Y
220	-0.01	2.05	44	2.2	Y
230	0.01	1.97	48	2.2	Y

M35042

MIS1

0	-1.66	1.69	0.00	3.08	Z
10	-1.49	1.71	2.84	3.08	Z
20	-1.63	1.62	6.00	3.08	Z
30	-0.95	1.73	10.00	3.08	Y

MIS 2

40	-0.07	1.66	14.00	2.16	Y
50	0.88	1.9	18.00	2.16	Y
60	0.7	1.99	23.00	2.16	Y

MIS 3

70	0.12	1.99	28.00	1.23	Y
80	0.14	1.92	36.33	1.23	Y
90	0	1.76	44.67	1.23	Y
100	-0.1	1.92	53.00	1.23	Y
110	0.23	1.78	57.80	1.23	Y

MIS 4

125	0.35	1.74	65.00	2.75	Y
130	0.08	1.9	67.14	2.75	Y
140	0.29	1.95	71.43	2.21	Y

MIS 5

160	-0.3	2.19	80.00	2.21	Y
170	-0.2	1.9	83.17	2.21	X
180	0.13	1.93	86.33	2.21	X
190	0.04	2	89.50	2.21	X
198	-0.2	1.91	92.03	2.21	X
220	-0.68	2.11	99.00	2.21	X
228	-0.57	1.89	101.79	2.21	X
250	-0.72	1.79	109.45	2.21	X
260	-1.22	1.72	112.94	2.21	X
270	-0.96	1.68	116.42	2.21	X
280	-1.37	1.7	119.91	2.21	X
286	-1.44	1.75	122.00	2.21	X
293.5	-0.99	1.58	126.06	2.21	X

MIS 6

300	-0.46	1.54	129.58	1.65	X
310	0.47	1.57	135.00	1.65	W
320	0.22	1.41	140.33	1.65	W
330	0.33	1.48	145.67	1.65	W
340	0.51	1.62	151.00	1.65	W
350	0.45	1.59	157.40	1.65	W
360	0.25	1.54	163.80	1.65	V
370	0.15	1.44	170.20	1.65	V
380	0.21	1.46	176.60	1.65	V
390	0.25	1.79	183.00	1.65	V
394.5	-0.09	1.79	184.65	1.65	V

Depth (cm) and Marine Isotope Stage (MIS)	$\delta^{18}O$ (*G. sacculifer*)	$\delta^{13}C$ (*G. sacculifer*)	Age (ky) Isotopes	Sedim. Rate (cm/ky)	*Globorotalia menardii* complex Zone
MIS 7					
414	-0.59	1.84	191.80	2.19	V
420	-0.99	1.81	194.00	2.19	V
430	-0.63	2.08	197.14	2.19	V
440	-0.95	1.72	200.29	2.19	V
450	-0.81	1.98	203.43	2.19	V
455	-0.59	2.14	205.00	2.19	V
460	-0.52	2.09	206.57	2.19	V
490	-1.03	1.92	216.00	2.19	V
500	-0.61	1.68	222.00	2.19	V
510	-0.31	1.68	228.00	2.19	V
520	-0.36	1.74	231.33	2.19	V
530	-0.42	1.96	234.67	2.19	V
540	-0.91	1.96	238.00	2.19	V

M35043

MIS 1					
0	-1.48	2.18	0.00	3.13	Z
10	-1.46	2.03	2.57	3.13	Z
20	-1.55	1.81	5.14	3.13	Z
30	-1.33	2.11	7.71	3.13	Z
40	-0.08	1.87	10.29	3.13	Y
MIS 2					
50	0.05	2.20	12.86	3.08	Y
60	0.32	2.13	15.43	3.08	Y
70	0.47	2.21	18.00	3.08	Y
MIS 3					
80	0.09	2.15	28.00	0.84	Y
90	0.28	1.92	40.50	0.84	Y
100	-0.06	1.73	53.00	0.84	Y
MIS 4					
110	0.11	2.03	59.00	2.58	Y
120	0.03	1.75	65.00	2.58	Y
MIS 5					
130	0.10	2.23	72.50	2.75	Y
140	-0.20	2.22	80.00	2.75	Y
150	0.04	1.97	83.23	2.75	X
160	-0.27	2.32	86.46	2.75	X
170	0.08	2.00	89.69	2.75	X
180	-0.03	2.09	92.92	2.75	X
190	-0.52	1.67	96.15	2.75	X
200	-0.67	2.03	99.38	2.75	X
210	-0.68	2.11	102.62	2.75	X
220	-0.67	2.08	105.85	2.75	X
240	-0.95	1.74	112.31	2.75	X
250	-1.02	1.75	115.54	2.75	X
260	-1.33	1.47	118.77	2.75	X
270	-1.48	1.58	122.00	2.75	X
280	-1.15	1.94	124.17	2.75	X
290	-1.21	1.69	126.33	2.75	X

Depth (cm) and Marine Isotope Stage (MIS)	$\delta^{18}O$ (*G. sacculifer*)	$\delta^{13}C$ (*G. sacculifer*)	Age (ky) Isotopes	Sedim. Rate (cm/ky)	*Globorotalia menardii* complex Zone
MIS 6					
300	-0.68	1.54	128.50	1.85	X
310	0.22	1.45	130.67	1.85	W
320	0.49	1.58	132.83	1.85	W
330	0.76	1.75	135.00	1.85	W
340	0.59	1.66	138.20	1.85	W
350	0.42	1.68	141.40	1.85	W
360	0.08	1.71	144.60	1.85	V
370	0.26	1.75	147.80	1.85	V
380	0.43	1.70	151.00	1.85	V
400	-0.60	1.89	171.00	1.85	V
410	-0.04	2.08	178.67	1.85	V
MIS 7					
420	-0.66	1.99	186.33	2.00	V
430	-0.67	1.92	194.00	2.00	V

M35048

MIS 1					
0	-1.81	n/a	0.00	5.40	Z
10	-1.59	n/a	1.20	5.40	Z
20	-1.73	n/a	2.40	5.40	Z
30	-1.96	n/a	3.60	5.40	Z
40	-1.61	n/a	4.80	5.40	Z
50	-1.73	n/a	6.00	5.40	Y
60	-0.59	n/a	9.00	5.40	Y
MIS 2					
70	-1.21	n/a	12.00	1.75	Y
90	-0.12	n/a	18.00	1.75	Y
MIS 3					
100	-0.28	n/a	53.00	0.32	Y
MIS 4					
110	-0.59	n/a	59.00	1.66	X
120	-0.58	n/a	65.00	1.66	X
130	-0.89	n/a	68.75	1.66	X
MIS 5					
140	-0.48	n/a	72.50	3.15	X
150	-0.05	n/a	76.25	3.15	X
160	-0.41	n/a	80.00	3.15	X
170	-0.46	n/a	83.17	3.15	X
180	-0.10	n/a	86.33	3.15	X
190	-0.30	n/a	89.50	3.15	X
200	-0.46	n/a	92.67	3.15	X
210	0.14	n/a	95.83	3.15	X
220	-0.97	n/a	99.00	3.15	X
230	0.56	n/a	102.29	3.15	X
240	-0.26	n/a	105.57	3.15	X
250	-0.58	n/a	108.86	3.15	X
260	-0.96	n/a	112.14	3.15	X
270	-0.42	n/a	115.43	3.15	X
280	0.52	n/a	118.71	3.15	X
290	0.49	n/a	122.00	3.15	X

Depth (cm) and Marine Isotope Stage (MIS)	$\delta^{18}O$ (*G. sacculifer*)	$\delta^{13}C$ (*G. sacculifer*)	Age (ky) Isotopes	Sedim. Rate (cm/ky)	*Globorotalia menardii* complex Zone
MIS 6					
300	0.47	n/a	129.25	0.41	X
310	1.05	n/a	136.50	0.41	W
330	0.57	n/a	151.00	0.41	W
340	0.51	n/a	165.33	0.41	W
350	-0.50	n/a	179.67	0.41	V
MIS 7					
360	-0.19	n/a	194.00	2.69	V
370	-0.23	n/a	196.75	2.69	V
380	0.50	n/a	199.50	2.69	V
390	1.12	n/a	202.25	2.69	V
400	-0.12	n/a	205.00	2.69	V
410	-0.97	n/a	207.75	2.69	V
420	0.30	n/a	210.50	2.69	V
430	-0.33	n/a	213.25	2.69	V
440	-0.09	n/a	216.00	2.69	V
450	0.35	n/a	220.40	2.69	V
460	-0.40	n/a	224.80	2.69	V
470	-0.51	n/a	229.20	2.69	V
480	-0.58	n/a	233.60	2.69	V
490	-0.34	n/a	238.00	2.69	V
500	-0.32	n/a	243.50	2.69	V
MIS 8					
510	0.15	n/a	249.00	2.69	V

M35049

MIS 1					
0	-1.678	2.19	0.00	4.42	Z
10	-1.923	1.97	2.00	4.42	Z
20	-2.168	2.03	4.00	4.42	Z
30	-2.302	2.05	6.00	4.42	Z
40	-1.859	2.13	9.00	4.42	Y
MIS 2					
50	-1.19	2.07	12.00	0.96	Y
60	0.249	2.24	15.00	0.96	Y
70	0.458	2.11	18.00	0.96	Y
MIS 3					
80	0.091	2.15	28.00	0.99	Y
90	0.34	2.21	33.00	0.99	Y
100	0.3	2.17	38.00	0.99	Y
110	0.206	2.07	43.00	0.99	Y
120	-0.356	2.37	48.00	0.99	Y
130	-0.499	2.17	53.00	0.99	Y
MIS 4					
140	-0.072	2.39	65.00	3.33	Y
150	-0.124	2.4	67.14	3.33	Y
160	n/a	n/a	69.29	3.33	Y

Depth (cm) and Marine Isotope Stage (MIS)	$\delta^{18}O$ (*G. sacculifer*)	$\delta^{13}C$ (*G. sacculifer*)	Age (ky) Isotopes	Sedim. Rate (cm/ky)	*Globorotalia menardii* complex Zone
MIS 5					
170	-0.672	2.23	71.43	2.72	X
180	-0.995	2.39	73.57	2.72	X
190	-1.128	2.5	75.71	2.72	X
200	-1.202	1.92	77.86	2.72	X
210	-1.478	2.05	80.00	2.72	X
220	-0.921	2.29	82.71	2.72	X
230	-1.185	2.32	85.43	2.72	X
250	-1.355	2.32	90.86	2.72	X
260	-1.484	2.05	93.57	2.72	X
270	-1.667	2.12	96.29	2.72	X
280	-1.69	1.86	99.00	2.72	X
290	-1.222	1.79	104.75	2.72	X
300	-1.926	1.81	110.50	2.72	X
310	-1.88	1.58	116.25	2.72	X
320	-1.992	1.81	122.00	2.72	X
330	-1.771	1.82	126.33	2.72	W
MIS 6					
340	-0.8	1.84	130.67	1.32	W
350	0.23	1.86	135.00	1.32	W
360	n/a	n/a	147.00	1.32	W
370	0.095	1.95	159.00	1.32	W
380	-0.156	1.86	171.00	1.32	V
390	0.228	1.9	183.00	1.32	V
400	0.227	1.74	184.22	1.32	V
410	0.086	2.01	185.44	1.32	V
MIS 7					
430	-0.874	1.58	187.89	3.73	V
440	n/a	n/a	189.11	3.73	V
450	-1.044	2.19	190.33	3.73	V
460	-1.164	2.21	191.56	3.73	V
470	-1.169	2.24	192.78	3.73	V
480	-1.449	2.42	194.00	3.73	V
490	-1.13	2.26	199.33	3.73	V
500	-1.167	2.13	204.67	3.73	V
510	-1.402	2.23	210.00	3.73	V

M35052

MIS 1					
0	-0.554	1.968	0.00	3.33	Z
20	-1.45	2.1	6.00	3.33	Z
30	-1.077	1.942	10.00	3.33	Y
MIS 2					
40	0.005	1.946	14.00	1.33	Y
50	1.434	2.227	18.00	1.33	Y
MIS 3					
60	0.317	2.059	28.00	3.41	Y
70	0.486	2.313	29.47	3.41	Y
80	0.613	2.312	30.94	3.41	Y
95	0.924	2.353	33.15	3.41	Y
100	0.843	2.28	33.88	3.41	Y

Depth (cm) and Marine Isotope Stage (MIS)	$\delta^{18}O$ (*G. sacculifer*)	$\delta^{13}C$ (*G. sacculifer*)	Age (ky) Isotopes	Sedim. Rate (cm/ky)	*Globorotalia menardii* complex Zone
110	0.737	2.217	35.35	3.41	Y
120	0.879	2.293	36.82	3.41	Y
130	0.743	2.308	38.29	3.41	Y
140	0.664	2.316	39.76	3.41	Y
150	0.456	2.162	41.24	3.41	Y
220	0.073	1.821	51.53	3.41	Y
230	-0.076	2.051	53.00	3.41	Y
MIS 4					
240	0.152	2.145	62.00	1.50	Y
250	-0.13	2.267	71.00	2.56	Y
MIS 5					
260	-0.441	2.267	80.00	2.56	Y
270	-0.326	2.399	82.38	2.56	X
280	-0.594	2.213	84.75	2.56	X
290	-0.579	1.944	87.13	2.56	X
300	0.125	1.757	89.50	2.56	X
310	-0.274	1.894	91.88	2.56	X
320	0.074	1.92	94.25	2.56	X
330	-0.32	2.172	96.63	2.56	X
340	-0.681	1.921	99.00	2.56	X
350	-0.364	2.068	104.75	2.56	X
370	-0.66	1.863	116.25	2.56	X
380	-0.972	1.645	122.00	2.56	X
390	-0.467	1.74	125.25	2.56	X
MIS 6					
400	0.386	1.535	128.50	1.53	X
410	0.623	1.652	131.75	1.53	W
420	1.481	1.599	135.00	1.53	W
430	1.019	1.85	137.53	1.53	W
440	0.371	1.801	140.05	1.53	W
495	0.423	1.738	153.95	1.53	W
500	0.054	1.893	155.21	1.53	W
590	0.717	1.629	177.95	1.53	V
600	0.315	1.685	180.47	1.53	V
610	0.938	1.712	183.00	1.53	V
MIS 7					
620	-0.174	1.772	186.67	2.07	V
630	-0.236	1.631	190.33	2.07	V
640	-0.842	1.772	194.00	2.07	V
650	-0.577	1.889	199.50	2.07	V
660	-0.676	1.751	205.00	2.07	V
670	-0.357	1.901	210.50	2.07	V
680	-0.605	1.984	216.00	2.07	V
690	-0.355	1.779	220.00	2.07	V
700	0.233	1.906	224.00	2.07	V
710	0.336	1.845	228.00	2.07	V
720	-0.761	1.9	238.00	2.07	V
730	-0.587	1.908	239.72	2.07	V
740	0.172	1.743	241.44	2.07	V
750	1.012	1.745	243.17	1.59	V
MIS 8					
870	1.096	1.67	263.83	1.59	V
880	0.258	1.667	265.56	1.59	V

Depth (cm) and Marine Isotope Stage (MIS)	$\delta^{18}O$ (*G. sacculifer*)	$\delta^{13}C$ (*G. sacculifer*)	Age (ky) Isotopes	Sedim. Rate (cm/ky)	*Globorotalia menardii* complex Zone
900	0.608	1.773	269.00	1.59	V
910	0.208	1.977	278.00	1.59	V
920	-0.191	1.858	287.00	1.59	V
930	0.14	1.823	293.00	1.59	V
940	0.621	2.088	299.00	1.59	V
MIS 9					
950	-0.148	1.822	304.50	3.14	V
960	-0.185	1.927	310.00	3.14	V

PC059

MIS 1					
0	n/a	n/a	0.00	0.54	Z
2.5	-1.32	1.61	4.52	0.54	Z
MIS 2					
10.5	0.02	1.73	19.00	0.92	Y
MIS 3					
20.5	-0.19	1.74	28.00	2.23	Y
30.5	-0.35	1.55	31.68	2.23	Y
40.5	0.19	1.81	35.35	2.23	Y
50.5	-0.10	2.06	39.03	2.23	Y
70.5	0.35	1.95	46.38	2.23	Y
80.5	-0.03	1.77	50.06	2.23	Y
83.5	n/a	n/a	51.16	2.23	Y
88.5	-0.14	1.71	53.00	2.23	Y
MIS 4					
96.5	0.06	1.94	65.00	1.46	Y
106.5	-0.15	1.99	68.00	1.46	Y
MIS 5					
116.5	0.00	1.93	71.00	1.9	Y
120.5	-0.47	2.07	72.20	1.9	Y
136.5	-0.35	2.25	77.00	1.9	Y
146.5	-0.54	2.06	80.00	1.9	X
156.5	-0.31	1.83	83.80	1.9	X
166.5	-0.12	1.99	87.60	1.9	X
176.5	-0.03	1.69	91.40	1.9	X
186.5	-0.40	1.72	95.20	1.9	X
196.5	-0.25	1.90	99.00	1.9	X
213.5	n/a	n/a	109.86	1.9	X
216.5	-0.40	1.56	111.78	1.9	X
226.5	-0.75	1.63	118.17	1.9	X
232.5	n/a	n/a	122.00	1.9	X
MIS 6					
238.5	0.72	1.71	135.00	0.96	W
246.5	0.58	1.52	145.11	0.96	W
256.5	0.56	1.49	157.74	0.96	W
266.5	0.47	1.41	170.37	0.96	V
276.5	0.48	1.32	183.00	0.96	V
MIS 7					
286.5	0.27	1.64	186.67	1.83	V
296.5	-0.32	1.57	190.33	1.83	V
306.5	-0.16	1.82	194.00	1.83	V

Depth (cm) and Marine Isotope Stage (MIS)	$\delta^{18}O$ (*G. sacculifer*)	$\delta^{13}C$ (*G. sacculifer*)	Age (ky) Isotopes	Sedim. Rate (cm/ky)	*Globorotalia menardii* complex Zone
316.5	-0.48	1.94	205.00	1.83	V
326.5	-0.68	2.02	216.00	1.83	V
336.5	-0.27	1.98	219.14	1.83	V
346.5	-0.60	1.87	222.29	1.83	V
356.5	-0.47	1.70	225.43	1.83	V
366.5	-0.05	1.72	228.57	1.83	V
373.5	-0.26	1.79	230.77	1.83	V
378.5	-0.45	1.65	232.34	1.83	V
386.5	-0.76	1.89	234.86	1.83	V
396.5	-0.59	1.74	238.00	1.83	V
MIS 8					
406.5	-0.26	1.40	249.00	1.46	V
426.5	0.70	1.44	261.67	1.46	V
436.5	0.19	1.46	268.00	1.46	V
446.5	0.59	1.48	274.33	1.46	V
456.5	0.41	1.47	280.67	1.46	V
466.5	-0.05	1.97	287.00	1.46	V
476.5	0.29	n/a	n/a	n/a	V
486.5	0.34	n/a	n/a	n/a	V
496.5	0.75	n/a	n/a	n/a	V
506.5	0.54	n/a	n/a	n/a	V
516.5	0.45	n/a	n/a	n/a	V
523.5	0.51	n/a	n/a	n/a	V

PC100

MIS 1					
0	-1.55	1.7	0.00	3.17	Z
6	-1.55	1.7	1.64	3.17	Z
16	-1.42	1.87	4.36	3.17	Z
26	-1.4	1.87	7.09	3.17	Z
36	-0.5	1.75	9.82	3.17	Y
MIS 2					
46	0.51	2.03	12.55	2.71	Y
56	0.38	1.95	15.27	2.71	Y
66	0.77	1.99	18.00	2.71	Y
MIS 3					
76	-0.04	1.74	28.00	1.31	Y
86	-0.05	1.99	34.25	1.31	Y
96	-0.14	2.25	40.50	1.31	Y
106	-0.11	1.94	46.75	1.31	Y
116	-0.16	1.83	53.00	1.31	Y
MIS 4					
126	0.45	2.01	65.00	1.45	Y
136	0.03	2.09	70.00	1.45	Y
MIS 5					
146	-0.21	2.23	75.00	1.94	Y
156	-0.47	1.99	80.00	1.94	Y
166	-0.05	1.98	84.22	1.94	X
174	-0.25	2.03	87.60	1.94	X
191	-0.3	1.88	94.78	1.94	X
201	-0.35	2.05	99.00	1.94	X

Depth (cm) and Marine Isotope Stage (MIS)		$\delta^{18}O$ (*G. sacculifer*)	$\delta^{13}C$ (*G. sacculifer*)	Age (ky) Isotopes	Sedim. Rate (cm/ky)	*Globorotalia menardii* complex Zone
MIS 6						
	210	0.93	1.56	135.00	1.1	W
	219	0.57	1.73	144.00	1.1	W
	228	0.54	1.64	153.00	1.1	W
	238	0.9	1.54	163.00	1.1	W
	248	0.69	1.47	173.00	1.1	V
	258	1.02	1.57	183.00	1.1	V
MIS 7						
	268	0.42	1.89	187.78	1.71	V
	275	0.2	2.09	191.13	1.71	V
	281	0.11	1.57	194.00	1.71	V
	286	0.18	2.02	195.67	1.71	V
	296	0.3	1.81	199.00	1.71	V
	304	0.27	1.94	201.67	1.71	V
	332	0.73	1.85	211.00	1.71	V
	341	0.41	1.75	214.00	1.71	V
	347	0.15	1.62	216.00	1.71	V
	351	0.63	1.63	217.76	1.71	V
	361	0.26	1.73	222.16	1.71	V
	365	0.36	1.89	223.92	1.71	V
	372	-0.11	1.81	227.00	1.71	V
	381	-0.3	1.9	230.96	1.71	V
	397	-0.67	1.68	238.00	1.71	V
	410	0.52	1.5	243.72	1.71	V
MIS 8						
	422	0.99	1.44	249.00	1.41	V
	435	0.58	1.52	259.40	1.41	V
	447	1.56	1.57	269.00	1.41	V
	458	1.25	1.84	278.00	1.41	V
	469	0.25	1.9	287.00	1.41	V
	474	0.6	1.89	289.22	1.41	V
	487	0.51	1.88	295.00	1.41	V
	496	0.63	2.01	299.00	1.41	V
MIS 9						
	507	0.09	1.69	305.05	2	V
	516	0	1.86	310.00	2	V

Appendix 4 - Mineralogy

Mineralogy Data	Carbonates vs. non-carbonates				Bulk Sediment					
Depth (cm) and Marine Isotope Stage (MIS)	$CaCO_3$ bulk (%)	$CaCO_3$ fine fraction (%)	Non-Carbonates bulk (%)	Non-Carbonates fine (%)	Bulk Aragonite (relative %)	Bulk HMC (relative %)	Bulk LMC (relative %)	Aragonite bulk (absolute %)	HMC bulk (absolute %)	LMC bulk (absolute %)
M35032										
MIS 1										
0	90.41	86.57	9.59	13.43	68.34	7.37	24.29	61.79	6.66	21.96
10	90.41	86.57	9.59	13.43	71.00	7.77	21.23	64.19	7.02	19.19
20	76.16	76.90	23.84	23.10	58.24	11.39	30.37	44.36	8.67	23.13
Average	85.66	83.35	14.34	16.65	65.86	8.84	25.30	56.78	7.45	21.43
Maximum	90.41	86.57	23.84	23.10	71.00	11.39	30.37	64.19	8.67	23.13
Minimum	76.16	76.90	9.59	13.43	58.24	7.37	21.23	44.36	6.66	19.19
MIS 2										
30	69.67	61.99	30.33	38.01	45.26	14.02	40.72	31.53	9.77	28.37
40	67.90	60.81	32.10	39.19	41.31	16.21	42.49	28.05	11.01	28.85
50	64.91	59.90	35.09	40.10	42.35	14.30	43.35	27.49	9.28	28.14
60	71.36	62.03	28.64	37.97	41.81	15.50	42.69	29.83	11.06	30.46
Average	68.46	61.18	31.54	38.82	42.68	15.01	42.31	29.23	10.28	28.96
Maximum	71.36	62.03	35.09	40.10	45.26	16.21	43.35	31.53	11.06	30.46
Minimum	64.91	59.90	28.64	37.97	41.31	14.02	40.72	27.49	9.28	28.14
MIS 3										
70	71.27	64.42	28.73	35.58	47.45	13.65	38.90	33.82	9.73	27.73
80	76.90	68.97	23.10	31.03	49.62	13.13	37.24	38.16	10.10	28.64
90	76.35	67.92	23.65	32.08	48.37	15.59	36.04	36.93	11.90	27.52
100	74.93	66.14	25.07	33.86	46.73	15.79	37.47	35.02	11.83	28.08
110	76.46	72.50	23.54	27.50	54.06	12.69	33.25	41.33	9.70	25.42
120	77.88	70.25	22.12	29.75	49.51	14.75	35.74	38.56	11.48	27.84
130	78.31	79.01	21.69	20.99	42.22	18.04	39.74	33.06	14.13	31.12
Average	76.02	69.89	23.98	30.11	48.28	14.80	36.91	36.70	11.27	28.05
Maximum	78.31	79.01	28.73	35.58	54.06	18.04	39.74	41.33	14.13	31.12
Minimum	71.27	64.42	21.69	20.99	42.22	12.69	33.25	33.06	9.70	25.42
MIS 4										
140	79.57	75.39	20.43	24.61	50.42	13.70	35.88	40.12	10.90	28.55
180	73.21	72.74	26.79	27.26	48.10	13.48	38.41	35.22	9.87	28.12
Average	76.39	74.07	23.61	25.93	49.26	13.59	37.15	37.67	10.39	28.34
Maximum	79.57	75.39	26.79	27.26	50.42	13.70	38.41	40.12	10.90	28.55
Minimum	73.21	72.74	20.43	24.61	48.10	13.48	35.88	35.22	9.87	28.12
MIS 5										
220	71.10	70.47	28.90	29.53	51.15	12.02	36.84	36.37	8.54	26.19
260	82.70	81.75	17.30	18.25	60.48	9.67	29.86	50.01	7.99	24.69
270	84.62	77.94	15.38	22.06	56.38	12.26	31.37	47.70	10.37	26.54
280	80.53	80.47	19.47	19.53	54.99	11.89	33.12	44.28	9.58	26.67
310	83.21	77.28	16.79	22.72	56.89	10.98	32.13	47.34	9.14	26.73
320	78.47	80.70	21.53	19.30	54.19	12.11	33.70	42.52	9.51	26.44
330	85.86	78.52	14.14	21.48	61.51	10.36	28.13	52.81	8.90	24.16
340	88.03	89.25	11.97	10.75	61.97	10.91	27.12	54.56	9.60	23.87
350	93.06	90.74	6.94	9.26	69.46	6.22	24.32	64.64	5.79	22.63
Average	83.06	80.79	16.94	19.21	58.56	10.71	30.73	48.91	8.82	25.33
Maximum	93.06	90.74	28.90	29.53	69.46	12.26	36.84	64.64	10.37	26.73
Minimum	71.10	70.47	6.94	9.26	51.15	6.22	24.32	36.37	5.79	22.63
Interglacials	84.36	82.07	15.64	17.93	62.21	9.78	28.01	52.85	8.14	23.38
Glacials	72.42	67.63	27.58	32.37	45.97	14.30	39.73	33.45	10.33	28.65
Stage 3	76.02	69.89	23.98	30.11	48.28	14.80	36.91	36.70	11.27	28.05

	Fine Fraction						Fine carbonates in bulk sediment			
Quartz Intensity bulk	Fine Aragonite (relative %)	HMC fine (relative %)	LMC fine (relative %)	Fine Aragonite (absolute %)	HMC fine (absolute %)	LMC fine (absolute %)	Fine Aragonite in bulk sedim. (%)	Fine HMC in bulk sedim. (%)	Fine LMC in bulk sedim. (%)	Fine Quartz Intensity
300	73.66	10.22	16.12	63.77	8.84	13.95	48.05	6.38	10.07	240
178	73.66	10.22	16.12	63.77	8.84	13.95	48.05	6.38	10.07	240
435	58.57	14.45	26.98	45.04	11.11	20.75	33.23	8.28	15.46	412
304	68.63	11.63	19.74	57.53	9.60	16.22	43.11	7.01	11.87	297
435	73.66	14.45	26.98	63.77	11.11	20.75	48.05	8.28	15.46	412
178	58.57	10.22	16.12	45.04	8.84	13.95	33.23	6.38	10.07	240
547	43.84	15.93	40.23	27.17	9.88	24.94	23.53	7.61	19.21	752
635	33.61	18.32	48.07	20.44	11.14	29.23	18.51	9.03	23.71	1017
680	35.64	23.81	40.55	21.35	14.27	24.29	19.82	12.22	20.81	799
647	37.07	16.59	46.34	22.99	10.29	28.75	20.43	7.95	22.21	748
627	37.54	18.66	43.80	22.99	11.39	26.80	20.57	9.20	21.48	829
680	43.84	23.81	48.07	27.17	14.27	29.23	23.53	12.22	23.71	1017
547	33.61	15.93	40.23	20.44	9.88	24.29	18.51	7.61	19.21	748
527	38.23	25.22	36.55	24.63	16.25	23.55	21.22	12.66	18.34	715
454	43.51	16.55	39.95	30.01	11.41	27.55	25.92	8.84	21.35	618
388	44.75	6.55	48.70	30.39	4.45	33.07	24.29	3.16	23.51	638
536	43.09	11.43	45.48	28.50	7.56	30.08	25.76	6.03	24.00	634
421	50.68	14.43	34.89	36.75	10.46	25.30	30.95	8.35	20.20	612
503	47.75	16.00	36.26	33.54	11.24	25.47	29.46	8.90	20.18	648
392	37.31	0.00	62.69	29.48	0.00	49.53	22.86	0.00	38.75	475
460	43.62	12.88	43.50	30.47	8.77	30.65	25.78	6.85	23.76	620
536	50.68	25.22	62.69	36.75	16.25	49.53	30.95	12.66	38.75	715
388	37.31	0.00	34.89	24.63	0.00	23.55	21.22	0.00	18.34	475
396	42.51	10.82	46.68	32.05	8.15	35.19	27.12	6.54	28.22	483
519	46.06	6.77	47.17	33.50	4.93	34.31	28.10	4.11	28.60	593
458	44.28	8.79	46.92	32.77	6.54	34.75	27.61	5.32	28.41	538
519	46.06	10.82	47.17	33.50	8.15	35.19	28.10	6.54	28.60	593
396	42.51	6.77	46.68	32.05	4.93	34.31	27.12	4.11	28.22	483
576	46.79	17.29	35.91	32.98	12.19	25.31	27.27	9.99	20.74	697
328	56.28	18.51	25.22	46.01	15.13	20.61	35.22	11.45	15.60	422
374	51.70	10.91	37.39	40.29	8.50	29.14	31.87	6.20	21.24	540
377	53.00	8.92	38.08	42.65	7.18	30.64	34.47	5.80	24.75	514
369	57.56	16.61	25.83	44.48	12.83	19.96	39.28	10.52	16.37	447
492	61.29	13.69	25.02	49.46	11.05	20.19	39.26	9.02	16.48	391
311	55.77	16.45	27.79	43.79	12.91	21.82	28.32	7.64	12.90	453
257	64.77	6.49	28.74	57.81	5.80	25.65	47.77	4.86	21.49	244
171	69.17	12.55	18.28	62.77	11.38	16.59	44.82	7.93	11.55	318
362	57.37	13.49	29.14	46.69	10.77	23.32	36.48	8.15	17.90	447
576	69.17	18.51	38.08	62.77	15.13	30.64	47.77	11.45	24.75	697
171	46.79	6.49	18.28	32.98	5.80	16.59	27.27	4.86	11.55	244
333	63.00	12.56	24.44	52.11	10.19	19.77	39.79	7.58	14.88	372
542	40.91	13.73	45.36	27.88	8.97	30.78	24.09	7.26	24.95	684
460	43.62	12.88	43.50	30.47	8.77	30.65	25.78	6.85	23.76	620

Mineralogy Data	Carbonates vs. non-carbonates				Bulk Sediment					
Depth (cm) and Marine Isotope Stage (MIS)	$CaCO_3$ bulk (%)	$CaCO_3$ fine fraction (%)	Non-Carbonates bulk (%)	Non-Carbonates fine (%)	Bulk Aragonite (relative %)	Bulk HMC (relative %)	Bulk LMC (relative %)	Aragonite bulk (absolute %)	HMC bulk (absolute %)	LMC bulk (absolute %)
Overall average	78.53	74.37	21.47	25.63	53.27	12.55	34.18	42.39	9.70	26.44
Glacial-to-Interglacial percentual deviation as shown in Fig. 7.2 and 7.3				**80.54**						
M35034										
Stage 1										
0	83.77	84.44	16.23	15.56	61.63	15.71	22.66	51.63	13.16	18.98
30	85.23	85.52	14.77	14.48	58.69	13.34	27.96	50.02	11.37	23.83
60	86.65	87.36	13.35	12.64	63.00	14.96	22.05	54.59	12.96	19.10
80	86.36	85.90	13.64	14.10	68.63	9.80	21.56	59.27	8.47	18.62
90	85.19	86.19	14.81	13.81	68.36	11.33	20.31	58.24	9.65	17.30
100	79.24	77.97	20.76	22.03	43.23	11.27	45.50	34.26	8.93	36.05
110	73.89	68.70	26.11	31.30	40.44	13.69	45.87	29.88	10.11	33.89
Average	86.61	83.99	17.09	17.70	57.71	12.87	29.42	48.27	10.67	23.97
Maximum	90.41	86.57	26.11	31.30	68.63	15.71	45.87	59.27	13.16	36.05
Minimum	76.16	76.90	13.35	12.64	40.44	9.80	20.31	29.88	8.47	17.30
Stage 2										
120	65.57	65.19	34.43	34.81	30.54	17.70	51.75	20.03	11.61	33.94
130	70.56	65.75	29.44	34.25	31.62	17.15	51.22	22.31	12.10	36.14
150	82.85	80.08	17.15	19.92	50.75	17.08	32.17	42.05	14.15	26.65
160	77.65	70.23	22.35	29.77	33.66	17.23	49.11	26.14	13.38	38.14
Average	69.02	61.29	25.84	29.69	36.64	17.29	46.06	27.63	12.81	33.72
Maximum	71.36	62.03	34.43	34.81	50.75	17.70	51.75	42.05	14.15	38.14
Minimum	64.91	59.90	17.15	19.92	30.54	17.08	32.17	20.03	11.61	26.65
Stage 3										
180	78.36	73.84	21.64	26.16	34.78	14.78	50.43	27.26	11.59	39.52
190	79.68	74.49	20.32	25.51	35.15	12.87	51.98	28.01	10.26	41.42
200	78.55	77.75	21.45	22.25	46.53	14.83	38.64	36.55	11.65	30.35
210	76.79	75.61	23.21	24.39	56.00	6.71	37.29	43.00	5.15	28.64
220	75.89	74.18	24.11	25.82	35.21	12.96	51.84	26.72	9.83	39.34
230	73.65	69.87	26.35	30.13	41.07	18.13	40.81	30.25	13.35	30.06
Average	76.66	70.95	22.85	25.71	41.46	13.38	45.16	31.96	10.30	34.89
Maximum	78.31	79.01	26.35	30.13	56.00	18.13	51.98	43.00	13.35	41.42
Minimum	74.93	66.14	20.32	22.25	34.78	6.71	37.29	26.72	5.15	28.64
Overall Average	78.82	76.65	21.18	23.35	47.02	14.09	38.89	37.66	11.04	30.12
Glacial-to-Interglacial percentual deviation as shown in Fig. 7.2 and 7.3				**67.71**						

	Fine Fraction						Fine carbonates in bulk sediment			
Quartz Intensity bulk	Fine Aragonite (relative %)	HMC fine (relative %)	LMC fine (relative %)	Fine Aragonite (absolute %)	HMC fine (absolute %)	LMC fine (absolute %)	Fine Aragonite in bulk sedim. (%)	Fine HMC in bulk sedim. (%)	Fine LMC in bulk sedim. (%)	Fine Quartz Intensity
433	50.65	13.55	35.80	38.54	9.83	25.99	31.02	7.59	20.23	546
							-39.46	**-4.24**	**67.61**	
56	79.39	11.31	9.30	67.04	9.55	7.86	52.52	7.48	6.15	91
73	80.30	8.48	11.22	68.68	7.25	9.59	51.72	5.46	7.23	148
48	81.35	12.41	6.24	71.07	10.84	5.45	53.53	8.17	4.10	92
61	85.55	8.40	6.05	73.49	7.22	5.20	59.09	5.80	4.18	105
59	85.01	9.72	5.27	73.28	8.37	4.54	64.11	7.33	3.97	109
222	72.63	9.34	18.02	56.63	7.29	14.05	44.53	5.73	11.05	267
250	60.03	18.65	21.32	41.24	12.81	14.64	28.38	8.82	10.08	370
110	77.75	11.19	11.06	64.49	9.05	8.76	50.55	6.97	6.68	169
250	85.55	18.65	21.32	73.49	12.81	14.64	64.11	8.82	11.05	370
48	60.03	8.40	5.27	41.24	7.22	4.54	28.38	5.46	3.97	91
445	53.61	21.09	25.30	34.95	13.75	16.49	28.99	11.41	13.68	552
446	45.45	22.49	32.06	29.88	14.79	21.08	22.58	11.18	15.93	618
251	71.21	15.34	13.45	57.03	12.29	10.77	37.83	8.15	7.14	317
321	53.87	16.34	29.79	37.83	11.48	20.92	27.89	8.46	15.42	514
366	56.03	18.82	25.15	39.92	13.08	17.31	29.32	9.80	13.04	500
446	71.21	22.49	32.06	57.03	14.79	21.08	37.83	11.41	15.93	618
251	45.45	15.34	13.45	29.88	11.48	10.77	22.58	8.15	7.14	317
258	49.85	23.77	26.38	36.81	17.55	19.48	25.48	12.15	13.48	411
288	55.30	13.51	31.18	41.19	10.06	23.23	29.22	7.14	16.48	432
273	59.18	12.16	28.66	46.01	9.45	22.28	36.70	7.54	17.77	382
331	50.47	9.11	40.42	38.16	6.89	30.56	30.47	5.50	24.40	406
294	55.67	8.56	35.77	41.30	6.35	26.54	31.37	4.82	20.16	368
383	58.10	11.57	30.32	40.60	8.09	21.19	32.34	6.44	16.88	540
305	54.76	13.11	32.12	40.68	9.73	23.88	30.93	7.27	18.20	423
383	59.18	23.77	40.42	46.01	17.55	30.56	36.70	12.15	24.40	540
258	49.85	8.56	26.38	36.81	6.35	19.48	25.48	4.82	13.48	368
239	64.53	13.66	21.81	50.30	10.24	16.11	38.63	7.74	12.24	337
							-41.99	**40.60**	**95.23**	

Mineralogy Data	Carbonates vs. non-carbonates				Bulk Sediment					
Depth (cm) and Marine Isotope Stage (MIS)	$CaCO_3$ bulk (%)	$CaCO_3$ fine fraction (%)	Non-Carbonates bulk (%)	Non-Carbonates fine (%)	Bulk Aragonite (relative %)	Bulk HMC (relative %)	Bulk LMC (relative %)	Aragonite bulk (absolute %)	HMC bulk (absolute %)	LMC bulk (absolute %)
M35042										
Stage1										
0	88.68	93.31	11.32	6.69	79.93	7.91	12.16	70.88	7.02	10.78
10	85.66	84.27	14.34	15.73	74.69	5.54	19.77	63.98	4.74	16.94
20	85.56	84.27	14.44	15.73	73.18	3.97	22.85	62.61	3.39	19.55
30	85.10	81.99	14.90	18.01	67.12	10.89	22.00	57.12	9.26	18.72
Average	86.25	85.96	13.75	14.04	73.73	7.08	19.20	63.65	6.10	16.50
Maximum	88.68	93.31	14.90	18.01	79.93	10.89	22.85	70.88	9.26	19.55
Minimum	85.10	81.99	11.32	6.69	67.12	3.97	12.16	57.12	3.39	10.78
Stage 2										
40	75.96	72.54	24.04	27.46	48.42	18.65	32.93	36.78	14.16	25.01
50	75.87	72.36	24.13	27.64	42.13	19.49	38.38	31.96	14.79	29.12
60	75.32	71.16	24.68	28.84	45.67	21.08	33.26	34.39	15.88	25.05
Average	75.71	72.02	24.29	27.98	45.41	19.74	34.85	34.38	14.94	26.39
Maximum	75.96	72.54	24.68	28.84	48.42	21.08	38.38	36.78	15.88	29.12
Minimum	75.32	71.16	24.04	27.46	42.13	18.65	32.93	31.96	14.16	25.01
Stage 3										
70	74.49	88.58	25.51	11.42	39.10	21.01	39.89	29.12	15.65	29.71
80	78.04	84.08	21.96	15.92	52.54	17.75	29.71	41.00	13.85	23.18
90	79.26	82.35	20.74	17.65	41.74	12.70	45.57	33.08	10.06	36.11
100	79.91	78.75	20.09	21.25	53.84	7.25	38.91	43.02	5.80	31.09
110	74.95	84.48	25.05	15.52	39.72	7.79	52.49	29.77	5.84	39.34
Average	77.33	83.65	22.67	16.35	45.39	13.30	41.31	35.20	10.24	31.89
Maximum	79.91	88.58	25.51	21.25	53.84	21.01	52.49	43.02	15.65	39.34
Minimum	74.49	78.75	20.09	11.42	39.10	7.25	29.71	29.12	5.80	23.18
Stage 4										
125	71.98	75.00	28.02	25.00	34.42	14.72	50.86	24.77	10.60	36.61
130	71.26	75.58	28.74	24.42	34.76	21.14	44.10	24.77	15.06	31.43
140	75.03	77.07	24.97	22.93	47.70	8.39	43.91	35.79	6.29	32.94
Average	72.76	75.88	27.24	24.12	38.96	14.75	46.29	28.44	10.65	33.66
Maximum	75.03	77.07	28.74	25.00	47.70	21.14	50.86	35.79	15.06	36.61
Minimum	71.26	75.00	24.97	22.93	34.42	8.39	43.91	24.77	6.29	31.43
Stage 5										
160	82.85	84.78	17.15	15.22	55.90	6.79	37.31	46.31	5.62	30.91
170	82.91	85.92	17.09	14.08	59.63	1.56	38.81	49.44	1.29	32.18
180	78.57	81.88	21.43	18.12	48.70	3.24	48.06	38.27	2.55	37.76
190	80.14	83.17	19.86	16.83	48.75	2.37	48.88	39.07	1.90	39.17
198	85.15	88.97	14.85	11.03	60.48	5.21	34.31	51.50	4.43	29.21
220	84.06	88.82	15.94	11.18	72.99	9.24	17.77	61.36	7.76	14.94
228	82.62	88.85	17.38	11.15	71.01	10.11	18.88	58.67	8.35	15.60
250	85.81	91.77	14.19	8.23	73.04	8.94	18.02	62.68	7.67	15.46
260	85.55	86.95	14.45	13.05	72.75	8.27	18.98	62.24	7.07	16.24
270	86.42	88.00	13.58	12.00	73.81	8.73	17.47	63.78	7.54	15.09
280	86.91	87.00	13.09	13.00	70.80	9.05	20.16	61.53	7.86	17.52
286	90.07	92.23	9.93	7.77	79.67	7.31	13.02	71.76	6.58	11.73
293.5	87.39	87.77	12.61	12.23	75.80	9.48	14.72	66.24	8.29	12.87
Average	84.50	87.39	15.50	12.61	66.41	6.94	26.64	56.37	5.92	22.21
Maximum	90.07	92.23	21.43	18.12	79.67	10.11	48.88	71.76	8.35	39.17
Minimum	78.57	81.88	9.93	7.77	48.70	1.56	13.02	38.27	1.29	11.73

	Fine Fraction						Fine carbonates in bulk sediment			
Quartz Intensity bulk	Fine Aragonite (relative %)	HMC fine (relative %)	LMC fine (relative %)	Fine Aragonite (absolute %)	HMC fine (absolute %)	LMC fine (absolute %)	Fine Aragonite in bulk sedim. (%)	Fine HMC in bulk sedim. (%)	Fine LMC in bulk sedim. (%)	Fine Quartz Intensity
129	81.06	8.01	10.93	75.64	7.48	10.20	64.23	6.35	8.66	133
190	73.13	6.26	20.61	61.63	5.27	17.37	47.77	4.09	13.46	193
170	73.10	9.24	17.66	61.60	7.79	14.88	48.17	6.09	11.64	218
230	67.60	6.73	25.68	55.42	5.51	21.05	42.11	4.19	15.99	252
180	73.72	7.56	18.72	63.57	6.51	15.87	50.57	5.18	12.44	199
230	81.06	9.24	25.68	75.64	7.79	21.05	64.23	6.35	15.99	252
129	67.60	6.26	10.93	55.42	5.27	10.20	42.11	4.09	8.66	133
398	38.06	25.30	36.65	27.60	18.35	26.58	22.83	15.18	21.99	466
364	34.48	28.45	37.07	24.95	20.59	26.83	20.95	17.29	22.53	456
400	39.05	18.32	42.62	27.79	13.04	30.33	23.54	11.05	25.70	484
387	37.20	24.02	38.78	26.78	17.33	27.91	22.44	14.50	23.40	469
400	39.05	28.45	42.62	27.79	20.59	30.33	23.54	17.29	25.70	484
364	34.48	18.32	36.65	24.95	13.04	26.58	20.95	11.05	21.99	456
357	36.75	21.63	41.62	32.55	19.16	36.86	27.53	16.20	31.17	507
383	43.19	16.54	40.27	36.32	13.91	33.86	31.02	11.88	28.92	414
366	39.08	17.82	43.10	32.19	14.67	35.49	27.70	12.63	30.55	385
324	40.73	14.42	44.86	32.07	11.35	35.33	28.31	10.02	31.19	473
269	41.02	5.05	53.93	34.66	4.27	45.56	29.66	3.65	38.99	383
340	40.16	15.09	44.75	33.56	12.67	37.42	28.85	10.88	32.16	432
383	43.19	21.63	53.93	36.32	19.16	45.56	31.02	16.20	38.99	507
269	36.75	5.05	40.27	32.07	4.27	33.86	27.53	3.65	28.92	383
454	32.01	22.25	45.74	24.01	16.69	34.31	21.80	15.15	31.15	536
489	41.04	22.53	36.43	31.02	17.03	27.53	29.31	16.08	26.01	486
399	45.14	7.97	46.89	34.79	6.14	36.14	31.31	5.53	32.53	478
447	39.40	17.58	43.02	29.94	13.28	32.66	27.47	12.25	29.90	500
489	45.14	22.53	46.89	34.79	17.03	36.14	31.31	16.08	32.53	536
399	32.01	7.97	36.43	24.01	6.14	27.53	21.80	5.53	26.01	478
266	56.84	4.67	38.49	48.19	3.96	32.63	40.71	3.35	27.56	286
255	59.00	3.41	37.59	50.69	2.93	32.30	44.52	2.57	28.37	271
319	50.10	5.86	44.04	41.02	4.80	36.06	35.84	4.19	31.50	469
273	51.39	2.76	45.86	42.74	2.29	38.14	36.67	1.97	32.72	312
231	61.38	10.23	28.40	54.61	9.10	25.27	46.11	7.68	21.34	207
243	66.47	9.14	24.39	59.04	8.12	21.66	50.73	6.98	18.61	248
265	70.71	10.09	19.20	62.83	8.97	17.06	55.69	7.95	15.12	284
200	79.00	8.92	12.08	72.50	8.19	11.09	56.35	6.36	8.62	211
218	77.95	5.68	16.37	67.78	4.94	14.23	58.19	4.24	12.22	225
222	74.73	9.18	16.09	65.77	8.07	14.16	54.36	6.67	11.70	230
177	77.85	5.96	16.19	67.74	5.18	14.09	52.33	4.00	10.88	
133	78.88	9.12	12.00	72.75	8.41	11.07	63.28	7.31	9.63	171
165	74.05	11.70	14.25	65.00	10.27	12.50	53.53	8.46	10.30	253
228	67.57	7.44	24.99	59.28	6.56	21.56	49.87	5.52	18.35	264
319	79.00	11.70	45.86	72.75	10.27	38.14	63.28	8.46	32.72	469
133	50.10	2.76	12.00	41.02	2.29	11.07	35.84	1.97	8.62	171

Mineralogy Data	Carbonates vs. non-carbonates				Bulk Sediment					
Depth (cm) and Marine Isotope Stage (MIS)	$CaCO_3$ bulk (%)	$CaCO_3$ fine fraction (%)	Non-Carbonates bulk (%)	Non-Carbonates fine (%)	Bulk Aragonite (relative %)	Bulk HMC (relative %)	Bulk LMC (relative %)	Aragonite bulk (absolute %)	HMC bulk (absolute %)	LMC bulk (absolute %)
Stage 6										
300	79.07	74.80	20.93	25.20	53.38	13.55	33.07	42.21	10.71	26.15
310	75.15	73.03	24.85	26.97	38.00	18.56	43.43	28.56	13.95	32.64
320	76.17	75.25	23.83	24.75	42.17	22.09	35.74	32.12	16.83	27.22
330	74.23	75.14	25.77	24.86	36.35	18.72	44.92	26.98	13.90	33.35
340	70.38	69.64	29.62	30.36	33.00	31.46	35.54	23.22	22.14	25.01
350	71.29	67.74	28.71	32.26	33.73	25.32	40.95	24.05	18.05	29.20
360	71.50	73.32	28.50	26.68	37.81	12.03	50.15	27.04	8.61	35.86
370	79.27	78.13	20.73	21.87	30.96	15.24	53.80	24.54	12.08	42.64
380	77.32	77.07	22.68	22.93	31.95	9.82	58.23	24.71	7.60	45.02
390	80.00	81.39	20.00	18.61	47.95	6.45	45.61	38.36	5.16	36.48
394.5	86.14	87.84	13.86	12.16	67.51	4.23	28.26	58.15	3.64	24.34
Average	76.41	75.76	23.59	24.24	41.16	16.14	42.70	31.81	12.06	32.54
Maximum	86.14	87.84	29.62	32.26	67.51	31.46	58.23	58.15	22.14	45.02
Minimum	70.38	67.74	13.86	12.16	30.96	4.23	28.26	23.22	3.64	24.34
Stage 7										
414	83.61	85.63	16.39	14.37	65.13	10.41	24.46	54.45	8.71	20.45
420	84.94	88.29	15.06	11.71	68.91	14.61	16.48	58.53	12.41	14.00
430	86.07	87.05	13.93	12.95	70.82	7.49	21.69	60.95	6.44	18.67
440	86.70	87.87	13.30	12.13	69.52	7.35	23.13	60.28	6.37	20.06
450	87.39	91.96	12.61	8.04	73.87	10.54	15.59	64.55	9.21	13.62
455	85.50	88.01	14.50	11.99	69.15	10.55	20.29	59.13	9.02	17.35
460	88.18	90.73	11.82	9.27	73.08	5.49	21.43	64.44	4.84	18.89
490	88.60	91.63	11.40	8.37	66.85	9.87	23.27	59.23	8.75	20.62
500	87.90	86.86	12.10	13.14	70.32	7.50	22.18	61.81	6.59	19.50
510	77.67	75.27	22.33	24.73	54.89	11.64	33.47	42.64	9.04	26.00
520	83.69	84.95	16.31	15.05	63.00	4.48	32.52	52.72	3.75	27.22
530	84.93	86.90	15.07	13.10	70.21	6.09	23.70	59.63	5.17	20.13
540	90.26	93.93	9.74	6.07	76.68	5.04	18.28	69.21	4.55	16.50
Average	85.80	87.62	14.20	12.38	68.65	8.54	22.81	59.05	7.30	19.46
Maximum	90.26	93.93	22.33	24.73	76.68	14.61	33.47	69.21	12.41	27.22
Minimum	77.67	75.27	9.74	6.07	54.89	4.48	15.59	42.64	3.75	13.62
Interglacials	85.52	86.99	14.48	13.01	69.60	7.52	22.88	59.69	6.44	19.39
Glacials	74.96	74.55	25.04	25.45	41.84	16.87	41.28	31.55	12.55	30.86
Stage 3	77.33	83.65	22.67	16.35	45.39	13.30	41.31	35.20	10.24	31.89
Overall Average	81.77	83.47	18.23	16.53	58.24	10.80	30.96	48.37	8.60	24.80
Glacial-to-Interglacial percentual deviation as shown in Fig. 7.2 and 7.3				**95.63**						
M35043										
Stage 1										
0	88.39	91.74	11.61	8.26	75.63	9.08	15.28	66.85	8.03	13.51
10	82.16	90.47	17.84	9.53	75.16	7.34	17.50	61.75	6.03	14.38
20	88.64	88.56	11.36	11.44	75.25	6.23	18.52	66.70	5.52	16.42

	Fine Fraction						Fine carbonates in bulk sediment			
Quartz Intensity bulk	Fine Aragonite (relative %)	HMC fine (relative %)	LMC fine (relative %)	Fine Aragonite (absolute %)	HMC fine (absolute %)	LMC fine (absolute %)	Fine Aragonite in bulk sedim. (%)	Fine HMC in bulk sedim. (%)	Fine LMC in bulk sedim. (%)	Fine Quartz Intensity
372	43.69	8.66	47.65	32.68	6.48	35.64	27.83	5.52	30.35	463
349	39.04	17.78	43.18	28.51	12.99	31.54	24.96	11.37	27.61	500
382	35.62	22.94	41.44	26.80	17.27	31.18	23.93	15.42	27.85	467
409	29.64	26.41	43.95	22.27	19.84	33.03	20.50	18.26	30.39	469
524	31.44	24.05	44.51	21.90	16.75	31.00	20.28	15.52	28.71	590
502	32.67	17.67	49.67	22.13	11.97	33.64	20.36	11.01	30.96	698
526	34.01	6.69	59.30	24.93	4.91	43.49	22.49	4.42	39.22	550
341	36.51	6.93	56.56	28.52	5.42	44.19	23.05	4.38	35.72	415
364	38.55	12.36	49.09	29.71	9.53	37.84	25.85	8.29	32.92	459
284	48.19	0.00	51.81	39.23	0.00	42.17	34.89	0.00	37.50	339
230	67.64	8.13	24.23	59.41	7.14	21.29	53.49	6.43	19.16	334
389	39.73	13.78	46.49	30.55	10.21	35.00	27.06	9.15	30.94	480
526	67.64	26.41	59.30	59.41	19.84	44.19	53.49	18.26	39.22	698
230	29.64	0.00	24.23	21.90	0.00	21.29	20.28	0.00	19.16	334
218	61.88	14.13	23.99	52.99	12.10	20.54	45.07	10.29	17.47	285
265	68.80	15.55	15.65	60.74	13.73	13.81	53.84	12.17	12.24	
235	66.85	8.97	24.18	58.19	7.81	21.05	46.83	6.28	16.94	287
233	69.70	10.90	19.40	61.24	9.58	17.05	48.84	7.64	13.60	221
197	75.35	11.77	12.88	69.29	10.83	11.84	57.32	8.95	9.80	206
232	68.79	13.36	17.86	60.54	11.76	15.71	49.47	9.61	12.84	323
206	74.95	6.42	18.62	68.01	5.83	16.90	58.40	5.01	14.51	223
146	68.36	9.76	21.88	62.63	8.95	20.05	52.32	7.47	16.75	188
171	63.50	9.43	27.07	55.15	8.19	23.51	47.25	7.02	20.15	258
335	46.92	13.93	39.16	35.31	10.48	29.47	30.81	9.15	25.72	474
254	66.19	10.63	23.18	56.23	9.03	19.69	48.19	7.74	16.88	345
226	68.13	7.17	24.71	59.20	6.23	21.47	50.64	5.33	18.37	281
137	75.57	8.77	15.66	70.99	8.23	14.71	63.74	7.39	13.21	150
220	67.31	10.83	21.86	59.27	9.44	18.91	50.21	8.00	16.04	270
335	75.57	15.55	39.16	70.99	13.73	29.47	63.74	12.17	25.72	474
137	46.92	6.42	12.88	35.31	5.83	11.84	30.81	5.01	9.80	150
209	69.53	8.61	21.86	60.71	7.50	18.78	50.22	6.23	15.61	244
408	38.77	18.46	42.76	29.09	13.61	31.86	25.66	11.97	28.08	483
340	40.16	15.09	44.75	33.56	12.67	37.42	28.85	10.88	32.16	432
280	56.98	11.91	31.11	48.45	9.69	25.32	41.04	8.33	21.75	326
							-48.91	**91.98**	**79.91**	
146	77.14	8.22	14.64	70.76	7.54	13.43	53.70	5.72	10.19	176
166	73.19	11.38	15.42	66.22	10.30	13.95	51.62	8.03	10.88	162
141	75.44	7.89	16.67	66.81	6.99	14.76	52.73	5.52	11.65	232

Mineralogy Data	Carbonates vs. non-carbonates				Bulk Sediment					
Depth (cm) and Marine Isotope Stage (MIS)	$CaCO_3$ bulk (%)	$CaCO_3$ fine fraction (%)	Non-Carbonates bulk (%)	Non-Carbonates fine (%)	Bulk Aragonite (relative %)	Bulk HMC (relative %)	Bulk LMC (relative %)	Aragonite bulk (absolute %)	HMC bulk (absolute %)	LMC bulk (absolute %)
30	89.38	93.56	10.62	6.44	77.75	7.20	15.05	69.49	6.44	13.45
40	87.61	86.27	12.39	13.73	63.88	9.66	26.46	55.97	8.47	23.18
Average	87.24	90.12	12.76	9.88	73.53	7.90	18.56	64.15	6.90	16.19
Maximum	89.38	93.56	17.84	13.73	77.75	9.66	26.46	69.49	8.47	23.18
Minimum	82.16	86.27	10.62	6.44	63.88	6.23	15.05	55.97	5.52	13.45
Stage 2										
50	87.74	87.59	12.26	12.41	59.94	13.39	26.66	52.60	11.75	23.40
60	85.19	88.65	14.81	11.35	63.65	13.45	22.91	54.22	11.46	19.51
70	84.99	88.82	15.01	11.18	55.41	16.13	28.46	47.09	13.71	24.19
Average	85.97	88.36	14.03	11.64	59.67	14.32	26.01	51.30	12.30	22.37
Maximum	87.74	88.82	15.01	12.41	63.65	16.13	28.46	54.22	13.71	24.19
Minimum	84.99	87.59	12.26	11.18	55.41	13.39	22.91	47.09	11.46	19.51
Stage 3										
80	82.55	87.29	17.45	12.71	58.45	12.88	28.67	48.25	10.63	23.67
90	80.37	84.93	19.63	15.07	52.68	9.40	37.92	42.34	7.56	30.48
100	79.41	84.47	20.59	15.53	49.27	11.04	39.69	39.12	8.77	31.52
Average	80.78	85.56	19.22	14.44	53.46	11.11	35.43	43.24	8.99	28.55
Maximum	82.55	87.29	20.59	15.53	58.45	12.88	39.69	48.25	10.63	31.52
Minimum	79.41	84.47	17.45	12.71	49.27	9.40	28.67	39.12	7.56	23.67
Stage 4										
110	81.95	87.40	18.05	12.60	50.09	9.45	40.47	41.05	7.74	33.16
120	82.14	85.96	17.86	14.04	57.88	4.24	37.88	47.54	3.48	31.11
Average	82.04	86.68	17.96	13.32	53.98	6.84	39.17	44.29	5.61	32.14
Maximum	82.14	87.40	18.05	14.04	57.88	9.45	40.47	47.54	7.74	33.16
Minimum	81.95	85.96	17.86	12.60	50.09	4.24	37.88	41.05	3.48	31.11
Stage 5										
130	81.11	86.62	18.89	13.38	60.65	8.84	30.50	49.20	7.17	24.74
140	81.53	88.87	18.47	11.13	57.53	6.79	35.68	46.91	5.54	29.09
150	84.64	92.01	15.36	7.99	63.17	1.29	35.55	53.47	1.09	30.09
160	78.90	90.66	21.10	9.34	62.52	7.64	29.84	49.33	6.03	23.55
170	82.20	85.42	17.80	14.58	57.40	6.76	35.84	47.19	5.56	29.46
180	83.55	88.16	16.45	11.84	59.37	4.70	35.93	49.61	3.92	30.02
190	84.46	86.79	15.54	13.21	61.49	4.16	34.35	51.93	3.51	29.01
200	88.25	91.61	11.75	8.39	70.67	2.54	26.79	62.37	2.24	23.64
210	87.67	92.14	12.33	7.86	73.60	7.91	18.50	64.52	6.93	16.22
220	86.29	91.46	13.71	8.54	75.96	10.48	13.56	65.55	9.05	11.70
240	86.67	90.60	13.33	9.40	72.94	7.95	19.12	63.21	6.89	16.57
250	87.92	92.84	12.08	7.16	77.53	8.23	14.24	68.16	7.23	12.52
260	88.37	93.81	11.63	6.19	76.03	9.32	14.66	67.19	8.23	12.95
270	87.75	93.05	12.25	6.95	78.13	2.73	19.14	68.56	2.39	16.79
280	88.25	93.15	11.75	6.85	74.05	6.07	19.87	65.35	5.36	17.54
290	90.21	95.42	9.79	4.58	79.02	8.34	12.64	71.28	7.53	11.40
Average	85.49	90.79	14.51	9.21	68.75	6.48	24.76	58.99	5.54	20.95
Maximum	90.21	95.42	21.10	14.58	79.02	10.48	35.93	71.28	9.05	30.09
Minimum	78.90	85.42	9.79	4.58	57.40	1.29	12.64	46.91	1.09	11.40
Stage 6										
300	81.92	85.41	18.08	14.59	47.62	14.22	38.15	39.01	11.65	31.26
310	82.17	82.93	17.83	17.07	54.20	14.68	31.11	44.54	12.07	25.57
320	84.54	86.69	15.46	13.31	56.54	19.42	24.04	47.80	16.42	20.32
330	80.87	83.13	19.13	16.87	44.86	19.16	35.97	36.28	15.50	29.09
340	79.08	78.78	20.92	21.22	52.74	18.62	28.64	41.71	14.73	22.65

	Fine Fraction						Fine carbonates in bulk sediment			
Quartz Intensity bulk	Fine Aragonite (relative %)	HMC fine (relative %)	LMC fine (relative %)	Fine Aragonite (absolute %)	HMC fine (absolute %)	LMC fine (absolute %)	Fine Aragonite in bulk sedim. (%)	Fine HMC in bulk sedim. (%)	Fine LMC in bulk sedim. (%)	Fine Quartz Intensity
168	80.04	10.04	9.92	74.89	9.39	9.28	63.25	7.93	7.84	148
188	60.05	14.63	25.31	51.81	12.62	21.84	31.58	7.70	13.31	280
162	73.17	10.43	16.39	66.10	9.37	14.65	50.57	6.98	10.77	200
188	80.04	14.63	25.31	74.89	12.62	21.84	63.25	8.03	13.31	280
141	60.05	7.89	9.92	51.81	6.99	9.28	31.58	5.52	7.84	148
173	56.52	20.51	22.97	49.51	17.96	20.12	29.58	10.73	12.02	310
189	59.79	23.58	16.63	53.01	20.90	14.74	29.91	11.80	8.32	263
177	60.91	17.94	21.15	54.11	15.93	18.79	31.43	9.26	10.91	322
180	59.08	20.68	20.25	52.21	18.27	17.88	30.31	10.59	10.42	298
189	60.91	23.58	22.97	54.11	20.90	20.12	31.43	11.80	12.02	322
173	56.52	17.94	16.63	49.51	15.93	14.74	29.58	9.26	8.32	263
233	54.86	17.95	27.19	47.89	15.67	23.73	32.37	10.59	16.04	318
262	51.48	11.38	37.15	43.72	9.66	31.55	34.59	7.64	24.96	354
292	48.67	11.83	39.50	41.11	9.99	33.37	34.03	8.27	27.62	333
262	51.67	13.72	34.61	44.24	11.78	29.55	33.66	8.84	22.87	335
292	54.86	17.95	39.50	47.89	15.67	33.37	34.59	10.59	27.62	354
233	48.67	11.38	27.19	41.11	9.66	23.73	32.37	7.64	16.04	318
441	45.73	2.53	51.74	39.97	2.21	45.22	32.63	1.81	36.92	292
256	52.80	9.01	38.19	45.39	7.74	32.83	35.65	6.08	25.79	350
349	49.26	5.77	44.97	42.68	4.98	39.03	34.14	3.94	31.35	321
441	52.80	9.01	51.74	45.39	7.74	45.22	35.65	6.08	36.92	350
256	45.73	2.53	38.19	39.97	2.21	32.83	32.63	1.81	25.79	292
267	57.09	8.12	34.80	49.45	7.03	30.14	40.28	5.73	24.55	365
257	59.86	5.37	34.77	53.19	4.77	30.90	46.64	4.19	27.10	265
203	64.87	1.97	33.16	59.68	1.82	30.51	51.28	1.56	26.21	174
193	63.08	2.59	34.33	57.19	2.35	31.12	49.09	2.02	26.72	198
251	61.66	1.97	36.37	52.67	1.68	31.07	40.31	1.29	23.78	303
231	60.46	1.39	38.15	53.30	1.23	33.63	44.73	1.03	28.22	263
210	63.34	4.24	32.42	54.97	3.68	28.14	45.05	3.01	23.06	280
134	72.32	5.24	22.44	66.26	4.80	20.56	56.20	4.07	17.44	166
196	76.50	9.90	13.60	70.49	9.12	12.53	59.20	7.66	10.53	210
187	77.71	6.55	15.74	71.08	5.99	14.39	62.45	5.26	12.65	210
179	75.12	7.97	16.91	68.06	7.22	15.32	56.17	5.96	12.64	251
159	81.10	6.78	12.12	75.29	6.29	11.25	67.03	5.60	10.02	185
176	79.63	7.03	13.34	74.70	6.59	12.51	65.42	5.77	10.96	195
157	78.04	7.33	14.63	72.62	6.82	13.61	62.13	5.84	11.64	210
166	76.62	6.18	17.20	71.37	5.75	16.02	56.57	4.56	12.70	164
125	78.55	9.07	12.38	74.95	8.65	11.82	64.10	7.40	10.11	145
193	70.37	5.73	23.90	64.08	5.24	21.47	54.17	4.43	18.02	224
267	81.10	9.90	38.15	75.29	9.12	33.63	67.03	7.66	28.22	365
125	57.09	1.39	12.12	49.45	1.23	11.25	40.28	1.03	10.02	145
404	55.75	11.55	32.71	47.61	9.86	27.93	37.76	7.82	22.15	376
420	44.85	25.65	29.49	37.20	21.27	24.46	26.68	15.26	17.54	406
230	52.35	14.04	33.61	45.38	12.17	29.14	31.02	8.32	19.92	322
350	39.57	32.28	28.16	32.89	26.83	23.41	25.99	21.20	18.49	426
392	46.29	21.37	32.34	36.47	16.84	25.48	28.35	13.09	19.80	571

Mineralogy Data	Carbonates vs. non-carbonates				Bulk Sediment					
Depth (cm) and Marine Isotope Stage (MIS)	$CaCO_3$ bulk (%)	$CaCO_3$ fine fraction (%)	Non-Carbonates bulk (%)	Non-Carbonates fine (%)	Bulk Aragonite (relative %)	Bulk HMC (relative %)	Bulk LMC (relative %)	Aragonite bulk (absolute %)	HMC bulk (absolute %)	LMC bulk (absolute %)
350	76.46	78.45	23.54	21.55	49.99	18.23	31.78	38.22	13.94	24.30
360	81.96	84.27	18.04	15.73	45.97	7.16	46.87	37.67	5.87	38.42
370	82.54	85.60	17.46	14.40	48.13	0.89	50.98	39.73	0.73	42.08
380	82.00	89.80	18.00	10.20	48.37	10.16	41.48	39.66	8.33	34.01
400	85.29	92.53	14.71	7.47	66.60	8.27	25.13	56.80	7.05	21.43
410	85.66	92.35	14.34	7.65	69.69	11.25	19.06	59.70	9.63	16.33
Average	82.04	85.45	17.96	14.55	53.16	12.92	33.93	43.74	10.54	27.77
Maximum	85.66	92.53	23.54	21.55	69.69	19.42	50.98	59.70	16.42	42.08
Minimum	76.46	78.45	14.34	7.47	44.86	0.89	19.06	36.28	0.73	16.33
Stage 7										
420	86.32	93.90	13.68	6.10	71.26	4.24	24.50	61.52	3.66	21.15
430	86.94	94.31	13.06	5.69	72.91	8.47	18.62	63.39	7.37	16.19
Average	86.63	94.11	13.37	5.89	72.09	6.36	21.56	62.45	5.51	18.67
Maximum	86.94	94.31	13.68	6.10	72.91	8.47	24.50	63.39	7.37	21.15
Minimum	86.32	93.90	13.06	5.69	71.26	4.24	18.62	61.52	3.66	16.19
Interglacials	86.45	91.67	13.55	8.33	71.46	6.91	21.63	61.86	5.98	18.60
Glacials	83.35	86.83	16.65	13.17	55.60	11.36	33.04	46.45	9.49	27.42
Stage 3	80.78	85.56	19.22	14.44	53.46	11.11	35.43	43.24	8.99	28.55
Overall Average	84.88	89.77	15.12	10.23	65.34	8.16	26.50	55.66	6.92	22.29
Glacial-to-Interglacial percentual deviation as shown in Fig. 7.2 and 7.3				**58.12**						
M35048										
MIS 1										
0	85.99	92.09	14.01	7.91	81.76	11.74	6.50	70.31	10.09	5.59
10	92.46	91.66	7.54	8.34	81.78	11.88	6.34	75.61	10.98	5.87
20	87.65	92.75	12.35	7.25	82.13	10.09	7.78	71.99	8.85	6.82
30	86.77	93.04	13.23	6.96	83.41	8.25	8.34	72.38	7.16	7.24
40	85.55	93.22	14.45	6.78	85.24	5.72	9.04	72.93	4.89	7.73
50	85.75	92.82	14.25	7.18	89.10	5.11	5.79	76.41	4.38	4.96
60	86.23	92.55	13.77	7.45	86.16	6.71	7.14	74.29	5.78	6.15
Average	87.20	92.59	12.80	7.41	84.23	8.50	7.27	73.42	7.45	6.34
Maximum	92.46	93.22	14.45	8.34	89.10	11.88	9.04	76.41	10.98	7.73
Minimum	85.55	91.66	7.54	6.78	81.76	5.11	5.79	70.31	4.38	4.96
MIS 2										
70	86.05	94.41	13.95	5.59	82.40	10.43	7.17	70.91	8.98	6.17
90	87.90	93.14	12.10	6.86	69.88	7.21	22.92	61.42	6.33	20.14
Average	86.97	93.78	13.03	6.22	76.14	8.82	15.04	66.16	7.66	13.15
Maximum	87.90	94.41	13.95	6.86	82.40	10.43	22.92	70.91	8.98	20.14
Minimum	86.05	93.14	12.10	5.59	69.88	7.21	7.17	61.42	6.33	6.17

	Fine Fraction						Fine carbonates in bulk sediment			
Quartz Intensity bulk	Fine Aragonite (relative %)	HMC fine (relative %)	LMC fine (relative %)	Fine Aragonite (absolute %)	HMC fine (absolute %)	LMC fine (absolute %)	Fine Aragonite in bulk sedim. (%)	Fine HMC in bulk sedim. (%)	Fine LMC in bulk sedim. (%)	Fine Quartz Intensity
411	51.07	15.48	33.45	40.07	12.15	26.24	33.36	10.11	21.84	512
290	47.89	7.09	45.02	40.35	5.97	37.94	33.15	4.91	31.17	321
252	52.54	9.55	37.92	44.97	8.17	32.46	38.05	6.92	27.47	294
243	51.77	8.17	40.07	46.48	7.33	35.98	38.85	6.13	30.07	332
209	65.09	4.75	30.16	60.23	4.40	27.91	51.24	3.74	23.74	250
195	70.02	6.22	23.76	64.67	5.75	21.94	54.93	4.88	18.64	253
309	52.47	14.19	33.33	45.12	11.89	28.44	36.31	9.31	22.80	369
420	70.02	32.28	45.02	64.67	26.83	37.94	54.93	21.20	31.17	571
195	39.57	4.75	23.76	32.89	4.40	21.94	25.99	3.74	17.54	250
161	71.15	4.60	24.25	66.82	4.32	22.77	55.42	3.58	18.88	234
179	73.96	7.05	18.99	69.75	6.65	17.91	58.50	5.58	15.02	198
170	72.56	5.83	21.62	68.28	5.48	20.34	56.96	4.58	16.95	216
179	73.96	7.05	24.25	69.75	6.65	22.77	58.50	5.58	18.88	234
161	71.15	4.60	18.99	66.82	4.32	17.91	55.42	3.58	15.02	198
175	72.03	7.33	20.64	66.15	6.70	18.82	53.90	5.33	15.25	213
279	53.60	13.55	32.85	46.67	11.71	28.45	33.58	7.95	21.52	330
262	51.67	13.72	34.61	44.24	11.78	29.55	33.66	8.84	22.87	335
207	65.61	8.57	25.83	59.13	7.65	22.99	47.44	5.75	18.38	253
							-37.69	**49.10**	**41.15**	
61	83.29	10.64	6.07	76.70	9.80	5.59	59.27	7.57	4.32	73
80	83.60	10.61	5.79	76.63	9.73	5.31	57.48	7.30	3.98	
0	84.95	8.75	6.30	78.79	8.12	5.84	54.85	5.65	4.07	61
55	86.83	7.16	6.01	80.79	6.66	5.59	58.18	4.80	4.03	69
0	88.61	6.70	4.69	82.60	6.25	4.38	62.65	4.74	3.32	64
56	91.75	4.09	4.17	85.16	3.79	3.87	71.08	3.17	3.23	
87	90.01	6.17	3.82	83.31	5.71	3.53	60.39	4.14	2.56	69
48	87.01	7.73	5.26	80.56	7.16	4.87	60.56	5.34	3.64	67
87	91.75	10.64	6.30	85.53	9.92	5.87	71.08	7.57	4.32	73
0	83.29	4.09	3.82	76.34	3.74	3.50	54.85	3.17	2.56	61
54	89.56	5.87	4.57	84.55	5.54	4.31	49.21	3.23	2.51	
78	69.43	5.14	25.43	64.67	4.79	23.69	40.59	3.00	14.87	143
66	79.49	5.51	15.00	74.55	5.16	14.07	44.90	3.12	8.69	143
78	89.56	5.87	25.43	84.55	5.54	24.01	49.21	3.23	14.87	143
54	69.43	5.14	4.57	64.67	4.79	4.26	40.59	3.00	2.51	143

Mineralogy Data	Carbonates vs. non-carbonates				Bulk Sediment					
Depth (cm) and Marine Isotope Stage (MIS)	$CaCO_3$ bulk (%)	$CaCO_3$ fine fraction (%)	Non-Carbonates bulk (%)	Non-Carbonates fine (%)	Bulk Aragonite (relative %)	Bulk HMC (relative %)	Bulk LMC (relative %)	Aragonite bulk (absolute %)	HMC bulk (absolute %)	LMC bulk (absolute %)
MIS 3										
100	90.39	94.17	9.61	5.83	74.32	4.85	20.83	67.18	4.39	18.83
Average	90.39	94.17	9.61	5.83	74.32	4.85	20.83	67.18	4.39	18.83
Maximum	90.39	94.17	9.61	5.83	74.32	4.85	20.83	67.18	4.39	18.83
Minimum	90.39	94.17	9.61	5.83	74.32	4.85	20.83	67.18	4.39	18.83
MIS 4										
110	84.49	92.37	15.51	7.63	76.94	7.68	15.39	65.00	6.49	13.00
120	85.78	92.64	14.22	7.36	76.26	6.95	16.79	65.41	5.96	14.40
130	84.74	92.30	15.26	7.70	78.43	7.93	13.64	66.46	6.72	11.56
Average	85.00	92.44	15.00	7.56	77.21	7.52	15.27	65.63	6.39	12.99
Maximum	85.78	92.64	15.51	7.70	78.43	7.93	16.79	66.46	6.72	14.40
Minimum	84.49	92.30	14.22	7.36	76.26	6.95	13.64	65.00	5.96	11.56
MIS 5										
140	88.15	93.76	11.85	6.24	83.58	2.35	14.08	73.67	2.07	12.41
150	88.69	92.73	11.31	7.27	82.00	4.79	13.21	72.72	4.25	11.72
160	88.16	94.12	11.84	5.88	84.54	1.81	13.65	74.53	1.59	12.04
170	88.20	93.48	11.80	6.52	85.29	4.60	10.11	75.22	4.06	8.92
180	89.78	93.55	10.22	6.45	86.11	2.93	10.96	77.31	2.63	9.84
190	87.65	93.71	12.35	6.29	83.88	5.46	10.66	73.51	4.79	9.34
200	86.66	92.78	13.34	7.22	82.45	6.34	11.21	71.45	5.50	9.71
210	86.09	93.12	13.91	6.88	82.65	5.31	12.04	71.15	4.57	10.36
220	84.68	91.83	15.32	8.17	84.41	0.85	14.73	71.48	0.72	12.48
230	83.24	92.45	16.76	7.55	80.59	3.63	15.78	67.09	3.02	13.14
240	86.51	93.25	13.49	6.75	82.19	1.91	15.90	71.11	1.65	13.76
250	87.26	93.74	12.74	6.26	81.24	3.30	15.46	70.89	2.88	13.49
260	86.62	93.82	13.38	6.18	81.82	2.36	15.82	70.87	2.05	13.70
270	87.25	94.43	12.75	5.57	87.89	1.42	10.69	76.68	1.24	9.33
280	89.52	94.30	10.48	5.70	87.27	3.37	9.35	78.13	3.02	8.37
290	89.03	91.60	10.97	8.40	92.90	2.29	4.81	82.71	2.04	4.28
Average	87.34	93.29	12.66	6.71	84.30	3.30	12.40	73.66	2.88	10.81
Maximum	89.78	94.43	16.76	8.40	92.90	6.34	15.90	82.71	5.50	13.76
Minimum	83.24	91.60	10.22	5.57	80.59	0.85	4.81	67.09	0.72	4.28
MIS 6										
300	86.84	93.01	13.16	6.99	89.57	3.65	6.78	77.78	3.17	5.89
310	86.82	92.10	13.18	7.90	78.02	10.98	11.01	67.74	9.53	9.56
330	84.29	94.00	15.71	6.00	66.91	1.83	31.26	56.40	1.54	26.35
340	87.25	94.73	12.75	5.27	72.82	1.88	25.30	63.54	1.64	22.08
350	87.60	93.33	12.40	6.67	79.25	3.83	16.92	69.43	3.36	14.82
Average	86.56	93.43	13.44	6.57	77.31	4.43	18.25	66.98	3.85	15.74
Maximum	87.60	94.73	15.71	7.90	89.57	10.98	31.26	77.78	9.53	26.35
Minimum	84.29	92.10	12.40	5.27	66.91	1.83	6.78	56.40	1.54	5.89
MIS 7										
360	82.46	93.89	17.54	6.11	79.80	3.39	16.80	65.81	2.80	13.86
370	87.67	93.27	12.33	6.73	82.82	4.52	12.66	72.61	3.96	11.10
380	86.28	93.92	13.72	6.08	89.55	5.12	5.33	77.27	4.42	4.60
390	83.17	95.66	16.83	4.34	78.16	2.09	19.75	65.00	1.74	16.43
400	83.61	94.54	16.39	5.46	79.44	4.19	16.37	66.42	3.50	13.69
410	86.69	93.65	13.31	6.35	78.17	3.75	18.09	67.76	3.25	15.68
420	85.47	94.39	14.53	5.61	80.64	4.39	14.97	68.92	3.75	12.80
430	85.22	94.37	14.78	5.63	82.55	3.22	14.23	70.35	2.74	12.13
440	87.70	94.70	12.30	5.30	80.92	2.15	16.93	70.97	1.89	14.85

	Fine Fraction						Fine carbonates in bulk sediment			
Quartz Intensity bulk	Fine Aragonite (relative %)	HMC fine (relative %)	LMC fine (relative %)	Fine Aragonite (absolute %)	HMC fine (absolute %)	LMC fine (absolute %)	Fine Aragonite in bulk sedim. (%)	Fine HMC in bulk sedim. (%)	Fine LMC in bulk sedim. (%)	Fine Quartz Intensity
60	77.57	2.35	20.08	73.05	2.22	18.91	60.88	1.85	15.76	67
60	77.57	2.35	20.08	73.05	2.22	18.91	60.88	1.85	15.76	67
60	77.57	2.35	20.08	73.05	2.22	18.91	60.88	1.85	15.76	67
60	77.57	2.35	20.08	73.05	2.22	18.91	60.88	1.85	15.76	67
85	75.44	11.67	12.89	69.69	10.78	11.91	49.28	7.62	8.42	120
111	80.77	9.13	10.10	74.83	8.46	9.36	44.50	5.03	5.56	102
74	81.26	5.03	13.71	75.00	4.64	12.66	61.02	3.78	10.30	74
90	79.16	8.61	12.23	73.17	7.96	11.31	51.60	5.48	8.09	99
111	81.26	11.67	13.71	75.28	10.81	12.70	61.02	7.62	10.30	120
74	75.44	5.03	10.10	69.63	4.64	9.32	44.50	3.78	5.56	74
51	83.84	4.64	11.52	78.61	4.35	10.81	64.62	3.57	8.88	54
61	84.13	3.86	12.02	78.01	3.58	11.14	65.96	3.02	9.42	70
57	85.30	4.52	10.18	80.29	4.25	9.58	70.15	3.72	8.37	65
62	86.13	4.35	9.52	80.51	4.07	8.90	60.34	3.05	6.67	65
52	88.03	5.21	6.76	82.35	4.88	6.32	66.24	3.92	5.08	72
55	86.74	2.46	10.80	81.29	2.30	10.12	62.20	1.76	7.75	69
67	85.73	5.54	8.74	79.54	5.14	8.10	64.77	4.19	6.60	60
59	84.66	5.29	10.05	78.84	4.92	9.36	67.02	4.19	7.96	70
69	86.36	2.05	11.58	79.31	1.89	10.64	68.16	1.62	9.14	68
67	86.33	2.24	11.42	79.82	2.07	10.56	60.07	1.56	7.95	65
61	85.17	3.90	10.93	79.42	3.64	10.19	65.30	2.99	8.38	61
50	83.40	2.21	14.39	78.18	2.07	13.49	63.69	1.69	10.99	74
59	83.96	3.80	12.24	78.77	3.57	11.48	67.80	3.07	9.89	65
59	87.17	2.12	10.71	82.32	2.00	10.11	68.30	1.66	8.39	51
52	89.25	3.61	7.14	84.16	3.41	6.73	75.69	3.06	6.06	63
41	89.97	3.24	6.79	82.42	2.97	6.22	76.97	2.77	5.81	72
58	86.01	3.69	10.30	80.24	3.44	9.61	66.70	2.87	7.96	65
69	89.97	5.54	14.39	84.97	5.23	13.59	76.97	4.19	10.99	74
41	83.40	2.05	6.76	76.40	1.88	6.19	60.07	1.56	5.08	51
60	88.30	4.54	7.15	82.13	4.22	6.65	67.87	3.49	5.50	54
67	84.18	6.81	9.01	77.53	6.27	8.29	44.45	3.60	4.75	97
66	65.20	4.55	30.25	61.29	4.28	28.44	30.73	2.15	14.26	93
55	75.42	1.75	22.83	71.44	1.66	21.63	51.68	1.20	15.65	70
74	83.01	1.80	15.18	77.48	1.68	14.17	59.86	1.30	10.95	84
64	79.22	3.89	16.89	74.02	3.64	15.78	50.92	2.35	10.22	80
74	88.30	6.81	30.25	83.65	6.45	28.65	67.87	3.60	15.65	97
55	65.20	1.75	7.15	60.04	1.61	6.59	30.73	1.20	4.75	54
73	80.70	1.64	17.66	75.77	1.54	16.58	63.95	1.30	13.99	96
79	80.83	4.15	15.02	75.39	3.87	14.01	62.20	3.20	11.56	64
61	82.33	2.61	15.06	77.33	2.45	14.14	61.65	1.95	11.28	60
78	81.46	0.37	18.17	77.93	0.35	17.38	60.85	0.28	13.57	84
79	79.19	2.26	18.55	74.87	2.14	17.54	65.14	1.86	15.26	101
62	80.02	2.79	17.19	74.93	2.62	16.10	64.18	2.24	13.79	83
82	79.63	3.55	16.82	75.17	3.35	15.87	64.40	2.87	13.60	60
70	80.19	4.61	15.20	75.67	4.35	14.34	66.53	3.83	12.61	75
52	85.13	2.54	12.32	80.62	2.41	11.67	68.98	2.06	9.98	69

Mineralogy Data	Carbonates vs. non-carbonates				Bulk Sediment					
Depth (cm) and Marine Isotope Stage (MIS)	$CaCO_3$ bulk (%)	$CaCO_3$ fine fraction (%)	Non-Carbonates bulk (%)	Non-Carbonates fine (%)	Bulk Aragonite (relative %)	Bulk HMC (relative %)	Bulk LMC (relative %)	Aragonite bulk (absolute %)	HMC bulk (absolute %)	LMC bulk (absolute %)
450	85.56	94.60	14.44	5.40	81.27	0.41	18.32	69.53	0.35	15.67
460	85.60	94.55	14.40	5.45	79.58	2.61	17.81	68.12	2.23	15.25
470	88.25	94.20	11.75	5.80	78.94	2.08	18.98	69.66	1.83	16.75
480	85.45	94.19	14.55	5.81	79.23	0.72	20.04	67.70	0.62	17.13
490	86.29	93.04	13.71	6.96	82.99	2.26	14.75	71.62	1.95	12.73
500	86.14	93.08	13.86	6.92	82.91	3.34	13.75	71.42	2.88	11.84
Average	85.70	94.14	14.30	5.86	81.13	2.95	15.92	69.54	2.53	13.63
Maximum	88.25	95.66	17.54	6.96	89.55	5.12	20.04	77.27	4.42	17.13
Minimum	82.46	93.04	11.75	4.34	78.16	0.41	5.33	65.00	0.35	4.60
MIS 8										
510	80.52	93.86	19.48	6.14	72.94	3.56	23.50	58.73	2.87	18.92
Average	80.52	93.86	19.48	6.14	72.94	3.56	23.50	58.73	2.87	18.92
Maximum	80.52	93.86	19.48	6.14	72.94	3.56	23.50	58.73	2.87	18.92
Minimum	80.52	93.86	19.48	6.14	72.94	3.56	23.50	58.73	2.87	18.92
Interglacials	86.75	93.34	13.25	6.66	83.22	4.91	11.87	72.21	4.28	10.26
Glacials	84.76	93.38	15.24	6.62	75.90	6.08	18.02	64.37	5.19	15.20
Stage 3	90.39	94.17	9.61	5.83	74.32	4.85	20.83	67.18	4.39	18.83
Overall Average	86.52	93.46	13.48	6.54	81.46	4.54	13.99	70.51	3.94	12.07
Glacial-to-Interglacial percentual deviation as shown in Fig. 7.2 and 7.3				**-0.57**						
M35049										
Stage 1										
0	91.90	88.99	8.10	11.01	80.22	6.70	13.08	73.72	6.16	12.02
10	91.22	89.57	8.78	10.43	79.35	7.63	13.02	72.38	6.96	11.87
20	93.22	88.86	6.78	11.14	77.03	6.51	16.46	71.81	6.06	15.34
30	92.38	90.05	7.62	9.95	80.05	7.09	12.86	73.96	6.55	11.88
40	91.93	91.49	8.07	8.51	82.17	6.59	11.24	75.54	6.06	10.33
Average	92.13	89.79	7.87	10.21	79.77	6.90	13.33	73.48	6.36	12.29
Maximum	93.22	91.49	8.78	11.14	82.17	7.63	16.46	75.54	6.96	15.34
Minimum	91.22	88.86	6.78	8.51	77.03	6.51	11.24	71.81	6.06	10.33
Stage 2										
50	92.32	90.06	7.68	9.94	72.04	8.27	19.70	66.51	7.63	18.18
60	90.80	87.12	9.20	12.88	61.73	13.52	24.74	56.06	12.28	22.47
70	90.87	88.01	9.13	11.99	59.85	13.12	27.03	54.38	11.92	24.56
Average	91.33	88.40	8.67	11.60	64.54	11.64	23.82	58.98	10.61	21.74
Maximum	92.32	90.06	9.20	12.88	72.04	13.52	27.03	66.51	12.28	24.56
Minimum	90.80	87.12	7.68	9.94	59.85	8.27	19.70	54.38	7.63	18.18
Stage 3										
80	89.99	88.37	10.01	11.63	59.97	11.92	28.10	53.97	10.73	25.29
90	86.41	88.32	13.59	11.68	56.87	9.79	33.34	49.14	8.46	28.81
100	88.41	86.48	11.59	13.52	54.26	9.79	35.95	47.97	8.65	31.78
110	88.31	86.58	11.69	13.42	58.73	10.32	30.95	51.87	9.11	27.33

	Fine Fraction						Fine carbonates in bulk sediment			
Quartz Intensity bulk	Fine Aragonite (relative %)	HMC fine (relative %)	LMC fine (relative %)	Fine Aragonite (absolute %)	HMC fine (absolute %)	LMC fine (absolute %)	Fine Aragonite in bulk sedim. (%)	Fine HMC in bulk sedim. (%)	Fine LMC in bulk sedim. (%)	Fine Quartz Intensity
61	79.91	0.29	19.79	75.60	0.28	18.72	62.41	0.23	15.46	384
61	78.07	1.91	20.02	73.82	1.80	18.93	61.98	1.51	15.89	95
70	73.40	0.00	26.60	69.14	0.00	25.06	62.64	0.00	22.70	
62	81.97	2.42	15.61	77.20	2.28	14.70	68.40	2.02	13.03	74
70	86.57	1.19	12.24	80.54	1.11	11.39	71.52	0.99	10.11	79
50	80.15	3.63	16.22	74.60	3.38	15.10	58.03	2.63	11.75	84
67	80.64	2.27	17.10	75.91	2.13	16.09	64.19	1.80	13.64	101
82	86.57	4.61	26.60	82.81	4.41	25.45	71.52	3.83	22.70	384
50	73.40	0.00	12.24	68.29	0.00	11.39	58.03	0.00	9.98	60
75	75.16	7.67	17.17	70.55	7.20	16.11	46.89	4.79	10.71	98
75	75.16	7.67	17.17	70.55	7.20	16.11	46.89	4.79	10.71	98
75	75.16	7.67	17.17	70.55	7.20	16.11	46.89	4.79	10.71	98
75	75.16	7.67	17.17	70.55	7.20	16.11	46.89	4.79	10.71	98
58	84.55	4.56	10.89	78.92	4.26	10.16	63.82	3.33	8.41	78
74	78.26	6.42	15.32	73.08	5.99	14.31	48.58	3.93	9.43	105
60	77.57	2.35	20.08	73.05	2.22	18.91	60.88	1.85	15.76	67
63	82.80	4.27	12.93	77.39	3.99	12.08	61.22	3.02	9.53	76
							-23.88	**17.94**	**12.07**	
114	79.17	7.47	13.36	70.46	6.65	11.89	55.35	5.22	9.34	153
125	77.54	9.55	12.90	69.45	8.56	11.56	55.57	6.85	9.25	151
108	79.37	7.59	13.04	70.53	6.74	11.59	56.46	5.40	9.28	153
112	80.99	7.07	11.94	72.93	6.37	10.75	58.29	5.09	8.59	153
97	81.97	8.54	9.49	75.00	7.81	8.68	59.60	6.21	6.90	146
111	79.81	8.04	12.15	71.67	7.23	10.89	57.05	5.75	8.67	151
125	81.97	9.55	13.36	75.00	8.56	11.89	59.60	6.85	9.34	153
97	77.54	7.07	9.49	69.45	6.37	8.68	55.35	5.09	6.90	146
139	74.21	12.81	12.97	66.84	11.54	11.68	46.84	8.09	8.19	185
156	55.64	20.67	23.69	48.47	18.00	20.64	26.16	9.72	11.14	382
185	61.61	15.97	22.42	54.23	14.05	19.73	35.36	9.16	12.87	295
160	63.82	16.48	19.70	56.51	14.53	17.35	36.12	8.99	10.73	287
185	74.21	20.67	23.69	66.84	18.00	20.64	46.84	9.72	12.87	382
139	55.64	12.81	12.97	48.47	11.54	11.68	26.16	8.09	8.19	185
183	53.63	18.90	27.47	47.39	16.70	24.28	32.68	11.52	16.74	271
219	51.83	12.86	35.31	45.77	11.36	31.19	35.99	8.93	24.52	311
192	51.99	3.84	44.17	44.97	3.32	38.20	36.68	2.71	31.16	290
254	53.63	13.96	32.41	46.44	12.09	28.06	37.48	9.76	22.65	310

Mineralogy Data	Carbonates vs. non-carbonates				Bulk Sediment					
Depth (cm) and Marine Isotope Stage (MIS)	$CaCO_3$ bulk (%)	$CaCO_3$ fine fraction (%)	Non-Carbonates bulk (%)	Non-Carbonates fine (%)	Bulk Aragonite (relative %)	Bulk HMC (relative %)	Bulk LMC (relative %)	Aragonite bulk (absolute %)	HMC bulk (absolute %)	LMC bulk (absolute %)
120	86.36	85.24	13.64	14.76	61.11	10.21	28.68	52.77	8.82	24.77
130	88.74	82.46	11.26	17.54	62.00	4.82	33.18	55.02	4.28	29.45
Average	88.04	86.24	11.96	13.76	58.82	9.48	31.70	51.79	8.34	27.91
Maximum	89.99	88.37	13.64	17.54	62.00	11.92	35.95	55.02	10.73	31.78
Minimum	86.36	82.46	10.01	11.63	54.26	4.82	28.10	47.97	4.28	24.77
Stage 4										
140	87.04	84.56	12.96	15.44	64.97	3.65	31.38	56.55	3.17	27.32
150	94.22	88.74	5.78	11.26	67.72	3.59	28.69	63.81	3.38	27.03
160	88.56	88.81	11.44	11.19	72.69	6.51	20.80	64.37	5.76	18.42
Average	89.94	87.37	10.06	12.63	68.46	4.58	26.96	61.58	4.11	24.26
Maximum	94.22	88.81	12.96	15.44	72.69	6.51	31.38	64.37	5.76	27.32
Minimum	87.04	84.56	5.78	11.19	64.97	3.59	20.80	56.55	3.17	18.42
Stage 5										
170	92.89	88.89	7.11	11.11	72.63	8.97	18.41	67.46	8.33	17.10
180	87.60	90.62	12.40	9.38	70.95	9.38	19.67	62.15	8.22	17.23
190	88.18	87.28	11.82	12.72	69.89	9.38	20.73	61.63	8.27	18.28
200	93.90	90.12	6.10	9.88	74.08	6.63	19.29	69.56	6.22	18.12
210	94.73	91.40	5.27	8.60	79.60	7.20	13.19	75.41	6.82	12.50
220	95.48	91.08	4.52	8.92	79.25	7.00	13.75	75.67	6.69	13.13
230	95.93	90.92	4.07	9.08	78.91	9.08	12.02	75.70	8.71	11.53
250	92.47	91.15	7.53	8.85	77.06	8.79	14.16	71.25	8.13	13.09
260	94.85	92.78	5.15	7.22	80.46	6.81	12.73	76.31	6.46	12.07
270	94.32	94.01	5.68	5.99	80.74	6.72	12.55	76.15	6.34	11.84
280	95.23	93.70	4.77	6.30	79.91	6.07	14.02	76.10	5.78	13.36
290	90.60	89.27	9.40	10.73	78.81	6.70	14.49	71.40	6.07	13.13
300	95.67	90.19	4.33	9.81	77.86	6.89	15.25	74.50	6.59	14.59
310	97.14	90.13	2.86	9.87	79.32	6.08	14.60	77.06	5.90	14.18
320	98.74	97.04	1.26	2.96	85.32	7.42	7.27	84.24	7.33	7.17
330	98.93	94.05	1.07	5.95	83.38	7.63	8.99	82.50	7.54	8.89
Average	94.17	91.41	5.83	8.59	78.01	7.55	14.44	73.57	7.09	13.51
Maximum	98.93	97.04	12.40	12.72	85.32	9.38	20.73	84.24	8.71	18.28
Minimum	87.60	87.28	1.07	2.96	69.89	6.07	7.27	61.63	5.78	7.17
Stage 6										
340	95.49	94.14	4.51	5.86	74.76	10.93	14.30	71.39	10.44	13.66
350	89.14	79.32	10.86	20.68	51.84	19.92	28.25	46.21	17.75	25.18
360	88.52	74.72	11.48	25.28	50.15	23.49	26.36	44.40	20.79	23.33
370	83.35	82.60	16.65	17.40	50.17	17.10	32.73	41.81	14.25	27.28
380	88.01	84.63	11.99	15.37	52.13	9.93	37.94	45.88	8.74	33.40
390	90.52	88.13	9.48	11.87	51.04	9.66	39.29	46.20	8.75	35.57
400	91.82	87.15	8.18	12.85	55.32	5.41	39.27	50.79	4.97	36.06
410	92.13	89.65	7.87	10.35	60.16	7.18	32.66	55.42	6.62	30.09
Average	89.87	85.04	10.13	14.96	55.70	12.95	31.35	50.26	11.54	28.07
Maximum	95.49	94.14	16.65	25.28	74.76	23.49	39.29	71.39	20.79	36.06
Minimum	83.35	74.72	4.51	5.86	50.15	5.41	14.30	41.81	4.97	13.66
Stage 7										
430	89.55	89.78	10.45	10.22	68.70	8.75	22.55	61.52	7.84	20.19
440	92.01	88.85	7.99	11.15	73.74	11.91	14.36	67.84	10.96	13.21
450	96.70	94.15	3.30	5.85	73.41	11.21	15.38	70.99	10.84	14.87
460	97.35	94.02	2.65	5.98	75.77	9.55	14.68	73.76	9.30	14.29
470	95.37	95.77	4.63	4.23	79.34	6.16	14.50	75.67	5.87	13.83
480	98.59	95.92	1.41	4.08	78.89	8.99	12.13	77.78	8.86	11.96
490	98.74	94.52	1.26	5.48	75.26	7.94	16.79	74.32	7.84	16.58

	Fine Fraction						Fine carbonates in bulk sediment			
Quartz Intensity bulk	Fine Aragonite (relative %)	HMC fine (relative %)	LMC fine (relative %)	Fine Aragonite (absolute %)	HMC fine (absolute %)	LMC fine (absolute %)	Fine Aragonite in bulk sedim. (%)	Fine HMC in bulk sedim. (%)	Fine LMC in bulk sedim. (%)	Fine Quartz Intensity
225	58.06	12.16	29.78	49.49	10.36	25.38	41.95	8.78	21.51	330
245	58.58	6.10	35.32	48.31	5.03	29.12	41.38	4.31	24.95	303
220	54.62	11.30	34.08	47.06	9.81	29.37	37.69	7.67	23.59	303
254	58.58	18.90	44.17	49.49	16.70	38.20	41.95	11.52	31.16	330
183	51.83	3.84	27.47	44.97	3.32	24.28	32.68	2.71	16.74	271
228	64.61	3.58	31.81	54.64	3.03	26.89	47.17	2.61	23.22	295
133	63.77	2.83	33.40	56.59	2.51	29.64	48.97	2.18	25.65	168
168				0.00	0.00	0.00	0.00	0.00	0.00	
176	64.19	3.21	32.60	37.08	1.85	18.84	32.05	1.60	16.29	232
228	64.61	3.58	33.40	56.59	3.03	29.64	48.97	2.61	25.65	295
133	63.77	2.83	31.81	0.00	0.00	0.00	0.00	0.00	0.00	168
173	74.21	10.01	15.79	65.96	8.90	14.03	53.74	7.25	11.43	226
182	69.65	9.94	20.40	63.12	9.01	18.49	52.15	7.44	15.28	253
192	68.87	11.62	19.51	60.11	10.15	17.03	51.51	8.69	14.59	277
138	74.46	5.28	20.26	67.11	4.75	18.26	58.16	4.12	15.82	132
107	79.98	5.84	14.18	73.10	5.34	12.96	63.79	4.66	11.31	132
131	79.68	7.64	12.68	72.58	6.96	11.55	61.20	5.87	9.74	175
138	80.56	7.63	11.81	73.25	6.93	10.74	65.41	6.19	9.59	167
153	80.70	7.33	11.97	73.55	6.68	10.91	63.62	5.78	9.44	187
142	82.07	7.54	10.39	76.14	7.00	9.64	69.66	6.40	8.82	145
104	82.76	5.12	12.12	77.80	4.82	11.39	71.51	4.43	10.47	130
181	79.10	7.56	13.34	74.12	7.09	12.50	65.50	6.26	11.04	162
122	79.79	6.37	13.85	71.22	5.68	12.36	61.96	4.94	10.75	155
127	75.73	6.15	18.12	68.30	5.54	16.34	56.88	4.62	13.61	164
109	77.70	7.59	14.70	70.03	6.84	13.25	58.00	5.67	10.97	144
89	84.17	9.48	6.35	81.68	9.20	6.16	64.88	7.31	4.89	90
93	83.30	7.66	9.05	78.34	7.20	8.51	56.48	5.19	6.13	114
136	78.30	7.67	14.03	71.65	7.01	12.76	60.90	5.93	10.87	166
192	84.17	11.62	20.40	81.68	10.15	18.49	71.51	8.69	15.82	277
89	68.87	5.12	6.35	60.11	4.75	6.16	51.51	4.12	4.89	90
182	74.73	9.94	15.33	70.36	9.35	14.43	53.49	7.11	10.97	200
291	49.88	22.81	27.31	39.56	18.09	21.66	30.69	14.04	16.80	400
328				0.00	0.00	0.00	0.00	0.00	0.00	
399	46.69	19.24	34.07	38.56	15.89	28.14	32.50	13.39	23.71	471
275	48.48	8.00	43.53	41.03	6.77	36.84	34.85	5.75	31.29	371
238	54.09	7.55	38.35	47.67	6.66	33.80	39.46	5.51	27.98	297
264	52.80	8.72	38.48	46.02	7.60	33.54	37.72	6.23	27.49	328
195	56.36	8.99	34.64	50.53	8.06	31.06	42.98	6.86	26.42	314
272	54.72	12.18	33.10	41.72	9.05	24.93	33.96	7.36	20.58	340
399	74.73	22.81	43.53	70.36	18.09	36.84	53.49	14.04	31.29	471
182	46.69	7.55	15.33	0.00	0.00	0.00	0.00	0.00	0.00	200
183	68.20	9.59	22.22	61.23	8.61	19.95	52.24	7.34	17.02	219
189	73.98	12.91	13.12	65.72	11.47	11.65	57.04	9.95	10.11	263
144	76.18	10.37	13.45	71.73	9.77	12.66	59.26	8.07	10.46	185
158	75.61	11.40	13.00	71.08	10.71	12.22	59.96	9.04	10.31	208
100	79.76	6.29	13.95	76.38	6.02	13.36	64.59	5.09	11.30	165
125	80.34	7.94	11.72	77.06	7.61	11.25	65.75	6.49	9.59	164
137	76.84	9.08	14.07	72.63	8.58	13.30	62.76	7.42	11.49	182

Mineralogy Data	Carbonates vs. non-carbonates				Bulk Sediment					
Depth (cm) and Marine Isotope Stage (MIS)	$CaCO_3$ bulk (%)	$CaCO_3$ fine fraction (%)	Non-Carbonates bulk (%)	Non-Carbonates fine (%)	Bulk Aragonite (relative %)	Bulk HMC (relative %)	Bulk LMC (relative %)	Aragonite bulk (absolute %)	HMC bulk (absolute %)	LMC bulk (absolute %)
500	98.22	97.33	1.78	2.67	78.85	8.43	12.72	77.45	8.28	12.50
510	98.36	98.85	1.64	1.15	83.12	10.21	6.67	81.75	10.04	6.56
Average	96.10	94.35	3.90	5.65	76.34	9.24	14.42	73.45	8.87	13.78
Maximum	98.74	98.85	10.45	11.15	83.12	11.91	22.55	81.75	10.96	20.19
Minimum	89.55	88.85	1.26	1.15	68.70	6.16	6.67	61.52	5.87	6.56
Interglacials	94.13	91.85	5.87	8.15	78.04	7.90	14.06	73.50	7.44	13.19
Glacials	90.38	86.94	9.62	13.06	62.90	9.72	27.38	56.94	8.75	24.69
Stage 3	88.04	86.24	11.96	13.76	58.82	9.48	31.70	51.79	8.34	27.91
Overall Average	92.47	89.72	7.53	10.28	70.63	8.95	20.42	65.60	8.23	18.63
Glacial-to-Interglacial percentual deviation as shown in Fig. 7.2 and 7.3				**60.35**						
M35052										
Stage 1										
0	70.73	69.47	29.27	30.53	56.98	7.69	35.33	40.30	5.44	24.99
20	76.49	76.88	23.51	23.12	58.64	5.81	35.55	44.85	4.44	27.19
30	71.59	68.24	28.41	31.76	50.91	6.86	42.24	36.45	4.91	30.24
Average	72.94	71.53	27.06	28.47	55.51	6.79	37.71	40.53	4.93	27.47
Maximum	76.49	76.88	29.27	31.76	58.64	7.69	42.24	44.85	5.44	30.24
Minimum	70.73	68.24	23.51	23.12	50.91	5.81	35.33	36.45	4.44	24.99
Stage 2										
40	61.47	56.99	38.53	43.01	42.92	12.16	44.92	26.39	7.47	27.61
50	55.78	52.56	44.22	47.44	35.50	10.83	53.67	19.80	6.04	29.94
Average	58.63	54.77	41.37	45.23	39.21	11.49	49.30	23.09	6.76	28.78
Maximum	61.47	56.99	44.22	47.44	42.92	12.16	53.67	26.39	7.47	29.94
Minimum	55.78	52.56	38.53	43.01	35.50	10.83	44.92	19.80	6.04	27.61
Stage 3										
60	52.56	59.35	47.44	40.65	35.90	10.30	53.80	18.87	5.41	28.28
70	50.47	48.43	49.53	51.57	34.10	12.43	53.47	17.21	6.27	26.98
80	49.81	50.62	50.19	49.38	34.22	16.93	48.85	17.05	8.43	24.33
95	58.46	56.32	41.54	43.68	42.79	7.40	49.81	25.01	4.33	29.12
100	62.53	58.01	37.47	41.99	43.15	8.46	48.40	26.98	5.29	30.26
110	62.27	59.14	37.73	40.86	42.91	9.31	47.78	26.72	5.80	29.75
120	61.20	59.31	38.80	40.69	44.52	8.50	46.97	27.25	5.20	28.75
130	61.71	59.01	38.29	40.99	43.71	7.16	49.12	26.98	4.42	30.32
140	61.33	59.98	38.67	40.02	44.79	7.58	47.63	27.47	4.65	29.21
150	70.92	70.67	29.08	29.33	41.10	9.38	49.52	29.15	6.66	35.12
220	72.62	65.16	27.38	34.84	49.25	12.63	38.12	35.77	9.17	27.68
230	52.34	51.37	47.66	48.63	37.37	17.63	45.00	19.56	9.23	23.55
Average	59.69	58.12	40.31	41.88	41.15	10.64	48.21	24.83	6.24	28.61
Maximum	72.62	70.67	50.19	51.57	49.25	17.63	53.80	35.77	9.23	35.12
Minimum	49.81	48.43	27.38	29.33	34.10	7.16	38.12	17.05	4.33	23.55
Stage 4										
240	49.83	47.83	50.17	52.17	35.95	16.13	47.92	17.91	8.04	23.88
250	53.82	50.34	46.18	49.66	43.09	11.58	45.34	23.19	6.23	24.40

	Fine Fraction						Fine carbonates in bulk sediment			
Quartz Intensity bulk	Fine Aragonite (relative %)	HMC fine (relative %)	LMC fine (relative %)	Fine Aragonite (absolute %)	HMC fine (absolute %)	LMC fine (absolute %)	Fine Aragonite in bulk sedim. (%)	Fine HMC in bulk sedim. (%)	Fine LMC in bulk sedim. (%)	Fine Quartz Intensity
114	79.56	10.68	9.75	77.44	10.40	9.49	70.36	9.45	8.63	148
53	83.21	9.89	6.90	82.26	9.77	6.82	66.88	7.95	5.55	56
134	77.08	9.79	13.13	72.84	9.22	12.30	62.09	7.87	10.49	177
189	83.21	12.91	22.22	82.26	11.47	19.95	70.36	9.95	17.02	263
53	68.20	6.29	6.90	61.23	6.02	6.82	52.24	5.09	5.55	56
127	78.39	8.50	13.10	72.05	7.82	11.98	60.02	6.52	10.01	165
203	60.91	10.62	28.47	45.10	8.48	20.38	34.04	5.98	15.87	286
220	54.62	11.30	34.08	47.06	9.81	29.37	37.69	7.67	23.59	303
169	67.52	9.20	19.28	61.14	8.23	17.07	50.42	6.62	13.98	210
							-43.28	**-8.19**	**58.50**	
317	57.64	7.18	35.18	40.04	4.99	24.44	29.99	3.74	18.30	435
231	58.87	11.10	30.03	45.25	8.53	23.09	27.43	5.17	13.99	361
348	46.60	12.99	40.41	31.80	8.86	27.58	22.34	6.23	19.37	507
299	54.37	10.42	35.21	39.03	7.46	25.03	26.59	5.05	17.22	434
348	58.87	12.99	40.41	45.25	8.86	27.58	29.99	6.23	19.37	507
231	46.60	7.18	30.03	31.80	4.99	23.09	22.34	3.74	13.99	361
640	36.81	14.92	48.27	20.98	8.50	27.51	16.59	6.73	21.76	755
694	22.99	17.55	59.46	12.08	9.22	31.25	9.66	7.37	24.99	877
667	29.90	16.23	53.87	16.53	8.86	29.38	13.13	7.05	23.38	816
694	36.81	17.55	59.46	20.98	9.22	31.25	16.59	7.37	24.99	877
640	22.99	14.92	48.27	12.08	8.50	27.51	9.66	6.73	21.76	755
834	26.90	19.75	53.35	15.97	11.72	31.66	13.39	9.83	26.55	838
826	26.63	19.32	54.05	12.90	9.36	26.18	10.73	7.78	21.77	944
896	29.06	19.46	51.49	14.71	9.85	26.06	12.77	8.55	22.63	918
664	32.61	14.74	52.64	18.37	8.30	29.65	14.94	6.75	24.11	737
556	35.50	14.38	50.12	20.59	8.34	29.07	16.13	6.53	22.77	679
648	34.45	12.08	53.47	20.37	7.14	31.62	15.76	5.53	24.46	723
603	35.56	15.36	49.08	21.09	9.11	29.11	16.65	7.19	22.97	790
586	38.46	11.06	50.48	22.70	6.53	29.79	17.37	4.99	22.79	670
632	37.18	10.59	52.23	22.30	6.35	31.33	18.54	5.28	26.04	766
462	36.50	8.42	55.07	25.80	5.95	38.92	19.75	4.56	29.80	512
453	38.03	13.40	48.57	24.78	8.73	31.65	15.38	5.42	19.63	653
875	27.85	21.88	50.28	14.31	11.24	25.83	11.95	9.39	21.58	1019
670	33.23	15.04	51.73	19.49	8.55	30.07	15.28	6.82	23.76	771
896	38.46	21.88	55.07	25.80	11.72	38.92	19.75	9.83	29.80	1019
453	26.63	8.42	48.57	12.90	5.95	25.83	10.73	4.56	19.63	512
935	27.08	18.56	54.36	12.95	8.88	26.00	11.21	7.68	22.50	1070
732	36.87	16.78	46.35	18.56	8.45	23.33	15.74	7.16	19.78	965

Mineralogy Data	Carbonates vs. non-carbonates				Bulk Sediment					
Depth (cm) and Marine Isotope Stage (MIS)	$CaCO_3$ bulk (%)	$CaCO_3$ fine fraction (%)	Non-Carbonates bulk (%)	Non-Carbonates fine (%)	Bulk Aragonite (relative %)	Bulk HMC (relative %)	Bulk LMC (relative %)	Aragonite bulk (absolute %)	HMC bulk (absolute %)	LMC bulk (absolute %)
Average	51.82	49.09	48.18	50.91	39.52	13.85	46.63	20.55	7.13	24.14
Maximum	53.82	50.34	50.17	52.17	43.09	16.13	47.92	23.19	8.04	24.40
Minimum	49.83	47.83	46.18	49.66	35.95	11.58	45.34	17.91	6.23	23.88
Stage 5										
260	62.99	57.79	37.01	42.21	51.44	10.95	37.61	32.40	6.90	23.69
270	64.01	64.96	35.99	35.04	49.18	10.80	40.01	31.48	6.92	25.61
280	70.89	71.47	29.11	28.53	49.57	7.17	43.26	35.14	5.08	30.67
290	62.20	59.79	37.80	40.21	48.83	8.39	42.78	30.37	5.22	26.61
300	70.56	70.45	29.44	29.55	43.75	8.37	47.88	30.87	5.90	33.78
310	69.47	71.05	30.53	28.95	40.43	6.00	53.57	28.09	4.17	37.21
320	74.96	74.29	25.04	25.71	38.86	2.07	59.07	29.13	1.55	44.28
330	72.67	73.21	27.33	26.79	41.96	3.04	55.00	30.49	2.21	39.96
340	66.83	67.49	33.17	32.51	48.28	4.84	46.88	32.26	3.23	31.33
350	67.90	68.73	32.10	31.27	52.06	4.73	43.21	35.35	3.21	29.34
370	71.17	71.90	28.83	28.10	51.06	3.94	44.99	36.34	2.81	32.02
380	73.28	73.00	26.72	27.00	52.57	5.52	41.91	38.53	4.04	30.71
390	77.12	77.34	22.88	22.66	45.93	3.86	50.21	35.42	2.98	38.73
Average	69.54	69.35	30.46	30.65	47.22	6.13	46.65	32.76	4.17	32.61
Maximum	77.12	77.34	37.80	42.21	52.57	10.95	59.07	38.53	6.92	44.28
Minimum	62.20	57.79	22.88	22.66	38.86	2.07	37.61	28.09	1.55	23.69
Stage 6										
400	66.56	66.19	33.44	33.81	27.22	2.08	70.69	18.12	1.39	47.06
410	53.17	55.37	46.83	44.63	25.02	9.82	65.16	13.30	5.22	34.64
420	61.45	61.19	38.55	38.81	20.11	5.33	74.56	12.36	3.28	45.82
430	58.05	58.74	41.95	41.26	28.35	10.80	60.85	16.46	6.27	35.32
440	60.84	63.47	39.16	36.53	26.30	10.75	62.95	16.00	6.54	38.30
495	60.62	62.20	39.38	37.80	37.85	18.54	43.61	22.95	11.24	26.43
500	55.01	51.43	44.99	48.57	43.29	11.51	45.20	23.82	6.33	24.87
590	66.59	61.92	33.41	38.08	40.57	11.23	48.21	27.01	7.47	32.10
600	68.11	61.84	31.89	38.16	41.01	8.55	50.44	27.93	5.82	34.36
610	66.22	56.16	33.78	43.84	38.49	9.19	52.32	25.48	6.09	34.65
Average	61.66	59.85	38.34	40.15	32.82	9.78	57.40	20.34	5.97	35.35
Maximum	68.11	66.19	46.83	48.57	43.29	18.54	74.56	27.93	11.24	47.06
Minimum	53.17	51.43	31.89	33.81	20.11	2.08	43.61	12.36	1.39	24.87
Stage 7										
620	62.46	60.00	37.54	40.00	35.39	9.38	55.23	22.11	5.86	34.50
630	67.13	61.21	32.87	38.79	38.46	9.54	52.00	25.82	6.41	34.91
640	64.27	61.08	35.73	38.92	45.67	9.71	44.62	29.35	6.24	28.68
650	75.30	69.06	24.70	30.94	42.31	4.44	53.25	31.86	3.34	40.09
660	70.97	68.60	29.03	31.40	40.21	6.35	53.43	28.54	4.51	37.92
670	75.73	70.66	24.27	29.34	42.53	4.28	53.19	32.21	3.24	40.29
680	77.29	74.45	22.71	25.55	40.13	5.26	54.62	31.01	4.06	42.21
690	74.25	74.28	25.75	25.72	36.57	3.76	59.66	27.16	2.79	44.30
700	66.17	63.62	33.83	36.38	38.00	7.82	54.18	25.14	5.17	35.85
710	63.37	60.46	36.63	39.54	31.41	6.93	61.66	19.91	4.39	39.07
720	73.68	69.57	26.32	30.43	42.08	2.40	55.52	31.01	1.77	40.90
730	77.89	77.47	22.11	22.53	39.86	2.98	57.16	31.04	2.32	44.52
740	68.03	68.40	31.97	31.60	32.71	2.54	64.74	22.26	1.73	44.05
750	64.34	64.12	35.66	35.88	23.98	4.74	71.28	15.43	3.05	45.86
Average	70.06	67.36	29.94	32.64	37.81	5.72	56.47	26.63	3.92	39.51
Maximum	77.89	77.47	37.54	40.00	45.67	9.71	71.28	32.21	6.41	45.86
Minimum	62.46	60.00	22.11	22.53	23.98	2.40	44.62	15.43	1.73	28.68

	Fine Fraction						Fine carbonates in bulk sediment			
Quartz Intensity bulk	Fine Aragonite (relative %)	HMC fine (relative %)	LMC fine (relative %)	Fine Aragonite (absolute %)	HMC fine (absolute %)	LMC fine (absolute %)	Fine Aragonite in bulk sedim. (%)	Fine HMC in bulk sedim. (%)	Fine LMC in bulk sedim. (%)	Fine Quartz Intensity
834	31.98	17.67	50.36	15.76	8.66	24.67	13.47	7.42	21.14	1018
935	36.87	18.56	54.36	18.56	8.88	26.00	15.74	7.68	22.50	1070
732	27.08	16.78	46.35	12.95	8.45	23.33	11.21	7.16	19.78	965
654	46.24	13.19	40.57	26.72	7.62	23.45	21.55	6.15	18.91	783
591	48.99	8.61	42.40	31.82	5.59	27.54	25.31	4.45	21.91	627
433	48.54	6.18	45.28	34.70	4.42	32.36	26.29	3.35	24.52	490
612	49.22	9.60	41.17	29.43	5.74	24.62	23.81	4.65	19.92	688
464	43.87	9.24	46.88	30.91	6.51	33.03	23.61	4.97	25.23	521
426	39.98	8.32	51.69	28.41	5.91	36.73	21.73	4.52	28.09	495
361	39.65	3.80	56.55	29.46	2.82	42.01	21.30	2.04	30.38	394
402	49.01	4.05	46.94	35.88	2.97	34.37	25.39	2.10	24.32	455
651	50.93	6.74	42.33	34.37	4.55	28.57	26.39	3.49	21.93	538
525	50.85	1.31	47.84	34.95	0.90	32.88	28.03	0.72	26.37	534
435	53.62	6.42	39.96	38.55	4.62	28.73	28.65	3.43	21.35	482
383	55.47	5.67	38.86	40.50	4.14	28.37	27.83	2.84	19.49	416
296	51.56	2.06	46.38	39.88	1.60	35.87	23.87	0.96	21.47	368
479	48.30	6.55	45.14	33.51	4.41	31.43	24.91	3.36	23.38	522
654	55.47	13.19	56.55	40.50	7.62	42.01	28.65	6.15	30.38	783
296	39.65	1.31	38.86	26.72	0.90	23.45	21.30	0.72	18.91	368
483	31.86	4.96	63.18	21.09	3.28	41.82	18.16	2.83	36.01	524
829	30.69	5.84	63.46	17.00	3.24	35.14	15.48	2.95	32.00	830
806	25.88	5.79	68.33	15.84	3.54	41.81	13.51	3.02	35.68	700
772	29.72	9.98	60.30	17.46	5.86	35.42	15.11	5.08	30.66	736
628	33.42	8.68	57.90	21.21	5.51	36.75	19.57	5.09	33.91	650
731	35.77	19.52	44.71	22.25	12.14	27.81	18.15	9.90	22.68	827
836	33.74	13.75	52.51	17.35	7.07	27.01	14.60	5.95	22.72	913
627	37.40	10.86	51.75	23.16	6.72	32.04	17.92	5.20	24.80	735
553	40.29	11.08	48.63	24.91	6.85	30.08	19.38	5.33	23.39	659
729	33.46	11.81	54.73	18.79	6.63	30.74	15.47	5.46	25.30	874
699	33.22	10.23	56.55	19.91	6.09	33.86	16.73	5.08	28.72	745
836	40.29	19.52	68.33	24.91	12.14	41.82	19.57	9.90	36.01	913
483	25.88	4.96	44.71	15.84	3.24	27.01	13.51	2.83	22.68	524
697	29.43	7.41	63.16	17.66	4.45	37.90	14.68	3.70	31.50	712
626	36.50	9.96	53.54	22.35	6.10	32.77	18.14	4.95	26.61	637
684	31.63	6.32	62.05	19.32	3.86	37.90	15.56	3.11	30.52	738
445	44.51	4.32	51.16	30.74	2.98	35.33	21.25	2.06	24.43	545
476	45.47	9.69	44.85	31.19	6.65	30.76	22.59	4.81	22.29	548
436	45.91	5.54	48.54	32.44	3.92	34.30	23.15	2.80	24.48	488
447	45.73	2.54	51.73	34.05	1.89	38.52	23.40	1.30	26.48	456
437	39.76	1.66	58.59	29.53	1.23	43.52	23.49	0.98	34.61	429
582	39.65	5.13	55.22	25.23	3.26	35.13	21.05	2.72	29.31	700
683	35.85	3.22	60.94	21.67	1.95	36.84	17.68	1.59	30.05	1014
438	46.04	5.01	48.94	32.03	3.49	34.05	23.80	2.59	25.29	518
315	40.99	4.97	54.04	31.75	3.85	41.86	24.07	2.92	31.74	421
546	34.90	1.45	63.64	23.87	0.99	43.53	20.69	0.86	37.72	552
593	25.70	4.87	69.43	16.48	3.12	44.52	14.32	2.71	38.70	721
529	38.72	5.15	56.13	26.31	3.41	37.64	20.28	2.65	29.55	606
697	46.04	9.96	69.43	34.05	6.65	44.52	24.07	4.95	38.70	1014
315	25.70	1.45	44.85	16.48	0.99	30.76	14.32	0.86	22.29	421

Mineralogy Data	Carbonates vs. non-carbonates				Bulk Sediment					
Depth (cm) and Marine Isotope Stage (MIS)	$CaCO_3$ bulk (%)	$CaCO_3$ fine fraction (%)	Non-Carbonates bulk (%)	Non-Carbonates fine (%)	Bulk Aragonite (relative %)	Bulk HMC (relative %)	Bulk LMC (relative %)	Aragonite bulk (absolute %)	HMC bulk (absolute %)	LMC bulk (absolute %)
Stage 8										
870	71.66	69.65	28.34	30.35	32.41	8.49	59.10	23.23	6.08	42.35
880	72.65	70.80	27.35	29.20	29.00	5.40	65.60	21.07	3.92	47.66
900	57.64	58.79	42.36	41.21	29.81	4.38	65.80	17.18	2.53	37.93
910	57.45	61.18	42.55	38.82	21.33	12.36	66.30	12.25	7.10	38.09
920	66.29	66.48	33.71	33.52	34.09	5.46	60.45	22.60	3.62	40.08
930	73.28	77.42	26.72	22.58	32.80	2.91	64.29	24.03	2.13	47.11
940	69.33	71.18	30.67	28.82	28.72	3.85	67.43	19.91	2.67	46.75
Average	66.90	67.93	33.10	32.07	29.74	6.12	64.14	20.04	4.01	42.85
Maximum	73.28	77.42	42.55	41.21	34.09	12.36	67.43	24.03	7.10	47.66
Minimum	57.45	58.79	26.72	22.58	21.33	2.91	59.10	12.25	2.13	37.93
Stage 9										
950	66.72	68.67	33.28	31.33	18.16	3.47	78.36	12.12	2.32	52.29
960	71.89	73.05	28.11	26.95	22.84	1.40	75.75	16.42	1.01	54.46
965	69.63	82.33	30.37	17.67	25.18	3.25	71.56	17.54	2.27	49.83
Average	69.42	74.68	30.58	25.32	22.06	2.71	75.23	15.36	1.86	52.19
Maximum	71.89	82.33	33.28	31.33	25.18	3.47	78.36	17.54	2.32	54.46
Minimum	66.72	68.67	28.11	17.67	18.16	1.40	71.56	12.12	1.01	49.83
Interglacials	70.49	70.73	29.51	29.27	40.65	5.34	54.01	28.82	3.72	37.95
Glacials	59.75	57.91	40.25	42.09	35.32	10.31	54.37	21.01	5.97	32.78
Stage 3	59.69	58.12	40.31	41.88	41.15	10.64	48.21	24.83	6.24	28.61
Overall Average	65.67	64.58	34.33	35.42	38.84	7.69	53.47	25.69	4.85	35.13
Glacial-to-Interglacial percentual deviation as shown in Fig. 7.2 and 7.3				**43.80**						
PC059										
Stage 1										
0	n/a	n/a	n/a	n/a	n/a	n/a	n/a	n/a	n/a	n/a
2.5	82.54	90.32	17.46	9.68	67.89	6.50	25.61	56.04	5.37	21.14
Average	82.54	90.32	17.46	9.68	67.89	6.50	25.61	56.04	5.37	21.14
Maximum	82.54	90.32	17.46	9.68	67.89	6.50	25.61	56.04	5.37	21.14
Minimum	82.54	90.32	17.46	9.68	67.89	6.50	25.61	56.04	5.37	21.14
Stage 2										
10.5	62.75	66.09	37.25	33.91	45.54	11.08	43.38	28.58	6.95	27.22
Average	62.75	66.09	37.25	33.91	45.54	11.08	43.38	28.58	6.95	27.22
Maximum	62.75	66.09	37.25	33.91	45.54	11.08	43.38	28.58	6.95	27.22
Minimum	62.75	66.09	37.25	33.91	45.54	11.08	43.38	28.58	6.95	27.22
Stage 3										
20.5	70.87	70.58	29.13	29.42	49.89	10.79	39.33	35.36	7.64	27.87
30.5	70.79	70.77	29.21	29.23	45.58	10.05	44.37	32.27	7.12	31.41
40.5	68.92	69.87	31.08	30.13	42.58	16.83	40.59	29.35	11.60	27.98
50.5	73.25	75.41	26.75	24.59	47.60	10.83	41.57	34.87	7.93	30.45
70.5	74.33	78.43	25.67	21.57	36.38	9.13	54.50	27.04	6.79	40.51
80.5	72.08	71.19	27.92	28.81	42.24	17.63	40.13	30.45	12.71	28.93

	Fine Fraction						Fine carbonates in bulk sediment			
Quartz Intensity bulk	Fine Aragonite (relative %)	HMC fine (relative %)	LMC fine (relative %)	Fine Aragonite (absolute %)	HMC fine (absolute %)	LMC fine (absolute %)	Fine Aragonite in bulk sedim. (%)	Fine HMC in bulk sedim. (%)	Fine LMC in bulk sedim. (%)	Fine Quartz Intensity
476	34.68	8.53	56.79	24.15	5.94	39.55	19.28	4.74	31.57	594
432	28.13	9.03	62.84	19.92	6.39	44.49	16.43	5.27	36.69	555
826	26.04	6.17	67.79	15.31	3.62	39.85	14.14	3.35	36.82	734
669	28.18	10.75	61.07	17.24	6.58	37.36	15.43	5.89	33.44	670
627	32.34	5.78	61.88	21.50	3.85	41.14	19.01	3.40	36.38	615
342	31.24	7.22	61.54	24.19	5.59	47.65	18.21	4.21	35.87	431
446	23.30	7.20	69.49	16.59	5.13	49.47	14.30	4.42	42.63	506
545	29.13	7.81	63.06	19.84	5.30	42.79	16.68	4.47	36.20	586
826	34.68	10.75	69.49	24.19	6.58	49.47	19.28	5.89	42.63	734
342	23.30	5.78	56.79	15.31	3.62	37.36	14.14	3.35	31.57	431
523	17.71	6.79	75.50	12.17	4.66	51.85	10.89	4.17	46.40	576
442	21.01	3.51	75.48	15.35	2.57	55.13	12.17	2.03	43.71	557
464	23.46	2.17	74.38	19.31	1.79	61.24	16.03	1.48	50.82	496
476	20.73	4.16	75.12	15.61	3.00	56.07	13.03	2.56	46.98	543
523	23.46	6.79	75.50	19.31	4.66	61.24	16.03	4.17	50.82	576
442	17.71	2.17	74.38	12.17	1.79	51.85	10.89	1.48	43.71	496
446	40.53	6.57	52.90	28.61	4.57	37.54	21.20	3.40	29.28	526
686	31.06	12.99	55.96	18.01	7.23	32.67	15.01	6.00	27.36	791
670	33.23	15.04	51.73	19.49	8.55	30.07	15.28	6.82	23.76	771
573	37.18	9.19	53.63	24.31	5.64	34.63	18.90	4.49	27.65	647
							-29.22	**76.40**	**-6.57**	
n/a	n/a	n/a	n/a	n/a	n/a	n/a	n/a	n/a	n/a	n/a
213	68.97	8.01	23.02	62.29	7.23	20.80	45.19	5.25	15.09	268
213	68.97	8.01	23.02	62.29	7.23	20.80	46.12	5.36	15.40	268
213	68.97	8.01	23.02	62.29	7.23	20.80	47.04	5.46	15.70	268
213	68.97	8.01	23.02	62.29	7.23	20.80	45.19	5.25	15.09	268
682	41.25	17.30	41.45	27.26	11.43	27.39	23.31	9.77	23.42	745
682	41.25	17.30	41.45	27.26	11.43	27.39	23.31	9.77	23.42	745
682	41.25	17.30	41.45	27.26	11.43	27.39	23.31	9.77	23.42	745
682	41.25	17.30	41.45	27.26	11.43	27.39	23.31	9.77	23.42	745
486	49.64	10.50	39.86	35.03	7.41	28.13	31.52	6.67	25.31	540
548	40.76	16.08	43.17	28.84	11.38	30.55	24.37	9.61	25.82	611
530	35.62	11.38	53.00	24.89	7.95	37.04	20.53	6.56	30.55	593
438	46.03	15.51	38.46	34.71	11.70	29.00	28.71	9.67	23.99	539
396	40.44	10.23	49.33	31.72	8.02	38.69	27.24	6.89	33.23	404
495	45.37	15.61	39.01	32.30	11.12	27.78	27.96	9.62	24.04	564

Mineralogy Data	Carbonates vs. non-carbonates				Bulk Sediment					
Depth (cm) and Marine Isotope Stage (MIS)	$CaCO_3$ bulk (%)	$CaCO_3$ fine fraction (%)	Non-Carbonates bulk (%)	Non-Carbonates fine (%)	Bulk Aragonite (relative %)	Bulk HMC (relative %)	Bulk LMC (relative %)	Aragonite bulk (absolute %)	HMC bulk (absolute %)	LMC bulk (absolute %)
83.5	68.58	75.15	31.42	24.85	50.17	13.31	36.52	34.41	9.13	25.05
88.5	71.87	72.81	28.13	27.19	45.34	10.80	43.86	32.59	7.77	31.52
Average	71.34	73.03	28.66	26.97	44.97	12.42	42.61	32.04	8.83	30.46
Maximum	74.33	78.43	31.42	30.13	50.17	17.63	54.50	35.36	12.71	40.51
Minimum	68.58	69.87	25.67	21.57	36.38	9.13	36.52	27.04	6.79	25.05
Stage 4										
96.5	71.87	72.81	28.13	27.19	40.50	12.72	46.78	29.11	9.14	33.62
106.5	63.37	64.25	36.63	35.75	46.87	10.96	42.16	29.71	6.95	26.72
Average	67.62	68.53	32.38	31.47	43.69	11.84	44.47	29.41	8.04	30.17
Maximum	71.87	72.81	36.63	35.75	46.87	12.72	46.78	29.71	9.14	33.62
Minimum	63.37	64.25	28.13	27.19	40.50	10.96	42.16	29.11	6.95	26.72
Stage 5										
116.5	70.08	74.24	29.92	25.76	54.06	8.43	37.51	37.89	5.91	26.29
120.5	71.87	73.21	28.13	26.79	56.66	11.53	31.81	40.72	8.29	22.86
136.5	76.04	79.20	23.96	20.80	54.82	6.70	38.47	41.69	5.10	29.26
146.5	77.71	83.48	22.29	16.52	59.99	8.30	31.71	46.61	6.45	24.64
156.5	69.25	75.71	30.75	24.29	60.85	11.02	28.13	42.14	7.63	19.48
166.5	74.00	78.92	26.00	21.08	48.42	6.92	44.66	35.83	5.12	33.05
176.5	78.37	82.56	21.63	17.44	49.75	9.73	40.51	38.99	7.63	31.75
186.5	83.75	89.72	16.25	10.28	65.07	1.17	33.76	54.50	0.98	28.27
196.5	82.08	88.79	17.92	11.21	66.23	4.44	29.33	54.36	3.65	24.07
213.5	77.46	82.03	22.54	17.97	67.19	5.39	27.42	52.04	4.18	21.24
216.5	79.42	85.49	20.58	14.51	62.85	5.83	31.32	49.91	4.63	24.87
226.5	81.67	86.82	18.33	13.18	60.42	1.40	38.18	49.35	1.14	31.18
232.5	84.62	88.23	15.38	11.77	70.09	1.23	28.67	59.31	1.04	24.27
Average	77.41	82.19	22.59	17.81	59.72	6.32	33.96	46.41	4.75	26.25
Maximum	84.62	89.72	30.75	26.79	70.09	11.53	44.66	59.31	8.29	33.05
Minimum	69.25	73.21	15.38	10.28	48.42	1.17	27.42	35.83	0.98	19.48
Stage 6										
238.5	68.71	68.94	31.29	31.06	29.76	3.67	66.58	20.44	2.52	45.74
246.5	68.92	70.13	31.08	29.87	45.66	10.33	44.01	31.47	7.12	30.33
256.5	66.04	63.12	33.96	36.88	41.97	6.31	51.72	27.72	4.17	34.15
266.5	65.75	65.25	34.25	34.75	34.58	10.20	55.22	22.73	6.71	36.31
276.5	72.29	70.14	27.71	29.86	40.82	1.85	57.33	29.51	1.33	41.44
Average	68.34	67.52	31.66	32.48	38.56	6.47	54.97	26.38	4.37	37.60
Maximum	72.29	70.14	34.25	36.88	45.66	10.33	66.58	31.47	7.12	45.74
Minimum	65.75	63.12	27.71	29.86	29.76	1.85	44.01	20.44	1.33	30.33
Stage 7										
286.5	69.33	70.12	30.67	29.88	41.10	6.79	52.12	28.49	4.70	36.14
296.5	78.37	78.65	21.63	21.35	55.57	7.23	37.20	43.56	5.67	29.15
306.5	81.29	82.04	18.71	17.96	67.77	1.52	30.71	55.09	1.24	24.96
316.5	81.13	83.51	18.87	16.49	60.08	7.35	32.57	48.74	5.96	26.42
326.5	79.72	84.48	20.28	15.52	72.89	4.15	22.96	58.10	3.31	18.31
336.5	82.20	86.44	17.80	13.56	73.31	9.60	17.10	60.26	7.89	14.05
346.5	80.99	85.34	19.01	14.66	61.30	8.66	30.04	49.65	7.02	24.33
356.5	77.50	82.11	22.50	17.89	53.32	8.37	38.31	41.33	6.49	29.69
366.5	70.64	70.20	29.36	29.80	52.71	7.54	39.75	37.23	5.33	28.08
373.5	74.47	73.78	25.53	26.22	63.62	10.21	26.17	47.38	7.61	19.49
378.5	73.31	75.73	26.69	24.27	56.86	2.32	40.82	41.69	1.70	29.93
386.5	82.77	87.43	17.23	12.57	69.30	3.44	27.26	57.36	2.85	22.56
396.5	86.96	92.28	13.04	7.72	77.69	6.45	15.86	67.55	5.61	13.79

	Fine Fraction						Fine carbonates in bulk sediment			
Quartz Intensity bulk	Fine Aragonite (relative %)	HMC fine (relative %)	LMC fine (relative %)	Fine Aragonite (absolute %)	HMC fine (absolute %)	LMC fine (absolute %)	Fine Aragonite in bulk sedim. (%)	Fine HMC in bulk sedim. (%)	Fine LMC in bulk sedim. (%)	Fine Quartz Intensity
500	47.55	12.87	39.58	35.73	9.67	29.74	30.24	8.19	25.16	473
565	52.91	13.22	33.87	38.52	9.63	24.66	33.25	8.31	21.29	619
495	44.79	13.18	42.04	32.72	9.61	30.70	27.98	8.19	26.17	543
565	52.91	16.08	53.00	38.52	11.70	38.69	33.25	9.67	33.23	619
396	35.62	10.23	33.87	24.89	7.41	24.66	20.53	6.56	21.29	404
801	38.22	19.72	42.05	27.83	14.36	30.62	25.26	13.03	27.79	832
689	45.51	15.11	39.38	29.24	9.71	25.30	25.82	8.57	22.34	724
745	41.87	17.42	40.72	28.54	12.03	27.96	25.54	10.80	25.06	778
801	45.51	19.72	42.05	29.24	14.36	30.62	25.82	13.03	27.79	832
689	38.22	15.11	39.38	27.83	9.71	25.30	25.26	8.57	22.34	724
509	47.32	11.93	40.75	35.13	8.86	30.25	30.57	7.70	26.32	525
484	55.10	4.57	40.33	40.34	3.35	29.52	33.16	2.75	24.27	541
338	58.32	9.07	32.60	46.19	7.19	25.82	39.81	6.19	22.25	404
306	60.04	4.73	35.23	50.12	3.95	29.41	42.97	3.38	25.22	355
573	57.87	5.27	36.86	43.82	3.99	27.91	38.09	3.47	24.26	526
397	48.29	8.27	43.44	38.11	6.53	34.28	33.48	5.73	30.13	469
292	52.82	10.67	36.51	43.60	8.81	30.14	36.49	7.37	25.22	365
188	65.63	0.83	33.54	58.88	0.75	30.09	46.00	0.58	23.51	253
197	69.41	4.17	26.42	61.63	3.70	23.46	50.06	3.01	19.06	220
289	69.79	3.52	26.69	57.25	2.89	21.90	46.49	2.34	17.78	352
327	68.41	6.08	25.51	58.48	5.20	21.81	50.96	4.53	19.00	292
212	63.50	5.01	31.50	55.13	4.35	27.35	46.25	3.65	22.94	247
179	72.43	4.82	22.74	63.91	4.26	20.07	54.40	3.62	17.08	225
330	60.69	6.07	33.24	50.20	4.91	27.08	42.21	4.18	22.85	367
573	72.43	11.93	43.44	63.91	8.86	34.28	54.40	7.70	30.13	541
179	47.32	0.83	22.74	35.13	0.75	20.07	30.57	0.58	17.08	220
520	35.15	6.83	58.03	24.23	4.71	40.00	21.40	4.16	35.32	597
612	43.54	17.58	38.88	30.54	12.33	27.27	29.03	11.72	25.93	603
674	41.01	16.39	42.60	25.89	10.35	26.89	22.92	9.16	23.81	788
640	40.39	10.73	48.88	26.35	7.00	31.90	23.34	6.20	28.25	858
464	34.82	3.46	61.72	24.42	2.43	43.29	20.83	2.07	36.92	508
582	38.98	11.00	50.02	26.29	7.36	33.87	23.50	6.66	30.05	671
674	43.54	17.58	61.72	30.54	12.33	43.29	29.03	11.72	36.92	858
464	34.82	3.46	38.88	24.23	2.43	26.89	20.83	2.07	23.81	508
558	46.56	5.03	48.41	32.65	3.53	33.95	29.54	3.19	30.71	574
305	57.80	6.38	35.82	45.46	5.02	28.17	35.48	3.92	21.99	359
352	62.93	5.21	31.86	51.63	4.28	26.14	41.60	3.45	21.06	340
235	63.04	4.56	32.40	52.65	3.80	27.06	38.69	2.80	19.89	274
287	73.36	7.00	19.63	61.98	5.92	16.59	53.74	5.13	14.38	308
237	70.07	2.93	27.00	60.57	2.53	23.34	52.40	2.19	20.19	203
222	65.94	3.13	30.92	56.28	2.67	26.39	46.81	2.22	21.95	266
295	58.46	7.54	33.99	48.00	6.19	27.91	41.32	5.33	24.03	283
463	53.79	8.72	37.48	37.77	6.12	26.32	33.20	5.38	23.14	568
477	60.03	5.03	34.94	44.29	3.71	25.78	37.24	3.12	21.67	496
444	59.02	6.33	34.65	44.69	4.80	26.24	37.30	4.00	21.90	484
221	72.40	4.84	22.76	63.30	4.24	19.90	53.35	3.57	16.77	210
171	72.46	2.52	25.02	66.87	2.33	23.09	54.93	1.91	18.97	216

Mineralogy Data	Carbonates vs. non-carbonates				Bulk Sediment					
Depth (cm) and Marine Isotope Stage (MIS)	$CaCO_3$ bulk (%)	$CaCO_3$ fine fraction (%)	Non-Carbonates bulk (%)	Non-Carbonates fine (%)	Bulk Aragonite (relative %)	Bulk HMC (relative %)	Bulk LMC (relative %)	Aragonite bulk (absolute %)	HMC bulk (absolute %)	LMC bulk (absolute %)
Average	78.36	80.93	21.64	19.07	61.96	6.43	31.60	48.96	5.03	24.38
Maximum	86.96	92.28	30.67	29.88	77.69	10.21	52.12	67.55	7.89	36.14
Minimum	69.33	70.12	13.04	7.72	41.10	1.52	15.86	28.49	1.24	13.79
Stage 8										
406.5	77.05	81.56	22.95	18.44	44.86	10.05	45.09	34.56	7.75	34.74
426.5	73.38	76.90	26.62	23.10	48.00	8.81	43.19	35.22	6.47	31.69
436.5	74.92	79.38	25.08	20.62	35.91	10.96	53.13	26.91	8.21	39.81
446.5	72.61	75.84	27.39	24.16	34.20	6.37	59.43	24.83	4.62	43.16
456.5	67.11	70.72	32.89	29.28	41.22	16.87	41.91	27.67	11.32	28.12
466.5	75.87	87.51	24.13	12.49	56.10	10.00	33.90	42.56	7.59	25.72
Average	73.49	78.65	26.51	21.35	43.38	10.51	46.11	31.96	7.66	33.87
Maximum	77.05	87.51	32.89	29.28	56.10	16.87	59.43	42.56	11.32	43.16
Minimum	67.11	70.72	22.95	12.49	34.20	6.37	33.90	24.83	4.62	25.72
Interglacials	79.44	84.48	20.56	15.52	63.19	6.42	30.39	50.47	5.05	23.92
Glacials	68.05	70.20	31.95	29.80	42.79	9.98	47.23	29.08	6.76	32.22
Stage 3	71.34	73.03	28.66	26.97	44.97	12.42	42.61	32.04	8.83	30.46
Overall Average	74.83	77.96	25.17	22.04	53.27	8.17	38.56	40.38	5.99	28.46
Glacial-to-Interglacial percentual deviation as shown in Fig. 7.2 and 7.3				**92.04**						
PC100										
Stage 1										
0	83.58	93.02	16.42	6.98	73.32	7.80	18.88	61.29	6.52	15.78
6	83.58	93.02	16.42	6.98	73.32	7.80	18.88	61.29	6.52	15.78
16	83.00	88.91	17.00	11.09	67.18	2.89	29.93	55.76	2.40	24.84
26	81.75	81.27	18.25	18.73	65.27	9.89	24.83	53.36	8.09	20.30
36	71.67	76.22	28.33	23.78	41.98	13.87	44.15	30.09	9.94	31.64
Average	80.72	86.49	19.28	13.51	64.22	8.45	27.33	52.36	6.69	21.67
Maximum	83.58	93.02	28.33	23.78	73.32	13.87	44.15	61.29	9.94	31.64
Minimum	71.67	76.22	16.42	6.98	41.98	2.89	18.88	30.09	2.40	15.78
Stage 2										
46	65.79	60.39	34.21	39.61	43.98	13.32	42.70	28.93	8.76	28.09
56	64.58	65.07	35.42	34.93	40.93	18.23	40.84	26.43	11.77	26.38
66	61.50	64.51	38.50	35.49	41.47	17.94	40.59	25.51	11.03	24.96
Average	63.96	63.32	36.04	36.68	42.13	16.50	41.38	26.96	10.52	26.48
Maximum	65.79	65.07	38.50	39.61	43.98	18.23	42.70	28.93	11.77	28.09
Minimum	61.50	60.39	34.21	34.93	40.93	13.32	40.59	25.51	8.76	24.96
Stage 3										
76	68.50	67.47	31.50	32.53	33.54	15.32	51.14	22.97	10.49	35.03
86	68.50	71.11	31.50	28.89	44.70	12.20	43.10	30.62	8.36	29.52
96	68.54	68.62	31.46	31.38	36.39	9.78	53.83	24.94	6.70	36.90
106	67.21	70.61	32.79	29.39	41.30	14.10	44.60	27.75	9.48	29.97
116	70.29	72.58	29.71	27.42	44.28	9.85	45.86	31.13	6.93	32.24

	Fine Fraction						Fine carbonates in bulk sediment			
Quartz Intensity bulk	Fine Aragonite (relative %)	HMC fine (relative %)	LMC fine (relative %)	Fine Aragonite (absolute %)	HMC fine (absolute %)	LMC fine (absolute %)	Fine Aragonite in bulk sedim. (%)	Fine HMC in bulk sedim. (%)	Fine LMC in bulk sedim. (%)	Fine Quartz Intensity
328	62.76	5.33	31.91	51.24	4.24	25.45	42.74	3.55	21.28	352
558	73.36	8.72	48.41	66.87	6.19	33.95	54.93	5.38	30.71	574
171	46.56	2.52	19.63	32.65	2.33	16.59	29.54	1.91	14.38	203
347	38.47	11.17	50.36	31.37	9.11	41.08	26.54	7.70	34.75	429
465	37.11	1.50	61.39	28.54	1.15	47.21	25.76	1.04	42.61	502
403	38.06	12.32	49.62	30.21	9.78	39.39	26.93	8.72	35.11	401
418	32.44	4.60	62.96	24.60	3.49	47.74	22.17	3.14	43.03	510
551	35.18	8.28	56.54	24.88	5.86	39.99	21.66	5.10	34.81	580
234	54.36	4.43	41.21	47.57	3.88	36.06	29.08	2.37	22.04	265
403	39.27	7.05	53.68	31.20	5.54	41.91	25.36	4.68	35.39	448
551	54.36	12.32	62.96	47.57	9.78	47.74	29.08	8.72	43.03	580
234	32.44	1.50	41.21	24.60	1.15	36.06	21.66	1.04	22.04	265
290	64.14	6.47	29.39	54.58	5.46	24.44	43.69	4.36	19.84	329
603	40.34	13.19	46.47	28.32	9.09	32.78	24.43	7.98	28.48	660
495	44.79	13.18	42.04	32.72	9.61	30.70	27.98	8.19	26.17	543
409	53.13	8.38	38.49	42.16	6.32	29.48	35.29	5.39	25.00	452
							-44.09	**82.86**	**43.54**	
216	74.86	7.78	17.35	69.64	7.24	16.14	53.29	5.54	12.35	232
216	74.86	7.78	17.35	69.64	7.24	16.14	53.29	5.54	12.35	232
220	69.49	5.80	24.71	61.79	5.15	21.97	44.80	3.74	15.93	244
264	68.97	10.43	20.61	56.05	8.47	16.75	41.61	6.29	12.43	271
485	39.40	12.61	47.99	30.03	9.61	36.58	24.54	7.86	29.89	495
280	65.52	8.88	25.60	57.43	7.54	21.52	43.50	5.79	16.59	295
485	74.86	12.61	47.99	69.64	9.61	36.58	53.29	7.86	29.89	495
216	39.40	5.80	17.35	30.03	5.15	16.14	24.54	3.74	12.35	232
674	31.85	17.82	50.33	19.23	10.76	30.40	16.14	9.03	25.51	776
622	34.30	20.18	45.52	22.32	13.13	29.62	19.19	11.29	25.47	748
702	35.68	19.89	44.43	23.02	12.83	28.66	20.11	11.21	25.04	724
666	33.94	19.30	46.76	21.52	12.24	29.56	18.48	10.51	25.34	749
702	35.68	20.18	50.33	23.02	13.13	30.40	20.11	11.29	25.51	776
622	31.85	17.82	44.43	19.23	10.76	28.66	16.14	9.03	25.04	724
693	48.91	12.90	38.19	33.00	8.70	25.77	30.49	8.04	23.81	573
541	37.42	13.77	48.81	26.61	9.79	34.71	21.73	8.00	28.34	672
574	39.61	17.10	43.29	27.18	11.73	29.71	22.14	9.56	24.20	557
521	42.27	12.49	45.24	29.85	8.82	31.95	25.96	7.67	27.78	565
497	40.09	0.00	59.91	29.10	0.00	43.49	26.84	0.00	40.12	497

Mineralogy Data	Carbonates vs. non-carbonates				Bulk Sediment					
Depth (cm) and Marine Isotope Stage (MIS)	$CaCO_3$ bulk (%)	$CaCO_3$ fine fraction (%)	Non-Carbonates bulk (%)	Non-Carbonates fine (%)	Bulk Aragonite (relative %)	Bulk HMC (relative %)	Bulk LMC (relative %)	Aragonite bulk (absolute %)	HMC bulk (absolute %)	LMC bulk (absolute %)
Average	68.61	70.08	31.39	29.92	40.04	12.25	47.71	27.48	8.39	32.73
Maximum	70.29	72.58	32.79	32.53	44.70	15.32	53.83	31.13	10.49	36.90
Minimum	67.21	67.47	29.71	27.42	33.54	9.78	43.10	22.97	6.70	29.52
Stage 4										
126	69.58	61.47	30.42	38.53	37.61	7.78	54.60	26.17	5.42	37.99
136	69.04	67.57	30.96	32.43	39.94	2.04	58.01	27.58	1.41	40.05
Average	69.31	68.96	31.22	31.04	39.60	10.84	49.58	27.27	7.44	34.09
Maximum	69.58	72.58	32.79	38.53	44.70	15.32	58.01	31.13	10.49	40.05
Minimum	69.04	61.47	29.71	27.42	33.54	2.04	43.10	22.97	1.41	29.52
Stage 5										
146	73.58	73.10	26.42	26.90	51.10	0.44	48.46	37.60	0.33	35.66
156	80.42	82.14	19.58	17.86	60.39	5.64	33.97	48.57	4.54	27.31
166	72.42	74.42	27.58	25.58	35.90	0.00	64.10	26.00	0.00	46.42
174	78.42	80.34	21.58	19.66	44.64	6.91	48.46	35.00	5.42	38.00
191	84.58	82.87	15.42	17.13	50.28	5.28	44.45	42.53	4.46	37.59
201	71.37	72.33	28.63	27.67	46.26	11.73	42.01	33.02	8.37	29.99
Average	76.80	77.53	23.20	22.47	48.09	5.00	46.91	37.12	3.85	35.83
Maximum	84.58	82.87	28.63	27.67	60.39	11.73	64.10	48.57	8.37	46.42
Minimum	71.37	72.33	15.42	17.13	35.90	0.00	33.97	26.00	0.00	27.31
Stage 6										
210	69.83	72.76	30.17	27.24	16.00	0.00	84.00	11.18	0.00	58.66
219	68.33	67.48	31.67	32.52	28.71	1.22	70.07	19.62	0.84	47.88
228	65.75	64.51	34.25	35.49	16.21	0.75	83.04	10.66	0.50	54.60
238	63.08	63.38	36.92	36.62	29.13	0.37	70.51	18.37	0.23	44.48
248	70.00	70.83	30.00	29.17	14.12	0.00	85.88	9.88	0.00	60.12
258	69.00	67.99	31.00	32.01	6.10	1.04	92.86	4.21	0.72	64.07
Average	67.67	67.83	32.33	32.17	18.38	0.56	81.06	12.32	0.38	54.97
Maximum	70.00	72.76	36.92	36.62	29.13	1.22	92.86	19.62	0.84	64.07
Minimum	63.08	63.38	30.00	27.24	6.10	0.00	70.07	4.21	0.00	44.48
Stage 7										
268	76.79	77.72	23.21	22.28	52.50	2.10	45.40	40.31	1.61	34.87
275	82.46	84.79	17.54	15.21	46.15	0.00	53.85	38.05	0.00	44.41
281	75.42	78.39	24.58	21.61	62.94	2.71	34.35	47.47	2.04	25.90
286	82.87	85.13	17.13	14.87	54.40	7.32	38.28	45.08	6.06	31.73
296	81.75	84.35	18.25	15.65	50.68	3.72	45.60	41.43	3.04	37.28
304	85.83	87.05	14.17	12.95	53.58	4.62	41.80	45.99	3.96	35.88
332	86.25	87.53	13.75	12.47	59.45	4.19	36.36	51.28	3.61	31.36
341	85.00	89.75	15.00	10.25	56.97	8.54	34.49	48.43	7.26	29.32
347	87.08	83.87	12.92	16.13	54.85	2.57	42.58	47.76	2.24	37.08
351	72.17	69.87	27.83	30.13	42.00	10.78	47.22	30.31	7.78	34.08
361	81.33	80.07	18.67	19.93	62.33	6.00	31.68	50.69	4.88	25.76
365	71.37	69.57	28.63	30.43	47.18	5.47	47.35	33.68	3.90	33.80
372	84.58	80.98	15.42	19.02	54.69	4.30	41.01	46.26	3.64	34.69
381	91.25	90.49	8.75	9.51	68.43	4.91	26.66	62.44	4.48	24.33
397	83.42	89.26	16.58	10.74	55.37	5.90	38.73	46.19	4.92	32.31
410	79.53	85.12	20.47	14.88	28.09	6.66	65.26	22.34	5.30	51.90
Average	81.69	82.75	18.31	17.25	53.10	4.99	41.91	43.61	4.05	34.04
Maximum	91.25	90.49	28.63	30.43	68.43	10.78	65.26	62.44	7.78	51.90
Minimum	71.37	69.57	8.75	9.51	28.09	0.00	26.66	22.34	0.00	24.33
Stage 8										
422	77.28	80.84	22.72	19.16	28.63	7.29	64.08	22.12	5.64	49.52

	Fine Fraction						Fine carbonates in bulk sediment			
Quartz Intensity bulk	Fine Aragonite (relative %)	HMC fine (relative %)	LMC fine (relative %)	Fine Aragonite (absolute %)	HMC fine (absolute %)	LMC fine (absolute %)	Fine Aragonite in bulk sedim. (%)	Fine HMC in bulk sedim. (%)	Fine LMC in bulk sedim. (%)	Fine Quartz Intensity
565	41.66	11.25	47.09	29.15	7.81	33.12	25.43	6.65	28.85	573
693	48.91	17.10	59.91	33.00	11.73	43.49	30.49	9.56	40.12	672
497	37.42	0.00	38.19	26.61	0.00	25.77	21.73	0.00	23.81	497
478	37.39	6.80	55.81	22.98	4.18	34.31	20.83	3.79	31.09	772
554	37.21	12.74	50.06	25.14	8.61	33.82	22.12	7.57	29.76	565
561	41.09	10.41	48.65	28.26	7.14	33.61	24.78	6.08	29.79	594
693	48.91	17.10	59.91	33.00	11.73	43.49	30.49	9.56	40.12	772
478	37.21	0.00	38.19	22.98	0.00	25.77	20.83	0.00	23.81	497
441	49.30	1.98	48.73	36.03	1.44	35.62	30.58	1.23	30.22	462
386	59.69	2.66	37.65	49.03	2.19	30.92	43.67	1.95	27.55	331
422	37.30	1.56	61.14	27.76	1.16	45.51	23.54	0.98	38.58	460
314	45.05	1.61	53.34	36.19	1.29	42.86	30.16	1.08	35.71	325
247	51.70	0.00	48.30	42.85	0.00	40.03	34.05	0.00	31.81	285
597	51.37	4.01	44.62	37.15	2.90	32.27	34.43	2.69	29.91	472
401	49.07	1.97	48.96	38.17	1.50	37.87	32.74	1.32	32.30	389
597	59.69	4.01	61.14	49.03	2.90	45.51	43.67	2.69	38.58	472
247	37.30	0.00	37.65	27.76	0.00	30.92	23.54	0.00	27.55	285
460	23.70	1.07	75.22	17.25	0.78	54.73	15.54	0.70	49.31	476
567	31.71	4.02	64.28	21.39	2.71	43.37	19.91	2.52	40.37	659
670	18.68	10.73	70.58	12.05	6.92	45.53	11.24	6.46	42.45	721
620	31.17	0.00	68.83	19.75	0.00	43.63	18.06	0.00	39.90	784
533	14.12	5.65	80.22	10.00	4.01	56.82	8.89	3.56	50.49	524
537	8.76	0.44	90.80	5.95	0.30	61.74	5.17	0.26	53.60	572
565	21.36	3.65	74.99	14.40	2.45	50.97	13.14	2.25	46.02	623
670	31.71	10.73	90.80	21.39	6.92	61.74	19.91	6.46	53.60	784
460	8.76	0.00	64.28	5.95	0.00	43.37	5.17	0.00	39.90	476
372	52.01	0.03	47.96	40.42	0.02	37.28	37.05	0.02	34.17	401
331	48.34	0.21	51.44	40.99	0.18	43.62	29.76	0.13	31.67	315
462	63.22	1.18	35.60	49.56	0.92	27.91	44.56	0.83	25.10	478
495	60.36	0.49	39.16	51.38	0.41	33.34	41.96	0.34	27.22	307
365	54.49	2.13	43.38	45.97	1.80	36.59	39.22	1.53	31.22	306
258	57.36	3.88	38.77	49.93	3.37	33.75	36.13	2.44	24.42	298
320	62.62	8.84	28.54	54.81	7.74	24.98	42.65	6.02	19.44	321
240	62.47	2.78	34.76	56.06	2.49	31.19	45.79	2.03	25.47	225
278	51.26	0.45	48.29	43.00	0.38	40.50	35.14	0.31	33.10	292
492	44.93	3.42	51.65	31.39	2.39	36.09	28.28	2.15	32.51	492
347	56.71	0.88	42.41	45.40	0.71	33.96	39.31	0.61	29.40	426
555	45.40	1.30	53.29	31.58	0.91	37.08	28.01	0.80	32.88	629
315	57.17	2.36	40.47	46.29	1.91	32.78	39.43	1.63	27.92	367
183	71.26	1.74	27.00	64.48	1.58	24.43	44.82	1.10	16.99	230
280	59.58	3.03	37.39	53.18	2.70	33.38	44.51	2.26	27.93	276
313	31.33	1.50	67.17	26.67	1.28	57.18	22.28	1.07	47.78	379
350	54.91	2.14	42.96	45.70	1.80	35.25	37.43	1.46	29.20	359
555	71.26	8.84	67.17	64.48	7.74	57.18	45.79	6.02	47.78	629
183	31.33	0.03	27.00	26.67	0.02	24.43	22.28	0.02	16.99	225
483	29.52	3.03	67.45	23.86	2.45	54.52	21.26	2.18	48.56	449

Mineralogy Data	Carbonates vs. non-carbonates				Bulk Sediment					
Depth (cm) and Marine Isotope Stage (MIS)	$CaCO_3$ bulk (%)	$CaCO_3$ fine fraction (%)	Non-Carbonates bulk (%)	Non-Carbonates fine (%)	Bulk Aragonite (relative %)	Bulk HMC (relative %)	Bulk LMC (relative %)	Aragonite bulk (absolute %)	HMC bulk (absolute %)	LMC bulk (absolute %)
435	79.52	82.45	20.48	17.55	23.16	0.11	76.73	18.42	0.09	61.02
447	74.84	77.46	25.16	22.54	25.43	0.12	74.45	19.04	0.09	55.72
458	66.79	69.90	33.21	30.10	18.87	6.33	74.80	12.60	4.23	49.96
469	79.90	85.22	20.10	14.78	43.57	6.62	49.81	34.81	5.29	39.80
474	85.23	90.03	14.77	9.97	39.76	3.10	57.14	33.89	2.64	48.70
487	79.57	83.44	20.43	16.56	35.73	2.21	62.06	28.43	1.76	49.38
496	80.07	84.43	19.93	15.57	41.28	1.42	57.30	33.06	1.14	45.88
Average	77.90	81.72	22.10	18.28	32.05	3.40	64.55	25.30	2.61	50.00
Maximum	85.23	90.03	33.21	30.10	43.57	7.29	76.73	34.81	5.64	61.02
Minimum	66.79	69.90	14.77	9.97	18.87	0.11	49.81	12.60	0.09	39.80
Stage 9										
507	80.24	84.47	19.76	15.53	35.24	3.98	60.78	28.28	3.19	48.77
516	84.07	90.30	15.93	9.70	33.95	7.37	58.68	28.55	6.20	49.33
Average	82.15	87.39	17.85	12.61	34.60	5.67	59.73	28.41	4.69	49.05
Maximum	84.07	90.30	19.76	15.53	35.24	7.37	60.78	28.55	6.20	49.33
Minimum	80.24	84.47	15.93	9.70	33.95	3.98	58.68	28.28	3.19	48.77
Interglacials	80.34	83.54	19.66	16.46	50.00	6.03	43.97	40.37	4.82	35.15
Glacials	69.71	70.46	30.42	29.54	33.04	7.83	59.14	22.96	5.24	41.38
Stage 3	68.61	70.08	31.39	29.92	40.04	12.25	47.71	27.48	8.39	32.73
Overall Average	76.20	77.86	23.80	22.14	43.38	5.93	50.68	33.72	4.42	38.06
Glacial-to-Interglacial percentual deviation as shown in Fig. 7.2 and 7.3				**79.47**						

	Fine Fraction						Fine carbonates in bulk sediment			
Quartz Intensity bulk	Fine Aragonite (relative %)	HMC fine (relative %)	LMC fine (relative %)	Fine Aragonite (absolute %)	HMC fine (absolute %)	LMC fine (absolute %)	Fine Aragonite in bulk sedim. (%)	Fine HMC in bulk sedim. (%)	Fine LMC in bulk sedim. (%)	Fine Quartz Intensity
385	24.43	3.45	72.12	20.14	2.84	59.47	17.17	2.42	50.71	369
480	26.54	4.59	68.87	20.56	3.55	53.34	18.63	3.22	48.33	400
607	20.21	0.00	79.79	14.13	0.00	55.77	13.24	0.00	52.25	621
362	44.75	0.59	54.66	38.14	0.50	46.58	32.25	0.42	39.39	365
261	45.33	6.74	47.93	40.82	6.07	43.15	33.26	4.95	35.16	314
359	29.16	8.36	62.48	24.33	6.98	52.13	21.78	6.25	46.67	363
415	36.97	4.94	58.09	31.22	4.17	49.04	28.48	3.81	44.74	363
419	32.12	3.96	63.92	26.65	3.32	51.75	23.26	2.91	45.73	406
607	45.33	8.36	79.79	40.82	6.98	59.47	33.26	6.25	52.25	621
261	20.21	0.00	47.93	14.13	0.00	43.15	13.24	0.00	35.16	314
350	38.96	5.07	55.97	32.91	4.28	47.28	29.28	3.81	42.06	448
254	36.98	10.69	52.33	33.40	9.65	47.25	28.88	8.35	40.87	248
302	37.97	7.88	54.15	33.15	6.97	47.26	29.08	6.08	41.46	348
350	38.96	10.69	55.97	33.40	9.65	47.28	29.28	8.35	42.06	448
254	36.98	5.07	52.33	32.91	4.28	47.25	28.88	3.81	40.87	248
333	51.87	5.22	42.92	43.61	4.45	35.48	35.69	3.66	29.89	348
553	32.13	9.33	58.58	22.71	6.29	41.47	19.91	5.44	36.72	593
565	41.66	11.25	47.09	29.15	7.81	33.12	25.43	6.65	28.85	573
427	44.27	5.54	50.19	35.31	4.14	38.41	29.46	3.49	33.02	447
							-44.20	**48.52**	**22.85**	

Appendix 5 - Grain size analyses

	Coarse vs. Fine Fraction		Coarse subfractions				
Depth (cm) and Marine Isotope Stage (MIS)	Coarse fraction (%)	Fine fraction (%)	63-125μm (% of coarse fraction)	125-250μm (% of coarse fraction)	250-500μm (% of coarse fraction)	500-1000μm (% of coarse fraction)	>1000μm (% of coarse fraction)
M35032							
MIS 1							
0	27.85	72.15	24.25	21.37	34.55	19.18	0.65
10	27.85	72.15	24.25	21.37	34.55	19.18	0.65
20	25.50	74.50	26.63	24.12	30.29	16.86	2.09
Average	27.06	72.94	25.05	22.28	33.13	18.40	1.13
Maximum	27.85	74.50	26.63	24.12	34.55	19.18	2.09
Minimum	25.50	72.15	24.25	21.37	30.29	16.86	0.65
MIS 2							
30	22.97	77.03	25.56	23.98	29.22	15.55	5.69
40	18.89	81.11	27.78	23.24	28.98	15.75	4.25
50	14.34	85.66	30.00	24.98	26.07	15.10	3.85
60	22.75	77.25	21.95	24.22	33.32	17.05	3.46
Average	19.74	80.26	26.32	24.11	29.40	15.86	4.31
Maximum	22.97	85.66	30.00	24.98	33.32	17.05	5.69
Minimum	14.34	77.03	21.95	23.24	26.07	15.10	3.46
MIS 3							
70	22.11	77.89	26.08	25.55	33.94	13.13	1.30
80	22.52	77.48	27.45	21.62	34.71	13.33	2.89
90	28.91	71.09	28.52	20.91	37.27	12.62	0.68
100	20.21	79.79	30.53	24.72	30.77	13.27	0.71
110	20.14	79.86	30.66	21.15	34.36	13.20	0.63
120	20.78	79.22	29.84	19.92	36.44	13.55	0.25
130	21.76	78.24	29.62	18.34	37.95	13.22	0.86
Average	22.35	77.65	28.96	21.74	35.06	13.19	1.05
Maximum	28.91	79.86	30.66	25.55	37.95	13.55	2.89
Minimum	20.14	71.09	26.08	18.34	30.77	12.62	0.25
MIS 4							
140	19.80	80.20	37.42	27.06	28.83	6.59	0.10
180	16.65	83.35	31.69	30.49	27.76	8.50	1.57
Average	18.23	81.77	34.55	28.78	28.29	7.54	0.83
Maximum	19.80	83.35	37.42	30.49	28.83	8.50	1.57
Minimum	16.65	80.20	31.69	27.06	27.76	6.59	0.10
MIS 5							
220	18.04	81.96	37.53	28.35	24.61	8.16	1.35
260	24.33	75.67	42.38	21.58	26.69	8.15	1.20
270	27.14	72.86	24.54	24.53	39.34	10.23	1.36
280	19.23	80.77	29.29	23.56	37.17	9.31	0.67
310	17.99	82.01	38.85	24.33	24.82	10.20	1.80
320	18.37	81.63	41.58	23.41	24.08	9.72	1.21
330	40.86	59.14	53.46	30.37	10.97	4.20	1.00
340	16.21	83.79	69.84	17.21	10.03	2.73	0.18
350	30.37	69.63	69.34	20.71	7.49	2.22	0.23
Average	23.61	76.39	45.20	23.78	22.80	7.21	1.00
Maximum	40.86	83.79	69.84	30.37	39.34	10.23	1.80
Minimum	16.21	59.14	24.54	17.21	7.49	2.22	0.18

	Coarse vs. Fine Fraction		Coarse subfractions				
Depth (cm) and Marine Isotope Stage (MIS)	Coarse fraction (%)	Fine fraction (%)	63-125µm (% of coarse fraction)	125-250µm (% of coarse fraction)	250-500µm (% of coarse fraction)	500-1000µm (% of coarse fraction)	>1000µm (% of coarse fraction)
Interglacials	25.34	74.66	35.12	23.03	27.97	12.81	1.07
Glacials	18.98	81.02	30.44	26.44	28.85	11.70	2.57
MIS 3	22.35	77.65	28.96	21.74	35.06	13.19	1.05
Overall Average	22.62	77.38	34.36	23.48	28.97	11.64	1.55
Glacial-to-Interglacial percentual deviation (%) as shown in Fig. 7.4 to 7.7	**-25.09**	**8.51**	**-13.34**	**14.79**	**3.14**	**-8.63**	**141.16**
M35034							
MIS 1							
0	21.66	78.34	67.98	18.16	8.23	3.93	1.70
30	24.69	75.31	53.17	26.18	14.21	5.43	1.00
60	24.67	75.33	62.05	22.73	10.26	4.45	0.51
80	19.59	80.41	31.09	24.81	31.22	11.48	1.41
90	12.51	87.49	32.75	29.77	27.78	8.51	1.18
100	21.38	78.62	38.27	30.05	23.23	7.34	1.11
110	31.18	68.82	48.36	28.23	14.99	6.74	1.68
Average	22.24	77.76	47.67	25.71	18.56	6.84	1.23
Maximum	31.18	87.49	67.98	30.05	31.22	11.48	1.70
Minimum	12.51	68.82	31.09	18.16	8.23	3.93	0.51
MIS 2							
120	17.03	82.97	46.67	26.40	17.37	6.73	2.83
130	24.44	75.56	47.70	31.77	13.94	5.29	1.29
150	33.65	66.35	65.47	25.14	6.91	2.10	0.37
160	26.29	73.71	45.20	27.79	15.71	7.69	3.61
Average	25.35	74.65	51.26	27.77	13.49	5.46	2.03
Maximum	33.65	82.97	65.47	31.77	17.37	7.69	3.61
Minimum	17.03	66.35	45.20	25.14	6.91	2.10	0.37
MIS 3							
180	30.77	69.23	33.64	39.97	20.21	5.22	0.96
190	29.06	70.94	39.06	26.45	24.09	8.84	1.56
200	20.24	79.76	52.95	22.08	18.46	5.94	0.57
210	20.16	79.84	39.02	25.77	28.15	6.77	0.29
220	24.04	75.96	40.78	24.42	26.60	7.65	0.55
230	20.34	79.66	53.37	29.90	13.09	3.41	0.24
Average	24.10	75.90	43.14	28.10	21.77	6.31	0.69
Maximum	30.77	79.84	53.37	39.97	28.15	8.84	1.56
Minimum	20.16	69.23	33.64	22.08	13.09	3.41	0.24
Overall Average	23.63	76.37	46.91	27.04	18.50	6.33	1.23
Glacial-to-Interglacial percentual deviation (%) as shown in Fig. 7.4 to 7.7	**14.00**	**-4.00**	**7.54**	**8.04**	**-27.34**	**-20.25**	**65.08**

	Coarse vs. Fine Fraction		Coarse subfractions				
Depth (cm) and Marine Isotope Stage (MIS)	Coarse fraction (%)	Fine fraction (%)	63-125μm (% of coarse fraction)	125-250μm (% of coarse fraction)	250-500μm (% of coarse fraction)	500-1000μm (% of coarse fraction)	>1000μm (% of coarse fraction)
M35042							
MIS1							
0	15.08	84.92	29.80	28.23	23.94	15.46	2.58
10	22.49	77.51	23.53	24.88	27.64	22.02	1.92
20	21.80	78.20	23.19	28.96	33.41	12.75	1.69
30	24.02	75.98	24.10	31.63	31.25	11.90	1.12
Average	20.85	79.15	25.15	28.42	29.06	15.53	1.83
Maximum	24.02	84.92	29.80	31.63	33.41	22.02	2.58
Minimum	15.08	75.98	23.19	24.88	23.94	11.90	1.12
MIS 2							
40	17.29	82.71	30.31	34.01	23.53	9.77	2.38
50	16.03	83.97	32.76	33.11	22.80	9.65	1.68
60	15.29	84.71	32.59	33.14	21.99	11.47	0.81
Average	16.20	83.80	31.89	33.42	22.77	10.30	1.62
Maximum	17.29	84.71	32.76	34.01	23.53	11.47	2.38
Minimum	15.29	82.71	30.31	33.11	21.99	9.65	0.81
MIS 3							
70	15.44	84.56	31.65	32.08	26.24	9.45	0.57
80	14.58	85.42	35.76	25.66	29.39	8.75	0.44
90	13.94	86.06	33.11	27.93	28.73	9.96	0.28
100	11.71	88.29	33.21	29.24	27.68	8.90	0.97
110	14.42	85.58	30.10	23.28	33.69	12.43	0.50
Average	14.02	85.98	32.77	27.64	29.14	9.90	0.55
Maximum	15.44	88.29	35.76	32.08	33.69	12.43	0.97
Minimum	11.71	84.56	30.10	23.28	26.24	8.75	0.28
MIS 4							
125	9.20	90.80	37.18	30.00	22.72	8.95	1.14
130	5.53	94.47	43.57	31.22	23.79	1.04	0.38
140	10.00	90.00	36.60	23.81	28.40	10.84	0.34
Average	8.25	91.75	39.12	28.34	24.97	6.95	0.62
Maximum	10.00	94.47	43.57	31.22	28.40	10.84	1.14
Minimum	5.53	90.00	36.60	23.81	22.72	1.04	0.34
MIS 5							
160	15.54	84.46	26.91	26.52	35.59	10.80	0.18
170	12.17	87.83	30.56	24.62	36.42	8.29	0.11
180	12.64	87.36	29.63	24.94	34.75	10.17	0.51
190	14.20	85.80	24.46	21.07	38.56	15.16	0.75
198	15.56	84.44	23.77	23.82	37.22	13.91	1.27
220	14.08	85.92	24.13	31.26	32.59	10.55	1.47
228	11.36	88.64	25.30	29.85	34.10	10.44	0.31
250	22.27	77.73	57.73	23.19	14.96	3.91	0.22
260	14.15	85.85	30.50	25.03	30.85	12.94	0.68
270	17.34	82.66	24.22	27.16	34.60	12.85	1.16
280	22.74	77.26	23.52	26.84	37.13	11.66	0.84
286	13.02	86.98	30.29	30.19	30.24	8.86	0.42
293.5	17.64	82.36	29.83	36.71	26.17	6.60	0.69
Average	15.59	84.41	29.30	27.02	32.55	10.47	0.66
Maximum	22.74	88.64	57.73	36.71	38.56	15.16	1.47
Minimum	11.36	77.26	23.52	21.07	14.96	3.91	0.11
MIS 6							
300	14.85	85.15	32.58	37.55	22.88	6.28	0.71
310	12.45	87.55	36.46	33.85	23.07	5.65	0.97
320	10.70	89.30	41.44	29.17	23.68	5.02	0.70
330	7.97	92.03	40.17	27.55	23.88	7.81	0.59

	Coarse vs. Fine Fraction		Coarse subfractions				
Depth (cm) and Marine Isotope Stage (MIS)	Coarse fraction (%)	Fine fraction (%)	63-125µm (% of coarse fraction)	125-250µm (% of coarse fraction)	250-500µm (% of coarse fraction)	500-1000µm (% of coarse fraction)	>1000µm (% of coarse fraction)
340	7.36	92.64	44.16	29.52	20.80	5.33	0.19
350	7.99	92.01	42.72	26.86	24.62	5.75	0.05
360	9.81	90.19	35.40	22.54	31.70	9.78	0.58
370	19.17	80.83	19.69	23.29	38.85	10.71	7.46
380	12.99	87.01	32.96	18.83	39.23	8.75	0.23
390	11.05	88.95	36.74	23.81	27.71	11.60	0.14
394.5	9.97	90.03	36.34	31.66	22.74	8.86	0.40
Average	11.30	88.70	36.24	27.69	27.20	7.78	1.09
Maximum	19.17	92.64	44.16	37.55	39.23	11.60	7.46
Minimum	7.36	80.83	19.69	18.83	20.80	5.02	0.05
MIS 7							
414	14.95	85.05	35.64	28.56	28.48	6.77	0.55
420	11.36	88.64	46.61	25.44	18.72	7.11	2.12
430	19.52	80.48	24.26	29.47	37.62	8.02	0.63
440	20.25	79.75	25.35	26.53	39.00	8.45	0.68
450	17.28	82.72	40.86	27.69	23.24	6.42	1.80
455	18.28	81.72	30.03	28.32	27.08	12.25	2.32
460	14.13	85.87	25.41	30.96	30.91	12.34	0.39
490	16.47	83.53	29.21	26.67	33.86	10.01	0.24
500	14.32	85.68	27.86	33.77	30.33	7.71	0.33
510	12.74	87.26	31.10	38.17	23.64	6.63	0.46
520	14.29	85.71	36.18	29.14	23.49	10.28	0.90
530	14.47	85.53	31.69	31.74	28.91	7.36	0.30
540	10.21	89.79	30.50	30.39	28.52	8.57	2.02
Average	15.25	84.75	31.90	29.76	28.75	8.61	0.98
Maximum	20.25	89.79	46.61	38.17	39.00	12.34	2.32
Minimum	10.21	79.75	24.26	25.44	18.72	6.42	0.24
Interglacials	17.23	82.77	28.78	28.40	30.12	11.54	1.16
Glacials	11.92	88.08	35.75	29.82	24.98	8.34	1.11
MIS 3	14.02	85.98	32.77	27.64	29.14	9.90	0.55
Overall Average	14.69	85.31	31.87	28.61	28.90	9.63	0.99
Glacial-to-Interglacial percentual deviation (%) as shown in Fig. 7.4 to 7.7	**-30.84**	**6.42**	**24.20**	**5.00**	**-17.07**	**-27.72**	**-3.73**
M35043							
MIS 1							
0	24.12	75.88	32.83	27.90	24.43	13.40	1.43
10	22.05	77.95	25.36	25.65	31.27	15.13	2.60
20	21.08	78.92	29.06	24.26	32.49	13.20	0.98
30	15.54	84.46	29.47	31.13	28.46	9.70	1.23
40	39.04	60.96	32.14	30.14	20.06	12.45	5.22
Average	24.37	75.63	29.77	27.82	27.34	12.78	2.29
Maximum	39.04	84.46	32.83	31.13	32.49	15.13	5.22
Minimum	15.54	60.96	25.36	24.26	20.06	9.70	0.98

	Coarse vs. Fine Fraction		Coarse subfractions				
Depth (cm) and Marine Isotope Stage (MIS)	Coarse fraction (%)	Fine fraction (%)	63-125μm (% of coarse fraction)	125-250μm (% of coarse fraction)	250-500μm (% of coarse fraction)	500-1000μm (% of coarse fraction)	>1000μm (% of coarse fraction)
MIS 2							
50	40.26	59.74	35.12	33.12	18.96	10.95	1.86
60	43.58	56.42	38.68	37.08	15.01	8.22	1.01
70	41.90	58.10	36.11	37.63	16.29	8.86	1.11
Average	41.91	58.09	36.63	35.94	16.75	9.34	1.33
Maximum	43.58	59.74	38.68	37.63	18.96	10.95	1.86
Minimum	40.26	56.42	35.12	33.12	15.01	8.22	1.01
MIS 3							
80	32.41	67.59	34.09	33.75	24.37	7.32	0.47
90	20.88	79.12	36.68	28.99	24.81	8.97	0.55
100	17.22	82.78	39.87	24.39	27.60	7.73	0.41
Average	23.51	76.49	36.88	29.04	25.60	8.01	0.47
Maximum	32.41	82.78	39.87	33.75	27.60	8.97	0.55
Minimum	17.22	67.59	34.09	24.39	24.37	7.32	0.41
MIS 4							
110	18.37	81.63	34.03	26.29	30.23	9.22	0.23
120	21.45	78.55	41.40	28.68	21.23	8.17	0.51
Average	19.91	80.09	37.72	27.48	25.73	8.69	0.37
Maximum	21.45	81.63	41.40	28.68	30.23	9.22	0.51
Minimum	18.37	78.55	34.03	26.29	21.23	8.17	0.23
MIS 5							
130	18.54	81.46	41.41	27.89	22.65	7.28	0.77
140	12.32	87.68	38.32	23.03	27.84	10.53	0.28
150	14.08	85.92	27.34	22.52	35.86	12.73	1.54
160	14.16	85.84	32.53	25.59	33.30	8.31	0.26
170	23.46	76.54	23.12	22.93	33.81	17.00	3.14
180	16.09	83.91	29.55	22.79	36.20	10.99	0.47
190	18.05	81.95	24.69	23.84	37.67	13.33	0.48
200	15.18	84.82	28.66	26.39	33.31	11.06	0.58
210	16.01	83.99	30.25	28.50	30.19	9.52	1.53
220	12.14	87.86	42.99	26.80	18.33	8.07	3.82
240	17.46	82.54	33.70	26.42	30.14	9.02	0.72
250	10.97	89.03	38.37	23.38	27.02	9.72	1.50
260	12.43	87.57	36.21	24.71	27.75	10.48	0.84
270	14.44	85.56	29.16	27.47	33.70	8.66	1.01
280	20.75	79.25	25.59	26.61	35.02	11.44	1.34
290	14.48	85.52	31.80	30.92	28.90	7.21	1.17
Average	15.66	84.34	32.11	25.61	30.73	10.34	1.22
Maximum	23.46	89.03	42.99	30.92	37.67	17.00	3.82
Minimum	10.97	76.54	23.12	22.52	18.33	7.21	0.26
MIS 6							
300	20.69	79.31	23.62	24.46	34.35	12.04	5.53
310	28.27	71.73	39.43	36.15	19.35	4.18	0.90
320	31.64	68.36	43.61	34.47	16.90	4.03	0.98
330	20.98	79.02	42.48	31.74	19.49	5.56	0.73
340	22.27	77.73	43.99	27.54	21.35	5.74	1.36
350	16.75	83.25	38.84	26.37	26.18	8.39	0.22
360	17.84	82.16	30.70	22.31	37.53	9.28	0.18
370	15.38	84.62	31.58	23.95	35.44	8.47	0.55
380	16.43	83.57	38.52	21.92	30.33	8.75	0.49
400	14.92	85.08	34.75	25.55	33.13	5.88	0.69
410	15.05	84.95	32.12	27.49	32.55	6.63	1.21
Average	20.02	79.98	36.33	27.45	27.87	7.18	1.17
Maximum	31.64	85.08	43.99	36.15	37.53	12.04	5.53
Minimum	14.92	68.36	23.62	21.92	16.90	4.03	0.18

	Coarse vs. Fine Fraction		Coarse subfractions				
Depth (cm) and Marine Isotope Stage (MIS)	Coarse fraction (%)	Fine fraction (%)	63-125µm (% of coarse fraction)	125-250µm (% of coarse fraction)	250-500µm (% of coarse fraction)	500-1000µm (% of coarse fraction)	>1000µm (% of coarse fraction)
MIS 7							
420	17.06	82.94	32.77	26.84	34.44	5.43	0.51
430	16.12	83.88	31.49	27.95	34.02	6.32	0.22
Average	16.59	83.41	32.13	27.40	34.23	5.87	0.37
Maximum	17.06	83.88	32.77	27.95	34.44	6.32	0.51
Minimum	16.12	82.94	31.49	26.84	34.02	5.43	0.22
Interglacials	18.87	81.13	31.34	26.94	30.77	9.66	1.29
Glacials	27.28	72.72	36.89	30.29	23.45	8.41	0.96
MIS 3	23.51	76.49	36.88	29.04	25.60	8.01	0.47
Overall Average	20.40	79.60	33.46	27.22	28.36	9.78	1.18
Glacial-to-Interglacial percentual deviation (%) as shown in Fig. 7.4 to 7.7	**44.56**	**-10.37**	**17.74**	**12.44**	**-23.78**	**-13.00**	**-26.05**
M35048							
MIS 1							
0	22.74	77.26	52.99	32.37	10.33	3.53	0.78
10	24.99	75.01	53.35	31.46	12.37	2.58	0.24
20	30.38	69.62	59.61	27.51	9.84	2.82	0.23
30	27.99	72.01	55.51	28.00	11.61	3.83	1.05
40	24.15	75.85	53.55	25.49	13.63	4.87	2.45
50	16.53	83.47	43.13	28.88	19.82	6.95	1.22
60	27.51	72.49	28.99	33.33	27.13	9.06	1.49
Average	24.90	75.10	49.59	29.58	14.96	4.80	1.06
Maximum	30.38	83.47	59.61	33.33	27.13	9.06	2.45
Minimum	16.53	69.62	28.99	25.49	9.84	2.58	0.23
MIS 2							
70	41.80	58.20	21.23	43.04	28.76	5.24	1.73
90	37.23	62.77	34.62	32.33	26.08	5.50	1.48
Average	39.52	60.48	27.93	37.68	27.42	5.37	1.60
Maximum	41.80	62.77	34.62	43.04	28.76	5.50	1.73
Minimum	37.23	58.20	21.23	32.33	26.08	5.24	1.48
MIS 3							
100	16.66	83.34	47.88	26.89	19.10	4.76	1.36
Average	16.66	83.34	47.88	26.89	19.10	4.76	1.36
Maximum	16.66	83.34	47.88	26.89	19.10	4.76	1.36
Minimum	16.66	83.34	47.88	26.89	19.10	4.76	1.36
MIS 4							
110	29.29	70.71	45.22	28.46	19.81	5.29	1.21
120	40.53	59.47	37.36	21.88	26.60	11.63	2.52
130	18.65	81.35	58.39	22.20	14.23	4.33	0.85
Average	29.49	70.51	46.99	24.18	20.22	7.08	1.53
Maximum	40.53	81.35	58.39	28.46	26.60	11.63	2.52
Minimum	18.65	59.47	37.36	21.88	14.23	4.33	0.85
MIS 5							
140	17.79	82.21	57.27	20.11	14.73	5.91	1.98
150	15.44	84.56	47.46	24.42	19.80	6.54	1.79
160	12.63	87.37	42.29	27.25	22.15	6.67	1.64

	Coarse vs. Fine Fraction		Coarse subfractions				
Depth (cm) and Marine Isotope Stage (MIS)	Coarse fraction (%)	Fine fraction (%)	63-125μm (% of coarse fraction)	125-250μm (% of coarse fraction)	250-500μm (% of coarse fraction)	500-1000μm (% of coarse fraction)	>1000μm (% of coarse fraction)
170	25.06	74.94	46.54	26.55	20.14	5.56	1.21
180	19.56	80.44	46.64	26.89	18.09	6.39	1.99
190	23.48	76.52	41.97	27.36	22.30	6.13	2.25
200	18.57	81.43	50.18	21.38	20.16	6.69	1.59
210	14.99	85.01	48.64	24.69	19.64	5.99	1.05
220	14.06	85.94	55.26	23.97	14.39	5.06	1.33
230	24.74	75.26	36.88	29.57	25.66	6.69	1.21
240	17.78	82.22	44.95	27.36	20.65	5.80	1.24
250	18.54	81.46	53.96	24.43	14.83	5.18	1.60
260	13.92	86.08	53.46	24.93	16.10	4.54	0.97
270	17.03	82.97	57.95	26.15	12.29	3.05	0.56
280	10.07	89.93	61.16	21.43	13.49	3.18	0.74
290	6.61	93.39	38.00	25.79	26.75	7.54	1.91
Average	16.89	83.11	48.91	25.14	18.82	5.68	1.44
Maximum	25.06	93.39	61.16	29.57	26.75	7.54	2.25
Minimum	6.61	74.94	36.88	20.11	12.29	3.05	0.56
MIS 6							
300	17.37	82.63	26.56	30.98	33.44	8.48	0.54
310	42.67	57.33	15.59	29.67	41.87	10.15	2.72
330	49.86	50.14	22.36	23.89	29.86	8.99	14.90
340	27.65	72.35	43.61	27.12	23.90	4.76	0.61
350	22.74	77.26	49.33	27.79	18.63	3.65	0.60
Average	32.06	67.94	31.49	27.89	29.54	7.21	3.87
Maximum	49.86	82.63	49.33	30.98	41.87	10.15	14.90
Minimum	17.37	50.14	15.59	23.89	18.63	3.65	0.54
MIS 7							
360	15.60	84.40	50.54	25.43	17.85	4.87	1.31
370	17.48	82.52	44.27	27.32	22.52	4.98	0.92
380	20.27	79.73	47.02	28.91	19.19	4.09	0.79
390	21.91	78.09	44.35	30.35	19.27	5.06	0.97
400	12.99	87.01	52.55	28.19	13.58	4.96	0.71
410	14.35	85.65	60.81	23.46	11.34	3.63	0.77
420	14.32	85.68	52.77	25.28	15.30	5.21	1.43
430	12.08	87.92	59.24	22.91	13.90	3.44	0.51
440	14.44	85.56	54.70	21.22	15.67	6.49	1.92
450	17.45	82.55	44.92	25.97	22.15	6.31	0.64
460	16.04	83.96	42.56	26.76	24.72	5.17	0.79
470	9.41	90.59	51.43	23.22	19.33	5.48	0.53
480	11.40	88.60	42.22	24.12	22.69	9.85	1.11
490	11.21	88.79	42.89	25.43	23.13	7.03	1.52
500	22.21	77.79	42.87	29.99	20.78	5.26	1.10
Average	15.41	84.59	48.88	25.90	18.76	5.46	1.00
Maximum	22.21	90.59	60.81	30.35	24.72	9.85	1.92
Minimum	9.41	77.79	42.22	21.22	11.34	3.44	0.51
MIS 8							
510	33.53	66.47	38.41	34.35	20.45	6.17	0.63
Average	33.53	66.47	38.41	34.35	20.45	6.17	0.63
Maximum	33.53	66.47	38.41	34.35	20.45	6.17	0.63
Minimum	33.53	66.47	38.41	34.35	20.45	6.17	0.63

	Coarse vs. Fine Fraction		Coarse subfractions				
Depth (cm) and Marine Isotope Stage (MIS)	Coarse fraction (%)	Fine fraction (%)	63-125μm (% of coarse fraction)	125-250μm (% of coarse fraction)	250-500μm (% of coarse fraction)	500-1000μm (% of coarse fraction)	>1000μm (% of coarse fraction)
Interglacials	19.07	80.93	49.13	26.87	17.52	5.31	1.17
Glacials	33.65	66.35	36.21	31.03	24.41	6.46	1.91
MIS 3	16.66	83.34	47.88	26.89	19.10	4.76	1.36
Overall Average	21.07	78.93	46.07	26.93	19.80	5.71	1.49
Glacial-to-Interglacial percentual deviation (%) as shown in Fig. 7.4 to 7.7	**76.47**	**-18.02**	**-26.30**	**15.44**	**39.34**	**21.49**	**63.16**
M35049							
MIS 1							
0	21.45	78.55	38.69	25.09	23.18	9.68	3.36
10	19.99	80.01	40.00	26.41	23.48	9.05	1.07
20	19.95	80.05	37.00	25.47	27.18	9.09	1.26
30	20.07	79.93	36.51	24.98	27.41	9.47	1.64
40	20.52	79.48	36.36	27.88	22.80	7.62	5.34
Average	20.40	79.60	37.71	25.97	24.81	8.98	2.53
Maximum	21.45	80.05	40.00	27.88	27.41	9.68	5.34
Minimum	19.95	78.55	36.36	24.98	22.80	7.62	1.07
MIS 2							
50	29.91	70.09	36.00	28.75	21.65	8.65	4.95
60	46.02	53.98	44.60	30.86	17.73	5.63	1.19
70	34.80	65.20	42.13	29.29	20.92	6.21	1.44
Average	36.91	63.09	40.91	29.63	20.10	6.83	2.53
Maximum	46.02	70.09	44.60	30.86	21.65	8.65	4.95
Minimum	29.91	53.98	36.00	28.75	17.73	5.63	1.19
MIS 3							
80	31.04	68.96	42.00	28.94	22.37	5.97	0.73
90	21.37	78.63	43.77	26.29	23.20	6.16	0.58
100	18.43	81.57	42.77	24.10	24.75	7.39	0.98
110	19.28	80.72	44.71	25.35	22.40	6.68	0.87
120	15.24	84.76	51.60	27.10	15.92	4.94	0.44
130	14.33	85.67	45.78	25.29	22.80	5.63	0.50
Average	19.95	80.05	45.11	26.18	21.91	6.13	0.68
Maximum	31.04	85.67	51.60	28.94	24.75	7.39	0.98
Minimum	14.33	68.96	42.00	24.10	15.92	4.94	0.44
MIS 4							
140	13.66	86.34	37.89	25.24	27.97	8.15	0.75
150	13.46	86.54	35.51	24.47	32.38	6.96	0.68
160	7.06	92.94	34.44	26.70	30.34	7.28	1.25
Average	11.40	88.60	35.94	25.47	30.23	7.46	0.89
Maximum	13.66	92.94	37.89	26.70	32.38	8.15	1.25
Minimum	7.06	86.34	34.44	24.47	27.97	6.96	0.68
MIS 5							
170	18.53	81.47	33.27	27.69	28.57	8.97	1.50
180	17.38	82.62	35.37	27.95	27.54	7.87	1.27
190	14.30	85.70	39.79	28.49	24.43	6.70	0.59
200	13.34	86.66	33.11	27.32	29.94	9.00	0.63
210	12.74	87.26	31.78	27.02	30.20	9.51	1.50
220	15.68	84.32	34.01	25.52	30.50	8.71	1.26
230	10.71	89.29	46.65	23.72	22.74	6.03	0.85

	Coarse vs. Fine Fraction		Coarse subfractions				
Depth (cm) and Marine Isotope Stage (MIS)	Coarse fraction (%)	Fine fraction (%)	63-125μm (% of coarse fraction)	125-250μm (% of coarse fraction)	250-500μm (% of coarse fraction)	500-1000μm (% of coarse fraction)	>1000μm (% of coarse fraction)
250	13.50	86.50	40.07	23.89	27.85	7.13	1.06
260	8.51	91.49	47.18	20.49	23.74	7.84	0.75
270	8.09	91.91	49.45	22.68	20.65	6.49	0.72
280	11.62	88.38	38.02	21.85	27.87	11.39	0.86
290	13.00	87.00	37.90	23.21	27.43	10.31	1.14
300	16.72	83.28	33.97	25.11	31.50	8.50	0.92
310	17.18	82.82	39.85	25.32	26.49	6.80	1.54
320	20.58	79.42	56.26	28.19	12.14	2.53	0.88
330	27.90	72.10	47.40	30.59	16.94	3.87	1.20
Average	14.99	85.01	40.25	25.57	25.53	7.60	1.04
Maximum	27.90	91.91	56.26	30.59	31.50	11.39	1.54
Minimum	8.09	72.10	31.78	20.49	12.14	2.53	0.59
MIS 6							
340	23.98	76.02	40.69	27.97	21.23	7.00	3.10
350	22.42	77.58	42.93	27.06	21.48	6.66	1.87
360	21.51	78.49	46.31	26.82	19.27	6.11	1.49
370	15.74	84.26	48.14	27.88	19.39	4.10	0.49
380	15.05	84.95	41.86	24.31	27.21	6.35	0.28
390	17.22	82.78	35.72	23.96	32.75	7.23	0.35
400	18.04	81.96	30.69	21.76	36.37	10.27	0.92
410	14.94	85.06	48.63	22.55	20.99	7.27	0.56
Average	18.61	81.39	41.87	25.29	24.84	6.87	1.13
Maximum	23.98	85.06	48.63	27.97	36.37	10.27	3.10
Minimum	14.94	76.02	30.69	21.76	19.27	4.10	0.28
MIS 7							
430	14.68	85.32	38.78	27.38	27.76	5.52	0.56
440	13.22	86.78	39.75	28.30	25.99	4.97	0.98
450	17.38	82.62	33.45	20.97	25.78	10.89	8.91
460	15.65	84.35	41.06	25.69	27.80	4.52	0.92
470	15.44	84.56	41.38	24.93	26.58	5.60	1.51
480	14.68	85.32	44.59	24.10	21.87	6.97	2.46
490	13.59	86.41	47.47	24.66	20.11	6.40	1.36
500	9.15	90.85	49.38	22.67	19.94	6.57	1.43
510	18.69	81.31	78.78	15.49	3.76	1.29	0.69
Average	14.72	85.28	46.07	23.80	22.18	5.86	2.09
Maximum	18.69	90.85	78.78	28.30	27.80	10.89	8.91
Minimum	9.15	81.31	33.45	15.49	3.76	1.29	0.56
Interglacials	16.70	83.30	41.34	25.11	24.17	7.48	1.89
Glacials	22.31	77.69	39.58	26.80	25.06	7.05	1.52
MIS 3	19.95	80.05	45.11	26.18	21.91	6.13	0.68
Overall Average	17.76	82.24	41.67	25.55	24.27	7.08	1.43
Glacial-to-Interglacial percentual deviation (%) as shown in Fig. 7.4 to 7.7	**33.57**	**-6.73**	**-4.28**	**6.72**	**3.65**	**-5.72**	**-19.69**

	Coarse vs. Fine Fraction		Coarse subfractions				
Depth (cm) and Marine Isotope Stage (MIS)	Coarse fraction (%)	Fine fraction (%)	63-125μm (% of coarse fraction)	125-250μm (% of coarse fraction)	250-500μm (% of coarse fraction)	500-1000μm (% of coarse fraction)	>1000μm (% of coarse fraction)
M35052							
MIS 1							
0	25.10	74.90	21.84	18.80	37.22	21.14	1.00
20	39.39	60.61	18.30	17.49	43.51	20.02	0.69
30	29.75	70.25	23.42	23.25	34.41	14.76	4.15
Average	31.41	68.59	21.19	19.85	38.38	18.64	1.95
Maximum	39.39	74.90	23.42	23.25	43.51	21.14	4.15
Minimum	25.10	60.61	18.30	17.49	34.41	14.76	0.69
MIS 2							
40	20.89	79.11	25.88	26.82	29.87	13.72	3.70
50	20.04	79.96	21.02	23.25	38.78	15.31	1.64
Average	20.46	79.54	23.45	25.03	34.33	14.52	2.67
Maximum	20.89	79.96	25.88	26.82	38.78	15.31	3.70
Minimum	20.04	79.11	21.02	23.25	29.87	13.72	1.64
MIS 3							
60	16.16	83.84	26.16	22.09	31.18	15.70	4.86
70	16.84	83.16	23.75	23.31	32.28	17.57	3.09
80	13.15	86.85	32.95	24.53	28.26	12.01	2.25
95	18.68	81.32	27.39	20.98	37.67	12.39	1.57
100	21.68	78.32	26.66	20.00	38.98	13.64	0.72
110	22.64	77.36	26.93	18.29	41.99	12.20	0.59
120	21.08	78.92	28.42	22.25	35.10	13.56	0.67
130	23.49	76.51	25.95	19.55	39.36	14.30	0.84
140	16.88	83.12	31.71	21.44	34.44	11.37	1.05
150	23.43	76.57	25.24	18.06	43.99	12.27	0.43
220	37.96	62.04	30.57	23.50	31.20	12.53	2.20
230	16.44	83.56	26.73	23.59	32.01	13.23	4.43
Average	20.70	79.30	27.71	21.47	35.54	13.40	1.89
Maximum	37.96	86.85	32.95	24.53	43.99	17.57	4.86
Minimum	13.15	62.04	23.75	18.06	28.26	11.37	0.43
MIS 4							
240	13.47	86.53	26.05	24.26	33.13	12.34	4.22
250	15.21	84.79	30.86	24.44	32.57	11.42	0.71
Average	14.34	85.66	28.46	24.35	32.85	11.88	2.46
Maximum	15.21	86.53	30.86	24.44	33.13	12.34	4.22
Minimum	13.47	84.79	26.05	24.26	32.57	11.42	0.71
MIS 5							
260	19.34	80.66	30.81	20.98	35.12	12.52	0.57
270	20.46	79.54	27.62	18.90	39.98	13.20	0.30
280	24.24	75.76	28.20	19.14	40.51	11.69	0.46
290	19.09	80.91	26.85	21.91	38.22	12.47	0.55
300	23.61	76.39	21.55	17.96	43.60	16.72	0.18
310	23.51	76.49	23.53	18.03	40.50	17.62	0.32
320	27.69	72.31	19.62	20.24	41.58	18.29	0.26
330	29.23	70.77	18.86	19.49	43.58	17.75	0.32
340	23.23	76.77	25.41	19.13	40.24	14.80	0.42
350	19.79	80.21	24.14	19.70	38.70	16.97	0.48
370	25.68	74.32	24.06	19.42	36.68	19.53	0.31
380	31.29	68.71	22.79	20.02	38.64	18.40	0.15
390	40.13	59.87	19.71	18.17	41.54	20.28	0.30
Average	25.18	74.82	24.09	19.47	39.91	16.17	0.36
Maximum	40.13	80.91	30.81	21.91	43.60	20.28	0.57
Minimum	19.09	59.87	18.86	17.96	35.12	11.69	0.15

	Coarse vs. Fine Fraction		Coarse subfractions				
Depth (cm) and Marine Isotope Stage (MIS)	Coarse fraction (%)	Fine fraction (%)	63-125μm (% of coarse fraction)	125-250μm (% of coarse fraction)	250-500μm (% of coarse fraction)	500-1000μm (% of coarse fraction)	>1000μm (% of coarse fraction)
MIS 6							
400	13.88	86.12	31.83	23.10	29.45	15.42	0.20
410	8.93	91.07	41.42	26.93	24.53	6.89	0.23
420	14.67	85.33	33.54	20.53	37.18	8.17	0.57
430	13.44	86.56	29.45	23.25	38.46	8.76	0.08
440	7.73	92.27	32.84	25.63	32.47	8.94	0.12
495	18.43	81.57	36.34	18.76	22.60	13.24	9.06
500	15.88	84.12	32.26	24.87	32.94	9.51	0.42
590	22.60	77.40	27.22	20.43	40.74	11.22	0.39
600	22.23	77.77	25.52	21.18	43.94	9.03	0.34
610	17.69	82.31	26.56	21.59	41.05	10.37	0.44
Average	15.55	84.45	31.70	22.63	34.34	10.16	1.18
Maximum	22.60	92.27	41.42	26.93	43.94	15.42	9.06
Minimum	7.73	77.40	25.52	18.76	22.60	6.89	0.08
MIS 7							
620	16.87	83.13	27.29	20.17	38.64	13.71	0.18
630	18.81	81.19	29.66	21.28	38.37	10.44	0.24
640	19.46	80.54	26.26	21.49	41.95	10.05	0.25
650	30.87	69.13	18.20	17.23	51.67	12.62	0.28
660	27.56	72.44	19.76	19.56	44.22	16.25	0.21
670	28.64	71.36	19.56	17.63	39.83	22.76	0.22
680	31.26	68.74	20.63	17.96	41.18	20.05	0.18
690	20.48	79.52	26.86	21.59	38.07	13.33	0.15
700	16.58	83.42	28.20	24.85	36.22	10.38	0.36
710	18.43	81.57	26.80	23.06	37.93	11.96	0.25
720	25.71	74.29	22.70	21.73	43.65	11.53	0.39
730	24.19	75.81	25.37	22.37	40.87	10.43	0.96
740	13.34	86.66	33.75	25.44	31.85	8.55	0.41
750	13.07	86.93	28.44	25.64	37.15	8.44	0.33
Average	21.81	78.19	25.25	21.43	40.11	12.89	0.32
Maximum	31.26	86.93	33.75	25.64	51.67	22.76	0.96
Minimum	13.07	68.74	18.20	17.23	31.85	8.44	0.15
MIS 8							
870	20.19	79.81	26.86	22.70	38.50	11.22	0.72
880	17.52	82.48	24.25	21.42	42.93	11.08	0.33
900	7.61	92.39	40.56	26.66	26.16	6.43	0.18
910	10.48	89.52	33.57	26.96	29.73	9.61	0.13
920	11.57	88.43	28.90	22.97	38.48	9.50	0.16
930	24.72	75.28	15.12	16.94	52.39	15.40	0.15
940	13.82	86.18	23.68	25.02	38.94	12.18	0.18
Average	15.13	84.87	27.56	23.24	38.16	10.77	0.26
Maximum	24.72	92.39	40.56	26.96	52.39	15.40	0.72
Minimum	7.61	75.28	15.12	16.94	26.16	6.43	0.13
MIS 9							
950	10.51	89.49	26.43	24.04	39.59	9.75	0.20
960	20.72	79.28	18.66	22.48	42.28	16.24	0.34
965	17.00	83.00	22.39	21.79	40.50	14.99	0.33
Average	16.08	83.92	22.49	22.77	40.79	13.66	0.29
Maximum	20.72	89.49	26.43	24.04	42.28	16.24	0.34
Minimum	10.51	79.28	18.66	21.79	39.59	9.75	0.20

	Coarse vs. Fine Fraction		Coarse subfractions				
Depth (cm) and Marine Isotope Stage (MIS)	Coarse fraction (%)	Fine fraction (%)	63-125μm (% of coarse fraction)	125-250μm (% of coarse fraction)	250-500μm (% of coarse fraction)	500-1000μm (% of coarse fraction)	>1000μm (% of coarse fraction)
Interglacials	23.62	76.38	23.25	20.88	39.80	15.34	0.73
Glacials	16.37	83.63	27.79	23.81	34.92	11.83	1.65
MIS 3	20.70	79.30	27.71	21.47	35.54	13.40	1.89
Overall Average	20.52	79.48	26.42	21.61	37.72	13.31	0.95
Glacial-to-Interglacial percentual deviation (%) as shown in Fig. 7.4 to 7.7	**-30.68**	**9.49**	**19.51**	**14.05**	**-12.26**	**-22.87**	**126.43**
PC059							
MIS 1							
0	24.48	75.52	23.89	24.23	33.97	16.75	1.18
2.5	27.46	72.54	24.27	26.41	34.36	14.49	0.47
Average	25.97	74.03	24.08	25.32	34.17	15.62	0.82
Maximum	27.46	75.52	24.27	26.41	34.36	16.75	1.18
Minimum	24.48	72.54	23.89	24.23	33.97	14.49	0.47
MIS 2							
10.5	14.50	85.50	31.44	29.67	21.80	12.43	4.66
Average	14.50	85.50	31.44	29.67	21.80	12.43	4.66
Maximum	14.50	85.50	31.44	29.67	21.80	12.43	4.66
Minimum	14.50	85.50	31.44	29.67	21.80	12.43	4.66
MIS 3							
20.5	10.02	89.98	40.14	29.64	21.10	7.05	2.06
30.5	15.49	84.51	39.98	29.07	24.26	6.04	0.66
40.5	17.52	82.48	38.70	30.62	22.10	8.42	0.16
50.5	17.29	82.71	39.46	28.12	22.31	7.61	2.51
70.5	14.13	85.87	39.02	22.84	28.35	9.78	0.00
80.5	13.43	86.57	42.14	24.32	25.08	8.20	0.27
83.5	15.38	84.62	36.59	23.11	28.34	11.72	0.24
88.5	13.68	86.32	40.51	24.11	25.89	8.09	1.40
Average	14.62	85.38	39.57	26.48	24.68	8.37	0.91
Maximum	17.52	89.98	42.14	30.62	28.35	11.72	2.51
Minimum	10.02	82.48	36.59	22.84	21.10	6.04	0.00
MIS 4							
96.5	9.25	90.75	40.82	32.00	19.95	6.58	0.65
106.5	11.71	88.29	41.29	28.04	22.20	8.21	0.27
Average	10.48	89.52	41.06	30.02	21.07	7.40	0.46
Maximum	11.71	90.75	41.29	32.00	22.20	8.21	0.65
Minimum	9.25	88.29	40.82	28.04	19.95	6.58	0.27
MIS 5							
116.5	13.00	87.00	43.33	23.50	23.41	9.75	0.02
120.5	17.80	82.20	42.00	25.88	22.69	8.91	0.52
136.5	13.82	86.18	36.25	24.50	29.36	9.76	0.14
146.5	14.26	85.74	36.45	22.82	30.79	9.91	0.03
156.5	13.06	86.94	39.73	26.61	24.31	9.30	0.05
166.5	12.13	87.87	34.35	19.71	34.57	11.25	0.13
176.5	16.32	83.68	28.85	21.82	36.09	13.25	0.00
186.5	21.88	78.12	40.59	24.20	23.85	9.66	1.70
196.5	18.77	81.23	30.97	21.28	33.00	14.40	0.34
213.5	18.79	81.21	25.49	16.20	26.73	14.13	17.45
216.5	12.87	87.13	36.38	22.57	28.86	11.98	0.21

	Coarse vs. Fine Fraction		Coarse subfractions				
Depth (cm) and Marine Isotope Stage (MIS)	Coarse fraction (%)	Fine fraction (%)	63-125µm (% of coarse fraction)	125-250µm (% of coarse fraction)	250-500µm (% of coarse fraction)	500-1000µm (% of coarse fraction)	>1000µm (% of coarse fraction)
226.5	16.10	83.90	28.71	21.35	38.11	11.68	0.15
232.5	14.87	85.13	35.36	21.96	32.96	9.64	0.07
Average	15.67	84.33	35.27	22.49	29.59	11.05	1.60
Maximum	21.88	87.87	43.33	26.61	38.11	14.40	17.45
Minimum	12.13	78.12	25.49	16.20	22.69	8.91	0.00
MIS 6							
238.5	11.69	88.31	38.62	23.07	31.54	6.75	0.02
246.5	4.92	95.08	47.08	25.66	20.56	6.69	0.00
256.5	11.45	88.55	35.08	30.93	22.88	10.56	0.55
266.5	11.42	88.58	36.10	21.17	29.26	12.15	1.31
276.5	14.72	85.28	28.79	21.00	40.61	9.51	0.10
Average	10.84	89.16	37.13	24.37	28.97	9.13	0.40
Maximum	14.72	95.08	47.08	30.93	40.61	12.15	1.31
Minimum	4.92	85.28	28.79	21.00	20.56	6.69	0.00
MIS 7							
286.5	9.53	90.47	44.52	19.90	24.88	10.70	0.00
296.5	21.95	78.05	34.32	27.24	30.81	7.64	0.00
306.5	19.41	80.59	31.55	29.50	31.90	6.90	0.16
316.5	26.50	73.50	25.98	23.96	41.15	8.84	0.07
326.5	13.30	86.70	37.62	27.98	25.47	8.58	0.34
336.5	13.49	86.51	40.04	25.48	24.84	9.61	0.03
346.5	16.82	83.18	29.49	20.57	36.01	13.88	0.05
356.5	13.92	86.08	39.39	26.56	26.28	7.52	0.25
366.5	12.08	87.92	40.10	25.84	26.19	7.87	0.00
373.5	15.93	84.07	34.42	27.86	28.28	9.17	0.27
378.5	16.54	83.46	32.90	27.63	29.45	10.02	0.00
386.5	15.71	84.29	54.49	25.67	17.50	2.31	0.01
396.5	17.85	82.15	33.65	27.44	32.81	5.36	0.74
Average	16.39	83.61	36.81	25.82	28.89	8.34	0.15
Maximum	26.50	90.47	54.49	29.50	41.15	13.88	0.74
Minimum	9.53	73.50	25.98	19.90	17.50	2.31	0.00
MIS 8							
406.5	15.41	84.59	41.22	35.61	19.46	3.71	0.00
426.5	9.74	90.26	45.60	22.52	27.48	4.40	0.00
436.5	10.86	89.14	41.90	22.36	28.09	7.18	0.48
446.5	9.88	90.12	41.30	19.95	28.33	10.39	0.03
456.5	12.94	87.06	47.85	26.15	21.03	4.98	0.00
466.5	38.87	61.13	21.07	19.12	46.44	11.14	2.23
Average	16.28	83.72	39.82	24.28	28.47	6.96	0.46
Maximum	38.87	90.26	47.85	35.61	46.44	11.14	2.23
Minimum	9.74	61.13	21.07	19.12	19.46	3.71	0.00
Interglacials	19.34	80.66	32.05	24.54	30.88	11.67	0.86
Glacials	13.03	86.97	37.36	27.08	25.08	8.98	1.49
MIS 3	14.62	85.38	39.57	26.48	24.68	8.37	0.91
Overall Average	15.46	84.54	36.80	24.95	28.11	9.30	0.84
Glacial-to-Interglacial percentual deviation (%) as shown in Fig. 7.4 to 7.7	**-32.65**	**7.83**	**16.58**	**10.36**	**-18.80**	**-23.02**	**74.06**

	Coarse vs. Fine Fraction		Coarse subfractions				
Depth (cm) and Marine Isotope Stage (MIS)	Coarse fraction (%)	Fine fraction (%)	63-125μm (% of coarse fraction)	125-250μm (% of coarse fraction)	250-500μm (% of coarse fraction)	500-1000μm (% of coarse fraction)	>1000μm (% of coarse fraction)
PC100							
MIS 1							
0	23.48	76.52	32.21	27.65	25.44	13.15	1.54
6	23.48	76.52	32.21	27.65	25.44	13.15	1.54
16	27.50	72.50	22.47	23.89	34.92	17.35	1.37
26	25.77	74.23	21.41	23.88	33.87	16.77	4.07
36	18.28	81.72	32.92	32.19	22.87	10.13	1.90
Average	23.70	76.30	28.24	27.05	28.51	14.11	2.09
Maximum	27.50	81.72	32.92	32.19	34.92	17.35	4.07
Minimum	18.28	72.50	21.41	23.88	22.87	10.13	1.37
MIS 2							
46	16.06	83.94	25.27	24.96	22.48	16.50	10.78
56	14.02	85.98	31.79	28.04	21.89	13.41	4.86
66	12.62	87.38	31.77	33.45	23.11	10.33	1.35
Average	14.24	85.76	29.61	28.81	22.49	13.42	5.67
Maximum	16.06	87.38	31.79	33.45	23.11	16.50	10.78
Minimum	12.62	83.94	25.27	24.96	21.89	10.33	1.35
MIS 3							
76	7.60	92.40	33.84	22.99	38.40	4.29	0.48
86	18.36	81.64	36.26	28.69	26.79	8.17	0.09
96	18.55	81.45	35.38	27.39	26.58	10.59	0.06
106	13.03	86.97	39.71	24.27	27.05	8.60	0.37
116	7.75	92.25	45.69	21.42	23.82	8.03	1.04
Average	13.06	86.94	38.18	24.95	28.53	7.94	0.41
Maximum	18.55	92.40	45.69	28.69	38.40	10.59	1.04
Minimum	7.60	81.45	33.84	21.42	23.82	4.29	0.06
MIS 4							
126	9.38	90.62	35.89	27.15	27.07	9.89	0.00
136	12.03	87.97	35.61	24.29	32.28	7.72	0.10
Average	12.59	87.41	38.01	25.13	29.28	8.01	0.36
Maximum	18.55	92.40	45.69	28.69	38.40	10.59	1.04
Minimum	7.60	81.45	33.84	21.42	23.82	4.29	0.00
MIS 5							
146	15.15	84.85	35.13	22.19	31.96	10.52	0.20
156	10.92	89.08	39.52	20.93	29.48	9.71	0.36
166	15.21	84.79	31.79	20.46	35.77	11.49	0.49
174	16.66	83.34	26.37	22.35	36.83	14.46	0.00
191	20.53	79.47	22.24	23.12	39.11	15.53	0.00
201	7.34	92.66	39.09	21.87	29.06	9.98	0.00
Average	14.30	85.70	32.36	21.82	33.70	11.95	0.18
Maximum	20.53	92.66	39.52	23.12	39.11	15.53	0.49
Minimum	7.34	79.47	22.24	20.46	29.06	9.71	0.00
MIS 6							
210	9.90	90.10	43.58	20.56	26.01	6.19	3.66
219	6.93	93.07	42.69	22.35	23.75	11.21	0.00
228	6.76	93.24	43.93	27.22	20.59	8.26	0.00
238	8.55	91.45	44.68	23.22	26.86	5.23	0.00
248	11.15	88.85	32.34	19.53	36.05	12.08	0.00
258	13.18	86.82	27.49	20.39	40.18	11.93	0.00
Average	9.41	90.59	39.12	22.21	28.91	9.15	0.61
Maximum	13.18	93.24	44.68	27.22	40.18	12.08	3.66
Minimum	6.76	86.82	27.49	19.53	20.59	5.23	0.00

	Coarse vs. Fine Fraction		Coarse subfractions				
Depth (cm) and Marine Isotope Stage (MIS)	Coarse fraction (%)	Fine fraction (%)	63-125μm (% of coarse fraction)	125-250μm (% of coarse fraction)	250-500μm (% of coarse fraction)	500-1000μm (% of coarse fraction)	>1000μm (% of coarse fraction)
MIS 7							
268	8.34	91.66	45.52	21.19	23.53	9.76	0.00
275	27.39	72.61	24.07	24.15	40.18	11.45	0.15
281	10.08	89.92	50.61	24.09	20.22	5.08	0.00
286	18.33	81.67	29.23	20.63	40.41	9.62	0.11
296	14.68	85.32	33.77	23.28	34.24	8.65	0.07
304	27.64	72.36	15.88	18.33	52.28	13.38	0.13
332	22.18	77.82	31.59	23.55	30.60	14.15	0.12
341	18.33	81.67	30.13	21.18	34.54	14.04	0.12
347	18.27	81.73	29.45	21.56	37.36	11.64	0.00
351	9.91	90.09	44.79	30.16	19.71	5.24	0.11
361	13.41	86.59	43.48	21.08	26.77	8.66	0.02
365	11.33	88.67	34.29	26.71	27.75	11.26	0.00
372	14.84	85.16	41.39	28.50	25.14	4.82	0.15
381	30.48	69.52	16.52	16.84	54.96	10.90	0.78
397	16.31	83.69	30.18	23.85	38.18	7.42	0.37
410	16.43	83.57	36.29	26.85	26.38	9.88	0.60
Average	17.37	82.63	33.57	23.24	33.27	9.75	0.17
Maximum	30.48	91.66	50.61	30.16	54.96	14.15	0.78
Minimum	8.34	69.52	15.88	16.84	19.71	4.82	0.00
MIS 8							
422	10.93	89.07	41.87	22.99	28.32	6.81	0.00
435	14.73	85.27	34.58	21.80	34.56	9.06	0.00
447	9.39	90.61	42.76	20.15	26.23	10.71	0.15
458	6.31	93.69	48.50	26.72	18.96	5.81	0.00
469	15.44	84.56	25.40	18.23	47.25	8.87	0.25
474	18.51	81.49	20.25	17.89	49.00	12.68	0.18
487	10.48	89.52	31.95	22.57	33.26	12.01	0.21
496	8.76	91.24	34.12	23.52	32.74	9.62	0.00
Average	11.82	88.18	34.93	21.73	33.79	9.45	0.10
Maximum	18.51	93.69	48.50	26.72	49.00	12.68	0.25
Minimum	6.31	81.49	20.25	17.89	18.96	5.81	0.00
MIS 9							
507	11.03	88.97	33.04	25.02	29.48	10.82	1.64
516	13.52	86.48	29.82	22.69	40.59	6.90	0.00
Average	12.27	87.73	31.43	23.85	35.04	8.86	0.82
Maximum	13.52	88.97	33.04	25.02	40.59	10.82	1.64
Minimum	11.03	86.48	29.82	22.69	29.48	6.90	0.00
Interglacials	16.91	83.09	31.40	23.99	32.63	11.17	0.81
Glacials	12.01	87.99	35.42	24.47	28.62	10.01	1.68
MIS 3	13.06	86.94	38.18	24.95	28.53	7.94	0.41
Overall Average	14.85	85.15	33.98	23.69	31.33	10.26	0.74
Glacial-to-Interglacial percentual deviation (%) as shown in Fig. 7.4 to 7.7	**-28.97**	**5.90**	**12.79**	**2.00**	**-12.29**	**-10.39**	**107.18**

Appendix 6 - Physical Properties & Mass accumulation rates

Physical Properties Data Sheet

Depth (cm) and Marine Isotope Stage (MIS)	Water Content (%)	Wet Bulk Density (g/cm^3)	Dry Bulk Density (g/cm^3)	MAR Bulk sediment ($g/cm^2/ky$)	MAR Coarse fraction ($g/cm^2/ky$)	MAR Fine fraction ($g/cm^2/ky$)	MAR Aragonite fine ($g/cm^2/ky$)	MAR HMC fine ($g/cm^2/ky$)	MAR LMC fine ($g/cm^2/ky$)	MAR Non Carbonates fine ($g/cm^2/ky$)
M35032										
MIS 1										
0	46.49	1.41	0.75	2.02	0.56	1.45	0.93	0.13	0.20	0.20
10	46.49	1.41	0.75	2.02	0.56	1.45	0.93	0.13	0.20	0.20
20	42.54	1.58	0.91	2.42	0.62	1.80	0.81	0.20	0.37	0.42
Average	45.17	1.47	0.81	2.15	0.58	1.57	0.89	0.15	0.26	0.27
Maximum	46.49	1.58	0.91	2.42	0.62	1.80	0.93	0.20	0.37	0.42
Minimum	42.54	1.41	0.75	2.02	0.56	1.45	0.81	0.13	0.20	0.20
MIS 2										
30	46.93	1.45	0.77	2.76	0.63	2.12	0.58	0.21	0.53	0.81
40	44.34	1.48	0.82	2.94	0.56	2.38	0.49	0.27	0.70	0.93
50	43.38	1.57	0.89	3.18	0.46	2.72	0.58	0.39	0.66	1.09
60	44.78	1.49	0.82	2.94	0.67	2.27	0.52	0.23	0.65	0.86
Average	44.86	1.49	0.82	2.95	0.58	2.37	0.54	0.27	0.63	0.92
Maximum	46.93	1.57	0.89	3.18	0.67	2.72	0.58	0.39	0.70	1.09
Minimum	43.38	1.45	0.77	2.76	0.46	2.12	0.49	0.21	0.53	0.81
MIS 3										
70	40.27	1.53	0.92	1.55	0.34	1.21	0.30	0.20	0.28	0.43
80	42.25	1.52	0.88	1.49	0.33	1.15	0.35	0.13	0.32	0.36
90	45.36	1.52	0.83	1.40	0.41	1.00	0.30	0.04	0.33	0.32
100	43.50	1.57	0.88	1.49	0.30	1.19	0.34	0.09	0.36	0.40
110	43.47	1.52	0.86	1.45	0.29	1.16	0.43	0.12	0.29	0.32
120	44.10	1.49	0.83	1.41	0.29	1.12	0.37	0.13	0.28	0.33
130	44.48	1.55	0.86	1.45	0.32	1.14	0.34	0.00	0.56	0.24
Average	43.35	1.53	0.87	1.46	0.33	1.14	0.35	0.10	0.35	0.34
Maximum	45.36	1.57	0.92	1.55	0.41	1.21	0.43	0.20	0.56	0.43
Minimum	40.27	1.49	0.83	1.40	0.29	1.00	0.30	0.00	0.28	0.24
MIS 4										
140	39.06	1.62	0.99	1.03	0.20	0.82	0.26	0.07	0.29	0.20
180	38.96	1.59	0.97	1.01	0.17	0.84	0.28	0.04	0.29	0.23
Average	39.01	1.61	0.98	1.02	0.19	0.83	0.27	0.05	0.29	0.22
Maximum	39.06	1.62	0.99	1.03	0.20	0.84	0.28	0.07	0.29	0.23
Minimum	38.96	1.59	0.97	1.01	0.17	0.82	0.26	0.04	0.29	0.20
MIS 5										
220	39.05	1.60	0.98	2.22	0.40	1.82	0.60	0.22	0.46	0.54
260	37.15	1.62	1.02	2.32	0.56	1.75	0.81	0.27	0.36	0.32
270	39.32	1.62	0.98	2.23	0.60	1.62	0.65	0.14	0.47	0.36
280	36.83	1.63	1.03	2.33	0.45	1.88	0.80	0.14	0.58	0.37
310	35.78	1.62	1.04	2.36	0.42	1.93	0.86	0.25	0.39	0.44
320	35.16	1.65	1.07	2.43	0.45	1.99	0.98	0.22	0.40	0.38
330	39.93	1.59	0.96	2.17	0.89	1.28	0.56	0.17	0.28	0.28
340	29.75	1.79	1.26	2.85	0.46	2.39	1.38	0.14	0.61	0.26
350	28.20	1.81	1.30	2.95	0.90	2.06	1.29	0.23	0.34	0.19
Average	35.69	1.66	1.07	2.43	0.57	1.86	0.88	0.20	0.43	0.35
Maximum	39.93	1.81	1.30	2.95	0.90	2.39	1.38	0.27	0.61	0.54
Minimum	28.20	1.59	0.96	2.17	0.40	1.28	0.56	0.14	0.28	0.19
Interglacials	40.43	1.56	0.94	2.29	0.58	1.71	0.89	0.17	0.35	0.31
Glacials	41.93	1.55	0.90	1.99	0.38	1.60	0.41	0.16	0.46	0.57
MIS 3	43.35	1.53	0.87	1.46	0.33	1.14	0.35	0.10	0.35	0.34
Overall Average	40.70	1.57	0.93	2.10	0.47	1.62	0.63	0.17	0.41	0.42
Glacial-to-Interglacial percentual deviation (%) as shown in Fig. 6.8				**-13.28**	**-33.59**	**-6.46**	**-53.99**	**-5.77**	**33.47**	**84.82**
M35034										
MIS 1										
0	42.51	1.50	0.86	5.55	1.20	4.35	2.92	0.42	0.34	0.68
30	36.24	1.61	1.02	6.62	1.63	4.98	3.42	0.36	0.48	0.72
60	31.48	1.80	1.23	7.95	1.96	5.99	4.26	0.65	0.33	0.76
80	33.13	1.72	1.15	7.44	1.46	5.98	4.40	0.43	0.31	0.84
90	36.87	1.59	1.01	6.49	0.81	5.68	4.16	0.48	0.26	0.78
100	36.04	1.62	1.04	6.70	1.43	5.27	2.98	0.38	0.74	1.16
110	34.21	1.74	1.14	7.38	2.30	5.08	2.09	0.65	0.74	1.59
Average	35.78	1.65	1.06	6.88	1.54	5.33	3.46	0.48	0.46	0.94
Maximum	42.51	1.80	1.23	7.95	2.30	5.99	4.40	0.65	0.74	1.88
Minimum	31.48	1.50	0.86	5.55	0.81	4.35	2.09	0.36	0.26	0.55

Physical Properties Data Sheet

Depth (cm) and Marine Isotope Stage (MIS)	Water Content (%)	Wet Bulk Density (g/cm³)	Dry Bulk Density (g/cm³)	MAR Bulk sediment (g/cm²/ky)	MAR Coarse fraction (g/cm²/ky)	MAR Fine fraction (g/cm²/ky)	MAR Aragonite fine (g/cm²/ky)	MAR HMC fine (g/cm²/ky)	MAR LMC fine (g/cm²/ky)	MAR Non Carbonates fine (g/cm²/ky)
MIS 2										
120	37.63	1.59	0.99	4.16	0.71	3.45	1.21	0.48	0.57	1.20
130	36.88	1.60	1.01	4.23	1.03	3.20	0.96	0.47	0.67	1.10
150	27.54	1.77	1.28	5.39	1.81	3.58	2.04	0.44	0.39	0.71
160	33.72	1.69	1.12	4.71	1.24	3.47	1.31	0.40	0.73	1.03
Average	33.94	1.66	1.10	4.62	1.20	3.42	1.38	0.45	0.59	1.02
Maximum	37.63	1.77	1.28	5.39	1.81	3.58	2.04	0.48	0.73	1.25
Minimum	27.54	1.59	0.99	4.16	0.71	3.20	0.96	0.40	0.39	0.64
MIS 3										
180	35.71	1.67	1.07	2.36	0.73	1.63	0.60	0.29	0.32	0.43
190	39.14	1.62	0.99	2.18	0.63	1.54	0.64	0.16	0.36	0.39
200	36.17	1.63	1.04	2.29	0.46	1.83	0.84	0.17	0.41	0.41
210	37.25	1.61	1.01	2.22	0.45	1.77	0.68	0.12	0.54	0.43
220	34.55	1.69	1.10	2.43	0.58	1.84	0.76	0.12	0.49	0.48
230	33.56	1.67	1.11	2.44	0.50	1.94	0.79	0.16	0.41	0.59
Average	36.06	1.65	1.05	2.32	0.56	1.76	0.72	0.17	0.42	0.45
Maximum	39.14	1.69	1.11	2.44	0.73	1.94	0.84	0.29	0.54	0.59
Minimum	33.56	1.61	0.99	2.18	0.45	1.54	0.60	0.12	0.32	0.34
Overall Average	35.45	1.65	1.07	4.74	1.11	3.62	2.00	0.36	0.48	0.85
Glacial-to-Interglacial percentual deviation (%) as shown in Fig. 6.8				**-32.77**	**-22.32**	**-35.79**	**-60.17**	**-7.23**	**28.78**	**-24.23**
M35042										
MIS1										
0	35.69	1.65	1.06	3.26	0.49	2.77	2.09	0.21	0.28	0.19
10	38.81	1.58	0.97	2.98	0.67	2.31	1.42	0.12	0.40	0.36
20	37.36	1.70	1.06	3.27	0.71	2.56	1.58	0.20	0.38	0.40
30	38.60	1.56	0.96	2.95	0.71	2.24	1.24	0.12	0.47	0.40
Average	37.61	1.62	1.01	3.11	0.65	2.47	1.58	0.16	0.38	0.34
Maximum	38.81	1.70	1.06	3.27	0.71	2.77	2.09	0.21	0.47	0.40
Minimum	35.69	1.56	0.96	2.95	0.49	2.24	1.24	0.12	0.28	0.19
MIS 2										
40	37.13	1.72	1.08	2.33	0.40	1.93	0.53	0.35	0.51	0.53
50	37.32	1.66	1.04	2.24	0.36	1.88	0.47	0.39	0.51	0.52
60	37.93	1.59	0.99	2.13	0.33	1.81	0.50	0.24	0.55	0.52
Average	37.46	1.65	1.03	2.24	0.36	1.87	0.50	0.33	0.52	0.52
Maximum	37.93	1.72	1.08	2.33	0.40	1.93	0.53	0.39	0.55	0.53
Minimum	37.13	1.59	0.99	2.13	0.33	1.81	0.47	0.24	0.51	0.52
MIS 3										
70	37.65	1.61	1.00	1.23	0.19	1.04	0.34	0.20	0.38	0.12
80	37.61	1.65	1.03	1.26	0.18	1.08	0.39	0.15	0.37	0.17
90	38.25	1.63	1.01	1.24	0.17	1.06	0.34	0.16	0.38	0.19
100	39.30	1.64	1.00	1.22	0.14	1.08	0.35	0.12	0.38	0.23
110	36.77	1.65	1.05	1.29	0.19	1.10	0.38	0.05	0.50	0.17
Average	37.92	1.64	1.02	1.25	0.18	1.07	0.36	0.14	0.40	0.18
Maximum	39.30	1.65	1.05	1.29	0.19	1.10	0.39	0.20	0.50	0.23
Minimum	36.77	1.61	1.00	1.22	0.14	1.04	0.34	0.05	0.37	0.12
MIS 4										
125	36.23	1.84	1.18	3.23	0.30	2.94	0.71	0.49	1.01	0.73
130	32.30	1.54	1.04	2.86	0.16	2.70	0.84	0.46	0.74	0.66
140	34.37	1.72	1.13	2.50	0.25	2.25	0.78	0.14	0.81	0.52
Average	34.30	1.70	1.12	2.86	0.24	2.63	0.78	0.36	0.85	0.64
Maximum	36.23	1.84	1.18	3.23	0.30	2.94	0.84	0.49	1.01	0.73
Minimum	32.30	1.54	1.04	2.50	0.16	2.25	0.71	0.14	0.74	0.52
MIS 5										
160	36.69	1.67	1.06	2.33	0.36	1.97	0.95	0.08	0.64	0.30
170	35.63	1.70	1.10	2.42	0.29	2.13	1.08	0.06	0.69	0.30
180	35.08	1.67	1.09	2.40	0.30	2.10	0.86	0.10	0.76	0.38
190	36.54	1.68	1.06	2.35	0.33	2.02	0.86	0.05	0.77	0.34
198	37.77	1.66	1.03	2.29	0.36	1.93	1.05	0.18	0.49	0.21
220	33.20	1.76	1.17	2.59	0.36	2.23	1.32	0.18	0.48	0.25
228	31.03	1.76	1.22	2.69	0.31	2.38	1.50	0.21	0.41	0.27
250	35.64	1.70	1.09	2.41	0.54	1.88	1.36	0.15	0.21	0.15
260	33.28	1.76	1.17	2.59	0.37	2.23	1.51	0.11	0.32	0.29
270	33.36	1.73	1.15	2.54	0.44	2.10	1.38	0.17	0.30	0.25
280	34.58	1.71	1.12	2.48	0.56	1.91	1.30	0.10	0.27	0.25
286	31.90	1.76	1.20	2.65	0.35	2.31	1.68	0.19	0.26	0.18
293.5	32.32	1.74	1.18	2.60	0.46	2.14	1.39	0.22	0.27	0.26

Physical Properties Data Sheet

Depth (cm) and Marine Isotope Stage (MIS)	Water Content (%)	Wet Bulk Density (g/cm^3)	Dry Bulk Density (g/cm^3)	MAR Bulk sediment ($g/cm^2/ky$)	MAR Coarse fraction ($g/cm^2/ky$)	MAR Fine fraction ($g/cm^2/ky$)	MAR Aragonite fine ($g/cm^2/ky$)	MAR HMC fine ($g/cm^2/ky$)	MAR LMC fine ($g/cm^2/ky$)	MAR Non Carbonates fine ($g/cm^2/ky$)
Average	34.39	1.72	1.13	2.49	0.39	2.10	1.25	0.14	0.45	0.26
Maximum	37.77	1.76	1.22	2.69	0.56	2.38	1.68	0.22	0.77	0.38
Minimum	31.03	1.66	1.03	2.29	0.29	1.88	0.86	0.05	0.21	0.15
MIS 6										
300	34.59	1.68	1.10	1.82	0.27	1.55	0.51	0.10	0.55	0.39
310	32.32	1.51	1.02	1.69	0.21	1.48	0.42	0.19	0.47	0.40
320	35.97	1.66	1.06	1.75	0.19	1.56	0.42	0.27	0.49	0.39
330	34.68	1.66	1.08	1.78	0.14	1.64	0.37	0.33	0.54	0.41
340	29.85	1.60	1.12	1.85	0.14	1.72	0.38	0.29	0.53	0.52
350	33.97	1.69	1.12	1.85	0.15	1.70	0.38	0.20	0.57	0.55
360	33.66	1.75	1.16	1.91	0.19	1.72	0.43	0.08	0.75	0.46
370	33.56	1.67	1.11	1.83	0.35	1.48	0.42	0.08	0.66	0.32
380	34.04	1.70	1.12	1.86	0.24	1.61	0.48	0.15	0.61	0.37
390	26.01	1.49	1.10	1.82	0.20	1.62	0.64	0.00	0.68	0.30
394.5	29.54	1.80	1.27	2.09	0.21	1.88	1.12	0.13	0.40	0.23
Average	32.56	1.66	1.12	1.84	0.21	1.63	0.50	0.17	0.57	0.39
Maximum	35.97	1.80	1.27	2.09	0.35	1.88	1.12	0.33	0.75	0.55
Minimum	26.01	1.49	1.02	1.69	0.14	1.48	0.37	0.00	0.40	0.23
MIS 7										
414	34.11	1.72	1.13	2.48	0.37	2.11	1.12	0.26	0.43	0.30
420	31.74	1.71	1.17	2.56	0.29	2.27	1.38	0.31	0.31	0.27
430	34.24	1.66	1.09	2.39	0.47	1.93	1.12	0.15	0.41	0.25
440	33.27	1.68	1.12	2.46	0.50	1.96	1.20	0.19	0.33	0.24
450	31.02	1.74	1.20	2.63	0.46	2.18	1.51	0.24	0.26	0.18
455	33.09	1.70	1.14	2.49	0.46	2.03	1.23	0.24	0.32	0.24
460	31.97	1.72	1.17	2.57	0.36	2.20	1.50	0.13	0.37	0.20
490	31.88	1.75	1.19	2.61	0.43	2.18	1.37	0.20	0.44	0.18
500	33.96	1.68	1.11	2.43	0.35	2.08	1.15	0.17	0.49	0.27
510	33.65	1.73	1.15	2.51	0.32	2.19	0.77	0.23	0.65	0.54
520	32.73	1.70	1.14	2.50	0.36	2.15	1.21	0.19	0.42	0.32
530	30.77	1.77	1.23	2.69	0.39	2.30	1.36	0.14	0.49	0.30
540	29.24	1.80	1.28	2.80	0.29	2.51	1.78	0.21	0.37	0.15
Average	32.44	1.72	1.16	2.55	0.39	2.16	1.28	0.20	0.41	0.27
Maximum	34.24	1.80	1.28	2.80	0.50	2.51	1.78	0.31	0.65	0.54
Minimum	29.24	1.66	1.09	2.39	0.29	1.93	0.77	0.13	0.26	0.15
Interglacials	34.81	1.69	1.10	2.72	0.47	2.24	1.37	0.17	0.41	0.29
Glacials	34.78	1.67	1.09	2.31	0.27	2.05	0.59	0.28	0.65	0.52
MIS 3	37.92	1.64	1.02	1.25	0.18	1.07	0.36	0.14	0.40	0.18
Overall Average	34.29	1.68	1.11	2.32	0.35	1.97	0.99	0.19	0.47	0.32
Glacial-to-Interglacial percentual deviation (%) as shown in Fig. 6.8				**-14.84**	**-43.25**	**-8.85**	**-56.74**	**69.19**	**56.73**	**79.04**
M35043										
MIS 1										
0	36.90	1.61	1.02	3.18	0.77	2.41	1.71	0.18	0.32	0.20
10	35.84	1.70	1.09	3.40	0.75	2.65	1.76	0.27	0.37	0.25
20	34.72	1.71	1.11	3.48	0.73	2.75	1.83	0.19	0.41	0.31
30	33.51	1.71	1.14	3.55	0.55	3.00	2.25	0.28	0.28	0.19
40	38.41	1.59	0.98	3.07	1.20	1.87	0.97	0.24	0.41	0.26
Average	35.88	1.66	1.07	3.34	0.80	2.54	1.70	0.23	0.36	0.24
Maximum	38.41	1.71	1.14	3.55	1.20	3.00	2.25	0.28	0.41	0.31
Minimum	33.51	1.59	0.98	3.07	0.55	1.87	0.97	0.18	0.28	0.19
MIS 2										
50	38.08	1.57	0.97	3.00	1.21	1.79	0.89	0.32	0.36	0.22
60	41.86	1.54	0.90	2.77	1.21	1.56	0.83	0.33	0.23	0.18
70	41.06	1.57	0.93	2.85	1.20	1.66	0.90	0.26	0.31	0.19
Average	40.33	1.56	0.93	2.87	1.20	1.67	0.87	0.30	0.30	0.19
Maximum	41.86	1.57	0.97	3.00	1.21	1.79	0.90	0.33	0.36	0.22
Minimum	38.08	1.54	0.90	2.77	1.20	1.56	0.83	0.26	0.23	0.18
MIS 3										
80	37.60	1.62	1.01	0.85	0.27	0.57	0.27	0.09	0.14	0.07
90	36.21	1.68	1.07	0.90	0.19	0.71	0.31	0.07	0.22	0.11
100	36.40	1.69	1.08	0.90	0.16	0.75	0.31	0.07	0.25	0.12
Average	36.74	1.66	1.05	0.88	0.21	0.68	0.30	0.08	0.20	0.10
Maximum	37.60	1.69	1.08	0.90	0.27	0.75	0.31	0.09	0.25	0.12
Minimum	36.21	1.62	1.01	0.85	0.16	0.57	0.27	0.07	0.14	0.07
MIS 4										
110	36.57	1.67	1.06	2.73	0.50	2.23	0.89	0.05	1.01	0.28

Physical Properties Data Sheet

Depth (cm) and Marine Isotope Stage (MIS)	Water Content (%)	Wet Bulk Density (g/cm^3)	Dry Bulk Density (g/cm^3)	MAR Bulk sediment ($g/cm^2/ky$)	MAR Coarse fraction ($g/cm^2/ky$)	MAR Fine fraction ($g/cm^2/ky$)	MAR Aragonite fine ($g/cm^2/ky$)	MAR HMC fine ($g/cm^2/ky$)	MAR LMC fine ($g/cm^2/ky$)	MAR Non Carbonates fine ($g/cm^2/ky$)
120	34.52	1.65	1.08	2.79	0.60	2.19	1.00	0.17	0.72	0.31
Average	35.55	1.66	1.07	2.76	0.55	2.21	0.94	0.11	0.86	0.29
Maximum	36.57	1.67	1.08	2.79	0.60	2.23	1.00	0.17	1.01	0.31
Minimum	34.52	1.65	1.06	2.73	0.50	2.19	0.89	0.05	0.72	0.28
MIS 5										
130	36.38	1.62	1.03	2.83	0.53	2.31	1.14	0.16	0.70	0.31
140	34.46	1.67	1.09	3.01	0.37	2.64	1.40	0.13	0.82	0.29
150	34.96	1.70	1.11	3.05	0.43	2.62	1.56	0.05	0.80	0.21
160	35.76	1.66	1.07	2.94	0.42	2.52	1.44	0.06	0.78	0.24
170	36.35	1.65	1.05	2.89	0.68	2.22	1.17	0.04	0.69	0.32
180	36.49	1.66	1.06	2.90	0.47	2.44	1.30	0.03	0.82	0.29
190	36.45	1.68	1.07	2.94	0.53	2.41	1.32	0.09	0.68	0.32
200	33.58	1.74	1.15	3.17	0.48	2.69	1.78	0.13	0.55	0.23
210	32.83	1.75	1.18	3.23	0.52	2.71	1.91	0.25	0.34	0.21
220	30.55	1.75	1.22	3.35	0.41	2.94	2.09	0.18	0.42	0.25
240	32.39	1.71	1.16	3.18	0.56	2.62	1.79	0.19	0.40	0.25
250	33.03	1.68	1.12	3.09	0.34	2.75	2.07	0.17	0.31	0.20
260	32.65	1.70	1.15	3.16	0.39	2.76	2.07	0.18	0.35	0.17
270	32.46	1.75	1.18	3.24	0.47	2.78	2.02	0.19	0.38	0.19
280	32.57	1.73	1.17	3.21	0.67	2.54	1.82	0.15	0.41	0.17
290	31.04	1.74	1.20	3.30	0.48	2.83	2.12	0.24	0.33	0.13
Average	33.87	1.70	1.13	3.09	0.48	2.61	1.69	0.14	0.55	0.24
Maximum	36.49	1.75	1.22	3.35	0.68	2.94	2.12	0.25	0.82	0.32
Minimum	30.55	1.62	1.03	2.83	0.34	2.22	1.14	0.03	0.31	0.13
MIS 6										
300	37.11	1.61	1.01	1.88	0.39	1.49	0.71	0.15	0.42	0.22
310	29.06	1.63	1.16	2.14	0.61	1.54	0.57	0.33	0.38	0.26
320	37.61	1.61	1.00	1.86	0.59	1.27	0.58	0.15	0.37	0.17
330	33.78	1.71	1.13	2.09	0.44	1.65	0.54	0.44	0.39	0.28
340	34.96	1.67	1.09	2.01	0.45	1.56	0.57	0.26	0.40	0.33
350	33.70	1.74	1.15	2.13	0.36	1.77	0.71	0.22	0.47	0.38
360	32.79	1.74	1.17	2.17	0.39	1.78	0.72	0.11	0.68	0.28
370	32.40	1.73	1.17	2.17	0.33	1.84	0.83	0.15	0.60	0.26
380	33.10	1.75	1.17	2.16	0.36	1.81	0.84	0.13	0.65	0.18
400	34.36	1.65	1.08	2.00	0.30	1.71	1.03	0.07	0.48	0.13
410	31.55	1.74	1.19	2.20	0.33	1.87	1.21	0.11	0.41	0.14
Average	33.68	1.69	1.12	2.07	0.41	1.66	0.75	0.19	0.47	0.24
Maximum	37.61	1.75	1.19	2.20	0.61	1.87	1.21	0.44	0.68	0.38
Minimum	29.06	1.61	1.00	1.86	0.30	1.27	0.54	0.07	0.37	0.13
MIS 7										
420	31.62	1.74	1.19	2.38	0.41	1.97	1.32	0.09	0.45	0.12
430	32.13	1.71	1.16	2.32	0.37	1.94	1.36	0.13	0.35	0.11
Average	31.88	1.72	1.17	2.35	0.39	1.96	1.34	0.11	0.40	0.12
Maximum	32.13	1.74	1.19	2.38	0.41	1.97	1.36	0.13	0.45	0.12
Minimum	31.62	1.71	1.16	2.32	0.37	1.94	1.32	0.09	0.35	0.11
Interglacials	33.87	1.70	1.12	2.93	0.56	2.37	1.58	0.16	0.43	0.20
Glacials	36.52	1.64	1.04	2.57	0.72	1.85	0.86	0.20	0.55	0.24
MIS 3	36.74	1.66	1.05	0.88	0.21	0.68	0.30	0.08	0.20	0.10
Overall Average	35.09	1.68	1.09	2.74	0.55	2.18	1.34	0.15	0.48	0.21
Glacial-to-Interglacial percentual deviation (%) as shown in Fig. 6.8				**-12.19**	**29.43**	**-21.99**	**-45.67**	**26.47**	**25.70**	**22.58**
M35048										
MIS 1										
0	34.33	1.67	1.10	5.92	1.35	4.57	3.51	0.45	0.26	0.36
10	31.29	1.75	1.21	6.51	1.63	4.88	3.74	0.47	0.26	0.41
20	33.02	1.71	1.14	6.18	1.88	4.30	3.39	0.35	0.25	0.31
30	29.78	1.80	1.26	6.83	1.91	4.92	3.97	0.33	0.27	0.34
40	30.18	1.73	1.21	6.53	1.58	4.95	4.09	0.31	0.22	0.34
50	29.24	1.85	1.31	7.05	1.17	5.89	5.01	0.22	0.23	0.42
60	28.47	1.82	1.30	7.04	1.94	5.11	4.25	0.29	0.18	0.38
Average	30.90	1.76	1.22	6.58	1.63	4.95	4.00	0.35	0.24	0.37
Maximum	34.33	1.85	1.31	7.05	1.94	5.89	5.01	0.47	0.27	0.42
Minimum	28.47	1.67	1.10	5.92	1.17	4.30	3.39	0.22	0.18	0.31

Physical Properties Data Sheet

Depth (cm) and Marine Isotope Stage (MIS)	Water Content (%)	Wet Bulk Density (g/cm^3)	Dry Bulk Density (g/cm^3)	MAR Bulk sediment ($g/cm^2/ky$)	MAR Coarse fraction ($g/cm^2/ky$)	MAR Fine fraction ($g/cm^2/ky$)	MAR Aragonite fine ($g/cm^2/ky$)	MAR HMC fine ($g/cm^2/ky$)	MAR LMC fine ($g/cm^2/ky$)	MAR Non Carbonates fine ($g/cm^2/ky$)
MIS 2										
70	29.03	1.77	1.26	2.20	0.92	1.28	1.08	0.07	0.06	0.07
90	29.36	1.80	1.27	2.22	0.83	1.40	0.90	0.07	0.33	0.10
Average	29.19	1.78	1.26	2.21	0.87	1.34	0.99	0.07	0.19	0.08
Maximum	29.36	1.80	1.27	2.22	0.92	1.40	1.08	0.07	0.33	0.10
Minimum	29.03	1.77	1.26	2.20	0.83	1.28	0.90	0.07	0.06	0.07
MIS 3										
100	27.63	1.83	1.33	0.42	0.07	0.35	0.26	0.01	0.07	0.02
Average	27.63	1.83	1.33	0.42	0.07	0.35	0.26	0.01	0.07	0.02
Maximum	27.63	1.83	1.33	0.42	0.07	0.35	0.26	0.01	0.07	0.02
Minimum	27.63	1.83	1.33	0.42	0.07	0.35	0.26	0.01	0.07	0.02
MIS 4										
110	28.86	1.91	1.36	2.25	0.66	1.59	1.11	0.17	0.19	0.12
120	27.58	1.87	1.35	2.25	0.91	1.34	1.00	0.11	0.13	0.10
130	27.71	1.80	1.30	2.15	0.40	1.75	1.31	0.08	0.22	0.13
Average	28.05	1.86	1.34	2.22	0.66	1.56	1.14	0.12	0.18	0.12
Maximum	28.86	1.91	1.36	2.25	0.91	1.75	1.31	0.17	0.22	0.13
Minimum	27.58	1.80	1.30	2.15	0.40	1.34	1.00	0.08	0.13	0.10
MIS 5										
140	28.32	1.80	1.29	4.06	0.72	3.34	2.62	0.15	0.36	0.21
150	28.02	1.81	1.30	4.11	0.63	3.48	2.71	0.12	0.39	0.25
160	27.85	1.81	1.31	4.13	0.52	3.60	2.89	0.15	0.35	0.21
170	26.86	1.80	1.31	4.14	1.04	3.10	2.50	0.13	0.28	0.20
180	28.09	1.85	1.33	4.19	0.82	3.37	2.77	0.16	0.21	0.22
190	27.40	1.86	1.35	4.25	1.00	3.25	2.64	0.07	0.33	0.20
200	28.83	1.80	1.28	4.05	0.75	3.30	2.62	0.17	0.27	0.24
210	27.55	1.84	1.33	4.19	0.63	3.57	2.81	0.18	0.33	0.25
220	28.86	1.76	1.25	3.94	0.55	3.38	2.68	0.06	0.36	0.28
230	27.67	1.88	1.36	4.28	1.06	3.22	2.57	0.07	0.34	0.24
240	28.87	1.80	1.28	4.02	0.72	3.31	2.63	0.12	0.34	0.22
250	28.38	1.80	1.29	4.07	0.75	3.31	2.59	0.07	0.45	0.21
260	27.69	1.82	1.32	4.15	0.58	3.57	2.81	0.13	0.41	0.22
270	24.78	1.86	1.40	4.40	0.75	3.65	3.01	0.07	0.37	0.20
280	29.09	1.79	1.27	4.00	0.40	3.59	3.03	0.12	0.24	0.20
290	28.08	1.80	1.30	4.08	0.27	3.81	3.14	0.11	0.24	0.32
Average	27.90	1.82	1.31	4.13	0.70	3.43	2.75	0.12	0.33	0.23
Maximum	29.09	1.88	1.40	4.40	1.06	3.81	3.14	0.18	0.45	0.32
Minimum	24.78	1.76	1.25	3.94	0.27	3.10	2.50	0.06	0.21	0.20
MIS 6										
300	27.12	1.84	1.34	0.55	0.10	0.45	0.37	0.02	0.03	0.03
310	26.81	1.80	1.32	0.54	0.23	0.31	0.24	0.02	0.03	0.02
330	27.36	1.82	1.32	0.54	0.27	0.27	0.17	0.01	0.08	0.02
340	26.31	1.98	1.46	0.60	0.17	0.43	0.31	0.01	0.09	0.02
350	28.98	1.83	1.30	0.53	0.12	0.41	0.32	0.01	0.06	0.03
Average	27.32	1.85	1.35	0.55	0.18	0.38	0.28	0.01	0.06	0.02
Maximum	28.98	1.98	1.46	0.60	0.27	0.45	0.37	0.02	0.09	0.03
Minimum	26.31	1.80	1.30	0.53	0.10	0.27	0.17	0.01	0.03	0.02
MIS 7										
360	28.44	1.82	1.30	3.51	0.55	2.96	2.24	0.05	0.49	0.18
370	27.28	1.85	1.35	3.62	0.63	2.99	2.25	0.12	0.42	0.20
380	27.10	1.84	1.34	3.62	0.73	2.88	2.23	0.07	0.41	0.18
390	27.47	1.86	1.35	3.63	0.80	2.84	2.21	0.01	0.49	0.12
400	26.91	1.83	1.34	3.60	0.47	3.13	2.35	0.07	0.55	0.17
410	28.79	1.80	1.28	3.45	0.50	2.96	2.21	0.08	0.48	0.19
420	26.62	1.87	1.37	3.68	0.53	3.15	2.37	0.11	0.50	0.18
430	28.80	1.81	1.29	3.47	0.42	3.05	2.31	0.13	0.44	0.17
440	28.12	1.82	1.31	3.52	0.51	3.01	2.43	0.07	0.35	0.16
450	29.12	1.80	1.28	3.43	0.60	2.83	2.14	0.01	0.53	0.15
460	28.49	1.81	1.29	3.48	0.56	2.92	2.16	0.05	0.55	0.16
470	28.70	1.78	1.27	3.42	0.32	3.10	2.14	0.00	0.78	0.18
480	28.13	1.78	1.28	3.45	0.39	3.05	2.36	0.07	0.45	0.18
490	27.78	1.82	1.32	3.55	0.40	3.15	2.54	0.03	0.36	0.22
500	28.97	1.82	1.29	3.47	0.77	2.70	2.02	0.09	0.41	0.19
Average	28.05	1.82	1.31	3.53	0.54	2.98	2.26	0.06	0.48	0.17
Maximum	29.12	1.87	1.37	3.68	0.80	3.15	2.54	0.13	0.78	0.22
Minimum	26.62	1.78	1.27	3.42	0.32	2.70	2.02	0.00	0.35	0.12
MIS 8										
510	30.80	1.78	1.23	3.31	1.11	2.20	1.55	0.16	0.35	0.14
Average	30.80	1.78	1.23	3.31	1.11	2.20	1.55	0.16	0.35	0.14
Maximum	30.80	1.78	1.23	3.31	1.11	2.20	1.55	0.16	0.35	0.14
Minimum	30.80	1.78	1.23	3.31	1.11	2.20	1.55	0.16	0.35	0.14

Physical Properties Data Sheet

Depth (cm) and Marine Isotope Stage (MIS)	Water Content (%)	Wet Bulk Density (g/cm^3)	Dry Bulk Density (g/cm^3)	MAR Bulk sediment (g/cm^2/ky)	MAR Coarse fraction (g/cm^2/ky)	MAR Fine fraction (g/cm^2/ky)	MAR Aragonite fine (g/cm^2/ky)	MAR HMC fine (g/cm^2/ky)	MAR LMC fine (g/cm^2/ky)	MAR Non Carbonates fine (g/cm^2/ky)
Interglacials	28.95	1.80	1.28	4.74	0.96	3.79	3.00	0.18	0.35	0.26
Glacials	28.84	1.82	1.29	2.07	0.70	1.37	0.99	0.09	0.20	0.09
MIS 3	27.63	1.83	1.33	0.42	0.07	0.35	0.26	0.01	0.07	0.02
Overall Average	28.42	1.82	1.30	3.65	0.73	2.92	2.29	0.12	0.32	0.19
Glacial-to-Interglacial percentual deviation (%) as shown in Fig. 6.8				**-56.31**	**-26.59**	**-63.84**	**-66.98**	**-48.54**	**-43.86**	**-64.83**
M35049										
MIS 1										
0	36.97	1.64	1.03	4.56	0.98	3.58	2.52	0.24	0.43	0.39
10	34.60	1.73	1.13	5.01	1.00	4.01	2.78	0.34	0.46	0.42
20	34.19	1.67	1.10	4.87	0.97	3.90	2.75	0.26	0.45	0.43
30	33.24	1.70	1.14	5.02	1.01	4.01	2.93	0.26	0.43	0.40
40	33.05	1.73	1.16	5.11	1.05	4.06	3.05	0.32	0.35	0.35
Average	34.41	1.69	1.11	4.91	1.00	3.91	2.80	0.28	0.42	0.40
Maximum	36.97	1.73	1.16	5.11	1.05	4.06	3.05	0.34	0.46	0.43
Minimum	33.05	1.64	1.03	4.56	0.97	3.58	2.52	0.24	0.35	0.35
MIS 2										
50	35.11	1.66	1.08	1.03	0.31	0.72	0.48	0.08	0.08	0.07
60	37.28	1.63	1.02	0.98	0.45	0.53	0.26	0.10	0.11	0.07
70	35.56	1.68	1.08	1.04	0.36	0.68	0.37	0.09	0.13	0.08
Average	35.98	1.66	1.06	1.02	0.37	0.64	0.37	0.09	0.11	0.07
Maximum	37.28	1.68	1.08	1.04	0.45	0.72	0.48	0.10	0.13	0.08
Minimum	35.11	1.63	1.02	0.98	0.31	0.53	0.26	0.08	0.08	0.07
MIS 3										
80	38.54	1.62	0.99	0.98	0.31	0.68	0.32	0.11	0.16	0.08
90	36.96	1.64	1.04	1.03	0.22	0.81	0.37	0.09	0.25	0.09
100	34.84	1.66	1.08	1.07	0.20	0.87	0.39	0.03	0.33	0.12
110	34.76	1.70	1.11	1.10	0.21	0.89	0.41	0.11	0.25	0.12
120	32.91	1.72	1.15	1.14	0.17	0.97	0.48	0.10	0.25	0.14
130	34.46	1.68	1.10	1.09	0.16	0.94	0.45	0.05	0.27	0.16
Average	35.41	1.67	1.08	1.07	0.21	0.86	0.40	0.08	0.25	0.12
Maximum	38.54	1.72	1.15	1.14	0.31	0.97	0.48	0.11	0.33	0.16
Minimum	32.91	1.62	0.99	0.98	0.16	0.68	0.32	0.03	0.16	0.08
MIS 4										
140	34.46	1.71	1.12	3.74	0.51	3.23	1.76	0.10	0.87	0.50
150	33.99	1.71	1.13	3.75	0.51	3.25	1.84	0.08	0.96	0.37
160	39.00	1.71	1.04	3.47	0.25	3.23	0.00	0.00	0.00	0.36
Average	35.82	1.71	1.10	3.65	0.42	3.23	1.20	0.06	0.61	0.41
Maximum	39.00	1.71	1.13	3.75	0.51	3.25	1.84	0.10	0.96	0.50
Minimum	33.99	1.71	1.04	3.47	0.25	3.23	0.00	0.00	0.00	0.36
MIS 5										
170	29.38	1.68	1.19	3.24	0.60	2.64	1.74	0.23	0.37	0.29
180	34.70	1.70	1.11	3.01	0.52	2.49	1.57	0.22	0.46	0.23
190	34.62	1.70	1.11	3.02	0.43	2.58	1.55	0.26	0.44	0.33
200	33.95	1.81	1.19	3.25	0.43	2.82	1.89	0.13	0.51	0.28
210	30.76	1.76	1.22	3.31	0.42	2.89	2.11	0.15	0.37	0.25
220	28.64	1.83	1.30	3.54	0.56	2.99	2.17	0.21	0.35	0.27
230	27.57	1.85	1.34	3.65	0.39	3.26	2.39	0.23	0.35	0.30
250	31.34	1.75	1.20	3.28	0.44	2.83	2.08	0.19	0.31	0.25
260	33.12	1.74	1.16	3.16	0.27	2.89	2.20	0.20	0.28	0.21
270	33.13	1.71	1.14	3.10	0.25	2.85	2.22	0.14	0.32	0.17
280	34.12	1.68	1.11	3.01	0.35	2.66	1.97	0.19	0.33	0.17
290	32.74	1.72	1.15	3.14	0.41	2.73	1.94	0.16	0.34	0.29
300	32.34	1.71	1.16	3.15	0.53	2.62	1.79	0.15	0.43	0.26
310	31.07	1.78	1.23	3.34	0.57	2.77	1.94	0.19	0.37	0.27
320	26.74	1.87	1.37	3.72	0.77	2.96	2.42	0.27	0.18	0.09
330	30.16	1.80	1.25	3.41	0.95	2.46	1.93	0.18	0.21	0.15
Average	31.52	1.75	1.20	3.27	0.49	2.78	1.99	0.19	0.35	0.24
Maximum	34.70	1.87	1.37	3.72	0.95	3.26	2.42	0.27	0.51	0.33
Minimum	26.74	1.68	1.11	3.01	0.25	2.46	1.55	0.13	0.18	0.09
MIS 6										
340	33.19	1.73	1.15	1.52	0.37	1.16	0.81	0.11	0.17	0.07
350	35.06	1.66	1.08	1.43	0.32	1.11	0.44	0.20	0.24	0.23
360	33.87	1.68	1.11	1.47	0.32	1.15	0.00	0.00	0.00	0.29
370	34.26	1.70	1.12	1.48	0.23	1.25	0.48	0.20	0.35	0.22
380	33.04	1.69	1.13	1.50	0.23	1.27	0.52	0.09	0.47	0.20
390	33.63	1.71	1.14	1.50	0.26	1.24	0.59	0.08	0.42	0.15
400	32.51	1.73	1.16	1.54	0.28	1.26	0.58	0.10	0.42	0.16
410	31.04	1.74	1.20	1.58	0.24	1.35	0.68	0.11	0.42	0.14

Physical Properties Data Sheet

Depth (cm) and Marine Isotope Stage (MIS)	Water Content (%)	Wet Bulk Density (g/cm^3)	Dry Bulk Density (g/cm^3)	MAR Bulk sediment (g/cm^2/ky)	MAR Coarse fraction (g/cm^2/ky)	MAR Fine fraction (g/cm^2/ky)	MAR Aragonite fine (g/cm^2/ky)	MAR HMC fine (g/cm^2/ky)	MAR LMC fine (g/cm^2/ky)	MAR Non Carbonates fine (g/cm^2/ky)
Average	33.33	1.71	1.14	1.50	0.28	1.22	0.51	0.11	0.31	0.18
Maximum	35.06	1.74	1.20	1.58	0.37	1.35	0.81	0.20	0.47	0.29
Minimum	31.04	1.66	1.08	1.43	0.23	1.11	0.00	0.00	0.00	0.07
MIS 7										
430	33.76	1.69	1.12	4.18	0.61	3.56	2.18	0.31	0.71	0.36
440	31.11	1.73	1.19	4.44	0.59	3.85	2.53	0.44	0.45	0.43
450	29.91	1.80	1.26	4.71	0.82	3.89	2.79	0.38	0.49	0.23
460	29.85	1.77	1.24	4.62	0.72	3.90	2.77	0.42	0.48	0.23
470	29.92	1.81	1.27	4.74	0.73	4.01	3.06	0.24	0.54	0.17
480	29.85	1.80	1.26	4.71	0.69	4.02	3.10	0.31	0.45	0.16
490	29.61	1.82	1.28	4.78	0.65	4.13	3.00	0.35	0.55	0.23
500	28.90	1.82	1.30	4.84	0.44	4.39	3.40	0.46	0.42	0.12
510	26.90	1.87	1.37	5.10	0.95	4.14	3.41	0.40	0.28	0.05
Average	29.98	1.79	1.25	4.68	0.69	3.99	2.92	0.37	0.48	0.22
Maximum	33.76	1.87	1.37	5.10	0.95	4.39	3.41	0.46	0.71	0.43
Minimum	26.90	1.69	1.12	4.18	0.44	3.56	2.18	0.24	0.28	0.05
Interglacials	31.97	1.75	1.19	4.29	0.73	3.56	2.57	0.28	0.42	0.29
Glacials	35.04	1.69	1.10	2.06	0.36	1.70	0.69	0.09	0.34	0.22
MIS 3	35.41	1.67	1.08	1.07	0.21	0.86	0.40	0.08	0.25	0.12
Overall Average	32.81	1.73	1.16	3.03	0.50	2.53	1.67	0.19	0.37	0.23
Glacial-to-Interglacial percentual deviation (%) as shown in Fig. 6.8				**-52.00**	**-50.86**	**-52.23**	**-73.00**	**-69.09**	**-18.31**	**-22.47**
M35052										
MIS 1										
0	44.06	1.53	0.85	2.84	0.71	2.13	0.85	0.11	0.52	0.65
20	43.13	1.51	0.86	2.86	1.13	1.73	0.78	0.15	0.40	0.40
30	41.42	1.49	0.87	2.91	0.87	2.05	0.65	0.18	0.56	0.65
Average	42.87	1.51	0.86	2.87	0.90	1.97	0.76	0.15	0.49	0.57
Maximum	44.06	1.53	0.87	2.91	1.13	2.13	0.85	0.18	0.56	0.65
Minimum	41.42	1.49	0.85	2.84	0.71	1.73	0.65	0.11	0.40	0.40
MIS 2										
40	42.01	1.56	0.90	1.20	0.25	0.95	0.20	0.08	0.26	0.41
50	41.67	1.57	0.92	1.22	0.24	0.98	0.12	0.09	0.31	0.46
Average	41.84	1.57	0.91	1.21	0.25	0.96	0.16	0.09	0.28	0.44
Maximum	42.01	1.57	0.92	1.22	0.25	0.98	0.20	0.09	0.31	0.46
Minimum	41.67	1.56	0.90	1.20	0.24	0.95	0.12	0.08	0.26	0.41
MIS 3										
60	42.94	1.58	0.90	3.08	0.50	2.58	0.41	0.30	0.82	1.05
70	43.19	1.55	0.88	3.01	0.51	2.50	0.32	0.23	0.65	1.29
80	42.26	1.56	0.90	3.07	0.40	2.67	0.39	0.26	0.70	1.32
95	42.87	1.54	0.88	3.00	0.56	2.44	0.45	0.20	0.72	1.07
100	40.45	1.59	0.95	3.23	0.70	2.53	0.52	0.21	0.73	1.06
110	43.27	1.54	0.87	2.97	0.67	2.30	0.47	0.16	0.73	0.94
120	43.84	1.53	0.86	2.94	0.62	2.32	0.49	0.21	0.67	0.94
130	43.63	1.51	0.85	2.90	0.68	2.22	0.50	0.15	0.66	0.91
140	44.16	1.54	0.86	2.93	0.49	2.44	0.54	0.15	0.76	0.98
150	42.27	1.56	0.90	3.07	0.72	2.35	0.61	0.14	0.92	0.69
220	40.35	1.57	0.94	3.19	1.21	1.98	0.49	0.17	0.63	0.69
230	41.40	1.55	0.91	3.10	0.51	2.59	0.37	0.29	0.67	1.26
Average	42.55	1.55	0.89	3.04	0.63	2.41	0.46	0.21	0.72	1.02
Maximum	44.16	1.59	0.95	3.23	1.21	2.67	0.61	0.30	0.92	1.32
Minimum	40.35	1.51	0.85	2.90	0.40	1.98	0.32	0.14	0.63	0.69
MIS 4										
240	42.76	1.53	0.88	1.32	0.18	1.14	0.15	0.10	0.30	0.59
250	42.17	1.65	0.96	2.45	0.37	2.08	0.39	0.18	0.48	1.03
Average	42.47	1.59	0.92	1.88	0.27	1.61	0.27	0.14	0.39	0.81
Maximum	42.76	1.65	0.96	2.45	0.37	2.08	0.39	0.18	0.48	1.03
Minimum	42.17	1.53	0.88	1.32	0.18	1.14	0.15	0.10	0.30	0.59
MIS 5										
260	43.22	1.57	0.89	2.28	0.44	1.84	0.49	0.14	0.43	0.78
270	42.64	1.56	0.89	2.29	0.47	1.82	0.58	0.10	0.50	0.64
280	42.01	1.55	0.90	2.31	0.56	1.75	0.61	0.08	0.57	0.50
290	41.02	1.58	0.93	2.39	0.46	1.93	0.57	0.11	0.48	0.78
300	40.26	1.57	0.94	2.40	0.57	1.83	0.57	0.12	0.61	0.54
310	41.00	1.53	0.90	2.31	0.54	1.77	0.50	0.10	0.65	0.51
320	38.45	1.64	1.01	2.58	0.72	1.87	0.55	0.05	0.78	0.48
330	39.87	1.62	0.97	2.50	0.73	1.77	0.63	0.05	0.61	0.47

Physical Properties Data Sheet

Depth (cm) and Marine Isotope Stage (MIS)	Water Content (%)	Wet Bulk Density (g/cm^3)	Dry Bulk Density (g/cm^3)	MAR Bulk sediment ($g/cm^2/ky$)	MAR Coarse fraction ($g/cm^2/ky$)	MAR Fine fraction ($g/cm^2/ky$)	MAR Aragonite fine ($g/cm^2/ky$)	MAR HMC fine ($g/cm^2/ky$)	MAR LMC fine ($g/cm^2/ky$)	MAR Non Carbonates fine ($g/cm^2/ky$)
340	38.68	1.59	0.98	2.50	0.58	1.92	0.66	0.09	0.55	0.62
350	39.99	1.56	0.94	2.39	0.47	1.92	0.67	0.02	0.63	0.60
370	38.96	1.59	0.97	2.48	0.64	1.84	0.71	0.09	0.53	0.52
380	41.99	1.56	0.91	2.32	0.73	1.60	0.65	0.07	0.45	0.43
390	40.81	1.56	0.93	2.37	0.95	1.42	0.57	0.02	0.51	0.32
Average	40.68	1.58	0.94	2.39	0.60	1.79	0.60	0.08	0.56	0.55
Maximum	43.22	1.64	1.01	2.58	0.95	1.93	0.71	0.14	0.78	0.78
Minimum	38.45	1.53	0.89	2.28	0.44	1.42	0.49	0.02	0.43	0.32
MIS 6										
400	37.48	1.62	1.02	1.55	0.22	1.34	0.28	0.04	0.56	0.45
410	39.62	1.55	0.94	1.43	0.13	1.30	0.22	0.04	0.46	0.58
420	36.77	1.60	1.01	1.55	0.23	1.32	0.21	0.05	0.55	0.51
430	40.26	1.61	0.96	1.47	0.20	1.27	0.22	0.07	0.45	0.52
440	43.54	1.68	0.95	1.45	0.11	1.34	0.28	0.07	0.49	0.49
495	39.92	1.62	0.97	1.49	0.27	1.21	0.27	0.15	0.34	0.46
500	43.12	1.52	0.87	1.32	0.21	1.11	0.19	0.08	0.30	0.54
590	40.59	1.57	0.93	1.42	0.32	1.10	0.25	0.07	0.35	0.42
600	39.94	1.60	0.96	1.47	0.33	1.15	0.29	0.08	0.34	0.44
610	39.74	1.58	0.95	1.46	0.26	1.20	0.23	0.08	0.37	0.53
Average	40.10	1.59	0.96	1.46	0.23	1.23	0.24	0.07	0.42	0.49
Maximum	43.54	1.68	1.02	1.55	0.33	1.34	0.29	0.15	0.56	0.58
Minimum	36.77	1.52	0.87	1.32	0.11	1.10	0.19	0.04	0.30	0.42
MIS 7										
620	39.03	1.57	0.96	1.98	0.33	1.65	0.29	0.07	0.62	0.66
630	40.85	1.58	0.93	1.93	0.36	1.57	0.35	0.10	0.51	0.61
640	41.85	1.56	0.90	1.87	0.36	1.51	0.29	0.06	0.57	0.59
650	40.11	1.59	0.95	1.97	0.61	1.36	0.42	0.04	0.48	0.42
660	39.90	1.61	0.97	2.01	0.55	1.45	0.45	0.10	0.45	0.46
670	39.94	1.56	0.94	1.94	0.56	1.39	0.45	0.05	0.48	0.41
680	39.61	1.59	0.96	1.98	0.62	1.36	0.46	0.03	0.53	0.35
690	37.89	1.60	1.00	2.06	0.42	1.64	0.48	0.02	0.71	0.42
700	37.20	1.66	1.04	2.16	0.36	1.80	0.45	0.06	0.63	0.66
710	40.23	1.58	0.94	1.95	0.36	1.59	0.35	0.03	0.59	0.63
720	38.25	1.59	0.98	2.03	0.52	1.51	0.48	0.05	0.51	0.46
730	37.43	1.65	1.03	2.14	0.52	1.62	0.51	0.06	0.68	0.37
740	36.78	1.66	1.05	2.17	0.29	1.88	0.45	0.02	0.82	0.60
750	38.66	1.64	1.00	1.59	0.21	1.39	0.23	0.04	0.62	0.50
Average	39.12	1.60	0.98	1.99	0.43	1.55	0.41	0.05	0.59	0.51
Maximum	41.85	1.66	1.05	2.17	0.62	1.88	0.51	0.10	0.82	0.66
Minimum	36.78	1.56	0.90	1.59	0.21	1.36	0.23	0.02	0.45	0.35
MIS 8										
870	39.25	1.60	0.97	1.54	0.31	1.23	0.30	0.07	0.49	0.37
880	38.70	1.62	0.99	1.58	0.28	1.30	0.26	0.08	0.58	0.38
900	38.33	1.60	0.99	1.57	0.12	1.45	0.22	0.05	0.58	0.60
910	39.83	1.55	0.93	1.48	0.16	1.33	0.23	0.09	0.50	0.51
920	39.43	1.60	0.97	1.54	0.18	1.37	0.29	0.05	0.56	0.46
930	39.51	1.64	0.99	1.57	0.39	1.18	0.29	0.07	0.56	0.27
940	37.97	1.62	1.01	1.60	0.22	1.38	0.23	0.07	0.68	0.40
Average	39.00	1.60	0.98	1.55	0.24	1.32	0.26	0.07	0.56	0.43
Maximum	39.83	1.64	1.01	1.60	0.39	1.45	0.30	0.09	0.68	0.60
Minimum	37.97	1.55	0.93	1.48	0.12	1.18	0.22	0.05	0.49	0.27
MIS 9										
950	38.37	1.60	0.99	3.10	0.33	2.78	0.34	0.13	1.44	0.87
960	39.98	1.58	0.95	2.97	0.62	2.36	0.36	0.06	1.30	0.64
965	38.06	1.62	1.00	0.00	0.00	0.00	0.00	0.00	0.00	0.00
Average	38.80	1.60	0.98	2.03	0.31	1.71	0.23	0.06	0.91	0.50
Maximum	39.98	1.62	1.00	3.10	0.62	2.78	0.36	0.13	1.44	0.87
Minimum	38.06	1.58	0.95	0.00	0.00	0.00	0.00	0.00	0.00	0.00
Interglacials	40.37	1.57	0.94	2.32	0.56	1.76	0.50	0.09	0.64	0.53
Glacials	40.85	1.59	0.94	1.53	0.25	1.28	0.23	0.09	0.41	0.54
MIS 3	42.55	1.55	0.89	3.04	0.63	2.41	0.46	0.21	0.72	1.02
Overall Average	40.53	1.58	0.94	2.15	0.46	1.69	0.41	0.10	0.57	0.61
Glacial-to-Interglacial percentual deviation (%) as shown in Fig. 6.8				**-34.12**	**-56.26**	**-27.02**	**-53.48**	**7.78**	**-35.06**	**1.89**

Physical Properties Data Sheet

Depth (cm) and Marine Isotope Stage (MIS)	Water Content (%)	Wet Bulk Density (g/cm^3)	Dry Bulk Density (g/cm^3)	MAR Bulk sediment ($g/cm^2/ky$)	MAR Coarse fraction ($g/cm^2/ky$)	MAR Fine fraction ($g/cm^2/ky$)	MAR Aragonite fine ($g/cm^2/ky$)	MAR HMC fine ($g/cm^2/ky$)	MAR LMC fine ($g/cm^2/ky$)	MAR Non Carbonates fine ($g/cm^2/ky$)
PC059										
MIS 1										
0	37.46	1.61	1.01	0.54	0.13	0.41	0.26	0.03	0.09	0.04
2.5	37.46	1.61	1.01	0.54	0.15	0.39	0.25	0.03	0.08	0.04
Average	37.46	1.61	1.01	0.54	0.14	0.40	0.25	0.03	0.08	0.04
Maximum	37.46	1.61	1.01	0.54	0.15	0.41	0.26	0.03	0.09	0.04
Minimum	37.46	1.61	1.01	0.54	0.13	0.39	0.25	0.03	0.08	0.04
MIS 2										
10.5	40.45	1.64	0.98	0.90	0.13	0.77	0.21	0.09	0.21	0.26
Average	40.45	1.64	0.98	0.90	0.13	0.77	0.21	0.09	0.21	0.26
Maximum	40.45	1.64	0.98	0.90	0.13	0.77	0.21	0.09	0.21	0.26
Minimum	40.45	1.64	0.98	0.90	0.13	0.77	0.21	0.09	0.21	0.26
MIS 3										
20.5	38.03	2.14	1.32	2.95	0.30	2.66	0.93	0.20	0.75	0.78
30.5	38.74	1.62	0.99	2.21	0.34	1.87	0.54	0.21	0.57	0.55
40.5	40.12	1.54	0.92	2.06	0.36	1.70	0.42	0.13	0.63	0.51
50.5	39.57	1.67	1.01	2.24	0.39	1.86	0.64	0.22	0.54	0.46
70.5	38.84	1.65	1.01	2.25	0.32	1.93	0.61	0.15	0.75	0.42
80.5	38.77	1.64	1.00	2.23	0.30	1.93	0.62	0.21	0.54	0.56
83.5	38.97	1.72	1.05	2.34	0.36	1.98	0.71	0.19	0.59	0.49
88.5	38.81	1.67	1.02	2.29	0.31	1.97	0.76	0.19	0.49	0.54
Average	38.98	1.71	1.04	2.32	0.33	1.99	0.66	0.19	0.61	0.54
Maximum	40.12	2.14	1.32	2.95	0.39	2.66	0.93	0.22	0.75	0.78
Minimum	38.03	1.54	0.92	2.06	0.30	1.70	0.42	0.13	0.49	0.42
MIS 4										
96.5	39.74	1.63	0.98	1.43	0.13	1.30	0.36	0.19	0.40	0.35
106.5	39.13	1.62	0.99	1.44	0.17	1.27	0.37	0.12	0.32	0.45
Average	39.43	1.62	0.98	1.44	0.15	1.29	0.37	0.16	0.36	0.40
Maximum	39.74	1.63	0.99	1.44	0.17	1.30	0.37	0.19	0.40	0.45
Minimum	39.13	1.62	0.98	1.43	0.13	1.27	0.36	0.12	0.32	0.35
MIS 5										
116.5	38.13	1.63	1.01	1.91	0.25	1.66	0.58	0.15	0.50	0.43
120.5	38.54	1.58	0.97	1.85	0.33	1.52	0.61	0.05	0.45	0.41
136.5	38.17	1.67	1.03	1.96	0.27	1.69	0.78	0.12	0.44	0.35
146.5	37.02	1.78	1.12	2.13	0.30	1.82	0.91	0.07	0.54	0.30
156.5	38.21	1.63	1.01	1.91	0.25	1.66	0.73	0.07	0.46	0.40
166.5	37.01	1.67	1.05	2.00	0.24	1.76	0.67	0.11	0.60	0.37
176.5	36.63	1.67	1.06	2.01	0.33	1.68	0.73	0.15	0.51	0.29
186.5	34.63	1.74	1.14	2.16	0.47	1.69	0.99	0.01	0.51	0.17
196.5	34.41	1.72	1.13	2.15	0.40	1.75	1.08	0.06	0.41	0.20
213.5	33.45	1.75	1.16	2.21	0.42	1.80	1.03	0.05	0.39	0.32
216.5	33.59	1.73	1.15	2.18	0.28	1.90	1.11	0.10	0.41	0.28
226.5	34.78	1.81	1.18	2.24	0.36	1.88	1.04	0.08	0.52	0.25
232.5	33.83	1.69	1.12	2.13	0.32	1.81	1.16	0.08	0.36	0.21
Average	36.03	1.70	1.09	2.07	0.32	1.74	0.88	0.09	0.47	0.31
Maximum	38.54	1.81	1.18	2.24	0.47	1.90	1.16	0.15	0.60	0.43
Minimum	33.45	1.58	0.97	1.85	0.24	1.52	0.58	0.01	0.36	0.17
MIS 6										
238.5	34.07	1.71	1.13	1.08	0.13	0.96	0.23	0.04	0.38	0.30
246.5	33.43	1.74	1.16	1.11	0.05	1.06	0.32	0.13	0.29	0.32
256.5	36.75	1.68	1.06	1.02	0.12	0.90	0.23	0.09	0.24	0.33
266.5	35.88	1.61	1.03	0.99	0.11	0.88	0.23	0.06	0.28	0.31
276.5	34.56	1.63	1.07	1.02	0.15	0.87	0.21	0.02	0.38	0.26
Average	34.94	1.67	1.09	1.05	0.11	0.93	0.25	0.07	0.31	0.30
Maximum	36.75	1.74	1.16	1.11	0.15	1.06	0.32	0.13	0.38	0.33
Minimum	33.43	1.61	1.03	0.99	0.05	0.87	0.21	0.02	0.24	0.26
MIS 7										
286.5	34.82	1.70	1.11	2.03	0.19	1.84	0.60	0.06	0.62	0.55
296.5	36.61	1.65	1.05	1.92	0.42	1.50	0.68	0.08	0.42	0.32
306.5	33.44	1.77	1.18	2.16	0.42	1.74	0.90	0.07	0.45	0.31
316.5	34.96	1.70	1.11	2.03	0.54	1.49	0.79	0.06	0.40	0.25
326.5	32.92	1.71	1.15	2.10	0.28	1.82	1.13	0.11	0.30	0.28
336.5	33.15	1.71	1.14	2.09	0.28	1.81	1.09	0.05	0.42	0.25
346.5	33.71	1.73	1.15	2.10	0.35	1.75	0.98	0.05	0.46	0.26
356.5	35.17	1.68	1.09	2.00	0.28	1.72	0.83	0.11	0.48	0.31
366.5	34.62	1.68	1.10	2.02	0.24	1.77	0.67	0.11	0.47	0.53
373.5	35.37	1.72	1.11	2.03	0.32	1.71	0.76	0.06	0.44	0.45
378.5	35.67	1.70	1.09	2.00	0.33	1.67	0.75	0.08	0.44	0.40
386.5	30.93	1.76	1.22	2.22	0.35	1.87	1.19	0.08	0.37	0.24
396.5	33.04	1.74	1.17	2.13	0.38	1.75	1.17	0.04	0.40	0.14
Average	34.19	1.71	1.13	2.06	0.34	1.73	0.89	0.07	0.44	0.33
Maximum	36.61	1.77	1.22	2.22	0.54	1.87	1.19	0.11	0.62	0.55
Minimum	30.93	1.65	1.05	1.92	0.19	1.49	0.60	0.04	0.30	0.14

Physical Properties Data Sheet

Depth (cm) and Marine Isotope Stage (MIS)	Water Content (%)	Wet Bulk Density (g/cm^3)	Dry Bulk Density (g/cm^3)	MAR Bulk sediment ($g/cm^2/ky$)	MAR Coarse fraction ($g/cm^2/ky$)	MAR Fine fraction ($g/cm^2/ky$)	MAR Aragonite fine ($g/cm^2/ky$)	MAR HMC fine ($g/cm^2/ky$)	MAR LMC fine ($g/cm^2/ky$)	MAR Non Carbonates fine ($g/cm^2/ky$)
MIS 8										
406.5	35.06	1.67	1.08	1.58	0.24	1.34	0.42	0.12	0.55	0.25
426.5	34.25	1.71	1.13	1.65	0.16	1.49	0.42	0.02	0.70	0.34
436.5	33.39	1.72	1.15	1.67	0.18	1.49	0.45	0.15	0.59	0.31
446.5	34.05	1.70	1.12	1.64	0.16	1.48	0.36	0.05	0.71	0.36
456.5	35.10	1.68	1.09	1.59	0.21	1.38	0.34	0.08	0.55	0.41
466.5	33.24	1.74	1.16	1.70	0.66	1.04	0.49	0.04	0.37	0.13
Average	34.18	1.70	1.12	1.64	0.27	1.37	0.42	0.08	0.58	0.30
Maximum	35.10	1.74	1.16	1.70	0.66	1.49	0.49	0.15	0.71	0.41
Minimum	33.24	1.67	1.08	1.58	0.16	1.04	0.34	0.02	0.37	0.13
Interglacials	35.89	1.67	1.07	1.56	0.27	1.29	0.67	0.06	0.33	0.22
Glacials	37.25	1.66	1.04	1.25	0.17	1.09	0.31	0.10	0.37	0.32
MIS 3	38.98	1.71	1.04	2.32	0.33	1.99	0.66	0.19	0.61	0.54
Overall Average	35.97	1.69	1.09	1.84	0.28	1.56	0.67	0.10	0.46	0.34
Glacial-to-Interglacial percentual deviation (%) as shown in Fig. 6.8				**-19.49**	**-38.26**	**-15.59**	**-53.95**	**55.75**	**10.70**	**40.69**
PC100										
MIS 1										
0	39.98	1.34	0.81	2.55	0.60	1.95	1.36	0.14	0.32	0.14
6	39.98	1.34	0.81	2.55	0.60	1.95	1.36	0.14	0.32	0.14
16	43.05	1.55	0.89	2.81	0.77	2.03	1.26	0.10	0.45	0.23
26	41.66	1.31	0.76	2.41	0.62	1.79	1.00	0.15	0.30	0.34
36	43.11	1.61	0.92	2.91	0.53	2.37	0.71	0.23	0.87	0.56
Average	41.56	1.43	0.84	2.65	0.62	2.02	1.14	0.15	0.45	0.28
Maximum	43.11	1.61	0.92	2.91	0.77	2.37	1.36	0.23	0.87	0.56
Minimum	39.98	1.31	0.76	2.41	0.53	1.79	0.71	0.10	0.30	0.14
MIS 2										
46	46.44	1.80	0.96	2.61	0.42	2.19	0.42	0.24	0.67	0.87
56	43.95	1.58	0.89	2.40	0.34	2.06	0.46	0.27	0.61	0.72
66	42.97	1.85	1.05	2.86	0.36	2.50	0.57	0.32	0.72	0.89
Average	44.45	1.74	0.97	2.62	0.37	2.25	0.49	0.28	0.66	0.82
Maximum	46.44	1.85	1.05	2.86	0.42	2.50	0.57	0.32	0.72	0.89
Minimum	42.97	1.58	0.89	2.40	0.34	2.06	0.42	0.24	0.61	0.72
MIS 3										
76	41.10	1.61	0.95	1.24	0.09	1.15	0.38	0.10	0.30	0.37
86	42.81	1.55	0.89	1.16	0.21	0.95	0.25	0.09	0.33	0.27
96	35.29	1.60	1.03	1.36	0.25	1.10	0.30	0.13	0.33	0.35
106	41.54	1.61	0.94	1.23	0.16	1.07	0.32	0.09	0.34	0.32
116	39.56	1.57	0.95	1.25	0.10	1.15	0.33	0.00	0.50	0.32
Average	40.06	1.59	0.95	1.25	0.16	1.08	0.32	0.08	0.36	0.32
Maximum	42.81	1.61	1.03	1.36	0.25	1.15	0.38	0.13	0.50	0.37
Minimum	35.29	1.55	0.89	1.16	0.09	0.95	0.25	0.00	0.30	0.27
MIS 4										
126	41.74	1.61	0.94	1.36	0.13	1.23	0.28	0.05	0.42	0.47
136	40.36	1.65	0.99	1.43	0.17	1.26	0.32	0.11	0.43	0.41
Average	40.05	1.60	0.96	1.28	0.16	1.11	0.31	0.08	0.38	0.35
Maximum	42.81	1.65	1.03	1.43	0.25	1.26	0.38	0.13	0.50	0.47
Minimum	35.29	1.55	0.89	1.16	0.09	0.95	0.25	0.00	0.30	0.27
MIS 5										
146	38.63	1.72	1.05	2.05	0.31	1.74	0.63	0.03	0.62	0.47
156	37.14	1.66	1.05	2.03	0.22	1.81	0.89	0.04	0.56	0.32
166	37.81	1.64	1.02	1.98	0.30	1.68	0.47	0.02	0.76	0.43
174	37.03	1.68	1.06	2.05	0.34	1.71	0.62	0.02	0.73	0.34
191	36.75	1.68	1.06	2.06	0.42	1.63	0.70	0.00	0.65	0.28
201	35.67	1.65	1.06	2.06	0.15	1.91	0.71	0.06	0.62	0.53
Average	37.17	1.67	1.05	2.04	0.29	1.74	0.67	0.03	0.66	0.39
Maximum	38.63	1.72	1.06	2.06	0.42	1.91	0.89	0.06	0.76	0.53
Minimum	35.67	1.64	1.02	1.98	0.15	1.63	0.47	0.00	0.56	0.28
MIS 6										
210	35.95	1.62	1.04	1.14	0.11	1.03	0.18	0.01	0.56	0.28
219	35.87	1.68	1.08	1.18	0.08	1.10	0.24	0.03	0.48	0.36
228	36.35	1.68	1.07	1.18	0.08	1.10	0.13	0.08	0.50	0.39
238	36.12	1.68	1.07	1.18	0.10	1.08	0.21	0.00	0.47	0.39
248	35.69	1.80	1.16	1.27	0.14	1.13	0.11	0.05	0.64	0.33
258	35.57	1.63	1.05	1.16	0.15	1.01	0.06	0.00	0.62	0.32

Physical Properties Data Sheet

Depth (cm) and Marine Isotope Stage (MIS)	Water Content (%)	Wet Bulk Density (g/cm^3)	Dry Bulk Density (g/cm^3)	MAR Bulk sediment ($g/cm^2/ky$)	MAR Coarse fraction ($g/cm^2/ky$)	MAR Fine fraction ($g/cm^2/ky$)	MAR Aragonite fine ($g/cm^2/ky$)	MAR HMC fine ($g/cm^2/ky$)	MAR LMC fine ($g/cm^2/ky$)	MAR Non Carbonates fine ($g/cm^2/ky$)
Average	35.92	1.68	1.08	1.19	0.11	1.07	0.16	0.03	0.55	0.35
Maximum	36.35	1.80	1.16	1.27	0.15	1.13	0.24	0.08	0.64	0.39
Minimum	35.57	1.62	1.04	1.14	0.08	1.01	0.06	0.00	0.47	0.28
MIS 7										
268	35.41	1.72	1.11	1.89	0.16	1.74	0.70	0.00	0.65	0.39
275	37.99	1.60	0.99	1.70	0.47	1.23	0.51	0.00	0.54	0.19
281	37.17	1.64	1.03	1.76	0.18	1.59	0.79	0.01	0.44	0.34
286	35.66	1.63	1.05	1.80	0.33	1.47	0.75	0.01	0.49	0.22
296	35.18	1.69	1.09	1.87	0.27	1.60	0.73	0.03	0.58	0.25
304	34.21	1.79	1.18	2.02	0.56	1.46	0.73	0.05	0.49	0.19
332	36.48	1.64	1.04	1.78	0.39	1.38	0.76	0.11	0.35	0.17
341	35.57	1.66	1.07	1.83	0.34	1.49	0.84	0.04	0.47	0.15
347	35.37	1.70	1.10	1.88	0.34	1.54	0.66	0.01	0.62	0.25
351	35.84	1.68	1.08	1.84	0.18	1.66	0.52	0.04	0.60	0.50
361	34.18	1.70	1.12	1.91	0.26	1.66	0.75	0.01	0.56	0.33
365	36.62	1.68	1.06	1.82	0.21	1.61	0.51	0.01	0.60	0.49
372	35.50	1.68	1.08	1.85	0.27	1.58	0.73	0.03	0.52	0.30
381	31.96	1.79	1.22	2.08	0.63	1.45	0.93	0.02	0.35	0.14
397	35.68	1.67	1.08	1.84	0.30	1.54	0.82	0.04	0.51	0.17
410	34.39	1.73	1.13	1.94	0.32	1.62	0.43	0.02	0.93	0.24
Average	35.45	1.69	1.09	1.86	0.33	1.54	0.70	0.03	0.54	0.27
Maximum	37.99	1.79	1.22	2.08	0.63	1.74	0.93	0.11	0.93	0.50
Minimum	31.96	1.60	0.99	1.70	0.16	1.23	0.43	0.00	0.35	0.14
MIS 8										
422	35.93	1.65	1.06	1.49	0.16	1.33	0.32	0.03	0.73	0.25
435	34.68	1.74	1.14	1.60	0.24	1.37	0.28	0.04	0.81	0.24
447	34.46	1.68	1.10	1.55	0.15	1.41	0.29	0.05	0.75	0.32
458	35.17	1.70	1.10	1.55	0.10	1.45	0.21	0.00	0.81	0.44
469	34.20	1.74	1.15	1.62	0.25	1.37	0.52	0.01	0.64	0.20
474	33.47	1.72	1.14	1.61	0.30	1.31	0.54	0.08	0.57	0.13
487	32.65	1.75	1.18	1.66	0.17	1.49	0.36	0.10	0.77	0.25
496	33.36	1.73	1.15	1.63	0.14	1.48	0.46	0.06	0.73	0.23
Average	34.24	1.71	1.13	1.59	0.19	1.40	0.37	0.05	0.73	0.26
Maximum	35.93	1.75	1.18	1.66	0.30	1.49	0.54	0.10	0.81	0.44
Minimum	32.65	1.65	1.06	1.49	0.10	1.31	0.21	0.00	0.57	0.13
MIS 9										
507	34.58	1.71	1.12	2.24	0.25	2.00	0.66	0.09	0.94	0.31
516	32.33	1.69	1.15	2.29	0.31	1.98	0.66	0.19	0.94	0.19
Average	33.45	1.70	1.13	2.27	0.28	1.99	0.66	0.14	0.94	0.25
Maximum	34.58	1.71	1.15	2.29	0.31	2.00	0.66	0.19	0.94	0.31
Minimum	32.33	1.69	1.12	2.24	0.25	1.98	0.66	0.09	0.94	0.19
Interglacials	36.91	1.62	1.03	2.20	0.38	1.82	0.79	0.09	0.65	0.30
Glacials	38.67	1.68	1.03	1.67	0.21	1.46	0.33	0.11	0.58	0.44
MIS 3	40.06	1.59	0.95	1.25	0.16	1.08	0.32	0.08	0.36	0.32
Overall Average	37.17	1.66	1.04	1.82	0.28	1.54	0.56	0.07	0.58	0.33
Glacial-to-Interglacial percentual deviation (%) as shown in Fig. 6.8				**-24.26**	**-45.11**	**-20.02**	**-58.12**	**23.84**	**-10.61**	**48.70**

Appendix 7 - Geochemistry analyses

Geochemistry Data Sheet

M35048

Depth (cm)	Age (ky)	Main elements in %										Trace elements in ppm				
		SiO_2	Al_2O_3	MnO	MgO	Na_2O	CaO	TiO_2	P_2O_5	K_2O	Fe_2O_3	Ba	Co	Cr	Cu	La
0	0.00	2.96	0.52	0.01	1.74	1.55	53.11	0.02	0.11	0.09	0.29	34	4	18	118	14
20	2.40	1.85	0.32	0.01	1.59	1.46	54.94	0.02	0.12	0.07	0.18	18	4	18	134	14
40	4.80	2.25	0.5	0.01	1.43	1.44	55.3	0.03	0.12	0.08	0.23	46	4	18	121	14
60	9.00	1.91	0.5	0.01	1.4	1.3	55.23	0.03	0.12	0.08	0.28	46	4	18	129	14
100	53.00	1.52	0.54	0.01	1.19	1.14	57.2	0.03	0.1	0.09	0.23	73	4	18	105	14
120	65.00	1.81	0.61	0.01	1.29	1.15	55.98	0.03	0.1	0.1	0.29	8	4	18	117	14
140	72.50	1.12	0.36	0.01	1.03	1.26	56.88	0.02	0.11	0.06	0.17	8	4	18	119	14
160	80.00	1.11	0.36	0.01	1.02	1.24	56.82	0.02	0.09	0.07	0.2	24	4	18	122	14
180	86.33	1.1	0.38	0.01	1.05	1.23	56.76	0.02	0.08	0.07	0.2	28	4	18	105	14
200	92.67	1.29	0.39	0.01	1.18	1.3	56.25	0.02	0.09	0.07	0.19	29	4	18	101	14
220	99.00	1.63	0.52	0.01	0.96	1.27	56.49	0.03	0.09	0.09	0.25	48	4	18	121	14
240	105.57	1.48	0.52	0.01	0.9	1.23	56.72	0.03	0.11	0.08	0.26	21	4	18	131	14
260	112.14	1.27	0.45	0.01	0.94	1.3	56.65	0.02	0.1	0.07	0.23	8	4	18	106	14
280	118.71	0.85	0.32	0.01	1.01	1.21	56.9	0.02	0.09	0.05	0.18	8	4	18	136	14
300	129.25	1.07	0.42	0.01	1.16	1.26	56.13	0.02	0.09	0.07	0.25	19	4	18	112	14
340	165.33	1.38	0.51	0.01	1.1	1.1	57.51	0.03	0.18	0.08	0.21	49	4	18	114	14
360	194.00	1.41	0.51	0.01	1.02	1.26	56.65	0.03	0.11	0.08	0.25	32	4	18	111	14
380	199.50	1.15	0.43	0.01	1.02	1.15	56.87	0.02	0.09	0.07	0.21	32	4	18	125	14
400	205.00	1.37	0.51	0.01	1.09	1.26	56.64	0.02	0.08	0.08	0.22	14	4	18	118	14
420	210.50	1.24	0.46	0.01	1.04	1.25	56.82	0.02	0.09	0.07	0.24	26	4	18	98	14
440	216.00	1.1	0.41	0.01	0.93	1.22	57.23	0.02	0.09	0.07	0.21	30	4	18	125	14
460	224.80	1.12	0.41	0.01	0.86	1.23	57.4	0.02	0.09	0.07	0.2	41	4	18	128	14
480	233.60	0.48	0.48	0.01	0.86	1.3	56.76	0.02	0.11	0.07	0.29	50	4	18	105	14
500	243.50	0.46	0.46	0.01	0.93	1.19	56.76	0.02	0.09	0.07	0.24	34	4	18	119	14
510	249.00	1.78	0.65	0.01	1.2	1.27	56.1	0.02	0.08	0.11	0.32	8	4	18	111	14

M35049

Depth (cm)	Age (ky)	Main elements in %										Trace elements in ppm				
		SiO_2	Al_2O_3	MnO	MgO	Na_2O	CaO	TiO_2	P_2O_5	K_2O	Fe_2O_3	Ba	Co	Cr	Cu	La
0	0.00	5.17	1.42	0.09	1.32	1.68	51.41	0.06	0.07	0.21	0.65	73	4	18	8	14
10	2.00	4.9	1.45	0.1	1.32	1.43	52.1	0.07	0.082	0.2	0.69	77	9	18	7	16
20	4.00	5.14	1.49	0.03	1.29	1.41	52.09	0.07	0.107	0.22	0.82	90	4	18	5	14
30	6.00	4.52	1.42	0.03	1.25	1.33	52.86	0.06	0.105	0.2	0.67	100	4	18	4	14
40	9.00	3.55	1.27	0.02	1.25	1.32	53.32	0.06	0.117	0.2	0.66	94	4	18	4	14
50	12.00	3.7	1.42	0.03	1.36	1.44	53.26	0.08	0.108	0.22	0.66	73	4	18	8	27
60	15.00	4.32	1.65	0.03	1.57	1.51	52.34	0.08	0.098	0.26	0.72	37	4	18	4	16
70	18.00	4.96	1.97	0.05	1.65	1.27	51.81	0.09	0.109	0.28	1.08	62	4	18	8	21
80	28.00	5.37	2.12	0.08	1.57	1.35	51.56	0.09	0.112	0.28	1.04	33	9	18	15	28
90	33.00	6.31	2.53	0.1	1.57	1.31	50.44	0.12	0.13	0.33	1.21	45	10	18	4	53
100	38.00	5.91	2.34	0.11	1.58	1.36	50.87	0.1	0.124	0.31	1.12	65	5	18	8	26
110	43.00	6.54	2.57	0.11	1.79	1.2	50.13	0.11	0.103	0.33	1.21	63	8	18	9	40
120	48.00	7.04	2.77	0.12	1.75	1.18	49.54	0.13	0.102	0.35	1.3	53	7	18	9	14
130	53.00	6.89	2.72	0.12	1.54	1.17	49.75	0.12	0.077	0.35	1.27	50	7	18	4	29
140	65.00	6.99	2.7	0.12	1.49	1.24	49.69	0.12	0.08	0.37	1.24	59	8	18	7	14
150	67.14	4.84	1.82	0.09	1.29	1.03	52.31	0.08	0.083	0.26	1.06	70	6	18	4	14
170	71.43	5.11	1.86	0.05	1.39	1.27	51.7	0.09	0.081	0.31	0.84	59	4	18	4	29
180	73.57	5.87	2.2	0.06	1.48	1.23	51.1	0.1	0.107	0.32	0.79	51	6	18	4	14
190	75.71	6.23	2.31	0.06	1.49	1.18	50.73	0.1	0.119	0.35	0.88	68	5	18	4	14
200	77.86	4.41	1.59	0.07	1.26	1.2	52.49	0.07	0.11	0.29	0.92	61	6	18	4	27
210	80.00	3.55	1.31	0.05	1.13	1.1	53.66	0.06	0.132	0.23	0.7	63	5	18	4	14
220	82.71	3.9	1.52	0.07	1.23	1	53.4	0.07	0.11	0.24	0.66	52	4	18	4	14
230	85.43	3.87	1.49	0.04	1.41	0.96	53.45	0.07	0.101	0.23	0.59	57	4	18	4	14
250	90.86	4.85	1.74	0.06	1.33	1.16	52.39	0.07	0.11	0.27	0.7	58	4	18	4	14
260	93.57	4.73	1.68	0.04	1.35	1.21	52.11	0.07	0.101	0.25	0.66	75	4	18	4	14
270	96.29	3.97	1.22	0.03	1.23	1.25	52.89	0.05	0.087	0.21	0.64	59	4	18	4	14
280	99.00	4.77	1.44	0.04	1.13	1.23	52.44	0.07	0.096	0.23	0.64	110	5	18	7	14
290	104.75	5.34	1.59	0.04	1.14	1.2	52.23	0.07	0.103	0.25	0.76	85	4	18	4	14
300	110.50	4.44	1.47	0.05	1.12	1.25	53.14	0.06	0.143	0.22	0.67	107	4	18	4	14
310	116.25	3.8	1.37	0.06	1.17	1.15	53.73	0.06	0.143	0.2	0.6	96	4	18	4	14
320	122.00	1.57	0.68	0.03	1.3	1.06	55.47	0.03	0.071	0.12	0.46	65	4	18	4	14
330	126.33	2.24	0.97	0.04	1.22	1.08	54.67	0.04	0.092	0.15	0.5	84	4	18	4	34
340	130.67	4.67	1.75	0.05	1.43	1.19	52.39	0.08	0.1	0.27	0.72	83	5	18	4	14
350	135.00	7.92	2.87	0.08	2.04	1.28	48.46	0.13	0.14	0.43	1.29	65	9	18	10	25
370	159.00	11.22	4.09	0.1	1.95	1.22	45.27	0.19	0.11	0.58	1.75	78	4	20	4	26
380	171.00	8.65	3.08	0.14	1.7	1.27	48.08	0.14	0.104	0.47	1.36	70	4	18	4	22
390	183.00	7.18	2.65	0.14	1.62	1.2	49.79	0.11	0.119	0.4	1.16	59	7	18	4	47
400	184.22	7.34	2.69	0.13	1.65	1.7	49.63	0.12	0.106	0.4	1.21	61	8	18	5	21
410	185.44	6.2	2.32	0.11	1.61	1.11	51.07	0.11	0.103	0.35	1.05	51	4	18	4	23
430	187.89	6.84	2.2	0.09	1.62	1.28	49.78	0.09	0.077	0.44	1.55	81	5	18	4	18
440	189.11	5.89	2.27	0.04	1.77	1.18	50.63	0.1	0.055	0.35	0.88	118	51	18	9	16
450	190.33	4.3	1.61	0.06	1.55	1.07	52.59	0.07	0.084	0.26	0.8	36	6	18	4	14
460	191.56	4.63	1.84	0.03	1.58	1.14	52.37	0.08	0.092	0.27	0.71	62	7	18	4	14
470	192.78	3.66	1.4	0.05	1.3	1.06	53.57	0.06	0.112	0.23	0.77	68	4	18	4	14
480	194.00	3.7	1.47	0.05	1.41	1.04	53.36	0.07	0.152	0.23	0.66	31	4	18	4	27
490	199.33	4.12	1.6	0.07	1.43	0.99	52.97	0.07	0.11	0.25	0.75	47	4	18	4	14
500	204.67	3.21	1.37	0.04	1.4	1.14	53.87	0.06	0.095	0.21	0.59	62	4	18	4	30
510	210.00	0.8	0.45	0.02	1.54	1.08	55.61	0.03	0.059	0.09	0.35	37	4	18	4	14

												High- vs. low-Sr-aragonite				
Nb	Ni	Ga	Pb	Pr	Rb	Sr	Th	V	Y	Zr	Zn	Aragonit fine (absol. %)	Aragonit bulk (absol. %)	Sr $CaCO_3$ basis (ppm)	High-Sr Aragonite (% of Arag. bulk)	Low-Sr Aragonite (% of Arag. bulk)
3	n/a	8	4	8	14	4767	4	21	15	179	15	76.70	70.31	5544	53.21	17.10
5	n/a	8	4	8	13	4710	5	14	15	182	20	78.79	71.99	5374	51.86	20.13
3	n/a	8	4	8	15	4862	4	22	14	187	15	82.60	72.93	5683	55.01	17.91
6	n/a	8	4	8	16	5523	4	16	15	211	17	83.31	74.29	6405	62.26	12.04
4	n/a	8	4	8	17	4598	4	17	17	189	15	73.05	67.18	5087	48.30	18.87
2	n/a	8	4	8	18	4755	4	24	18	189	16	74.83	65.41	5543	52.30	13.11
4	n/a	8	4	8	16	5914	4	15	12	225	20	78.61	73.67	6709	65.09	8.58
2	n/a	8	4	8	17	6130	4	19	14	234	15	80.29	74.53	6953	67.63	6.90
2	n/a	8	4	8	19	5693	4	23	13	216	15	82.35	77.31	6341	62.17	15.13
3	n/a	8	4	8	13	5569	4	21	18	216	15	79.54	71.45	6426	61.91	9.54
4	n/a	8	4	8	17	5403	4	24	14	213	15	79.31	71.48	6381	61.48	10.00
4	n/a	8	4	8	15	5376	4	21	18	211	15	79.42	71.11	6214	59.80	11.30
3	n/a	8	4	8	16	5597	4	17	15	215	15	78.77	70.87	6462	62.14	8.73
2	n/a	8	4	8	17	6703	4	21	11	252	15	84.16	78.13	7488	73.58	4.54
2	n/a	8	4	8	19	6767	4	22	14	252	15	82.13	77.78	7793	76.51	1.27
3	n/a	8	4	8	15	3827	4	18	18	154	15	71.44	63.54	4386	41.09	22.45
7	n/a	8	4	8	16	5195	4	13	18	206	15	75.77	65.81	6300	59.53	6.28
5	n/a	8	4	8	16	5558	4	15	15	215	15	77.33	77.27	6442	63.15	14.11
3	n/a	8	4	8	17	5253	4	20	15	209	15	74.87	66.42	6283	59.50	6.93
3	n/a	8	4	8	17	5330	4	23	18	205	15	75.17	68.92	6236	59.58	9.33
3	n/a	8	4	8	15	5515	4	22	17	217	15	80.62	70.97	6288	60.49	10.47
3	n/a	8	4	8	12	5011	4	18	15	194	15	73.82	68.12	5854	55.78	12.34
3	n/a	8	4	8	14	4802	4	22	17	194	15	77.21	67.70	5620	53.47	14.23
4	n/a	8	4	8	14	5176	4	19	19	219	15	74.57	71.42	6009	57.89	13.53
4	n/a	8	4	8	13	3908	4	23	19	160	15	69.97	58.73	4854	44.55	14.18

												High- vs. low-Sr-aragonite				
Nb	Ni	Ga	Pb	Pr	Rb	Sr	Th	V	Y	Zr	Zn	Aragonit fine (abs. %)	Aragonit bulk (asol. %)	Sr $CaCO_3$ basis (ppm)	High-Sr Aragonite (% of Arag. bulk)	Low-Sr Aragonite (% of Arag. bulk)
4	4	8	4	10	20	4176	4	14	2	4	18	70.46	73.72	4544	44.09	29.63
6	7	8	4	8	17	4175	4	18	2	4	25	69.45	72.38	4577	44.23	28.15
5	2	8	4	8	16	3923	4	12	2	4	28	70.53	71.81	4208	40.59	31.22
2	13	8	4	8	16	4345	4	12	2	4	19	72.93	73.96	4703	45.67	28.29
2	4	8	4	8	15	4705	4	12	2	4	20	75.00	75.54	5118	49.93	25.61
6	6	8	4	8	15	3306	4	20	2	4	25	66.84	66.51	3581	33.92	32.59
4	2	8	4	8	16	2366	4	24	2	4	24	48.47	56.06	2606	23.62	32.44
9	8	8	5	11	17	2497	4	21	2	4	31	54.23	54.38	2748	24.70	29.69
2	8	8	10	8	17	2472	4	29	2	4	30	47.39	53.97	2747	24.64	29.33
2	13	9	6	8	17	2334	4	27	2	4	37	45.77	49.14	2701	23.57	25.57
5	9	8	8	8	15	2232	4	19	2	4	34	44.97	47.97	2525	21.87	26.10
10	12	8	4	11	20	2633	4	34	2	4	32	46.44	51.87	2981	26.44	25.43
7	15	8	5	8	21	2866	4	27	2	6	50	49.49	52.77	3319	29.57	23.20
6	14	8	4	8	19	2909	4	27	2	4	32	48.31	55.02	3278	29.56	25.46
4	13	8	4	8	22	3139	4	32	2	4	30	54.64	56.55	3606	32.77	23.78
12	7	8	7	8	16	3328	6	19	2	4	15	56.59	63.81	3532	33.12	30.68
2	8	8	4	12	20	3892	4	47	2	4	20	65.96	67.46	4190	39.83	27.64
7	7	8	4	8	23	3793	4	24	2	4	23	63.12	62.15	4330	40.33	21.82
4	6	8	4	11	21	3639	4	28	2	4	29	60.11	61.63	4127	38.36	23.27
2	5	8	4	8	20	4216	4	22	2	4	15	67.11	69.56	4490	42.99	26.57
3	2	8	4	8	19	5136	4	18	2	4	17	73.10	75.41	5422	52.87	22.54
2	2	8	4	11	20	4906	4	19	2	4	26	72.58	75.67	5138	50.14	25.52
4	2	8	4	10	20	5060	4	21	2	4	22	73.25	75.70	5274	51.48	24.22
7	3	8	4	8	21	4598	4	18	2	4	26	73.55	71.25	4973	47.88	23.37
5	2	8	4	8	20	4962	4	26	2	4	21	76.14	76.31	5231	51.15	25.16
8	4	8	4	8	20	5113	4	23	2	4	35	77.80	76.15	5421	52.98	23.18
4	5	8	4	8	20	4782	4	18	2	4	27	74.12	76.10	5021	49.07	27.03
3	7	8	4	8	18	4695	4	12	2	4	19	71.22	71.40	5182	49.92	21.48
5	2	8	4	8	18	4653	4	22	2	4	29	68.30	74.50	4863	47.30	27.20
6	6	8	7	8	17	4766	4	16	2	4	23	70.03	77.06	4906	48.07	28.99
2	2	8	4	8	17	6084	4	12	2	4	15	81.68	84.24	6162	61.50	22.74
2	4	8	4	8	17	5546	4	13	2	4	15	78.34	82.50	5606	55.72	26.78
6	8	8	4	8	18	3987	4	15	2	4	28	70.36	71.39	4175	40.22	31.17
3	12	8	8	8	21	2031	4	40	2	10	35	39.56	46.21	2279	19.51	26.70
9	10	8	8	8	29	1983	4	45	2	15	43	38.56	41.81	2379	19.72	22.09
4	11	8	6	8	23	2145	4	29	2	4	33	41.03	45.88	2437	20.82	25.06
10	5	8	4	8	21	2190	4	26	2	5	31	47.67	46.20	2419	20.71	25.49
9	9	8	6	8	22	2340	6	33	2	4	37	46.02	50.79	2549	22.46	28.33
3	2	8	6	8	19	2772	4	25	2	4	34	50.53	55.42	3009	27.19	28.24
7	7	8	4	8	25	3472	4	25	2	4	24	61.23	61.52	3877	36.02	25.50
3	113	8	4	9	23	4339	4	44	2	4	22	65.72	67.84	4716	44.89	22.95
9	8	8	4	8	20	4372	4	24	2	4	24	71.73	70.99	4521	43.50	27.49
9	2	8	4	8	21	4525	4	39	2	4	23	71.08	73.76	4648	45.11	28.66
3	4	10	4	8	19	4770	4	14	2	4	18	76.38	75.67	5001	48.81	26.86
5	2	8	4	8	20	4958	4	23	2	4	18	77.06	77.78	5029	49.37	28.40
3	8	8	8	8	21	4645	4	25	2	4	22	72.63	74.32	4704	45.73	28.59
7	2	8	4	8	17	5139	4	26	2	4	20	77.44	77.45	5232	51.32	26.13
6	2	8	4	8	16	6048	4	13	2	4	15	82.26	81.75	6149	61.01	20.75

Geochemistry Data Sheet

M35052

Depth (cm)	Age (ky)	Main elements in %										Trace elements in ppm				
		SiO_2	Al_2O_3	MnO	MgO	Na_2O	CaO	TiO_2	P_2O_5	K_2O	Fe_2O_3	Ba	Co	Cr	Cu	La
0	0.00	11.43	3.91	0.11	1.44	1.87	45.26	0.16	0.078	0.5	1.75	242	7	24	12	38
20	6.00	7.87	2.77	0.09	1.29	1.78	49.02	0.12	0.07	0.36	1.29	264	5	18	10	14
30	10.00	11.31	3.9	0.07	1.55	1.7	45.32	0.18	0.104	0.51	1.81	212	5	18	4	29
40	14.00	17.63	5.86	0.08	1.99	1.93	38.88	0.27	0.092	0.74	2.82	204	14	41	31	16
50	18.00	20.93	7	0.11	2.22	1.94	35.46	0.34	0.106	0.86	3.35	194	20	46	28	40
60	28.00	22.26	7.31	0.13	2.34	2.05	33.89	0.35	0.112	0.92	3.58	185	20	50	37	43
70	29.47	22.79	7.64	0.12	2.37	2.01	33.17	0.36	0.112	0.95	3.61	196	19	49	31	27
80	30.94	23.38	7.93	0.15	2.41	1.99	32.49	0.37	0.105	0.99	3.72	194	23	55	39	24
90	33.15	17.58	5.94	0.16	2.06	1.87	38.71	0.28	0.093	0.75	2.89	123	15	43	25	23
100	33.88	16.68	5.6	0.17	1.93	1.85	40.03	0.26	0.097	0.72	2.72	158	11	46	19	50
110	35.35	16.51	5.67	0.12	1.91	1.91	40.04	0.25	0.09	0.71	2.68	180	15	32	29	54
120	36.82	17.07	5.74	0.11	2.01	1.93	39.34	0.28	0.093	0.72	2.73	139	14	46	25	33
130	38.29	17.11	5.88	0.12	1.99	1.93	39.3	0.27	0.093	0.73	2.8	121	13	44	23	39
140	39.76	18.08	6.3	0.16	1.97	1.96	38.12	0.29	0.105	0.78	2.94	150	18	45	25	17
150	41.24	12.02	4.2	0.13	1.6	1.66	44.79	0.2	0.107	0.54	1.99	125	9	22	12	32
220	51.53	11.15	3.71	0.07	1.77	1.78	45.71	0.17	0.068	0.51	1.65	142	6	18	4	22
230	53.00	23.83	8.04	0.07	2.41	1.99	32.21	0.38	0.091	1.02	3.66	166	11	55	34	53
240	62.00	25.12	8.49	0.07	2.49	2.15	30.69	0.39	0.099	1.07	4.02	153	18	63	35	23
250	71.00	22.46	7.49	0.09	2.2	1.99	33.62	0.34	0.103	0.97	3.74	133	15	47	30	20
260	80.00	17.16	6.22	0.1	1.86	1.93	38.96	0.27	0.09	0.8	2.59	152	10	32	8	27
270	82.38	16.16	5.72	0.11	1.83	1.77	40.25	0.25	0.085	0.77	2.54	181	12	31	18	28
290	87.13	16.75	6.08	0.08	1.77	1.72	39.81	0.26	0.092	0.79	2.66	178	10	35	13	28
300	89.50	12.92	4.66	0.15	1.52	1.62	43.88	0.2	0.097	0.61	2.14	138	9	24	18	25
320	94.25	9.81	3.62	0.14	1.23	1.4	47.67	0.15	0.088	0.47	1.61	126	6	18	11	21
330	96.63	10.65	3.88	0.14	1.29	1.47	46.79	0.17	0.091	0.5	1.72	146	9	18	9	14
340	99.00	14.52	5.14	0.12	1.6	1.62	42.64	0.24	0.087	0.66	2.35	204	12	27	16	37
350	104.75	13.77	4.9	0.11	1.61	1.6	43.09	0.22	0.094	0.65	2.22	177	17	24	7	14
370	116.25	11.48	4.33	0.1	1.41	1.6	45.5	0.18	0.077	0.59	1.66	183	11	18	13	19
380	122.00	10.63	3.84	0.08	1.27	1.64	46.58	0.17	0.076	0.54	1.63	257	12	18	10	20
390	125.25	8.58	3.13	0.11	1.26	1.55	48.86	0.13	0.093	0.41	1.37	368	9	18	4	36
400	128.50	15.08	4.88	0.13	1.85	1.57	42.24	0.24	0.092	0.67	2.46	282	13	37	19	42
410	131.75	22.79	7.61	0.1	2.15	1.82	34.1	0.37	0.112	0.97	3.74	158	14	51	25	33
420	135.00	18.39	6.06	0.14	1.97	1.72	38.53	0.28	0.125	0.79	3	175	14	39	26	20

PC100

Depth (cm)	Age (ky)	Main elements in %										Trace elements in ppm				
		SiO_2	Al_2O_3	MnO	MgO	Na_2O	CaO	TiO_2	P_2O_5	K_2O	Fe_2O_3	Ba	Co	Cr	Cu	La
6	1.64	6.68	2.18	0.11	1.33	1.71	49.78	0.09	0.11	0.26	0.99	120	4	18	115	14
26	7.09	7.61	2.67	0.1	1.41	1.8	48.48	0.11	0.12	0.31	1.23	145	4	18	101	14
46	12.55	16.67	6.17	0.18	1.87	2.05	37.77	0.26	0.13	0.7	2.79	246	9	18	89	14
66	18.00	18.48	6.9	0.24	2.01	1.96	35.93	0.29	0.13	0.79	3.16	232	11	18	87	14
86	34.25	15.03	5.68	0.21	1.76	1.78	40.17	0.24	0.13	0.64	2.64	191	8	18	91	14
106	46.75	14.19	5.36	0.22	1.73	1.7	41.62	0.22	0.14	0.6	2.42	157	7	18	91	14
136	70.00	15.33	5.86	0.25	1.77	1.78	40.45	0.24	0.13	0.66	2.62	128	7	18	93	14
156	80.00	8.95	3.36	0.12	1.55	1.48	47.52	0.13	0.11	0.38	1.53	117	4	18	110	14
174	87.60	9.05	3.46	0.17	1.44	1.4	48.02	0.14	0.12	0.4	1.61	135	4	18	103	14
201	99.00	13.7	5.17	0.18	1.69	1.51	42.41	0.21	0.12	0.6	2.35	165	7	18	96	14
219	144.00	15.41	5.91	0.18	1.82	1.49	40.23	0.24	0.14	0.66	2.73	171	7	18	90	14
238	163.00	16.76	6.42	0.23	1.77	1.53	39.02	0.27	0.13	0.7	2.95	160	8	18	89	16
258	183.00	15.4	5.74	0.2	1.69	1.49	40.82	0.24	0.13	0.65	2.7	166	8	18	90	14
275	191.13	8.23	3.11	0.18	1.45	1.47	48.74	0.12	0.11	0.38	1.51	167	4	18	104	14
296	199.00	9.33	3.45	0.14	1.47	1.42	47.54	0.14	0.13	0.43	1.78	103	4	18	97	14
332	211.00	7.7	2.93	0.12	1.27	1.47	49.69	0.12	0.12	0.38	1.2	133	4	18	110	14
351	217.76	14.74	5.37	0.13	1.83	1.54	41.01	0.23	0.12	0.69	2.7	131	7	18	90	14
365	223.92	15.12	5.82	0.14	1.68	1.56	40.34	0.24	0.11	0.71	2.65	154	7	18	90	14
410	243.72	10.12	3.66	0.19	1.58	1.25	47.32	0.16	0.12	0.47	1.81	171	4	18	110	14
435	259.40	10.04	3.69	0.18	1.46	1.33	47.48	0.16	0.13	0.46	1.69	120	4	18	113	14
458	278.00	17.16	6.39	0.15	1.78	1.48	38.58	0.26	0.12	0.79	3.19	121	8	18	88	14
474	289.22	7.81	2.93	0.21	1.37	1.28	50.25	0.12	0.12	0.37	1.33	105	4	18	108	70
507	305.05	10.31	3.91	0.15	1.39	1.35	46.71	0.16	0.11	0.5	1.82	151	4	18	95	14
516	310.00	7.6	2.82	0.15	1.36	1.32	50.46	0.11	0.12	0.35	1.38	37	4	18	114	14

												High- vs. low-Sr-aragonite				
Nb	Ni	Ga	Pb	Pr	Rb	Sr	Th	V	Y	Zr	Zn	Aragonit fine (abs. %)	Aragonit bulk (asol. %)	Sr $CaCO_3$ basis (ppm)	High-Sr Aragonite (% of Arag. bulk)	Low-Sr Aragonite (% of Arag. bulk)
7	26	8	13	8	24	2133	6	43	2	10	59	40.04	40.30	3016	24.68	15.62
8	21	8	4	8	16	2089	4	35	2	4	52	45.25	44.85	2731	23.16	21.69
8	18	8	4	10	21	1817	4	42	2	14	62	31.80	36.45	2538	20.04	16.41
5	28	9	8	10	28	1523	4	67	2	28	71	20.98	26.39	2477	17.15	9.23
9	36	8	9	8	32	1305	4	74	6	34	75	12.08	19.80	2340	14.11	5.70
9	44	8	10	8	32	1254	4	82	9	40	78	15.97	18.87	2386	14.03	4.84
11	37	8	8	9	36	1267	4	82	11	40	78	12.90	17.21	2511	14.04	3.17
2	49	8	8	8	36	1369	4	85	7	44	82	14.71	17.05	2749	15.29	1.75
5	39	8	5	8	27	1455	4	64	2	26	63	18.37	25.01	2489	16.82	8.19
5	38	9	4	8	29	1446	4	56	3	30	67	20.59	26.98	2313	16.17	10.81
6	28	8	5	8	26	1419	4	65	2	24	64	20.37	26.72	2279	15.87	10.85
9	30	8	7	8	28	1411	4	60	2	29	73	21.09	27.25	2305	16.19	11.06
10	28	8	7	8	29	1418	4	68	3	26	64	22.70	26.98	2298	16.07	10.91
2	33	8	7	8	32	1544	4	72	3	32	67	22.30	27.47	2518	17.74	9.72
5	22	8	4	11	23	1396	4	45	2	20	54	25.80	29.15	1968	14.23	14.92
2	15	8	7	9	22	1877	4	60	2	13	35	24.78	35.77	2585	20.27	15.50
5	47	8	4	12	44	1367	4	75	11	41	64	14.31	19.56	2612	15.65	3.91
10	45	14	8	8	45	1315	4	90	10	50	68	12.95	17.91	2639	15.09	2.83
9	41	8	19	8	38	1373	5	76	7	39	59	18.56	23.19	2551	16.64	6.55
10	28	9	11	8	36	1656	4	90	2	30	52	26.72	32.40	2629	19.85	12.55
8	25	8	10	8	35	1777	4	63	2	27	52	31.82	31.48	2776	20.72	10.76
6	26	8	10	11	35	1742	4	72	3	27	57	29.43	30.37	2801	20.60	9.77
7	23	8	4	8	27	1570	4	51	2	22	36	30.91	30.87	2225	16.47	14.39
12	15	8	5	8	22	1631	4	31	2	13	35	29.46	28.09	2176	15.48	12.60
9	13	8	6	8	22	1708	4	45	2	14	37	35.88	29.13	2350	16.99	12.14
10	26	8	8	8	29	1803	4	53	2	24	44	34.37	30.49	2698	19.87	10.62
9	17	8	8	8	29	1849	4	51	2	20	47	34.95	32.26	2723	20.52	11.74
6	23	8	9	8	27	1878	9	59	2	16	38	38.55	35.35	2639	20.60	14.75
6	18	8	8	10	24	1912	4	49	2	15	40	40.50	38.53	2609	21.02	17.51
6	10	8	7	8	19	1823	4	443	2	9	34	39.88	35.42	2364	18.47	16.95
10	30	8	7	8	23	1317	4	59	6	29	46	21.09	18.12	1979	11.38	6.74
13	40	10	11	8	37	1191	12	76	7	43	59	17.00	13.30	2240	10.78	2.52
7	32	8	6	8	30	1084	4	57	8	33	51	15.84	12.36	1764	8.11	4.25

												High- vs. low-Sr-aragonite				
Nb	Ni	Ga	Pb	Pr	Rb	Sr	Th	V	Y	Zr	Zn	Aragonit fine (absol. %)	Aragonit bulk (asol. %)	Sr $CaCO_3$ basis (ppm)	High-Sr Aragonite (% of Arag. bulk)	Low-Sr Aragonite (% of Arag. bulk)
7	n/a	8	4	8	19	3487	4	35	13	150	21	69.64	61.29	4172	38.72	22.56
4	n/a	8	4	8	21	3054	4	37	17	140	24	56.05	53.36	3736	33.40	19.96
8	n/a	8	4	8	37	1681	4	78	27	117	56	19.23	28.93	2555	18.41	10.52
6	n/a	8	4	8	39	1578	6	85	27	115	57	23.02	25.51	2566	17.50	8.01
5	n/a	8	4	8	34	1650	4	70	22	114	47	26.61	30.62	2409	17.77	12.84
4	n/a	8	4	8	31	1954	4	70	22	120	45	29.85	27.75	2907	20.58	7.17
4	n/a	8	4	8	35	1547	6	70	23	106	47	25.14	27.58	2241	15.82	11.76
5	n/a	8	4	8	22	2906	4	51	19	130	31	49.03	48.57	3614	31.42	17.14
6	n/a	8	4	8	24	1903	7	45	20	111	33	36.19	35.00	2427	18.88	16.13
7	n/a	8	4	8	33	2066	6	66	23	121	47	37.15	33.02	2895	22.01	11.00
4	n/a	8	4	8	33	1303	4	74	28	104	53	21.39	19.62	1907	11.44	8.18
6	n/a	8	4	8	35	1375	4	86	22	111	53	19.75	18.37	2180	12.63	5.74
6	n/a	11	4	8	34	1151	6	65	24	100	47	5.95	4.21	1668	3.45	0.76
3	n/a	8	4	8	21	1704	4	41	17	96	29	40.99	38.05	2066	16.57	21.48
7	n/a	8	4	8	23	2354	4	45	22	126	29	45.97	41.43	2880	23.79	17.64
2	n/a	8	4	8	22	2476	4	55	16	124	23	54.81	51.28	2871	25.37	25.91
5	n/a	8	4	8	34	1773	4	60	24	113	43	31.39	30.31	2457	18.05	12.26
7	n/a	8	4	8	36	1804	4	79	23	117	46	31.58	33.68	2527	19.37	14.31
5	n/a	8	4	8	24	1537	4	59	20	102	32	26.67	22.34	1933	12.38	9.96
7	n/a	8	4	8	25	1472	4	43	21	100	35	20.14	18.42	1851	10.74	7.67
7	n/a	8	4	8	38	1454	4	70	26	112	53	14.13	12.60	2177	10.13	2.47
2	n/a	8	4	8	20	1892	4	34	14	107	27	40.82	33.89	2220	17.05	16.83
5	n/a	8	4	8	25	1780	4	50	21	108	36	32.91	28.28	2218	15.83	12.45
3	n/a	8	4	8	19	1819	4	34	18	106	28	33.40	28.55	2164	15.50	13.04

Appendix 8 - Turbidite analyses

Turbidite Data Sheet			Carbonate Mineralogy									
Depth (cm)	What type of turbidite or turbidite section was sampled? (Based on the coarse vs. fine fraction content)	Deposited during MIS	$CaCO_3$ bulk (%)	$CaCO_3$ fine (%)	Aragonite bulk (absolute %)	HMC bulk (absolute %)	LMC bulk (absolute %)	Quartz Intensity bulk	Fine Aragonite (absolute %)	HMC fine absolute %	LMC fine absolute %	Fine Aragonite in bulk sedim. (%)
M35032												
150	middle of TB to base	4	93.58	98.67	76.79	2.91	13.88	102	82.29	10.29	6.10	35.14
160	base	4	93.83	99.06	74.87	3.42	15.54	66	78.73	14.27	6.06	12.12
170	middle to base	4	95.19	100.00	78.13	2.98	14.09	53	85.83	10.25	3.92	64.41
190	Fine tail	5	78.27	81.46	47.96	7.67	22.64	438	51.80	8.32	21.34	47.06
205	middle to top	5	97.33	93.45	73.16	5.42	18.74	100	67.78	8.51	17.16	39.90
210	base of TB	5	94.00	96.33	69.19	4.50	20.31	91	72.48	12.47	11.38	18.84
230	middle to top	5	88.90	91.31	58.22	7.91	22.78	196	55.08	8.16	28.07	36.03
240	base	5	95.38	99.46	74.90	3.81	16.66	57	78.97	12.02	8.47	24.32
250	base	5	95.98	94.99	72.77	4.89	18.32	85	71.60	13.99	9.40	23.51
290	middle to base	5	92.94	94.39	67.57	5.76	19.62	172	69.54	8.16	16.70	41.36
300	base	5	95.63	90.18	72.86	3.80	18.97	208	66.06	15.55	8.56	22.69
M35034												
10	middle to base	1	86.39	83.98	54.18	15.28	16.93	76	69.11	9.21	5.66	42.50
40	base	1	90.35	87.18	59.57	16.04	14.74	26	72.66	8.38	6.14	35.98
50	base	1	88.77	86.85	52.80	11.21	24.75	50	69.69	9.19	7.97	20.99
70	base	1	91.10	87.18	53.11	21.56	16.43	62	68.56	10.63	8.00	25.45
140	base	2	90.28	77.23	48.84	22.27	19.17	127	51.28	13.98	11.97	12.31
170	base	2	92.57	88.03	51.93	25.41	15.23	46	65.03	12.69	10.31	21.32
M35042												
120	middle to fine endtail	4	85.52	88.92	51.01	3.99	30.52	214	53.83	10.42	24.67	47.81
150	middle to fine endtail	5	88.82	95.53	61.83	4.35	22.64	141	69.21	2.52	23.79	61.99
203	middle to fine endtail	5	89.76	93.89	66.37	2.28	21.11	159	65.34	3.21	25.35	57.53
207.5	middle to base	5	88.35	92.69	62.66	5.38	20.30	193	63.13	6.92	22.65	54.05
236	fine endtail	5	91.58	97.25	68.34	10.99	12.26	85	75.37	6.55	15.33	74.14
243	middle to fine endtail	5	95.24	100.00	79.88	6.63	8.72	47	86.12	7.49	6.39	76.67
290	fine endtail	5	94.55	98.16	82.78	6.02	5.76	79	83.77	7.04	7.36	79.99
400	fine endtail	7	95.19	98.71	73.57	11.95	9.68	82	77.77	10.40	10.54	74.87
410	base	7	98.06	99.00	79.97	12.58	5.51	0	81.58	11.77	5.65	55.97
463	middle to fine endtail	7	91.20	94.44	71.48	6.50	13.22	154	71.84	8.97	13.64	66.09
467	fine endtail	7	98.86	99.36	82.86	8.02	7.98	0	81.49	10.02	7.85	78.51
470	fine endtail	7	99.62	99.65	84.06	7.94	7.62	0	84.64	5.97	9.04	82.87
480	fine endtail	7	99.97	100.00	83.13	8.59	8.25	0	83.93	8.30	7.77	80.07
M35043												
230	base to middle of TB	5	93.08	98.48	75.85	4.94	12.29	52	82.93	7.18	8.37	45.12
390	base to middle of TB	7	91.33	98.91	67.64	5.45	18.24	109	76.73	6.29	15.90	44.89
M35048												
80	middle to base of TB	2	85.22	92.72	58.91	9.32	16.99	63	65.44	5.56	21.73	32.86
320	middle to base of TB	6	79.49	93.00	52.88	11.95	14.66	75	67.58	6.71	19.58	29.11
516	middle to base of TB	8	86.39	93.86	60.55	3.52	22.31	70	68.67	0.84	24.36	34.50
M35049												
240	middle to base of TB	5	97.70	93.48	76.66	8.02	13.03	52	77.56	9.63	6.29	26.31
420	middle to base of TB	> 6/7	96.19	100.75	76.18	11.01	9.01	57	79.54	11.32	9.89	34.71
M35052												
10	fine endtail	1	76.53	83.50	47.65	11.02	17.86	235	55.67	13.88	13.94	46.51
160	transition into peripl. ooze	3	64.31	66.01	26.30	5.72	32.29	593	27.57	5.72	32.72	24.21
170	fine endtail	3	69.65	74.52	34.84	6.49	28.31	411	37.28	5.86	31.38	37.08
180	fine endtail	3	73.31	81.08	45.06	6.10	22.15	284	48.85	6.76	25.48	48.60
190	middle	3	87.42	93.49	63.83	12.55	11.05	96	71.10	12.66	9.73	55.83
200	base	3	86.86	92.66	60.20	15.50	11.15	80	66.51	14.77	11.37	26.23
210	base	3	85.18	88.99	59.31	13.16	12.71	166	62.51	13.00	13.48	26.57
360	fine endtail	5	70.23	74.67	39.18	3.07	27.99	394	40.88	2.85	30.93	38.26
450	fine endtail	6	65.81	73.03	29.35	1.83	34.63	493	33.89	4.36	34.77	33.79
460	fine endtail	6	73.31	80.40	41.36	3.59	28.36	321	45.79	3.51	31.10	45.37
470	middle of TB	6	81.28	88.97	54.01	6.48	20.79	246	60.46	6.03	22.48	53.05
480	base of TB	6	87.35	91.48	61.20	9.62	16.53	76	61.16	15.52	14.80	14.47
510	fine endtail	6	74.72	81.84	24.55	3.54	46.64	304	26.38	2.60	52.86	25.71
520	fine endtail	6	76.58	84.20	24.77	0.00	51.81	301	27.94	0.14	56.12	27.75
535	fine tail	6	79.23	85.52	39.29	1.70	38.24	236	43.19	2.54	39.79	38.18

			Grain Size analysis									Physical Properties		
HMC fine in bulk sedim. (%)	LMC fine in bulk sedim. (%)	Fine Quartz Intensity	Coarse fraction (%)	Fine fraction (%)	63-125μm (% of the coarse fraction)	125-250μm (% of the coarse fraction)	Fine Sand fraction (% of the coarse fraction)	250-500μm (medium sand fraction)	500-1000μm (% of the coarse fraction)	>1000μm (% of the coarse fraction)	Coarse Sand fraction (% of the coarse fraction)	Water Content (%)	Wet Bulk Density (g/cm^3)	Dry Bulk Density (g/cm^3)
4.63	2.74	129	54.98	45.02	65.36	30.58	95.94	2.93	1.09	0.04	1.12	23.55	1.72	1.31
2.32	0.98	165	83.75	16.25	16.98	58.38	75.37	23.84	0.78	0.01	0.80	28.60	1.67	1.19
8.08	3.09	53	21.16	78.84	61.49	33.81	95.30	4.40	0.29	0.01	0.30	28.72	1.74	1.24
7.86	20.18	402	5.44	94.56	39.15	24.77	63.92	22.88	10.20	2.99	13.19	34.46	1.65	1.08
4.81	9.70	211	43.48	56.52	26.47	11.28	37.75	8.72	19.55	33.98	53.53	36.85	1.61	1.02
3.32	3.03	215	73.36	26.64	38.69	43.68	82.37	16.33	1.02	0.28	1.30	41.21	1.46	0.86
5.48	18.86	314	32.82	67.18	53.78	21.65	75.43	18.72	5.38	0.47	5.85	32.60	1.64	1.10
3.86	2.72	135	67.88	32.12	57.50	30.61	88.11	10.00	1.70	0.18	1.89	35.82	1.56	1.00
4.55	3.05	177	67.50	32.50	32.20	31.45	63.65	30.18	5.45	0.72	6.17	40.91	1.55	0.92
4.93	10.09	207	39.59	60.41	73.18	18.46	91.63	6.09	1.83	0.44	2.28	28.90	1.71	1.22
5.04	2.77	302	67.61	32.39	53.10	32.18	85.29	10.96	3.17	0.58	3.76	38.96	1.59	0.97
5.67	3.48	103	38.50	61.50	46.89	37.47	84.37	13.26	2.19	0.17	2.37	35.50	1.69	1.09
4.15	3.04	71	50.49	49.51	36.24	42.28	78.52	14.50	5.41	1.58	6.98	33.33	1.81	1.21
2.77	2.40	114	69.88	30.12	29.57	49.50	79.07	15.92	4.55	0.46	5.01	32.87	1.83	1.23
3.95	2.97	152	62.87	37.13	16.84	39.88	56.72	25.18	17.76	0.34	18.10	23.77	1.97	1.50
3.36	2.87	349	76.00	24.00	32.63	53.40	86.04	12.31	1.26	0.39	1.65	31.24	1.62	1.12
4.16	3.38	163	67.21	32.79	54.07	38.47	92.54	5.95	1.16	0.36	1.51	28.23	1.98	1.42
9.26	21.91	214	11.19	88.81	37.50	25.65	63.15	27.79	8.87	0.19	9.05	31.49	1.73	1.19
2.26	21.31	179	10.43	89.57	35.35	23.13	58.47	29.06	12.31	0.16	12.47	32.57	1.72	1.16
2.83	22.32	164	11.95	88.05	27.08	26.17	53.24	33.82	12.73	0.20	12.93	32.47	1.72	1.16
5.92	19.39	191	14.37	85.63	26.25	27.41	53.67	33.60	12.54	0.19	12.73	28.71	1.62	1.16
6.44	15.08	127	1.63	98.37	57.47	11.75	69.21	12.70	10.04	8.04	18.08	24.81	1.91	1.43
6.67	5.69	57	10.97	89.03	96.02	3.68	99.70	0.21	0.04	0.05	0.08	28.16	1.89	1.36
6.72	7.03	83	4.50	95.50	53.46	22.31	75.77	16.30	5.45	2.47	7.92	25.89	1.83	1.36
10.01	10.15	436	3.74	96.26	91.50	7.49	98.99	0.76	0.17	0.08	0.25	25.43	1.84	1.37
8.08	3.88		31.39	68.61	82.87	16.66	99.53	0.41	0.06	0.00	0.06	31.24	1.74	1.20
8.25	12.54	147	8.00	92.00	37.36	29.03	66.39	25.00	8.25	0.36	8.61	29.52	1.77	1.25
9.65	7.56	104	3.66	96.34	50.53	21.41	71.94	19.21	7.93	0.92	8.85	29.31	1.80	1.27
5.84	8.85	85	2.10	97.90	77.67	11.12	88.79	8.13	3.08	0.00	3.08	28.78	1.81	1.29
7.91	7.42	85	4.60	95.40	79.09	12.18	91.27	6.85	1.83	0.06	1.88	27.97	1.80	1.29
3.91	4.55	93	45.59	54.41	59.30	34.35	93.65	5.94	0.37	0.04	0.41	34.46	1.68	1.10
3.68	9.30	129	41.49	58.51	32.38	20.59	52.97	37.02	9.19	0.83	10.02	34.22	1.63	1.07
2.79	10.91	119	49.78	50.22	23.32	42.43	65.75	25.23	4.51	4.51	9.02	27.95	1.74	1.25
2.89	8.43	123	56.52	43.48	24.94	34.75	59.69	34.16	5.73	0.42	6.15	25.80	1.84	1.37
0.42	12.24	98	49.76	50.24	23.78	23.40	47.18	18.10	10.62	24.10	34.72	27.52	1.67	1.21
3.27	2.13	121	66.07	33.93	29.41	27.44	56.85	32.83	9.72	0.61	10.32	34.32	1.52	1.00
4.94	4.31	94	56.36	43.64	53.40	29.82	83.22	14.97	1.76	0.05	1.81	35.39	1.72	1.11
11.60	11.65	258	16.45	83.55	73.40	14.85	88.25	8.46	3.20	0.08	3.28	33.62	1.77	1.18
5.02	28.73	606	12.19	87.81	33.98	23.71	57.69	34.13	7.82	0.35	8.18	41.71	1.56	0.91
5.83	31.20	381	0.55	99.45	46.04	27.73	73.77	22.14	3.83	0.26	4.09	37.30	1.64	1.03
6.73	25.35	289	0.50	99.50	96.02	2.29	98.31	0.72	0.96	0.00	0.96	32.67	1.71	1.15
9.94	7.64	116	21.47	78.53	95.16	4.45	99.61	0.30	0.05	0.04	0.09	32.88	1.81	1.22
5.83	4.48	149	60.57	39.43	72.80	22.89	95.69	2.67	1.09	0.54	1.64	36.36	1.69	1.08
5.53	5.73	216	57.49	42.51	52.63	38.31	90.94	8.47	0.57	0.02	0.59	39.44	1.93	1.17
2.67	28.95	394	6.41	93.59	27.44	18.59	46.03	35.63	18.20	0.15	18.35	37.69	1.64	1.02
4.35	34.66	455	0.32	99.68	53.13	25.06	78.19	18.17	3.63	0.00	3.63	35.99	1.63	1.05
3.48	30.81	329	0.92	99.08	90.80	7.65	98.46	1.29	0.25	0.00	0.25	32.67	1.72	1.16
5.29	19.73	212	12.25	87.75	97.70	1.63	99.33	0.41	0.18	0.08	0.26	28.40	1.78	1.27
3.67	3.50	234	76.34	23.66	49.37	47.26	96.63	3.28	0.07	0.02	0.09	37.04	1.58	0.99
2.53	51.52	280	2.53	97.47	34.09	22.59	56.68	33.38	9.88	0.06	9.94	33.11	1.72	1.15
0.14	55.73	254	0.70	99.30	39.69	23.35	63.04	25.94	8.19	2.83	11.02	29.96	1.77	1.24
2.25	35.18	221	11.59	88.41	89.75	8.39	98.14	1.39	0.46	0.01	0.47	28.96	1.80	1.28

Turbidite Data Sheet			Carbonate Mineralogy									
Depth (cm)	What type of turbidite or turbidite section was sampled? (Based on the coarse vs. fine fraction content)	Deposited during MIS	$CaCO_3$ bulk (%)	$CaCO_3$ fine (%)	Aragonite bulk (absolute %)	HMC bulk (absolute %)	LMC bulk (absolute %)	Quartz Intensity bulk	Fine Aragonite (absolute %)	HMC fine absolute %	LMC fine absolute %	Fine Aragonite in bulk sedim. (%)
540	fine tail	6	86.65	91.77	47.36	2.63	36.66	99	49.81	2.95	39.01	47.04
M35052 continued												
550	middle to base	6	85.59	93.74	45.75	0.89	38.95	113	52.78	0.67	40.29	42.18
560	upper base	6	85.45	89.18	50.91	4.82	29.72	89	56.47	2.53	30.18	20.88
570	middle base	6	82.77	83.53	47.89	10.12	24.76	150	49.39	5.71	28.43	12.84
580	lower base	6	84.46	81.51	47.20	8.01	29.25	100	47.16	8.17	26.19	8.01
765	fine endtail	8	72.61	77.86	31.02	3.35	38.23	412	31.31	1.80	44.75	31.25
770	fine endtail	8	76.89	78.23	34.35	5.43	37.11	332	35.98	3.95	38.30	35.48
780	fine endtail	8	77.92	84.20	42.38	3.90	31.65	316	47.31	7.54	29.35	46.79
790	fine endtail	8	86.45	93.74	60.02	7.25	19.18	159	67.88	6.99	18.87	63.59
800	fine endtail	8	87.34	95.23	62.31	8.46	16.58	139	69.96	7.58	17.69	63.15
810	middle part of TB	8	85.49	94.49	62.08	8.16	15.25	85	67.39	10.00	17.09	48.33
820	middle part of TB	8	88.79	93.77	64.42	9.92	14.46	69	67.86	9.32	16.58	41.30
830	middle part of TB	8	87.06	94.45	61.67	10.05	15.34	96	66.44	12.21	15.80	34.82
840	Base of TB	8	80.15	91.97	53.93	11.30	14.91	92	59.52	10.38	22.07	24.39
850	Base of TB	8	88.78	93.52	62.07	11.11	15.60	73	62.24	12.60	18.68	24.55
860	Base of TB	8	84.86	89.87	56.64	10.77	17.46	110	56.72	10.53	22.63	17.32
890	middle of fine endtail of TB	8	77.45	81.15	37.59	6.65	33.21	320	38.31	6.78	36.06	34.26
PC059												
23.5	middle to base of TB	3	72.83	78.22	40.09	7.22	25.53	427	43.06	8.45	26.72	29.20
60.5	middle to base of TB	3	81.04	84.62	51.63	9.37	20.04	280	49.95	10.46	24.21	32.72
63.5	base of TB	3	83.17	86.94	48.83	9.98	24.36	241	52.67	8.52	25.75	19.38
124.5	middle to base of TB	5	81.37	84.54	56.15	3.43	21.79	281	54.94	3.24	26.36	42.19
126.5	middle to base of TB	5	81.00	88.18	57.39	4.03	19.58	252	62.40	4.71	21.08	46.89
129.5	middle to base of TB	5	84.25	89.00	67.45	3.52	13.28	192	66.38	6.55	16.07	44.60
201	upper fine tail of TB	5	86.67	93.14	69.25	4.57	12.85	163	74.92	3.22	15.00	64.88
294.5	upper fine tail of TB	6	85.00	88.52	66.19	2.82	15.99	219	66.86	5.29	16.37	57.84
312	base of TB	7	87.33	89.13	63.39	8.02	15.93	161	66.18	2.37	20.58	33.82
415.5	upper fine tail of TB	8	62.93	87.41	39.45	6.63	16.86	250	53.55	7.09	26.77	46.00
418	middle to base of TB	8	83.60	89.90	58.75	5.74	19.10	194	58.24	10.35	21.32	46.28
PC 076												
0	fine tail	n/a	n/a	83.50	n/a	n/a	n/a	n/a	51.44	9.77	22.29	33.56
290	fine tail	n/a	n/a	85.80	n/a	n/a	n/a	n/a	49.85	0.00	35.95	34.95
300	middle to Base of TB	n/a	n/a	84.00	n/a	n/a	n/a	n/a	45.36	2.52	36.12	30.58
310	middle to Base of TB	n/a	n/a	83.80	n/a	n/a	n/a	n/a	35.87	2.51	45.42	22.21
340	middle to Base of TB	n/a	n/a	84.30	n/a	n/a	n/a	n/a	41.56	2.53	40.21	25.60
350	middle to Base of TB	n/a	n/a	84.70	n/a	n/a	n/a	n/a	47.18	0.00	37.52	26.11
430	fine tail	n/a	n/a	85.10	n/a	n/a	n/a	n/a	33.27	0.00	51.83	23.79
440	Fine tail	n/a	n/a	84.70	n/a	n/a	n/a	n/a	33.29	0.00	51.41	24.94
490	middle to Base of TB	n/a	n/a	85.90	n/a	n/a	n/a	n/a	34.79	0.00	51.11	16.43
PC 100												
181	Fine tail	5	85.21	92.78	63.05	0.78	21.38	169	69.97	2.12	20.69	59.71
187.5	middle to Base of TB	5	86.83	86.79	61.13	1.39	24.32	181	60.56	2.26	23.97	30.59
271	middle to Base of TB	7	88.75	94.77	63.59	0.84	24.32	148	74.30	3.76	16.71	46.47
310	base of TB (very small TB)	7	98.33	95.25	51.01	3.94	43.38	73	70.63	0.74	23.87	6.51
314	base of TB (very small TB)	7	95.83	88.10	51.35	3.27	41.22	87	57.02	0.75	30.34	10.68
319	base of TB (very small TB)	7	95.00	94.24	58.85	7.02	29.13	94	66.35	0.03	27.86	17.53
324	base of TB (very small TB)	7	90.42	93.52	54.14	3.60	32.68	75	67.47	2.50	23.55	15.14
328	middle to Base of TB	7	93.75	93.68	63.89	5.12	24.73	112	68.09	0.29	25.30	24.53
386	base of TB	7	96.67	92.71	48.32	11.00	37.34	88	64.21	0.17	28.33	12.19
389	middle to Base of TB	7	93.33	92.45	66.72	1.80	24.81	137	63.48	0.00	28.97	30.56
392	middle to Base of TB	7	92.08	95.05	65.91	2.47	23.70	118	67.75	1.64	25.65	25.57
415	middle to Base of TB	8	89.31	90.30	61.24	0.00	28.06		50.18	0.00	40.11	29.30
419	middle to Base of TB	8	90.43	90.28	62.36	0.12	27.95	155	55.67	1.99	32.63	27.48
492	middle to Base of TB	8	80.82	90.61	45.60	3.50	31.72	304	54.87	3.79	31.96	26.63

			Grain Size analysis									Physical Properties		
HMC fine in bulk sedim. (%)	LMC fine in bulk sedim. (%)	Fine Quartz Intensity	Coarse fraction (%)	Fine fraction (%)	63-125μm (% of the coarse fraction)	125-250μm (% of the coarse fraction)	Fine Sand fraction (% of the coarse fraction)	250-500μm (medium sand fraction)	500-1000μm (% of the coarse fraction)	>1000μm (% of the coarse fraction)	Coarse Sand fraction (% of the coarse fraction)	Water Content (%)	Wet Bulk Density (g/cm^3)	Dry Bulk Density (g/cm^3)
2.79	36.84	123	5.56	94.44	97.51	1.91	99.42	0.58	0.00	0.00	0.00	25.44	1.85	1.38
0.54	32.20	142	20.08	79.92	93.16	6.71	99.87	0.10	0.03	0.00	0.03	26.50	1.87	1.38
0.93	11.16	175	63.02	36.98	45.79	36.00	81.79	17.12	1.06	0.03	1.09	33.53	1.65	1.09
1.49	7.39	269	74.00	26.00	23.28	42.90	66.18	29.53	4.16	0.14	4.29	36.90	1.56	0.98
1.39	4.45	311	83.01	16.99	9.13	29.37	38.50	51.02	9.43	1.05	10.48	34.30	1.53	1.01
1.80	44.67	386	0.18	99.82	56.64	25.66	82.30	12.68	5.01	0.00	5.01	36.67	1.63	1.03
3.90	37.77	437	1.38	98.62	75.67	17.90	93.57	5.83	0.61	0.00	0.61	35.67	1.68	1.08
7.46	29.02	271	1.10	98.90	66.99	17.99	84.98	13.03	1.99	0.00	1.99	34.32	1.70	1.12
6.55	17.68	149	6.31	93.69	96.66	2.31	98.97	0.67	0.36	0.00	0.36	28.33	1.85	1.32
6.84	15.97	119	9.74	90.26	96.08	3.30	99.38	0.44	0.18	0.00	0.18	27.74	1.85	1.34
7.17	12.26	126	28.29	71.71	91.72	8.01	99.73	0.21	0.07	0.00	0.07	29.74	1.73	1.21
5.67	10.09	133	39.14	60.86	83.54	15.81	99.35	0.57	0.08	0.00	0.08	31.47	1.78	1.22
6.40	8.28	133	47.60	52.40	71.57	26.11	97.68	1.91	0.40	0.01	0.41	33.78	1.65	1.09
4.25	9.04	179	59.03	40.97	44.62	38.63	83.25	13.86	2.88	0.01	2.89	38.62	1.56	0.96
4.97	7.37	178	60.55	39.45	44.24	46.90	91.15	8.74	0.12	0.00	0.12	34.04	1.63	1.08
3.21	6.91	547	69.46	30.54	19.69	44.39	64.08	33.82	1.94	0.17	2.11	35.40	1.58	1.02
6.06	32.24	353	10.58	89.42	53.31	19.52	72.83	21.20	5.85	0.12	5.97	47.38	2.03	1.07
5.73	18.12	497	32.19	67.81	21.33	26.48	47.81	27.37	19.66	5.16	24.82	42.24	1.60	0.93
6.85	15.86	495	34.49	65.51	42.67	32.69	75.36	19.23	5.18	0.23	5.41	33.28	1.74	1.16
3.14	9.47	328	63.20	36.80	21.57	26.42	47.99	37.92	13.51	0.58	14.09	36.17	1.50	0.96
2.49	20.24	331	23.20	76.80	48.22	23.80	72.02	20.84	7.12	0.02	7.14	34.96	1.80	1.17
3.54	15.84	242	24.85	75.15	60.38	22.59	82.97	11.91	4.64	0.47	5.12	34.99	1.76	1.15
4.40	10.80	267	32.81	67.19	65.70	20.13	85.83	9.99	4.04	0.14	4.19	33.95	1.70	1.13
2.79	12.99	155	13.41	86.59	69.40	17.61	87.01	10.24	2.51	0.23	2.75	30.54	1.81	1.26
4.58	14.16	251	13.49	86.51	69.57	18.54	88.10	8.61	3.15	0.14	3.28	30.50	1.84	1.28
1.21	10.52	223	48.89	51.11	42.72	39.76	82.48	15.74	1.74	0.04	1.78	31.91	1.76	1.20
6.09	22.99	259	14.10	85.90	60.68	22.93	83.61	12.43	3.95	0.02	3.96	32.20	1.78	1.21
8.22	16.94	243	20.54	79.46	74.41	19.18	93.59	4.85	1.51	0.06	1.57	31.66	1.71	1.17
6.37	14.55	n/a	34.75	65.25	29.60	24.20	53.80	32.69	12.56	0.95	13.51	36.13	n/a	n/a
0.00	25.20	n/a	29.90	70.10	26.30	22.97	49.27	37.68	12.88	0.16	13.05	32.40	n/a	n/a
1.70	24.35	n/a	32.58	67.42	23.14	29.96	53.10	36.00	10.67	0.23	10.90	31.53	n/a	n/a
1.56	28.12	n/a	38.09	61.91	18.13	20.45	38.58	30.02	13.97	17.43	31.40	29.80	n/a	n/a
1.56	24.77	n/a	38.40	61.60	20.77	35.39	56.16	41.55	2.29	0.00	2.29	29.85	n/a	n/a
0.00	20.77	n/a	44.66	55.34	23.97	32.18	56.15	40.04	3.67	0.13	3.81	29.65	n/a	n/a
0.00	37.06	n/a	28.49	71.51	19.51	29.94	49.45	38.07	9.80	2.69	12.48	30.14	n/a	n/a
0.00	38.52	n/a	25.07	74.93	22.74	25.81	48.55	42.96	8.08	0.41	8.49	29.97	n/a	n/a
0.00	24.13	n/a	52.78	47.22	14.22	29.62	43.84	50.91	5.14	0.10	5.25	30.20	n/a	n/a
1.81	17.65	156	14.66	85.34	17.89	13.86	31.76	40.56	27.37	0.31	27.68	33.26	1.76	1.17
1.14	12.11	240	49.48	50.52	13.77	20.74	34.52	36.06	28.24	1.18	29.42	41.61	1.48	0.86
2.35	10.45	177	37.46	62.54	47.72	32.42	80.14	17.09	2.76	0.02	2.78	35.19	1.65	1.07
0.07	2.20	245	90.78	9.22	3.69	5.83	9.51	65.07	23.33	2.09	25.42	31.08	1.14	0.79
0.14	5.68	216	81.26	18.74	5.46	6.89	12.34	35.59	48.35	3.71	52.07	36.36	1.35	0.86
0.01	7.36	208	73.58	26.42	7.83	11.04	18.87	42.09	38.71	0.32	39.04	38.53	1.43	0.88
0.56	5.28	180	77.56	22.44	8.51	14.14	22.65	52.31	24.69	0.35	25.05	39.31	1.38	0.84
0.11	9.11	219	63.98	36.02	16.32	23.98	40.30	43.26	16.39	0.06	16.44	41.16	1.47	0.87
0.03	5.38	205	81.02	18.98	6.29	10.27	16.55	56.91	26.08	0.45	26.53	38.32	1.46	0.90
0.00	13.95	236	51.86	48.14	17.97	26.68	44.65	41.21	12.93	1.22	14.14	39.90	1.47	0.88
0.62	9.68	208	62.26	37.74	15.39	24.80	40.19	54.34	5.40	0.07	5.47	40.06	1.53	0.92
0.00	23.42	323	58.38	41.62	15.75	24.12	39.87	30.21	19.93	9.99	29.91	41.80	1.41	0.82
0.98	16.11	310	50.63	49.37	21.55	28.15	49.70	30.51	17.11	2.68	19.79	38.28	1.58	0.97
1.84	15.51	417	51.46	48.54	15.84	11.87	27.71	41.25	29.68	1.36	31.04	39.40	1.49	0.91

Appendix 9 - Seismic analyses

Seismic Profiles Data

3.5 kHz Seismic Line Number	Start Point Longitude (°N)	Start Point Latitude (°N)	End Point Longitude (°N)
(CH0288-48) PB48	-	-	-
(CH0288-49) PB49	-	-	-
(CH0288-52) PB52	17° 54.65	78° 55.49	17° 33.50
(CH0288-53) PB53	17° 33.50	78° 54.25	17° 42.62
(CH0288-58) PB58	17° 57.58	78° 50.84	17° 35.50
(CH0288-59) PB59	17° 35.50	78° 50.80	17° 51.00
(CH0288-60) PB60	17° 51.00	79° 06.50	17° 41.10
(CH0288-61) PB61	17° 41.10	79° 11.50	17° 29.50
(CH0288-63) PB63	17° 27.10	79° 07.00	17° 41.60
(CH0288-64) PB64	17° 46.75	78° 52.75	17°32.50

Parasound Line Number	Start Point Longitude (°N)	Start Point Latitude (°N)	End Point Longitude (°N)
PS Line A Part 1	17° 29.92	78° 08.15	17° 25.11
PS Line A Part 2	17° 25.11	79° 00.97	17° 24.69
PS Line B	17° 41.42	78° 58.44	17° 36.07
PS Line C	16° 49.47	78° 38.04	16° 56.17
PS Line D	16° 50.30	78° 33.17	16° 46.61

End Point Latitude (°N)	Heading (°)	Annotations
-	0° (N)	No exact positions available
-	315° (NW)	No exact positions available
78° 54.25	180° (S)	± perpendicular towards platform margin
79° 06.00	315° (NW)	± perpendicular from platform margin
78° 50.80	180° (S)	± perpendicular towards platform margin
79° 06.50	315° (NW)	± perpendicular from platform margin
79° 11.50	210° (SSW)	± parallel to platform margin (distal)
78° 59.50	130° (SE)	± perpendicular towards platform margin
78° 52.75	45° (NE)	± parallel to platform margin (± proximal)
78° 29.25	120° (SE)	± parallel to platform margin (distal)

End Point Latitude (°N)	Heading (°)	Annotations
79° 00.97	130° (SE)	± perpendicular towards platform margin
79° 00.57	45° (NE)	± parallel along upper slope
78° 52.07	130° (SE)	± perpendicular towards platform margin
78° 38.04	0° (SSW)	± perpendicular towards platform margin
78° 35.95	210° (SSW)	± perpendicular from platform margin

Appendix 10 - Age correlation (Specmap- and Bassinot-Stack)

Specmap and Bassinot Stack

Isotope Event	Specmap-age (ky)	Bassinot-age (ky)
1.1	6	
2.0	12	11
2.2	19	17
3.0	24	24
3.1	28	30
3.3	53	52
4.0	59	57
4.2	65	62
5.0	71	71
5.1	80	79
5.2	87	86
5.3	99	97
5.4	107	106
5.5	122	122
6.0	128	127
6.2	135	133
6.3	146	
6.4	151	
6.5	171	
6.6	183	
7.0	186	186
7.1	194	194
7.2	205	202
7.3	216	213
7.4	228	225
7.5	238	236
8.0	245	242
8.2	249	248
8.3	257	258
8.4	269	266
8.5	287	287
8.6	299	295
9.0	303	301
9.1	310	309
9.2	320	315
9.3	331	328
10.0	339	334
10.2	339	340

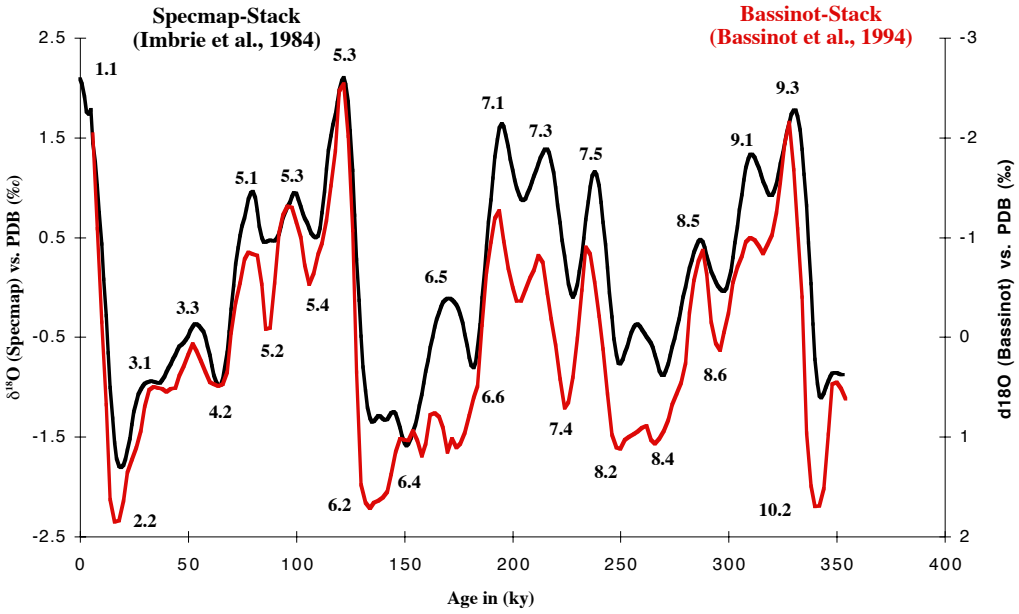

Appendix 11 - Pointcount Data

Pointcount Data **All values in absolute percentages (counting was done using the grain-bulk counting method)**

Depth (cm)	Type of sediment	Micrite	Planktic Foraminifera	Pteropods	Calcispheres	Deep water benthic foraminifera	Shallow water Foraminifera	"Coralgal"	Peloids
1	Intergl. periplatform sediment	45	7	0	2	0.5	1	0	1
10	Intergl. periplatform sediment	44.5	7	0.5	1.5	0.5	1	0	4
30	Intergl. periplatform sediment	59.5	8.5	3	1	1.5	0.5	0	1.5
40	Intergl. periplatform sediment	41.5	4.5	0	1	0	0	0	2.5
50	Turbidite layer	2.5	7	0	0	1	0.5	0	1.5
60	Intergl. periplatform sediment	60	4	1	2	0	0	0	0
70	Turbidite layer	15.5	3.5	0	0	0	2	2.5	15.5
80	Intergl. periplatform sediment	56.5	10	3.5	0.5	0.5	0	0	2
90	Intergl. periplatform sediment	66.5	10	3.5	1	0	0	0	1
100	Intergl. periplatform sediment	54	18.5	8.5	1	0	0	0	0
110	Intergl. periplatform sediment	56.5	14.5	8	0	0	0	0	0
120	Glacial periplatform sediment	63.5	15	7	0	0	0	0	0
130	Glacial periplatform sediment	65.5	10	10	0	0	0	0	1.5
140	Turbidite layer	26.5	12.5	4.5	0.5	0	1.5	0	27.5
150	Glacial periplatform sediment	52.5	5.5	3.5	0.5	0	0	1	4.5
160	Glacial periplatform sediment	75.5	8.5	5	0.5	0	0	0	0
170	Turbidite layer	17	4.5	4	1.5	0	2	4	15
180	Stage 3 periplatform sediment	73.5	11	4.5	0	0	0.5	0	0
190	Stage 3 periplatform sediment	61	14	8	0	0	0.5	0.5	0
200	Stage 3 periplatform sediment	62	14	5.5	0.5	0.5	0	0	0
210	Stage 3 periplatform sediment	60	25	5	0	0	0.5	0.5	0
220	Stage 3 periplatform sediment	61.5	22.5	3.5	0.5	0	0.5	1	2.5
230	Stage 3 periplatform sediment	68	5.5	1.5	0.5	0	0.5	0	3.5

Red algae (Corallinacaea)	Green algae (predominantly *Halimeda)*	Mollusc	Bryozoa	Echinoderms	Ooids	Sparite	Porosity	Unidentifiable grains	"black" Peloids	Intraclasts	Other
0	0	1.5	0	2.5	0	19.5	4	9	4.5	2.5	0
0.5	0	1.5	1	1	0	16.5	4.5	10.5	3.5	2	0
0	0	1	0	0	0	9.5	2.5	6	3.5	1	1
1	0	1	0	1.5	0	22.5	5	13	3	3	0.5
0.5	0	2	0.5	3	0	7.5	20.5	53	0	0	0.5
0	0.5	1	0	1.5	0	11	4	5.5	8	1	0.5
0	0	2.5	0	2	0.5	13.5	12.5	28	0.5	0	1.5
0	0	0.5	0	1	0	9.5	4	1.5	9.5	0	1
0	0	2	0	0	0	7.5	2	1	5	0.5	0
0	0	0.5	0	0	0	7.5	2.5	2.5	5	0	0
0	0	0.5	0	0	0	7	2.5	5	5	1	0
0	0	1.5	0	1.5	0	1.5	2	4	3.5	0.5	0
0.5	0	2	0.5	0	0	1.5	2.5	4.5	1.5	0	0
1.5	0.5	1	0	0.5	0	10.5	4.5	8	0.5	0	0
0	0	2	0	1	1	7	6	13	0	2.5	0
0	0	0	0	0	0	0.5	4	5.5	0	0.5	0
0.5	1.5	3	0	1.5	0	8.5	11	15	0	10.5	0.5
0	0	1	0	1.5	0	1	1	5.5	0	0.5	0
0	0	3	0	0	0	0.5	7	5.5	0	0	0
0	0	2.5	0	1	0	1	3.5	6.5	3	0	0
0	0	4	0	0	0	0	3	1.5	0.5	0	0
0	0	0	0	0	0	2.5	2	2.5	0	0.5	0.5
0	0	1.5	0	0.5	0.5	1	1.5	5.5	7	3	0